WOODHEAD PUBLISHING SERIES IN ELECTRONIC AND OPTICAL MATERIALS

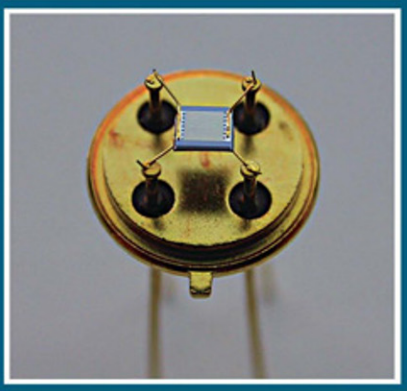

Nanosensors for Chemical and Biological Applications

Sensing with Nanotubes, Nanowires and Nanoparticles

Edited by Kevin C. Honeychurch

WP
WOODHEAD PUBLISHING

Nanosensors for Chemical and Biological Applications

Related titles:

Smart sensors and MEMS
(ISBN 978-0-85709-502-2)

Nanostructured semiconductor oxides for the next generation of electronics and functional devices
(ISBN 978-1-78242-220-4)

Laser spectroscopy for sensing
(ISBN 978-0-85709-273-1)

Woodhead Publishing Series in Electronic and Optical Materials:
Number 61

Nanosensors for Chemical and Biological Applications

Sensing with Nanotubes, Nanowires and Nanoparticles

Edited by
Kevin C. Honeychurch

AMSTERDAM • BOSTON • CAMBRIDGE • HEIDELBERG • LONDON
NEW YORK • OXFORD • PARIS • SAN DIEGO
SAN FRANCISCO • SINGAPORE • SYDNEY • TOKYO
Woodhead Publishing is an imprint of Elsevier

Woodhead Publishing is an imprint of Elsevier
80 High Street, Sawston, Cambridge, CB22 3HJ, UK
225 Wyman Street, Waltham, MA 02451, USA
Langford Lane, Kidlington, OX5 1GB, UK

British Library Cataloguing-in-Publication Data
A catalogue record for this book is available from the British Library.

Library of Congress Control Number: 2014931603

ISBN 978-0-85709-660-9 (print)
ISBN 978-0-85709-672-2 (online)

For information on all Woodhead Publishing publications visit our website at http://store.elsevier.com/

Typeset by Newgen Knowledge Works Pvt Ltd, India

Printed and bound in the United Kingdom

Contents

This page intentionally left blank

Contributor contact details

(* = main contact)

Editor

Kevin C. Honeychurch
Centre for Research in Biosciences
Department of Biological, Biomedical and Analytical Sciences
University of the West of England, Bristol
BS16 1QY, UK

E-mail: kevin.honeychurch@uwe.ac.uk

Chapter 1

Mohammed Boujtita
University of Nantes
Faculty of Science
Department of Chemistry CEISAM-UMR 6230
2 rue de la Houssinière
BP 92208, F-44322 Nantes cedex 3, France

E-mail: mohammed.boujtita@univ-nantes.fr

Chapter 2

Frank Davis and Séamus P. J. Higson*
Cranfield Health
Cranfield University
Bedford, MK43 0AL, UK

E-mail: f.davis@cranfield.ac.uk; s.p.j.higson@cranfield.ac.uk

Chapter 3

Jonathan P. Metters and Craig E. Banks*
Faculty of Science and Engineering
School of Science and the Environment
Division of Chemistry and Environmental Science
Manchester Metropolitan University
Chester Street
Manchester
M1 5GD, Lancs, UK

E-mail: c.banks@mmu.ac.uk

Chapter 4

Frankie James Rawson
Laboratory of Biophysics and Surface Analysis
School of Pharmacy
University of Nottingham
University Park
Nottingham, NG7 2RD, UK

E-mail: frankie.rawson@nottingham.ac.uk

Chapter 5

Luca Francioso
CNR-IMM
Institute for Microelectronics and Microsystems
Unit of Lecce
Via Monteroni, University Campus
73100 Lecce, Italy

E-mail: luca.francioso@imm.cnr.it

Chapter 6

Aysu Yarman
Fraunhofer Institute for Biomedical Engineering IBMT
14476 Potsdam, Germany

and

Institute of Biochemistry and Biology
University of Potsdam
Karl-Liebknecht-Str. 24-25
14476 Potsdam, Germany

Anthony P. F. Turner*
Biosensors & Bioelectronics Centre
IFM-Linköping University
S-58183, Sweden

E-mail: anthony.turner@liu.se

Frieder W. Scheller
Fraunhofer Institute for Biomedical Engineering IBMT
14476 Potsdam, Germany

and

Institute of Biochemistry and Biology
University of Potsdam
Karl-Liebknecht-Str. 24-25
14476 Potsdam, Germany

Chapter 7

Kelly Westmacott and
Anthony J. Killard*
Centre for Research in Biosciences
Department of Biological, Biomedical and Analytical Sciences
University of the West of England
Coldharbour Lane
Bristol
BS16 1QY, United Kingdom

E-mail: Tony.killard@uwe.ac.uk

Bo Weng and
Gordon G. Wallace
Intelligent Polymer Research Institute
University of Wollongong
New South Wales, 2522 Australia

Chapter 8

Laura Rodriguez-Lorenzo
Bio-Nanomaterials, Adolphe Merkle Institute
University of Fribourg
Rte de l'Ancienne Papeterie
P.O. Box 209 CH-1723 Marly 1, Switzerland

E-mail: laura.rodriguez-lorenzo@unifr.ch

Ramón A. Alvarez-Puebla*
Departmento de Ingenieria Electronica
Universitat Rovira i Virgili
Avda. Països Catalans 26
43007 Tarragona, Spain

and

Centro de Tecnologia Quimica de Cataluña
Carrer de Marcel•lí Domingo s/n
43007 Tarragona, Spain

and

ICREA, Passeig Lluís Companys 23
08010 Barcelona, Spain

E-mail: ramon.alvarez@urv.cat

Chapter 9

Nathan Lazarus*
Formerly of Carnegie Mellon University
Currently US Army Research Laboratory
RDRL-SED-E
2800 Powder Mill Rd
Adelphi, MD 20783 United States of America

E-mail: nathan.lazarus2.ctr@mail.mil; nlazarus1@gmail.com

R. Jin
Department of Chemistry
Carnegie Mellon University
1201 Hamburg Hall
5000 Forbes Ave
Pittsburgh
Pennsylvania 15213, USA

G. K. Fedder
Department of Electrical and Computer Engineering
Carnegie Mellon University
1201 Hamburg Hall
5000 Forbes Ave
Pittsburgh
Pennsylvania 15213, USA

Chapter 10

Takeshi Shimomura
Funai Electric Advanced Applied Technology Research Institute Inc. (FEAT)
TCI 37A, 2-1-6, Sengen,
Tsukuba-shi
Ibaraki 305-0047, Japan

E-mail: shimomura.t@funai-atri.co.jp

Chapter 11

Nikos Chaniotakis* and Raluca Buiculescu
Department of Chemistry
University of Crete
Vassilika Voutes
70013, Iraklion
Crete, Greece

E-mail: nchan@chemistry.uoc.gr; raluca@chemistry.uoc.gr

Chapter 12

Yolanda Picó*
Food and Environmental Safety Research Group
Facultat de Farmàcia
Universitat de València
Av. Vicent Andrés Estellés
s/n, 46100 Burjassot
València, Spain

E-mail: Yolanda.Pico@uv.es

Vicente Andreu
Landscape Chemistry and Environmental Forensics Group
Research Center on Desertification-CIDE (CSIC-UV-GV)
Carretera Moncada-Náquera
Km 4.5 Apartado Oficial.
46113 – Moncada
Valencia, Spain

Woodhead Publishing Series in Electronic and Optical Materials

1 **Circuit analysis**
J. E. Whitehouse
2 **Signal processing in electronic communications: For engineers and mathematicians**
M. J. Chapman, D. P. Goodall and N. C. Steele
3 **Pattern recognition and image processing**
D. Luo
4 **Digital filters and signal processing in electronic engineering: Theory, applications, architecture, code**
S. M. Bozic and R. J. Chance
5 **Cable engineering for local area networks**
B. J. Elliott
6 **Designing a structured cabling system to ISO 11801: Cross-referenced to European CENELEC and American Standards Second edition**
B. J. Elliott
7 **Microscopy techniques for materials science**
A. Clarke and C. Eberhardt
8 **Materials for energy conversion devices**
Edited by C. C. Sorrell, J. Nowotny and S. Sugihara
9 **Digital image processing: Mathematical and computational methods Second edition**
J. M. Blackledge
10 **Nanolithography and patterning techniques in microelectronics**
Edited by D. Bucknall
11 **Digital signal processing: Mathematical and computational methods, software development and applications Second edition**
J. M. Blackledge
12 **Handbook of advanced dielectric, piezoelectric and ferroelectric materials: Synthesis, properties and applications**
Edited by Z.-G. Ye
13 **Materials for fuel cells**
Edited by M. Gasik

14 **Solid-state hydrogen storage: Materials and chemistry**
Edited by G. Walker
15 **Laser cooling of solids**
S. V. Petrushkin and V. V. Samartsev
16 **Polymer electrolytes: Fundamentals and applications**
Edited by C. A. C. Sequeira and D. A. F. Santos
17 **Advanced piezoelectric materials: Science and technology**
Edited by K. Uchino
18 **Optical switches: Materials and design**
Edited by S. J. Chua and B. Li
19 **Advanced adhesives in electronics: Materials, properties and applications**
Edited by M. O. Alam and C. Bailey
20 **Thin film growth: Physics, materials science and applications**
Edited by Z. Cao
21 **Electromigration in thin films and electronic devices: Materials and reliability**
Edited by C.-U. Kim
22 ***In situ* characterization of thin film growth**
Edited by G. Koster and G. Rijnders
23 **Silicon-germanium (SiGe) nanostructures: Production, properties and applications in electronics**
Edited by Y. Shiraki and N. Usami
24 **High-temperature superconductors**
Edited by X. G. Qiu
25 **Introduction to the physics of nanoelectronics**
S. G. Tan and M. B. A. Jalil
26 **Printed films: Materials science and applications in sensors, electronics and photonics**
Edited by M. Prudenziati and J. Hormadaly
27 **Laser growth and processing of photonic devices**
Edited by N. A. Vainos
28 **Quantum optics with semiconductor nanostructures**
Edited by F. Jahnke
29 **Ultrasonic transducers: Materials and design for sensors, actuators and medical applications**
Edited by K. Nakamura
30 **Waste electrical and electronic equipment (WEEE) handbook**
Edited by V. Goodship and A. Stevels
31 **Applications of ATILA FEM software to smart materials: Case studies in designing devices**
Edited by K. Uchino and J.-C. Debus
32 **MEMS for automotive and aerospace applications**
Edited by M. Kraft and N. M. White

33 **Semiconductor lasers: Fundamentals and applications**
Edited by A. Baranov and E. Tournie
34 **Handbook of terahertz technology for imaging, sensing and communications**
Edited by D. Saeedkia
35 **Handbook of solid-state lasers: Materials, systems and applications**
Edited by B. Denker and E. Shklovsky
36 **Organic light-emitting diodes (OLEDs): Materials, devices and applications**
Edited by A. Buckley
37 **Lasers for medical applications: Diagnostics, therapy and surgery**
Edited by H. Jelínková
38 **Semiconductor gas sensors**
Edited by R. Jaaniso and O. K. Tan
39 **Handbook of organic materials for optical and (opto)electronic devices: Properties and applications**
Edited by O. Ostroverkhova
40 **Metallic films for electronic, optical and magnetic applications: Structure, processing and properties**
Edited by K. Barmak and K. Coffey
41 **Handbook of laser welding technologies**
Edited by S. Katayama
42 **Nanolithography: The art of fabricating nanoelectronic and nanophotonic devices and systems**
Edited by M. Feldman
43 **Laser spectroscopy for sensing: Fundamentals, techniques and applications**
Edited by M. Baudelet
44 **Chalcogenide glasses: Preparation, properties and applications**
Edited by J.-L. Adam and X. Zhang
45 **Handbook of MEMS for wireless and mobile applications**
Edited by D. Uttamchandani
46 **Subsea optics and imaging**
Edited by J. Watson and O. Zielinski
47 **Carbon nanotubes and graphene for photonic applications**
Edited by S. Yamashita, Y. Saito and J. H. Choi
48 **Optical biomimetics: Materials and applications**
Edited by M. Large
49 **Optical thin films and coatings**
Edited by A. Piegari and F. Flory
50 **Computer design of diffractive optics**
Edited by V. A. Soifer

51 **Smart sensors and MEMS: Intelligent devices and microsystems for industrial applications**
Edited by S. Nihtianov and A. Luque
52 **Fundamentals of femtosecond optics**
S. A. Kozlov and V. V. Samartsev
53 **Nanostructured semiconductor oxides for the next generation of electronics and functional devices: Properties and applications**
S. Zhuiykov
54 **Nitride semiconductor light-emitting diodes (LEDs): Materials, performance and applications**
Edited by J. J. Huang, H. C. Kuo and S. C. Shen
55 **Sensor technologies for civil infrastructures Volume 1: Sensing hardware and data collection methods for performance assessment**
Edited by M. Wang, J. Lynch and H. Sohn
56 **Sensor technologies for civil infrastructures Volume 2: Applications in structural health monitoring**
Edited by M. Wang, J. Lynch and H. Sohn
57 **Graphene: Properties, preparation, characterisation and devices**
Edited by V. Skákalová and A. B. Kaiser
58 **Handbook of silicon-on-insulator (SOI) technology**
Edited by O. Kononchuk and B.-Y. Nguyen
59 **Biological identification: DNA amplification and sequencing, optical sensing, lab-on-chip and portable systems**
Edited by P. Schaudies
60 **High performance silicon imaging: Fundamentals and applications of CMOS and CCD sensors**
Edited by D. Durini
61 **Nanosensors for chemical and biological applications: Sensing with nanotubes, nanowires and nanoparticles**
Edited by K. C. Honeychurch
62 **Composite magnetoelectrics: Materials, structures, and applications**
G. Srinivasan, S. Priya, and N. Sun
63 **Quantum information processing with diamond: Principles and applications**
Edited by S. Prawer and I. Aharonovich
64 **Advances in nonvolatile memory and storage technology**
Edited by Y. Nishi
65 **Laser surface engineering: Processes and applications**
Edited by J. Lawrence, C. Dowding, D. Waugh and J. Griffiths
66 **Power ultrasonics: A handbook of materials, design and applications of high power ultrasound transducers**
Edited by J. A. Gallego-Juárez

67 **Advances in delay-tolerant networks (DTNs): Architectures, routing and challenges**
Edited by J. Rodrigues
68 **Handbook of flexible organic electronics: Materials, manufacturing and applications**
Edited by S. Logothetidis
69 **Machine-to-machine (M2M) communications: Architecture, performance and applications**
Edited by C. Anton-Haro and M. Dohler
70 **Ecological design of smart home networks: Technologies, social impact and sustainability**
Edited by N. Saito and D. Menga
71 **Industrial tomography: Systems and applications**
Edited by M. Wang
72 **Vehicular communications and networks: Architectures, protocols, operation and deployment**
Edited by W. Chen
73 **Modeling, characterization, and production of nanomaterials: Electronics, photonics and energy applications**
Edited by V. Tewary and Y. Zhang
74 **Reliability characterisation of electrical and electronic systems**
Edited by J. Swingler
75 **Handbook of industrial wireless sensor networks: Monitoring, control and automation**
Edited by R. Budampati S. Kolavennu
76 **Epitaxial growth of complex metal oxides: Techniques, properties and applications**
Edited by G. Koster and G. Rijnders
77 **Semiconductor nanowires: Materials, synthesis, characterization and applications**
Edited by J. Arbiol and Q. Xiong

Introduction

KEVIN C. HONEYCHURCH,
B.Sc. (Hons), M.Sc. Ph.D. MRSC, CChem,
University of the West of England, UK

Nano-sized materials have been shown to have a number of novel and interesting physical and chemical properties. These can have marked differences from those of the bulk material, offering the possibility of new applications and improved performance. This book comprises a set of in-depth monographs which seek to provide an overview of some of the important and recent developments brought about by the application of nanotechnology for both chemical and biological sensor development. Up-to-date information on the fabrication, properties and operating mechanisms of these sensors is given. Progress in the field, fundamental issues and challenges facing researchers, and prospects for future development are discussed. The book will be of interest to those with a general interest in the area, researchers actively engaged in one or more of the areas covered, and research students who are just entering into the field. It is hoped that the book will also provide insights into the direction of future developments.

The book is organised into two sections: firstly the electrochemical and secondly the spectrographic application of nanosensors technology. Chapter 1 describes the synthesis of both single-wall and multi-wall carbon nanotubes and their application in electrochemical biosensor systems. The second chapter continues this theme, concentrating on the application of nanotechnology for the electrochemical glucose biosensor. The chapter discusses how nano-sized materials have been incorporated into conventional enzymatic and non-enzymatic electrochemical glucose sensors, and the construction of complete sensors on the micro/nanometre scale. Chapter 3 examines some of the analytical advantages that metal nanoparticles provide for stripping voltammetric electroanalysis, discussing several analytical applications of the technology. A great deal of interest has focused on exploring the biochemistry of living cells, and Chapter 4 reports on the development and application of nano-sized electrochemical sensors capable of interfacing directly with living cells. This chapter shows that such an approach can allow for previously unattainable insights into intracellular and extracellular purposes to be monitored. Chapter 5 reviews the determination of

gases with low dimensional and semi-conductive nanoparticle-based metal oxide chemiresistor-based sensors. The fundamentals of these sensors are explored with descriptions of techniques typically adopted for their preparation. New research trends, and low cost and alternative substrates are also discussed. In Chapters 6 and 7 the possibility of integrating nanotechnology and polymer science is investigated. In the first of these chapters, electropolymerised molecularly imprinted polymers are investigated as biomimetic sensors. The integration of nanomaterials into the sensing layer of these devices is reported to have a number of advantages, such as increased surface area, mass transport and conductivity allowing for the electrochemical preparation of catalytically active molecularly imprinted polymers. Chapter 7 discusses the available methods for fabricating conducting polymer nanomaterials, and looks at their application to electrochemical sensing and biosensing of a range of different analytes.

In the second section, developments of nanotechnology for spectrographic-based sensors are discussed. In the first chapter in this section, Chapter 8, nanoparticle-based sensors utilising the enhancement of spontaneous Raman scattering are described. The following chapter describes the application of coated gold nanoparticles for creating high performance chemiresistive sensors. The chapter reviews their use, synthesis, and the choice of coating material, and gives a review of present applications. Chapter 10 explores both the theory and practical possibilities of enzyme encapsulation into the pores of nanoporous silicon material as an effective method for obtaining enzymatic biosensors. The chapter then illustrates the application of this approach for the determination of formaldehyde. The penultimate chapter explores the application of quantum dots for the development of sensors and biosensors based on Förster fluorescence resonance energy transfer detection of proteins and enzymatic activities and nucleic acids. In the final chapter, the environmental fate, behaviour, disposition and toxicity of nanoparticles are discussed. An overview of the present analytical methods and sample preparation used for their determination is given.

I would like to thank all the authors who have contributed to the successful completion of this book and the very high standard of the contributions made, as well as for their dedication, professionalism and the friendly manner in which all this has been achieved. I would also like to thank all the staff at Woodhead for their helpful assistance throughout the development of this project.

Part I

Electrochemical nanosensors

This page intentionally left blank

1

Chemical and biological sensing with carbon nanotubes (CNTs)

M. BOUJTITA, University of Nantes, France

DOI: 10.1533/9780857096722.1.3

Abstract: Carbon nanotubes (CNTs) modified with biorecognition elements constitute an ideal material for tailoring nanostructured surfaces for sensor devices. This chapter focuses on recent advances in analytical tools based on CNTs. Firstly, the main approaches for the fabrication of CNTs are described including single-wall and multi-wall CNTs. Recent advances in functionalizing CNTs are also reported and discussed. Subsequently, the chapter discusses various configurations of biosensors, including their integration in analytical devices. The chapter concludes with a discussion on the future challenges and prospects of the application of CNTs in analytical devices.

Key words: CNT-based biosensors, bioanalytical applications, surface functionalization, electrochemical biosensing, analytical nanodevices.

1.1 Introduction

Carbon nanotubes (CNTs)[1,2] have a one-dimensional cylindrical shape with nanometer scale diameters and micrometre scale lengths. They are formed from rolling up single or multiple sheets of graphene. Depending on the number of layers of graphene sheets and their chirality, CNTs may have properties as conductors, semiconductors or superconductors. Due to their unique properties, CNTs may find a number of potential and varied applications in analytical and bioanalytical fields. Consequently, a great deal of attention has been focused on optical biosensors,[3–8] electrochemical biosensors,[9–11] and FET biosensors.[12–14] To exploit the remarkable properties of this nanomaterial in biosensor development, CNTs need to be purified and functionalized with biosensing elements. The design of the biosensing interface constitutes the key challenge in biosensor development. It needs to take into account both the functionalization and transduction steps. In order to achieve this, the immobilization of the biosensing element must be optimized so that the analyte can be selectively recognized at the biosensor surface. Transduction must also be optimized so that small changes in the

biorecognition element resulting from the presence of the target analyte can be rapidly and sensitively detected.

Since 1996 there have been more than 1300 papers reported on CNT-based biosensors, and 165 reviews since 2003. This chapter will include an overview of CNT-based biosensors, but the main focus will be on the most notable advances in the field of CNT-based biosensors. It will begin by describing the main synthesis methods of CNTs. Then it will go onto explain the important strategies used for functionalizing CNTs and how they can be used in the preparation of biosensors. To conclude, technical and industrial challenges for the integration of CNTs in analytical and bioanalytical devices will be discussed.

1.2 Synthesis of carbon nanotubes (CNTs)

CNTs can be grouped into two main forms,[2,15] single-walled carbon nanotubes[16] (SWCNTs) and multi-walled carbon nanotubes[17] (MWCNTs), as shown in Fig. 1.1. In the latter, a number of SWCNTs are assembled in a concentric disposition to form MWCNTs with variable diameters. The diameter of the MWCNT depends on the number of concentric nanotubes. The external diameter is generally less than 2 nm for SWCNTs. Various authors consider SWCNTs as a single large molecule, whereas MWCNTs are considered as a mesoscale graphite system with diameters ranging between 2 and 200 nm.

Four methods are identified for synthesizing CNTs:

- arc discharge
- laser ablation

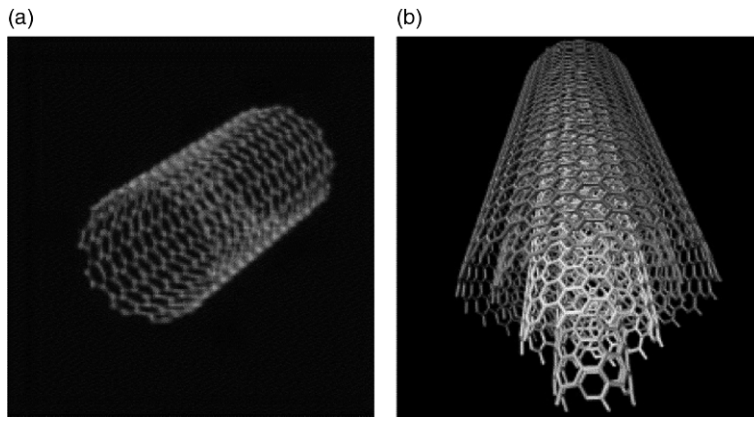

1.1 Schematic presentation of (a) SWCNT and (b) MWCNT. (*Source*: Reprinted from reference 15 with permission from Elsevier.)

- chemical vapour deposition
- plasma enhanced vapour deposition.

The arc discharge method consists of applying a voltage of about 20 V between two graphite electrodes held 1–3 mm apart. The synthesis is carried out in an inert atmosphere, typically argon. The arc discharge evaporates the graphite on the anode, which leads to an increase in local temperature. The graphite then condenses onto the cathode, forming the CNTs. The arc discharge method was first used to synthesize fullerenes; it was also regarded as a simple method for synthesizing CNTs.[1] MWCNTs are synthesized when pure graphite is used as an electrode. The arc discharge evaporation method was the first method used for synthesizing SWCNTs. Since 1991, a large amount of research has been directed towards attempts to synthesize homogeneous SWCNTs. SWCNTs are obtained when a graphite anode containing a metal catalyst, Fe, Ni or Co, is used with a cathode comprising pure graphite. However, the arc discharge method is incapable of controlling the purity of CNTs; chemical refinement is required to obtain pure CNTs.

It has been demonstrated that CNTs can be synthesized using a high power laser beam with a pulsed laser. Consequently, in 1996, the related SWCNTs were reported to be made by laser ablation.[17–22] In this method, a target containing a mixture of graphite and metal catalyst, Co or Ni, was used under a flow of inert gas, such as argon. The laser causes the evaporation of graphite, and the graphite then condenses on the cooler surface, which forms the CNTs. However, this method also leads to the formation of impure CNTs that also require chemical refinement.

The chemical vapour deposition (CVD)[23,24] process has been found to be a very promising approach to synthesize CNTs. This method uses a carbon precursor gas that decomposes on a metal catalyst surfaces under thermal heating. Various gases can be used, including CO, C_2H_2 and CH_4. According to the CVD method, MWCNTs present an inner diameter of about 1–3 nm and outer diameter varying from 2 to 20 nm. SWCNTs may also be obtained by using CVD; however, their synthesis has been found difficult to control.

The CVD process has been improved by adding an additional plasma process: plasma enhanced CVD (PECVD).[25–32] In this method, the activation of gas is carried out by using electron impact instead of thermal energy. This presents an important advantage, leading to the possibility of synthesis at low temperatures. The PECVD process is now considered the most appropriate method for synthesizing interfaces modified with CNTs on various substrates (glass, silicon) as it does not damage them. It is interesting to note that PECVD is used to synthesize vertically aligned CNTs at temperatures ranging from 400°C to 650°C.[33–41]

1.3 Functionalization of CNTs

There has been significant interest in developing methods to functionalize CNTs for a variety of applications including biosensing transducers.[42–49] The functionalization of CNTs is required for three reasons: (i) to modify the electrode surface with ordered anchoring of CNTs, (ii) to immobilize biosensing elements on CNTs and (iii) to change the optical and electronic properties of CNTs for a desired application. One of the major difficulties of making CNTs functional is their poor solubility in most solvents, including organic and aqueous media. There are three methods to minimize the π-staking of CNTs and their aggregation: the first is based on covalent modification by grafting functional group via sp^2 carbon atoms of CNTs;[50,51] in the second method, the functionalization is based on non-covalent modification by adsorbing functional groups via hydrophobic chemical structures;[52] finally, the third method is completed by creating defect groups of functionalization on the ends and sidewalls of CNTs.[53] The most used approaches for the functionalization of CNTs are based on chemical, physical or electrochemical processes.

1.3.1 Chemical functionalization

There are many methods to increase the bio-applications of CNTs, but the acid-oxidized treatment was probably the most used method in the past for introducing oxygenated chemical groups namely –COOH, –CO and –OH. The functionalization of CNTs using a nitric or nitric/sulfuric acid mixture was found to be effective for increasing the oxygenated functional groups of both ends and sidewalls of CNTs.[54,55] Despite the fact that the hydrophilic character of CNTs is found to be increased by oxidative treatment, the effects on the deterioration of electrical, optical and electrochemical properties of CNTs are often difficult to control. For instance, depending on the size and nature of CNTs (single or multi-wall), oxidative treatment may introduce defect sites, leading to undesired chemical and physical properties after treating CNTs. The effect of oxidative treatment could vary greatly.

Sidewall damage due to the introduction of defect sites in the SWCNTs sp^2 structure may lead to a change in hybridization of the carbon to sp^3. This change causes a significant change in both conductivity and optical properties of SWCNTs.[56] Selective oxidation of SWCNTs[57–59] can be obtained by controlling the temperature, the concentration of oxidant reagents, the heating time, and by monitoring the functionalization degree via spectrometric measurements (Raman, IR, etc.).

The preparation of carboxylated CNTs constitutes an interesting further chemical modification of CNTs. Carboxyl groups may be used as precursors

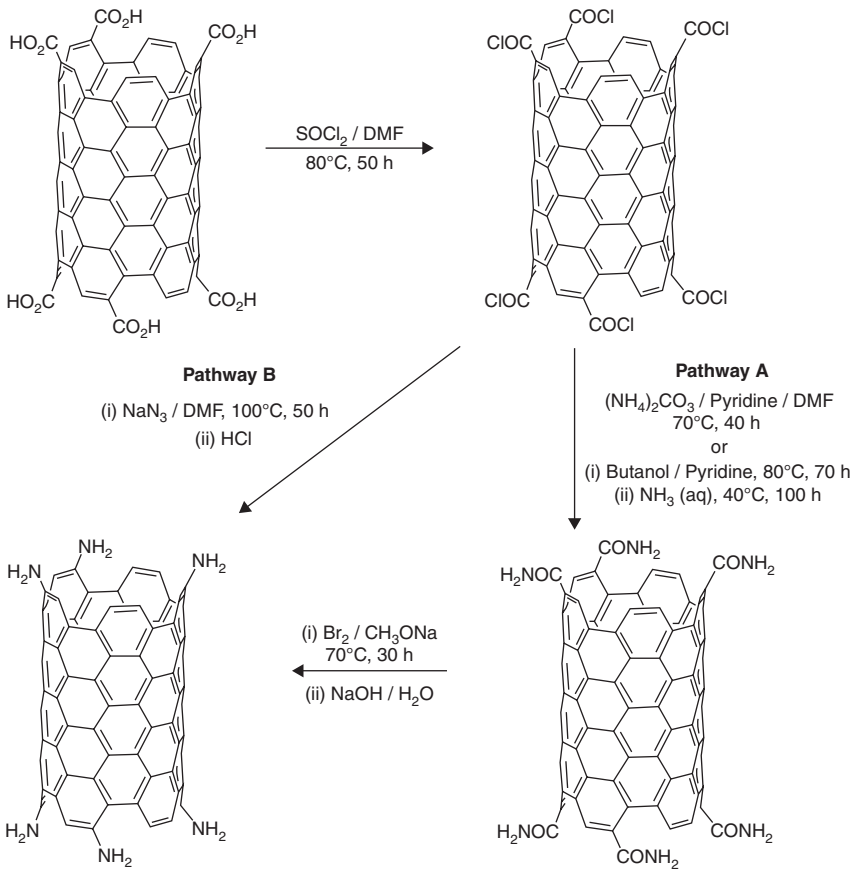

1.2 Preparation of amino-functionalized SWCNTs via Hofmann rearrangement of carboxylic acid amide (pathway A) and via Curtius reaction of carboxylic acid chloride with sodium azide (pathway B). (*Source*: Reprinted from reference 61 with permission from American Chemical Society.)

to obtain new functionalities as amine or amide groups. For that purpose, amino groups were obtained by using two methods:[60,61] (i) the Hofmann rearrangement of the corresponding amides and (ii) the Curtius reaction of carboxylic acid chloride with an azide group (Fig. 1.2).

Most of the strategies reported in the literature indicate the difficulty in integrating an ordered molecular structure onto the CNT surface. This difficulty is often due to the incompatibility between the functionality of the chemical structure desired and the experimental conditions required for CNT functionalization. The use of the click chemistry concept offers some interesting possibilities for CNT functionalization for different

applications.[62–74] The best known reaction of click chemistry is the Cu(I)-catalysed azide-alkyne 1,3-dipolar cycloaddition (CuAAc), which was successfully used in the preparation of biosensors. This method may be achieved in mild experimental conditions and coupled to the diazonium method. The major advantage of this method is the control of the molecular architecture of the electrode surface (Fig. 1.3).[75]

Chemical functionalization of CNTs is still challenging, due to the difficulty of obtaining a well-ordered molecular architecture of the electrode surface in a reproducible way and under mild experimental conditions. A well-organized molecular architecture, based on supramolecular chemistry, can be obtained by combining various methods including the diazotation process, click chemistry and incorporation of metal NPs. It is worth noting that the effect of the functionalization of both electronic and optical properties is different depending on the nature of the CNTs: SWCNTs or MWCNTs. For instance, a compromise must be found between increasing the functionalization coverage and decreasing SWCNTs' conductivity. Covalent functionalization of SWCNTs may be replaced by non-covalent functionalization in order to minimize the change in network resistivity of CNTs. The resistivity of MWCNTs is generally less sensitive to the effect of

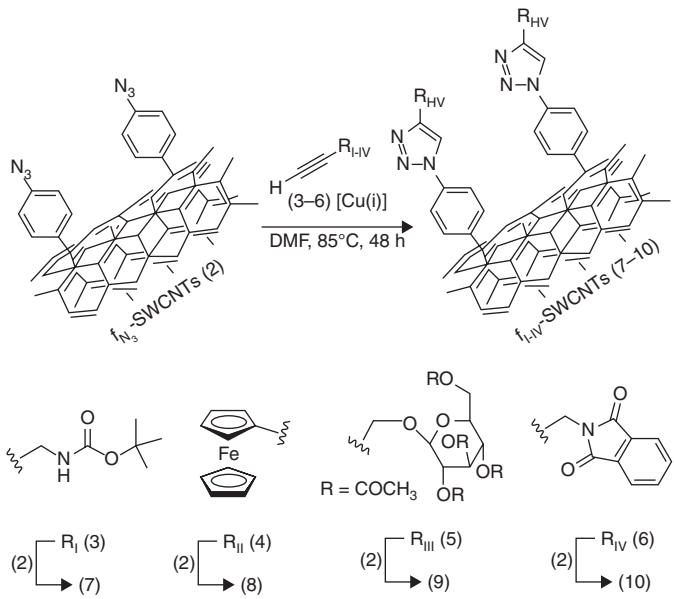

1.3 CuAAc reaction between arylazido-decorated fN3-SWCNTs (2) and alkyne-terminated organic/organometallic compounds (3–6). (*Source*: Reprinted from reference 75 with permission from John Wiley and Sons.)

functionalization processes; the conductivity is kept through the inner walls even if the MWCNTs are modified.

1.3.2 Physical functionalization

Strong acid-treatments used in chemical processes for CNTs modifications were found to be not only effective to introduce oxygen-containing functional groups,[76–82] but also demonstrated to be effective to remove metallic catalysts[83–85] from CNTs. However, the acid oxidation of CNTs is limited by the time required for the process. This is often considered inappropriate in industrial applications. Alternative approaches have been explored for functionalizing CNTs by introducing oxygen-containing groups on the end and sidewall of CNTs.

Among these approaches, plasma processes have been explored to graft various functional groups as carboxylic, hydroxyl or amine groups. For those purposes, a series of plasma gases could be used, such as oxygen, air, mixture of hydrogen/nitrogen, or carbon dioxide. Plasma processes have also demonstrated an effective way of increasing the hydrophilic character of CNTs, thus facilitating the immobilization of bio-recognizing systems for the fabrication of biosensors.

In the case of an aligned configuration of CNTs, microwave plasma treatment using CO_2 or N_2/H_2 not only permitted the functionalization of the CNTs but also avoided the aggregation phenomena, thus retaining the alignment structure of the electrode surface.[82] The authors demonstrated that the resulting treated materials based on CNTs were found to be suitable to develop high sensitivity enzyme biosensors operating on a direct electron transfer process. The atmospheric plasma treatment was demonstrated to be more appropriate for functionalization of CNTs with aligned configuration compared to the classical oxidative treatment which occurred in the solution.

1.3.3 Non-covalent functionalization

Non-covalent functionalization is very useful since it offers the possibility to modify CNTs without damaging the sp^2 structure. This may cause a significant change in both the conductivity and optical properties of CNTs. The exploitation of π–π interaction for stabilizing the dispersion of CNTs in suspensions was often reported. For instance, current monovalent functionalization of CNTs includes π–π stacking of aromatic groups (e.g. pyrene) and sidewalls of CNTs. 1-pyrene-butanoic acid succinimidyl ester was used to covalently bind biomolecules to CNTs (Fig. 1.4).[52] The non-covalent functionalization of SWCNTs could be considered to be the most suitable for preparing biosensors based on luminophor systems.[86,87]

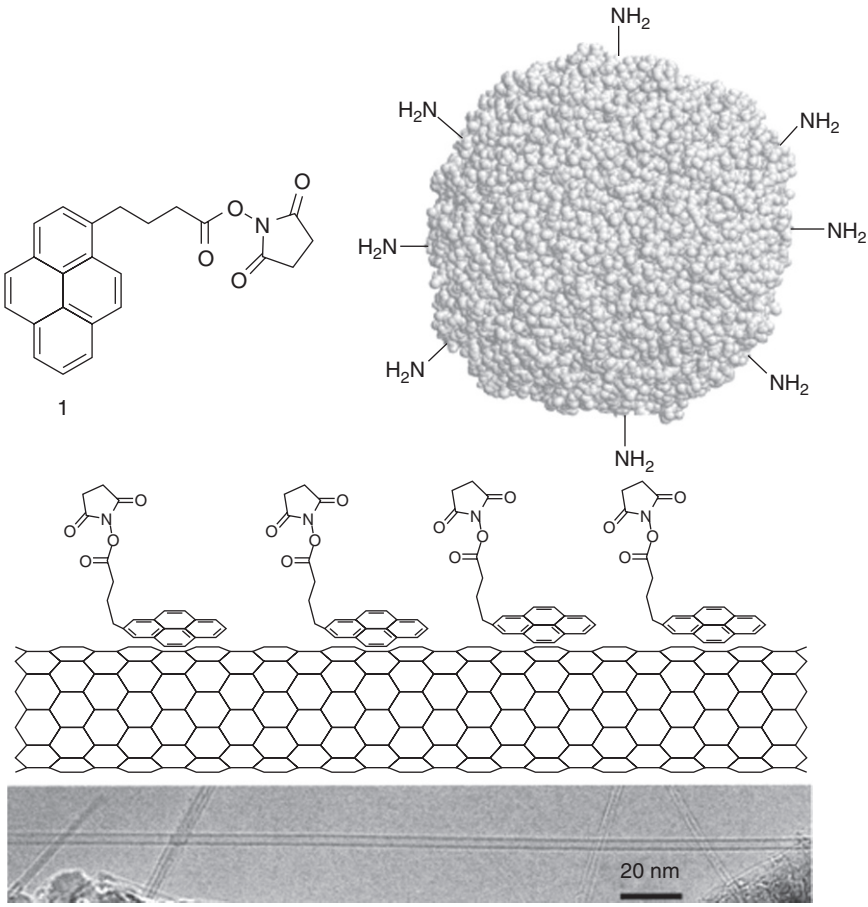

1.4 Pyrenebutanoic acid succinimidyl ester irreversibly adsorbed onto the sidewall of a SWCNT via π-stacking. (*Source*: Reprinted from reference 52 with permission from American Chemical Society.)

1.3.4 Electrochemical functionalization

Electrochemistry may offer the possibility to functionalize CNTs under mild reaction conditions while avoiding undesired and uncontrolled reactions. Diazonium salt reactions provide interesting approaches for functionalizing the end-tip and sidewall of CNTs.[88–102] Interesting results have been obtained with diazonium salts for functionalizing CNTs; however, obtaining monolayers with a well-controlled architecture remains a challenge due to the spontaneous polymerization process of radical species which are formed from the decomposing diazonium salts. The diazonium salt method can

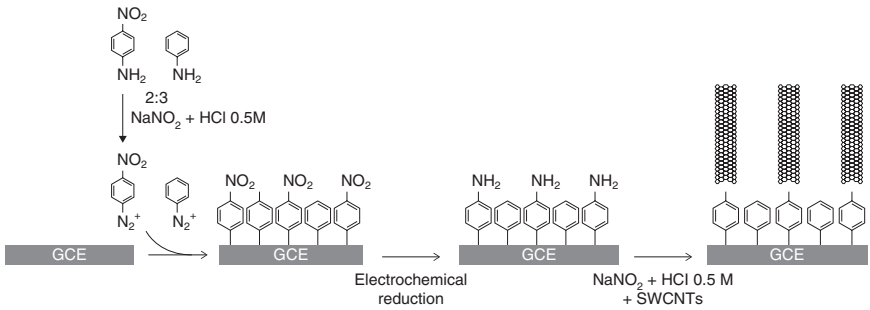

1.5 Schematic representation of SWCNT assembly on glassy carbon electrode (GCE). Immobilization of unfunctionalized SWCNTs on a GCE modified by a mixed monolayer of phenyl/aniline groups 3:2, obtained by the diazonium reaction. (*Source*: Reprint from reference 89 with permission from John Wiley and Sons.)

cause the CNTs to anchor on an electrode surface (Fig. 1.5).[89] The authors demonstrated that a well-organized assembly of CNTs is obtained, which provided a simple approach for modifying electrode surfaces with CNTs. The advantage of aryl diazonium salt derivatives is that they can be applied to a variety of surfaces, such as CNTs decorated with metal nanoparticles.

The modification of electrode surfaces with aryl diazonium salts is obtained by the reductive adsorption of one electron from the radical aryl diazonium. The electrochemical regeneration of the radical species is achieved at a working potential value of about 0 V vs saturated calomel electrode (SCE), either in acetonitrile or in aqueous acid solutions with a pH of below 2.[103,104] A covalent stable C–C bond with the carbon electrode is formed. However, the formation of the radical aryl diazonium often leads to multilayer structures instead of a well-ordered monolayer. This is the most important drawback to electrochemical functionalization using diazonium salts.

The side reactions in which radical aryl diazonium is involved are not only dependent on applied potentials or electrolysis time, but are also dependent on the nature of radical group R and the reactivity of the electrode surface. Depending on the nature of R, the radical aryl diazonium may undergo a polymerization process involving attacks on the ortho-position. An appropriate control of the charge passed during the electrochemical functionalization may be used to avoid the formation of multilayers.[105] The functionalization of CNTs by aryl diazoniums was suggested as a way to facilitate their solubility in organic and aqueous solutions. Tour *et al*.[106] reported that by using a variety of diazonium salts, modification of the sidewalls of SWCNTs occurred. The functionalization was studied and the chemical structure of carbon surface was monitored by IR, XPS, ETM and Raman. It is worth noting that the Raman D-band measurements

indicated that multilayers could easily be grown on the sidewalls of CNTs. The intensity of the D-band is often used as an indicator to access the number of carbon of SWCNTs transformed from sp^2 to sp^3. The authors demonstrated that the intensity of the D-band remained constant after the functionalization process, proving that aryl diazonium rings were not grafted to the sidewalls of CNTs but to the aromatic itself.

On the whole, various studies on electrografting of molecules and biomolecules have been reviewed by using several precursors including amines, carboxylic groups, alcohols, vinylics, diazonium salts, etc. Generally, any precursor can be grafted onto the CNTs' surface as long as it is able to generate radical species. The *in situ* generation of aryl radical species was found very useful for the functionalization of CNTs, but this process needs to be improved to better control the formation of multilayers;[107] this often leads to a significant passivation of electrode surface. The nature of precursors is primordial for minimizing polymerization process and optimizing the homogeneity of the structure of the surface. It is obvious that a better understanding of both the chemistry and electrochemistry of precursors will provide valuable knowledge in the field of electrochemical functionalization. This will lead on to more reliable control to obtain a homogeneous and monolayer structure.

1.3.5 CNTs/nanoparticles (NPs) as nanohybrid materials

CNTs may be used as appropriate materials for the incorporation of noble metal nanoparticles (NPs).[61,108–110] Since the first report dealing with noble metal NP/CNT nanohybrid materials, a series of manuscripts have been focused on approaches for assembling NPs on CNTs. Some of these approaches[111–114] are based on layer-by-layer methods by exploiting positively charged AuNPs. These are able to be anchored in functionalized CNTs. Other approaches lead to self-assembled anchoring of CNTs[115–118] on electrode surfaces by using gold NPs.

Development of new methods to prepare nanostructured hybrid material-based AuNPs–CNTs systems was reported in the literature, each method providing specific properties in terms of size and density of NPs. These methods include electrochemical deposition, chemical deposition, interaction of NPs with functionalized CNTs and physical methods. For instance, a simple method based on *in situ* growth of AuNPs on CNTs under mild experimental conditions has been studied, and uniform dispersion of AnNPs with low size decorating CNTs was obtained.

From an analytical point of view, the combination of CNTs and metal NPs leads to a synergistic effect in terms of sensitivity and electrical connection. The functionalization of AuNPs integrated into CNTs leads to a high surface-to-volume ratio, which is suitable for the preparation of better

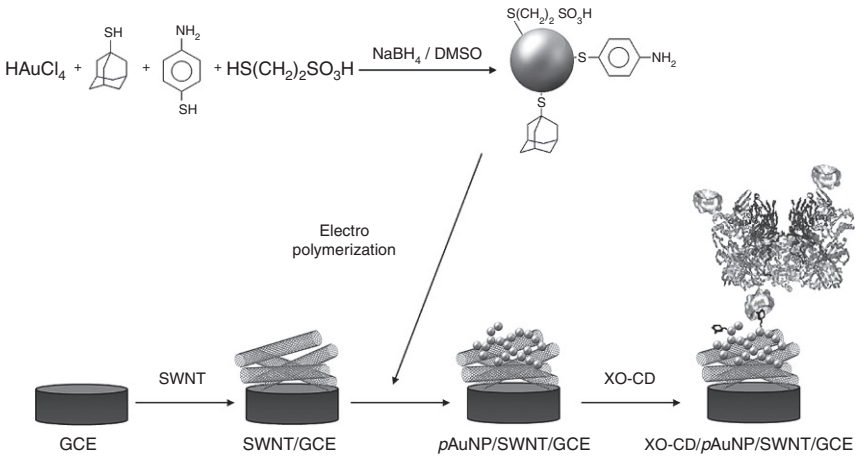

1.6 Main steps involved in the preparation of XO-CD/pAuNP/SWNT/GCE enzyme biosensors. (*Source*: Reprinted from reference 119 with permission from American Chemical Society.)

performing biosensors. Furthermore, surfaces with CNTs/AuNPs based on the use of host–guest supramolecular interactions constitute an effective way for immobilizing enzymes on AuNPs.[119] The preparation of nanostructured electrode surfaces by electropolymerizing polyfunctionalized AuNPs with 2-mercaptoethanesulfonic acid, 1-adamantanethiol and p-aminothiophenol was carried out (Fig. 1.6).

1.4 Biosensors based on multi-walled carbon nanotubes (MWCNTs)

Carbon nanotubes are a promising electrochemical material for biosensors due to its high specific area surface and excellent electrochemical reactivity. Within this context, the use of CNTs as a platform for immobilizing redox enzyme and exploiting their ability to promote electron transfer reactions is considered as an interesting strategy for enhancing analytical performances of biosensors.

1.4.1 Enzymatic biosensors with aligned configurations

The modification of electrodes with CNTs can be achieved in two ways. The first method is based on random distribution of CNTs on the electrode surface; this method is probably the most studied, because it is easy to carry out. The second method involves self-assembled CNTs or aligned CNTs on

the electrode surface. This latter approach represents an attractive advantage for preparing more selective and sensitive biosensors.

The establishment of direct electron transfer (DET) between the redox enzyme and the electrode surface is still considered, until now, to be difficult to achieve, due to the location of a redox site inside the insulated protein shell. Self-assembled monolayers (SAMs) using functionalized thiols on gold constitute, probably, the most explored way to promote DET.[120–125] The introduction of the concept of the electron relays[126–128] to the study of the electrochemistry of the redox enzyme has enabled the reduction of the electron distance.

Various strategies have been reported to promote the direct electrochemistry redox enzymes[129–133] and for that purpose we can cite the concept of 'molecular wire' introduced by Hess *et al*.[134] This is where a conjugated molecular wire poly-(phenylethynyl) terminated with aniline and thiol functionalities was assembled on a gold electrode. The wire was connected to the enzyme by the amino-group. The supra-chemistry is now able to provide a series of molecular wires with a well-defined architecture appropriate for modifying electrode surfaces with specific aligned and spaced configurations.[102,135] Another model of molecular wire which is attractive and appropriate for micro/nanotechnology fabrication is CNTs. Electrode surfaces modified with CNTs may also provide an interesting way to establish an electrical communication between the redox enzyme centre and the electrode. Both the nanoscale size and conductive properties of CNTs may facilitate an efficient DET.

Furthermore, CNTs, as nanoscale materials, may offer various attractive advantages, in that they offer the possibility to increase the analytical performance in terms of selectivity and sensitivity. For instance, a better selectivity could be obtained by achieving DET from the redox enzymes to the electrode surface using a relatively simple chemistry.

The use of CNTs may offer a large surface for enzyme binding, which is beneficial for increasing the biosensor sensitivity. Gooding's group has demonstrated that shortened CNTs may be immobilized via cysteamine with an aligned configuration on a gold electrode by self-assembly.[102] Microperoxidase attached to the ends of CNTs showed an efficient DET, demonstrating that CNTs act as molecular wires to establish electrical contact between the electrode surface and the redox proteins.

Vertically aligned configurations of CNTs could be obtained either by self-assembly or by using CVD techniques with direct synthesis of CNTs on the electrode surface. Clearly, modified electrodes based on an oriented CNT standing perpendicularly on a conductive substrate should offer the advantage of greater electrochemical reactivity. Consequently, the aligned configuration of CNTs has to provide a higher electrochemical reactivity and a better DET. However, one of the primordial issues in the preparation

of electrochemical biosensors based on CNTs is how to avoid both the non-specific immobilization of redox enzymes and its random orientations on the electrode surface. A random distribution of enzymes on the electrode surface often leads to an inefficient DE, so a controlled and optimized orientation of the redox proteins constitutes a crucial step and should promote the DET.

It is worth noting that some elegant strategies for achieving effective electrical contact between a redox enzyme and the electrode surface have been reported in the literature.[136] The authors have proposed an effective method to orientate glucose oxidase for establishing DET. According to this strategy, the enzyme is immobilized with an optimal orientation maintaining a redox site in proximity of the electrode surface. The resulting methodology is based on a reconstitution method in which a redox centre is first separated from the enzyme. Firstly, the isolated redox centre (e.g. flavin–adenine dinucleotide, FAD) is linked to the CNTs with an aligned configuration. Secondly, the bioelectrocatalytic activity is reconstituted by adding the apoenzyme to the already modified electrode surface, as is schematically displayed in Fig. 1.7.

Gooding's group compared the DET involving CNTs plugged to GOD using two methods.[133] In the first method, GOD was immobilized directly to the ends of CNTs without immobilizing FAD. In the second method, FAD was first linked to the ends of the CNTs and apoenzyme was then added to reconstitute the active GOD around CNTs containing FAD. The authors demonstrated that this latter way permits more efficient DET.

In another example, an electrically contacted cellobiose (CDH) with CNTs showed that CDH is able to transfer its electron to the electrode surface.[137] The authors stipulated that the electrons are transferred directly from the FAD to acceptors (haemic structure cofactor) which can act as a redox mediator between CDH and CNTs. The modification of the electrode was achieved via adsorbed CNTs on a glassy carbon surface. The adsorbed CNTs were modified using aryl diazonium salts generated *in situ* from p-aminobenzoic and p-phenylenediamine, leading to negative or positive charges depending on the pH value (Fig. 1.8). The adsorption of CDH on both electrode types led to an efficient DET.

1.4.2 DNA-biosensors

Because of the emergence nanomaterials in the bioelectrochemistry field, the DNA-biosensor developments have taken advantage of CNTs to increase the sensitivity.[10,45,50,138–142] For that purpose, CNTs were used for immobilizing DNA molecules amplifying the signal of hybridization detection.[143] Generally, an ssDNA probe is attached to the CNTs (single- or multi-wall) and the hybridization process between the DNA probe and its

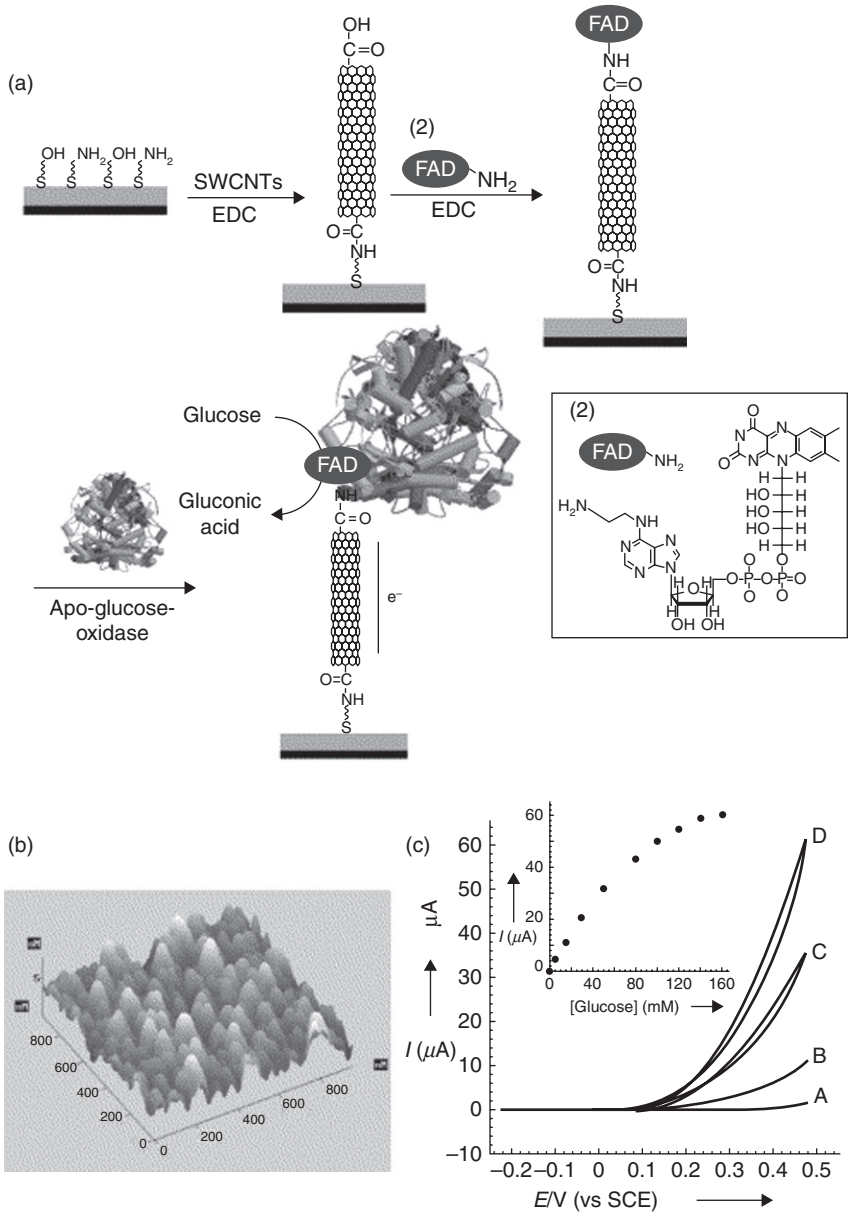

1.7 Electrical contacting of glucose oxidase with a gold electrode using carbon nanotubes as connectors. (a) The reconstitution of apo-glucose oxidase (apo-GOx) on FAD-functionalized SWCNTs associated with an electrode in the presence of EDC (1-ethyl-3-[3-dimethylaminopropyl] carbodiimide). (b) Atomic force microscopy image of the reconstituted GOx on the FAD-functionalized SWCNTs. (c) Cyclic voltammograms corresponding to the bioelectrocatalytic anodic currents generated by GOx reconstituted on the SWCNT-modified electrode, using 25–30 nm

(*Continued*)

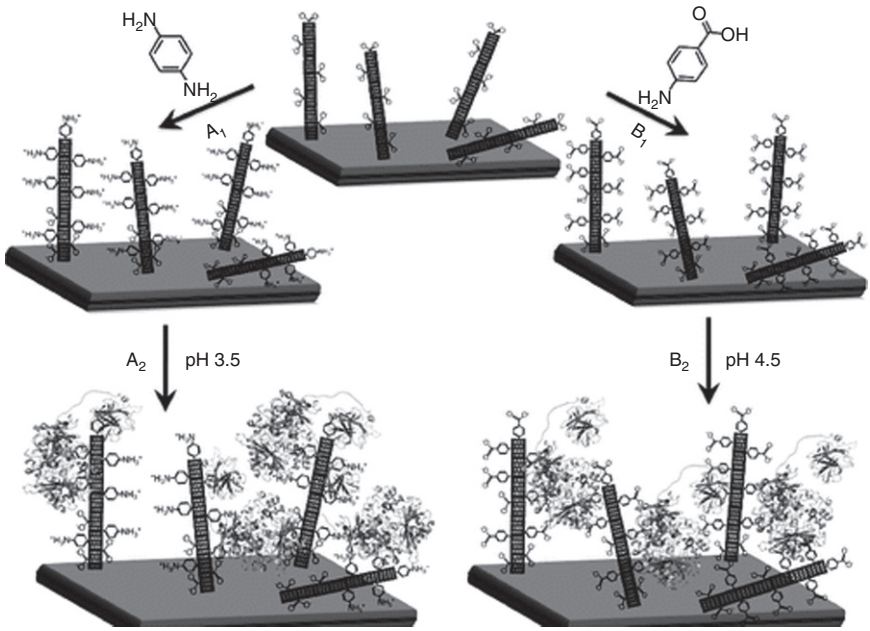

1.8 SWCNTs-GC electrodes modified with p-phenylenediamine or p-aminobenzoic acid. After the modification, the orientation of redox enzyme is influenced by the charged surfaces: The highly negatively charged redox enzyme is attracted by the positive charges of A2 or repulsed by the negative charges on B2. (*Source*: Reprinted from reference 137 with permission from American Chemical Society.)

complementary target is detected by using several transducing modes. The most reported are electrochemical, including cyclic voltammetry or electrochemical impedance spectrometry, piezoelectric quartz-crystal impedance (PQCI) and fluorescence spectroscopy. Redox intercalators as derivatives of Ru complex (e.g. $Ru(bpy)_3^{2+}$) have been introduced to amplify the electrochemical signal[144] of the hybridization process. A new approach has been used by combining NPs and CNTs; in this way NPs were used as relays for the DNA attachment to CNTs [145–148] and enabled reaching a low LOD in the pM range.

1.7 Continued

long SWCNTs, in the presence of variable concentrations of glucose: A. 0 mM, B. 20 mM, C. 60 mM and D. 160 mM. Inset: Calibration curve corresponding to the amperometric responses of the GOx–SWCNT electrode at different concentrations of glucose (the electrode comprised 20–30 nm long SWCNTs). I, current; *E*/V, potential in volts; SCE, standard calomel electrode. (*Source*: Reprinted from reference 136 with permission from Elsevier.)

SWCNTs may present a semiconductor behaviour and constitute a promising material for preparing biosensors using the field effect transistor (FET biosensors).[149] Dekker's group reported the possibility of using an individual SWCNT as a FET device.[150] The possibility of inducing a variation in the conductance of SWCNTs by simple molecular interactions has been significantly reported in the literature for developing biosensors.[108,151–154] Biosensors using an individual or a network of SWCNTs that have been reported demonstrated the possibility to exploit the FET for detecting the DNA hybridization in the pico- and micro-molar level range. In the most popular configuration, the SWCNT operates as a gate in the DNA–FET sensor and is connected to two electrodes, namely source and drain, according to the FET principle. Increasing the sensitivity of the SWCNT–FET biosensors can be achieved by integrating gold nanoparticles (AuNP) which will permit it to detect DNA hybridization at the femtomolar level.[108]

1.5 Technical and industrial challenge for the integration of CNTs in analytical and bioanalytical devices

As was shown from significant reported publications in the literature, the use of CNTs for preparing biosensors is of great interest, due to their unique characteristics in terms of conductivity, electrocatalytic activity and nanometric size. However, in order to achieve commercially available biosensors, CNTs require to be integrated into a given configuration on a substrate, even if various strategies and techniques for modifying surfaces are now well known. Commercially available biosensors based on CNTs still face the difficulty of fabricating bio-interfaces at an industrial scale in a reproducible way. For instance, the integration of CNTs in analytical devices often requires their treatment with an oxidizing agent, as was discussed above. The introduction of oxygenated groups on the CNT surface, to increase the hydrophilic properties or to immobilize biosensing elements by using chemical reagents, may present various disadvantages. One of these disadvantages is that oxidative treatment is not compatible with industrial processes because of its time consumption and its dependency on the mode of the CNT synthesis. Another disadvantage involves the purification of CNTs from metal catalysts. Even after abundant acidic washing, the CNTs still contain metal nanoparticles. Even at a trace concentration, this may drastically affect the electrochemical activity of CNTs, as well as the activity of biosensing elements.

Plasma processing has been reported as a very promising strategy to integrate CNTs directly onto substrates. However, classical plasma processing operating at temperatures higher than 600°C limits the use of some

substrates with a low melting-point. In the arc discharge method, CNTs can be synthesized with a yield of up to 60–70%; however, the synthesized CNTs show significant defects such as amorphous carbon and catalyst residues. In the laser ablation method, carried out at 1200°C, will have a yield of about 80–90%, and only small cleaned CNTs free from catalyst are obtained. The synthesis of CNTs by chemical vapour deposition (CVD) using CO, C_2H_2 or CH_4 as a carbon precursor gas and a catalyst surface leads to MWCNTs and SWCNTs. Generally, the CVD method requires high temperatures, which can damage the substrates. Thus a lower temperature (<600°C) for CNT synthesis is needed. The combination of CVD and the photolithography process has also been reported on glass substrates with oxygen-plasma treatment of the transferred SWCNTs.[155,156] The SWCNT films are three-electrode systems comprising a CNT working electrode, an Ag/AgCl reference electrode and a Pt counter electrode. These were fabricated on low melting-point glass substrates using the plasma process. The resulting three-electrode systems were successfully used for preparing an SWCNT-based DNA biosensor. The authors demonstrated that a plasma approach may be used for the full integration of the functionalization of CNTs film electrode. This is done by the oxygen-plasma process for batch fabrication of miniaturized electrochemical biosensors.

Plasma enhanced CVD (PECVD) may present an opportunity to develop more adequate methods for industrial preparations of biosensors. An advantage of PECVD is that it can purify the CNTs to form metal catalyst, by using the etching process followed by their functionalization. The synthesis temperature for PECVD is in the range of 400–600°C and constitutes an appropriate method for an industrial platform for biosensing surfaces. It is worth noting that the synthesis of CNTs, with the possibility of their *in situ* functionalization, offers significant advantages in terms of cost preparation, and fabrication at high scale. In the case of Si substrate, the synthesis of aligned CNTs followed by their functionalization has been reported and the use in HRP biosensors was also demonstrated. PECVD seems more appropriate for controlling the location of CNTs at a desired placement on the electrode surface.

From various results and discussions reported in the literature, some difficulties are seldom discussed: for instance, the possibility to synthesize CNTs with full control of electronic properties, size (both diameter and length) and chirality. The problem of producing homogeneous CNTs seems to be more present for SWCNTs than MWCNTs. In fact, MWCNTs are metallic conductors, but SWCNTs may present conductor or semiconductor properties depending on their size (diameter) and chirality. For instance, in the same batch of CNTs (SW or MW), even prepared under the same experimental conditions, we observe different lengths and electronic structures. So we still have a significant heterogeneity in the fabrication of SWCNTs

or MWCNTs and only an average number of properties are observed. This may affect the reproducibility of the preparation of biosensors; the effect may be more pronounced in the case of a one-dimensional SWCNT-based nanobiosensors. On the whole, the integration of CNTs under optimized configuration, vertically aligned or one-dimension (1-D), makes the fabrication of CNT biosensors difficult and complex. The three-dimension (3-D) CNTs which are vertically aligned facilitate the collapsing effect leading to a significant decrease of an effective surface area. Moreover, it is worth noting that in the field of biosensors, most studies were carried out without taking into account the effect of some of the impurities present in the bulk or surfaces of CNTs. For instance, the electrochemical reactivity of metal nanoparticles used as catalyst for CNTs growth is seldom discussed. Only few papers have been reported that metal nanoparticles may be responsible for the electrocatalysis observed for CNTs. Significant ameliorations in fabrication of clean and homogenous CNTs are still waiting to reach commercial biosensors.

Beyond the challenges related to the control of the homogeneity, physical properties and low-cost fabrication limit the commercialization of CNT-based biosensors. The toxic effect of CNTs on human health is still not clear and may also restrict the development of CNT-based biological sensors. So the toxicology study of CNTs on human and animal cells is required, mainly for development of disposable implantable biosensors.

1.6 Conclusion and future trends

CNTs offer many various advantages, for instance the increase of biosensor selectivity by facilitating the DET with redox enzymes. They also offer the advantage, depending on their electrical properties, whether MWCNTs or SWCNTs, to use various types of transducers including electrochemical, FET and optical. Despite their potentialities reported through various papers, CNT-based biosensors face various challenges, and probably the most crucial concern is the transposition of their fabrication to an industrial scale. Various methods have been reported in the literature for the characterization of CNTs and have highlighted interesting insights that permit better understanding of the electrochemical, electrical and optical properties of CNTs.

In terms of future prospects, the miniaturization of CNT-based biosensors presents many advantages in various fields including clinical analytical chemistry and biochemistry, pollutant-monitoring, or agri-food quality. For instance, commercially available CNT-based biosensors are expected in 'tailored or personalized medicine'[157] for examining the oxidative drug metabolism. Rapid detection and identification of metabolites are important for the assessment of toxic effects of various

drugs. In environment chemistry, the rapid detection of various emerging pollutants and their oxidative degradations may provide a better understanding of the fate of various emerging pollutants, and also their toxic effects. The use of CNTs in monitoring devices for living cells is used to evaluate drug treatments or to study phagocytosis phenomena in real time. It should be very useful for examining cellular activities with relatively easy detection.[13]

There are many applications that the resulting biosensors may offer to improve the quality of life. So full-integration processes comprising the synthesis with the *in situ* purification and functionalization have to be improved in order to meet the high scale fabrication. The use of CNTs in FET devices also constitutes a promising direction for integrating CNTs in biosensors. The coupling of SWCNT and FET technology constitutes one of the most important strategies appropriate with mass production and the fabrication of a generic platform for the biosensor's fabrication. The PECVD method, already used in integrated circuit fabrication, may also offer interesting solutions for the fabrication of CNT interfaces. Undoubtedly, the micro- and nano-electronic process will give an important contribution to provide appropriate solutions for reaching commercial CNT-based biosensors.

1.7 References

1. Iijima, S. (1991) *Nature*, **354**, 56.
2. Ando, Y., Iijima, S. (1993) *Japanese Journal of Applied Physics, Part 2: Letters*, **32**, L107.
3. Bandaru, N. M., Voelcker, N. H. (2012) *Journal of Materials Chemistry*, **22**, 8748.
4. Cha, T. G., Baker, B. A., Sauffer, M. D., Salgado, J., Jaroch, D., Rickus, J. L., Porterfield, D. M., Choi, J. H. (2011) *ACS Nano*, **5**, 4236.
5. Chen, Z., Zhang, X., Yang, R., Zhu, Z., Chen, Y., Tan, W. (2011) *Nanoscale*, **3**, 1949.
6. Deryabin, D. G., Aleshina, E. S., Efremova, L. V. (2012) *Microbiology (Russian Federation)*, **81**, 492.
7. Felhofer, J. L., Caranto, J. D., Garcia, C. D. (2010) *Langmuir*, **26**, 17178.
8. Ximenes, J. C. M., Melo, G. C., Melo, V. M. M., Mendes Filho, J., Souza Filho, A. G. (2012) *Journal of Physics and Chemistry of Solids*, **73**, 232.
9. Saleh Ahammad, A. J., Lee, J. J., Rahman, M. A. (2009) *Sensors*, **9**, 2289.
10. Umasankar, Y., Thiagarajan, S., Chen, S. M. (2008) *Sensors*, **8**, 7191.
11. Vashist, S. K., Zheng, D., Al-Rubeaan, K., Luong, J. H. T., Sheu, F. S. (2011) *Biotechnology Advances*, **29**, 169.
12. Lee, M., Lucero, A., Kim, J. (2012) *Transactions on Electrical and Electronic Materials*, **13**, 165.
13. Liu, S., Guo, X. (2012) *NPG Asia Materials*, **4**, 1–10.

14. Wang, X. N., Hu, P. A. (2012) *Frontiers of Materials Science*, **6**, 26.
15. Merkoçi, A., Pumera, M., Llopis, X., Pérez, B., Del Valle, M., Alegret, S. (2005) *TrAC – Trends in Analytical Chemistry*, **24**, 826.
16. Iijima, S., Ichihashi, T. (1993) *Nature*, **363**, 603.
17. Zhao, X., Ohkohchi, M., Wang, M., Iijima, S., Ichihashi, T., Ando, Y. (1997) *Carbon*, **35**, 775.
18. Yudasaka, M., Ichihashi, T., Iijima, S. (1998) *Journal of Physical Chemistry B*, **102**, 10201.
19. Yudasaka, M., Ichihashi, T., Komatsu, T., Iijima, S. (1999) *Chemical Physics Letters*, **299**, 91.
20. Yudasaka, M., Komatsu, T., Ichihashi, T., Achiba, Y., Iijima, S. (1998) *Journal of Physical Chemistry B*, **102**, 4892.
21. Zhang, Y., Gu, H., Iijima, S. (1998) *Applied Physics Letters*, **73**, 3827.
22. Zhang, Y., Iijima, S. (1998) *Philosophical Magazine Letters*, **78**, 139.
23. Li, W. Z., Xie, S. S., Qian, L. X., Chang, B. H., Zou, B. S., Zhou, W. Y., Zhao, R. A., Wang, G. (1996) *Science*, **274**, 1701.
24. José-Yacamán, M., Terrones, H., Rendón, L., Domínguez, J. M. (1995) *Carbon*, **33**, 669.
25. Choi, Y. C., Bae, D. J., Lee, Y. H., Lee, B. S., Han, I. T., Choi, W. B., Lee, N. S., Kim, J. M. (2000) *Synthetic Metals*, **108**, 159.
26. Choi, Y. C., Shin, Y. M., Lee, Y. H., Lee, B. S., Park, G. S., Choi, W. B., Lee, N. S., Kim, J. M. (2000) *Applied Physics Letters*, **76**, 2367.
27. Han, J. H., Yang, W. S., Yoo, J. B., Park, C. Y. (2000) *Journal of Applied Physics*, **88**, 7363.
28. Murakami, H., Hirakawa, M., Tanaka, C., Yamakawa, H. (2000) *Applied Physics Letters*, **76**, 1776.
29. Park, K. H., Choi, S., Lee, K. M., Oh, S. G., Lee, S., Koh, K. H. (2000) *Journal of the Korean Physical Society*, **37**, L153.
30. Ren, Z. F., Huang, Z. P., Wang, D. Z., Wen, J. G., Xu, J. W., Wang, J. H., Calvet, L. E., Chen, J., Klemic, J. F., Reed, M. A. (1999) *Applied Physics Letters*, **75**, 1086.
31. Tsai, S. H., Chao, C. W., Lee, C. L., Shih, H. C. (1999) *Applied Physics Letters*, **74**, 3462.
32. Zhang, Q., Yoon, S. F., Ahn, J., Gan, B., Rusli, Yu, M. B. (2000) *Journal of Physics and Chemistry of Solids*, **61**, 1179.
33. Amama, P. B., Ogebule, O., Maschmann, M. R., Sands, T. D., Fisher, T. S. (2006) *Chemical Communications*, **27**, 2899–2901.
34. Bell, M. S., Teo, K. B. K., Milne, W. I. (2007) *Journal of Physics D: Applied Physics*, **40**, 2285.
35. Gohier, A., Djouadi, M. A., Dubosc, M., Granier, A., Minea, T. M., Sirghi, L., Rossi, F., Paredez, P., Alvarez, F. (2007) *Journal of Nanoscience and Nanotechnology*, **7**, 3350.
36. Kato, T., Jeong, G. H., Hirata, T., Hatakeyama, R., Tohji, K., Motomiya, K. (2003) *Chemical Physics Letters*, **381**, 422.
37. Kyung, S. J., Lee, Y. H., Kim, C. W., Lee, J. H., Yeom, G. Y. (2006) *Carbon*, **44**, 1530.
38. Sato, H., Hata, K. (2006) *New Diamond and Frontier Carbon Technology*, **16**, 163.

39. Shiratori, Y., Hiraoka, H., Yamamoto, M. (2004) *Materials Chemistry and Physics*, **87**, 31.
40. Dubosc, M., Minea, T., Besland, M. P., Cardinaud, C., Granier, A., Gohier, A., Point, S., Torres, J. (2006) *Microelectronic Engineering*, **83**, 2427.
41. Gohier, A., Minea, T. M., Djouadi, M. A., Jiménez, J., Granier, A. (2007) *Physica E: Low-Dimensional Systems and Nanostructures*, **37**, 34.
42. Gong, K., Yan, Y., Zhang, M., Su, L., Xiong, S., Mao, L. (2005) *Analytical Sciences*, **21**, 1383.
43. Moulton, S. E., Minett, A. I., Wallace, G. G. (2005) *Sensor Letters*, **3**, 183.
44. Sánchez-Pomales, G., Santiago-Rodríguez, L., Cabrera, C. R. (2009) *Journal of Nanoscience and Nanotechnology*, **9**, 2175.
45. Santiago-Rodríguez, L., Sánchez-Pomales, G., Cabrera, C. R. (2010) *Israel Journal of Chemistry*, **50**, 277.
46. Umasankar, Y., Chen, S. M. (2008) *Analytical Letters*, **41**, 210.
47. Fam, D. W. H., Palaniappan, A., Tok, A. I. Y., Liedberg, B., Moochhala, S. M. (2011) *Sensors and Actuators, B: Chemical*, **157**, 1.
48. Lei, J., Ju, H. (2010) *Wiley Interdisciplinary Reviews: Nanomedicine and Nanobiotechnology*, **2**, 496.
49. Yeom, S. H., Kang, B. H., Kim, K. J., Kang, S. W. (2011) *Frontiers in Bioscience*, **16**, 997.
50. Daniel, S., Rao, T. P., Rao, K. S., Rani, S. U., Naidu, G. R. K., Lee, H. Y., Kawai, T. (2007) *Sensors and Actuators, B: Chemical*, **122**, 672.
51. Zeng, Y. L., Huang, Y. F., Jiang, J. H., Zhang, X. B., Tang, C. R., Shen, G. L., Yu, R. Q. (2007) *Electrochemistry Communications*, **9**, 185.
52. Chen, R. J., Zhang, Y., Wang, D., Dai, H. (2001) *Journal of the American Chemical Society*, **123**, 3838.
53. Yu, J., Shapter, J. G., Johnston, M. R., Quinton, J. S., Gooding, J. J. (2007) *Electrochimica Acta*, **52**, 6206.
54. Park, K. C., Hayashi, T., Tomiyasu, H., Endo, M., Dresselhaus, M. S. (2005) *Journal of Materials Chemistry*, **15**, 407.
55. Park, T. J., Banerjee, S., Hemraj-Benny, T., Wong, S. S. (2006) *Journal of Materials Chemistry*, **16**, 141.
56. Bergeret, C., Cousseau, J., Fernandez, V., Mevellec, J. Y., Lefrant, S. (2008) *Journal of Physical Chemistry C*, **112**, 16411.
57. Ziegler, K. J., Gu, Z., Peng, H., Flor, E. L., Hauge, R. H., Smalley, R. E. (2005) *Journal of the American Chemical Society*, **127**, 1541.
58. Ziegler, K. J., Gu, Z., Shaver, J., Chen, Z., Flor, E. L., Schmidt, D. J., Chan, C., Hauge, R. H., Smalley, R. E. (2005) *Nanotechnology*, **16**, S539.
59. Marega, R., Accorsi, G., Meneghetti, M., Parisini, A., Prato, M., Bonifazi, D. (2009) *Carbon*, **47**, 675.
60. Gromov, A., Dittmer, S., Svensson, J., Nerushev, O. A., Perez-García, S. A., Licea-Jiménez, L., Rychwalski, R., Campbell, E. E. B. (2005) *Journal of Materials Chemistry*, **15**, 3334.
61. Karousis, N., Tagmatarchis, N., Tasis, D. (2010) *Chemical Reviews*, **110**, 5366.
62. Campidelli, S. (2011) *Current Organic Chemistry*, **15**, 1151.
63. Campidelli, S., Ballesteros, B., Filoramo, A., Díaz, D. D., De La Torre, G., Torres, T., Rahman, G. M. A., Ehli, C., Kiessling, D., Werner, F., Sgobba, V., Guldi, D.

M., Cioffi, C., Prato, M., Bourgoin, J. P. (2008) *Journal of the American Chemical Society*, **130**, 11503.
64. Clavé, G., Campidelli, S. (2011) *Chemical Science*, **2**, 1887.
65. Coates, M., Griveau, S., Bedioui, F., Nyokong, T. (2012) *Electroanalysis*, **24**, 1833.
66. Guo, Z., Liang, L., Liang, J. J., Ma, Y. F., Yang, X. Y., Ren, D. M., Chen, Y. S., Zheng, J. Y. (2008) *Journal of Nanoparticle Research*, **10**, 1077.
67. Han, J., Gao, C. (2010) *Nano-Micro Letters*, **2**, 213.
68. Jing, L., Liang, C., Shi, X., Ye, S., Xian, Y. (2012) *Analyst*, **137**, 1718.
69. Kumar, I., Rana, S., Rode, C. V., Cho, J. W. (2008) *Journal of Nanoscience and Nanotechnology*, **8**, 3351.
70. Li, H., Cheng, F., Duft, A. M., Adronov, A. (2005) *Journal of the American Chemical Society*, **127**, 14518.
71. Liu, J., Nie, Z., Cao, Y., Adronov, A., Li, H. (2008) *Journal of Polymer Science, Part A: Polymer Chemistry*, **46**, 7187.
72. Palacin, T., Le Khanh, H., Jousselme, B., Jegou, P., Filoramo, A., Ehli, C., Guldi, D. M., Campidelli, S. (2009) *Journal of the American Chemical Society*, **131**, 15394.
73. Qi, H., Ling, C., Huang, R., Qiu, X., Shangguan, L., Gao, Q., Zhang, C. (2012) *Electrochimica Acta*, **63**, 76.
74. Rana, S., Kumar, I., Yoo, H. J., Cho, J. W. (2009) *Journal of Nanoscience and Nanotechnology*, **9**, 3261.
75. Tuci, G., Vinattieri, C., Luconi, L., Ceppatelli, M., Cicchi, S., Brandi, A., Filippi, J., Melucci, M., Giambastiani, G. (2012) *Chemistry – A European Journal*, **18**, 8454.
76. Chen, C., Liang, B., Lu, D., Ogino, A., Wang, X., Nagatsu, M. (2010) *Carbon*, **48**, 939.
77. Kim, J. H., Lee, M. J., Park, E. J., Lee, J. Y., Lee, C. J., Min, N. K. (2012) *Plasma Processes and Polymers*, **9**, 873.
78. Lee, J. Y., Park, E. J., Lee, C. J., Kim, S. W., Pak, J. J., Min, N. K. (2009) *Thin Solid Films*, **517**, 3883.
79. Park, E. J., Lee, J. Y., Kim, J. H., Kim, S. K., Lee, C. J., Min, N. K. (2010) *Japanese Journal of Applied Physics*, **49**, 08JH01–08JH01-5.
80. Wang, S. C., Chang, K. S., Yuan, C. J. (2009) *Electrochimica Acta*, **54**, 4937.
81. Yeo, S., Choi, C., Jang, C. W., Lee, S., Jhon, Y. M. (2013) *Applied Physics Letters*, **102**, art. no. 073108.
82. Luais, E., Thobie-Gautier, C., Tailleur, A., Djouadi, M. A., Granier, A., Tessier, P. Y., Debarnot, D., Poncin-Epaillard, F., Boujtita, M. (2010) *Electrochimica Acta*, **55**, 7916.
83. Huber, T. A., Kopac, M. C., Chow, C. (2008) *Canadian Journal of Chemistry*, **86**, 1138.
84. Ying, L. S., Bin Mohd Salleh, M. A., B. Mohamed Yusoff, H., Abdul Rashid, S. B., B. Abd. Razak, J. (2011) *Journal of Industrial and Engineering Chemistry*, **17**, 367.
85. Yuan, D., Liu, J. (2007) *Small*, **3**, 366.
86. Ding, X., Li, H., Deng, L., Peng, Z., Chen, H., Wang, D. (2011) *Biosensors and Bioelectronics*, **26**, 4596.

87. Zhang, Y., Li, B., Yan, C., Fu, L. (2011) *Biosensors and Bioelectronics*, **26**, 3505.
88. Abdula, D., Nguyen, K. T., Shim, M. (2007) *Journal of Physical Chemistry C*, **111**, 17755.
89. Arias De Fuentes, O., Ferri, T., Frasconi, M., Paolini, V., Santucci, R. (2011) *Angewandte Chemie – International Edition*, **50**, 3457.
90. Balasubramanian, K., Burghard, M., Kern, K. (2008) *Physical Chemistry Chemical Physics*, **10**, 2256.
91. Chakraborty, A. K., Coleman, K. S., Dhanak, V. R. (2009) *Nanotechnology*, **20**, art no 155704.
92. Ellison, M. D., Gasda, P. J. (2008) *Journal of Physical Chemistry C*, **112**, 738.
93. Fantini, C., Usrey, M. L., Strano, M. S. (2007) *Journal of Physical Chemistry C*, **111**, 17941.
94. Floch, F. L., Thuaire, A., Bidan, G., Simonato, J. P. (2009) *Nanotechnology*, **20**, art no 145705.
95. Gohier, A., Nekelson, F., Helezen, M., Jegou, P., Deniau, G., Palacin, S., Mayne-L'Hermite, M. (2011) *Journal of Materials Chemistry*, **21**, 4615.
96. Gross, M. L., Hickner, M. A. (2010) *Electrochemical and Solid-State Letters*, **13**, K5.
97. Karousis, N., Ali-Boucetta, H., Kostarelos, K., Tagmatarchis, N. (2008) *Materials Science and Engineering B: Solid-State Materials for Advanced Technology*, **152**, 8.
98. Kim, S. K., Jeon, S. (2012) *Electrochemistry Communications*, **22**, 141.
99. Lipińska, M. E., Rebelo, S. L. H., Pereira, M. F. R., Gomes, J. A. N. F., Freire, C., Figueiredo, J. L. (2012) *Carbon*, **50**, 3280.
100. Mévellec, V., Roussel, S., Tessier, L., Chancolon, J., Mayne-L'Hermite, M., Deniau, G., Viel, P., Palacin, S. (2007) *Chemistry of Materials*, **19**, 6323.
101. Ungureanu, E. M., Pilan, L., Meghea, A., Le Floch, F., Simonato, J. P., Bidan, G. (2008) *Revista de Chimie*, **59**, 400.
102. Bahr, J. L., Yang, J., Kosynkin, D. V., Bronikowski, M. J., Smalley, R. E., Tour, J. M. (2001) *Journal of the American Chemical Society*, **123**, 6536.
103. Downard, A. J. (2000) *Electroanalysis*, **12**, 1085.
104. Pinson, J., Podvorica, F. (2005) *Chemical Society Reviews*, **34**, 429.
105. Combellas, C., Delamar, M., Kanoufi, F., Pinson, J., Podvorica, F. I. (2005) *Chemistry of Materials*, **17**, 3968.
106. Doyle, C. D., Rocha, J. D. R., Weisman, R. B., Tour, J. M. (2008) *Journal of the American Chemical Society*, **130**, 6795.
107. Brooksby, P. A., Downard, A. J. (2005) *Journal of Physical Chemistry B*, **109**, 8791.
108. Ko, J. W., Woo, J. M., Jinhong, A., Cheon, J. H., Lim, J. H., Kim, S. H., Chun, H., Kim, E., Park, Y. J. (2011) *ACS Nano*, **5**, 4365.
109. Wei, G., Pan, C., Reichert, J., Jandt, K. D. (2010) *Carbon*, **48**, 645.
110. Zhou, J., Barbara, P., Paranjape, M. (2010) *Journal of Nanoscience and Nanotechnology*, **10**, 3890.
111. Lai, Y., Bai, J., Shi, X., Zeng, Y., Xian, Y., Hou, J., Jin, L. (2013) *Talanta*, **107**, 176.
112. Pan, Y., Zhang, Y. Z., Li, Y. (2013) *Journal of Applied Polymer Science*, **128**, 647.

113. Siqueira Jr, J. R., Gabriel, R. C., Zucolotto, V., Silva, A. C. A., Dantas, N. O., Gasparotto, L. H. S. (2012) *Physical Chemistry Chemical Physics*, **14**, 14340.
114. Yu, A., Wang, Q., Yong, J., Mahon, P. J., Malherbe, F., Wang, F., Zhang, H., Wang, J. (2012) *Electrochimica Acta*, **74**, 111.
115. Chu, X., Duan, D., Shen, G., Yu, R. (2007) *Talanta*, **71**, 2040.
116. Flavel, B. S., Yu, J., Ellis, A. V., Quinton, J. S., Shapter, J. G. (2008) *Nanotechnology*, **19**, art no 445301.
117. Lee, K. P., Gopalan, A. I., Santhosh, P., Manesh, K. M., Kim, J. H., Kim, K. S. (2006) *Journal of Nanoscience and Nanotechnology*, **6**, 1575.
118. Rao, S. G., Huang, L., Murray, J. (2011) *Applied Surface Science*, **258**, 1519.
119. Villalonga, R., Díez, P., Eguílaz, M., Martínez, P., Pingarrón, J. M. (2012) *ACS Applied Materials and Interfaces*, **4**, 4312.
120. Alvarez-Paggi, D., Martín, D. F., Debiase, P. M., Hildebrandt, P., Martí, M. A., Murgida, D. H. (2010) *Journal of the American Chemical Society*, **132**, 5769.
121. Ferapontova, E. E., Ruzgas, T., Gorton, L. (2003) *Analytical Chemistry*, **75**, 4841.
122. Frasconi, M., Favero, G., Di Fusco, M., Mazzei, F. (2009) *Biosensors and Bioelectronics*, **24**, 1424.
123. Murata, K., Nakamura, N., Ohno, H. (2007) *Electroanalysis*, **19**, 530.
124. Yang, M., Kabulski, J. L., Wollenberg, L., Chen, X., Subramanian, M., Tracy, T. S., Lederman, D., Gannett, P. M., Wu, N. (2009) *Drug Metabolism and Disposition*, **37**, 892.
125. Gooding, J. J., Mearns, F., Yang, W., Liu, J. (2003) *Electroanalysis*, **15**, 81.
126. Heering, H. A., Wiertz, F. G. M., Dekker, C., De Vries, S. (2004) *Journal of the American Chemical Society*, **126**, 11103.
127. Hill, H. A. O. (2006) *Australian Journal of Chemistry*, **59**, 231.
128. Mogharrab, N., Ghourchian, H. (2005) *Electrochemistry Communications*, **7**, 466.
129. Cai, C., Chen, J. (2004) *Analytical Biochemistry*, **332**, 75.
130. Cai, C., Chen, J., Lu, T. (2004) *Science in China, Series B: Chemistry*, **47**, 113.
131. Guiseppi-Elie, A., Lei, C., Baughman, R. H. (2002) *Nanotechnology*, **13**, 559.
132. Liang, W., Zhuobin, Y. (2003) *Sensors*, **3**, 544.
133. Liu, J., Chou, A., Rahmat, W., Paddon-Row, M. N., Gooding, J. J. (2005) *Electroanalysis*, **17**, 38.
134. Hess, C. R., Juda, G. A., Dooley, D. M., Amii, R. N., Hill, M. G., Winkler, J. R., Gray, H. B. (2003) *Journal of the American Chemical Society*, **125**, 7156.
135. Liu, G., Gooding, J. J. (2006) *Langmuir*, **22**, 7421.
136. Willner, B., Katz, E., Willner, I. (2006) *Current Opinion in Biotechnology*, **17**, 589.
137. Tasca, F., Harreither, W., Ludwig, R., Gooding, J. J., Gorton, L. (2011) *Analytical Chemistry*, **83**, 3042.
138. He, P., Xu, Y., Fang, Y. (2006) *Microchimica Acta*, **152**, 175.
139. Cao, C., Kim, J. H., Yoon, D., Hwang, E. S., Kim, Y. J., Baik, S. (2008) *Materials Chemistry and Physics*, **112**, 738.
140. Higashi, T., Nakajima, Y., Kojima, M., Ishii, K., Inoue, A., Maekawa, T., Hanajiri, T. (2011) *Chemical Physics Letters*, **501**, 451.
141. Martínez, M. T., Tseng, Y. C., González, M., Bokor, J. (2012) *Journal of Physical Chemistry C*, **116**, 22579.

142. Shi, J., Cha, T. G., Claussen, J. C., Diggs, A. R., Choi, J. H., Porterfield, D. M. (2011) *Analyst*, **136**, 4916.
143. Berti, F., Lozzi, L., Palchetti, I., Santucci, S., Marrazza, G. (2009) *Electrochimica Acta*, **54**, 5035.
144. Li, J., Ng, H. T., Cassell, A., Fan, W., Chen, H., Ye, Q., Koehne, J., Han, J., Meyyappan, M. (2003) *Nano Letters*, **3**, 597.
145. Dong, X. Y., Mi, X. N., Zhang, L., Liang, T. M., Xu, J. J., Chen, H. Y. (2012) *Biosensors and Bioelectronics*, **38**, 337.
146. Li, L., Wang, S., Yang, T., Huang, S., Wang, J. (2012) *Biosensors and Bioelectronics*, **33**, 279.
147. Moghaddam, M. J., Yang, W., Bojarski, B., Gengenbach, T. R., Gao, M., Zareie, H., McCall, M. J. (2012) *Nanotechnology*, **23**, art no 425503.
148. Zhu, N., Chang, Z., He, P., Fang, Y. (2005) *Analytica Chimica Acta*, **545**, 21.
149. Star, A., Tu, E., Niemann, J., Gabriel, J. C. P., Joiner, C. S., Valcke, C. (2006) *Proceedings of the National Academy of Sciences of the United States of America*, **103**, 921.
150. Besteman, K., Lee, J. O., Wiertz, F. G. M., Heering, H. A., Dekker, C. (2003) *Nano Letters*, **3**, 727.
151. Byon, H. R., Kim, S., Choi, H. C. (2008) *Nano*, **3**, 415.
152. Cha, M., Jung, S., Cha, M. H., Kim, G., Ihm, J., Lee, J. (2009) *Nano Letters*, **9**, 1345.
153. Kinm, S., Kim, T. G., Byon, H. R., Shin, H. J., Ban, C., Choi, H. C. (2009) *Journal of Physical Chemistry B*, **113**, 12164.
154. Staii, C., Johnson Jr, A. T., Chen, M., Gelperin, A. (2005) *Nano Letters*, **5**, 1774.
155. Kim, J. H., Lee, J. Y., Jin, J. H., Park, E. J., Min, N. K. (2013) *Japanese Journal of Applied Physics*, **52** (1 Part 2), art. no. 01AE02.
156. Kim, J. H., Song, M. J., Lee, C. J., Lee, J. H., Kim, J. H., Min, N. K. (2013) *Carbon*, **52**, 398.
157. De Micheli, G., Boero, C., Baj-Rossi, C., Taurino, I., Carrara, S. (2012) *Proceedings of the 49th Design Automation Conference (DAC)*, San Francisco, California, USA, 3–7 June 2012, pp. 6–11.

2

Electrochemical nanosensors for blood glucose analysis

F. DAVIS and S. P. J. HIGSON, Cranfield University, UK

DOI: 10.1533/9780857096722.1.28

Abstract: We begin by reviewing the need for blood glucose sensing, and follow this with a brief history of the development of the glucose sensor. The use of nanotechnology to enhance the performance of glucose sensors is reviewed with special attention paid to the use of such systems as carbon nanotubes (CNTs) and noble metal nanoparticles. Their use in the direct detection of glucose without the need for enzymes is discussed. One of the potential advantages of nanotechnology would be the development of miniaturised sensors that are capable of being implanted within patients. The chapter concludes with a section of potential future trends and the applications of the advances made in glucose sensing towards the detection of a range of other clinical targets.

Key words: nanotechnology, carbon nanotubes CNTs, nanoparticles, glucose sensing, enzyme-free.

2.1 Introduction

The detection and quantification of glucose in blood or other physiological fluids is one of the success stories of the biosensor world. The driving force for this research has of course been the prevalence and increase of diabetes within the Western world. At present diabetes is experienced by 346 million sufferers world-wide and this is estimated to double between 2005 and 2030 (World Health Organisation, 2012). The world market for biosensors is predicted to reach $15–16bn by 2016; in 2009 approximately 32% of this market was for blood glucose monitoring (Thusu, 2010). A complete review of the field of glucose sensing is outside the scope of this chapter; however, much of the work up to 2008 is summarised here (Wang, 2008). The application of nanomedicine to diabetes research and practice has been recently reviewed (Pickup *et al.,* 2008; Cash and Clark, 2010).

Nanotechnology has become somewhat of a buzz-word in recent times, and the biosensing field is no exception. It is thought that the utilisation of such technologies, as well as the use of nanosized materials, could well have beneficial effects for the performance of biosensors. For example, a simple

reduction in size would lead to the lowering of the sample size necessary for analysis, and this would be especially of benefit for invasive processes such as blood sampling. The smaller size and enhanced surface areas of such devices would also reduce the effects of diffusion, leading to higher sensitivities and faster response times. Since many glucose biosensors use enzymes as the active component, nanosized materials can be used which, because of their similarity of size to the enzymes, allow such intimate contact to be used to directly 'wire' the enzyme to the electrode, thereby removing the need for mediators. Many nanomaterials display unique catalytic activities which enable the non-enzymatic determination of glucose as an alternative to conventional enzyme-based systems. Finally the reductions in size possibly using these technologies open up the possibly of analysing for biochemical events within individual cells rather than the organism as a whole.

This chapter will be split into two main parts. The first analyses how nanosized materials are being incorporated into conventional electrochemical glucose sensors, both enzymatic and non-enzymatic in nature. The second discusses the construction of complete sensors on the micro/nanometre scale and their use in interrogating localised biological conditions.

2.2 Nanosized materials: enzymatic detection of glucose

Ever since Clark's pioneering work, which first proposed the use of glucose oxidase modified electrodes to determination glucose concentrations (Clark and Lyons, 1962), the majority of electrochemical glucose sensors have been enzymatic in nature. Initially, these were based on glucose oxidase which catalysed the reaction of glucose and oxygen to gluconolactone and hydrogen peroxide, with either the loss of oxygen or creation of peroxide being measured electrochemically; these are now termed first-generation glucose biosensors. Later work utilised mediator compounds such as ferrocene derivatives to mediate this reaction (Cass *et al.,* 1984), resulting in a reduction in the electrochemical potentials required to determine glucose levels; these mediated biosensors are known as second-generation biosensors. Other workers examined the possibility of 'wiring' the enzyme to the electrode, for example by using osmium containing polymers (Degani and Heller, 1987); these are now known as third-generation biosensors.

There is a wide range of nanosized materials that can be utilised in the construction of biosensors, many of which are reviewed here (Pandey *et al.,* 2008; Siangprob *et al.,* 2011). Two of the most commonly used are metal nanoparticles and carbon nanotubes (CNTs). A number of different metal nanoparticles have been utilised; however, gold nanoparticles are easily the most common. Gold nanoparticles can be easily synthesised in a wide variety of shapes and sizes, are relatively inert to air and water, are highly

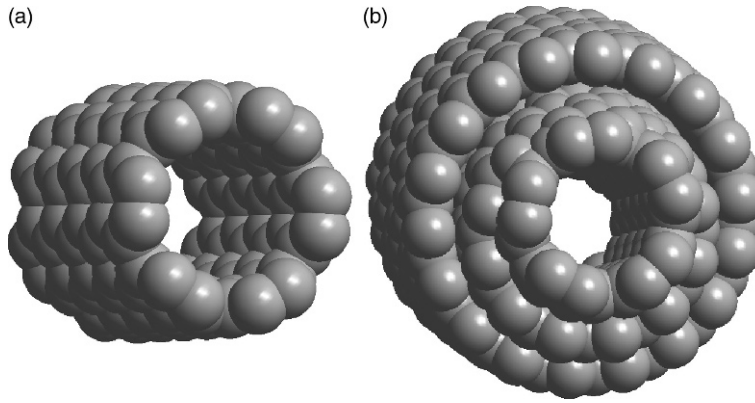

2.1 Structures of (a) single-walled and (b) multi-walled carbon nanotubes.

electrically conductive, and can be immobilised by a variety of chemistries, the most popular using thiols due to formation of strong Au–S bonds (Pandey *et al.,* 2008; Siangprob *et al.,* 2011).

CNTs are allotropes of carbon which can be thought of as one or several graphene sheets rolled into a cylinder (Fig. 2.1). They display a range of interesting properties such as electrical conductivity and are capable of catalysing chemical and electrochemical reactions, such as the oxidation of hydrogen peroxide. CNTs can also be selectively chemically modified along their sides or ends, allowing them to be used as supports for the immobilisation or biological molecules and with potential use as molecular 'wires'. It is possible to incorporate CNTs into sensors by simple methods such as casting from suspension, or they can actually be grown from catalytic seeds to give vertically orientated CNT 'forests'. Much of the work on CNTs in electrochemical biosensors has been extensively reviewed elsewhere (Pandey *et al.,* 2008; Ahammad *et al*., 2009; Siangprob *et al.,* 2011).

The earliest work on utilising nanosized materials came by simply synthesising the nanomaterial separately and then incorporating it into a biologically active film on a classic electrode such as gold or glassy carbon by simple casting or other methods. Because of its relative inertness and capability to be substituted with thiols, gold has been widely studied and a detailed description would be outside of the scope of this chapter. One of the earliest studies involved the reconstitution of apo-glucose oxidase onto a 1.4 nm Au_{55} nanoparticle which had already been functionalised with the co-factor flavin adenine dinucleotide (FAD) and immobilised onto gold electrodes (Xiao *et al.,* 2003). This could then be used to detect glucose with a rapid electron transfer turnover rate, the gold nanoparticle acting to 'plug' the enzyme into the electrode.

Other examples include the modification of gold electrodes to which a monolayer of gold nanoparticles can be immobilised and then used as a substrate onto which glucose oxidase can be covalently attached. The use of these nanoparticles in sensors not only led to enhanced electron transfer between enzyme and electrode but also gave enhanced stability for up to 30 days (Zhang *et al.,* 2005). Similar studies immobilised colloidal gold on gold and carbon electrodes, onto which films of crosslinked glucose oxidase was grafted. The composite films demonstrated higher sensitivity and stability compared to sensors without the colloid (Mena *et al.,* 2005). Gold nanoparticles have also been utilised in composite electrodes along with the electron transfer compounds tetrathiafulvalene-tetracyanoquinodimethane (Sanchez-Obrero *et al.,* 2009). Glucose oxidase could be crosslinked onto these electrodes and used for glucose sensing; composite electrodes containing gold were found to give enhanced performance compared to those that did not.

As well as gold nanoparticles, other nanostructures made from gold can be used to enhance electron transfer between enzymes and electrodes. Track-etched polycarbonate membrane containing regular pores could be used as a matrix to form arrays of gold nanotubes onto which glucose oxidase could be immobilised (Delvaux and Champagne, 2003) with the resulting sensor demonstrating extremely high sensitivity (400 nA mM^{-1} cm^{-2}) to glucose. One challenge was that the electrochemical potential required for the detection of glucose allowed interference from other electrooxidisable compounds; however, in later work incorporation of a second enzyme, horseradish peroxidase, lowered the potential required to only –200 mV vs Ag/AgCl where interference effects are minimal (Delvaux *et al.,* 2005).

Metal nanoparticles are not limited to gold, with for example silver nanoparticles and glucose oxidase having been encapsulated within a crosslinked polymer film on a platinum electrode with a 60-fold increase in electrochemical response in comparison to systems without nanoparticles (Ren *et al.,* 2005). Platinum nanoparticles encapsulated with poly(amidoamine) dendrimers were assembled along with glucose oxidase using a layer-by-layer technique onto platinum electrodes. The resultant sensors displayed a 5 μM to 1.0 mM linear range to glucose with a 5 s response time (Zhu *et al.,* 2007).

Magnetic nanoparticles are becoming a topic of increasing interest within the sensing world because of their ability to be controllably moved and concentrated using magnetic fields, and in this context for example a suspension of these particles can be placed on an electrode and a magnetic field can be used to pull the particles onto the electrode rather than having to dry off the solvent or wait for gravity or diffusion. Gold-coated Fe_3O_4 nanoparticles could be assembled using magnetic fields onto a gold electrode to form vertical 'nanowires' along magnetic field lines (Fig. 2.2). These could then be

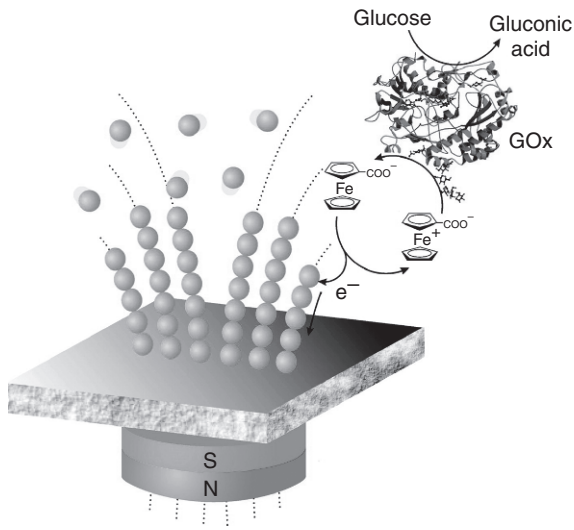

2.2 Self-assembly of Au-coated magnetic nanoparticles along magnetic field lines to form a nanostructured electrode. Glucose oxidase, GOx. (*Source*: Reprinted with permission from Jiminez *et al.,* 2008. Copyright 2008. American Chemical Society.)

used to determine levels of glucose by using soluble glucose oxidase and a ferrocene carboxylic acid mediator (Jimenez *et al.,* 2008).

Glucose sensors using other magnetic particles have been described such as for example mixtures of Fe_3O_4 nanoparticles with chitosan and glucose oxidase which could be crosslinked onto platinum electrodes. The nanoparticles have a chemistry that mimics peroxidase and leads to the development of a sensor with good sensitivity and largely free from the effect of interferences which could be used in determination of glucose in clinical samples (Yang *et al.,* 2009a). More complex materials comprising Fe_3O_4, Prussian blue and glucose oxidase could be immobilised on a carbon electrode by magnetic attraction and covalent linking (Li *et al.,* 2009a) to give a biosensor which could be used in human blood. Other workers have similarly used nickel iron oxide (Luo *et al.,* 2010) nanoparticles as a basis for a biosensor.

Carbon has been widely used within biosensors for many years so once CNTs became available in usable quantities, it was inevitable that they would be incorporated into sensors. They display high aspect ratios along with a high surface area to volume ratio and good electrical conductivity. They also can be chemically modified in a number of selective procedures, meaning recognition species can be easily covalently attached to these substrates. Nanotubes exist in single-walled (SWCNTs) and multi-walled varieties (MWCNTs) as shown in Fig. 2.1. Initial experiments using these materials often simply cast them onto conventional electrodes because of

their potential to greatly increase surface area, leading to higher binding levels of enzyme and easier access of substrate. Much of the work on the use of CNTs in a wide variety of electrochemical biosensors is outside of the scope of this chapter, but has been reviewed elsewhere (Wang and Lin, 2008).

A composite of glucose oxidase, chitosan and MWCNTs, for example, can be cast onto a glassy carbon electrode to give a glucose sensor which displays direct enzyme–electrode electron transfer without need for a mediator (Liu *et al.,* 2005a). An advantage of CNTs is that they can often act as a catalyst for various electrochemical reactions. Much of the early enzyme biosensor work utilised oxidase enzymes, the use of dehydrogenase enzymes being much less common because of the requirement for co-factors such as NAD/NADH (nicotinamide adenine dinucleotide) which require high oxidation overpotentials. CNTs cast onto glassy carbon electrodes have been shown to catalyse this reaction, allowing the use of much lower (reduced by 490 mV) potentials (Musameh *et al.,* 2002), thereby opening up the possibility of utilising dehydrogenase enzymes as components of sensitive, low operating potential amperometric biosensors.

The ability to chemically modify CNTs has allowed workers to enhance their performance by grafting electroactive species onto the tube. Ferrocene units could be covalently linked onto CNTs which were cast onto electrodes and then coated with a glucose oxidase/chitosan composite to give systems which demonstrated enhanced electron transfer kinetics (Qiu *et al.,* 2009). Polyaniline could be grafted onto MWCNTs to give composites which, when encapsulated into a silica/Nafion matrix, could be used as a substrate for glucose oxidase immobilisation and sensor construction (Gopalan *et al.,* 2009). An ionic liquid could be used as a dispersant to construct cellulose–MWCNT composites into which glucose oxidase could be encapsulated, leading to the development of a biosensor (Wu *et al.,* 2009). Glucose oxidase and anionic carboxylic acid modified CNTs could be electrochemically co–deposited in a conductive polypyrrole matrix as a simple method of constructing CNT containing biosensors (Wang and Musameh, 2005).

Combinations of CNTs with a number of other nanomaterials such as metal nanoparticles have also been utilised; Nafion, glucose oxidase, Pt nanoparticles and SWCNTs, for example, could be mixed together to give biosensors with enhanced sensitivity over systems which contained either Pt or SWCNTs alone (Hrapovic *et al.,* 2004). Glassy carbon electrodes could be modified with SWCNTs and gold nanoparticles using a layer-by-layer technique with an increase in sensitivity to H_2O_2 for up to eight layers, the resulting system being able to be coated with a glucose oxidase/chitosan composite to give a glucose biosensor (Wang *et al.,* 2009a). CNTs, Ag nanoparticles, glucose oxidase and horseradish peroxidase were combined in solution and deposited onto indium tin oxide electrodes to give

an amperometric biosensor with a linear range of 0.5–50 μM glucose and a detection limit of 0.1 μM (Lin *et al.,* 2009).

MWCNTs could be cast onto glassy carbon and composite Au/Pt nanoparticles electrodeposited directly onto this substrate with glucose oxidase being adsorbed onto this surface (Zhang *et al.,* 2010). The resultant biosensor gave good performance and was successfully used to analyse human serum. Alumina membranes could be used as matrices for the simultaneous hydrothermal polymerisation of glucose and the reductive deposition of Pt salts to give a mixture of carbohydrate and Pt nanoparticles. Heating these to 750°C carbonised the polymer and upon dissolution of the membrane with 10% HF, novel Pt/CNT composites were obtained which were cast onto glassy carbon (Wen *et al.,* 2009). The Pt/CNT composites displayed superior activity towards H_2O_2 compared to CNT/glassy carbon or bulk Pt electrodes, as well as being able to be used as the basis for a glucose sensor.

Other more complex combinations have also been used. MWCNTs have been decorated with Fe_3O_4 nanoparticles which had been coated with silica to improve biocompatibility (Baby and Ramaprabhu, 2010), cast onto glassy carbon and coated with a glucose oxidase/Nafion mixture to give a glucose sensor. Composites of MWCNTs with platinum, silica and alumina could be cast onto glassy carbon and used as substrates for glucose oxidase, with the resultant sensor showing higher sensitivity than sensors made with just platinum and MWCNTs (Tsai and Tsai, 2009). Composites of platinum nanoparticles, CNTs and TiO_2 have also been studied (Pang *et al.,* 2009). Gold and gold/platinum nanoparticles have also been deposited using a chemical reduction method onto a planar form of carbon; graphene nanosheets (Baby *et al.,* 2010). The resultant composites have a large surface area, since the metal nanoparticles prevent 'stacking' of the graphene sheets and, when combined with glucose oxidase and Nafion, can be used in the development of glucose sensors.

One of the recent focuses of CNT use in biosensors is the possibility to arrange them in a more controlled manner than obtained by simple casting or other adsorption techniques, and to actually use the CNTs as controlled 'molecular wires'. Early work in this field involved chemically modifying the ends of the CNT and then binding one end to an electrode to give vertical CNTs. Some of the earlier applications to the biosensing field involved binding carboxylic acid functionalised, 50 nm long SWCNTs to an amino–modified gold electrode (Patolsky *et al.,* 2004), substituting the free end of the CNT with the FAD co-factor and then using this to bind apo-glucose oxidase (Fig. 2.3). Other workers (Liu *et al*., 2005b) also used this technique to immobilise either glucose oxidase or apo-glucose oxidase onto vertical SWCNTs, with the latter approach proving more successful. In both studies the CNTs were shown to act as nanoelectrodes and to allow direct 'wiring' of the enzyme to the electrode.

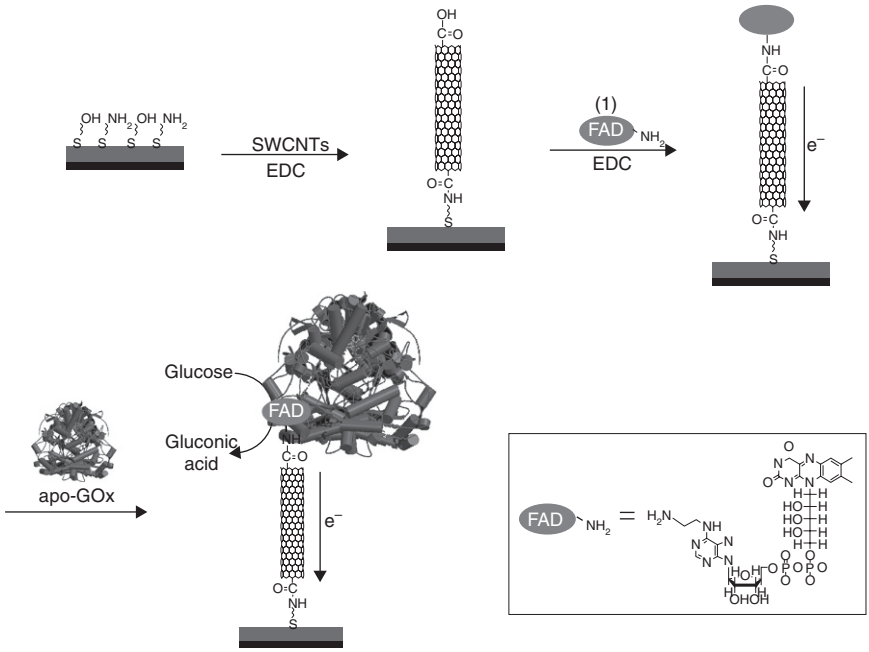

2.3 Long-range electrical contacting of redox enzymes by SWCNT connectors. ((1) = the amino derivative of the FAD co-factor, EDC = 1-ethyl-3-(3-dimethylaminopropyl) carbodiimide hydrochloride). (*Source*: Copyright Wiley-VCH Verlag GmbH & Co. KGaA. Reproduced with permission from Patolsky *et al.,* 2004.)

A number of techniques have been developed for growing CNTs vertically from a surface, for example by chemical vapour deposition. Often 'seeds' such as metal nanoparticles can be used and the disposal of these seeds on the surface affects the final nature of the nanotube array. Tightly packed 'forests' of nanotubes can be grown or alternatively the individual nanotubes can be widely spaced, thereby allowing each nanotube to act as an isolated nanoelectrode and the system as a whole as a nanoelectrode array. For example, vapour deposition onto a chromium electrode 'seeded' with nickel nanoparticles allowed development of low density nanoelectrode patterned arrays (Lin *et al.,* 2004). These arrays could be encapsulated in epoxy and polished so that the tips of the CNTs were showing; these were then selectively modified to allow covalent immobilisation of glucose oxidase just on the ends of the nanotubes (Lin *et al.,* 2004). The nanoelectrode was shown to be capable of detecting the reduction of enzymatically produced H_2O_2 in the presence of glucose at –0.2 V vs Ag/AgCl with no need for a mediator and minimal interference being observed from ascorbate, acetaminophen or uric acid. Other workers have grown horizontal SWCNTs on silicon

substrates using vapour deposition and then electrodes were deposited on top of the SWCNTs with electron-beam lithography (Besteman *et al.,* 2003). These systems acted as field effect transistors, and glucose oxidase could be immobilised onto the sides of the SWCNTs. The resultant system could detect the presence of glucose, which opens up the possibility of using single CNTs as sensors.

Although much less popular than CNTs, carbon nanofibres have also been utilised in biosensors (Wang and Lin, 2008). By a combination of photolithographic and chemical or electrochemical techniques (shown schematically in Fig. 2.4) it has proven possible to spatially control functionalisation across both the surface of an array and along the length of the vertical nanofibres

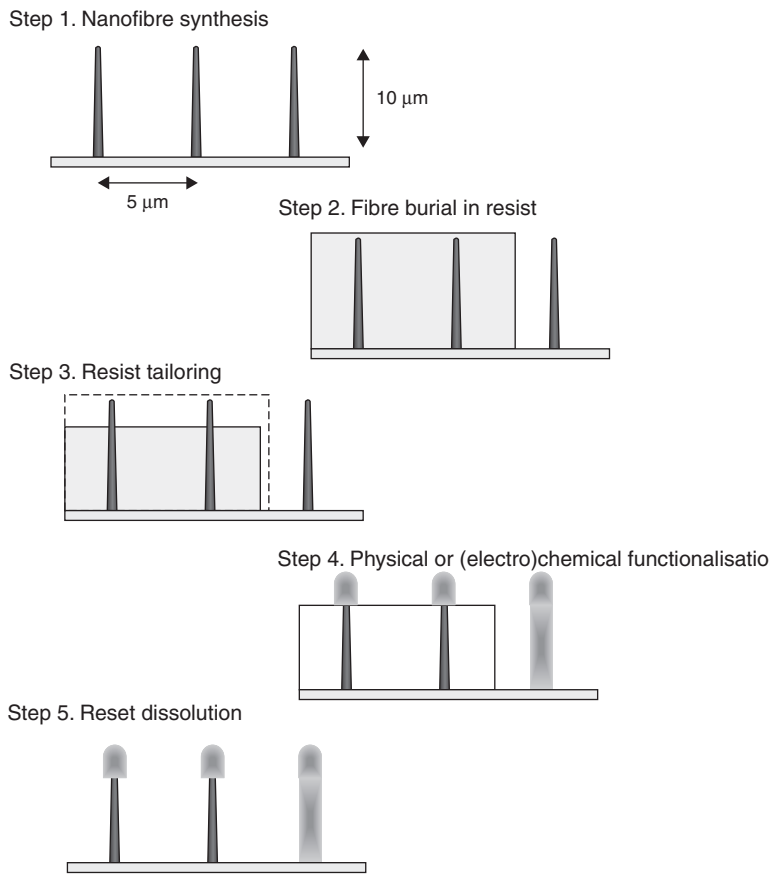

2.4 General scheme for photoresist-based blocking of chemical or electrochemical functionalisation of arrays of vertically aligned carbon nanofibres. (*Source*: Reprinted with permission from McKnight *et al.,* 2006. Copyright 2006. American Chemical Society.)

(McKnight *et al.,* 2006). In a similar manner to that reported above for CNTs, the possible control of structure, as visualised using fluorescent and electron microscopy, opens up scope for the development of nanosized biosensors. Commercial carbon nanofibres could be modified with glucose oxidase and then cast onto platinum electrodes and used in glucose sensing. The authors reported that comparison experiments showed the carbon nanofibres to be the best matrix, being superior to CNTs or graphite powder (Vamvakaki *et al.,* 2006). Other workers (Wu *et al.,* 2007) functionalised carbon nanofibres with carboxylic acid groups using a simple nitric acid treatment, cast them onto a glassy carbon electrode and coated with glucose oxidase/Nafion to give a glucose biosensor which could be operated at a low operating potential (–0.3 V vs a standard calomel electrode (SCE)).

Besides the carbon based systems discussed above, a range of metal oxide nanowires and nanotubes have also been investigated for use in biosensors; incorporation of all the materials that have been utilised in these systems is beyond the scope of this work but has been reviewed extensively elsewhere (Liu, 2008), so only a few examples will be given. ZnO nanotube arrays could be formulated by chemical etching onto gold electrodes and used as substrates to immobilise glucose oxidase (Kong *et al*., 2009) with the nanotube assemblies giving higher performance than either planar or ZnO nanorod substrates. Similar ZnO arrays could be deposited electrochemically and modified with glucose oxidase/Nafion to give biosensors (Yang *et al.,* 2009b). Thin (250 μm diameter) silver wires could be used as substrates to grow ZnO nanowires 1.2 μm × 250 nm in size, onto which glucose oxidase could then be immobilised. The resultant device could sense glucose in the range 0.5 μM to 10 mM, and is potentially small enough to be inserted into single cells (Ali *et al.,* 2010).

Other nanowires have also been used; gold nanowire arrays, for example, could be deposited using template-assisted electrodeposition on gold disc electrodes and used to immobilise glucose oxidase (Liu *et al.,* 2009a). The resultant arrays (shown in Fig. 2.5) had much higher (37-fold) activities than the planar electrodes. Other workers electrochemically deposited nanowires of an inorganic complex salt, ruthenium purple (Chi *et al.,* 2009), with the resultant electrode displaying high reactivity to H_2O_2 at a low potential of –0.1 V vs SCE. Depositing a crosslinked film of glucose oxidase/chitosan on the substrate allowed the construction of a glucose sensor.

The materials described above have been either metallic or inorganic in nature. However, organic conducting polymers have been utilised in a similar manner since they can often be synthesised as nanofibres or other nanostructures, with the same advantages as those observed for inorganic species. For example, within our own group we have used a combined electrochemical and sonochemical method to design arrays of micron-sized polyaniline 'mushrooms' into which glucose oxidase can be entrapped, giving a glucose

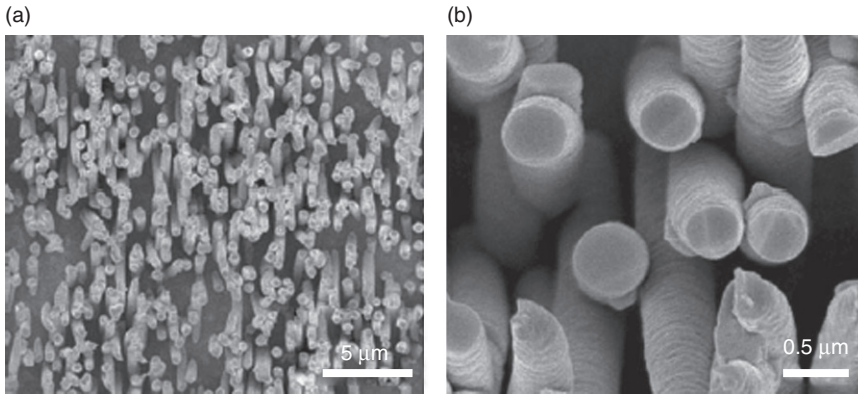

2.5 SEM images of a gold nanowire array on an electrode. (*Source*: Reproduced from Liu *et al.,* 2009a with kind permission from Springer Science + Business Media.)

sensor (Barton *et al.,* 2004). Alumina membranes could also be used as a template into which polyaniline nanotubes could be grown, allowing glucose oxidase to then be electrochemically trapped on the inside of these tubes. The resultant sensor displayed direct enzyme to electrode transfer, good sensitivity and could be run at a low potential (–0.3 V vs SCE) in clinical samples, thereby eliminating the effects of many interferents (Wang *et al.,* 2009b). Other workers have used a montmorillonite clay template inside which they polymerised diphenylamine (Santhosh *et al.,* 2009a). Separation of the clay and polymer gave a polymeric product consisting of nanostructured hollow spheres, and these could be immobilised on an electrode along with glucose oxidase and Nafion to give a sensitive glucose sensor with low interference from common compounds such as ascorbate. Again composite materials have also been studied containing polymer – and other nanosized objects such as nanofibres of the conducting polymer poly(3,4-ethylenedioxythiophene) could be electrodeposited onto glassy carbon and then a further electrodeposition step used to deposit palladium nanoparticles onto the nanofibres (Santhosh *et al.,* 2009b). Further deposition of glucose oxidase and Nafion gave rise to a sensitive glucose sensor with minimal susceptibility to electroactive interfering species.

A novel method of synthesising enzyme/conductive polymer nanocomposites has been reported (Ramanavicius *et al.,* 2005). Combining within solution glucose, glucose oxidase and pyrrole caused the enzymatic production of hydrogen peroxide, which in turn caused oxidative polymerisation of pyrrole with the resultant formation of polypyrrole/glucose oxidase nanoparticles (Fig. 2.6). Casting the enzyme/polymer suspension onto carbon electrodes and crosslinking with glutaraldehyde led to formation of glucose

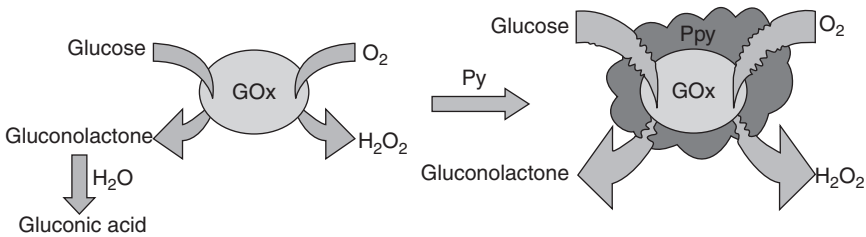

2.6 Synthesis of polypyrrole encapsulated glucose oxidase nanoparticles. (*Source*: Reproduced from Ramanavicius *et al.,* 2005 with permission from Elsevier.)

sensors with enhanced stability compared to controls manufactured from crosslinked enzyme only.

2.3 Nanosized materials: direct detection of glucose

Although glucose oxidase-based biosensors are widely used in academia and are the basis of the home-glucose testing market, they do suffer some disadvantages, such as for example that the enzyme can potentially leach out from the matrix or become denatured, and that the biological molecules can often be relatively challenging to isolate and purify to the same standard and reactivity every time. There has therefore been work on developing methods of detecting glucose that do not require enzymes. Many of these are either based on chemical assays or are optical or spectroscopic in nature and are outside the scope of this chapter. However, the direct electrochemical detection of glucose is a possible alternative to enzyme-based electrodes (Cash and Clark, 2010).

Glucose can undergo electro-oxidation reactions directly at electrodes and for example in this context, workers have studied the electrochemistry of glucose at platinum electrodes (Vassilyev *et al.,* 1985), showing that glucose can be detected at these electrodes. However, challenges to this simple approach include selectivity, with clinical samples containing many other oxidisable compounds and the deposition of reaction products on the electrode. Other limitations include slow reaction kinetics and the requirement for large overpotentials, thereby compromising specificity. Other workers have used gold electrodes, which have shown better activity and lower levels of electrode poisoning (Adzic *et al.,* 1989). A variety of other electrode systems have been utilised, and in this context a wide range of metal alloys, for example, were screened, with the most effective electrodes being found to contain both Pt and Pb (Sun *et al.,* 2001); these operated at lower potentials, minimised the effects of potential interferences, and also lowered poisoning. Metal carbon composites have also been used; for instance a nickel

powder/ceramic carbon/Nafion electrode displayed low levels of interference and long lifetime, and was demonstrated for the determination of glucose in human serum samples (Salimi and Roushani, 2005). However, many of these methods still require the samples to be run in highly alkaline conditions (Cash and Clark, 2010), thereby complicating any assay and making *in vivo* measurements problematic.

Nanosized materials, again for their potential beneficial catalytic effects, electron transfer and increased surface areas, have been applied to this challenge, and we will discuss some of the most recent work. Nanoparticles of a variety of substances have been incorporated into electrodes. Gold nanoparticle/chitosan complexes, for example, could be deposited on glassy carbon and were successfully used to quantify glucose in rat serum (Feng *et al.,* 2009). Silver nanoparticles could be incorporated into carbon black electrodes and be shown to catalyse glucose oxidation as well as being able to be used in a flow injection analysis for glucose using pulsed amperometric detection (Quan *et al.,* 2010). Nickel hexacyanoferrate nanoparticles could be used to develop a non-enzymatic glucose sensor with modest selectivity over ascorbic acid (Wang *et al.,* 2010a) while nickel–palladium nanoparticles could be deposited onto an electrochemically etched silicon microchannel plate and in alkaline solutions were shown to give good responses to glucose with minimal interference from ascorbic acid (Miao *et al.,* 2009).

Carbon nanostructured materials have also been of interest, usually as composites with other nanosized electrocatalytic materials. MWCNTs could be cast onto glassy carbon electrodes, modified with nickel oxide, and then used to detect glucose in alkaline solution, the CNT modified electrode showing much higher reactivity than the control electrodes without the CNT, thereby allowing this to be used to assess glucose in human serum (Shamsipur *et al.,* 2010). Composites of SWCNTs and Pd nanoparticles could be cast onto glassy carbon electrodes, which displayed a high catalytic activity towards glucose in phosphate buffer (pH = 7.4) and a low oxidation potential (−0.35 V vs SCE), which minimised the effect of common interferents (Meng *et al.,* 2009). Palladium/CNT composites have also been shown to catalyse oxidation of glucose at 0.4 V vs SCE, as well as being suitable for measuring glucose in urine samples with good resistance to poisoning by common interferents (Chen, 2010).

Other workers compared double-walled CNTs coated with Pt, CuS or SnO_2 nanoparticles (Myung *et al.,* 2009) and demonstrated the highest activity for the Pt modified electrodes. Self-assembled layers of CNTs interleaved with layers of polyoxometallates could be deposited onto indium tin oxide electrodes and then used as a substrate to electrodeposit copper nanoparticles, to give a glucose sensor with greater sensitivity than Cu/CNT composites (Li *et al.,* 2009b). Vertical forests of MWCNTs could be grown on tantalum foil sputtered with cupric oxide to give CuO nanoparticle

modified substrates which could directly catalyse the oxidation of glucose with excellent sensitivity, high resistance to chloride poisoning, and minimal effects from common interferents (Jiang and Zhang, 2010), which together allowed the sensor to be used for the assessment of human serum samples.

Chemical functionalisation of CNTs has also been successful; in this context boronic acids are known to readily form boronate esters with 1,2-diols, of which glucose is an example. CNTs could be modified by a number of chemical moieties, one of which was vinyl phenyl boronic acid which could be grafted using radiation induced polymerisation onto MWCNTs (Yang *et al.,* 2010). These, when cast along with Nafion onto glassy carbon, allowed construction of a sensor with linear response to glucose concentration in the range 1.0–10 mM. Carbon nanofibres have also been studied. Composite paste electrodes of carbon nanofibres and Ni/NiO nanoparticles, for example, were used to construct renewable glucose sensors with strong and rapid amperometric responses, with no evidence of poisoning by chloride ions and displaying a linear range from 2 μM to 2.5 mM and a detection limit of 1 μM (Liu *et al.,* 2009b). Other workers compared CNTs, carbon nanofibres and activated carbon based sensors, all modified with platinum nanoparticles, with the nanofibre-based electrodes showing the highest sensitivity (Rathod *et al.,* 2010).

A variety of other nanosized materials have been recently incorporated into enzyme-free glucose biosensors. Copper-based materials have been studied and Cu-CuO nanowires, for example, could be deposited onto glassy carbon to give electrodes capable of amperometric detection of glucose in 0.1 M NaOH with a linear range from 0.1 to 12 mM and minimal interference from ascorbic and uric acid (Wang *et al.,* 2010b). Other work (Wang and Fan, 2010c) compared CuO nanoflowers and nanorods immobilised on graphite electrodes; these systems both showed catalytic ability towards glucose with good selectivity over ascorbate and dopamine, with the CuO nanoflowers imparting higher sensitivity, although the nanorods displayed a larger linear range of glucose concentration and a shorter response time. Copper oxalate-modified copper electrodes also gave good results, with linear ranges up to 15 mM, and could be used to assess glucose levels in serum (Babu and Ramachandran, 2010).

Both voltammetric and amperometric methods could be used to determine the concentration of glucose on gold nanowire-modified electrodes (Cherevko and Chung, 2009). Simple mixing of carbon powder, nanosized $Ni(OH)_2$ and an ionic liquid also gave a relatively quick and inexpensive method of making electrodes which could determine glucose rapidly with low levels of interference from ascorbic and uric acid (Safavi *et al.,* 2009). Hydrothermal methods could be used to grow bimetallic Pb/Pt networks on titanium electrodes to give glucose sensors suitable for use in neutral media at low operating potentials (−0.08 V vs Ag/AgCl) with

minimal chloride poisoning and low sensitivity to common interferents (Wang *et al.,* 2008). Highest sensitivities were obtained for a 50:50 mix of the two metals. Vertical forests of silicon nanowires on a Si substrate could be fabricated and boron doped diamond could be grown on these using chemical vapour deposition to give a nanorod modified electrode. This could be used as a selective, enzyme-free sensor for glucose in 0.1 M NaOH with minimal effects from interfering compounds (Luo *et al.,* 2009).

As can be seen, there exist a number of possibilities for the use of direct glucose oxidation sensors. They have the advantages that they do not require expensive biological materials and often display superior storage characteristics due to there being no denaturation of enzymes. They can, however, require high oxidation potentials and, in the majority of the cases described, samples must be in an alkaline solution, making their use in *in vivo* applications challenging if not impossible. They have been shown to be capable of assaying clinical samples with good sensitivity, although again most of these require the sample to be diluted in an alkaline solution, typically 0.1 M NaOH.

2.4 Nanosized sensors

One of the most interesting areas of research is that of developing actual nanosized sensors. These would be especially useful in either monitoring the conditions inside individual cells or in *in vivo* applications, such as continuous monitoring of glucose in diabetic patients. One of the more promising applications is that of using nanosized, fluorescent species such as quantum dots or fluorescent polymer nanoparticles, perhaps within a 'smart tattoo'. These would allow direct interrogation through the skin rather than having to implant an electrode system. However, since this chapter is focused on electrochemical detection we will not cover this subject further, and the reader is referred to another review (Cash and Clark, 2010).

Implantable glucose sensors for continuous monitoring, such as the Minimed™ system are already commercially available and use subcutaneous needle sensors to detect glucose. They can be coupled with an insulin pump to allow much greater levels of control for blood glucose levels, especially important in Type 1 diabetes. Challenges to their use still exist, however, including for example that they are generally usable only for a week or so at a time before needing to be replaced.

The construction of glucose sensors for *in vivo* applications is an intensely active field of research, so we will again confine ourselves to recent advances. One relatively simple method is to enclose the sensor inside a catheter to allow monitoring of clinical samples. Major issues

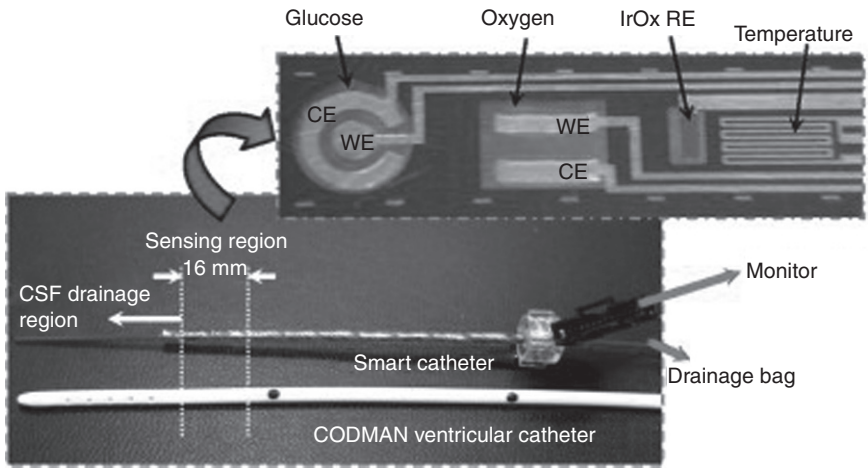

2.7 Photographs of a smart catheter with glucose, oxygen and temperature sensors (WE = working electrode, CE = counter electrode, RE = reference electrode, CSF = cerebrospinal fluid). (*Source*: reproduced from Li *et al.*, 2009c with permission from Elsevier.)

with any sensor of this type are biocompatibility and potential toxicity. The common reference electrodes used, for example, are the SCE and Ag/AgCl, both containing toxic metals. In recent work, glucose, oxygen and temperature sensors could be constructed on a Kapton polymer film. The glucose sensor consisted of a gold electrode modified with glucose oxidase and platinum nanoparticles, which catalysed the electrochemical detection of hydrogen peroxide, along with an indium oxide reference electrode (Li *et al.,* 2009c). The sensors could then be rolled up inside an intraventricular catheter (Fig. 2.7) and used to assess glucose, oxygen and temperature in extracted cerebrospinal fluid. Other workers utilised a 3 mm diameter catheter electrode that had been modified to have a paste working electrode made from fluorinated CNTs to measure glucose in human urine without the need for enzyme catalysis (Ly and Lee, 2009). The catheter could be inserted into rats bladders for *in vivo* measurement of glucose in urine.

Reducing these devices in size further to produce true nanobiosensors has proved problematic. The development of micro- and nano biosensors is being very actively researched, however, as reviewed elsewhere (Urban, 2009). One potential approach has been the use of nanowire arrays (Ali *et al.,* 2011) and, for example, a zinc oxide nanowire array modified with glucose oxidase/Nafion film could be fabricated on a silver wire (250 μm diameter). This not only gave good responses to glucose with minimal effects from interferents, but was also successfully integrated with standard mobile phone technology to allow for potential remote monitoring applications such as point-of-care

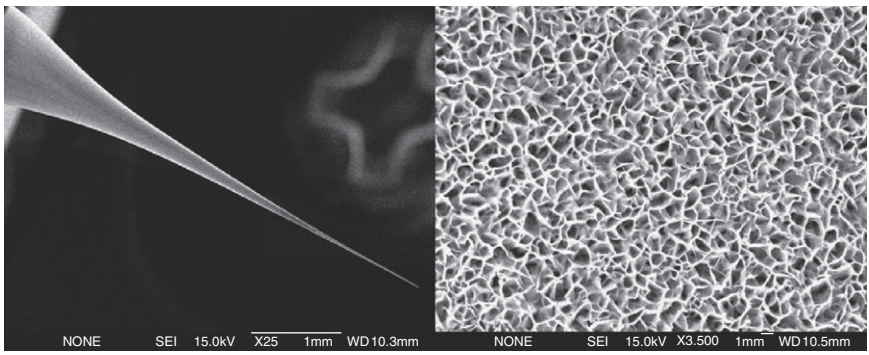

2.8 Typical scanning electron microscopy images of the nanoflake ZnO grown on an aluminium-coated glass capillary before enzyme coating. The electron microscope image of nanoflake ZnO is on the right, the image on the left is that of the capillary. (*Source*: Reproduced from Fulati *et al.,* 2010 with permission from Elsevier.)

testing. In other work by the same group, ZnO 'nanoflakes' could be grown onto aluminium-coated glass capillaries (0.7 μm diameter, Fig. 2.8), coated with glucose oxidase/Nafion and used to electrochemically determine glucose concentrations in individual human adipocytes and frog oocytes (Fulati *et al.,* 2010). The intracellular glucose concentration in individual human adipocytes could be measured to be 60 ± 15 μM (n = 5), increasing to 130 ± 15 μM (n = 5) upon addition of insulin, which is expected as insulin stimulates cellular glucose uptake.

Other workers spin-coated polymethyl methacrylate onto platinum-coated indium tin oxide to give a 30 nm thick layer of polymer. Nanochannels 80 nm in width were then dug into the film using an atomic force microscope (Tsai *et al.,* 2009). These could then be filled with glucose oxidase using electrodeposition to give glucose nanobiosensors with much higher sensitivity per unit area than similar macroelectrodes.

Field effect transistors have been widely used in the biosensor field. Workers successfully created silicon nanowires of 50 nm height and 50–100 nm width by electron-beam lithography onto a Si/SiO_2 microneedle (Fig. 2.9) to create a field effect transistor that could measure pH (Park *et al.,* 2007). Deposition of a suitable biological recognition moiety such as glucose oxidase onto the surface of this nanowire would give a system which could be used as a biosensor, since oxidation of glucose leads to formation of gluconic acid and a resultant pH change. Other workers used glucose oxidase to coat a region ion sensitive field effect transistor to give a nanobiosensor for glucose (Risveden *et al.,* 2007). The use of these silicon nanowires systems in label-free biosensors has been reviewed recently (Chen *et al.,* 2011).

A major advance would be incorporation of these nanosensors into living systems. Recently, biofuel cells containing CNTs which utilise glucose as a

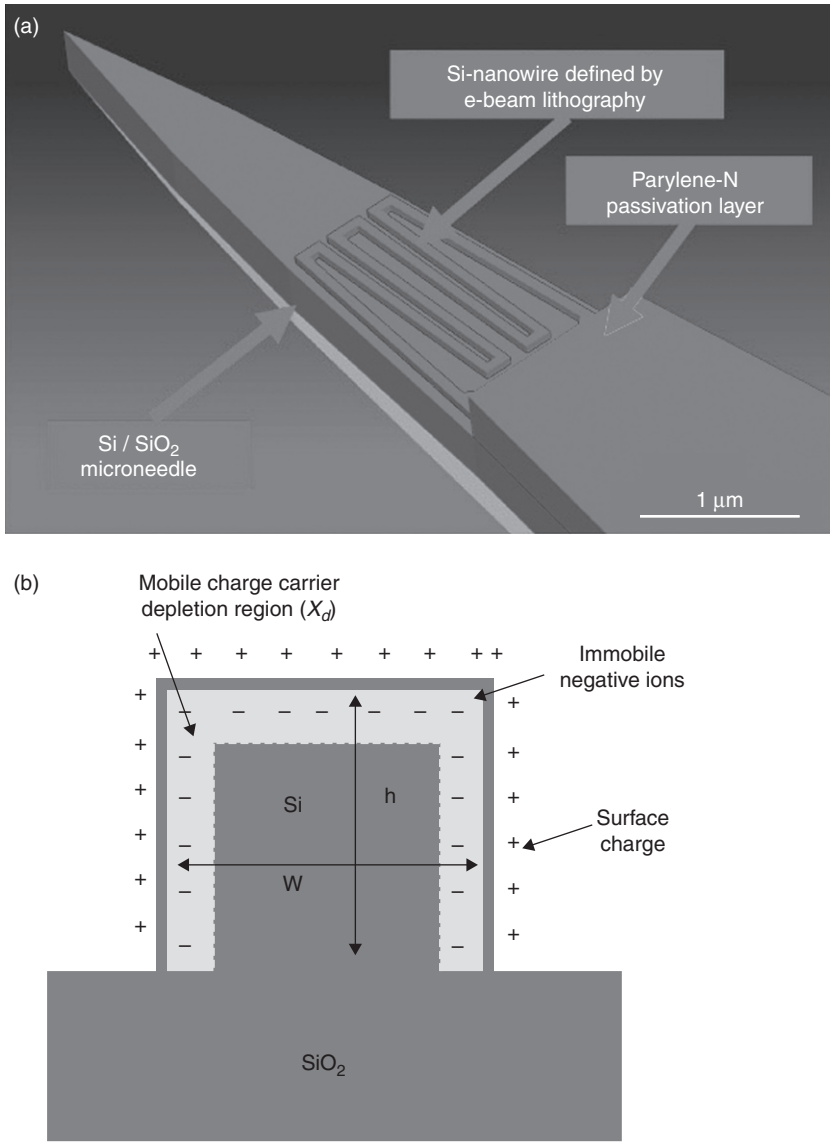

2.9 (a) Design of microneedle tip with integrated serpentine silicon nanowire structure on top surface (b) Cross-sectional view of silicon nanowire fabricated by e-beam lithography on silicon-on-insulator (SOI) substrate. (*Source*: Reproduced from Park *et al.*, 2007 with permission from Elsevier.)

fuel to produce electrical energy have been successfully implanted for up to 2 weeks within a snail (Halámková *et al.*, 2012). Other workers have utilised a computational approach to simulate the application of medical nanorobotics for diabetes using clinical data (Cavalcanti *et al.*, 2008).

2.5 Conclusion and future trends

We have described above how the use of nanomaterials in glucose sensors is becoming much more common and is also demonstrating improved sensitivities and selectivities over sensors that do not contain these materials. This is especially relevant in the development of enzyme-free glucose sensors, which use nanomaterials to directly catalyse electrochemical reactions. However, it is difficult to see how these technologies will impinge on much of the current commercial glucose sensing market due to factors such as cost. Currently the single-shot disposable electrodes which are widely used within the management of diabetes are constructed using screen printing methods which are relatively inexpensive and allow the mass production of large numbers of these electrodes. Another major advantage of using single-shot electrodes is that problems such as biofouling and cleaning of electrodes simply do not exist. Since these electrodes are entirely fit for their required purpose, it is difficult to envisage much more complex electrodes with the attendant higher costs making any impact in this market.

However a second field in which nanotechnology could potentially make a major impact is that of continuous monitoring. The stick-pin method of glucose sensing, where the patient takes a blood sample at regular intervals and determines the glucose level, suffers from several disadvantages. Firstly the process is painful and invasive, thereby carrying the risk on non-compliance by the patient. Also, it only provides snapshots of glucose concentration, whereas trends in glucose levels would be of greater interest. Finally, it cannot provide warnings of dangerously high/low glucose levels unless the patient actually happens to test at that particular time. It is obvious that a much better system would be one where the patient's glucose levels are essentially continuously monitored. Such commercial systems exist, such as the Minimed™ system; however, these do not display long term stability, requiring to be changed on an approximately weekly basis. The desired system would be a small 'glucose chip' which could be implanted subcutaneously, had a long (preferably months or even years) lifetime, was resistant to processes such as biofouling which can affect accuracy, and could communicate its results via wireless technology.

Nanobiosensors and nanomaterials potentially offer solutions to some if not all of these problems. The lowering in size that is possible with using such materials means that biochips small enough and with low power requirements could be implanted. Direct enzyme-free measurement of glucose could offer a solution to the problem of enzyme degradation and denaturation. The small size, and the potential to tailor the surface chemistry of such sensors, could offer a solution to biofouling. However, there are still major issues to be addressed.

Many of the sensors described have only been tested in laboratory conditions, and in simple media such as phosphate buffer. Extensive testing with clinical samples and over long time periods would be required before any sensor could even be submitted for medical trials on human patients. The long term stability of any implanted sensor is vital, not only for the need for it to retain accuracy and to ensure biocompatibility but also the possibility that components of the sensor could 'escape' into the wider human system. Many nanomaterials could potentially display high toxicity, with for example CNTs having been shown in many cases to display toxicology issues similar to those of asbestos. Many metallic nanoparticles have also been shown to be toxic to living organisms. Any materials used in implanted sensors must be proven to be benign or be encapsulated so securely, that release is essentially impossible.

Research into these fields is continuing apace despite these challenges, and it is easy to see why. Development of a stable, implantable sensor with a long lifetime would have a major positive effect of the life of diabetic patients. Coupling this together with an insulin pump, such as the Minimed™ system, would essentially allow the development of an 'artificial pancreas' and remove the need for constant testing and injections.

A further potential use for nanobiosensors would be for investigating localised conditions. Because of their small size, devices such as these could be used for localised monitoring of glucose, perhaps at a particular site in the body where there may be injury or surgical intervention is occurring. The extreme example of this would be glucose monitoring in individual cells. Although this may not be of interest in a direct clinical use, on a patient it could still be used to assess cell reactions. For example cells from a biopsy could be monitored upon exposure to individual or mixtures of anticancer drugs. The cells that 'die' most rapidly could be used to evaluate the efficiency of the various drugs and mixtures and allow the patient to be treated with the optimum drug 'cocktail' for their individual cancer.

The existence of these potential applications means that research into these nanosized systems will continue and hopefully will lead to advances that will enhance survival and quality of life for people suffering from a variety of clinical conditions.

2.6 Sources of further information and advice

Irudayaraj J M (2012) '*Biomedical Nanosensors (Pan Stanford Series on Biomedical Nanotechnology)*', Pan Stanford.

Lim T-C (2010) '*Nanosensors: Theory and Applications in Industry, Healthcare and Defense*', CRC Press.

Muhandiramlage T P (2011) '*Preparation and Characterization of Glucose Nanosensors for Intracellular Applications*. Proquest, Umi Dissertation Publishing.

Nagahara L, Tao N and Thundat T (2007) '*Introduction to Nanosensors (Nanostructure Science and Technology)*', Springer-Verlag, New York.

Khanna V K (2011) '*Nanosensors: Physical, Chemical, and Biological (Series in Sensors)*', Taylor and Francis.

Tibbals H F (2010) '*Medical Nanotechnology and Nanomedicine (Perspectives in Nanotechnology)*', CRC Press. Also see the review articles by Wang (2008), Cash and Clark (2010) and Pickup (2008).

2.7 References

Adzic R R, Hsiao M W and Yeager E B (1989) 'Electrochemical oxidation of glucose on single crystal gold surfaces', *J. Electroanal. Chem.* **260**, 475–485

Ahammad A J S, Lee J -J and Rahman M D (2009) 'Electrochemical sensors based on carbon nanotubes', *Sensors*, **9**, 2289–2319.

Ali S M U, Aijazi T, Axelsson K, Nur O and Willander M (2011) 'Wireless remote monitoring of glucose using a functionalized ZnO nanowire arrays based sensor', *Sensors* **11**, 8485–8496.

Ali S M U, Nur O, Willander M and Danielsson B (2010) 'A fast and sensitive potentiometric glucose microsensor based on glucose oxidase coated ZnO nanowires grown on a thin silver wire', *Sens. Actuat. B* **145**, 869–874.

Babu T G S and Ramachandran T (2010) 'Development of highly sensitive non-enzymatic sensor for the selective determination of glucose and fabrication of a working model', *Electrochim. Acta* **55**, 1612–1618.

Baby T T and Ramaprabhu S (2010) 'SiO_2 coated Fe_3O_4 magnetic nanoparticle dispersed multiwalled carbon nanotubes based amperometric glucose biosensor', *Talanta* **80**, 2016–2022.

Baby T T, Jyothirmayee Aravind S S, Arockiadoss T, Rakhi R B and Ramaprabhu S (2010) 'Metal decorated graphene nanosheets as immobilization matrix for amperometric glucose biosensor', *Sens. Actuat. B* **145**, 71–77.

Barton A C, Collter S D, Davis F, Gornall D D, Law K A, Lawrence E C, Mills D W, Myler S, Pritchard J A, Thompson M and Higson S P (2004) 'Sonochemically fabricated microelectrode arrays for biosensors offering widespread applicability. Part I', *Biosens. Bioelec*. **20**, 328–337.

Besteman K, Lee J, Wiertz F G M, Heering H A and Dekker C (2003) 'Enzyme-coated carbon nanotubes as single-molecule biosensors', *Nano Lett*. **3**, 727–730.

Cash K J and Clark H A (2010) 'Nanosensors and nanomaterials for monitoring glucose in diabetes', *Trends Mol. Med.* **16**, 584–593.

Cass A E, Davis G, Francis G D, Hill H A O, Aston W J, Higgins J, Plotkin E V, Scott L D L and Turner A P F (1984) 'Ferrocene-mediated enzyme electrode for amperometric determination of glucose', *Anal. Chem*. **56**, 667–671.

Cavalcanti A, Shirinzadeh B and Kretly L C (2008) 'Medical nanorobotics for diabetes control', *Nanomed: Nanotech. Biol. Med*. **4**, 127–138.

Chen X M (2010) 'Nonenzymatic amperometric sensing of glucose by using palladium nanoparticles supported on functional carbon nanotubes', *Biosens. Bioelec*. **25**, 1803–1808.

Chen K I, Li B R and Chen Y T (2011) 'Silicon nanowire field-effect transistor-based biosensors for biomedical diagnosis and cellular recording investigation', *Nano Today* **6**, 131–154.

Cherevko S and Chung C H (2009) 'Gold nanowire array electrode for non-enzymatic voltammetric and amperometric glucose detection', *Sens. Actuat. B* **142**, 216–223.

Chi B Z, Zeng Q, Jiang J-H, Shen G -L and Yu R-Q (2009) 'Synthesis of ruthenium purple nanowire array for construction of sensitive and selective biosensors for glucose detection', *Sens. Actuat. B* **140**, 591–596.

Clark L and Lyons C (1962) 'Electrode systems for continuous monitoring in cardiovascular surgery', *Ann. NY Acad. Sci*. **102**, 29–45.

Degani Y and Heller A (1987) 'Direct electrical communication between chemically modified enzymes and metal electrodes. I. Electron transfer from glucose oxidase to metal electrodes via electron relays, bound covalently to the enzyme', *J. Phys. Chem*. **91**, 1285–1289.

Delvaux M and Champagne S D (2003) 'Immobilisation of glucose oxidase within metallic nanotubes arrays for application to enzyme biosensors', *Biosens. Bioelec*. **18**, 943–951.

Delvaux M, Walcaarius A and Champagne S D (2005) 'Bienzyme HRP–GOx-modified gold nanoelectrodes for the sensitive amperometric detection of glucose at low overpotentials', *Biosens. Bioelec*. **20**, 1587–1594.

Feng D, Wang F and Chen Z (2009) 'Electrochemical glucose sensor based on one-step construction of gold nanoparticle-chitosan composite film', *Sens. Actuat. B* **138**, 539–544.

Fulati A, Usman Ali S M, Asif M H, Naveed ul Hassan Alvi, Willander M, Brännmark C, Strålfors P, Börjesson S I, Elinder F and Danielsson B (2010) 'An intracellular glucose biosensor based on nanoflake ZnO', *Sens. Actuat. B* **150**, 673–680.

Gopalan, A I, Lee K P, Ragupathy D, Lee S H and Lee J W (2009) 'An electrochemical glucose biosensor exploiting a polyaniline grafted multiwalled carbon nanotube/perfluorosulfonate ionomer-silica nanocomposite', *Biomaterials* **30**, 5999–6005.

Halámková L, Halámek J, Bocharova V, Szczupak A, Alfonta L, and Katz E (2012) 'Implanted biofuel cell operating in a living snail', *J. Am. Chem. Soc.* **134**, 5040–5043.

Hrapovic S, Liu Y L, Male K B and Luong J H T (2004) 'Electrochemical biosensing platforms using platinum nanoparticles and carbon nanotubes', *Anal. Chem*. **76**, 1083–1088.

Jiang L C and Zhang W D (2010) 'A highly sensitive nonenzymatic glucose sensor based on CuO nanoparticles-modified carbon nanotube electrode', *Biosens. Bioelec*. **25**, 1402–1407.

Jimenez J, Sheparovych R, Pita M, García A N, Dominguez E, Minko S and Katz E (2008) 'Magneto-induced self-assembling of conductive nanowires for biosensor applications', *J. Phys. Chem. C* **112**, 7337–7344

Kong T, Chen Y, Ye Y, Zhang K, Wang Z and Wang X (2009) 'An amperometric glucose biosensor based on the immobilization of glucose oxidase on the ZnO nanotubes', *Sens. Actuat. B* **138,** 344–350.

Li J P, Wei X P and Yuan Y (2009a) 'Synthesis of magnetic nanoparticles composed by Prussian blue and glucose oxidase for preparing highly sensitive and selective glucose biosensor', *Sens. Actuat. B* **139**, 400–406.

Li X, Zhu Q, Tong S, Wang W and Song W (2009b) 'Self-assembled microstructure of carbon nanotubes for enzymeless glucose sensor', *Sens. Actuat. B* **136,** 444–450.

Li C, Ahn C H, Shutter L A and Narayan R K (2009c) 'Toward real-time continuous brain glucose and oxygen monitoring with a smart catheter', *Biosens. Bioelec*. **25**, 173–178.

Lin Y, Lu F, Tu Y and Ren Z (2004) 'Glucose biosensors based on carbon nanotube nanoelectrode ensembles', *Nano Lett*. **4**, 191–195.

Lin J H, He C, Zhao Y and Zhang S (2009) 'One-step synthesis of silver nanoparticles/carbon nanotubes/chitosan film and its application in glucose biosensor', *Sens. Actuat B* **137**, 768–773.

Liu Y, Wang M, Zhao F, Xu Z and Dong S (2005a) 'The direct electron transfer of glucose oxidase and glucose biosensor based on carbon nanotubes/chitosan matrix', *Biosens. Bioelec.* **21**, 984–988.

Liu J Q, Chou A, Rahmat W, Paddon Row M N and Gooding J J (2005b) 'Achieving direct electrical connection to glucose oxidase using aligned single walled carbon nanotube arrays', *Electroanalysis* **17**, 38–46.

Liu A. (2008) 'Towards development of chemosensors and biosensors with metal-oxide based nanowires or nanotubes', *Biosens. Bioelec*. **24**, 167–177.

Liu Y, Zhu Y, Zeng Y and Xu F (2009a) 'An effective amperometric biosensor based on gold nanoelectrode arrays', *Nanoscale Res Lett.* **4,** 210–215.

Liu Y, Teng H, Hou H and You T (2009b) 'Nonenzymatic glucose sensor based on renewable electrospun Ni nanoparticle-loaded carbon nanofiber paste electrode', *Biosens. Bioelec*. **24**, 3329–3334.

Luo D B, Wu L and Zhi J (2009) 'Fabrication of boron-doped diamond nanorod forest electrodes and their application in nonenzymatic amperometric glucose biosensing', *ACS Nano* **3**, 2121–2128.

Luo L Q, Li Q, Xu Y, Ding Y, Wang X, Deng D and Xu Y (2010) 'Amperometric glucose biosensor based on $NiFe_2O_4$ nanoparticles and chitosan', *Sens. Actuat. B* **145**, 293–298.

Ly S Y and Lee J H (2009) 'Human-urine diabetes assay and in vivo rat bladder assay using a fluorine-doped carbon nanotube catheter sensor', *Ann. Biomed. Eng*. **37**, 2028–2033.

McKnight T E, Peeraphatdit C, Jones S W, Fowlkes J D, Fletcher B L, Klein K L, Melechko A V, Doktycz M J and Simpson M L (2006) 'Site-specific biochemical functionalization along the height of vertically aligned carbon nanofiber arrays', *Chem. Mater.* **18**, 3203–3211.

Mena M L, Yanez-Sedeno P, Pingarron J M (2005) 'A comparison of different strategies for the construction of amperometric enzyme biosensors using gold nanoparticle-modified electrodes', *Anal. Biochem.* **336**, 20–27.

Meng L, Jin J, Yang G, Lu T, Zhang H and Cai C (2009) 'Nonenzymatic electrochemical detection of glucose based on palladium-single-walled carbon nanotube hybrid nanostructures', *Anal. Chem*. **81**, 7271–7280.

Miao F J, Tao B, Sun L, Liu T, You J, Wang L and Chu P K (2009) 'Amperometric glucose sensor based on 3D ordered nickel-palladium nanomaterial supported by silicon MCP array', *Sens Actuat B* **141**, 338–342.

Musameh M, Wang J, Merkoci A and Lin Y H (2002)'Low-potential stable NADH detection at carbon-nanotube-modified glassy carbon electrodes', *Electrochem. Commun*. **4**, 743–746.

Myung Y, Jang D M, Cho Y J, Kim H S and Park J (2009) 'Nonenzymatic amperometric glucose sensing of platinum, copper sulfide, and tin oxide nanoparticle-carbon nanotube hybrid nanostructures', *J. Phys. Chem. C* 2009, **113**, 1251–1259.

Pandey P, Datta M and Malhotra B D (2008) 'Prospects of nanomaterials in biosensors', *Anal. Lett*. **41**, 159–209.

Pang X Y, He D, Luo S and Cai Q (2009) 'An amperometric glucose biosensor fabricated with Pt nanoparticle-decorated carbon nanotubes/TiO_2 nanotube arrays composite', *Sens. Actuat. B* **137**, 134–138.

Park I, Li Z, Li X, Pisano A P and Williams R S. (2007) 'Towards the silicon nanowire-based sensor for intracellular biochemical detection', *Biosens. Bioelec*. **22**, 2065–2070.

Patolsky F, Weizmann Y and Willner I (2004) 'Long-range electrical contacting of redox enzymes by SWCNT connectors', *Angew. Chem. Int. Ed*. **43**, 2113–2117.

Pickup J C, Zhi Z -L, Khan F, Saxl T and Birch D J S (2008) 'Nanomedicine and its potential in diabetes research and practice', *Diabetes Met. Res. Rev*. **24**, 604–610.

Qiu J D, Zhou W M, Guo J, Wang R and Liang RP. (2009) 'Amperometric sensor based on ferrocene modified multi-walled carbon nanotube nanocomposites as electron mediator for the determination of glucose', *Anal. Biochem.* **385**, 264–269.

Quan H, Park S and Park J (2010) 'Electrochemical oxidation of glucose on silver nanoparticle-modified composite electrodes', *Electrochim. Acta* **55**, 2232–2237.

Ramanavicius A, Kausaite A and Ramanaviciene A (2005) 'Polypyrrole-coated glucose oxidase nanoparticles for biosensor design', *Sens. Actuat. B* **111**, 532–539.

Rathod D, Dickinson C, Egan D and Dempsey E (2010) 'Platinum nanoparticle decoration of carbon materials with applications in non-enzymatic glucose sensing', *Sens. Actuat. B* **143**, 547–554.

Ren X L, Meng. M, Chen D, Tang F Q and Jiao J (2005) 'Using silver nanoparticle to enhance current response of biosensor', *Biosens. Bioelec*. **21**, 433–437.

Risveden K, Pontén J F, Calander N, Willander M and Danielsson B (2007) 'The region ion sensitive field effect transistor, a novel bioelectronic nanosensor', *Biosens. Bioelec*. **22**, 3105–3112.

Safavi A, Maleki N and Farjami E (2009) 'Fabrication of a glucose sensor based on a novel nanocomposite electrode', *Biosens. Bioelec*. **24,** 1655–1660.

Salimi A and Roushani M (2005) 'Non-enzymatic glucose detection free of ascorbic acid interference using nickel powder and Nafion sol–gel dispersed renewable carbon ceramic electrode', *Electrochem. Comm*. **7**, 879–887.

Sanchez-Obrero G, Cano M, Avila J L, Mayen M, Mena M L, Pingarron J M and Rodriguez-Amaro R (2009) 'A gold nanoparticle-modified PVC/TTF-TCNQ composite amperometric biosensor for glucose determination'. *J. Electroanal. Chem.* **634**, 59–63.

Santhosh P, Manesh K M, Uthayakumar S, Gopalan A I and Lee K-P (2009a) 'Hollow spherical nanostructured polydiphenylamine for direct electrochemistry and glucose biosensor', *Biosens. Bioelec*. **24**, 2008–2014.

Santhosh P, Manesh K M, Uthayakumar S, Komathi S, Gopalan A I and Lee K -P (2009b) 'Hollow spherical nanostructured polydiphenylamine for direct electrochemistry and glucose biosensor', *Bioelectrochemistry* **75**, 61–66.

Shamsipur M, Najafi M and Hosseini M R M (2010) 'Highly improved electrooxidation of glucose at a nickel(II) oxide/multi-walled carbon nanotube modified glassy carbon electrode', *Bioelectrochemistry* **77**, 120–124.

Siangprob W, Dungchai W and Chaailpakul O (2011) 'Nanoparticle-based electrochemical detection in conventional and miniaturised systems and their bioanalytical applications, A review', *Anal. Chim. Acta* **690**, 10–25.

Sun Y, Buck H and Mallouk T E (2001) 'Combinatorial discovery of alloy electrocatalysts for amperometric glucose sensors', *Anal. Chem*. **73**, 1599–1604.

R. Thusu (2010) Available at: http//www.sensorsmag.com/specialty-markets/medical/strong-growth-predicted-biosensors-market-7640, accessed 14 Feb 2012.

Tsai M C and Tsai Y C (2009) 'Adsorption of glucose oxidase at platinum-multiwalled carbon nanotube-alumina-coated silica nanocomposite for amperometric glucose biosensor', *Sens. Actuat. B* **141**, 592–598.

Tsai Y C, Ho C L and Liao S W (2009) 'Nanobiosensors prepared by electrodeposition of glucose oxidase in PMMA nanochannels produced by atomic force microscopy nanolithography', *Electrochem. Comm*. **11**, 1316–1319.

Urban G A (2009) 'Micro- and nanobiosensors – state of the art and trends', *Meas. Sci. Technol*. **20**, 012001

Vamvakaki V, Tsagaraki K and Chaniotakis N (2006) 'Carbon nanofiber-based glucose biosensor', *Anal. Chem*. **78,** 5538–5542.

Vassilyev Y B, Khazova O A and Nikolaeva N N (1985) 'Kinetics and mechanism of glucose electrooxidation on different electrode-catalysts part I. Adsorption and oxidation on platinum', *J. Electroanal. Chem*. **196**, 105–125

Wang J (2008) 'Electrochemical glucose biosensors', *Chem. Rev.* **108**, 814–825.

Wang J and Lin Y H (2008) 'Functionalized carbon nanotubes and nanofibres for biosensing applications', *Trends Anal. Chem*. **27**, 619–626.

Wang J and Musameh M (2005) 'Carbon-nanotubes doped polypyrrole glucose biosensor', *Anal. Chim. Acta* **539**, 209–213.

Wang J, Thomas D F and Chen A (2008) 'Nonenzymatic electrochemical glucose sensor based on nanoporous PtPb networks', *Anal. Chem*. **80**, 997–1004.

Wang Y, Wei W, Liu X and Zeng X (2009a) 'Carbon nanotube/chitosan/gold nanoparticles based glucose biosensor prepared by a layer-by-layer technique', *Mater. Sci. Eng. C-Biomim. Supramol. Syst*. **29**, 50–54.

Wang Z, Liu S, Wu P and Cai C (2009b) 'Detection of glucose based on direct electron transfer reaction of glucose oxidase immobilized on highly ordered polyaniline nanotubes', *Anal. Chem*. **81**, 1638–1645.

Wang X, Zhang Y, Banks C E, Chen Q and Ji X (2010a) 'Non-enzymatic amperometric glucose biosensor based on nickel hexacyanoferrate nanoparticle film modified electrodes', *Coll. Surf. B: Biointerfaces* **78**, 363–366.

Wang G F, Wei Y, Zhang W, Zhang X, Fang B and Wang L (2010b) 'Enzyme-free amperometric sensing of glucose using Cu-CuO nanowire composites', *Microchim. Acta* **168**, 87–92.

Wang X and Fan C-G (2010c) 'Synthesis of CuO nanostructures and their application for nonenzymatic glucose sensing', *Sens. Actuat*. B **144**, 220–225.

Wen Z H, Ci S Q and Li J H (2009) 'Pt nanoparticles inserting in carbon nanotube arrays: nanocomposites for glucose biosensors', *J. Phys. Chem. C* **113**, 13482–13487.

World Health Organisation (2012), Available at: www.who.org, accessed 12 Feb 2012.

Wu L, Zhang X and Ju H (2007) 'Amperometric glucose sensor based on catalytic reduction of dissolved oxygen at soluble carbon nanofiber', *Biosens. Bioelec*. **23**, 479–484.

Wu X E, Zhao F, Varcoe J R, Thumser A E, Avignone-Rossa C and Slade R C (2009) 'Direct electron transfer of glucose oxidase immobilized in an ionic

liquid reconstituted cellulose-carbon nanotube matrix', *Bioelectrochemistry* **77**, 64–68.

Xiao Y, Patolsky F, Katz E, Hainfeld J F and Willner I (2003) "Plugging into enzymes': nanowiring of redox enzymes by a gold nanoparticle', *Science* **299**, 1877–1881.

Yang L Q, Ren X L, Tang F Q and Zhang L (2009a) 'A practical glucose biosensor based on Fe_3O_4 nanoparticles and chitosan/nafion composite film', *Biosens. Bioelec*. **25**, 889–895.

Yang K, She G-W, Wang H, Ou X-M, Zhang X-H, Lee C-S and Lee S-T (2009b) 'ZnO nanotube arrays as biosensors for glucose', *J. Phys. Chem. C* **113**, 20169–20172.

Yang D S, Jung D J and Choi S H (2010) 'One-step functionalization of multi-walled carbon nanotubes by radiation-induced graft polymerization and their application as enzyme-free biosensors', *Radiat. Phys. Chem*. **79**, 434–440.

Zhang S X, Wang N, Yu H J, Niu Y M and Sun C Q (2005) 'Covalent attachment of glucose oxidase to an Au electrode modified with gold nanoparticles for use as glucose biosensor', *Bioelectrochemistry* **67**, 15–22.

Zhang Y F, Guo G, Zhao F, Mo Z, Xiao F and Zeng B (2010) 'A novel glucose biosensor based on glucose oxidase immobilized on AuPt nanoparticle – carbon nanotube – ionic liquid hybrid coated electrode', *Electroanalysis* **22**, 223–228.

Zhu L H, Zhu H Y, Yang X L, Xu L H and Li C Z (2007) 'Sensitive biosensors based on (dendrimer encapsulated pt nanoparticles)/enzyme multilayers', *Electroanalysis* **19**, 698–703.

3

Nanoparticle modified electrodes for trace metal ion analysis

J. P. METTERS and C. E. BANKS, Manchester Metropolitan University, UK

DOI: 10.1533/9780857096722.1.54

Abstract: This chapter overviews the use of metallic nanoparticle modified electrodes for the electroanalytical sensing of trace metal ions. Consideration is first given to theoretical aspects of nanoparticle modified architectures followed by an overview of progress made towards the sensing of pertinent heavy metal ions using nanoparticle constructed electrochemical sensing platforms.

Key words: heavy metals, nanoparticles, modified electrodes, sensing, electrochemistry.

3.1 Introduction

In today's current scientific arena, the use of 'nano' appears to be a prerequisite in order for the said scientific work to be published. In the field of electrochemistry this is particularly true, with the use of nanoparticles proclaiming significant improvements when applied to new fields of research. The use of bulk metals in electrochemistry is well known, such as in industrial electrolytic processes and in electroanalytical uses, as well as in energy storage/production. In certain cases, the beneficial use of nanoparticles is well documented; for example, in the case of gold, the bulk material is relatively non-reactive, whereas gold nanoparticles/crystals are reported to be highly catalytic (Hughes *et al.*, 2005; Hutchings, 2008).

In electrochemistry the nature of the electrode, that is, its size and composition, significantly influences the electrochemical performance, which can allow one to tailor the electrode surface/composition to achieve the desired electrochemical outcome. Metal nanoparticles have been reported to provide four unique advantages over macroelectrodes for electroanalysis: enhancement of mass transport, catalysis, highly effective surface area, and control over electrode microenvironment conductivity (Hernandez-Santos *et al.*, 2002; Cavicchioli *et al.*, 2004; Welch and Compton, 2006).

This chapter overviews the use of metallic nanoparticles in electrochemistry, with consideration of the fundamental changes upon electrode

reactions, before highlighting pertinent applications for the sensing of metal ions. Given that the range of nanoparticle materials is diverse, rather than consider each possible nanoparticle we consider instead pertinent target metal ion species that are '*hot topics*' for researchers.

3.2 Nanoparticle modified electrodes: basic principles

Electrode surfaces are usually modified by casting the desired nanoparticles onto the chosen electrode substrate. Provided that they are in electrical contact with the underlying electrode surface, the nanoparticles are 'electrically wired'. In this case, each nanoparticle can be considered as a nanoelectrode, such that the modified electrode surface has the electrochemical properties of the nanoparticle material rather than that of the supporting electrode substrate. Note that this is usually the desired case; for example, in the electroanalytical sensing of arsenic (III) ions, gold nanoparticle modified electrodes are utilised (see later) since gold exhibits beneficial electroanalytical properties while the underlying electrode, usually carbon, is electrochemically inert. If this were not the case, and the underlying electrode had electrochemical activity towards the analyte, there would be no real advantage in the modification of the electrode with the gold nanoparticles. An alternative to casting nanoparticles upon electrode substrates via drop-coating, which involves solutions of nanoparticles which are deposited upon the electrode surface and allowed to dry such that the solvent evaporates leaving the nanoparticles immobilised, involves the 'growing' the nanoparticles via electrodeposition. Figure 3.1 shows the case of a nanoparticle modified electrode surface, as typically used in the field by researchers.

Let us first consider the case of an isolated nanoparticle immobilised upon an electrode surface. Streeter and Compton (2007b) have considered the case of a single isolated nanoparticle using numerical simulations, the results of which are shown in Fig. 3.2.

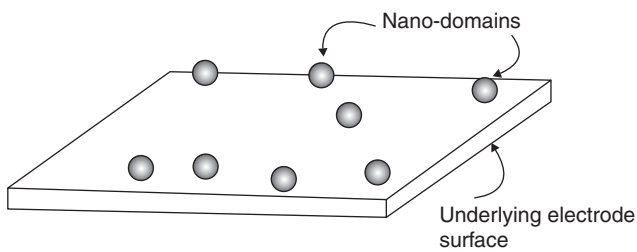

3.1 Nanoparticles immobilised on an electrode surface.

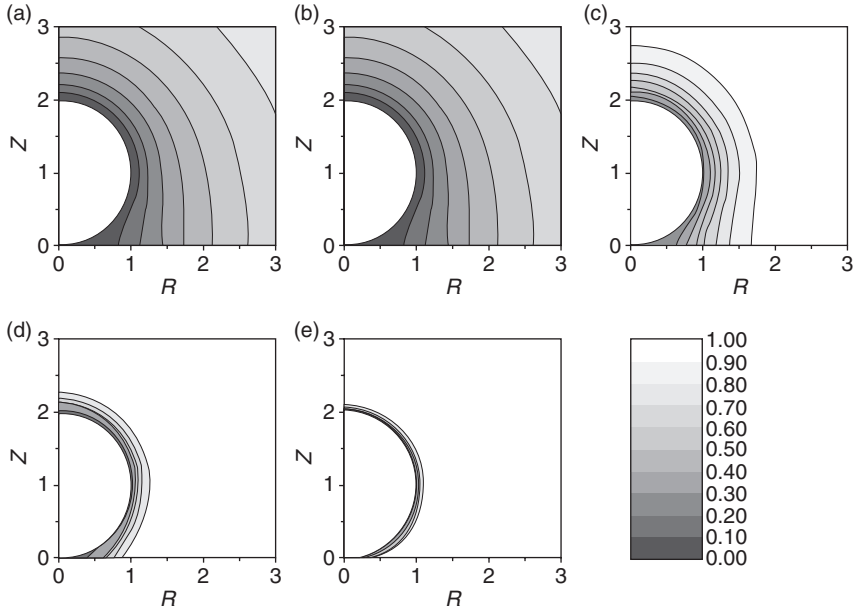

3.2 Simulated concentration profiles at the spherical particle: (a) $\sigma = 0.1$, (b) $\sigma = 1$, (c) $\sigma = 10$, (d) $\sigma = 100$, (e) $\sigma = 1000$. (*Source*: Reproduced from Streeter and Compton (2007b). Copyright 2010 The American Chemical Society.)

As electrolysis occurs, the electroactive species is consumed at the electrode surface with a depletion zone, viz. diffusion layer, formed. Figure 3.2 shows the case of a single spherical nanoparticle undergoing a simple electron transfer process ($A + ne^- \leftrightarrow B$), with the effect of the diffusion layer arising from changing the voltammetric scan rate, where the dimensionless scan rate, σ, is defined as:

$$\sigma = \left(\frac{F}{RT}\right)\left(\frac{\upsilon r_{np}^2}{D}\right) \qquad [3.1]$$

where T is the temperature, r_{np} is the radius of the nanoparticle sitting on an infinite plane, F is the Faraday constant, υ is the scan rate applied, R is the universal gas constant and D is the diffusion coefficient of the electroactive species 'A'. The corresponding voltammetric profiles are also shown in Fig. 3.3.

It is evident that a near-steady-state response is observed at a slow scan rate (Fig. 3.3a), which transitions to near planar diffusional behaviour as the experimental timescale is changed, resulting in a change of the diffusion layer thickness. In the case of a single spherical nanoparticle, the limiting current has been reported by Streeter and Compton (2007b):

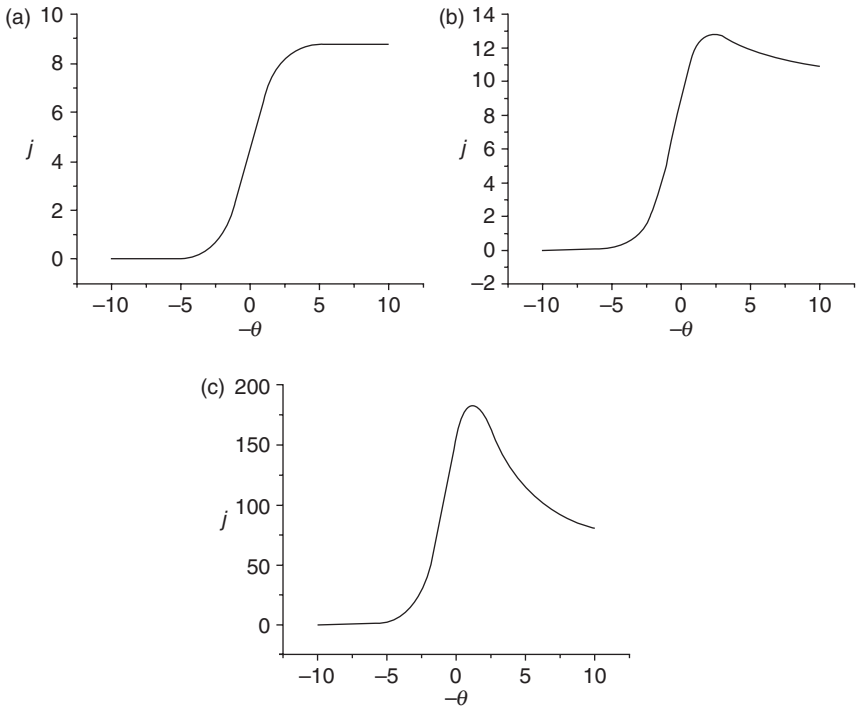

3.3 Simulated voltammetry for a reversible electrode transfer at the spherical particle. The following scan rates are used: (a) $\sigma = 10^{-3}$, (b) $\sigma = 1$, (c) $\sigma = 1000$. Note that j on the y-axis is the electrode flux ($j = -i/(nFD[A]_{bulk}r)$. (*Source*: Reproduced from Streeter and Compton (2007b). Copyright 2010 The American Chemical Society.)

$$i_{\lim} = 8.71 nFDr_{np}\left[A\right]_{bulk} \qquad [3.2]$$

where n is the number of electrons transferred in the electrochemical process. The benefit of nanoparticle modified electrodes can be realised through the consideration that, typically, one has a surface comprising many nanoparticles. In this particular case Equation [3.2] becomes:

$$i_{\lim} = 8.71 nFDr_{np}\left[A\right]_{bulk} N \qquad [3.3]$$

where N is the total number of nanoparticles comprising the modified electrode surface. Hence, as can be seen from inspection of Equation [3.3], the current is multiplied by the total number of nanoparticles, such that the extremely low levels of detection with a high analytical sensitivity should be realised. However, Equation [3.3] is only viable in the case where diffusional independence ensues.

Streeter *et al.* (2007a) have considered the case of neighbouring spherical particles which are not completely isolated from one another. Figure 3.4 shows the four diffusional categories that can arise as a result of this. In the case of Category 1, the particles are diffusionally independent and the diffusion layer thickness is much smaller than the particle radius (r_{np}). Under such conditions, diffusion to the particle surface is approximately planar in nature. In Category 1, cyclic voltammetric profiles are peak shaped, due to the diffusion layers being small and each nanoparticle thus being diffusionally independent. In Category 2, the diffusion layers are larger but still independent, with steady-state responses observed. In this regime, Equation [3.3] applies. In Category 3, diffusion layers overlap and are small in comparison to nanoparticle separation. In such cases, the cyclic voltammetric profile is

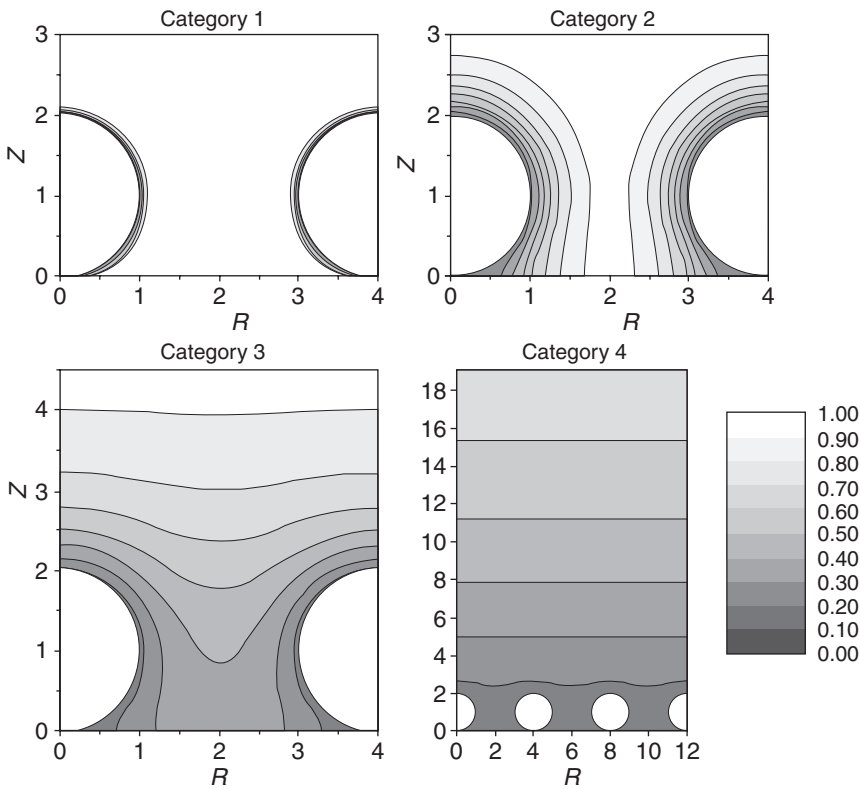

3.4 Simulated concentration profiles at a diffusion domain containing a spherical particle. Category 1: $\sigma = 1000$. Category 2: $\sigma = 10$. Category 3: $\sigma = 1$. Category 4: $\sigma = 0.01$. For all categories $R_0 = 2$. Concentration profiles were taken at the linear sweep's peak potential. (*Source*: Reproduced from Streeter *et al.* (2007a). Copyright 2010 The American Chemical Society.)

peak shaped, with the current smaller than would be derived from Equation [3.3]. Finally, in Category 4, diffusion layers heavily overlap and mass transport is linear and, as seen, the peak limit is governed by the Randles-Sevčík Equation. It has also been shown that gold nanoparticle modified electrodes can be used per se to allow mechanistic insights to be derived, such as has been shown for the case of arsenic (III) ion deposition, where the gold nanoparticles provide an alternative to expensive single crystal electrodes, which require extensive surface pretreatment (Khairy *et al.*, 2010b). Interestingly, in the case of the electrochemical reduction of hydrogen peroxide with silver nanoparticles, as the nanoparticle coverage was reduced, the electrochemical reduction of hydrogen peroxide was found to shift, demonstrating that the size of the nanoparticles dominated the observed peak potential. In the case of slow electrode kinetics, the peak potential has been shown to be dependent upon the radius of the nanoparticle (r_{np}) given by (Campbell *et al.*, 2009):

$$\frac{\partial E_P}{\partial \ln\left(r_{np}\right)} = \frac{2.3RT}{\left(n' + \alpha\right)F} \qquad [3.4]$$

where α is the transfer coefficient in the electrochemical process, and n' is the number of electrons transferred before the rate determining step. The observed dependence of E_p upon r_{np} is due to the mass transport being the rate limiting factor. In the case of a nanoparticle modified electrode, a large overpotential will be observed compared to the case of the corresponding macroelectrode. Essentially, the smaller the nanoparticle size, the greater is the observed overpotential. Additionally, it has also been shown that the electrochemical processes can quantitatively change (Rodriguez-Vazquez *et al.*, 2008; Campbell *et al.*, 2010b; Jeyabharathi *et al.*, 2010; Zhou *et al.*, 2010), such that the expected mechanism reported upon a macroelectrode quantitatively changes at a nanoparticle modified electrode; clearly, the use of nanoparticle modified electrodes can give rise to some unique and beneficial responses. Consequently, we next turn to considering the effect of the use of metallic nanoparticles to quantify heavy metal ion analytes of key interest.

3.3 Electroanalytical applications of nanoparticle modified electrodes: detection of arsenic

Arsenic sensing receives attention due to its global presence in groundwater resulting in arsenic-contaminated drinking water (Mays and Hussam, 2009). It is, however, important to note that arsenic is not just a geochemical problem; it is also widely used in industry. It is used as a doping agent

in solid state devices such as transistors (Gilbert, 2012). It is also used for manufacturing germanium-arsenide-selenide optical materials, and was previously used for short wave infrared technology. A large amount of arsenic is also used for treating wood to prevent decay or insect damage. Several compounds are used, but the vast majority of wood is treated with what is referred to as chromated copper arsenate (Gilbert, 2012). Exposure to arsenic is reported to result in hyperkeratosis, fatigue and cancer (Mays and Hussam, 2009). Because of this, WHO (WHO, 2012) has set the maximum level in drinking water to 10 $\mu g\ L^{-1}$. The total arsenic content is of interest, that is the measurement of both arsenic (III) and (V), but given that the former is more toxic for acute or short exposure times, research tends to focus on the sensing of arsenic (III). The poisoning of water with arsenic is a 'geological' problem, and contaminates drinking wells in third world countries. There is, therefore, a requirement for an extremely sensitive protocol which is economical and portable. As it is a geological problem, the level of arsenic in the drinking water can potentially vary and, as such, routine monitoring is necessary. Of all the techniques available, it appears that electrochemistry provides a real potential avenue to meet such criteria most effectively. A thorough overview of voltammetric methods is given by Mays and Hussam (2009), but here we focus only on the use of nanoparticle modified electrodes.

The sensing of arsenic (III) typically involves a gold surface, due to favourable electrode kinetics, but other metallic surfaces can be employed, such as silver (Simm *et al*., 2005a). Anodic stripping voltammetry (ASV) is usually applied to sense arsenic (III), with a substantial volume of literature reporting upon the use of macroelectrodes through to ultra-microelectrodes (Forsberg *et al*., 1975; Hamilton and Ellis, 1980; Hua *et al*., 1987; Simm *et al*., 2004; Simm *et al*., 2005b; Simm *et al*., 2005c; Dai and Compton, 2006d). The use of nanoparticle modified electrodes is also extensive, and therefore Table 3.1 summarises the most current state-of-the-art configurations. For example, gold nanoparticles deposited upon indium tin oxide film coated glass have been shown to be viable with a detection limit of 5 $\mu g\ L^{-1}$, but the supporting indium tin oxide substrate is quite fragile, which will probably limit any 'real world' applications. Other work describing gold nanoparticles supported upon glassy carbon electrodes (Dai *et al*., 2004; Hossain *et al*., 2008) has also shown detection limits below that of the pre-defined WHO limit. Notable work by Dai *et al.* (2006a, 2006b) has shown that gold nanoparticle modified glassy carbon microspheres bound together and 'wired' using multi-walled carbon nanotubes allow the sensing of arsenic (III) down to 2.5 $\mu g\ L^{-1}$; a drawback of this approach is the elaborate and time-consuming electrode preparation. The construction of the electrode is shown in Fig. 3.5, critically the gold modified glassy carbon sphere can be tailored to incorporate different metals, allowing designer,

Table 3.1 A compilation of techniques utilised for the sensing of arsenic through the incorporation of nanoparticles

Technique	Working electrode	Linear range	Limit of detection	Comments	Reference
CV, LSV, SWV	AuCNT	7.5–52.4 μg L^{-1}	0.1 μg L^{-1}		Xiao *et al.*, 2008
ASV	Au NP on GC and Au NP on BPPG	ND	GC: 0.45 μg L^{-1} BPPG: 17.26 μg L^{-1}		Dai and Compton, 2005b
LSV	Au NP on GC	ND	9.75 μg L^{-1}		Dai and Compton, 2005a
AS-SWV	Au nanoelectrode	0.2–3.0 μg L^{-1}	0.005 μg L^{-1}		Mardegan *et al.*, 2012
SW-ASV	Citrate stabilised Au NP on GC	0.05–1.0 μg L^{-1}	0.025 μg L^{-1}		Lan *et al.*, 2012
DPP	Au nanodendrite porous network	0.1–7.0 μg L^{-1}	ND		Huan *et al.*, 2011
ASV	Pt-Fe (II) NP modified CNT on GC	ND	0.75 μg L^{-1}		Shin and Hong, 2010
ASV	Au NP on a graphite screen printed electrode	18–94 μg L^{-1}	0.4 μg L^{-1}	Analysis in the presence of Cu (II) and proof-of-concept through detection in canal water samples	Khairy *et al.*, 2010a

ND: Not disclosed; ASV: Anodic stripping voltammetry; CV: Cyclic voltammetry; DPP: Differential pulse polarography; LSV: Linear sweep voltammetry; SWV: Square-wave voltammetry; NP: Nanoparticle; GC: Glassy carbon electrode; CNT: Carbon nanotube; BPPG: Basal plane pyrolytic graphite electrode.

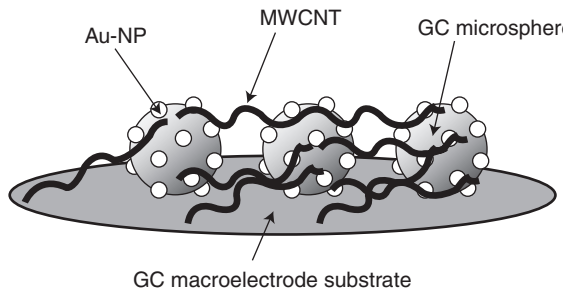

3.5 A schematic showing the construction of the Au-NP-GC microspheres deposited as a film onto the surface of a glassy carbon macroelectrode, where the film is stabilised and wired together using multi-walled carbon nanotubes (MWCNTs). (*Source*: Reproduced from Dai *et al.* (2006a). Copyright 2006 The American Chemical Society.)

task specific, electrode interfaces to be realised (Dai *et al.*, 2006b). In their work, Dai *et al.* (2006a) demonstrate, as shown in Fig. 3.6, that this novel architecture allows the nanoparticles to behave *like* an equivalent gold microdisc, since each gold nanoparticle acts as an individual nanoelectrode which is fabricated such that heavy diffusional overlap occurs between neighbouring nanoparticles, resulting in the electrode behaving in the manner of Category 4 (as discussed earlier). As such, the diffusional regime of the nanoparticle architecture exhibits planar diffusion equivalent to a microdisc comprising the same metallic composition; only 1% of the required gold macroelectrode is being used to give useful voltammetric responses and clearly the cost implications are evident. In other work, carbon nanotubes have been demonstrated to be useful as electrode supports for metallic nanoparticles and applied to the sensing of arsenic (III) in model solutions (Xiao *et al.*, 2008).

Finally, the real, beneficial use of nanoparticle modified electrodes has been reported by Dai and co-workers (Dai and Compton, 2005b). In the case of real samples, copper (II) ions pose a great problem and limit many potential electroanalytical applications. Figure 3.7 shows ASV profiles, in 1 M HCl, when 30 mM copper (II) was present alone (Fig. 3.7a), where the peak at ~ + 0.37 V (vs SCE) corresponds to the underpotential dissolution of copper (Bonfil *et al.*, 1999). Following the additions of arsenic (III), three peaks are observed (Fig. 3.7a). The peak at ~ + 0.12 V (vs SCE) is the stripping peak of arsenic (III) from arsenic metal while the curves at + 0.25 V to + 0.45 V (vs SCE) show two maxima corresponding to two peaks overlapping. The peak at ~ + 0.37 V (vs SCE) is observed when only copper (II) is present in the solution, while the other at ~ + 0.27 V (vs SCE) is due to the intermetallic species of arsenic and copper (Cu_3As_2). The stripping peak of pure copper in 1 M HNO_3 (Fig. 3.7b) was observed to occur

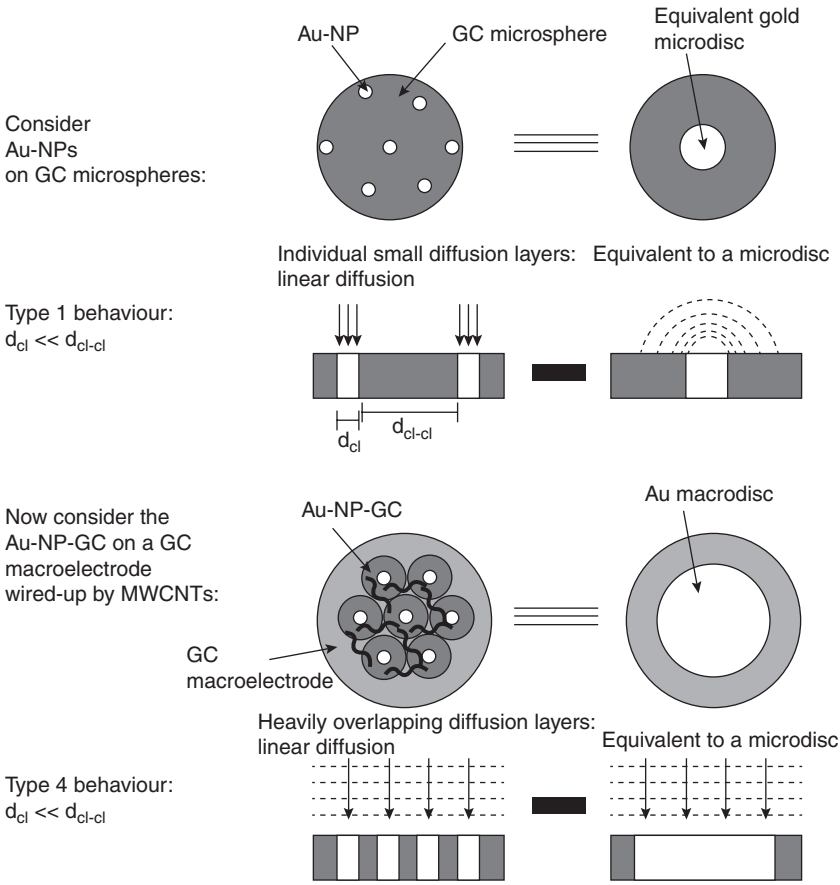

3.6 Schematic illustration of how intelligent chemical architectural design can take advantage of the synergy between Type 1 and Type 4 behaviour at nano- and microelectrode arrays to produce macroelectrode behaviour while using a fraction of the electrode material required. (*Source*: Reproduced from Dai *et al.* (2006a). Copyright 2006 The American Chemical Society.)

at more negative potentials than in 1 M HCl as shown in Fig. 3.7. A similar observation relates to the stripping peak of Cu_3As_2. When arsenic (III) and copper (II) were both in the solution, only two peaks were seen if HNO_3 was used as the electrolyte; one was the stripping peak of arsenic (III) at ~ + 0.15 V (vs SCE) and the other one at ~ + 0.30 V (vs SCE) arose from the copper (II) species and was also hidden under the voltammetric profile, the response arising from the intermetallic species. In comparing the curves in 1 M HCl and in 1 M HNO_3, the arsenic stripping feature is further separated from the possible interfering peaks observed in 1 M HCl (Dai and Compton, 2005b). Clearly, the presence of copper (II) can detrimentally

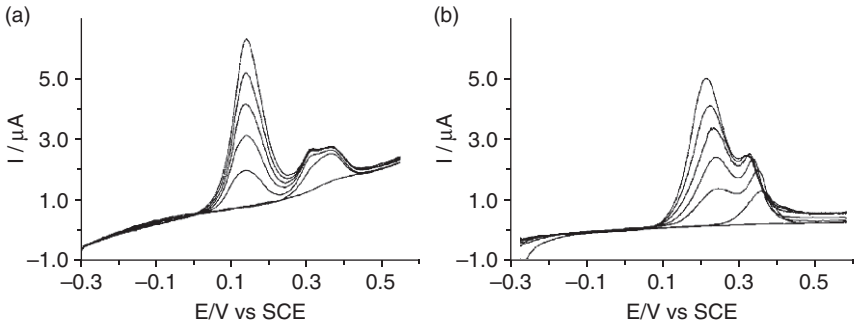

3.7 LSV curves of As (III) additions (10 μM each) to 30 mM Cu (II) on a macro gold electrode in different electrolyte: 1 M HCl (a) and 1 M HNO_3 (b). LSV parameters: predeposition at + 0.3 V (vs saturated calomel electrode, SCE) for 60 s, potential scan rate 100 mV s^{-1}. (*Source*: Reproduced from Dai and Compton (2005b) with permission from Wiley.)

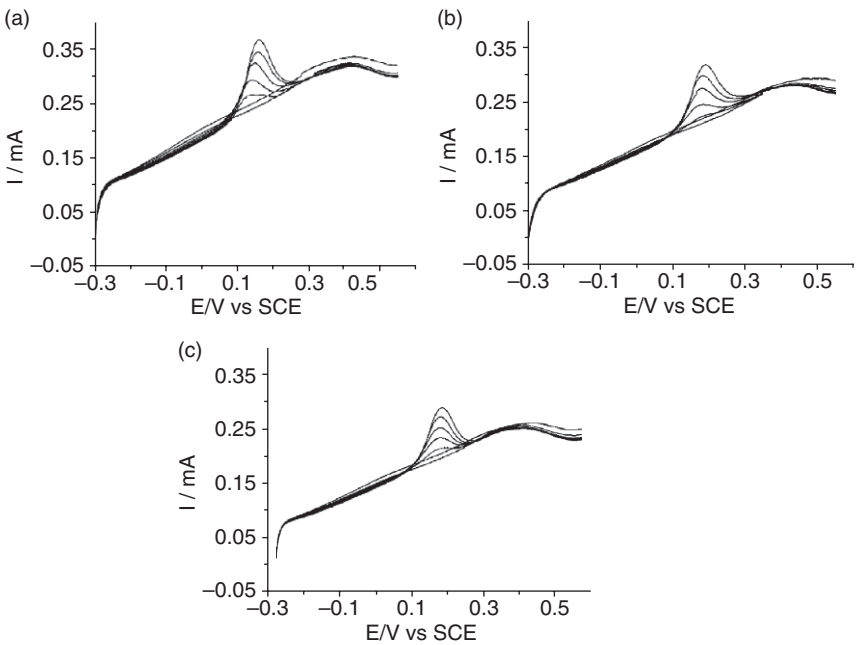

3.8 LSV response of arsenic (III) additions to 1 M HCl containing copper (II) on a gold nanoparticle modified basal plane pyrolytic electrode. From (a) to (c), copper (II) concentrations are 2 μM, 5 μM and 10 μM respectively. The arsenic (III) addition was 5 mM each. (*Source*: Reproduced from Dai and Compton (2005b) with permission from Wiley.)

affect the sensing of arsenic (III), which is why researchers do not report real sample analysis in their papers! The response of the nanoparticle modified electrode is shown in Fig. 3.8, where no effect from copper is evident over the concentration ranges studied, clearly highlighting the benefit of using such a nanoparticle modified electrode.

In a fixed copper (II) solution (2 μM), a limit of detection of 1.18 μg L^{-1} was reported to be achievable. Clearly, the change in mass transport, and/or the differing electrode kinetics of the arsenic (III) and copper (II), potentially allow sensing in real water samples using gold nanoparticle modified electrodes (Dai and Compton, 2005b).

Another exciting approach is to use the direct electrochemical oxidation of arsenic (III) to (V). Dai and Compton were the first to demonstrate that this is a viable approach using platinum nanoparticle modified glassy carbon electrodes. A limit of detection of 2.1 μg L^{-1} was shown to be achievable, which is substantially below the 10 μg L^{-1} set by the WHO (Dai and Compton, 2006c). Critically, it is also key to note that the method did not suffer from the presence of copper (II) ions.

3.4 Electroanalytical applications of nanoparticle modified electrodes: detection of chromium

A further heavy metal ion of great interest is chromium (VI) (Welch *et al.*, 2004; Bielicka *et al.*, 2005). The chromium (VI) species poses a great environmental threat, being around 100–1000 times more toxic than chromium (III) (Crespon-Romero *et al.*, 1996). This increased hazardous status is attributed to the high oxidation potential and, as a result, the World Health Organisation (WHO) recommends chromium (VI) to be limited to 50 μg L^{-1} within groundwater (WHO, 1993). Due to the previously discussed imposed restrictions relating to chromium (VI) levels within water, areas of industry such as plating, cooling towers, timber treatment, leather tanning, wood preservation and steel manufacturing require sensitive and reliable techniques to monitor anthropogenic chromium pollution in ground water (Golub and Oren, 1989; Kieber *et al.*, 2002). In addition to chromium (VI), a second chromium species of key interest exists: chromium (III). Although chromium (III) poses no significant threat, being relatively harmless, it maintains an important biological role (Vincent, 2003) and as such the monitoring of this species is still of significant interest.

Liu *et al.* have reported the use of gold nanoparticle modified electrodes for the sensing of chromium (VI), with a limit of detection of 5 μg L^{-1}, with the technique also being demonstrated to be useful for the sensing of chromium (VI) within water samples (Liu *et al.*, 2007). The recovery of

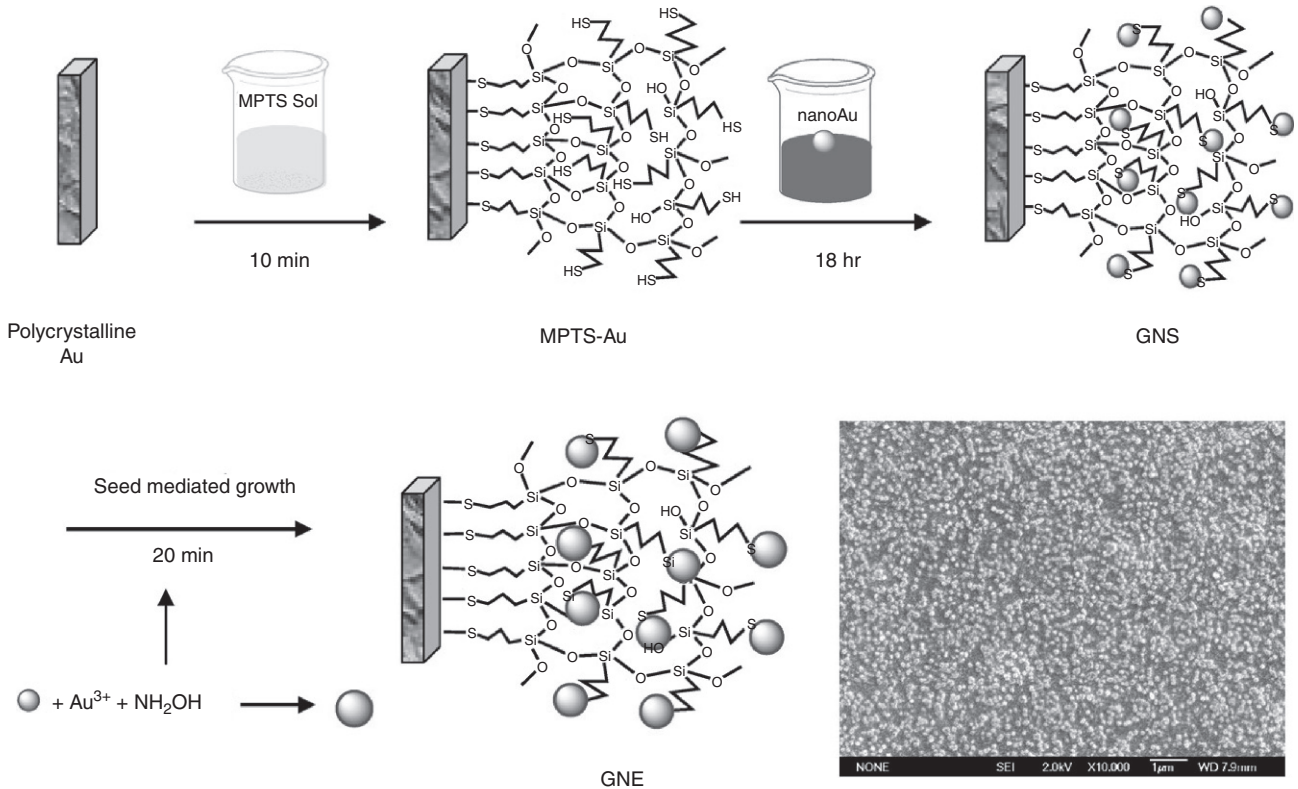

3.9 A scheme illustrating the preparation of the gold nanoelectrode ensemble and the Field Emission Scanning Electron Microscopy image of the gold nanoelectrode on the silicate network. (*Source*: Reproduced from Jena and Raj (2008) with permission from Elsevier.)

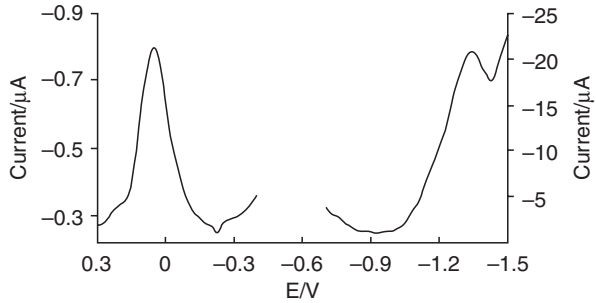

3.10 Differential pulse voltammograms for the simultaneous determination of chromium (III) and chromium (VI) using a mercury film modified screen printed electrode (right side) and a gold nanoparticle modified screen printed electrode (left side). Acetic-acetate pH 4, [chromium (III)] = 7.3×10^{-4} M, [chromium (VI)] = 1.8×10^{-5} M. (*Source*: Reproduced from Calvo-Perez *et al.* (2010) with permission from Wiley.)

chromium (VI) from river water samples is shown to be highly reliable and in excellent agreement with independent ICP-MS studies demonstrating the reliable and robust nature of the nanoparticle sensor reported by Liu *et al*. (2007).

The trend of using gold nanoparticles has been followed by Jena and Raj (2008), who demonstrated sub-ppb sensing of chromium (VI) utilising an electrode fabricated as shown in Fig. 3.9. Their method was validated using a certified reference material. The electrode was shown to be highly stable, and can be used for repeated measurements. The nanoparticles on the silicate network behave as an ensemble of gold nanoelectrodes. The ultra-sensitivity of the electrode towards chromium (VI) is ascribed to (i) enhanced mass transport to the electrode, (ii) high catalytic activity of the nanoparticles, and (iii) the large surface area of the nanoparticles on the electrode surface (Jena and Raj, 2008).

Other work has reported indium tin oxide electrodes modified with gold nanoparticles (Tsai and Chen, 2008), in addition to flower-like gold nanoparticles (Ouyang *et al*., 2012), and gold nanoparticles (Liu *et al*., 2008) on glassy carbon electrodes. However, the limitations of these studies are the underlying electrode, and the use of alternative electrode fabrication techniques such as screen printing can overcome this limitation and, provide an economical electrode substrate which can be used and disposed of following a single measurement, the cost-effective nature of such sensors off-setting any potential memory effects (Metters and Kadara, 2012).

To this end, Dominguez-Renedo *et al.* (2008) have used silver and gold nanoparticles immobilised upon screen printed electrodes via electrochemical deposition, reporting detection limits of 63.8 and 30.0 μg L^{-1} chromium (VI) with silver and gold nanoparticle modified electrodes, respectively. This

Table 3.2 A compilation of techniques utilised for the sensing of chromium (VI) through the incorporation of nanoparticles

Technique	Working electrode	Linear range	Limit of detection	Reference
DPV	Au NP on screen printed electrode	ND	20.85 μg L^{-1}	Dominguez-Renedo *et al.*, 2008
DPV	Ag NP on screen printed electrode	ND	44.28 μg L^{-1}	Dominguez-Renedo *et al.*, 2008
CV	Au NP on indium tin oxide	0.26–5.2 mg L^{-1}	0.10 mg L^{-1}	Tsai and Chen, 2008
SWV	Au NP on screen printed electrode	1.56–855 μg L^{-1}	0.78 μg L^{-1}	Liu *et al.*, 2007
DPV	Bi NP on GC	50–300 ng L^{-1}	0.12 ng L^{-1}	Saturno *et al.*, 2011
Chronoamperometry	Au NP on Au	0.2–3 μg L^{-1}	0.1 μg L^{-1}	Jena and Raj, 2008

ND: Not disclosed; CV: Cyclic voltammetry; DPV: Differential pulse voltammetry; SWV: Square-wave voltammetry; NP: Nanoparticle; GC: Glassy carbon electrode.

application of silver and gold nanoparticles has been thoroughly studied, with Xing *et al.* (2011) reporting the possibility of a silver nanoparticle/Nafion composite with a limit of detection of 0.67 μg L^{-1}, shown to be visible in real water samples. Clearly, the use of nanoparticles other than gold can be beneficially utilised in the sensing of chromium (VI).

Finally, of note is the work by Calvo-Perez and co-workers (Calvo-Perez *et al.*, 2010) who have reported the sensing of total chromium, that is, chromium (III) and chromium (VI), *via* differential pulse voltammetry at a mercury film modified screen printed electrode, and additionally at a gold nanoparticle modified carbon screen printed electrode array.

Figure 3.10 shows the voltammograms for the sensing of both chromium (III) and (VI) where limits of detections of 9.9 and 0.25 μg L^{-1} respectively were found to be viable. The application of the sensor to real samples obtained from a tannery factory is also reported and compared with ICP-MS, demonstrating that the proposed electrochemical configuration provided results in excellent agreement with those obtained via ICP-MS (Calvo-Perez *et al.*, 2010). Further applications of nanoparticle modified electrodes to the sensing of chromium (VI) are detailed in Table 3.2.

3.5 Electroanalytical applications of nanoparticle modified electrodes: detection of lead (II) and cadmium (II)

Two analytes of real interest, due to their toxicity, are the heavy metals lead and cadmium (Pohl *et al*., 2006; Toghill *et al*., 2008). With the continued and expansive use of both lead and cadmium within industrial applications and society as a whole, there is an ever increasing quantity of metal ions being released into the environment. Accurate quantification of the concentrations of these metal ions, within both environmental samples such as ground waters and clinical and industrial samples is of real necessity (Prado *et al*., 2002; Kefala *et al*., 2003; Demetriades *et al*., 2004; Kruusma *et al*., 2004; Manivannan *et al*., 2004; Economou, 2005; Hocevar *et al*., 2005; McGaw and Swain, 2006; Pohl *et al*., 2006; Kachoosangi *et al*., 2007; Cao *et al*., 2008). The two analytes are commonly studied in unison, as typically in real samples they co-exist. Table 3.3 highlights a non-exhaustive listing of some of the prevalent and key applications of nanoparticle-based electrodes utilised for the sensing of lead and cadmium.

Toghill and co-workers have reported the simultaneous electroanalytical determination of lead (II) and cadmium (II) utilising square-wave anodic stripping voltammetry (SW-ASV), using a random nanoparticle array bismuth modified boron-doped diamond electrode (Toghill *et al*., 2008). The bismuth nanoparticle modified electrode substrate was fabricated through utilisation of *in situ* electrodeposition. It was reported that detection limits of 1.9 μg L^{-1} and 2.3 μg L^{-1} for lead (II) and cadmium (II) were achieved, respectively. Comparisons between the performance of the nanoparticle modified electrode and a bulk bismuth macroelectrode determined that the bismuth nanoparticle electrode exhibited a more beneficial analytical response than the bulk electrode, indicating the benefits of a nanoparticle array as opposed to a polycrystalline bulk surface (Toghill *et al*., 2008).

Further detailed studies by Toghill *et al.* (2009) focused upon the application of antimony nanoparticles for the sensing of cadmium (II) and lead (II). Once again, a boron-doped diamond electrode was selected as the underlying electrode substrate, which was consequently modified with antimony nanoparticles being deposited *in situ* from a solution of 1 mg L^{-1} $SbCl_3$ in 0.1 M HCl (pH 1). It was found that simultaneous detection of the two analytes was not viable using the bare, unmodified boron-doped diamond electrode, whereas the modification of the same electrode material with antimony nanoparticles allowed for readily discernible and quantifiable measurement of the two analytes over the linear range 50–500 μg L^{-1} (Toghill *et al*., 2009).

Development of the study of nanoparticle utilisation for the monitoring of the two key metal ions was continued by the same research group using

Table 3.3 A compilation of techniques utilised for the sensing of lead (II) and cadmium (II) through the incorporation of nanoparticles

Technique	Working electrode	Linear range	Limit of detection	Comments	Reference
DPV	Bi NP on GC	Lead: 60–400 μg L^{-1} Cadmium: 60–400 μg L^{-1}	Lead: 18 μg L^{-1} Cadmium: 11 μg L^{-1}		Saturno *et al.*, 2011
ASV	Polymeric film of dipicolinic acid onto Au NP-cysteine-Au electrode	Cadmium: 0.0022–2.815 mg L^{-1}	Cadmium: 1.69 μgL^{-1}	Simultaneous detection with zinc	Gholivand *et al.*, 2011
ASV	Graphite NP screen printed electrode	Lead: 5–100 μg L^{-1} Cadmium: 5–100 μg L^{-1}	Lead: < 7 μg L^{-1} Cadmium: < 7 μg L^{-1}	Time-effect studies in sea water carried out	Aragay *et al.*, 2011
ASV	Sb NP on BDD electrode	Lead: 50–500 μg L^{-1} Cadmium: 50–500 μg L^{-1}	Lead: 25.4 μg L^{-1} Cadmium: 38.1 μg L^{-1}		Toghill *et al.*, 2009
SW-ASV	Bi NP on BDD electrode	Lead: 20–200 μg L^{-1} Cadmium: 20–200 μg L^{-1}	Lead: 1.9 μg L^{-1} Cadmium: 2.3 μg L^{-1}		Toghill *et al.*, 2008
SWV	L-Aspartic acid/L-cysteine/Au NP on a gold microelectrode	Lead: 5–2000 μg L^{-1}	Lead: 1.0 μg L^{-1}		Wang *et al.*, 2012

ASV: Anodic stripping voltammetry; DPV: Differential pulse voltammetry; SWV: Square-wave voltammetry; NP: Nanoparticle; GC: Glassy carbon electrode; BDD: Boron-doped diamond electrode.

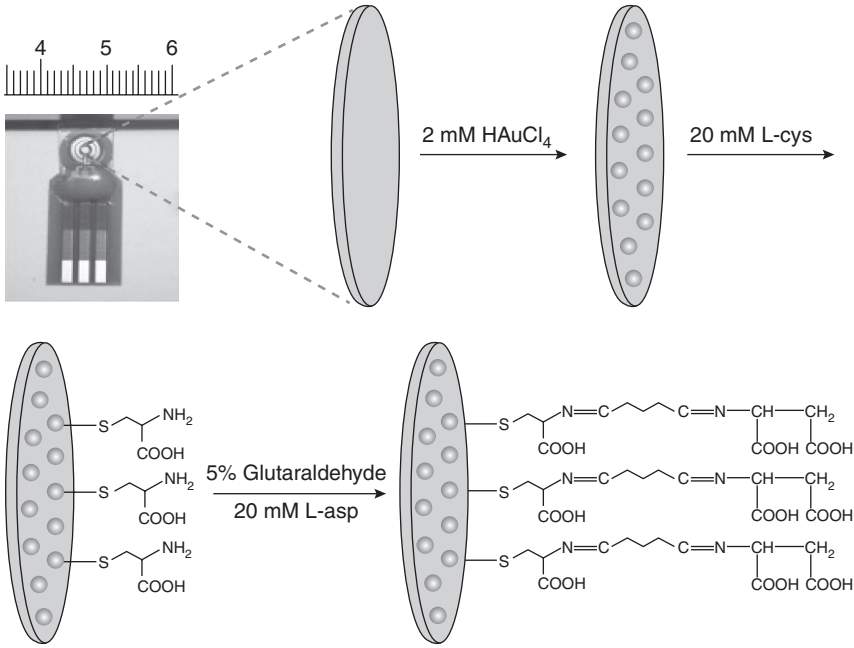

3.11 A schematic illustration of preparation of modified microelectrode. (*Source*: Reproduced from Wang *et al.* (2012) with permission from Elsevier.)

a silver nanoparticle modified electrode (Campbell and Compton, 2010a). Underpotential deposition of lead and cadmium was observed at macro- and nanoparticle silver electrodes with diameter greater than ~50 nm; however, the same behaviour was absent for nanoparticles with a diameter below ~50 nm. Investigation of the electrochemical deposition of the heavy metals lead and cadmium on silver nanoparticles indicated that a minimum diameter of ~50 nm is required in order to clearly observe the underpotential deposition and corresponding stripping processes for both deposits; both lead and cadmium deposition where the array was composed of small silver nanoparticles (less than ~50 nm) did not exhibit such behaviour. The group interpreted this to suggest that this is a general behaviour with underpotential deposition of heavy metals on silver nanomaterials; in particular, the change of surface structure and/or work function at the nanoscale qualitatively alters the observed electrochemistry, and a similar situation has previously been reported for the underpotential deposition of thallium on large and small silver nanoparticles (Campbell and Compton, 2010a).

Nanostructured bismuth film electrodes applied to the monitoring of lead (II) and cadmium (II) have also been described by Saturno *et al.* (2011) The bismuth nanoparticles were electrodeposited on a hydrated aluminium oxide template, which was previously coated upon a glassy carbon electrode surface.

Scanning electron microscopy revealed the resultant surface, after soaking in 0.1 M NaOH, to be particulate in appearance. The analysis of aqueous solutions of cadmium and lead determined that the bismuth nanoparticle modified electrodes enabled improved limits of detection and sensitivity over conventional bismuth film modified glassy carbon electrodes (Saturno *et al.*, 2011).

One interesting report describes the modification of microelectrodes using gold nanoparticles for the monitoring of lead (II) and cadmium (II) (Wang *et al.*, 2012). The microelectrode was fabricated as depicted in Fig. 3.11, whereby gold nanoparticles were first deposited on the electrode surface via electrodeposition. Next, the L-cysteine layer was assembled on the gold nanoparticle surface by immersing the microelectrode in an aqueous solution of L-cysteine in the absence of light. Following this, the microelectrode was immersed in glutaraldehyde and then, finally, L-aspartic.

The electrochemical microsensor modified L-aspartic acid/L-cysteine and gold nanoparticles was used as the selective ligand for metal ions, and exhibited an excellent linear range from 5 μg L^{-1} to 2000 μg L^{-1} with a detection limit of 1 μg L^{-1}, offering a simple and sensitive measurement of the two analytes, and it could be used for electrochemical analysis of copper (II) and lead (II) (Wang *et al.*, 2012).

Finally, screen printed sensors modified with carbon nanoparticles have been reported for the monitoring of various heavy metals, including cadmium (II) and lead (II) (Aragay *et al.*, 2011). Both lead (II) and cadmium (II) were monitored using the sensors over the range of 5–100 μg L^{-1}. The size of the graphite nanoparticles was found to range from 25 to 60 nm with some individual particles larger than 60 nm found in the ink matrix (average particle size of 38 nm with a RSD of 17%). By using this ink, the resulting electrode was expected to have a homogeneous and nanostructured surface area, enabling improved reproducibility between the disposable sensors. Critically, the robust nature of the economical screen oriented sensor has been demonstrated through long-term stability studies in sea water at a set concentration of lead (II) (Aragay *et al.*, 2011).

3.6 Electroanalytical applications of nanoparticle modified electrodes: detection of antimony

Antimony is a toxic heavy metal, and its prevalence is due to industrial applications (Toghill and Compton, 2011). At high dosages, symptoms are similar to those observed for arsenic poisoning, and it has been linked to autism and sudden infant death syndrome (SIDS). The trivalent species is reported to be more toxic than the pentavalent species, though the total antimony concentration is required to be monitored. Consequently, the maximum acceptable level of antimony in drinking water is reported to be 5 μg L^{-1} in the EU (Council of the European Union, 1998) and 20 μg L^{-1} in other continents

(WHO, 2003). In recent years, antimony has also become a focus of concern and research in relation to the toxic gas hypothesis (i.e. SbH_3 production by fungi) for SIDS (Thompson and Faull, 1995; Department of Health, 1998; Craig *et al*., 2001).

An authoritative review by Toghill and Compton (2011) provides a thorough overview of the electroanalytical methods used for the sensing of antimony, showing that mercury, gold and carbon are viable electrode materials. However, it is highly surprising to note that there are very limited reports of nanoparticle modified electrodes (Dominguez-Renedo and Arcos-Martinez, 2007a, 2007b; Toghill and Compton, 2011). Gold (Dominguez-Renedo and Arcos-Martinez, 2007a), and silver (Dominguez-Renedo and Arcos-Martinez, 2007b) nanoparticle modified screen printed sensors have been reported by Dominguez-Renedo and Arcos-Martinez for the sensing of antimony (III), providing detection limits of 0.08 and 0.11 μg L^{-1} at the gold and silver surfaces, respectively.

In addition, sensing of antimony (V) using electrochemical techniques is an under-explored area. Existing studies in the literature show that antimony (V) sensing is achievable using mercury, gold and various modified electrodes; Lu *et al*. (2012) give a thorough overview. Surprisingly, it has only been shown that the sensing of antimony (V) is a viable approach using unmodified edge plane pyrolytic graphite electrodes exhibiting a detection limit of 0.71 μg L^{-1} (Lu *et al*., 2012). Clearly, this analyte is ripe for exploration using nanoparticle modified electrodes.

3.7 Conclusion

We have seen in this chapter that nanoparticle modified electrodes have been reported to provide some extremely significant analytical outputs. However, what is surprising is that nanoparticle modified electrodes have still to really fulfil their potential, and generally micron-sized particle modified electrodes are more commonly reported and utilised due to the ease of fabrication. The benefit of nanoparticle modified electrodes appears to be that a sprinkling of nanoparticles can recreate the electrochemical performance of a macroelectrode comprising the same electrode material, but at a fraction of the cost.

If the nanoparticle modified electrode is designed/fabricated more intelligently, such that sufficient spacing occurs between neighbouring nanoparticles, significant analytical improvements will be realised, due to enhancements in mass transport (see Introduction) arising from the nanoparticle structure. The use of nanoparticle modified electrodes has the potential to allow the sensing of analytes at very low levels, and we expect this area of research to continue to grow with a plethora of potential avenues for further exploration.

3.8 Sources of further information and advice

For background information regarding nanoparticles fabrication and characterisation see:

Gerbec J. A., D. Magana, A. Washington and G. F. Strouse (2005) Microwave-enhanced reaction rates for nanoparticle synthesis, *J. Am. Chem. Soc*., **127**, 15791.

Grzelczak M., J. Perez-Juste, P. Mulvaney and L. M. Liz-Marza´n (2008) Shape control in gold nanoparticle synthesis, *Chem. Soc. Rev*., **37**, 1783.

Kimling J., M. Maier, B. Okenve, V. Kotaidis, H. Ballot and A. Plech (2006) Turkevich method for gold nanoparticle synthesis revisited, *J. Phys. Chem. B*, **110**, 15700.

For background information regarding the toxicity of heavy metals see:

European Environment Agency, http://www.eea.europa.eu/ (Accessed November 2012).

Gilbert G. (2012) *A Small Dose of Toxicology: The Health Effects of Common Chemicals*, 2nd Edn., Healthy World Press.

The World Health Organisation, http://www.who.int/en/ (Accessed November 2012).

US Environmental Protection Agency, http://www.epa.gov/ (Accessed November 2012).

For background information upon electrochemical characterisation see:

Compton R. G. and C. E. Banks (2010) *Understanding Voltammetry*, 2nd Edn., Imperial College.

Wang J. (2006) *Analytical Electrochemistry*, 3rd Edn., Wiley.

Other background material of use is as follows:

Campbell F. W. and R. G. Compton (2010) The use of nanoparticles in electroanalysis: An updated review, *Anal. Bioanal. Chem*., **396**, 241.

Murray R. W. (2008) Nanoelectrochemistry: Metal nanoparticles, nanoelectrodes and nanopores, *Chem. Rev*., **108**, 2688.

Oyama M. (2010) Recent nanoarchitectures in metal nanoparticle-modified electrodes for electroanalysis, *Anal. Sci*., **26**, 1.

3.9 References

Aragay G., J. Pons and A. Merkoci (2011) Enhanced electrochemical detection of heavy metals at heated graphite nanoparticle-based screen-printed electrodes. *J. Mater. Chem.,* **21**, 4326.

Bielicka A., I. Bojanowska and A. Wisniewski (2005) Two faces of chromium – Pollutant and bioelement. *Pol. J. Environ. Stud.,* **14**, 5.

Bonfil Y., M. Brand and E. Kirowa-Eisner (1999) Determination of sub-μg l−1 concentrations of copper by anodic stripping voltammetry at the gold electrode. *Anal. Chim. Acta,* **387**, 85.

Calvo-Perez A., O. Dominguez-Renedo, M. A. Alonso-Lomillo and M. J. Arcos-Martinez (2010) Simultaneous determination of Cr(III) and Cr(VI) by differential pulse voltammetry using modified screen-printed carbon electrodes in array mode. *Electroanalysis,* **22**, 2924.

Campbell F. W. and R. G. Compton (2010a) Contrasting underpotential depositions of lead and cadmium on silver macroelectrodes and silver nanoparticle electrode arrays. *Int. J. Electrochem. Sci.,* **5**, 407.

Campbell F. W., S. R. Belding, L. Xiao and R. G. Compton (2010b) A changed electrode reaction mechanism between the nano- and macroscales. *ChemPhysChem,* **11**, 2820.

Campbell F. W., S. R. Belding, R. Baron, L. Xiao and R. G. Compton (2009) Hydrogen peroxide electroreduction at a silver-nanoparticle array: Investigating nanoparticle size and coverage effects. *J. Phys. Chem. C,* **113**, 9053.

Cao L., J. Jia and Z. Wang (2008) Facile synthesis of nearly monodispersed copper sulfide nanocrystals. *Electrochim. Acta,* **53**, 217.

Cavicchioli A., M. A. Scalea and R. G. R. Gutz (2004) Analysis and speciation of traces of arsenic in environmental, food and industrial samples by voltammetry: A review. *Electroanalysis,* **16,** 697.

Council of the European Union (1998) The quality of water intended for human consumption. Council Directive 98/83/EC.

Craig P. J., T. Sergeeva and R. O. Jenkins (2001) Determination of inorganic Sb(V) and methylantimony species by HPLC with hydride generation-atomic fluorescence spectrometric detection. *Mikrochim. Acta,* **137**, 221.

Crespon-Romero R. M., M. C. Yebra-Biurrun and M. P. Bermejo-Barrera (1996) Preconcentration and speciation of chromium by the determination of total chromium and chromium(III) in natural waters by flame atomic absorption spectrometry with a chelating ion-exchange flow injection system. *Anal. Chim. Acta,* **327**, 37.

Dai X., G. G. Wildgoose, C. Salter, A. Crossley and R. G. Compton (2006a) Electroanalysis using macro-, micro-, and nanochemical architectures on electrode surfaces. Bulk surface modification of glassy carbon microspheres with gold nanoparticles and their electrical wiring using carbon nanotubes. *Anal. Chem.,* **78**, 6102.

Dai X., G. G. Wildgoose and R. G. Compton (2006b) Designer electrode interfaces simultaneously comprising three different metal nanoparticle (Au, Ag, Pd)/carbon microsphere/carbon nanotube composites: progress towards combinatorial electrochemistry. *Analyst,* **131**, 1241.

Dai X., M. E. Hyde and R. G. Compton (2004) Anodic stripping voltammetry of arsenic(III) using gold nanoparticle-modified electrodes. *Anal. Chem.,* **76**, 5924.

Dai X. and R. G. Compton (2005a) Determination of copper in the presence of various amounts of arsenic with L-Cysteine modified gold electrodes. *Electroanalysis,* **17**, 1835.

Dai X. and R. G. Compton (2005b) Gold nanoparticle modified electrodes show a reduced interference by Cu(II) in the detection of As(III) using anodic stripping voltammetry. *Electroanalysis,* **17**, 1325.

Dai X. and R. G. Compton (2006c) Detection of As(III) via oxidation to As(V) using platinum nanoparticle modified glassy carbon electrodes: arsenic detection without interference from copper. *Analyst,* **131**, 516.

Dai X. and R. G. Compton (2006d) Direct electrodeposition of gold nanoparticles onto indium tin oxide film coated glass: Application to the detection of arsenic(III). *Anal. Sci.,* **22**, 567.

Demetriades D., A. Economou and A. Voulgaropoulos (2004) A study of pencil-lead bismuth-film electrodes for the determination of trace metals by anodic stripping voltammetry. *Anal. Chim. Acta,* **519**, 167.

Department of Health (1998) Expert group to investigate cot death theories: Toxic gas hypothesis: Final report. In: L. S. Limerick (ed.), *Chair*, HMSO, London.

Dominguez-Renedo O. and M. J. Arcos-Martinez (2007a) Anodic stripping voltammetry of antimony using gold nanoparticle-modified carbon screen-printed electrodes. *Anal. Chim. Acta,* **589**, 255.

Dominguez-Renedo O. and M. J. Arcos-Martinez (2007b) A novel method for the anodic stripping voltammetry determination of Sb(III) using silver nanoparticle-modified screen-printed electrodes. *Electrochem. Commun.,* **9**, 820.

Dominguez-Renedo O., L. Quiz-Espelt, N. Garcia-Astorgano and M. J. Arcos-Martinez (2008) Electrochemical determination of chromium(VI) using metallic nanoparticle-modified carbon screen-printed electrodes. *Talanta,* **76**, 854.

Economou A. (2005) Bismuth-film electrodes: recent developments and potentialities for electroanalysis. *Trends Anal. Chem.,* **24**, 334.

Forsberg G., J. W. O'laughlin and R. G. Megargle (1975) Determination of arsenic by anodic stripping voltammetry and differential pulse anodic stripping voltammetry. *Anal. Chem.,* **47**, 1586.

Gholivand M. B., A. Azadbakht and A. Pashabadi (2011) Simultaneous determination of trace zinc and cadmium by anodic stripping voltammetry using a polymeric film nanoparticle self-assembled electrode. *Electroanalysis,* **23**, 364.

Gilbert S. G. (2012) A small dose of toxicology: The health effects of common chemicals. Second Ed., Healthy World Press.

Golub D. and Y. Oren (1989) Removal of chromium from aqueous solutions by treatment with porous carbon electrodes: Electrochemical principles. *J. Appl. Electrochem.,* **19**, 3115.

Hamilton T. W. and J. Ellis (1980) Determination of arsenic and antimony in electrolytic copper by anodic stripping voltammetry at a gold film electrode. *Anal. Chim. Acta,* **119**, 225.

Hernandez-Santos D., M. B. Gonzalez-Garcia and A. C. Garcia (2002) Metal-nanoparticles based electroanalysis. *Electroanalysis,* **14**, 1225.

Hocevar S. B., I. Svancara, K. Vytras and B. Ogorevc (2005) Novel electrode for electrochemical stripping analysis based on carbon paste modified with bismuth powder. *Electrochim. Acta,* **51**, 706.

Hossain M., M. Islam, S. Ferdousi, T. Okajima and T. Oshaka (2008) Anodic stripping voltammetric detection of arsenic(III) at gold nanoparticle-modified glassy carbon electrodes prepared by electrodeposition in the presence of various additives. *Electroanalysis,* **20**, 2435.

Hua C., D. Jagner and L. Renman (1987) Automated determination of total arsenic in sea water by flow constant-current stripping analysis with gold fibre electrodes. *Anal. Chim. Acta,* **201**, 263.

Huan T. N., T. Ganesh, K. S. Kin, S. Kim and S.-H. Han (2011) A three-dimensional gold nanodendrite network porous structure and its application for an electrochemical sensing. *Biosens. Bioelectron.,* **27**, 183.

Hughes M. D., Y-J. Xu, P. Jenkins, P. Mcmorn, P. Landon, D. I. Enache, A. F. Carley, G. A. Attard, G. J. Hutchings, F. King, E, H. Stitt, P. Johnston, K. Griffin and

C. J. Kiely (2005) Tunable gold catalysts for selective hydrocarbon oxidation under mild conditions. *Nature,* **437**, 1132.

Hutchings G. J. (2008) Nanocrystalline gold and gold palladium alloy catalysts for chemical synthesis. *Chem. Commun.*, 1148.

Jena B. K. and C. R. Raj (2008) Highly sensitive and selective electrochemical detection of sub-ppb level chromium(VI) using nano-sized gold particle. *Talanta,* **76**, 161.

Jeyabharathi C., S. S. Kumar, G. V. M. Kiruthika and K. L. N. Phani (2010) Aqueous CTAB-assisted electrodeposition of gold atomic clusters and their oxygen reduction electrocatalytic activity in acid solutions. *Angew. Chem. Int. Ed.,* **49**, 2925.

Kachoosangi R. T., C. E. Banks, X. Ji and R. G. Compton (2007) Electroanalytical determination of cadmium(II) and lead(II) using an in-situ bismuth film modified edge plane pyrolytic graphite electrode. *Anal. Sci.,* **23**, 283.

Kefala G., A. Economou, A. Voulgaropoulos and M. Sofoniou (2003) A study of bismuth-film electrodes for the detection of trace metals by anodic stripping voltammetry and their application to the determination of Pb and Zn in tapwater and human hair. *Talanta,* **61**, 603.

Khairy M., D. K. Kampouris, R. O. Kadara and C. E. Banks (2010a) Gold nanoparticle modified screen printed electrodes for the trace sensing of arsenic(III) in the presence of copper(II). *Electroanalysis,* **22**, 2496.

Khairy M., N. A. Choudry, M. Ouasti, D. K. Kampouris, R. O. Kadara and C. E. Banks (2010b) Gold nanoparticle ensembles allow mechanistic insights into electrochemical processes. *ChemPhysChem,* **11**, 875.

Kieber R. J., J. D. Willey and S. D. Zvalaren (2002) Chromium speciation in rainwater: Temporal variability and atmospheric deposition. *Environ. Sci. Technol.,* **36**, 5321.

Kruusma J., C. E. Banks and R. G. Compton (2004) Mercury-free sono-electroanalytical detection of lead in human blood by use of bismuth-film-modified boron-doped diamond electrodes. *Anal. Bioanal. Chem.,* **379**, 700.

Lan Y., H. Luo, X. Ren, Y. Wang and L. Wang (2012) Glassy carbon electrode modified with citrate stabilized gold nanoparticles for sensitive arsenic (III) detection. Anal. Lett., 45, 1184.

Liu B., L. Lu, M. Wang and Y. Zi (2008) A study of nanostructured gold modified glassy carbon electrode for the determination of trace Cr(VI). *J. Chem. Sci.,* **120**, 493.

Liu G., Y.-Y. Lin, H. Wu and Y. Lin (2007) Voltammetric detection of Cr(VI) with disposable screen-printed electrode modified with gold nanoparticles. *Environ. Sci. Technol.,* **41**, 8129.

Lu M., N. V. Rees and R. G. Compton (2012) Determination of Sb(V) using differential pulse anodic stripping voltammetry at an unmodified edge plane pyrolytic graphite electrode. *Electroanalysis,* **24**, 1306.

Manivannan A., R, Kawasaki, D. A. Tryk and A. Fujishima (2004) Interaction of Pb and Cd during anodic stripping voltammetric analysis at boron-doped diamond electrodes. *Electrochim. Acta,* **49**, 3313.

Mardegan A., P. Scopece, F. Lamberti, M. Meneghetti, L. M. Moretto and P. Ugo (2012) Methods for estimation of generalized diffusion parameter at membrane–solution interface. *Electroanalysis* **24**, 789.

Mays D. E., and A. Hussam (2009) Voltammetric methods for determination and speciation of inorganic arsenic in the environment—A review. *Anal. Chim. Acta,* **646**, 6.

McGaw E. A. and Swain G. M. (2006) A comparison of boron-doped diamond thin-film and Hg-coated glassy carbon electrodes for anodic stripping voltammetric determination of heavy metal ions in aqueous media. *Anal. Chim. Acta,* **575**, 180.

Metters J. P., R. O. Kadara and C. E. Banks (2012) Electroanalytical sensing of chromium(III) and (VI) utilising gold screen printed macro electrodes. *Analyst,* **137**, 896.

Ouyang R., S. A. Bragg, J. Q. Chambers and Z.-L. Xue (2012) Flower-like self-assembly of gold nanoparticles for highly sensitive electrochemical detection of chromium(VI). *Analytica Chimica Acta,* **722**, 1.

Pohl H. R., H. G. Abadin and J. F. Risher (2006) Neurotoxicity of cadmium, lead, and mercury. *Metal Ions Life Sci.,* **1**, 395.

Prado C., S. J. Wilkins, F. Marken and R. G. Compton (2002) Simultaneous electrochemical detection and determination of lead and copper at boron-doped diamond film electrodes. *Electroanalysis* **14**, 262.

Rodriguez-Vazquez M. J., M. C. Blanco, R. Lourido, C. Vazquez-Vazquez, E. Pastor, G. A. Planes, J. Rivas and M. A. Lopez-Quintela (2008) Synthesis of atomic gold clusters with strong electrocatalytic activities. *Langmuir,* **24**, 12690.

Saturno J., D. Valera, H. Carrero and L. Fernandez (2011) Electroanalytical detection of Pb, Cd and traces of Cr at micro/nano-structured bismuth film electrodes. *Sens. Actuators B,* **159**, 92.

Shin S. H. and H. G. Hong (2010) Anodic stripping voltammetric detection of arsenic(III) at platinum–iron(III) nanoparticle modified carbon nanotube on glassy carbon electrode. *Bull. Korean Chem. Soc.,* **31**, 3077.

Simm A. O., C. E. Banks and R. G. Compton (2004) Sonically assisted electroanalytical detection of ultratrace arsenic. *Anal. Chem.,* **76**, 5051.

Simm A. O., C. E. Banks and R. G. Compton (2005a) The electrochemical detection of arsenic(III) at a silver electrode. *Electroanalysis,* **17**, 1727.

Simm A. O., C. E. Banks and R. G. Compton (2005b) Sonoelectroanalytical detection of ultra-trace arsenic. *Electroanalysis,* **17**, 335.

Simm A. O., C. E. Banks, S. J. Wilkins, N. G. Karousos, J. Davis and R. G. Compton (2005c) A comparison of different types of gold-carbon composite electrode for detection of arsenic(III). *Anal. Bioanal. Chem.,* **381**, 979.

Streeter I., R. Baron and R. G. Compton (2007a) Voltammetry at nanoparticle and microparticle modified electrodes: Theory and experiment. *J. Phys. Chem. C* **111**, 17008.

Streeter I. and R. G. Compton (2007b) Diffusion-limited currents to nanoparticles of various shapes supported on an electrode; spheres, hemispheres, and distorted spheres and hemispheres. *J. Phys. Chem. C,* **111**, 18049.

Thompson M. and J. L. Faull (1995) Do microbiota cause emission of stibine from cot mattresses? *Lancet,* **346**, 1557.

Toghill K. E., G. G. Wildgoose, A. Moshar, C. Mulcahy and R. G. Compton (2008) The fabrication and characterization of a bismuth nanoparticle modified boron doped diamond electrode and its application to the simultaneous determination of cadmium(II) and Llead(II). *Electroanalysis,* **20**, 1731.

Toghill K. E., L. Xiao, G. G. Wildgoose and R. G. Compton (2009) Electroanalytical determination of cadmium(II) and lead(II) using an antimony nanoparticle modified boron-doped diamond electrode. *Electroanalysis,* **21**, 1113.

Toghill K. E., M. Lu and R. G. Compton (2011) Electroanalytical determination of antimony. *Int. J. Electrochem. Sci.,* **6**, 3057.

Tsai M.-C. and P.-Y. Chen (2008) Voltammetric study and electrochemical detection of hexavalent chromium at gold nanoparticle-electrodeposited indium tinoxide (ITO) electrodes in acidic media. *Talanta,* **76**, 533.

Vincent J. B. (2003) Trace elements in viral hepatitis. *J. Trace Elem. Med. Biol.,* **16**, 227.

Wang J. F., C. Bian, J. H. Tong, J. Z. Sun and S. H. Xia (2012) L-Aspartic acid/L-cysteine/gold nanoparticle modified microelectrode for simultaneous detection of copper and lead. *Thin Sol. Films,* **520**, 6658.

Welch C. E. and R. G. Compton (2006) The use of nanoparticles in electroanalysis: A review. *Anal. Bioanal. Chem,* **384**, 601.

Welch C. M., M. E. Hyde, O. Nekrassova and R. G. Compton (2004) The oxidation of trivalent chromium at polycrystalline gold electrodes. *Phys. Chem. Chem. Phys.,* **6**, 3153.

WHO (1993) Guidance for Drinking Water Quality. Second Edition, Vol. 1 Recommendations, Geneva.

WHO (2003) Antimony in drinking-water. Background document for preparation of WHO Guidelines for drinking-water quality. WHO/SDE/WSH/03.04/74, Word Health Organisation, Geneva.

WHO (2012) Arsenic in drinking water. http://www.who.int/water_sanitation_health/dwq/arsenic/en/; Accessed November 2012.

Xiao L., G. G. Wildgoose and R. G. Compton (2008) Sensitive electrochemical detection of arsenic (III) using gold nanoparticle modified carbon nanotubes via anodic stripping voltammetry. *Anal. Chim. Acta,* **620**, 44.

Xing S., H. Xu, J. Chen, G. Shi and L. Jin (2011) Nafion stabilized silver nanoparticles modified electrode and its application to Cr(VI) detection. *J. Electroanal. Chem.,* **652**, 60.

Zhou Y.-G., F. W. Campbell, S. R. Belding and R. G. Compton (2010) Nanoparticle modified electrodes: Surface coverage effects in voltammetry showing the transition from convergent to linear diffusion. The reduction of aqueous chromium (III) at silver nanoparticle modified electrodes. *Chem. Phys. Lett.,* **497**, 200.

4

Interfacing cells with nanostructured electrochemical sensors for enhanced biomedical sensing

F. J. RAWSON, University of Nottingham, UK

DOI: 10.1533/9780857096722.1.80

Abstract: In recent years there has been a surge in research geared towards developing nanostructured and nanosized sensors for the purpose of interfacing with cells. This technology provides unprecedented temporal and spatial sensing for intracellular and extracellular purposes, enabling a greater understanding of the biochemical events that underpin a cell's behaviour. Various methods have been used to fabricate nanosensors, and a brief overview of these is provided in this chapter, including a discussion of the application of electrochemical nanosensors and their importance in providing new tools to understand cells on a molecular level by sensing biomolecules, bioelectricity and ions.

Key words: nanosensor, nanostructured electrochemical sensors, intracellular sensing, extracellular sensing, cell-sensor interface.

4.1 Introduction

Understanding cell function and identifying the various signalling pathways involved in controlling cell behaviour is crucial in providing insights into human pathology. Most cell-based biological assays are notorious for yielding data averaged across large groups of cells, despite the now common knowledge that individual cells, even those identical in appearance, differ in numerous characteristics. Variability in gene expression, concentration of a critical metabolite, ion, and relationship of multi-responses to a given stimulus are but a few familiar examples of cellular heterogeneity (Sims and Allbritton, 2007). Due to the differences between individual cells, traditional biochemical assays which analyse cells in bulk often overlook the rich information available when single cells are studied. For this reason, much emphasis has been placed on technical advances to enable biologists to peer into the molecular machinery of individual cells as well as populations of cells. Several bioanalytical tools are now available for single-cell analysis, including lab-on-a-chip technologies, microelectrode-based

electrochemical methods, fluorescent probes and mass spectrometric techniques (Lin *et al*., 2011). Despite important developments, the biochemical processes of a single cell can only be poorly quantified, limiting the ability to resolve the dynamic molecular processes that underlie important cell-fate decisions such as differentiation, cell division and cell death (Spiller *et al*., 2010).

To date, such bioanalytical tools have been limited in their ability to collect spatial and temporal information that enable us to study the intracellular environment on an equivalent level to the molecular event of interest. The search began to address this key issue with use of nanostructured electrochemical sensors, because they can interact with biomolecules on the equivalent scale. This therefore makes it possible to sense molecular events, both spatially and temporally, occurring inside and on the surface of cells. This approach of interfacing cells with nanostructured devices is in its infancy. It therefore has the potential to revolutionise our understanding of cell behaviour and give rise to new sensing strategies for the pharmaceutical and agrochemical industries. Consequently, it has the capability of impacting on human health and well-being. The aim of this chapter is to introduce the reader to common fabrication techniques used to construct nanostructured sensors, and to describe their application, offering an insight into how nanosensors provide new tools for biologists.

4.2 Designing and constructing nanostructured surfaces for cellular sensing

When designing nanosensors for the purpose of interfacing cells and sensing, there are a number of factors to consider, including the cell type, the nature of where the molecules/components of the cell that will be sensed are, and what is to be sensed. Another important component to consider is electrode fouling, to ensure sensing cellular events can be sensed reliably over time.

A key consideration is the structural differences that exist between most prokaryotes and eukaryotic cells. Prokaryotic cells that consist largely of bacteria possess no membrane-bound organelles, which can make sensing intracellular cell signalling less complicated since techniques to access membrane-bound organelles with electrochemical sensors selectively is yet to be achieved. The ultrastructure of most prokaryotic and a limited number of eukaryotic cells can consist of a cell wall. The cell wall is distinctly different from the plasma membrane. Examples of typical prokaryotes that contain a cell wall include gram negative and positive bacteria, although there are structural differences between the two classes; and a typical eukaryotic cell that has a cell wall is yeast. This means there is a necessity to consider how and where these structures will be interfaced with such cells either

directly, or penetrated which of course depends on the user's application. This is because the chemistry of these surfaces differs; for example, the cell wall is largely made of carbohydrates compared to the plasma membrane where the composition is largely based on phospholipids and proteins. A detailed explanation of exploiting different chemistries and cell surfaces can be found in a recent perspective review written by (Mager *et al*., 2011).

4.2.1 Engineering nanostructured surfaces

Engineering surfaces with nanostructures is of paramount importance to give a high degree of understanding of interactions on a molecular level (Pappas *et al*., 2006; Kleps *et al*., 2007; Koehne *et al*., 2009; Simmel, 2009; Jiang *et al*., 2010; Shalek *et al*., 2010; Yeung *et al*., 2010; Pranzetti *et al*., 2012). Research into the fabrication procedures used in nanotechnology was recently reviewed (Iqbal *et al*., 2012) and they define a nanostructured material as having a structured component with at least one dimension < 100 nm range, and this definition will be used for nanostructured sensors in this chapter. A number of fabrication techniques have been employed to produce nanostructured devices, including chemical vapour deposition (CVD) of metals (Ben-Jacob and Hanein, 2008; Koehne *et al*., 2009), CVD growth of carbon nanotubes (CNTs), and subsequent patterning using lithography (Ben-Jacob and Hanein, 2008). Another example is a surface nanostructured with indium arsenide nanowires; these were fabricated by molecular-beam epitaxy (MBE) (Berthing *et al*., 2011); photolithography (Kleps *et al*., 2007; Jiang *et al*., 2010), and electron beam patterning of metal electrodes (Jiang *et al*., 2010), microsphere lithography and microcontact stamping (Shalek *et al*., 2010). In addition, Mendes *et al*. utilised a mixed self-assembled monolayer (SAM) of thiol molecules on gold (Yeung *et al*., 2010). A detailed description of these techniques can be found in the writings of Iqbal *et al*. (2012).

4.2.2 Nanowires

A nanowire can be thought of as a nanostructure that can conduct electricity, therefore making them highly relevant to cell sensing. A variety of materials have been used to construct surfaces modified with nanowires including ZnO nano rods (Al-Hilli *et al*., 2007), CNTs (Garrett *et al*., 2009; Rawson *et al*., 2011), silicon nanowires (Shalek *et al*., 2010) and double stranded DNA acting as a biomolecular nanowire (Meng *et al*., 2009). It has been well highlighted in reviews by McCreery *et al*. (2008) and Yang *et al*. (2010) that carbon-based nanostructures such as CNTs display excellent high aspect ratios, high mechanical strength, superb thermal and chemical stability and

superior electronic properties. Vertically aligned carbon nanostructures have been functionalised with a number of biomolecules including DNA (Lee *et al*., 2004), and proteins (Gooding *et al*., 2003; Yu *et al*., 2005), consisting of immunoglobulins (Yu *et al*., 2005), and enzymes that allow for direct electron transfer (Gooding *et al*., 2003). They have also been modified with electrocatalysts, which are important for catalysing biologically relevant electron transfer events (Rawson *et al*., 2011). It was established that proteins could be covalently tethered to vertically aligned carbon nanotubes (VACNTs) (Gooding *et al*., 2003). This opens up the realm of biosensing opportunities and the ability to communicate with individual biomolecules via wiring into enzyme active sites, enabling direct electron transfer (Gooding *et al*., 2003). The ability to couple enzymes and immunoglobulins to nanostructures can enable specific sensing of important cellular chemistry due to the enzyme and antibodies binding biomolecules selectively. Silicon can also be modified with the above biomolecules; however, while carbon has preferential electronic properties, the advantage of using silicon is that the current electronics industry is set up to mass produce this.

4.2.3 Nanostructuring surfaces using self-assembled molecular layers

The rational design of surfaces for immobilisation of biomolecules is of paramount importance for a wide variety of applications, ranging from the development of model substrates for mechanistic studies of cell behaviour to high-throughput protein assays for drug discovery, clinical diagnostics, and proteomics (Christof, 2000). Molecular surface science has greatly contributed to the advancement of this area by providing platforms for bio-engineering surfaces on a molecular level (Sagiv, 1980; Nuzzo and Allara, 1983). For instance, SAMs, which form spontaneously by the adsorption of an active surfactant onto a solid surface, possess important properties of self-organisation and adaptability to a number of technologically relevant surface substrates, in which they can form a well-ordered monolayer. Additionally, diazonium chemistry has opened up a realm of possibilities with regards to the range of substrates that can be used as a surface substrate (Brooksby and Downard, 2004; Pinson and Podvorica, 2005; Yu and Downard, 2007). Electrochemical and non-electrochemical grafting of diazonium leads to covalently modified surfaces and, like SAMs, these can have head groups consisting of hydroxyl, carboxylic acid, maleimide, azide, amine and biotin groups. These functional groups give rise to the ability to attach biological functional biomolecules that can be used to control and sense cellular signalling processes (Rawson *et al*., 2011, 2012).

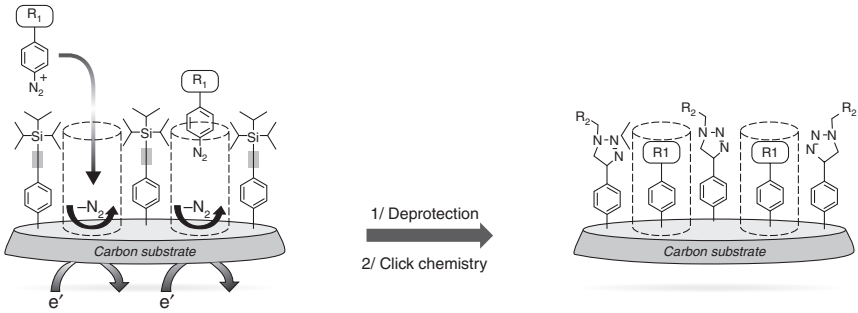

4.1 Strategy for electrochemically grafting multifunction diazonium surfaces. (*Source*: Approved for reproduction Leroux *et al.,* 2011.)

The properties of a SAM and films constructed using diazonium grafting can be easily controlled and specific functionalities can also be introduced into the building blocks. For instance, SAMs of thiols on gold and triethoxysilanes on silicon dioxide have been exploited (Lee *et al*., 2002; Mrksich, 2005; Christman *et al*., 2006; Lee *et al*., 2006; Mendes *et al*., 2007) to provide the surfaces, not only with active groups that interact with specific moieties of the biomolecules to be immobilised, but also with biomolecule-resistant groups such as oligoethyleneglycol (OEG). Biomolecules have been immobilised onto these surfaces by adsorption (Mrksich, 2005) molecular recognition between the biomolecules, immobilised ligands, or covalent coupling to the SAM surface (Lee *et al*., 2002, 2006). An important recent development for the surface modification using diazonium molecules was showing that multifunctional diazonium could be grafted (Fig. 4.1) (Leroux *et al*., 2010, 2011; Arias de Fuentes *et al*., 2011). The use of such bi-functional surfaces for biomolecular cellular sensing is yet to be achieved, but it can be envisaged how this could be used to pattern surfaces allowing for the spatial separation of components that can be electrochemically switched in a similar manner to that shown by Mendes and co-workers (Yeung *et al*., 2010; Pranzetti *et al*., 2012).

4.3 Electrochemical sensing using nanoelectronic sensing devices

The development of nanofabrication procedures has led to a flurry of important bioelectrochemical measurements utilising sensors, with at least one dimension on the nanoscale, which can sense and detect biological events on a molecular level yielding novel information about cellular events and new tools for biosensing (Huang *et al*., 2009). The materials used to construct nanostructured sensing devices include silicon (Patolsky *et al*., 2006), carbon-based nanostructures (Huang and Chen, 2010), and metals of various types.

The nature of the nanostructured sensors used can be categorised into three groups:

1. field effect transducers (FETs), based on monitoring conductance and current drain (Patolsky *et al.*, 2006)
2. potentiometric sensors, based on measuring voltages (Yamamoto *et al.*, 2003)
3. amperometric sensors, relying on measuring faradaic events and the electrical current they generate (Rawson *et al.*, 2011).

In the near future there will also be new ways of using electrochemical functional surfaces to probe biology by sensing with surface plasma resonance spectroscopy which can be coupled with electrochemistry (Pranzetti *et al.*, 2013).

A most interesting development in the field has been recently reported, where smart electrochemical functional surfaces were developed (Fig. 4.2). These consisted of biotin containing oligolysine and a spacer unit of alkane thiol, which was self-assembled onto a gold surface. It was shown that these surfaces could be electrochemically switched from an on- to an off-state. This was achieved by applying –0.4 V, the head biotin group was concealed and thus it was shown to prevent NeutrAvidin adsorption (off-state). Subsequently, when +0.3 V was applied the biotin was exposed, allowing adsorption (on-state) (Yeung *et al.*, 2010). The adsorption process was sensed using surface plasmon resonance spectroscopy (SPR). The surfaces were then adapted in which an alkane thiol with a carboxylic head

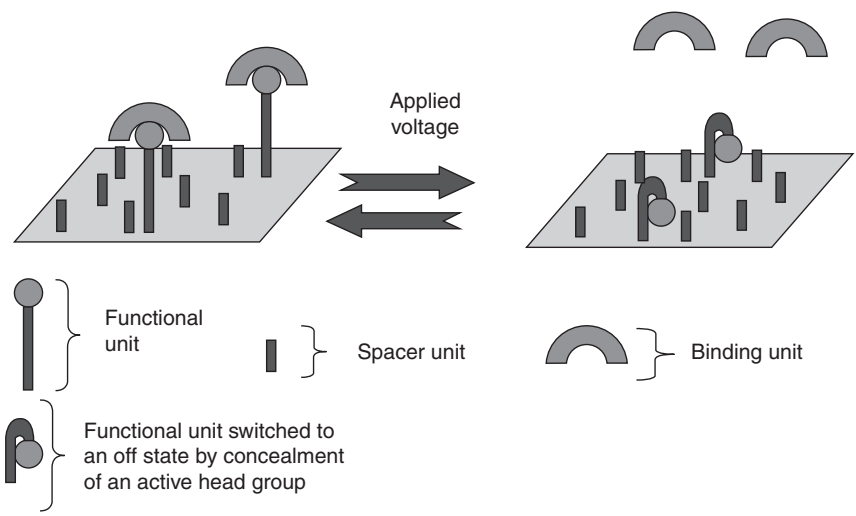

4.2 Diagrammatic representation of how an electrochemical functional surface for control and sensing of cell adhesion operates.

group (COOH) was self-assembled onto a gold surface instead of the oligolysine. In this instance, on application of an applied potential of +0.25 V the COOH is concealed (off) and on application of a –0.25 V it was revealed (on) (Pranzetti *et al.*, 2012). This platform was then used to control bacterial adhesion in an on/off fashion with the electrochemical concealment and expression of a bacterial pro-adhesive group. This opens up the realm of functional sensing surfaces, and can be used for investigating biological dynamic processes such as biofilm formation.

The following sections review:

- Interfacing nanostructured sensors for extracellular sensing
- Interfacing amperometric nanostructured sensors with cells for bioelectricity and biomolecules detection
- Interfacing nanostructured sensors for intracellular sensing.

4.4 Interfacing nanostructured sensors for extracellular sensing

Cells sense and respond to their external environment in order to survive and benefit one another. For example bacteria use quorum sensing in which, molecules are released into the external matrix and are then detected by other bacteria. The detection of such quorum molecules causes the bacteria detecting them to have a certain response such as transcription of a specific gene. This allows them to respond in a certain way to survive, such as the stimulation and release of a plasmid conveying antibiotic resistance. Additionally, eukaryotic cells also sense and communicate with other cells. For example, nerve cells can release and detect neurotransmitters such as dopamine. The release of dopamine can then be detected by other nerve cells which, then causes them to be stimulated. Cells also have membrane-bound proteins capable of expelling electrons to the external environment. For instance, cells use trans plasma membrane transport systems to reduce iron ions so that they can be transported across the cell membrane. Consequently, researchers have pioneered the development of sensors that are interfaced with or close to the plasma membrane to sense such events. By doing so this has enabled researchers to delve into these signalling events giving a deeper understanding of how they may control cell function. In this section, I will review key examples of such nanoelectrochemical sensors.

4.4.1 Sensing using carbon-based field effect transducers (FETs)

FETs have a source, drain and gate terminal, with the gate controlling the electron flow, via its conductance (Wang *et al.*, 2007). The surface that

constitutes the gate of a FET is sensitive to surface alterations, which manifests in changes of conductance and flow of electrons. They are sensitive to small changes and are ideal for sensing cellular events on a molecular level. FETs have been constructed in which the gate consisted of single walled carbon nanotubes (SWCNTs), modified with antibodies. These were sandwiched between two silicon oxide nanostructures, acting as the source and drain components (Wang *et al.*, 2007; Tsai *et al.*, 2008). The electrodes were fabricated by patterning silicon using photolithography and CNTs were dispersed from solution forming the gate component. The FETs were interfaced with cortical and chromaffin cells and detected the release of chromogranin A (CgA). The configuration of the FETs and their function can be seen in Fig. 4.3 where an antibody for CgA acts to provide a sensor specific for CgA detection. The cortical cells were stimulated to release CgA by adding glutamate, and chromaffin cells were stimulated to release CgA by histamine. In both cases, the CgA bound to the antibody and caused the conductance of the FET to increase. This led to a rise in the current flow which was used as the analytical signal reflecting the concentration of CgA release, and a detection limit of approximately 1 nM was achieved (Wang *et al.*, 2007).

Huang *et al.* (2009) have tried to make the FETs containing CNTs more suitable for mass production by using mats of CNTs drop-coated on glass substrates with silver paste. The FETs were interfaced with hundreds of

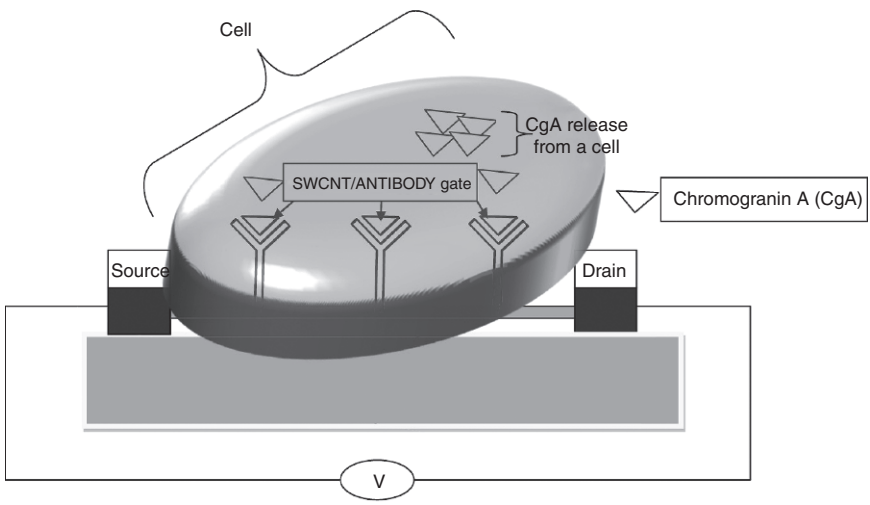

4.3 Schematic of how FET with a SWCNT-antibody gate would function to detect chromogranin A (CgA). The FET operates by CgA binding with the antibodies which increases the conductance that is detected as a rise in the current drain.

cells, and the release of adenosine triphosphate (ATP) from astrocytes in response to glutamate was monitored. They sensed catecholamine release from PC12 cells stimulated by membrane depolarisation (Sudibya *et al.*, 2009). The mechanism of signal transduction was through the aromatic carbon groups that are found within ATP and catecholamine forming pi–pi interactions with the CNTs increasing the current drain. Nets of SWCNTs drop-coated onto a glass slide were also used to detect direct electron transfer for myocytes in response to depolarisation of the myocytes cell membrane. In this case, FETs were interfaced with cardiac cells. The cardiac cells were exposed to 500 nM of tetrodotoxin, a toxin which blocks sodium channels essential for stimulation of an action potential, which led to a reduction in the electrical current drain (Pui *et al.*, 2010).

Graphene, acting as the gate component, has also been used in FET devices for interfacing with cells (Mohanty and Berry, 2008; Kempaiah *et al.*, 2011). In the first example, the gram positive bacteria *Bacillus cereus* was adhered to the graphene by functionalising with positive amine groups, which electrostatically adhere to the bacteria, which have a negatively charged surface. On attachment of the cells to the surface, the conductivity of the FET increased. They attributed this to a rise in the hole density caused by the negatively charged bacteria interfacing with the p-type characteristic of the graphene (Mohanty and Berry, 2008). Additionally, graphene was incorporated in FETs for monitoring conductance generation in chicken cardiomyocytes (Cohen-Karni *et al.*, 2010). Moreover, Kempaiah *et al.* (2011) used graphene, which was chemically reduced, and enabled yeast cells to adsorb on the FET surface. Yeast were subsequently exposed to ethanol and propanol. It was reported that their device could monitor the physiological effect of these alcohols. The mechanism of signal transduction was attributed to shrinkage in the cell volume in response to the alcohols, which caused increased wrinkles in the graphene sheets, leading to a decrease in conductance measurements. They were able to differentiate conductance measurements dependent on the toxin used, highlighting the selectivity of the device.

4.4.2 Sensing using silicon-based FETs

FETs incorporating graphene and CNTs have been used successfully when applied as sensors for electron generation and neurotransmitter release when interfaced with cells; however, the synthesis of well-defined CNTs into a single manufacturing procedure is yet to be achieved. Consequently, using silicon nanowire-based FETs that can be fabricated using standard lithographic equipment which is already in place in the electronics industry may prove to be a more appropriate method of manufacture and will

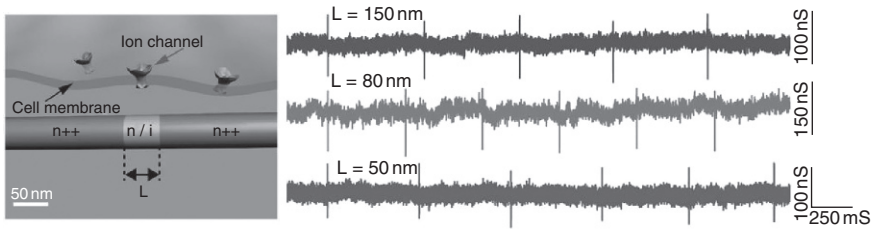

4.4 Diagram showing an ultrashort-channel nanowire transistor interfaced with cardiomyocytes and the detection of its beat (Cohen-Karni *et al.,* 2012).

allow for commercialisation and mass production. Examples of interfacing cells with silicon nanowire FETs have recently been shown to be useful both for bioelectricity monitoring (Pui *et al*., 2009a) and for monitoring cytokines where dysregulation has been linked to a number of diseases (Pui *et al*., 2009b, 2011). These silicon nanowire FETs were functionalised with antibodies against the cytokines interleukin-6 (IL-6) and tumour necrosis factor-alpha (TNF-alpha) on one chip, meaning their release could be monitored simultaneously and selectively. They inferred that measuring two cytokines simultaneously could help understand how a cell elicits an immune response. The analytical signal was generated in a similar manner to that described in Fig. 4.3 and the cytokine release was monitored in response to a bacterial endotoxin lipopolysaccharide (Pui *et al*., 2011). Femto-molar levels of secreted cytokines could be monitored which, when compared to other techniques, is unprecedented. Chang *et al*. (2012) also used silicon nanowire FETs to monitor extracellular potassium flux from chromaffin cells. They achieved the selective sensing of potassium ions by coating the silicon nanowire in valinomycin. The sensors were utilised to monitor the cellular response to nicotine. It was demonstrated that in nicotine's presence the potassium concentration was increased leading to a rise in the current drain.

A different approach to constructing FET sensors to enable point-like detection of individual ion channel function was achieved by fabrication of nano-channel FETs, and they measured beats of cardiomyocytes with increased conductance observed when channels were open (Cohen-Karni *et al*., 2012); this is illustrated in Fig. 4.4. More recently, Tian (Tian *et al*., 2012) took the technology further forward by fabricating 3D-meshes of FETs to allow for unprecedented spatial and temporal measurement of electrical stimuli of cardiomyocytes cultured on 3D-biomimetic surface. This raises the possibility of bio-mimicking the internal environment of organisms *in vitro* because 3D cell constructs more closely mimic the behaviour of equivalent cells *in vivo*.

4.5 Interfacing amperometric nanostructured sensors with cells for bioelectricity and biomolecule detection

Recent research has led to the development of novel nanostructured surfaces as electrochemical platforms to study electron transfer by wiring into bacterial membrane redox sites (Timur *et al*., 2007a, 2007b; Rawson *et al*., 2011). Moreover, investigating the mechanism of electron transfer from cells allows for a greater understanding of fundamental biology behind such processes (Reguera *et al*., 2005; Coman *et al*., 2009). However, little research has been performed on investigating direct electron transfer to electrodes from eukaryotic cells. The electrochemical research that has occurred has largely been performed by using soluble hydrophilic/lipophilic mediators. These diffuse to the cell, are reduced, and are either directly detected at an electrode, or the mediator reduces an intermediate molecule which is electrochemically detected (Baronian *et al*., 2002; Spégel *et al*., 2007; Heiskanen *et al*., 2009; Kostesha *et al*., 2009). This signal is dependent on a number of factors, including diffusion, ability to cross the membrane, stereochemistry, and because they are not attached to an electrode, they cannot be subjected to a constant potential and consequently this method is not the most appropriate for monitoring electron transfer events from cells.

All cells have transplasma membrane electron transport (tPMET) systems (also known as the plasma membrane oxidoreductase (PMOR) systems). tPMET systems are involved in the transportation of nutrients such as iron (Lesuisse and Labbe, 1992), cell regulation, cell signalling, cell growth, apoptosis and proton pumping, by transferring electrons to the external environment. Therefore elucidating their role and function is essential to understanding cellular control and behaviour (Baker and Lawen, 2000). There are three examples indicating that yeast can transfer electrons directly to an electrode and tPMETs were a likely source of these electrons (Prasad *et al*., 2007; Ducommun *et al*., 2010; Hubenova *et al*., 2010). It has also been reported that direct electron transfer from PC12 cells could be achieved using a gold electrode modified with an oligopeptide. However, in this report no mechanistic information was given (Kafi *et al*., 2011), but it is highly likely that the electron transfer occurs via a tPMET system. Overall, very little insight into the mechanisms of such events is known and nanostructured sensors will help in this manner. Therefore, by carefully designing and controlling nanostructured sensors on the nanoscale, it is feasible that some of these events can be understood in more detail.

One recent example of such a method was to show for the first time that electron transfer occurs directly across the yeast cell wall (Rawson *et al*., 2012), while others have alluded to the fact that intimate direct contact of nanostructured electrode with tPMETs was required to give rise to external

expulsion and detection of electrons (Shkil *et al*., 2011). By rational design, a nanostructured sensor with an electrochemically grafted tether diazonium layer, which was used as an anchor, to chemically couple an electrochemical mediator molecule osmium bipyridine was fabricated. This enabled the group to investigate the mechanism of electron transfer from yeast in a controlled manner for the first time (Rawson *et al*., 2012). This was achieved as the osmium complex acted as a mediator, allowing for direct electron transfer from *Saccharomyces cerevisiae*. It was shown that the maximum surface roughness of the nanomodified film was 25 nm. Considering the yeast cell wall is between 100 and 200 nm, there was no possible way the electrode could be in direct contact with tPMETs. It was concluded that electron transfer was occurring across the yeast cell wall; however, the elucidation of the exact mechanism requires further research. The technology developed shows how nanostructured sensors can offer new cellular insights, they concluded from their experimental observations that the biological role and function of the yeast cell wall needs revisiting.

Other examples of nanostructured sensors have included nanostructuring electrode surfaces both with mats (Timur *et al*., 2007a, 2007b; Coman *et al*., 2009) and vertically aligned CNTs (Rawson *et al*., 2011) to sense direct charge transfer from bacteria cells. Timur *et al*. (2007a) used mats of CNTs mixed with a carbon paste electrode that were functionalised with an osmium complex. This enabled the efficient wiring of bacterium *Pseudomonas putida* and the generated current reflected their metabolic rate. Subsequently, the sensors were wired into a genetically modified *Pseudomonas putida* that was sensitive to phenol. They used this biosensor to detect phenol in contaminated water, in which an increased concentration of phenol led to a higher current. This was attributed to the increased metabolic flux caused by the phenol-sensitive bacteria. Others have used MWCNTs drop-coated onto the surface of a glassy carbon electrode (Peng *et al*., 2010). Investigations into the ability of detecting direct electron transfer from the electrogenic organism *Shewanella oneidensis* was performed. It was discovered that the MWCNTs enhanced electron transfer rates by 82 times compared to bare glassy carbon electrodes. They also attribute the charge transfer events to the membrane-bound cytochrome c complex, which had its electron transfer rate constant calculated to be 1.25 s^{-1}. Such information may prove vital in comparing other organisms and how external electron transfer events are involved in the cell metabolism.

Rawson *et al.* (2011) were the first to use chemical assembly of vertically aligned SWCNTs onto a diazonium tether layer to study electron expulsion from non-electrogenic bacteria. The SWCNTs were further functionalised with an osmium bipyridine complex, via carbodiimide chemistry, and they demonstrated that electron transfer events could be seen from *Proteus vulgaris* and that the electron transfer represented the metabolic rate of

the bacteria. The group then utilised this to develop a rapid toxicity sensor in which three different toxins were appraised, ethanol, ampicillin and sodium azide. All showed that in the presence of the toxins the electron transfer rates decreased and this was also validated by plate viability counts (Rawson *et al*., 2011).

4.6 Interfacing nanostructured sensors for intracellular sensing

When interfacing cells with nanostructured sensors for application of intracellular monitoring, it is ideal that the nanostructures that traverse the plasma membrane to access the cytoplasm are introduced non-invasively to avoid causing undue stress or altering the cell function. Examples of non-invasive methods include culturing cells on Si nanowire fabricated using standard lithographic procedures (Kim *et al*., 2007; Pearton *et al*., 2007; Shalek *et al*., 2010) which naturally protrude through the cell membrane after 1 h of culture (Kim *et al*., 2007). A silicon-based nanoFET modified with phospholipid bilayers could penetrate the plasma membrane (Tian *et al*., 2010). Additionally, molecular biology techniques in which calcium is used to enable transformation of the cells with DNA has been utilised to enable non-invasive insertion of DNA nanowires (Meng *et al*., 2009) and vertically aligned SWCNT-DNA nanostructures inside eukaryotic cells (Rawson *et al*., 2013). They showed that the internalised SWCNT-DNA nanostructures could electrochemically communicate with the inside of a cell by sensing the redox dye methylene blue. DNA wires were thiolated allowing for the fabrication of DNA nanostructured surfaces via their self-assembly by formation of a gold-sulphur bond (Meng *et al*., 2009). The SWCNT were modified with ssDNA via its physioadsorption. These were self-assembled onto an electrochemically grafted diazonium tether layer (Rawson *et al*., 2013). Another method of cellular insertion of nanostructures without using any external force was by using the migration forces caused by cells themselves. Hoshino utilised this technique by fabricating microwells on glass and modifying these via the self-assembly of the cell adhesive protein fibronectin (Hoshino *et al*., 2008). The wells also contained a tungsten nano-needle that was used to penetrate the cell. This was achieved as the cells migrated across the fibronectin down into the well and the locomotive force is sufficiently higher than 10^{-9} N, which is the force required for a nano-needle to pierce the cell membrane (Obataya *et al*., 2005).

Examples of nanostructures being inserted into the cells by the application of external force include piercing of the membrane by electrodes under control of an atomic force microscope (Amemiya *et al*., 2012; Wang *et al*.,

2012) as well as by the manual insertion of silicon nano-needles (Patolsky *et al.*, 2006; Ferguson *et al.*, 2012).

4.6.1 Application of electrochemical sensors for intracellular studies

The application of inserting nanostructured electrochemical sensors that enable a deeper understanding of biology that control cell behaviour has yet to be fully exploited. However, in recent years there have been a few examples of such sensors highlighting the possibilities of using this technology. Recently an intracellular sensing assay was developed in which the sensing of reactive oxygen species (ROS) and reactive nitrogen species (RNS) production in response to mechanical stress was achieved (Wang *et al.*, 2012). This was made possible by inserting a platinum-black nanoelectrode encased in a micrometre-sized glass, and positioned into a single cell from a mouse macrophage cell line and poising the electrode at 850 mV vs Ag/AgCl reference electrode. The current was monitored amperometrically which was attributed to ROS/RNS generation only. Additionally, a platinised carbon fibre microelectrode was used to monitor extracellular ROS/RNS release in a similar manner. With the intracellular sensor, it was found that in response to mechanical stimulation ROS and RNS leakage from phagolysomes was detected. This adds further evidence to the literature that intracellular leakage occurs, although this remains highly controversial. It was observed that ROS/RNS bursts only resulted in higher currents for seconds, and was likely to have been dealt with by the cells antioxidant mechanisms which ensured no cellular damage occurred. The sensor developed allowed for the detection of such events on the time scale that was previously impossible to monitor and demonstrates how nanosensors can be used as new tools for biologists.

Measuring metal ions is important for many applications; for example, calcium ions have been linked to cell signalling, and magnesium ions have been linked to metabolic control. Therefore measuring ions such as these can be important for elucidating their biochemical role. Zinc oxide nanostructured electrodes were developed and used as potentiometric sensors to monitor intracellular glucose and metal ions (Asif *et al.*, 2011). They initially sensed calcium in both frogs eggs and human fat cells (Asif *et al.*, 2009), followed by magnesium ions (Asif *et al.*, 2010b). Selectivity was achieved by coating the nanostructured electrode with membranes selective for magnesium and calcium. It was shown that increased concentrations in these ions resulted in an increase in the electron motive force which was proportional to their intracellular concentration (Asif *et al.*, 2010a). Further research was

performed in which the zinc oxide nanostructured surfaces were functionalised, via ionic interactions with glucose oxidase. This provided a selective sensor that was capable of detecting intracellular glucose. The method of signal transduction was by the enzymatic oxidation of glucose to gluconolactone and hydrogen peroxide. Gluconolactone forms gluconic acid spontaneously which dissociates yielding a proton. This ionic change around the zinc oxide nanostructures causes a modification to the overall potential which is proportional to the glucose concentration. The biosensor was applied to monitor the change in intracellular glucose concentration in human fat and frog oocyte single cells. On application of 10 nM insulin, which acts as a key to allow glucose uptake into the cell (Asif *et al*., 2010a), they observed an increase in the electron motive force. The authors commented that the zinc oxide nanolayer was not very stable and this requires further work to improve the long term monitoring to ensure that it is ideal for pharmaceutical applications.

4.7 Conclusion

Significant advances have been made for the rational nanoscale design and fabrication of electrochemical nanosensors and biosensors for interfacing with cells. These range from the nanoscale fabrication of surfaces with SAMs which have been functionalised with various components from simple carboxylic groups to CNTs, through to nanofabricated surfaces fabricated by lithography forming well-defined nano-patterned areas, including amperometric, potentiometric and FET-based electrochemical sensors. These have been used to monitor extracellular secretion of biomolecules and generation of bioelectricity to intracellular monitoring of biomolecules, bioelectricity and metal ions. Importantly, nanostructured electrodes have been used to sense various components that provide new information regarding the biological behaviour of cells. These include the identification for a need to redefine the function of the yeast cell wall to most recently monitoring intracellular ROS which shed new light on their leakage from vacuoles. These examples highlight that the interfacing of nanosensors with cells can play a crucial role in understanding cell function and fate. This has the potential to revolutionise diagnostic sensing for biomedicine. However, we are in the infancy of this technology and there are still some significant problems to be solved, including how to provide long-term stability of sensors from biofouling and the ability to design surfaces to target and sense events at the surface of, and within, specific organelles within eukaryotic cells that can provide not only qualitative but also quantitative data. Looking forward, I envisage sensing systems that have the ability not only to sense but also to have functionality allowing for a deeper understanding of the dynamic environment of cells and what controls their behaviour. The

field will continue to expand and I expect it will make significant contributions to human health and well-being.

4.8 References

Al-Hilli, S. M., Willander, M., Ost, A. and Stralfors, P. (2007) ZnO nanorods as an intracellular sensor for pH measurements. *Journal of Applied Physics,* **102**, 084304–5.

Amemiya, Y., Kawano, K., Matsusaki, M., Akashi, M., Nakamura, N. and Nakamura, C. (2012) Formation of nanofilms on cell surfaces to improve the insertion efficiency of a nanoneedle into cells. *Biochemical and Biophysical Research Communications*, **420**, 662–665.

Arias de Fuentes, O., Ferri, T., Frasconi, M., Paolini, V. and Santucci, R. (2011) Highly-ordered covalent anchoring of carbon nanotubes on electrode surfaces by diazonium salt reactions. *Angewandte Chemie*, **123**, 3519–3523.

Asif, M., Elinder, F. and Willander, M. (2011) Electrochemical biosensors based on ZnO nanostructures to measure intracellular metal ions and glucose. *Analytical and Bioanalytical Techniques*, **S7**, 1–9.

Asif, M. H., Ali, S. M. U., Nur, O., Willander, M., Brännmark, C., Strålfors, P., Englund, U. H., Elinder, F. and Danielsson, B. (2010a) Functionalised ZnO-nanorod-based selective electrochemical sensor for intracellular glucose. *Biosensors and Bioelectronics,* **25**, 2205–2211.

Asif, M. H., Ali, S. M. U., Nur, O., Willander, M., Englund, U. H. and Elinder, F. (2010b) Functionalized ZnO nanorod-based selective magnesium ion sensor for intracellular measurements. *Biosensors and Bioelectronics*, **26**, 1118–1123.

Asif, M. H., Fulati, A., Nur, O., Willander, M., Brannmark, C., Stralfors, P., Borjesson, S. I. and Elinder, F. (2009) Functionalized zinc oxide nanorod with ionophore-membrane coating as an intracellular Ca[sup 2+] selective sensor. *Applied Physics Letters,* **95**, 023703.

Baker, M. A. and Lawen, A. (2000) Plasma membrane NADH-oxidoreductase system: A critical review of the structural and functional data. *Antioxidants and Redox Signaling,* **2**, 197–212.

Baronian, K., Downard, A., Lowen, R. and Pasco, N. (2002) Detection of two distinct substrate-dependent catabolic responses in yeast cells using a mediated electrochemical method. *Applied Microbiology and Biotechnology,* **60**, 108–113.

Ben-Jacob, E. and Hanein, Y. (2008) Carbon nanotube micro-electrodes for neuronal interfacing. *Journal of Materials Chemistry,* **18**, 5181–5186.

Berthing, T., Bonde, S., Sørensen, C. B., Utko, P., Nygård, J. and Martinez, K. L. (2011) Intact mammalian cell function on semiconductor nanowire arrays: New perspectives for cell-based biosensing. *Small,* **7**, 640–647.

Brooksby, P. A. and Downard, A. J. (2004) Electrochemical and atomic force microscopy study of carbon surface modification via diazonium reduction in aqueous and acetonitrile solutions. *Langmuir,* **20**, 5038–5045.

Chang, K.-S., Sun, C.-J., Chiang, P.-L., Chou, A.-C., Lin, M.-C., Liang, C., Hung, H.-H., Yeh, Y.-H., Chen, C.-D., Pan, C.-Y. and Chen, Y.-T. (2012) Monitoring extracellular K+ flux with a valinomycin-coated silicon nanowire field-effect transistor. *Biosensors and Bioelectronics,* **31**, 137–143.

Christman, K. L., Enriquez-Rios, V. D. and Maynard, H. D. (2006) Nanopatterning proteins and peptides. *Soft Matter,* **2**, 928–939.

Cohen-Karni, T., Casanova, D., Cahoon, J. F., Qing, Q., Bell, D. C. and Lieber, C. M. (2012) Synthetically encoded ultrashort-channel nanowire transistors for fast, pointlike cellular signal detection. *Nano Letters,* **12**, 2639–2644.

Cohen-Karni, T., Qing, Q., Li, Q., Fang, Y. and Lieber, C. M. (2010) Graphene and nanowire transistors for cellular interfaces and electrical recording. *Nano Letters,* **10**, 1098–1102.

Coman, V., Gustavsson, T., Finkelsteinas, A., von Wachenfeldt, C., Hägerhäll, C. and Gorton, L. (2009) Electrical wiring of live, metabolically enhanced *Bacillus subtilis* cells with flexible osmium-redox polymers. *Journal of the American Chemical Society*, **131**, 16171–16176.

Ducommun, R., Favre, M. F., Carrard, D. and Fischer, F. (2010) Outward electron transfer by *Saccharomyces cerevisiae* monitored with a bi-cathodic microbial fuel cell-type activity sensor. *Yeast,* **27**, 139–148.

Ferguson, J. E., Boldt, C., Puhl, J. G., Stigen, T. W., Jackson, J. C., Crisp, K. M., Mesce, K. A., Netoff, T. I. and Redish, A. D. (2012) Nanowires precisely grown on the ends of microwire electrodes permit the recording of intracellular action potentials within deeper neural structures. *Nanomedicine* **7**, 847–853.

Garrett, D. J., Flavel, B. S., Shapter, J. G., Baronian, K. H. R. and Downard, A. J. (2009) Robust forests of vertically aligned carbon nanotubes chemically assembled on carbon substrates. *Langmuir* **26**, 1848–1854.

Gooding, J. J., Wibowo, R., Liu, Yang, W., Losic, D., Orbons, S., Mearns, F. J., Shapter, J. G. and Hibbert, D. B. (2003) Protein electrochemistry using aligned carbon nanotube arrays. *Journal of the American Chemical Society*, **125**, 9006–9007.

Heiskanen, A., Spégel, C., Kostesha, N., Lindahl, S., Ruzgas, T. and Emnéus, J. (2009) Mediator-assisted simultaneous probing of cytosolic and mitochondrial redox activity in living cells. *Analytical Biochemistry*, **384**, 11–19.

Hoshino, T., Konno, T., Ishihara, K. and Morishima, K. (2008) A nano-needle interface self-assembled by using cell migration for recording intracellular activity: Nano-needle durability. *Biomedical Robotics and Biomechatronics, BioRob 2008. 2nd IEEE RAS and EMBS International Conference*, Scottsdale, AZ, 19–22 October 2008, 506–510.

Huang, Y. and Chen, P. (2010) Nanoelectronic biosensing of dynamic cellular activities based on nanostructured materials. *Advanced Materials,* **22**, 2818–2823.

Huang, Y., Sudibya, H. G., Fu, D., Xue, R., Dong, X., Li, L.-J. and Chen, P. (2009) Label-free detection of ATP release from living astrocytes with high temporal resolution using carbon nanotube network. *Biosensors and Bioelectronics,* **24**, 2716–2720.

Hubenova, Y. V., Rashkov, R. S., Buchvarov, V. D., Arnaudova, M. H., Babanova, S. M. and Mitov, M. Y. (2010) Improvement of yeast–biofuel cell output by electrode modifications. *Industrial and Engineering Chemistry Research,* **50**, 557–564.

Iqbal, P., Preece, J. A. and Mendes, P. M. (2012) Nanotechnology: The 'top-down' and 'bottom-up' approaches. *Supramolecular Chemistry.* Oxford: John Wiley & Sons, Ltd.

Jiang, X., Hu, J., Fitzgerald, L. A., Biffinger, J. C., Xie, P., Ringeisen, B. R. and Lieber, C. M. (2010) Probing electron transfer mechanisms in *Shewanella oneidensis* MR-1 using a nanoelectrode platform and single-cell imaging. *Proceedings of the National Academy of Sciences,* **107**, 16806–16810.

Kafi, M. A., Kim, T.-H., An, J. H. and Choi, J.-W. (2011) Fabrication of cell chip for detection of cell cycle progression based on electrochemical method. *Analytical Chemistry*, **83**(6), 2104–2111.

Kempaiah, R., Chung, A. and Maheshwari, V. (2011) Graphene as cellular interface: electromechanical coupling with cells. *ACS Nano,* **5**, 6025–6031.

Kim, W., Ng, J. K., Kunitake, M. E., Conklin, B. R. and Yang, P. (2007) Interfacing Silicon Nanowires with mammalian cells. *Journal of the American Chemical Society,* **129**, 7228–7229.

Kleps, I., Miu, M., Craciunoiu, F. and Simion, M. (2007) Development of the micro- and nanoelectrodes for cells investigation. *Microelectronic Engineering,* **84**, 1744–1748.

Koehne, J. E., Chen, H., Cassell, A., Liu, G.-Y., Li, J. and Meyyappan, M. (2009) Arrays of carbon nanofibers as a platform for biosensing at the molecular level and for tissue engineering and implantation. *Bio-Medical Materials and Engineering,* **19**, 35–43.

Kostesha, N., Heiskanen, A., Spégel, C., Hahn-Hägerdal, B., Gorwa-Grauslund, M.-F. and Emnéus, J. (2009) Real-time detection of cofactor availability in genetically modified living *Saccharomyces cerevisiae* cells – Simultaneous probing of different geno- and phenotypes. *Bioelectrochemistry,* **76**, 180–188.

Lee, C.-S., Baker, S. E., Marcus, M. S., Yang, W., Eriksson, M. A. and Hamers, R. J. (2004) Electrically addressable biomolecular functionalization of carbon nanotube and carbon nanofiber electrodes. *Nano Letters,* **4**, 1713–1716.

Lee, K.-B., Park, S.-J., Mirkin, C. A., Smith, J. C. and Mrksich, M. (2002) Protein nanoarrays generated by dip-pen nanolithography. *Science,* **295**, 1702–1705.

Lee, S. W., Oh, B. K., Sanedrin, R. G., Salaita, K., Fujigaya, T. and Mirkin, C. A. (2006) Biologically active protein nanoarrays generated using parallel dip-pen nanolithography. *Advanced Materials,* **18**, 1133–1136.

Leroux, Y. R., Fei, H., NOËL, J.-M., Roux, C. M. and Hapiot, P. (2010) Efficient covalent modification of a carbon surface: use of a silyl protecting group to form an active monolayer. *Journal of the American Chemical Society,* **132**, 14039–14041.

Leroux, Y. R., Hui, F., NOËL, J.-M., Roux, C. M., Downard, A. J. and Hapiot, P. (2011) Design of robust binary film onto carbon surface using diazonium electrochemistry. *Langmuir,* **27**, 11222–11228.

Lesuisse, E. and Labbe, P. (1992) Iron reduction and trans plasma membrane electron transfer in the yeast *Saccharomyces cerevisiae. Plant Physiology,* **100**, 769–777.

Lin, Y., Trouillon, R., Safina, G. and Ewing, A. G. (2011) Chemical analysis of single cells. *Analytical Chemistry,* **83**, 4369–4392.

Mager, M. D., Lapointe, V. and Stevens, M. M. (2011) Exploring and exploiting chemistry at the cell surface. *Nature Chemisty,* **3**, 582–589.

Mccreery, R. L. (2008) Advanced carbon electrode materials for molecular electrochemistry. *Chemical Reviews,* **108**, 2646–2687.

Mendes, P., Yeung, C. and Preece, J. (2007) Bio-nanopatterning of surfaces. *Nanoscale Research Letters,* **2**, 373–384.

Meng, F., Yang, J., Liu, T., Zhu, X. and Li, G. (2009) Electric communication between the inner part of a cell and an electrode: the way to look inside a cell. *Analytical Chemistry,* **81**, 9168–9171.

Mohanty, N. and Berry, V. (2008) Graphene-based single-bacterium resolution biodevice and DNA transistor: interfacing graphene derivatives with nanoscale and microscale biocomponents. *Nano Letters,* **8**, 4469–4476.

Mrksich, M. (2005) Dynamic substrates for cell biology. *MRS Bulletin,* **30**, 180–184.

Niemeyer, C. M. (2000) Self-assembled nanostructures based on DNA: towards the development of nanobiotechnology. *Current Opinion in Chemical Biology,* **4**, 609–618.

Nuzzo, R. G. and Allara, D. L. (1983) Adsorption of bifunctional organic disulfides on gold surfaces. *Journal of the American Chemical Society,* **105**, 4481–4483.

Obataya, I., Nakamura, C., Han, S., Nakamura, N. and Miyake, J. (2005) Mechanical sensing of the penetration of various nanoneedles into a living cell using atomic force microscopy. *Biosensors and Bioelectronics,* **20**, 1652–1655.

Pappas, T. C., Wickramanyake, W. M. S., Jan, E., Motamedi, M., Brodwick, M. and Kotov, N. A. (2006) Nanoscale engineering of a cellular interface with semiconductor nanoparticle films for photoelectric stimulation of neurons. *Nano Letters,* **7**, 513–519.

Patolsky, F., Timko, B. P., Yu, G., Fang, Y., Greytak, A. B., Zheng, G. and Lieber, C. M. (2006) Detection, stimulation, and inhibition of neuronal signals with high-density nanowire transistor arrays. *Science,* **313**, 1100–1104.

Pearton, S. J., Lele, T., Tseng, Y. and Ren, F. (2007) Penetrating living cells using semiconductor nanowires. *Trends in Biotechnology,* **25**, 481–482.

Peng, L., You, S.-J. and Wang, J.-Y. (2010) Carbon nanotubes as electrode modifier promoting direct electron transfer from *Shewanella oneidensis*. *Biosensors and Bioelectronics,* **25**, 1248–1251.

Pinson, J. and Podvorica, F. (2005) Attachment of organic layers to conductive or semiconductive surfaces by reduction of diazonium salts. *Chemical Society Reviews,* **34**, 429–439.

Pranzetti, A., Mieszkin, S., Iqbal, P., Rawson, F. J., Callow, M. E., Callow, J. A., Koelsch, P., Preece, J. A. and Mendes, P. M. (2013) An electrically reversible switchable surface to control and study early bacterial adhesion dynamics in real-time. *Advanced Materials*, **25**(15), 2181–2185.

Pranzetti, A., Salaün, S., Mieszkin, S., Callow, M. E., Callow, J. A., Preece, J. A. and Mendes, P. M. (2012) Model organic surfaces to probe marine bacterial adhesion kinetics by surface plasmon resonance. *Advanced Functional Materials,* **22**, 3672–368.

Prasad, D., Arun, S., Murugesan, M., Padmanaban, S., Satyanarayanan, R. S., Berchmans, S. and Yegnaraman, V. (2007) Direct electron transfer with yeast cells and construction of a mediatorless microbial fuel cell. *Biosensors and Bioelectronics,* **22**, 2604–2610.

Pui, T.-S., Agarwal, A., Ye, F., Balasubramanian, N. and Chen, P. (2009a) CMOS-compatible nanowire sensor arrays for detection of cellular bioelectricity. *Small,* **5**, 208–212.

Pui, T.-S., Agarwal, A., Ye, F., Huang, Y. and Chen, P. (2011) Nanoelectronic detection of triggered secretion of pro-inflammatory cytokines using CMOS compatible silicon nanowires. *Biosensors and Bioelectronics,* **26**, 2746–2750.

Pui, T.-S., Agarwal, A., Ye, F., Tou, Z.-Q., Huang, Y. and Chen, P. (2009b) Ultrasensitive detection of adipocytokines with CMOS-compatible silicon nanowire arrays. *Nanoscale,* **1**, 159–163.

Pui, T.-S., Sudibya, H. G., Luan, X., Zhang, Q., Ye, F., Huang, Y. and Chen, P. (2010) Non-invasive detection of cellular bioelectricity based on carbon nanotube devices for high-throughput drug screening. *Advanced Materials,* **22**, 3199–3203.

Rawson, F. J., Garrett, D. J., Leech, D., Downard, A. J. and Baronian, K. H. R. (2011) Electron transfer from Proteus vulgaris to a covalently assembled, single walled carbon nanotube electrode functionalised with osmium bipyridine complex: Application to a whole cell biosensor. *Biosensors and Bioelectronics* **26**, 2383–2389.

Rawson, F. J., Gross, A. J., Garrett, D. J., Downard, A. J. and Baronian, K. H. R. (2012) Mediated electrochemical detection of electron transfer from the outer surface of the cell wall of *Saccharomyces cerevisiae*. *Electrochemistry Communications,* **15**, 85–87.

Rawson, F. J., Yeung, C. L., Jackson, S. K. and Mendes, P. M. (2013) Tailoring 3D single-walled carbon nanotubes anchored to indium tin oxide for natural cellular uptake and intracellular sensing. *Nano Letters,* **13**, 1–8.

Reguera, G., Mccarthy, K. D., Mehta, T., Nicoll, J. S., Tuominen, M. T. and Lovley, D. R. (2005) Extracellular electron transfer via microbial nanowires. *Nature,* **435**, 1098–1101.

Sagiv, J. (1980) Organized monolayers by adsorption. 1. Formation and structure of oleophobic mixed monolayers on solid surfaces. *Journal of the American Chemical Society,* **102**, 92–98.

Shalek, A. K., Robinson, J. T., Karp, E. S., Lee, J. S., Ahn, D.-R., Yoon, M.-H., Sutton, A., Jorgolli, M., Gertner, R. S., Gujral, T. S., Macbeath, G., Yang, E. G. and Park, H. (2010) Vertical silicon nanowires as a universal platform for delivering biomolecules into living cells. *Proceedings of the National Academy of Sciences,* **107**, 1870–1875.

Shkil, H., Schulte, A., Guschin, D. A. and Schuhmann, W. (2011) Electron transfer between genetically modified hansenula polymorpha yeast cells and electrode surfaces via os-complex modified redox polymers. *ChemPhysChem,* **12**, 806–813.

Simmel, F. C. (2009) Bioelectronics: Wiring-up ion channels. *Nature Physics,* **5**, 783–784.

Sims, C. E. and Allbritton, N. L. (2007) Analysis of single mammalian cells on-chip. *Lab on a Chip,* **7**, 423–440.

Spégel, C. F., Heiskanen, A. R., Kostesha, N., Johanson, T. H., Gorwa-Grauslund, M.-F., Koudelka-Hep, M., Emnéus, J. and Ruzgas, T. (2007) Amperometric response from the glycolytic versus the pentose phosphate pathway in *Saccharomyces cerevisiae* cells. *Analytical Chemistry,* **79**, 8919–8926.

Spiller, D. G., Wood, C. D., Rand, D. A. and White, M. R. H. (2010) Measurement of single-cell dynamics. *Nature,* **465**, 736–745.

Sudibya, H. G., Ma, J., Dong, X., Ng, S., Li, L.-J., Liu, X.-W. and Chen, P. (2009) Interfacing glycosylated carbon-nanotube-network devices with living cells to detect dynamic secretion of biomolecules. *Angewandte Chemie International Edition,* **48**, 2723–2726.

Tian, B., Cohen-Karni, T., Qing, Q., Duan, X., Xie, P. and Lieber, C. M. (2010) Three-dimensional, flexible nanoscale field-effect transistors as localized bioprobes. *Science,* **329**, 830–834.

Tian, B., Liu, J., Dvir, T., Jin, L., Tsui, J. H., Qing, Q., Suo, Z., Langer, R., Kohane, D. S. and Lieber, C. M. (2012) Macroporous nanowire nanoelectronic scaffolds for synthetic tissues. *Nat Mater,* **11**, 986–994.

Timur, S., Anik, U., Odaci, D. and Gorton, L. (2007a) Development of a microbial biosensor based on carbon nanotube (CNT) modified electrodes. *Electrochemistry Communications,* **9**, 1810–1815.

Timur, S., Haghighi, B., Tkac, J., Pazarlioglu, N., Telefoncu, A. and Gorton, L. (2007b) Electrical wiring of Pseudomonas putida and Pseudomonas fluorescens with osmium redox polymers. *Bioelectrochemistry,* **71**, 38–45.

Tsai, C.-C., Yang, C.-C., Shih, P.-Y., Wu, C.-S., Chen, C.-D., Pan, C.-Y. and Chen, Y.-T. (2008). Exocytosis of a single bovine adrenal chromaffin cell: the electrical and morphological studies. *The Journal of Physical Chemistry B,* **112**, 9165–9173.

Wang, C.-W., Pan, C.-Y., Wu, H.-C., Shih, P.-Y., Tsai, C.-C., Liao, K.-T., Lu, L.-L., Hsieh, W.-H., Chen, C.-D. and Chen, Y.-T. (2007) In situ detection of chromogranin a released from living neurons with a single-walled carbon-nanotube field-effect transistor. *Small,* **3**, 1350–1355.

Wang, Y., Noël, J.-M., Velmurugan, J., Nogala, W., Mirkin, M. V., Lu, C., Guille Collignon, M., Lemaître, F. and Amatore, C. (2012) Nanoelectrodes for determination of reactive oxygen and nitrogen species inside murine macrophages. *Proceedings of the National Academy of Sciences,* **109**, 11534–11539.

Yamamoto, K., Shi, G., Zhou, T., Xu, F., Zhu, M., Liu, M., Kato, T., Jin, J.-Y. and Jin, L. (2003) Solid-state pH ultramicrosensor based on a tungstic oxide film fabricated on a tungsten nanoelectrode and its application to the study of endothelial cells. *Analytica Chimica Acta,* **480**, 109–117.

Yang, W., Ratinac, K. R., Ringer, S. P., Thordarson, P., Gooding, J. J. and Braet, F. (2010) Carbon nanomaterials in biosensors: should you use nanotubes or graphene? *Angewandte Chemie International Edition,* **49**, 2114–2138.

Yeung, C. L., Iqbal, P., Allan, M., Lashkor, M., Preece, J. A. and Mendes, P. M. (2010) Tuning specific biomolecular interactions using electro-switchable oligopeptide surfaces. *Advanced Functional Materials,* **20**, 2657–2663.

Yu, S. S. C. and Downard, A. J. (2007) Photochemical grafting and activation of organic layers on glassy carbon and pyrolyzed photoresist films. *Langmuir,* **23**, 4662–4668.

Yu, X., Kim, S. N., Papadimitrakopoulos, F. and Rusling, J. F. (2005) Protein immunosensor using single-wall carbon nanotube forests with electrochemical detection of enzyme labels. *Molecular BioSystems,* **1**, 70–78.

5

Chemiresistor gas sensors using semiconductor metal oxides

L. FRANCIOSO, Institute for Microelectronics and Microsystems, Italy

DOI: 10.1533/9780857096722.1.101

Abstract: This chapter presents a review of metal-oxide-based chemical sensors and chemiresistors with low dimensional semiconducting structures and nanoparticles, and examines recent developments in these fields. The fundamentals of sensors are discussed first, together with a description of the typical techniques adopted for the preparation of low dimensional structures. The final part looks at new research trends, low cost, and alternative substrate sensors. A comprehensive list of online resources completes the chapter.

Key words: metal oxide chemiresistor, low dimensional chemical sensors, nanowires, nanoparticles.

5.1 Introduction

This chapter will review the different kinds of chemical gas sensors based on metal oxide (MOX) sensitive semiconductor materials. These devices are used mainly in applications where low cost detection and miniaturized dimensions are required. Although the properties of these MOX materials have been known since the early 1970s and the conduction mechanism is well understood, some phenomena are still under investigation. It has been known for a long time that the charge-carrier concentration near the surface of a semiconductor exposed to gas is sensitive to the composition of the surrounding environment. In 1962, Seiyama *et al*. demonstrated that thin films of zinc oxide (ZnO), heated to 300°C in air, showed a conductivity sensitive to traces of different gases in the air. Taguchi in 1962 (Chiba, 1992) demonstrated similar properties for sintered SnO_2, a material characterized by enhanced stability.

Since the publication of these pioneering works, semiconductor gas sensors have been investigated extensively in order to develop practical applications such as gas leak detectors and environmental monitoring, and significant technological efforts have been made to improve gas response,

selectivity, and stability of devices. Numerous kinds of gases are emitted from various sources into our living and working spaces, or outdoors. Many of them, such as air pollutants, are hazardous to human beings and the environment, while others can be used to diagnose the state of their sources, such as ethanol and acetone in the breath and flavor components of foods. Most of these gases are present at very low concentrations, so extremely reliable sensing characteristics are required for their monitoring.

However, the selectivity of MOX sensors, in some cases and applications is poor, and over the past few years several different approaches have been taken to increase sensor selectivity. These approaches include the study of sensitive layers (Zarcomb and Stretter, 1984) and advanced sensor array architectures for electronic noses (Shurmer *et al*., 1990; Gardner, 1991), as well as identifying the gas by modulating the MOX temperature (Currie *et al*., 1991; Heilig *et al*., 1997). Over the last few decades, micromachined gas sensors based on semiconducting MOX have benefited from a parallel evolution in fabrication technologies for micro electro-mechanical-systems (MEMS). These technologies have been added to on-board sensor electronics to improve signal conditioning, improving the response, and decreasing the power consumption of the sensors. Furthermore, in recent years there has been a marked interest in integrated or harvesting-type power sources and an impressive amount of power density research, as well as coupling of different energy sources (vibration or thermoelectric) with sensor devices.

Recent interest in quasi one-dimensional MOX nanostructures versus polycrystalline forms is driven by different advantages with regard to thin- and thick-film-based devices:

- Highest crystallinity and limited aging;
- Large aspect ratio and surface-to-volume ratio;
- Easy functionalization of surface;
- Simple preparation methods by chemical or physical means.

This chapter will give details on the working principles and focused analysis of devices based on low dimensional chemical sensitive structures and their properties. New research directions and results for chemical sensor structures on flexible structures will also be presented.

5.2 The development of semiconductor metal oxide gas sensors

State-of-the-art commercial MOX gas sensors rely mostly on thick-film materials, mainly screen-printed onto bulk ceramic heater substrates. These thick-film MOX gas sensors have found wide commercial use in a variety of gas monitoring and home alarm applications (Moseley and Tofield, 1987;

Williams, 1987; Ikohura and Watson, 1994; Gopel and Schierbaum, 1995). Thick-film deposition of MOX materials is an industrial technology that offers low cost and considerable versatility toward different application needs.

Disadvantages of this technology include the low resolution of the technique and its low compatibility with MEMS foundry facilities (Kamp, 2002). As a result of the bulky ceramic substrate, such gas-sensing elements require several hundred mW/device in heating power, which is a big disadvantage for battery-supplied sensors. Moreover, the high power consumption of commercial MOX gas sensors also presents a serious obstacle in the achievement of gas-sensor arrays consisting of gas-sensing elements with systematically varying cross-sensitivity profiles.

In order to enable solutions ranging from simple low power consumption gas-sensing elements to complete sensor arrays, state-of-the-art MOX sensors are becoming increasingly smaller in size, while the sensor processing needs to be compatible with standard silicon foundry processing routines. Physical methods for thin films deposition, such as evaporation, sputtering, and laser ablation have been well developed (Phillips *et al*., 1996; Karapatnitski *et al*., 2002; Stryhal *et al*., 2002); however, so far fewer studies have been devoted to chemical deposition routes such as sol-gel. Chemical routes present different advantages, including simple and low-cost deposition equipment, easy modification of precursors and, as a result, efficient control over the morphology and composition of the produced sensitive materials. Epifani *et al*. (2007) proposed an alternative deposition process from Sn(II) 2-ethylhexanoate (SnEtEs) solutions; it is a modified process, with the addition of a surfactant to improve the wettability of the sensor substrates (Savianu *et al*., 1999).

From the perspective of operative parameters, the working temperature at which MOX sensors are more efficient can vary depending on the gas atmosphere and the properties of the sensor material selected in each case. As these temperatures range from 200°C to 800°C, far from room temperatures, it is necessary to implement a heating system in sensor devices. A simple MOX sensor will be composed of a substrate (where the sensor material will be supported), the electrodes (to measure the conductivity changes) and the heaters (to heat the device at optimum sensing temperatures). Figure 5.1 shows a packaged thin film MOX sensor realized at CNR-IMM institute in Lecce (Italy).

A different type of sensor can be achieved by processing the device in full front-side approach, like the devices showed in Fig. 5.2; the top panel shows a scanning electron microscopy (SEM) image of a complete device where the stacked structure is composed of platinum heater, the sensitive film square-like patterned and centered on the middle part of heater, and the electrical contacts deposited on top are all visible. The bottom panel

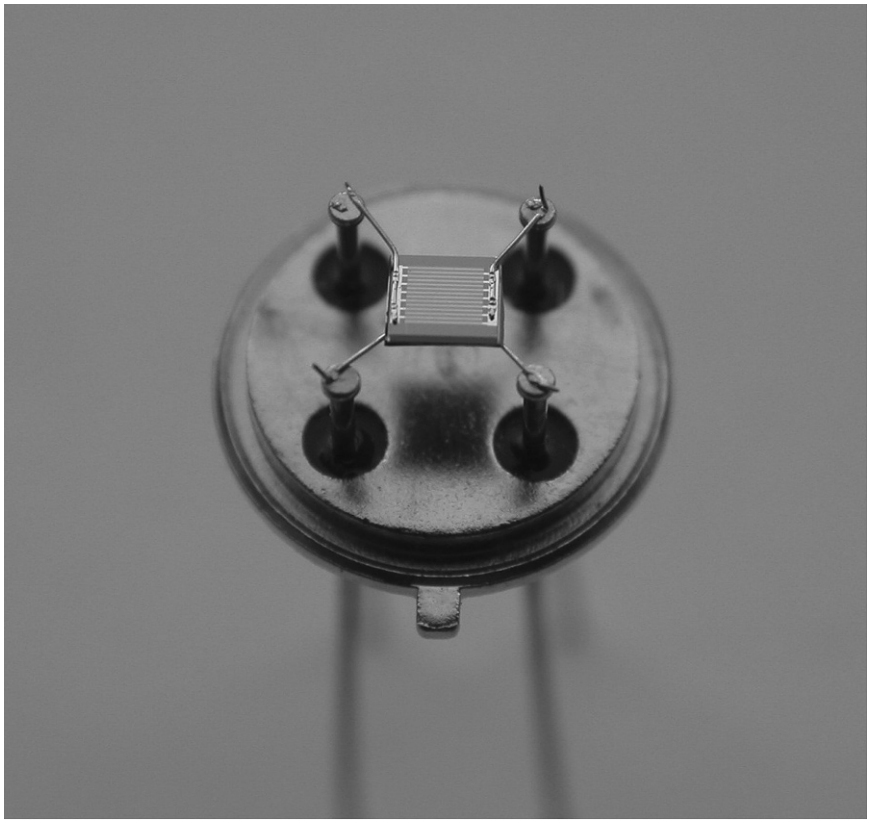

5.1 Packaged thin film gas sensor on silicon substrate (die 2 × 2 mm²). (*Source*: Courtesy of L. Francioso.)

shows the cross-section of a device where the paths of the heater, the SiO_2 passivation sandwich, the sensitive film, and the platinum fingers of electrical contacts can be seen.

Semiconductor gas sensors have been developed based on limited kinds of n-type MOXs, such as SnO_2, In_2O_3,WO_3, ZnO, and Fe_2O_3. The mobility of majority charge carriers is of primary importance for base semiconductors in these materials because it provides the proportionality constant of the change of electrical conductivity when the number of main carriers changes as a result of gas–solid interactions. The mobility of conduction electrons (n-type oxides) is reported between 10 and 200 cm^2/Vs for n-type MOX typically used in gas sensors. The mobility of p-type oxides such as NiO is usually much less (about 0.2 cm^2/Vs), and this is one of the reasons why p-type oxides are less frequently utilized in the discussed applications.

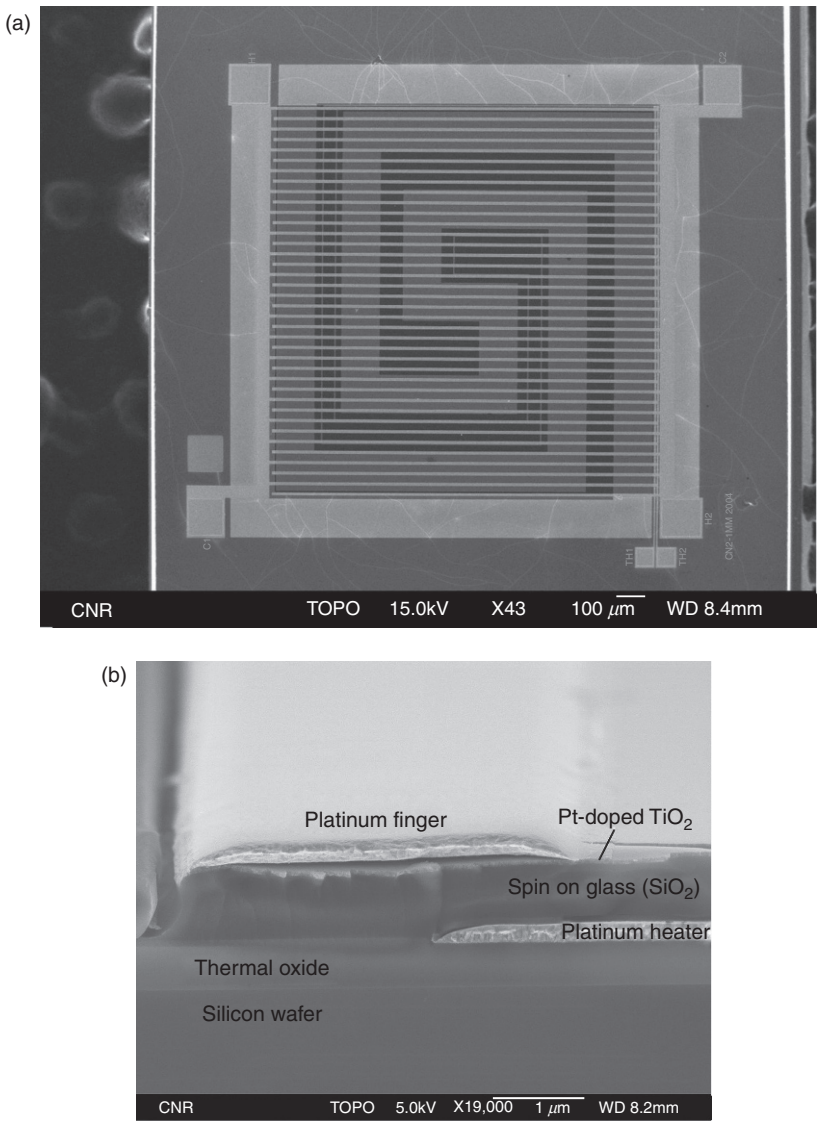

5.2 SEM micrograph of full front type gas sensor (a) and cross-section of stacked structure (b). (*Source*: Courtesy of L. Francioso.)

As mentioned above, the interest in sensing materials is due to the change of their electrical properties in the presence of a determinate gas, and the interaction with the gas species can lead to different surface conductance effects or bulk effects; bulk effects become important when material stability must be considered and studied.

5.3 The gas-sensing process in semiconductor metal oxide sensors

The gas-sensing process of a semiconductor device is controlled by two principal interactions: (a) the gas–solid interaction, which modifies physical properties of the surface (also called 'receptor function') and (b) the transduction of the surface effects into an electrical resistance change of the sensor (the so-called 'transducer function'). It is quite well accepted in the scientific community that the receptor function is related to the surface's chemical properties of semiconductor grains, while the transducer function is related to the surface's space charge layers on oxide grains and relative gas-dependent barriers.

This understanding has been strengthened by the elucidation of oxygen adsorptive properties of oxides and the findings of remarkable sensitizing actions played by various foreign receptors introduced into the grains (Yamazoe *et al*., 1979, 1983; Xu *et al*., 1991).

When the MOX sensor is exposed to a particular target gas with part per million (ppm) level concentration in air, the sensor changes its electrical resistance. When this experiment is carried out in a gas-sensing test bench, we can obtain response transients like those shown in Fig. 5.3.

This change in the electrical resistance is from a level in the baseline gas (typically named R_a or R_{air}) to a steady level (gas injection window, called R_g or R_{gas}) on exposure to the target gas (and vice versa) on cutting off the gas flow.

The output response of a given sensor is the representation of its output as a function of the measurand (M) applied to its input. It is called the sensor-response curve but is sometimes known, erroneously, as the sensitivity curve. A variety of quantities can correctly represent the sensor output response, and in the case of a chemical sensor based on the conductivity or resistance variation with respect to changing the input concentration of a given volatile compound, it is recommended to use one of the following possibilities, with G_0 and R_0 reference values considered for the normalization:

- R (resistance)
- $R–R_0$ (relative resistance)
- $(R–R_0)/R_0$ (relative change of resistance)
- G (conductance)
- G/G_0 (relative conductance)
- $(G–G_0)/G_0$ (relative change of conductance).

The sensor response is dependent on the effective substrate temperature. Naturally, R_g, as well as (R_a/R_g), depend on the kind and concentration of the target gas alongside other conditions. Typically, R_g and gas concentration

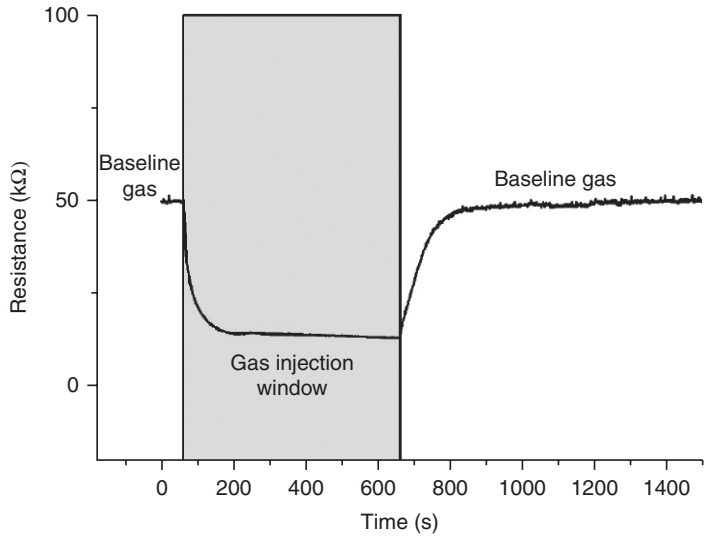

5.3 Typical dynamic response of a metal oxide gas sensor during a target gas injection.

are usually correlated linearly in a log–log scale. The sensitivity curve of a sensor can be produced by a derivative procedure from the response curve, and the indication along the sensitivity axes must specify the change of the output with respect to the input, such as, for instance, $S = \left(\partial\left(R/R_0\right)/\partial M\right)$. D'Amico and Di Natale (2001) also outlined different types of sensitivities in introducing the definition of an offset parameter.

In n-type semiconductors, the structure of energy bands levels (when a MOX surface is free of adsorbates) presents the conduction band and the valence band separated by an energy gap, in which discrete energetic levels are permitted. These energy levels are characterized from the donor levels, acceptor levels, and recombination and trapping centers.

Close to the surface, the energy levels of band results, modified as a fundamental property of the surface, are the inter-energetic levels in the forbidden gap, induced from the interruption of the crystalline lattice. They can act like donor centers or acceptors, capturing or donating electrons or can behave like recombination centers. Generally, these superficial levels can be generated by gaseous adsorption of species, foreign bodies to the surface of the material (Smith, 1964).

Ionisorption is the most important adsorption process in the working mechanisms of gas sensors. It does not create local bonds between atoms of the adsorbate's surface, but the adsorbate behaves as a superficial state and remains bonded to the surface by the electrostatic force. A gaseous species will obviously be chemisorbed to the surface of the single sensor if a certain

amount of energy is supplied. The Lennard-Jones model gives a simple model of the activation energy ΔE_a behavior for chemisorption. Figure 5.4 shows the behavior of the physisorption energy and chemisorption energy versus the distance from the surface of the sensor.

A molecule that, approximating to sensor surface with null total energy as indicated in curve (1) of Fig. 5.4, reaches the point in which the curves of physisorption and chemisorption of the Lennard-Jones model are intersected can be chemisorbed if thermally supplied with an energy equal to ΔE_a. This desorption is represented in the Lennard-Jones model by $\Delta E_a + \Delta H_{\text{chem}}$ energy. At thermal equilibrium, the probability of its occupation of the superficial intrinsic states is given from Fermi's statistics, as for the bulk states. The extraction and electron injection from acceptors and donors involves the formation of a layer of charge space under the surface of the semiconductor; the carrier concentration near the surface depends on the presence of donor states and acceptors from their occupation state. For MOX chemiresistors the density of the states is related to the interactions that exist between the gaseous species and the surface of the semiconductor.

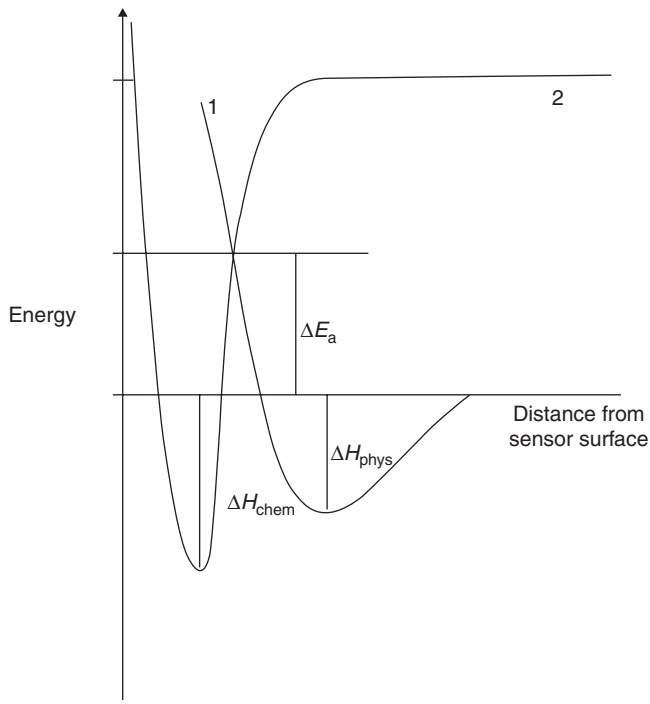

5.4 System energy as function of adsorbate-surface distance: (1) physisorption curve and (2) chemisorption curve. (*Source*: Adapted from Shiraiwa *et al.*, 2011.)

The dependence of the electrical conductivity σ on hydrogen partial pressure p_{H_2} can be characterized by a parameter m_σ, as defined by Radecka *et al.* (1998) as:

$$m_\sigma = \left(\frac{\partial \log \sigma}{\partial \log p_{H_2}} \right)^{-1} \quad [5.1]$$

It is possible to find the theoretical values of m_σ, depending on the gas solid-state interaction that occurred on the semiconductor's surface. In the presence of O_2 in the atmosphere, the sensing material chemisorbs it on its surface. Oxygen can be adsorbed in several forms, such as: O_2^-, O^{2-}, O^-.

Nevertheless, it has been generally recognized that at elevated temperatures SnO_2 has poor selectivity and low thermodynamic stability (Radecka *et al.*, 1998). On the other hand, materials such as TiO_2 can work at high temperatures because they base their sensing properties in the changes on volume-related conduction.

TiO_2 will be the perfect candidate for O_2 sensing in combustion processes where the MOX sensor device has to work at high temperatures (600–1000°C) (Sharma and Bhatnagar, 1999). TiO_2 shows high sensitivity toward oxygen gas, especially when it is doped with such metal impurities as Nb (Sharma *et al.*, 1998). TiO_2 responds to changes in oxygen partial pressure in the upper temperature range (700°C and above) and reflects the equilibrium between the atmosphere and its bulk stoichiometry (Kirner *et al.*, 1990; Moseley, 1992).

As reported in the Introduction, first approaches to MOX sensor research were oriented toward understand the influence of grain diameter on sensor performance for the detection of different reducing gases by n-type SnO_2 films. Semiconducting MOXs have long been known as efficient gas-sensing elements, and their electrical conductivity varies by many orders of magnitude with the changes in surrounding gas atmosphere (Franke *et al.*, 2006; Comini *et al.*, 2009; Kanan *et al.*, 2009; Lee, 2009; Fine *et al.*, 2010; Tricoli *et al.*, 2010; Korotcenkov and Cho, 2011). These reactions occur at the SnO_2 surface and can change the surface's charge state, which influences the accumulation or depletion of electrons within each grain.

Choi and Jang (2010) observed a large increase in the amplitude of the MOX sensor response when the mean grain diameter, D_{ave}, was reduced across the range from 30 to 5 nm. This enhanced sensitivity was attributed (Xu *et al.*, 1991) to the reduction of D_{ave} (mean grain diameter) to values less than the twice the Debye length, $2\lambda_D$. The discovery of this impressive influence of grain diameter encouraged the study and experimental investigation into chemical sensors of single-crystal nanowires (NWs), which

effectively constrict the conduction pathway to a single grain that is longer than it is wide; it is clear that the NW diameter was functionally equivalent to D_{ave} of standard grains.

Low dimensional structures such as NWs and nanoparticles (NPs) play a crucial role in the growing interest in materials synthesis and target-engineered devices. MOX chemical sensors generally show poor selectivity in a single gas or target compound; the possibilities of enhancing selectivity differ, and are typically based on physical filters on top of the sensor's package or material surface decoration, with noble metal particles or temperature-modulated working conditions (on micro-hotplate-based devices).

Different approaches can be cited for array-based solutions to reduce selectivity of MOX-based gas sensors. The Institute of Instrumental Analysis of the Karlsruhe Research Center proposed a gas-sensor array system (Karlsruher Mikronase, KAMINA) where the sensory properties of the elements are differentiated using a surface temperature gradient and/or a gradient of the thickness of a gas permeable SiO-coating on top of the MOX film (Goschnick, 2001).

Adami *et al*. (2006) outlined a MEMS technology-integrated chemiresistor array, using a monolithic multisensor chip and an array of sensor elements on a very small area implemented on membrane-based microhotplates (Lorenzelli, 2006), and the different sensing properties and sensor elements' selectivity have been performed at different operating temperatures in the array area. This approach has allowed for the recognition of distinct gases by analyzing the signal patterns produced by the sensors. The device has been used on a thin silicon oxide and nitride multilayer membrane, which allows for low power consumption, proper temperature control, and fast heating. In addition, the possibility of using such a microsystem for the discrimination of NO_2, CO and SO_2 has also been investigated. Principal component analysis (PCA) score plots (Fig. 5.5) show a good discrimination of different gases.

5.4 Gas sensors using novel low dimensional metal oxides

Recent developments in nanotechnology, as well as clean room fabrication methods and chemical routes synthesis, have made it easier to grow low dimensional MOXs with controlled morphology, electrical properties, and surface-to-volume ratios.

Yang *et al*. (2002) were among the first to demonstrate MOX NW-based chemical sensors. In 2002 they showed that bandgap-illuminated SnO_2 nanoribbons can detect NO_2 down to 3 ppm at room temperature. In the experiment, the authors postulated that NO_2 adsorption yields a surface NO_3 species that bridges two tin centers (Maiti *et al*., 2003), and nowadays researchers in the gas-sensor field are oriented toward this kind of

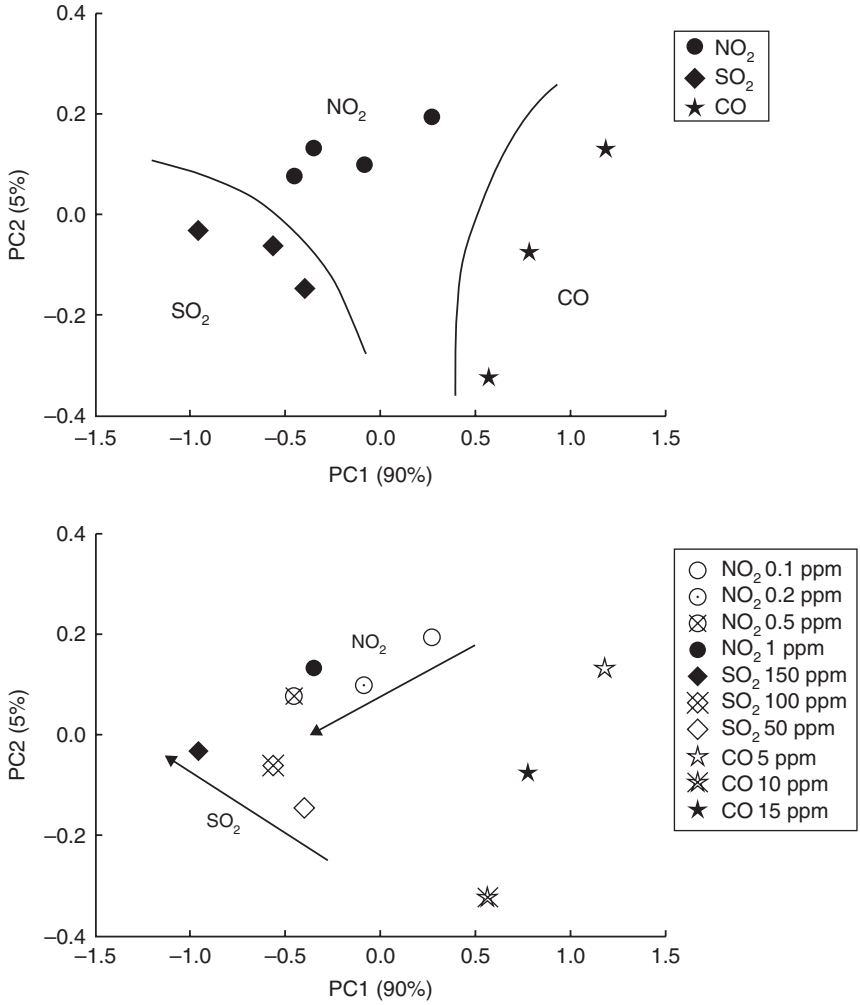

5.5 PCA chemical discrimination score plot of integrated gas sensor array. Top and bottom panels represents the PCA score plots for different gases, upper one simply showing the gases discrimination without concentration labelling; the bottom, PCA discrimination performance for different gases and different concentrations. (*Source*: Reprinted with permission from Adami *et al.*, 2006.)

nanometric structure. This is in order to investigate the real capabilities of these new low dimensional structures and to improve the performance of bulk and thin-/thick-film gas-sensor devices.

Several experimental techniques to prepare MOX NWs have been proposed and are well established. They can initially be classified as:

- Top-down approach
- Bottom-up approach.

The top-down approach is based on standard microfabrication methods, consisting of the reduction of the lateral dimensions of the films to nanometer size. When working with the top-down approach, Francioso and Siciliano (2006) focused on the implementation and experimental validation of a cheap top-down microfabrication process for large titania MOX NW arrays, electrically insulated on a silicon oxide mesa and micromachined by means of isotropic plasma processing (Fig. 5.6). This kind of NW array may be usefully implemented to realize gas-sensing experiments on the transport properties of MOX materials, as reported in Comini *et al*. (2002) and Faglia *et al*. (2005). Understanding a gas-sensor device based on MOX NWs may allow for localized modifications in terms of the charge-carrier population after additional exposure to the gas environment. Advantages of this can be seen in the use of the well-developed technology within the semiconductor industry and the ability to work on planar surfaces; however, its elevated costs and time-consuming processes are the main disadvantages. Furthermore, top-down processes still have problems creating structures smaller than 10 nm, and at the moment this technology does not fulfill the industrial requirements for the production of large numbers of low-cost devices. Additionally, the nanostructures produced with these techniques are generally polycrystalline.

The implementation of a cheap and fast process for producing nanometer-size semiconductor channels may result in a useful tool for this kind of structure; a 100 nm large gas-sensitive strip with lateral surfaces exposed

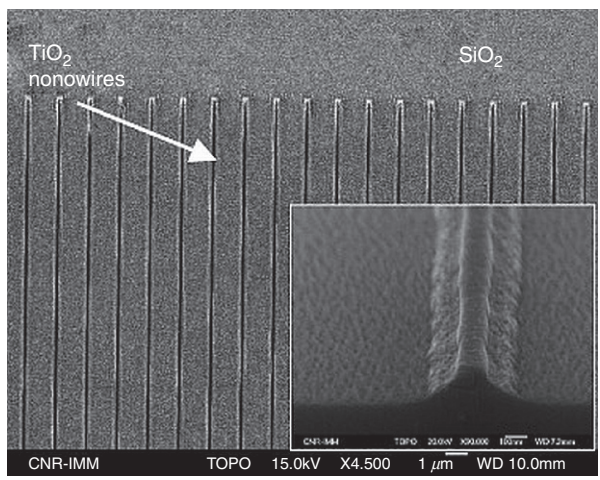

5.6 Top-down fabricated TiO_2 NWs. (*Source*: Reprinted with permission from Francioso and Siciliano, 2006.)

to gases may be affected by enhanced diffusion toward the so-called film 'sensing body,' resulting in improved responses (Sakai *et al*., 2001).

The bottom-up approach consists of chemical synthesis by vapor phase transport or chemical vapor deposition, electrochemical deposition, solution-based techniques, or template growth. One of the main disadvantages of this technique is the poor growth control and scarce integration capability into fully functional devices; also, the high temperature required for growth may be a limitation for process substrates or wafers with metals already on top. Advantages of this technique include the low cost of the experimental set-up, the reduced diameter of structures, and the high purity of materials. As pioneering work, Comini *et al*. (2002) detected ethanol (250 ppm, 400°C), NO_2 (0.50 ppm, 200°C), and CO (250 ppm, 400°C) by using heated single-crystal SnO_2 nanobelts. Many papers describing gas detection using different MOXs such as In_2O_3 (Lu and Fan, 2005; Zhou *et al*., 2009; Metha, 2010), TiO_2 (Rothschild, 2006; Francioso *et al*., 2008; Joshi *et al*., 2009), and ZnO (Ahn *et al*., 2008; Law and Thong, 2008; Yong and Kwak, 2008) have been published.

5.5 Metal oxide nanostructure surface modification and doping

In many gas sensors, the real response is determined by the efficiency of catalytic reactions with detected gas participation taking place at the surface of the gas-sensing material. As a result, the control of the catalytic activity of gas-sensor material is one of the most commonly used means of enhancing the performances of gas sensors. Noble metals are highly effective oxidation catalysts, and this capability can be used to enhance the reactions on gas-sensor surfaces. The pure SnO_2 thin film exhibits a very poor sensitivity (~3) without a catalyst (Haridas *et al*., 2008). From the point of view of the application of nanostructures for sensing properties' modification, MOX NWs have been chemically modified to achieve selectivity for a particular molecule or family of molecules.

Typically, two different approaches are adopted:

1. Doping of the semiconductor material.
2. Surface decoration by noble metals particles.

A wide diversity of methods, including impregnation, sol-gel, sputtering, and thermal evaporation, have been used to introduce noble metal additives into oxide semiconductors. A mixture of noble metal particles and MOXs may be obtained by the sol-gel method, while MOXs modified by noble metal particles on the surface may be obtained by sputtering or thermal evaporation. In the field of NW structures, the adoption of dopant elements

in a MOX NW and the subsequent modification of the function of SnO_2 NW-based ethanol sensors have been achieved (Wu, 2010) by p-doping the NWs with antimony. P-type NWs prepared by Wu (Wu, 2010) show an inverted response that is both rapid and highly sensitive, and has an observed limit of detection of 40 ppm.

The second method of modifying detection properties of MOXs, by physical deposition of transition metals, such as Pt or Pd, on sensing structures has a mass of reported literature. Lin *et al.* (2007) reported Pd decoration of ZnO NWs confers sensitivity to ethanol with a 5 ppm detection limit. Lee and co-workers (Hwang *et al.*, 2011a) studied the detection of ethanol at ZnO NW mats as a function of the loading of silver NPs onto these NWs (diameter 50–100 nm). These authors examined the sensor's selectivity to ethanol versus NH_3, H_2, and CO for three different silver loadings of the NWs (Fig. 5.7).

Significantly, an optimum silver loading controlled by electron-beam evaporation was observed in this study (Fig. 5.7b) in regard to both the sensor's sensitivity to ethanol and its selectivity for ethanol versus the other three gases. Response and recovery times were weakly affected by silver modification of the ZnO NWs; raw sensor-response data shows that the addition

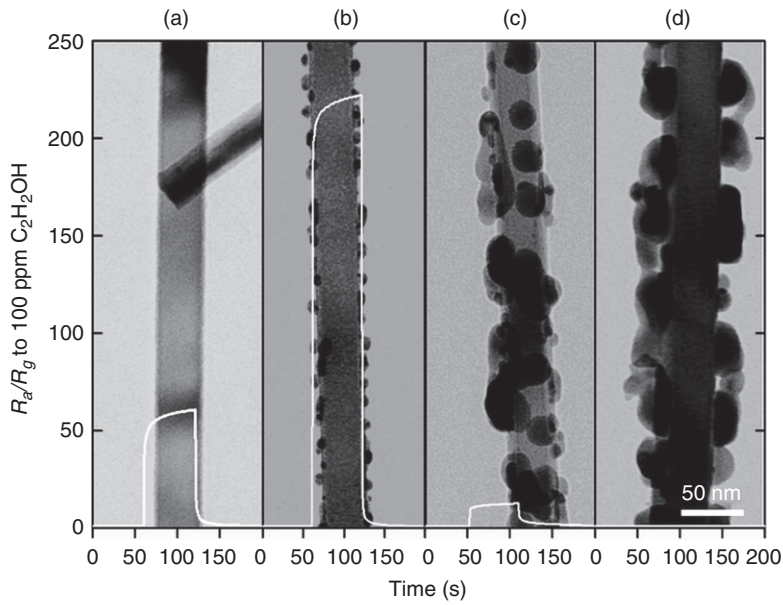

5.7 Transmission electron micrographs of (a) a pure SnO_2 NW, (b) a 5 Ag-SnO_2 NW, (c) a 10 Ag-SnO_2 NW, and (d) a 50 Ag-SnO_2 NW following heat treatment at 450°C for 2 h. (*Source*: Reprinted with permission from Hwang, 2011). Copyright (2011) American Chemical Society.)

of silver to the NW surface has an influence on the amplitude of the sensor response; however, the response and recovery times are unaffected. At the optimum silver loading (ZnO NWs decorated with a high density of 3–8 nm diameter silver nanoclusters) response to ethanol was about 228 at 100 ppm (versus 5–8 for the other three gases).

A relatively straightforward comparison can be made between typical thin-/thick-film-based chemiresistors and nanostructure-based ones, in order to highlight detection enhancement versus reliability and production cost.

Brunet *et al*. (2012) performed a comparison of detection performances between SnO_2 thin film and single crystalline SnO_2 NW sensors toward different gases, such as CO, CH_4, H_2, CO_2, SO_2, and H_2S.

At optimum operating temperature – varying from 250°C to 400°C – the SnO_2 thin film sensor detects CO, CH_4, CO_2, and SO_2 with responses in the range of 23–34%, and H_2 and H_2S with responses above 80%. The SnO_2 NW sensor shows responses in the range of 1–8% for CO, H_2, and SO_2, 29% for H_2S, while CH_4 and CO_2 are not detected (Fig. 5.8).

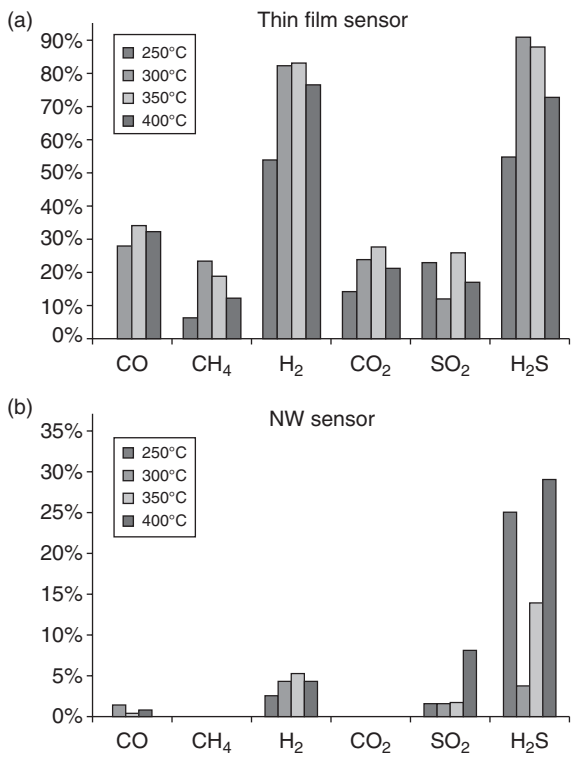

5.8 Temperature-dependent responses of (a) thin film and (b) NW sensors. (*Source*: Reprinted with permission from Brunet *et al.*, 2012.)

Authors estimated that in thin film sensors a single detected electron requires roughly 2760 gas molecules impinging on the sensor's surface, while for NW sensors only 86 gas molecules are required for a single detected electron. The SnO_2 NW sensor shows detection efficiency more than 30 times higher than the SnO_2 thin film sensor, probably due to a lack of grain boundaries (Brunet *et al.*, 2012). Zappa *et al.* (2011) investigated other materials as possible sensitive semiconductors for chemical detection, including prepared copper oxide NWs by thermal oxidation of metallic Cu thin layer deposited by RF sputtering on various substrates. The response of this alternative p-type sensing material, using a NW-based device, to various oxidizing and reducing target gases, has been evaluated by authors in order to check the functional properties of the CuO NWs as a chemical-sensing material.

Zappa *et al.* reported that the measured current decreased in the presence of reducing gases, a typical behavior observed for p-type oxide semiconductors. This observation is in line with the results of compositional and structural analyses, indicating the presence of p-type CuO as the main phase in the analyzed samples.

Nb-containing titania nanotubular arrays at room temperature by electrochemical anodization were investigated by Galstyan *et al.* (2012), and were, for the first time, gas-sensing characteristics of Nb-doped TiO_2 nanotubes; they were investigated and compared to those of undoped nanotubes. The functional properties of nanotubular arrays toward CO, H_2, NO_2, ethanol, and acetone were tested in a wide range of operating temperatures, and the introduction of Nb largely improves conductivity and enhances the gas-sensing performance of TiO_2 nanotubes.

The sensitive structures that can be realized and based on NWs of MOXs were also compared with sensing properties of NPs; I.S. Hwang *et al.* (2011b) realized a network of SnO_2 NWs gas sensors fabricated on a micro-electrode and heater suspended in a cavity. The gas response and the response speed of the SnO_2 NW sensor to 100 ppm C_2H_5OH were 4.6- and 4.7-fold greater, respectively, than those of the SnO_2 NPs sensors with the same electrode geometry. These enhanced gas-sensing characteristics were attributed to the rapid and effective diffusion of analyte gases through the porous SnO_2 NW network coated on the thermally insulated suspended hotplate.

Wang and co-workers (Sheng Xu *et al.*, 2010) have built a range of ZnO NWs in order to form a nanogenerator that can convert mechanical energy into a 1.2 V electrical output. Their fabrication method uses a low-temperature (<100°C) chemical process that can use flexible polymer substrates and is inexpensive to manufacture. Wang and co-workers measured a peak power density of 2.7 mW/cm^3.

5.6 Recent developments and future trends

This section will address recent results from the scientific community in the MOX sensor field, particularly the investigation of low dimensional exotic structures, the coupling of traditional MOX materials with strategic gallium nitride (GaN) or SiC semiconductors, and recent trends in hybrid structures, such as cutting-edge and interesting materials such as graphene. Different methods of investigating properties of NPs or NWs were looked into, including the possibility of growing low dimensional structures from different materials from MOXs that serve as structural devices, ready to be functionalized by chemical sensitive layers or coatings. Dobrokhotov *et al*. (2012) constructed chemical sensors for implementing novel nanomaterials (such as silica nanosprings) as structural devices. Authors coated the silica nanosprings with ZnO using atomic layer deposition (ALD) and decorated them with metal NPs. Working at optimum operational conditions ($T = 400°C$, ZnO grain size 15 nm), the nanospring-based sensors showed well-defined spikes in conductance upon exposure to explosives (trinitrotoluene, TNT and triacetone triperoxide, TATP) and flammable vapors. A complete and functional sensor array for simultaneous real-time resistance scans was realized and tested, and finally the linear discriminant analysis (LDA) data analysis method allowed for the identification of various chemical vapors at ppm level.

The most widely used MOX semiconductors (such as SnO_2) have been extensively tested and used as nanocomposites with graphene in lithium-ion storage and cataluminescence, but the gas-sensor performances of this composite has attracted attention from many research groups. Since its discovery, it has become clear that graphene is an interesting material, thanks to its electric and transport properties and the fact that it is characterized by high surface activity and sensitivity. F-L. Meng *et al*. (2012) developed an interesting study on the assembly of nanocomposites, where the SnO_2/graphene nanocomposite is composed of 4–5 nm SnO_2 NPs synthesized by a wet chemical method on graphene. Authors claimed that SnO_2/graphene nanocomposites showed an improved sensitivity to benzene, more than traditional tin oxide. The responses of this SnO_2/graphene nanocomposite to benzene reached an impressive 5 ppb detection limit.

As reported above for the nanospring-based detector, surface nanoclusters and NPs have been used as transducers for chemically inert NWs. Below is another example, as reported by R. Bajpai *et al*. (2012), who found a chemiresistor from GaN NWs functionalized with sputter-deposited tin dioxide (SnO_2) NPs. The authors used the change in photoconductivity of the hybrid SnO_2-nanocrystals/GaN-NW devices when exposed to analytes as a sensing function. The photoconductive properties of GaN and SnO_2 give a rapid response of this assembly compared to thin films, which enhances

the sensitivity and lowering response time. The UV illumination enables sensors to operate at room temperature instead of the typical 300–400°C operating temperature.

Hollow spheres are also considered to be a hot topic in nanostructures-based chemiresistors; both NiO and SnO_2 hollow structures are well-documented devices in literature. H-J. Kim (2012) prepared NiO and Fe-doped NiO hollow spheres with approximately 12 nm shell thickness by applying uniform coatings of Ni- and Fe-precursors onto Ni spheres, followed by partial oxidation of Ni spheres near their surfaces at 300°C and final core Ni dissolution.

The response to 100 ppm C_2H_5OH of Fe-doped NiO hollow spheres at 350°C ($R_g/R_a = 172.5$) was 31.4 times higher than that of NiO hollow spheres ($R_g/R_a = 5.5$). The reason for the significant improvement in C_2H_5OH response by doping Fe into NiO hollow spheres were discussed by the authors in relation to the incorporation of Fe components into the NiO lattice and their consequent impact on the gas-sensing reaction.

Nevertheless, the selectivity of these devices remains an open issue in the sensor field. Zhang *et al*. (2009) reported high selectivity of SnO_2 hollow spheres for NO_2 and reduced cross-sensitivity toward ethanol.

The impressive innovations in the field of NW and nanocomposite gas sensors, as reported in this chapter, open a new scenario of technological needs in terms of cost reduction and very low power consumption of devices, such as the single NWs of chemically sensitive materials that can work at room temperature or with few mW of power consumption to be heated at operating temperature. In a similar way, low power devices and sensor networks enable new solutions for monitoring environmental pollution. One of the required characteristics of sensor nodes is the low cost of devices, and costs can be drastically reduced when using printed electronics on foils/substrates such as polyimide, polyethylene naphthalate, or polyethylene-terephthalate (PET). Moving toward these kinds of substrates presents different advantages, such as flexibility, conformability, and wearing of complete sensor nodes.

Courbat *et al*. published examples of chemiresistor devices (Courbat *et al*., 2012) and examined highly miniaturized low power drop-coated MOX gas sensors on polyimide foil (Fig. 5.9). Drop-coating of SnO_2-based material was successfully achieved on transducers as small as 15 m on polyimide, and the sensors showed a very good chemo-resistive response when exposed to CO and NO_2.

In the area of realized sensors based on NWs, the main challenge for fabricating flexible devices using polymer-based substrates and oxide-based NWs lies in significantly different processing temperatures. As reported in literature, flexible devices using NWs require typically a two-step approach. First, NWs are synthesized on substrates that are resistant to high temperatures, then, after growth and dispersion of NWs in a solution, the NWs are transferred onto the flexible substrate and/or aligned in some way.

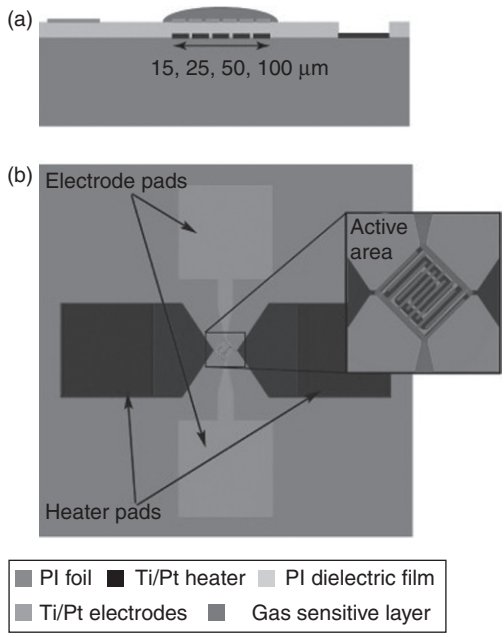

5.9 (a) Cross-sectional and (b) top schematic views of the drop-coated MOX gas sensor on polyimide foil. (*Source*: Reprinted with permission from Courbat *et al.,* 2012.)

To date, various patterning and transfer techniques to form NW arrays on the required substrates have been investigated, including contact printing, Langmuir–Blodgett, E-beam lithography, electric-field-assisted alignment, optical trapping, and micrometric ink-jet.

H-S. Woo *et al*. (2012) proposed a fast and cheap method for the fabrication of flexible devices with tin oxide NW; they used a commercial transparent polyester film with an acrylic adhesive to collect SnO_2-NW on a patterned Si substrate applying a controlled pressure. The film with the transferred NWs was fixed onto a glass substrate with the adhesive side facing upward, therefore using it as a support for silver contact deposition on NWs.

The reliability of the fabrication process, cost, and lifetime of these devices is a crucial challenge for chemiresistor innovation and for new applications to enter the field.

5.7 Sources of further information and advice

http://www.appliedsensor.com/
http://www.microsens.ch/

http://www.e2v.com/
http://www.neroxis.ch
http://www.aimsafety.com
http://www.biosystems.com
http://www.gasmonitors.com
http://www.crowcon.com
http://www.generalmonitors.com
http://www.honeywellanalytics.com
http://www.indsci.com
http://www.raesystems.com
http://www.rkiinstruments.com
http://www.scottinstruments.com
http://www.sierramonitor.com
http://bluestonegt.com/grat-filmtm
http://www.nanowerk.com/phpscripts/n_dbsearch.php
http://www.epluse.com/
http://www.sensorelectronics.com
http://english.hwsensor.com

5.8 References

Adami A., Lorenzelli L., Guarnieri V., Francioso L., Forleo A., Agnusdei G., Taurino A.M., Zen M. and Siciliano P. (2006) A WO_3-based gas sensor array with linear temperature gradient for wine quality monitoring, *Sensor. Actuat. B* **117**, 115–122.

Ahn M.W., Park K.S., Heo J.H., Park J.G., Kim D.W. *et al*. (2008) Gas sensing properties of defect-controlled ZnO-nanowire gas sensor, *Appl. Phys. Lett*. **93**, 263103.

Bajpaia R., Motayed A., Davydov A.V., Oleshko V.P., Aluri G.S., Bertnesse K.A., Rao M.V. and Zaghloula M.E. (2012) UV-assisted alcohol sensing using SnO_2 functionalized GaN nanowire devices, *Sensor. Actuat. B* **171–172**, 499–507.

Brunet E., Maier T., Mutinati G.C., Steinhauer S., Köck A., Gspan C. and Grogger W. (2012) Comparison of the gas sensing performance of SnO_2 thin film and SnO_2 nanowire sensors, *Sensor. Actuat. B* **165**, 110–118.

Chiba A. (1992) *Chemical Sensor Technology*, Vol. 4 Edn. Yamauchi S., Part 1 'Development of TGS gas sensor', ISBN 0-444-98680-4.

Choi K.J. and Jang H.W. (2010) One-dimensional oxide nanostructures as gas sensing materials: review and issues, *Sensors* **10** 4083–4099.

Comini E., Faglia G., Sberveglieri G., Pan Z. and Zhong L.W. (2002) Stable and highly sensitive gas sensors based on semiconducting oxide nanobelts, *Appl. Phys. Lett*. **81** 10.

Comini E., Baratto C., Faglia G., Ferroni M., Vomiero A. and Sberveglieri G. (2009) Quasi one dimensional metal oxide semiconductors: preparation, characterization and application as chemical sensors, *Prog. Mater. Sci.* **54** 1–67.

Courbat J., Briand D., Yue L., Raible S. and De Rooij N.F. (2012) Drop-coated metal-oxide gas sensor on polyimide foil with reduced power consumption for wireless applications, *Sensor. Actuat. B* **161** 862–868.

Currie J.F., Essalik A., and Marusic J.-C. (1999) Micromachined thin film solid state electrochemical CO_2, NO_2 and SO_2 gas sensors, *Sensor. Actuat. B* **59**, 235–241.

D'Amico A. and Di Natale C. (2001) A contribution on some basic definitions of sensors properties, *IEEE Sens. J.* **1**(3), 183.

Dobrokhotov V., Oakes L., Sowell D., Larin A., Hall J., Kengne A., Bakharev P., Corti G., Cantrell T., Prakashb T., Williams J. and McIlroy D.N. (2012) Toward the nanospring-based artificial olfactory system for trace-detection of flammable and explosive vapors, *Sensor. Actuat. B* **168**, 138–148.

Epifani M., Francioso L. and Siciliano P. (2007) SnO_2 thin films from metalorganic precursors, *Sensor. Actuat. B* **124**, 217–226.

Faglia G., Baratto C., Sberveglieri G., Zha M. and Zappettini A. (2005) Adsorption effects of NO_2 at ppm level on visible photoluminescence response of SnO_2 nanobelts, *Appl. Phys. Lett*. **86**, 011923.

Fine G.F., Cavanagh L.M., Afonja A. and Binions R. (2010) Metal oxide semiconductor gas sensors in environmental monitoring, *Sensors* **10**, 5469–5502.

Francioso L. and Siciliano P. (2006) Top-down contact lithography fabrication of a TiO_2 nanowire array over a SiO_2 mesa, *Nanotechnology* **17**, 3761–3767.

Francioso L., Taurino A.M., Forleo A. and Siciliano P. (2008) TiO_2 nanowires array fabrication and gas sensing properties, *Sensor. Actuat. B Chem*. **130**, 70–76.

Franke M.E., Koplin T.J. and Simon U. (2006) Metal and metal oxide nanoparticles in chemiresistors: does the nanoscale matter, *Small* **2**, 36–50.

Galstyan V., Comini E., Faglia G., Vomiero A., Borgese L., Bontempi E. and Sberveglieri G. (2012) Fabrication and investigation of gas sensing properties of Nb-doped TiO_2 nanotubular arrays, *Nanotechnology* **23**, 235706.

Gardner J.W. (1991) Detection of vapors and odors from multisensor array using pattern recognition, *Sensor. Actuat. B* **4**, 109–115.

Gopel W. and Schierbaum K.D. (1995) SnO_2 sensors: current status and future prospects, *Sensor. Actuat. B* **26–27**, 1–12.

Goschnick J.(2001) An electronic nose for intelligent consumer products based on a gas analytical gradient microarray, *Microelectron. Eng*. **57–58**, 693–704.

Haridas D., Gupta V. and Sreenivas K. (2008) Enhanced catalytic activity of nanoscale platinum islands loaded onto SnO_2 thin film for sensitive LPG gas sensors, *Bull. Mater. Sci*. **31**, 397–400.

Heilig A., Barsan N., Weimar U., Schweizer-Berberich M., Gardner J.W. and Gopel W. (1997) Gas identification by modulating temperatures of SnO_2-based thick film sensors, *Sensor. Actuat. B* **43**, 45–51.

Hwang I.S., Choi J.K., Woo H.S., Kim S.J., Jung S.Y. Seong T.Y., Kim I.D. and Lee J.H. (2011a) Facile control of C_2H_5OH sensing characteristics by decorating discrete Ag nanoclusters on SnO_2 nanowire networks, *Am. Chem. Soc. Appl. Mater. Interfaces* **3**, 3140–3145.

Hwang I.S., Lee E.B, Kim S.J., Choi J.K., Cha J.H., Lee H.J., Ju B.K. and Lee J.H. (2011b) Gas sensing properties of SnO_2 nanowires on micro-heater, *Sensor. Actuat. B* **154**, 295–300.

Ikohura K. and Watson J. (1994) *The Stannic Oxide Gas Sensor*, CRC Press, Boca Raton.

Joshi R.K., Hu Q., Am F., Joshi N. and Kumar A. (2009) Au decorated zinc oxide nanowires for CO sensing, *J. Phys. Chem. C* **113**, 16199–16202.

Kamp B. (2002) *Beitrage zur Sensorik Redox-aktiver Gase*, Ph.D. Thesis, University of Stuttgart.

Kanan S.M., El-Kadri O.M., Abu-Yousef I.A. and Kanan M.C. (2009) Semiconducting metal oxide based sensors for selective gas pollutant detection, *Sensors* **9**, 8158–8196.

Karapatnitski I.A., Mit K.A., Mukhamedshina D.M. and Beisenkhanov N.B. (2002) Optical, structural and electrical properties of tin oxide films prepared by magnetron sputtering, *Surf. Coat. Technol*. **151–152**, 76–81.

Kim H.J., Choi K.I., Kim K.M., Na C.W. and Lee J.-H. (2012) Highly sensitive C_2H_5OH sensors using Fe-doped NiO hollow spheres, *Sensor. Actuat. B: Chem* **171–172**, 1029–1037.

Kirner U., Schierbaum K.D., Göpel W., Leibold B., Nicoloso N., Weppner W., Fischer D. and Chu W.F. (1990) Low and high temperature TiO_2 oxygen sensors, *Sensor. Actuat. B* **1**, 103–107.

Korotcenkov G. and Cho B.K. (2011) Instability of metal oxide-based conductometric gas sensors and approaches to stability improvement (short survey), *Sensor. Actuat. B* **156**, 527–538.

Law J.B.K. and Thong J.T.L. (2008) Improving the NH_3 gas sensitivity of ZnO nanowire sensors by reducing the carrier concentration, *Nanotechnology* **19**, 205502.

Lee J.H. (2009) Gas sensors using hierarchical and hollow oxide nanostructures: overview, *Sensor. Actuat. B* **140**, 319–336.

Lin Y.R., Hsueh T.J., Chang S.J., Hsu C.L. and Chen I.C. (2007) Highly sensitive ZnO nanowire ethanol sensor with Pd adsorption, *Appl. Phys. Lett*. **91**, 053111.

Lu J.G. and Fan Z.Y. (2005) Gate-refreshable nanowire chemical sensors, *Appl. Phys. Lett*. **86**, 123510.

Maiti A., Rodriguez J.A., Law M., Kung P., McKinney J.R. and Yang P.D. (2003) SnO_2 nanoribbons as NO_2 sensors: insights from first principles calculations, *Nano Lett*. **3**, 1025–1028.

Mehta B.R., Kumar M., Singh V.N., Chatterjee R., Milikisiyants S., Lakshmi K.V. and Singh J.P. (2010) The role of stoichiometry of indium and oxygen on gas sensing properties of indium oxide nanostructures, *Appl. Phys. Lett*. **96**, 123114.

Meng F. Lli., H.H., Kong L.T., Liu J.Y., Jim Z., Li W., Jia Y., Liu J.H. and Huang X.J. (2012) Parts per billion-level detection of benzene using SnO_2/graphene nanocomposite composed of sub-6 nm SnO_2 nanoparticles, *Anal. Chim. Acta.* **736**, 100–107.

Moseley P.T. (1992) Materials selection for semiconductor gas sensors, *Sensor. Actuat. B* **6**, 149–156.

Moseley P.T. and Tofield B.C. (1987) *Solid State Gas Sensors*, Adam Hilger, Bristol.

Phillips H.M., Li Y., Bi Z. and Zhang B. (1996) Reactive pulsed laser deposition and laser induced crystallization of SnO_2 transparent conducting thin films, *Appl. Phys. A* **63**, 347–351.

Radecka M., Zakrzewska K. and Rekas M. (1998) SnO_2-TiO_2 solid solutions for gas sensors, *Sensor. Actuat. B* **47**, 194–204.

Rothschild A., Kim I.D., Lee B.H., Kim D.Y., Jo S.M. and Tuller H.L. (2006) Ultrasensitive chemiresistors based on electrospun TiO_2 nanofibers, *Nano Lett*. **6**, 2009–2013.

Sakai G., Matsunaga N., Shimanoe K. and Yamazoe N. (2001) Theory of gas-diffusion controlled sensitivity for thin film semiconductor gas sensor, *Sensor. Actuat. B* **80**, 125–131.

Savianu C., Arnautu A., Cobianu C., Craciun G., Flueraru C., Zaharescu M., Parlog C., Pasztic F. and Van den Berg A. (1999) Tin dioxide sol–gel derived films doped with platinum and antimony deposited on porous silicon, *Thin Solid Films* **349**, 29–35.

Seiyama T., Kato A., Fulishi K. and Nagatani M. (1962) A new detector for gaseous components using semiconductive thin films, *Anal. Chem*. **34**, 1502.

Sharma R. K. and Bhatnagar M. C. (1999) Improvement of the oxygen gas sensitivity in doped TiO_2 thick films, *Sensor. Actuat. B* **56**, 215–219.

Sharma R.K., Bhatnagar M.C. and Sharma G. L. (1998) Mechanism in Nb doped titania oxygen gas sensor, *Sensor. Actuat. B*, **46**, 194–201.

Sheng Xu, Yong Qin, Chen Xu, Yaguang Wei, Rusen Yang, Zhong Lin Wang (2010) Self-powered nanowire devices, *Nature Nanotechnology*, doi://10.1038/nnano.2010.46.

Shiraiwa M., Sosedova Y., Rouvière A., Yang H., Zhang Y., Abbatt J. P. D., Ammann M. and Pöschl U. (2011) The role of long-lived reactive oxygen intermediates in the reaction of ozone with aerosol particles, *Nat. Chem.* **3**, 291–295.

Shurmer H.V., Gardener J.W. and Corcoran P. (1990) Intelligent vapor discrimination using a composite 12-element sensor array, *Sensor. Actuat. B* **1**, 256–260.

Smith R.A. (1964) *Semiconductors*, Cambridge University Press.

Stryhal Z., Pavlik J., Novak S., Mackova A., Perina V. and Veltruska K. (2002) Investigations of SnO_2 thin films prepared by plasma oxidation, *Vacuum* **67**, 665–671.

Tricoli A., Righettoni M. and Teleki A. (2010) Semiconductor gas sensors: dry synthesis and applications, *Angew. Chem. Int. Ed.* **49**, 7632–7659.

Williams D.E.(1987) In: Moseley P.T., Tofield B.C. (Eds), *Solid State Gas Sensors*, Adam Hilger, Bristol, pp. 71–123.

Woo H.S., Hwang I.S., Na C.W., Kim S.J., Choi J.K., Lee J.S., Choi J., Kim G.T. and Lee J.H. (2012) Simple fabrication of transparent flexible devices using SnO_2 nanowires and their optoelectronic properties, *Mater. Lett.* **68**, 60–63.

Wu J.M. (2010) A room temperature ethanol sensor made from p-type Sb-doped SnO_2 nanowires, *Nanotechnology* **21**, 235501.

Xu C.N., Tamaki J., Miura N. and Yamazoe N. (1991) Grain-size effects on gas sensitivity of porous SnO_2-based elements, *Sensor. Actuat. B* **3**, 147–155.

Yamazoe N., Kurokawa Y. and Seiyama T. (1983) *Proc. of Int. Meet. Chem. Sens.*, 35.

Yamazoe N., Fuchigami J., Kishikawa M. and Seiyama T. (1979) Interactions of tin oxide surface with O_2, H_2O and H_2, *Surf. Sci*. **86**, 335.

Yang P.D., Law M., Kind H., Messer B. and Kim F. (2002) Photochemical sensing of NO_2 with SnO_2 nanoribbon nanosensors at room temperature, *Angew. Chem. Int. Ed*. **41**, 2405–2408.

Yong K.J. and Kwak G. (2008) Adsorption and reaction of ethanol on ZnO nanowires, *J. Phys. Chem. C* **112**, 3036–3041.

Zappa D., Comini E., Zamani R., Arbiol J., Morante J.R. and Sberveglieri G. (2011) Copper oxide nanowires prepared by thermal oxidation for chemical sensing, *Proc. Eng.* **25**, 753–756.

Zarcomb S. and Stretter J.R. (1984) Theoretical basis for identification and measurement of air contaminants using an array of sensors having partially overlapping sensitivities, *Sensor. Actuat. B* **6**, 225–243.

Zhang J., Wang S., Wang Y., Wang Y., Zhu B., Xia H., Guo X., Zhang S., Huang W. and Wu S. (2009) NO_2 sensing performance of SnO_2 hollow sphere sensor, *Sensor. Actuat. B* **135**, 610–617.

Zhou W.L., Zeng Z.M., Wang K., Zhang Z.X. and Chen J.J. (2009) The detection of H_2S at room temperature by using individual indium oxide nanowire transistors, *Nanotechnology* **20**, 045503.

6

Electropolymers for (nano-)imprinted biomimetic biosensors

A. YARMAN, Fraunhofer Institute for Biomedical Engineering, Germany and University of Potsdam, Germany,
A. P. F. TURNER, IFM-Linköping University, Sweden and
F. W. SCHELLER, Fraunhofer Institute for Biomedical Engineering, Germany and University of Potsdam, Germany

DOI: 10.1533/9780857096722.1.125

Abstract: Synthetic functional and cross-linking monomers may be electropolymerised in the presence of the target analyte to create polymers that mimic the active sites of biopolymers, e.g. antibodies, enzymes or nucleic acids. In a biomimetic sensor the molecularly imprinted polymer (MIP) must be in close proximity to the surface of the signal-generating electrode. By using electropolymerisation, thin MIP films can be obtained directly on the surface of the transducer. Integration of nanomaterials into the sensing layer has several advantages, such as increase of the surface area, mass transport and conductivity. These materials also provide a foundation for the electrochemical preparation of catalytically active MIPs.

Key words: molecularly imprinted polymer (MIP), electropolymerisation, biomimetic sensors, nanomaterials, enzyme mimics.

6.1 Introduction

Natural evolution has resulted in biopolymers based on amino acids and nucleotides, which display remarkable chemical selectivity and catalytic activity. Molecular recognition and catalytic conversion of the target molecules by antibodies and enzymes takes place in so-called epitopes or catalytic centres of the macromolecule, which comprise typically 10–15 amino acids. Nucleic acids bind complementary single-stranded nucleic acids by base pairing (hybridisation), but also interact highly specifically with proteins, e.g. transcription factors and low-molecular weight molecules, and even with ions.

The high specificity of biological macromolecules such as enzymes and antibodies has been exploited for more than 50 years, in clinical analysis, food processing and environmental analysis. More recently, alternative

biomimetic binders and catalysts have been generated using 'evolution in the test tube' of non-natural nucleotides or total synthesis of (molecularly imprinted) polymers. According to IUPAC: 'Biomimetic' refers to a laboratory procedure designed to imitate a natural chemical process and also to a compound that mimics a biological material in structure or function' (http://old.iupac.org/goldbook/BT06768.pdf).

Based on the technologies of laboratory analysers and test strips, a new generation of analytical tools, biosensors and biochips has been created. According to the IUPAC definition, a biosensor is an integrated receptor–transducer device, which is capable of providing selective quantitative or semi-quantitative analytical information using a biological recognition element (Thévenot *et al.*, 1999). The biosensor definition may be applied to biomimetic sensors which are based on (semi)synthetic and biomimetic recognition elements (Turner, 1989), e.g. 'minienzymes', synzymes, aptamers and molecularly imprinted polymers (MIPs).

6.2 Potential and limitations of molecularly imprinted polymers (MIPs)

In order to mimic the active sites of biopolymers, e.g. antibodies, enzymes or nucleic acids, synthetic functional and cross-linking monomers are copolymerised in the presence of the target analyte. In the pre-polymerisation mixture, the dissolved target interacts by covalent (pre-organised approach) or non-covalent (self-assembly approach) binding with the functional monomer. As conceptualised by Wulff, Shea and Mosbach (see below), this imprint molecule acts as a molecular template by the interaction with the complementary groups of the functional monomer and the cross-linker fixes the molecular image of the target molecules during copolymerisation. After polymerisation the template molecules are removed, providing binding sites ideally complementary in size, shape and functionality to the template, so that the template preferentially rebinds to the cavity (Fig. 6.1).

There are two main approaches as described above for the preparation of the pre-polymerisation complex in MIPs. In the covalent approach, which was introduced by Wulff and Sarhan (1972) and Shea and Thompson (1978), the template-functional monomer complex is formed by reversible covalent bonds. In order to remove the template, chemical bonds must be cleaved and binding occurs via the same covalent bonds (Tse Sum Bui and Haupt, 2010; Meier and Mizaikoff, 2011; Pietrzyk-Le *et al.*, 2011).

By contrast, in the non-covalent approach which was developed by Arshady and Mosbach, a complex between template and functional monomer is formed by non-covalent interactions such as hydrogen bonds, ionic bonds, van der Waals forces and hydrophobic interactions. This resembles the molecular recognition that occurs in nature. After polymerisation,

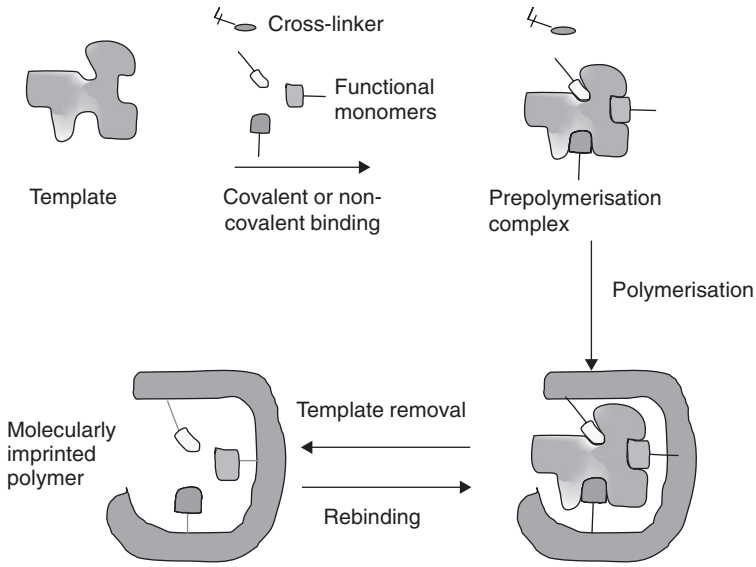

6.1 Schematic representation of the preparation of MIPs (Scheller and Yarman, 2012). (*Source*: With kind permission of Springer Science+Business Media.)

template molecules can be removed by simple solvent extraction. Binding of the analyte molecule is again obtained by the same non-covalent interactions. However, the yield of the binding sites is quite low in this method (Arshady and Mosbach, 1981; Tse Sum Bui and Haupt, 2010; Pietrzyk-Le *et al.*, 2011).

In practice the non-covalent approach is easier to apply and a larger variety of template molecules can be used, but in some respects the covalent approach is superior. The obvious advantage is that the monomer–template complex is stable and stoichiometric. This results in a more homogeneous population of binding sites. On the other hand, binding kinetics are slower as compared to non-covalent binding (Pérez-Moral and Mayes, 2006; Tse Sum Bui and Haupt, 2010; Meier and Mizaikoff, 2011).

To overcome the slow binding kinetics Whitcombe *et al.* have developed a procedure (called the semi-covalent approach) which is a hybrid of the two approaches described above. It is based on covalent bonds during the formation of the pre-polymerisation complex while rebinding of the template is by non-covalent interaction (Whitcombe *et al.*, 1995).

MIPs are easy to produce, more stable under harsh conditions such as high temperature, extreme pHs and organic solvents, and they are potentially cheaper to produce compared to biological molecules (Piletsky and Turner, 2006). Therefore, they have found applications as the stationary phase in chromatography (Sellergen and Shea, 1993; Nicholls *et al.*, 1995;

Turiel and Martin-Esteban, 2004), in solid-phase extraction (Sellergen, 1994; Andersson, 2000; Barahona *et al.*, 2011), environmental (Xie *et al.*, 2010) and clinical analysis (Viswanathan *et al.*, 2012), and also as recognition elements in sensors (Hedborg *et al.*, 1993; Haupt and Mosbach, 2000; Piletsky and Turner, 2008; Kang *et al.*, 2009; Berti *et al.,* 2010; Li *et al*., 2011).

Among the different formats for the preparation of MIPs, bulk polymerisation is most frequently used historically. This technique produces monolithic structures, which are then grounded and sieved. The most common functional monomers applied in thermal or photopolymerisation are methacrylic acid, vinylimidazole, vinylpyridine and their derivatives (Whitcombe *et al.*, 1995; Meier and Mizaikoff, 2011). The disadvantages of this method are that it is time consuming and slow binding kinetics is obtained. To overcome these drawbacks, other methods for the preparation of MIPs have been introduced including suspension, emulsion or precipitation polymerisation, which lead to the formation of micro- or nano-beads (Ansell and Mosbach, 1997; Meier and Mizaikoff, 2011); MIP nanomaterials such as nanoparticles (NPs), nanospheres (Ciardelli *et al.*, 2006; Guan *et al.*, 2008; Poma *et al.*, 2010; Yoshimatsu *et al.*, 2012); MIP nanomaterial composites (Díaz-Díaz *et al.*, 2012); self-assembled monolayers of thiols (Chou and Liu, 2005); and spreader-bar technique (Mirsky *et al.*, 1999). With the exception of the last two formats, the MIPs have to be immobilised on the transducer surface after preparation.

The first electrochemical MIP sensor was reported by Kröger *et al*. (1999). For the realisation of a biomimetic electrochemical sensor, the analyte recognition by the MIP must be in close proximity to the surface of the signal-generating electrode. The integration of MIPs to the transducers can be achieved by several methods, such as (i) drop-coating, spin coating or spray coating, (ii) preparation of composite membranes (iii) grafting and (iv) layer-by-layer-approach (Merkoçi and Alegret, 2002; Suryanarayanan *et al.,* 2010; Malitesta *et al.,* 2012; Sharma *et al.,* 2012).

6.3 Preparation and performance of molecularly imprinted electropolymers

In addition to the methods described above, electropolymerisation is an elegant way to prepare MIPs directly on the surface of a transducer, and one which provides some advantages. Such electrodes are quick and easy to prepare. Furthermore, highly reproducible results can be obtained by simply controlling the experimental conditions. For example, adjusting the charge passed during the electropolymerisation process allows control of the film thickness. In addition, the morphology of the surface can be controlled by the selection of an appropriate solvent and supporting electrolyte

(Suryanarayanan *et al.,* 2010; Meier and Mizaikoff, 2011 Malitesta *et al.*, 2012; Sharma *et al.*, 2012).

The first successful attempts to electropolymerise MIPs were performed by Malitesta *et al.* (1999) using o-phenylenediamine (o-PD) for the neutral template, glucose, and in the same year Panasyuk *et al.* used phenol for the template phenylalanine (Panasyuk *et al.,* 1999). Various different types of electroactive monomers or monomer mixtures have since been applied. Table 6.1 shows some examples of these monomers for the imprinting of low or high molecular weight substances. It is crucial to choose the right monomer according to the transducer applied. For example, for capacitive sensors, electrically insulating layers are preferred in order to improve the diffusion of the analyte to increase the sensitivity (Díaz-Díaz *et al.,* 2012). Therefore, monomers such as o-PD (Cheng *et al.,* 2001) or phenol (Blanco-López *et al.,* 2004) have been used to form non-conducting films for the imprinting of glucose and rifamycin SV, respectively.

In the case of MIP-sensors based on voltammetric or amperometric transduction, monomers which can either form non-conducting films or conducting films can be used. If a molecularly imprinted non-conducting film is formed, an electroactive template can be measured in three ways. The first method is based on direct measurement, in which signals are generated by diffusion of the template through the pores formed by the MIP process. However, some templates are not electroactive, in which case indirect measurement by using redox probes such as ferricyanide, or competitive assays can be applied. Upon filling of imprinted cavities by template molecules, the signal due to a redox probe is suppressed, i.e. an increase in the template concentration leads to a decrease in signal. In competitive assays, a non-electroactive competitor for electroactive templates, or an electroactive competitor for the non-electroactive templates, is used to compete with the template and this generates the signal (Liu *et al.,* 2009, 2011; Suryanarayanan *et al.,* 2010; Díaz-Díaz *et al.,* 2012).

6.3.1 Pyrrole

Pyrrole is one of the most frequently used monomers in electropolymerisation, since it can be used at neutral pH and its films are stable and compatible with various substrates. Electropolymerisation leads to the formation of conducting polymeric film (Fig. 6.2). However, high positive potentials lead to the overoxidation of the polymeric film and irreversible loss of the conductivity. Both polypyrrole and overoxidised polypyrrole have been applied in molecular imprinting for different templates such as caffeine (Ebarvia *et al.,* 2005), ascorbic acid (Özcan *et al.,* 2008), L-glutamic acid (Deore *et al.,* 1999), sodium dodecyl sulphate (SDS) (Albano and Sevilla, 2007), adenosine triphosphate (ATP) (Takeda *et al.,* 2008), paracetamol (Özcan

Table 6.1 MIP-sensors based on electropolymerisation

Functional monomer	Analyte/template	Electrochemical technique	Linear range(M), LOD(M)	Reference
o-PD	Triclosan	Amperometry	2×10^{-7}–3×10^{-6}, 8×10^{-8}	Liu *et al.*, 2009
o-PD	Oxytetracycline	Voltammetry	Up to 1×10^{-7}, 6.49×10^{-10}	Li *et al.*, 2010
o-PD	Glucose	QCM	Up to 20×10^{-3}	Malitesta *et al.*, 1999
o-PD/Resorcinol	Dopamine	Voltammetry	5×10^{-7}–4×10^{-5}, 13×10^{-4}	Song *et al.*, 2010
o-PD/Dopamine	L- and D- glutamic acid	Voltammetry, Capacitance	16.7×10^{-6}–250×10^{-6}, 5.9×10^{-6}	Ouyang *et al.*, 2007
Py	Paracetamol	Voltammetry	5×10^{-6}–5×10^{-4}, 7.9×10^{-7}	Özcan and Şahin, 2007
o-Py	L-aspartic acid	Piezoelectric microgravimetry	–	Syritski *et al.*, 2008
Phenol	Theophylline	Capacitance	Up to 15×10^{-6}, 10^{-6}	Wang *et al.*, 2007
o-AP	Dopamine	Voltammetry	2×10^{-8}–0.25×10^{-6}, 1.98×10^{-9}	Li *et al.*, 2009
m-AP	Tegafur	EIS and QCM	Up to 8×10^{-5}, ~10^{-5}	Liao *et al.*, 2004
EDOT	Morphine	Amperometry	0.1×10^{-3}–1×10^{-3}, 0.2×10^{-3}	Yeh and Ho, 2005
Aminophenyl boronic acid	D-fructose	Potentiometry	–	Deore and Freund, 2003
pABA	Melamine	Voltammetry, EIS	4.0×10^{-6}–4.5×10^{-4}, 3.6×10^{-7}	Liu *et al.*, 2011
Aminophenyl boronic acid	Lysozyme Cytochrome c	Voltammetry	Up to 37.5 mg L^{-1} Up to 60 mg L^{-1}	Rick and Chou, 2006
Pyrrole	Bovine haemoglobin	Voltammetry, EIS	–	Kan *et al.*, 2012
Phenol	Ovarian cancer antigen-125 (CA 125)	Voltammetry, EIS	0.5–400 U mL^{-1}, 0.5 U mL^{-1}	Viswanathan *et al.*, 2012

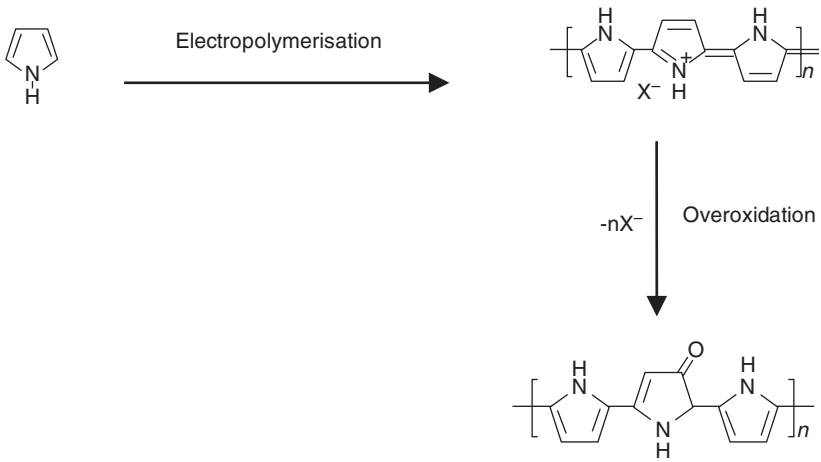

6.2 Electropolymerisation and overoxidation of pyrrole.

and Şahin, 2007), trichloroacetic acid (Suedee *et al.*, 2007) and biomacromolecules (Ramanaviciene and Ramanavicius, 2004; Namvar and Warriner, 2007).

In one approach, a caffeine-imprinted gold electrode was prepared using galvanostatic electropolymerisation of pyrrole monomers (Ebarvia *et al.,* 2005). Template molecules were removed with water and caffeine rebinding was detected with quartz crystal microbalance (QCM). The frequency shift increased linearly with the concentration of caffeine between 0.1 and 10 mg/mL. The sensitivity of the sensor was determined to be about 255 Hz/In concentration (mg/mL).

The first successful attempt with overoxidised polypyrrole was demonstrated by Deore *et al.* (1999) for the imprinting of L-glutamic acid. This approach was used by several later workers, for example, Percin Özkorucuklu *et al.* (2008) prepared sulphamethoxazole imprinted pencil graphite electrodes by using cyclic voltammetry with an overoxidised polypyrrole film in the presence of the supporting electrolyte tetrabutylammonium perchlorate (TBAP). Sulphamethoxazole was detected by differential pulse voltammetry (DPV) with a linear measuring range between 25×10^{-3} and 0.75 mM. The limit of detection (LOD) was determined to be 3.59×10^{-4} mM.

Ramanaviciene and Ramanavicius (2004) described an imprinted polymer for the bovine leukaemia virus (BLV) glycoprotein gp51 (gp51) on a platinum-black electrode applying 20 potential pulses between 950 (for 1 s) and 350 mV (for 10 s). Then gp51 was removed from the surface by 5 min. extraction with 1M H_2SO_4, followed by incubation in 0.1M phosphate buffer (pH 7.2) with 0.5 M KCl for at least 10 min. Pulse amperometry was applied to detect the protein up to 15 mg mL^{-1}. Another example for biological

imprinting is the determination of *Bacillus subtilus* endospores on a glassy carbon electrode (GCE) (Namvar and Warriner, 2007). The films were prepared as follows: GCEs were covered with polypyrrole, and endospores were then adsorbed onto this film. In the next step, 3-methylthiophene was potentiostatically electrodeposited on this layer. Endospores were removed by treating with dimethyl sulphoxide (DMSO). Rebinding studies were detected by electrochemical impedance spectroscopy (EIS) in $MnCl_2$ solution. However, regeneration of the MIP films was not possible.

6.3.2 Boronic acid derivatives

Selective interactions between boronic acid derivatives and vicinal diols have also been used in the molecular imprinting process, especially for saccharides and (glyco)proteins.

Deore and Freund (2003) described D-fructose imprinting by using 3-aminophenylboronic acid. Electropolymerisation was performed in the presence of fluoride at pH 5 or 7.4 by continuous sweeping between –0.1 and +1.0 V, until a cathodic charge of ~0.9 mC cm^2 was obtained. The last scan was stopped at +0.8 V and the potential held for 10 s. Then the template was removed by phosphate buffer for 24 h. Fluoride was used to disturb the intermolecular B-N interactions between monomers and resulted in complexation between the monomer and the template. It was found that the sensor was more sensitive to D-fructose as compared to D-glucose.

In another approach phenol was electropolymerised on an Au electrode in the presence of 3-hydroxyphenyl boronic acid–monosaccharide (D-glucose or D-mannose) complex under alkaline conditions (pH = 10.3) (Granot *et al.,* 2008). The analysis of the monosaccharides was based on a competitive electrochemical assay that employed ferrocene-modified monosaccharides as the redox label. Furthermore, enantioselective determination of D-glucose and L-glucose was shown.

Rick and Chou (2006) described lysozyme or cytochrome c imprinted electrodes by using electropolymerisation of p-aminophenylboronic acid (p-APBA) on a screen-printed Pt electrode at which the initial layer was polypyrrole and the second layer was poly(p-APBA). Electropolymerisation of pyrrole or p-APBA was performed by cyclic voltammetry. Proteins were extracted by washing in water containing glacial acetic acid (3%, v/v) and Tween®20 (0.1%, v/v). Rebinding studies showed two-phase binding profile of the respective proteins. However, RNAse A and myoglobin failed to produce imprinted sites when they were used as templates.

Apart from saccharides and proteins, 3-aminophenylboronic acid was used to prepare a toxin T-2 imprinted electropolymer on surface plasmon resonance (SPR) chips (Gupta *et al.,* 2011). The MIP showed a linear response for T-2 from 2.1 to 33.6 fM with a detection limit of 0.1 fM (0.05 pg/mL).

6.3.3 o-Phenylenediamine

Phenylenediamines are aniline derivatives whose properties differ from aniline. Reports showed that the electropolymerisation of o-PD is strongly affected by the polymerisation conditions such as pH and potential range (Camurri *et al.,* 2005). o-PD forms non-conducting film. Losito *et al.* (2003) formulated for the first time the mechanistic pathway for poly(phenylenediamine) formation at different pHs and potentials by using cyclic voltammetry and electrospray ionisation-ion trap mass spectrometry. According to this, the first stage of polymerisation is independent from the pH. Chain propagation by oxidative coupling competes with intramolecular oxidations, forming phenazine (at low pH and potential) or 1,4-benzoquinonediimine (at high pH and potential) units or both.

Liu *et al.* (2009) described a molecularly imprinted sensor on a GCE prepared by the electropolymerisation of o-PD for the detection of triclosan. Template could be removed by treatment of NaOH solution for 15 min. The response was linearly increased with triclosan concentration between 2.0×10^{-7} and 3.0×10^{-6} mol/L with a LOD of 8.0×10^{-8} mol/L. Furthermore, the response of the sensor was more influenced by smaller interfering substances than by larger ones.

Another example is the sensor for salicylic acid which was prepared by the electropolymerisation of o-PD by cyclic voltammetry on GCE (Kang *et al.,* 2009). Template was removed with sodium hydroxide solution. Rebinding studies were monitored by square wave voltammetry (SWV). The response of the sensor was linear between 6.0×10^{-5} and 1.0×10^{-4} mol/L with an LOD of about 2.0×10^{-5} mol/L. The sensor had a good selectivity to salicylic acid as compared to structurally similar interfering substances.

Electropolymerisation of o-PD with a functional co-monomer has also been successfully applied for the preparation of the MIP. Peng *et al.* (2000) described for the first time an atropine sulphate-imprinted sensor using o-PD with the co-monomer aniline. In this way branched chains could be produced, making the film more rigid and compact. Later the same copolymers were used for the imprinting of several substances, including paracetamol (Gómez-Caballero *et al.,* 2005). The response of this imprinted microsensor was linearly dependent on the concentration in the range between 6.5×10^{-6} and 2.0×10^{-3} M, with a good stability and reproducibility (RSD < 5.6%). In another piece of work, o-PD-dopamine co-monomers were used for the first time for the preparation of a glutamic acid imprinted sensor by electropolymerisation (Ouyang *et al.,* 2007). Furthermore, these are the first reported MIP capacitive sensors for the enantioselective determination of L- and D-glutamic acid. The response of the sensor was linearly dependent between 16.7 and 250 μM for both enantiomers.

In addition to the co-monomers with o-PD described above, Weetall and Rogers (2004) used resorcinol (Res) for the preparation and characterisation of imprinted electrodes for fluorescein, rhodamine and 2,4-dichlorophenoxyacetic acid (2,4-D). They found that the rhodamine-imprinted electrode was more sensitive to rhodamine as compared to fluorescein. Dyes were detected by fluorescence spectroscopy. 2,4-D was detected by SWV, but selectivity studies were not performed. Later the same group published a more detailed study on 2,4-D (Weetall *et al.*, 2005). The response of the imprinted electrode was found to be selective to 2,4-D in comparison to 2,4-dichlorophenol and benzoic acid. Fourier transform infrared spectroscopy (FTIR) studies showed that in the absence of the template H-bonding was significant in the o-PD-Res film. However, H-bonding was reduced when 2,4-D was doped to the film and template removal was not demonstrated.

In 2010, Song *et al.* successfully prepared a dopamine (DA)-imprinted sensor by using a mixture of o-PD with resorcinol by electropolymerisation. The response of the sensor was linearly dependent with the DA concentration between 5.0×10^{-7} M and 4×10^{-5} M with a LOD of 0.13 μM (S/N = 3).

6.3.4 Scopoletin

Scopoletin is a naturally occurring coumarin derivative which was established as an electromonomer by Gajovic-Eichelmann *et al.* in 2003 (Fig. 6.3). It offers some advantages over pyrrole, such as good solubility of the monomer in aqueous solution, no pre-purification or the deoxygenation of the monomer solution, and hydrophilicity of the deposited polymer.

Based on Shea's approaches, a new molecular imprinting workflow which combines the concepts of epitope imprinting, surface imprinting and electropolymerisation was demonstrated by the group of Scheller (Dechtrirat *et al.*, 2012). Cytochrome c was imprinted using its C-terminal nona-peptide as the template. The imprinted polymer film was grown directly on the electrode surface, including all processing steps. This facilitated the integration with electrochemical, SPR or QCM transducers. The imprinted, thin (6.7 nm, by ellipsometry), hydrophilic poly-scopoletin film possessed a moderately high affinity towards the imprinted peptide (Kd = 2.5 μM), and cytochrome c was detected in buffered solution in the micromolar concentration range in aqueous solution.

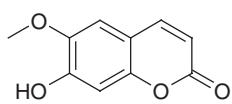

6.3 Structure of scopoletin.

6.3.5 Thiophene derivatives

Thiophene and its derivatives are also frequently used monomers for the preparation of molecularly imprinted electropolymers due to their high conductivity, chemical and mechanical stability (Sharma *et al.,* 2012). They have been used for either low-molecular weight substances such as DA, morphine, atrazine, folic acid, histamine, adenine, or high molecular substances such as *Bacillus subtilus* endospores, living cells (Malitesta *et al.,* 2012; Sharma *et al.,* 2012).

Yeh and Ho prepared potentiostatically a MIP-based indium tin oxide (ITO) electrode for the amperometric detection of morphine by using 3,4-ethylenedioxythiophene (EDOT) as a functional monomer (Yeh and Ho, 2005). Since poly(3,4-ethylenedioxythiophene) poly(styrenesulphonate) (PEDOT) is electroactive, it catalyses the oxidation of morphine. Furthermore, the sensor could discriminate between morphine and its analogues, such as codeine. Later the same group developed a microfluidic system containing a MIP for the detection of morphine by the electropolymerisation of EDOT on a microelectrode (Weng *et al.*, 2007). In one set up, Nylon 6 was incorporated into the MIP in order to prevent the interference of ascorbic acid. It was shown that the developed morphine–MIP microfluidic system successfully detected morphine in the concentrations ranging from 0.01 to 0.2 mM.

In another work, Pernites *et al.* (2011) developed an ultrathin film SPR sensor for the detection of the drugs paracetamol, naproxen and theophylline, using terthiophene and carbazole monomers. A novel feature was the application of a constant potential during the template removal procedure. This washing process was postulated to improve the template removal especially in the case of paracetamol. Furthermore, MIP films showed a greater binding response to the original imprinted molecule and only a limited response to the other analytes.

6.4 Combination of analyte-binding MIPs with nanomaterials

Electropolymerisation can be used to obtain thin MIP films, but the sensitivity of these sensors is limited. The amount of effective imprinted sites can be increased by increasing the thickness, but this can lead to slow diffusion of the analytes to the recognition sites and inefficient communication with the transducers (Riskin *et al.*, 2008). This drawback can be overcome by using nanomaterials. Integration of nanomaterials into the sensing systems has several advantages, such as increase of the surface area, mass transport, conductivity and improving the signal-to-noise ratio (Willner and Katz, 2005; Vamvakaki *et al.,* 2007; Pingarrón *et al.,* 2008; Campbell and Compton, 2010;

Table 6.2 Combination of nanomaterials with molecularly imprinted electropolymers

Electrode configuration	Analyte/template	Electrochemical technique	Linear range(M), LOD(M)	Reference
PQu-PRe-AuNP/GCE	Methyl parathion	EIS, voltammetry	7×10^{-8}–1×10^{-6}, 3.4×10^{-10}	Li *et al.*, 2012a
AuNPs-TL-PoAT/Au	Tolazoline	Voltammetry, EIS	0.05–5.0 $\mu g L^{-1}$ and 5–240 $\mu g L^{-1}$, LOD: 0.016 $\mu g L^{-1}$	Zhang *et al.*, 2010
AuNPs/MIP/GCE	Theophylline	Voltammetry, EIS	4×10^{-7}–1.5×10^{-7} and 2.4×10^{-4}–3.4×10^{-3}, LOD: 1×10^{-7}	Kan *et al.*, 2010
AgNPs-PoPD/GCE	Dimethoate	Voltammetry, EIS	1–1000 ng mL^{-1} and 1–5 $\mu g mL^{-1}$, LOD: 0.5 ng mL^{-1}	Du *et al.*, 2008
PATP-AuNP/PATP/Au	TNT	SPR, voltammetry, amperometry	LOD: 2×10^{-10}	Riskin *et al.*, 2008
PATP-AuNP-GCE	Chlorpyrifos	Voltammetry	5×10^{-7}–1×10^{-5}, 3.3×10^{-7}	Xie *et al.*, 2010
MIPs/MWCNTs/GCE	Dopamine	Voltammetry, EIS	6.25×10^{-7}–1×10^{-4}, 6×10^{-8}	Kan *et al.*, 2012
CNT-MIPPy	Caffeine	Potential pulse, amperometric pulse	–	Choong *et al.*, 2009
PHP/AuNP/CNT/GCE	Triazophos	Voltammetry	2×10^{-7}–1×10^{-5}, 9.3×10^{-8}	Li *et al.*, 2012b
HA-MWCNTs/PPy-SG/GCE	Tryptamine	Chronoamperometry, voltammetry, EIS	9×10^{-8}–7×10^{-5}, 7.4×10^{-8}	Xing *et al.*, 2012
CS-PtNPs /GR-AuNPs/MIP-AuNPs /Au	Erythromycin	Voltammetry, amperometry	7×10^{-8}–9×10^{-5}, 2.3×10^{-8}	Lian *et al.*, 2012

Feng and Ji, 2011; Kuila *et al.,* 2011; Ratinac *et al.,* 2011). Different nanomaterials, such as NPs, carbon nanotubes (CNTs) and graphene (GP) which have been used to immobilise biological substances, have also been applied to MIP film-based sensors (Table 6.2).

6.4.1 Nanoparticles

Much work has been performed with metallic NPs which are generally defined as isolable particles between 1 and 50 nm in size. Protecting shells are used to prevent the agglomeration of the particles. They have different chemical, physical or electronic properties due to their small size as compared with the bulk metals (Wang, 2005). Among these metallic NPs, AuNPs have been used most frequently. Different approaches have been applied for the preparation of molecularly imprinted electropolymer-nanoparticle combinations.

Li *et al.* (2012a) deposited AuNPs on a GCE and performed the electropolymerisation in a mixture of quercetin (Qu) and resorcinol (Re) for the imprinting of methyl parathion. The presence of AuNPs increased the response of imprinted PQu-PRe-AuNP/GCE (P=Poly) 2.6-fold as compared with the imprinted PQu-PRe/GCE in the absence of AuNPs. The LOD for imprinted PQu-PRe-AuNP/GCE was approximately one order of magnitude lower than the imprinted PQu-PRe/GCE.

In another approach, electropolymerisation was performed in the presence of the template, followed by template removal and deposition of AuNPs (Kan *et al*., 2010; Zhang *et al*., 2010). For example, Kan *et al.* (2010) described a theophylline-imprinted electrode using o-PD as monomer. Two linear ranges were obtained (Table 6.2) with a 10 μM LOD. Furthermore, the sensor was selective towards structurally similar substances and was applied in real samples. A similar approach was applied by Du *et al.* (2008) using silver NPs for the detection of dimethoate.

Willner's group developed a sensitive and selective method for the detection of trinitrotoluene (TNT) combining functionalised AuNPs with molecular imprinting technique (Riskin *et al.,* 2008). Figure 6.4 illustrates this technique. (However, the size of template and AuNPs in the figure does not reflect the almost ten-fold larger dimensions of the NPs!). At first, an Au electrode was modified by using p-aminothiophenol (PATP), which decreased the LOD from 10 μM (on bare Au) to 74 nM. In order to further increase the sensitivity of the electrode, AuNPs (functionalised with PATP and 2-mercaptoethane sulphonic acid) were electropolymerised on a PATP modified gold electrode. A 2 nM LOD was obtained by this modification. In the last modification, the MIP was formed by electropolymerisation in the presence of the TNT analogue picric acid. The LOD was determined to be

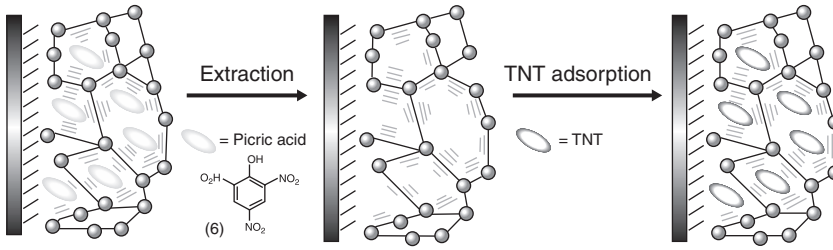

6.4 TNT imprinted electrode. (*Source*: Reprinted with permission from Riskin *et al.,* 2008. Copyright (2012) American Chemical Society.)

200 pM, which showed that the imprinting process not only increased the sensitivity, but also the selectivity of the electrode to the analyte TNT (20-fold more selective to TNT than dinitrotoluene and mononitrotoluene) was increased. Furthermore, the same group used bis-aniline-cross-linked AuNPs to imprint amino acids (Frasconi *et al.,* 2010) and boronic acid-bisaniline-cross-linked AuNPs to imprint antibiotics (Riskin *et al.,* 2010) (Table 6.2).

Xie *et al.* (2010) reported the detection of chlorpyrifos (CPF) by a surface assembly strategy for electropolymerised molecular imprinting at the AuNP modified GCE. The imprinted electrode was prepared as follows: electrodeposition of AuNPs on GCE, self-assembly of PATP on that layer for 24 h, incubation in CPF solution for 6 h, followed by the electropolymerisation in a solution containing PATP and CPF and removal of the template molecules. The presence of AuNPs increased the cyclic voltammetry (CV) response of the imprinted electrode 3.2-fold as compared with CPF-imprinted PATP/Au and the LOD was two orders of magnitude lower than for the latter CPF-imprinted electrode.

6.4.2 Carbon nanomaterials

Like NPs, carbon nanostructures are ideal for sensor preparation for molecularly imprinted electropolymer films. The carbon family includes 0 dimensional (0D) fullerenes, 1D CNTs, 2D GP, and 3D graphite (Geim and Novoselov, 2007).

Since their discovery in 1991, carbon nanotubes have been widely used. Nanotubes are composed of sp^2 hybrid carbon atoms arranged in hexagons, which form a layer of graphite and in turn, fold to a cylindrical sheet. Depending on their structures they are divided into two groups: single-walled carbon nanotubes (SWCNT) and multi-walled carbon nanotubes (MWCNT). Their tensile strength is 100-fold higher than that of steel and their thermal conductivity is higher than that of diamond. Furthermore, they have similar electrical conductivity to copper (Vamvakaki *et al*., 2007).

Among the other sensor applications, CNTs were also used for the molecular imprinting process. For example, Kan *et al.* (2012) used carboxyl functionalised multi-walled CNTs. These were electrodeposited on a GCE before electropolymerisation of pyrrole in the presence of the template, DA, for molecular imprinting. The LOD of the sensor was determined to be 6.8×10^{-8} M. Furthermore, the sensor showed good selectivity in the presence of epinephrine, ascorbic acid and uric acid.

Cai *et al.* (2010) developed human ferritin (hFtn) and the human papillomavirus E7 protein imprinted nanosensors on the tips of a carbon nanotube array by electropolymerisation of phenol. Rebinding studies were performed by EIS. Addition of hFtn in the concentration range from 1×10^{12} to 1×10^{-7} g L^{-1} revealed a concentration-dependent increase in impedance. Furthermore, analysis revealed the detection of the E7 protein at sub-pg L^{-1} levels. Human papillomavirus E6 protein (type-16) did not give a response to the E7 imprint electrode.

After the discovery of GP in 2004, by Novoselov and Geim, it also found application in sensor configurations (Shao *et al.*, 2010; Kuila *et al.*, 2011; Ratinac *et al.*, 2011). The idealised structure of GP is completely two-dimensional, comprising a single layer of carbon atoms joined by sp^2 covalent bonds to form a flat hexagonal lattice (Ratinac *et al.*, 2012). GP composites have also been used for the preparation of MIP-based sensors (Mao *et al.*, 2011).

6.4.3 Combination of different nanomaterials

In order to enhance the sensitivity and selectivity, different nanomaterials were combined to develop sensors based on electropolymerised MIPs. Some examples are described below.

A gold nanoparticle carbon nanotube-modified GCE was used to detect the pesticide triazophos (TAP) (Li *et al.*, 2012b). The electrode was prepared by the deposition of gold NPs on a CNT-modified GCE followed by the electropolymerisation of o-hydroxyphenol in the presence of triazophos via cyclic voltammetry. The cyclic voltammetric response of triazophos on this imprinted electrode was determined to be 10-fold higher than AuNP/CNT/GCE and 2.8-fold higher than the imprinted electrode prepared in the absence of AuNPs. Furthermore, the sensor showed selectivity to TAP over some other pesticides.

Xing *et al.* (2012) used GP with CNTs to detect tryptamine. The imprinted composite PolyPy-SG/HA-MWCNT/GCE was prepared as follows: after dropping sulphonated graphene (SG) on the pretreated GCE, pyrrole was electropolymerised on that layer (SG-PPy/GCE). Then SG-PPy/GCE was modified by casting a hyaluronic acid (HA)-MWCNT composite. The imprinted electrode was prepared on this electrode by electropolymerisation of p-aminobenzoic acid in the presence of tryptamine. According to

the amperometric measurements, the current linearly increased between 9×10^{-8} M and 7×10^{-5} M with a LOD of 7.4×10^{-8} M.

Recently, Lian *et al.* (2012) described a method for the detection of erythromycin using a combination of GP-AuNPs and chitosan (CH)-PtNPs. An Au electrode was modified with CH-PtNPs and GP-AuNPs successively by drop-coating. Erythromycin and the monomer, 2-mercaptonicotinic acid (MNA), (at pH 4) were self-assembled for 24 h on this layer. After that, the modified electrode was electropolymerised in $HAuCl_4$, MNA and the template solution to form a MIP. The template was removed by ethanol. It was found that the presence of AuNPs during MIP formation enhanced the response of the sensor and that the sensor was selective over three structurally analogues. Furthermore, analytical performance of the sensor was investigated by amperometry (Table 6.2) and applied to real samples.

6.5 Integration of analyte recognition with catalysis in MIPs

As an alternative to the generation of catalysts on the basis of amino acids, the concept of catalytically active antibodies (abzymes) has been transferred to totally synthetic MIPs. In analogy to the generation of abzymes, stable analogues of the postulated transition state (TSA) of the catalysed reaction are used as the template to mimic the active centre of the enzyme. (Wulff, 1995; Lettau *et al*., 2006). Another approach is the incorporation of transition metals or mimics of the catalytic centre of enzymes. (Sode *et al*., 2003; Cheng *et al.*, 2004; de Jesus Rodrigues Santos *et al*., 2007; Lakshmi *et al*, 2009; Díaz- Díaz *et al*., 2011).

Only a few sensor configurations based on catalytically active MIPs have been published to date. Lakshmi *et al.* (2009) developed an electrochemical sensor for catechol and DA using hybrid materials which was capable of oxidising the template. In this approach, a first conducting layer on a gold electrode was formed from a new monomer, N-phenylethylene diamine methacrylamide. After this the MIP was grafted by UV light from a monomer solution containing Cu^{2+}. The Cu^{2+} containing MIP mimics the active site of the enzyme tyrosinase, which can oxidise catechol. The signals increased linearly up to 144 μM with a LOD of 228 nM in the presence of atmospheric oxygen. This group (Berti *et al.*, 2010) went on to graft the same MIP on electrochemically grown conductive polyaniline nanotubes. As compared with the macroscopic electrode, the lower LOD was decreased by one order of magnitude (29 nM). Below 10 μM of catechol, no discernible difference in the catechol signal for the MIP and the non-imprinted polymer (NIP) modified electrodes could be observed. No detectable interference by resorcinol, hydroquinone and serotonin in the potential window of catechol oxidation

was found. The regeneration of the MIP sensor required the removal of the immobilised catechol with ethylenediaminetetraacetic acid (EDTA) and the re-loading of the MIP-catalyst with Cu(II).

Kubota's group (Neto *et al*., 2011) covered a GCE with a suspension of the heme-based bulk polymer. Methacrylic acid was used as functional monomer and p-aminophenol (pAP) as the template. Under optimised conditions the sensor responded linearly to pAP between 10 and 90 μM with a LOD of 3 μM and surprisingly no interfering signals were found for o-AP, catechol and guaiacol. A GP oxide modified screen-printed electrode has been grafted with a heme-containing MIP for the determination of the cancer marker 5-hydroxyindoleacetic acid (5-HIAA). The heme-catalysed oxidation of 5-HIAA produces a product, which is electroactive at lower potential. By using DPV a lower LOD of 36 μM was achieved (Antuña-Jiménez *et al.,* 2012).

Recently, a novel combination of a molecularly imprinted electropolymer with the minienzyme-microperoxidase-11 (MP-11) or horseradish peroxidase (HRP) as a catalyst was reported (Yarman *et al.* 2012). The peroxide-dependent conversion of the analgetic drug aminopyrine occurred in a layer on top of a product-imprinted electropolymer on the indicator electrode. This architecture allowed the optimisation of both parts before combining them in a hierarchical architecture. The amperometric responses for aminopyrine linearly increased between 1 and 13 μM with a regression coefficient of 0.9957 and with a LOD of 190 nM. The interference from ascorbic was completely suppressed by the action of the MIP layer and oxidation with peroxide. An advantage of this new hierarchical structure is the separation of MIP formation by electropolymerisation and immobilisation of the catalyst. This combination has the potential to be transferred to other enzymes, e.g. Cytochrome P450, opening up a way to measure other clinically important analytes.

6.6 Conclusion and future trends

The generation of MIPs on the basis of electropolymers offers several advantages such as straight forward procedure by one-step preparation, control of thickness and spatial addressability. On the other hand, the restriction in the thickness of the MIP layer and the signal generation at the electrode surface limits the number of 'separation plates' as compared with MIP columns containing bulk polymers.

The integration of nanomaterials into the imprinted electropolymer leads to a marked increase of the 'active surface'. This advantage has been elegantly demonstrated by Willner's group for several low-molecular weight analytes.

On the other hand, the number of MIPs based on electropolymers for proteins is still very small. In this field electro-inactive silane-based or acrylic

monomers dominate and the loading of the transducer requires a successive grafting procedure. The integration of nanomaterials with MIPs for biopolymers is still at an early stage. A key problem is the accessibility of the binding cavities for the macromolecules during template removal and rebinding. The modification of the electrode surface with conductive nanofilaments or nanocavities could lead to pronounced improvements.

For catalytically active MIPs, the integration of nanomaterials enhances the specific activity, as demonstrated by grafting of polyaniline (PANI) filaments. These principles should also work for the electrochemical preparation of catalytically active MIPs.

6.7 References

Albano, D.R. and Sevilla, F. III (2007) 'Piezoelectric quartz crystal sensor for surfactant based on molecularly imprinted polypyrrole', *Sens Act B-Chem,* **121**, 129–134.

Andersson, L.I. (2000) 'Molecular imprinting for drug analysis: A review on the application of molecularly imprinted polymers to solid-phase extraction and binding assay', *J Chromatogr B Biomed Sci Appl,* **739**, 163–173.

Ansell, R.J. and Mosbach K. (1997) 'Molecularly imprinted polymers by suspension polymerisation in perfluorocarbon liquids, with emphasis on the influence of the porogenic solvent', *J Chromatogr A* **787**, 55–66.

Antuña-Jiménez, D., Blanco-López, C., Miranda-Ordieres, A.J., Tuñón-Blanco, P. and Lobo-Castañón, M.J. (2012) 'Electrochemical detection of 5-hydroxyindoleacetic acid based on magnetic catalytic MIP at nanostructured electrodes', 14th International Conference on Electroanalysis, Slovenia.

Arshady, R. and Mosbach K. (1981) 'Synthesis of substrate-selective polymers by host-guest polymerization', *Makromol Chem,* **182**, 687–692.

Barahona, F., Turiel, E. and Martin-Esteban, A. (2011) 'Molecularly imprinted polymer grafted to porous polyethylene frits: A new selective solid-phase extraction format', *J Chromatogr A,* **1218**, 7065–7070.

Berti, F., Todros, T., Lakshmi, D., Whitcombe, M.J., Chianella, I., Ferroni, M., Piletsky, S.A., Turner, A.P.F. and Marrazza, G. (2010) 'Quasi-monodimensional polyaniline nanostructures for enhanced molecularly imprinted polymer-based sensing', *Biosens Bioelectron,* **26**, 497–503.

Blanco-López, M.C., Gutiérrez-Fernández, S., Lobo-Castañón, M.J., Miranda-Ordieres, A.J. and Tuñón-Blanco P. (2004) 'Electrochemical sensing with electrodes modified with molecular imprinted polymer films', *Anal Bioanal Chem*, **378**, 1922–1928.

Cai, D., Ren, L., Zhao, H., Xu, C., Zhang, L., Yu, Y., Wang, H., Lan, Y., Roberts, M.F., Chuang, J.H., Naughton, M.J., Ren, Z. and Chiles, T. (2010) 'A molecular-imprint nanosensor for ultrasensitive detection of proteins', *Nat Nanotech,* **5**, 597–601.

Campbell, F.W. and Compton, R.G. (2010) 'The use of nanoparticles in electroanalysis: an updated review', *Anal Bioanal Chem,* **396**, 241–259.

Camurri, G., Ferrarini, P., Giovanardi, R., Benassi, R. and Fontanesi, C. (2005) 'Modelling of the initial stages of the electropolymerization mechanism of the o-phenylenediamine', *J Electroanal Chem,* **585**, 181–190.

Cheng, Z., Wang, E. and Yang, X. (2001) 'Capacitive detection of glucose using molecularly imprinted polymers', *Biosens Bioelectron,* **16**, 179–185.

Cheng, Z., Zhang, L. and Li, Y. (2004) 'Synthesis of an enzyme-like imprinted polymer with the substrate as the template, and its catalytic properties under aqueous conditions', *Chem Eur J,* **10**, 3555–3561.

Choong, C.-L., Bendal, J.S. and Milne, W.I. (2009) 'Carbon nanotube array: A new MIP platform', *Biosens Bioelectron,* **25**, 625–656.

Chou, L.C.-S. and Liu, C.-C. (2005) 'Development of a molecular imprinting thick film electrochemical sensor for cholesterol detection', *Sensor Actuat B-Chem,* **110**, 204–208.

Ciardelli, G., Borrelli, C., Silvestri, D., Cristallini, C., Barbani, N. and Giusti, P. (2006) 'Supported imprinted nanospheres for the selective recognition of cholesterol', *Biosens Bioelectron,* **21**, 2329–2338.

Dechtrirat, D., Jetzschmann, K.J., Stöcklein, W.F.M., Scheller, F.W. and Gajovic-Eichelmann. (2012) 'Protein rebinding to a surface-confined imprint', *Adv Funct Mater*, **22**(24), 5231–5237, doi: 10.1002/adfm.201201328.

Deore, B., Chen, Z. and Nagaoka, T. (1999) 'Overoxidized polypyrrole with a dopant complementary cavities as a new molecularly imprinted matrix', *Anal Sci*, **15**, 827–828.

Deore, B. and Freund, M.S. (2003) 'Saccharide imprinting of poly(aniline boronic acid) in the presence of fluoride', *Analyst,* **128**, 803–806.

Díaz-Díaz, G., Antuña-Jiménez, D., Blanco-López, M.C., Lobo-Castañón, M.J., Miranda-Ordieres, A.J. and Tuñón-Blanco, P. (2012) 'New materials for analytical biomimetic assays based on affinity and catalytic receptors prepared by molecular imprinting', *Trends Anal Chem*, **33**, 68–80.

Du, D., Chen, S., Cai, J., Tao, Y., Tu, H. and Zhang, A. (2008) 'Recognition of dimethoate carried by bi-layer electrodeposition of silver nanoparticles and imprinted poly-o-phenylenediamine', *Electrochim Acta*, **53**, 6589–6595.

Ebarvia, B.S., Cabanilla, S. and Sevilla, F III. (2005) 'Biomimetic properties and surface studies of a piezoelectric caffeine sensor based on electrosynthesized polypyrrole', *Talanta,* **66**, 145–152.

Feng, W. and Ji, P. (2011) 'Enzymes immobilized on carbon nanotubes', *Biotechnol Adv*, **29**, 889–895.

Frasconi, M., Tel-Vered, R., Riskin, M. and Willner, I. (2010) 'Stereoselective and chiroselective surface plasmon resonance (SPR) analysis of amino acids by molecularly imprinted au-nanoparticle composites', *Chem Eur J,* **16**, 7114–7120.

Gajovic-Eichelmann, N., Ehrentreich-Förster, E. and Bier, F.F. (2003) 'Directed immobilization of nucleic acids at ultramicroelectrodes using a novel electrodeposited polymer', *Biosens Bioelectron*, **19**, 417–422.

Geim, A.K. and Novoselov, K.S. (2007) 'The rise of graphene', *Nat Mater*, **6**, 183–191.

Gómez-Caballero, A., Aranzazu, Goicolea, M. and Barrio, R. J. (2005) 'Paracetamol voltammetric microsensors based on electrocopolymerized–molecularly imprinted film modified carbon fiber microelectrodes', *Analyst*, **130**, 1012–1018.

Granot, E., Tel-Vered R., Lioubashevski, O. and Willner, I. (2008) 'Stereoselective and enantioselective electrochemical sensing of monosaccharides using imprinted boronic acid-functionalized polyphenol films', *Adv Funct Mater*, **18**, 478–484.

Guan, G., Liu, B., Wang, Z. and Zhang, Z. (2008) 'Imprinting of molecular recognition sites on nanostructures and its applications in chemosensors', *Sensors*, **8**, 8291–8320.

Gupta, G., Bhaskar, A.S., Tripathi, B.K., Pandey, P., Boopathi, M., Rao, P.V., Singh, B. and Vijayaraqhavan, R. (2011) 'Supersensitive detection of T-2 toxin by the in situ synthesized π-conjugated molecularly imprinted nanopatterns. An in situ investigation by surface plasmon resonance combined with electrochemistry', *Biosens Bioelectron,* **26**, 2534–2540.

Haupt, K and Mosbach, K. (2000) 'Molecularly imprinted polymers and their use in biomimetic sensors', *Chem Rev*, **100**, 2495–2504.

Hedborg, E., Winquist, F., Lundstrom, I., Andersson, L.I. and Mosbach, K. (1993) 'Some studies of molecularly-imprinted polymer membranes in combination with field-effect devices', *Sens Actuators A* **37–38**, 796–799.

http://old.iupac.org/goldbook/BT06768.pdf

Kan, X., Liu, T., Zhou, H., Li, C. and Fang, B. (2010) 'Molecular imprinting polymer electrosensor based on gold nanoparticles for theophylline recognition and determination', *Microchim Acta*, **171**, 423–429.

Kan, X., Xing, Z., Zhu, A., Zhao, Z., Xu, G., Li, C. and Zhou, H. (2012) 'Molecularly imprinted polymers based electrochemical sensor for bovine hemoglobin recognition', *Sensor Actuat B-Chem*, **168**, 395–401.

Kang, J., Zhang, H., Wang, Z., Wu, G. and Lu, X. (2009) 'A novel amperometric sensor for salicylic acid based on molecularly imprinted polymer-modified electrodes', *Polym Plast Technol Eng*, **48**, 639–645.

Kröger, S., Turner, A.P.F., Mosbach, K. and Haupt, K. (1999) 'Imprinted polymer-based sensor system for herbicides using differential-pulse voltammetry on screen-printed electrodes', *Anal Chem,* **71**, 3698–3702.

Kuila, T., Bose, S., Khanra, P., Mishra, A.K., Kim, N.H. and Lee, J.H. (2011) 'Recent advances in graphene-based biosensors', *Biosens Bioelectron,* **26**, 4637–4648.

Lakshmi, D., Bossi, A., Whitcombe, M.J., Chianella, I., Fowler, S.A., Subrahmanyam, S., Piletska, E.V. and Piletsky, S.A. (2009) 'Electrochemical sensor for catechol and dopamine based on catalytic molecularly imprinted polymer-conducting polymer hybrid recognition element', *Anal Chem,* **81**, 3576–3584.

Lettau, K., Warsinke, A., Katterle, M., Danielsson, B. and Scheller, F.W. (2006) 'A bifunctional molecularly imprinted polymer (MIP): Analysis of binding and catalysis by a thermistor', *Angew Chem Int Ed Engl*, **45**, 6986–6990.

Li, J., Zhao, J. and Wei, X. (2009) 'A sensitive and selective sensor for dopamine determination based on a molecularly imprinted electropolymer of o-aminophenol', *Sensor Actuat B-Chem*, **140**, 663–669.

Li, J., Jiang, F. and Wei, X. (2010) 'Molecularly imprinted sensor based on an enzyme amplifier for ultratrace oxytetracycline determination', *Anal Chem*, **82**, 6074–6078.

Li, J., Jiang, F. and Wei, X. (2011) 'Fabrication of an oxytetracycline molecular-imprinted sensor based on the competition reaction via GOD-enzymatic amplifier', *Biosens Bioelectron*, **26**, 2097–2101.

Li, H., Wang, Z., Wu, B., Liu, X., Xue, Z. and Lu, X. (2012a) 'Rapid and sensitive detection of methyl-parathion pesticide with an electropolymerized, molecularly imprinted capacitive sensor', *Electrochim Acta,* **62**, 319–326.

Li, H., Xie, C., Li, S. and Xu, K. (2012b) 'Electropolymerized molecular imprinting on gold nanoparticle-carbon nanotube modified electrode for electrochemical detection of triazophos' *Colloids Surf B Biointerfaces,* **89**, 175–181.

Lian, W., Liu, S., Yu, J., Xing, X., Li, J., Cui, M. and Huang, J. (2012) 'Electrochemical sensor based on gold nanoparticles fabricated molecularly imprinted polymer film at chitosan-platinum nanoparticles/graphene-gold nanoparticles double nanocomposites modified electrode for detection of erythromycin', *Biosens Bioelectron* **38**, 163–169.

Liao, H., Zhang, Z., Lie, H., Nie, L. and Yao, S. (2004) 'Preparation of the molecularly imprinted polymers-based capacitive sensor specific for tegafur and its characterization by electrochemical impedance and piezoelectric quartz crystal microbalance', *Electrochim Acta,* **49**, 4101–4107.

Liu, Y., Song, Q.-J. and Wang, L. (2009) 'Development and characterization of an amperometric sensor for triclosan detection based on electropolymerized molecularly imprinted polymer', *Microchem J,* **91**, 222–226.

Liu, Y.T., Deng, J., Xiao, X.L., Ding, L., Yuan, Y.L., Li, H. and Li, X.T. (2011) 'Electrochemical sensor based on a poly(para-aminobenzoic acid) film modified glassy carbon electrode for the determination of melamine in milk', *Electrochim Acta,* **56**, 4595–4602.

Losito, I., Palmisano, F. and Zambonin, P.G. (2003) 'o-Phenylenediamine electropolymerization by cyclic voltammetry combined electrospray ionization-ion trap mass spectrometry', *Anal Chem,* **75**, 4988–4995.

Malitesta, C., Losito, I. and Zambonin, P.G. (1999) 'Molecularly imprinted electrosynthesized polymers: New materials for biomimetic sensors', *Anal Chem,* **71**, 1366–1370.

Malitesta, C., Mazotta, E., Picca, R.A., Poma, A., Chianella, I. and Piletsky, S.A. (2012) 'MIP sensors: the electrochemical approach', *Anal Bioanal Chem,* **402**, 1827–1846.

Mao, Y., Bao, Y., Gan, S., Li, F. and Niu, L. (2011) 'Electrochemical sensor for dopamine based on a novel graphene-molecular imprinted polymers composite recognition element', *Biosens Bioelectron,* **28**, 291–297.

Meier, F. and Mizaikoff, B. (2011) 'Molecularly imprinted polymers as artificial receptors', in Mirsky V and Yatsimirsky, *Artificial Receptors for Chemical Sensors*, Weinheim, Germany, Wiley-VCH Verlag&Co. KGaA.

Merkoçi, A. and Alegret S. (2002) 'New materials for electrochemical sensing IV. Molecular imprinted polymers', *Trends Anal Chem*, **21**, 717–725.

Mirsky, V.M., Hirsch, T., Piletsky, S. A. and Wolfbeis, O.S. (1999) 'A spreader-bar approach to molecular architecture: Formation of stabil artificial chemoreceptors', *Angew Chem Int Ed Engl*, **38**, 1108–1110.

Namvar, A. and Warriner, K. (2007) 'Microbial imprinted polypyrrole/poly(3-methylthiophene) composite films for the detection of *Bacillus* endospores', *Biosens Bioelectron*, **22**, 2018–2024.

Neto, J.R.M., Santos, W.J.R., Lima, P.R., Tanaka, S.M.C.N., Tanaka, A.A. and Kubota, L.T. (2011) 'A hemin-based molecularly imprinted polymer (MIP) grafted onto a glassy carbon electrode as a selective sensor for 4-aminophenol amperometric', *Sensor Actuat B-Chem,* **152**, 220–225.

Nicholls, I.A., Ramström, O. and Mosbach, K. (1995) 'Insights into the role of the hydrogen bond and hydrophobic effect on recognition in molecularly imprinted polymer synthetic peptide receptor mimics', *J Chromatogr A*, **691**, 349–353.

Ouyang, R., Lei, J., Ju, H. and Xue, Y. (2007) 'A molecularly imprinted copolymer designed for enantioselective recognition of glutamic acid', *Adv Funct Mater*, **17**, 3223–3230.

Özcan, L., and Şahin, Y. (2007) 'Determination of paracetamol based on electropolymerized-molecularly imprinted polypyrrole modified pencil graphite electrode', *Sens Act B-Chem*, **127**, 362–369.

Özcan, L., Şahin, M. and Şahin, Y. (2008) 'Electrochemical preparation of a molecularly imprinted polypyrrole-modified pencil graphite electrode for determination of ascorbic acid', *Sensors,* **8**, 5792–5805.

Panasyuk, T.L., Mirsky, V.M., Piletsky, S.A. and Wolfbeis, O.S. (1999) 'Electropolymerized molecularly imprinted polymers as receptor layers in capacitive chemical sensors', *Anal Chem*, **71**, 4609–4613.

Peng, H., Liang, C., Zhou, A., Zhang, Y., Xie, Q. and Yao, S. (2000) 'Development of new atropine sulfate bulk acoustic wave sensor based on a molecularly imprinted electrosynthesized copolymer of aniline with *o*-phenylenediamine', *Anal Chim Acta*, **423**, 221–228.

Percin Özkorucuklu, S., Şahin, Y. and Alsancak, G. (2008) 'Voltammetric behaviour of sulfamethoxazole on electropolymerized-molecularly imprinted overoxidized polypyrrole', *Sensors,* **8**, 8463–8478.

Pernites, R. Ponnapati, R., Felipe, M.J. and Advincula, R. (2011) 'Electropolymerization molecularly imprinted polymer (E-MIP) SPR sensing of drug molecules: Pre-polymerization complexed terthiophene and carbazole electroactive monomers', *Biosens Bioelectron*, **26**, 2766–2771.

Pérez-Moral, N. and Mayes, A.G. (2006) 'MIP formats for analytical applications', in Piletsky S and Turner A, *Molecular Imprinting of Polymers*, Georgetown, TX, USA, Landes Bioscience.

Pietrzyk-Le, A., D´Souza, F. and Kutner, W. (2011) 'Supramolecular self-assembly governed molecularly imprinted polymers for selective chemical sensing', in Schneider H J, *Applications of Supramolecular Chemistry for 21st Century Technology*, London/Boca Raton, Taylor&Francis/CRC.

Piletsky, S. and Turner, A. (2006) 'A new generation of chemical sensors based on MIPs', in Piletsky S and Turner A, *Molecular Imprinting of Polymers*, Georgetown, TX, USA, Landes Bioscience.

Piletsky, S.A and Turner, A.P.F. (2008) 'Imprinted polymers and their application in optical sensors', in Ligler F S and Taitt C R, *Optical Biosensors: Today and Tomorrow*, Amsterdam, Elsevier Science B.V.

Pingarrón, J.M., Yáñez-Sedeño, P. and González-Cortés, A. (2008) 'Gold nanoparticle-based electrochemical biosensors', *Electrochim Acta*, **53**, 5848–5866.

Poma, A., Turner, A.P.F. and Piletsky, S. (2010) 'Advances in the manufacture of MIP nanoparticles', *Trends Biotechnol,* **28**, 629–637.

Ramanaviciene, A. and Ramanavicius, A. (2004) 'Molecularly imprinted polypyrrole-based synthetic receptor for direct detection of bovine leukemia virus glycoproteins', *Biosens Biolectron*, **20**, 1076–1082.

Ratinac, K.R., Yang, W., Gooding, J.J., Thordarson, P. and Braet, F. (2011) 'Graphene and related materials in electrochemical sensing', *Electroanalysis,* **23**, 803–826.

Rick, C. and Chou, T.-C. (2006) 'Using protein templates to direct the formation of thin-film polymer surfaces', *Biosens Biolectron,* **22**, 544–549.

Riskin, M., Tel-Vered, R., Bourenko, T., Granot, E. and Willner, I. (2008) 'Imprinting of molecular recognition sites through electropolymerization of functionalized

Au nanoparticles: Development of an electrochemical TNT sensor based on л-donor-acceptor interactions', *J Am Chem Soc,* **130**, 9726–9733.

Riskin, M., Tel-Vered, R., Frasconi, M., Yavo, N. and Willner, I. (2010) 'Surface plasmon resonance analysis of antibiotics using imprinted boronic acid Au-nanoparticle composites', *Anal Chem*, **82**, 2512–2519.

Scheller, F.W. and Yarman, A. (2012) 'Biomimetic sensors', in Bard A, Inzelt G, and Scholz F, *Electrochemical Dictionary 2nd edition*, Berlin-Heilderberg, Springer-Verlag.

Sellergen, B. and Shea, K.J. (1993) 'Influence of polymer morphology on the ability of imprinted network polymers to resolve enantiomers', *J Chromatogr A*, **635**, 31–49.

Sellergen, B. (1994) 'Direct drug determination by selective enrichment on an imprinted polymer', *Anal Chem*, **66**, 1578–1582.

Shao, Y., Wang, J., Wu, H., Liu, J., Aksay, I.A. and Lin, Y. (2010) 'Graphene-based electrochemical sensors and biosensors: A review', *Electroanalysis*, **22**, 1027–1036.

Sharma, P.S., Pietrzyk-Le, A., D´Souza, F. and Kutner, W. (2012) 'Electrochemically synthesized polymers in molecular imprinting for chemical sensing', *Anal Bioanal Chem*, **402**, 3177–3204.

Shea, K.J. and Thompson, E.A. (1978) 'Template synthesis of macromolecules. Selective functionalization of an organic polymer', *J Org Chem*, **43**, 4253–4255.

Sode, K., Ohta, S., Yanai, Y. and Yamazaki, T. (2003) 'Construction of a molecular imprinting catalyst using target anologue template and its application for an amperometric fructosylamine sensor', *Biosens Bioelectron*, **18**, 1485–1490.

Song, W., Chen, Y., Xu, J., Yang, X.-R. and Tian, D.-B. (2010) 'Dopamine sensor based on molecularly imprinted electrosynthesized polymers', *J Solid State Electrochem,* **14**, 1909–1914.

Suedee, R., Intakong, W., Lieberzeit, P.A., Wanichapichart, P., Chooto, P. and Dickert, F.L. (2007) 'Trichloroacetic acid-imprinted polypyrrole film and its property in piezoelectric quartz crystal microbalance and electrochemical sensors to application for determination of haloacetic acids disinfection by-product in drinking water', *J Appl Polym Sci*, **106**, 3861–3871.

Suryanarayanan, V., Wu, C.-T. and Ho, K.-C. (2010) 'Molecularly imprinted electrochemical sensors', *Electroanalysis*, **22**, 1795–1811.

Syritski, V., Reut, J., Menaker, A., Gyurcsányi, R.E. and Öpik, A. (2008) 'Electrosynthesized molecularly imprinted polypyrrole films for enantioselective recognition of L-aspartic acid', *Electrochim Acta*, **53**, 2729–2736.

Takeda, S., Yagi, H., Mizuguchi, S., Funahashi, H., Shiigi, H. and Nagaoka, T. (2008) 'A highly sensitive amperometric adenosine triphosphate sensor based on molecularly imprinted overoxidized polypyrrole', *J Flow Injection Anal*, **25**, 77–79.

Thévenot, D. R., Toth, K., Durst, R.A. and Wilson, G.S. (1999) 'Electrochemical biosensors: Recommended definitions and classification', *Pure Appl Chem*, **71**, 2333–2348.

Tse Sum Bui, B. and Haupt, K. (2010) 'Molecularly imprinted polymers: synthetic receptors in bioanalysis', *Anal Bioanal Chem,* **398**, 2481–2492.

Turiel, E. and Martin-Esteban, A. (2004) 'Molecularly imprinted polymers: towards selective stationary phases in liquid chromatography and capillary electrophoresis', *Anal Bioanal Chem*, **378**, 1876–1886.

Turner, A.P.F. (1989) 'Current trends in biosensor research and development', *Sensor Actuat B-Chem,* **17**, 433–450.

Vamvakaki, V., Fouskaki, M. and Chaniotakis, N. (2007) 'Electrochemical biosensing systems based on carbon nanotubes and carbon nanofibers', *Anal Lett*, **40**, 2271–2287.

Viswanathan, S., Rani, C., Riberio, S. and Delerue-Matos, C. (2012) 'Molecular imprinted nanoelectrodes for ultrasensitive detection of ovarian cancer marker', *Biosens Bioelectron*, **33**, 179–183.

Wang, J. (2005) 'Nanomaterial-based electrochemical biosensor', *Analyst,* **130**, 421–426.

Wang, Z., Kang, J., Liu, X. and Ma, Y. (2007) 'Capacitive detection of theophylline based on electropolymerized molecularly imprinted polymer', *Int J Polym Anal Char*, **12**, 131–142.

Weetall, H.H. and Rogers, K.R. (2004) 'Preparation and characterization of molecularly imprinted electropolymerized carbon electrodes', *Talanta*, **62**, 329–335.

Weetall, H.H., Hatcchett, D.W. and Rogers, K.R. (2005) 'Electrochemically deposited polymer-coated gold electrodes selective for 2,4-dichlorophenoxyacetic acid', *Electroanalysis,* **19**, 1789–1794.

Weng, C.-H., Yeh, W.-M., Ho, K.-C. and Lee, G.-B. (2007) 'A microfluidic system utilizing molecularly imprinted polymer films for amperometric detection of morphine', *Sens Act B-Chem*, **121**, 576–582.

Whitcombe, M.J., Rodriguez, M.E., Villar, P. and Vulfson, E.N. (1995) 'A new method for the introduction of recognition site functionality into polymers prepared by molecular imprinting: synthesis and characterization of polymeric receptors for cholesterol', *J Am Chem Soc*, **117**, 7105–7111.

Willner, I. and Katz, E. (2005) ' Bioelectronics-an introduction', in Willner I and Katz E, *Bioelectronics: From Theory to Applications,* Winheim Wiley-VCH.

Wulff, G. and Sarhan, A. (1972) 'The use of polymers with enzyme-analogous structures for the resolution of racemates', *Angew Chem Int. Ed Engl*, **11**, 341.

Wulff, G. (1995) 'Molekulares Prägen (Imprinting) in vernetzten Materialen mit Hilfe von Matrizenmolekülen-auf dem Weg zu künstlichen Antikörpern', *Angew Chem*, **107**, 1958–1979.

Xie, C., Li, H., Li, S., Wu, J. and Zhang Z. (2010) 'Surface molecular self-assembly for organophosphate pesticide imprinting in electropolymerized poly(p-aminothiophenol) membranes on a gold nanoparticle modified glassy carbon electrode', *Anal Chem*, **82**, 241–249.

Xie, C., Li, H., Li, S. and Gao, S. (2011) 'Surface molecular imprinting for chemiluminescence detection of organophosphate pesticide chlorpyrifos', *Microchim Acta*, **174**, 311–320.

Xing, X., Liu S., Yu, J., Lian, W. and Huang, J. (2012) 'Electrochemical sensor based on molecularly imprinted film at polypyrrole-sulfonated graphene/hyaluronic acid-multiwalled carbon nanotubes modified electrode for determination of tryptamine', *Biosens Bioelectron*, **31**, 277–283.

Yeh, W.-M. and Ho, K.-C. (2005) 'Amperometric morphine sensing using a molecularly imprinted polymer-modified electrode', *Anal Chim Acta*, **542**, 76–82.

Yarman, A., Neumann, B., Gajovic-Eichelmann, N., Wollenberger, U. and Scheller F.W. (2012) 'Intelligent biosensors unifying bioelectrocatalysis by minizymes with MIP-based selectivity', *Biosensors 2012*, 15–18 May 2012, Cancun, Mexico (Elsevier).

Yoshimatsu, K., Yamazaki, T., Chronakis, I.S. and Ye, L. (2012) 'Influence of template/functional monomer ratio on particle size and binding properties off molecularly imprinted nanoparticles', *J Appl Polym Sci*, **124**, 1249–1255.

Zhang, J., Wang, Y., Lv, R. and Xu, L. (2010) 'Electrochemical tolazoline sensor based on gold nanoparticles and imprinted poly-o-aminothiophenol film', *Electrochim Acta*, **55**, 4039–4044.

7

Nanostructured conducting polymers for electrochemical sensing and biosensing

K. WESTMACOTT, University of the West of England, UK, B. WENG and G. G. WALLACE, University of Wollongong, Australia and A. J. KILLARD, University of the West of England, UK

DOI: 10.1533/9780857096722.1.150

Abstract: Conducting polymers have found widespread use in the development of electrochemical sensors and biosensors. This chapter discusses the available methods for fabricating conducting polymer nanomaterials and looks at their application to electrochemical sensing and biosensing.

Key words: conducting polymers, nanomaterials, electrochemical, sensors, biosensors.

7.1 Introduction

Conducting polymers (CP) have received considerable attention since they were first reported in the 1970s, due to their interesting electronic and physical properties, chemical stability, and potential technological applications. The significant application potential of CPs in chemical and biological sensors is one of the main reasons for the intensive investigation and development of these materials. Their unique structure with high conjugated polymer chain can be assigned reversible chemical, electrochemical and physical properties controlled by a doping/de-doping process, which makes these polymers very attractive as transducer materials in various sensing devices. Meanwhile, nanotechnology, as one of most exciting forefront fields in recent materials research, brings further merits in designing and fabricating novel chemical and biological sensors for its ability to tailor the size and structure and hence the properties of nanomaterials, offering excellent prospects for enhancing the performance of the sensing devices.

The method of polymer synthesis at the nanoscale is vital to the materials sensing performance as the structural configuration achieved during synthesis can vary tremendously. This configuration could be film, fibre, wire, or particle, all of which can demonstrate different analytical advantages such

as response/recovery time, limit of detection (LOD), and extent of sensing range. This specific polymer configuration has a large role in the enhancing influence a secondary component can provide; a few examples of secondary components are: dopants, metals, metal oxides and carbon nanotubes (CNT). These can be used to enhance conductivity, stability, sensitivity, and the immobilisation characteristics of the polymeric matrix. Synthesis methods are continuously progressing, and this progress has come with the advanced control of the polymer structure: length, diameter, uniformity and porosity have all been manipulated to improve metrological performance.

In this chapter, the synthetic methods used to prepare a range of nanostructured conducting polymer materials and their application in chemical and biological sensing will be discussed. Many methods have been described in the literature to achieve CP nanostructures. The key methodologies can be categorised as follows (Huang and Kaner, 2006; Xia *et al.*, 2010):

1. Hard-template synthesis
2. Soft-template synthesis
3. Physical methodologies, including electrospinning and dip-pen coating techniques.

The following sections describe these techniques.

7.2 Hard-template synthesis of conducting polymer nanomaterials

In general, the preparation of CP nanostructures by a hard-template method is carried out by either chemical or electrochemical polymerisation. It can be divided into three types according to the function of the template and whether the template needs to be removed. In the template-only method, the template is useful solely during the polymerisation period, and is subsequently removed by solvents, reactions or other methods during or after synthesis. Thus, the template will not be present in the polymer after polymerisation. In other methods, the template may remain as part of the material. In this situation, the template, which creates nanogaps or nanojunctions for polymerisation, often acts as a physical support part, such as electrodes, in sensor devices. Alternatively, the template can become part of the nanocomposite. Nanostructured materials including CNTs, graphene, metal particles and metal oxide particles are often used as templates to create CPs nanostructures as well as becoming a composite component to enhance the properties of the materials.

Hard-template synthesis can easily control the shape and size of CP nanostructures by simply tailoring the morphology and diameter of the templates. The length and thickness of the nanostructure can be adjusted by changing polymerisation time (Xia *et al.*, 2010). In addition, the advantage of hard

templates is their availability in relatively large amounts, and availability in a wide range of sizes from commercial sources is also essential (Zhang *et al.,* 2006). Thus, the hard-template method is the most commonly used and the most efficient approach for preparing well-controlled and highly oriented nanostructures.

7.2.1 Template-only method

The template-only approach was first proposed by Martin's group to prepare nanofibres, nanotubes and nanowires of CPs (Hulteen and Martin, 1997; Martin, 1998). This method firstly grows CPs within the pores or channels of the template, or outside template nanoparticles and nanofibres. The template is then removed by solvent, reactions after the polymerisation, or even work as reactants in the synthesis (Fig. 7.1).

Chemical synthesis of nanostructured CPs with hard templates often involves placing a template membrane into the reaction mixture which contains monomer, dopant and oxidant that utilises the template as nano size reactors for polymerisation. Martin's group has synthesised polypyrrole (PPy), polyaniline (PANI) (Xiong *et al.,* 2004; Tai *et al.,* 2007), and poly(thiophene) (PTH) nanostructures using polycarbonate particle track-etched membranes (PC-PTM) and anodic aluminium oxide (AAO) membranes as templates (Martin *et al.,* 1993; Martin, 1994; Parthasarathy and Martin, 1994; Hulteen and Martin, 1997). Recently, a series of one dimensional structures of poly(3,4-ethylenedioxythiophene) (PEDOT) nanotubes, nanorods, nanothimbles, and nanobelts have been synthesised with Al_2O_3 membrane (AAO, Whatman Anodisc 47, pore size 250 nm, thickness 60 mm) as template (Han and Foulger, 2005). The AAO membrane was first filled with 3,4-ethylenedioxythiophene (EDOT) monomer under negative pressure, and then the EDOT-filled AAO membrane was quickly transferred to an aqueous oxidant solution to initiate the polymerisation. Due to the extremely low solubility of EDOT in the reaction solution, the monomer was retained in the pore of the AAO. In addition, the solvophobic properties of the PEDOT polymer led to its preferential growth on the

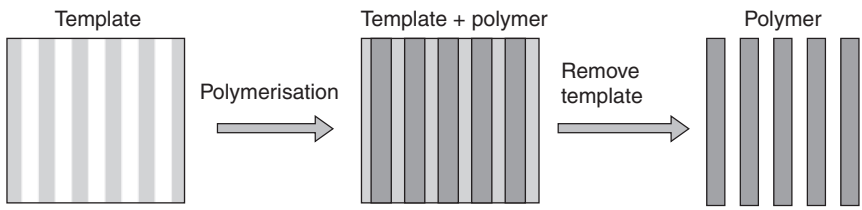

7.1 Schematic of the hard-template synthesis of CP nanostructures.

pore wall. After polymerisation, the nanostructured PEDOT was separated from the AAO membrane by dissolving the AAO in a 20 vol.% hydrofluoric acid (HF) aqueous solution and washing the residue with an excess of HF, deionised water, methanol, and then again with deionised water. Control of the geometric aspects of the structures was obtained through modifications of the synthetic conditions including oxidant concentrations and polymerisation temperature (Fig. 7.2).

A two-dimensional (2D) ordered, large-area, liftable, and patterned PANI nanobowl monolayer containing Au nanoparticles has been demonstrated by Jiang *et al.* (2009) with the monolayer self-assembled polystyrene (PS) spheres at the aqueous/air interface as template. Tetrachloroauric acid has been used as an oxidising agent for the polymerisation of aniline in aqueous

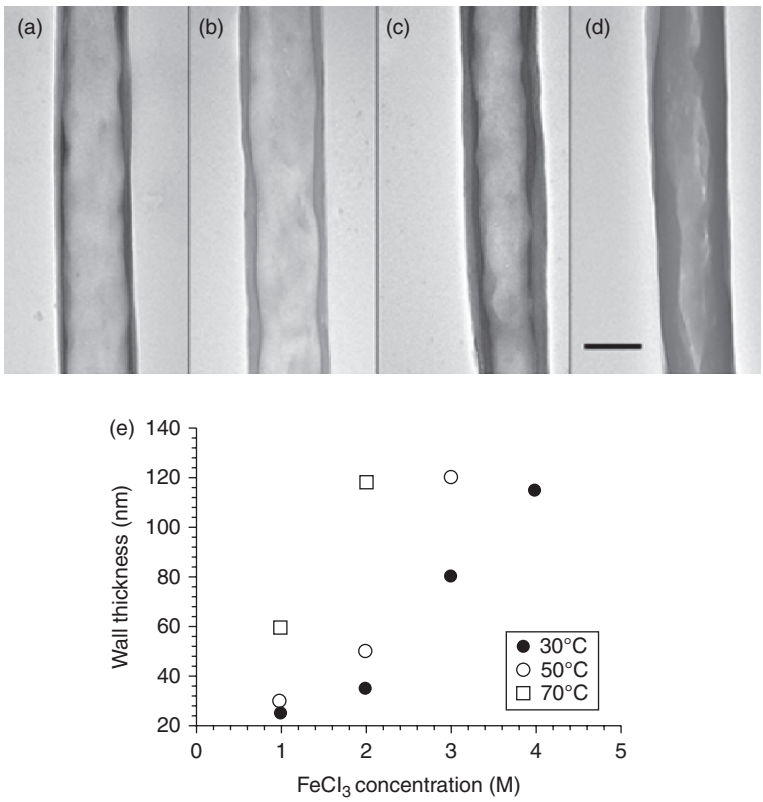

7.2 TEM images of PEDOT nanotubes synthesised under various conditions: (a) in 1 M $FeCl_3$ solution at 30°C; (b) in 1 M $FeCl_3$ solution at 50°C; (c) in 2 M $FeCl_3$ solution at 50°C; (d) in 3 M $FeCl_3$ solution at 30°C; and (e) tube wall thickness as a function of $FeCl_3$ concentration and polymerisation temperature. Polymerisation time was 1.5 h for each sample (Han and Foulger, 2005).

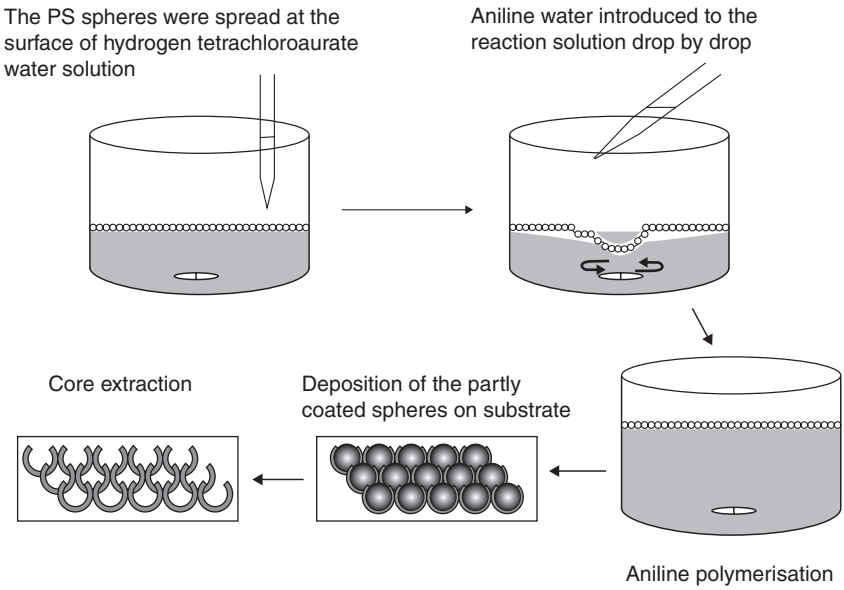

7.3 Schematic illustration of the process for fabrication 2D patterned conducting PANI–gold composite nanobowl sheet with PS spheres as template (Jiang *et al.,* 2009).

solution. The schematic of polymerisation is described in Fig. 7.3. The opening at the top of the nanobowl (420 ± 20 nm) is determined by the size of PS nanoparticles and the Au nanoparticle size, and the thickness of the PANI layer can be adjusted by changing aniline concentration from 50 ± 5 to 100 ± 10 nm (Fig. 7.4).

Zhang and Manohar (2004b) described a direct, one-step bulk chemical synthetic route to PPy nanofibres using seed as a template. The seed in this method served as both the hard-template and oxidant simultaneously and converted into soluble salt in reaction solution, which eliminates the post-process of removing the template. Fibre diameter can be controlled by reaction time. The fibre thickness can range from 30 to 100 nm.

CP nanostructures can also be achieved by using monomer-dopant salt as template. Wan's group explored a novel approach to prepare PANI nanostructures with many convolutions (140–170 nm in average diameter), which resemble the cerebral cortex of the brain, using aniline/citric acid (CA) salts as the template by a gas/solid reaction using chlorine gas as the oxidant (Zhu *et al.,* 2007). The aniline/CA salts were prepared in an organic solution by an acid/base reaction at room temperature. After the solvent had completely evaporated at room temperature, the white brain like aniline/CA salt crystal was grown. The average diameter of aniline/CA nanocrystals can be controlled by the polarity of the solvent used. The thickness and

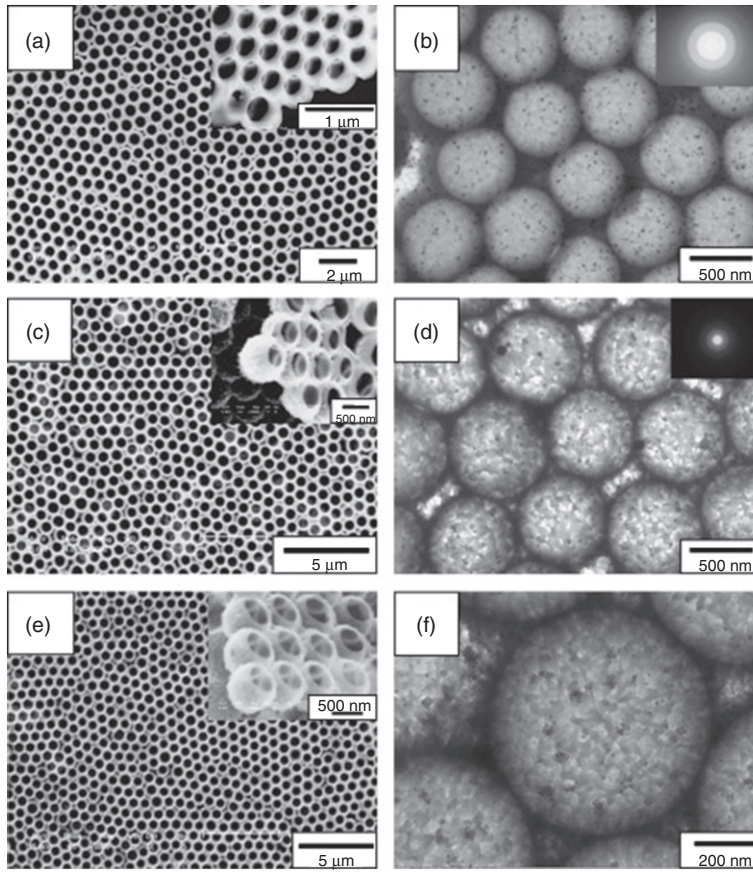

7.4 SEM and TEM images of the PANI–Au nanobowl sheet synthesized with different concentration of aniline. (a) and (b) [An] = 0.15 mol/L; (c) and (d) [An] = 0.1 mol/L; (e) and (f) [An] = 0.15 mol/L. Other conditions: [An]:[HAuCl4] = 3:1 (Jiang *et al.*, 2009).

detailed morphology of PANI films is determined by the exposure time to oxidant chlorine gas (Fig. 7.5).

7.2.2 Template as a part of the device

A series of nanostructured sensors including nanogaps and nanojunction sensors have been created by this method. In this method, a nanojunction must be prepared before deposition of CPs. Generally, it is created using gold electrodes through standard photolithographic techniques or milling to form gap junctions from 500 to 60 nm (Killard, 2010). Then, CPs are deposited electrochemically to bridge the gaps in two electrodes. Forzani *et al.*

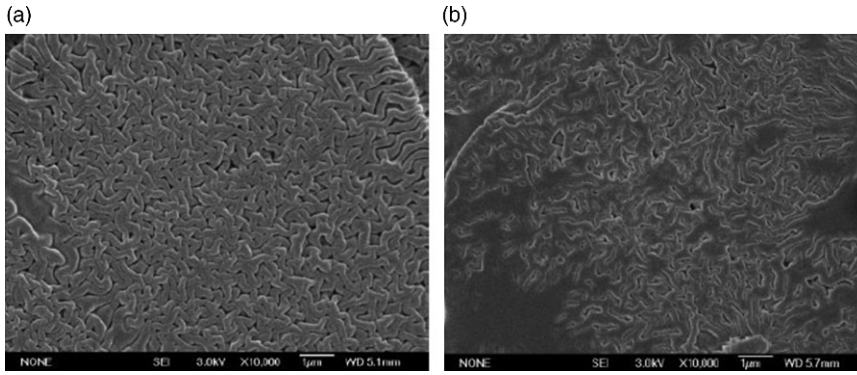

7.5 SEM images of brain-like nanostructured PANI produced by a gas/solid reaction using chlorine gas as oxidant with different polymerisation times: (a) 5 s and (b) 60 s (Zhu *et al.,* 2007).

(2004) fabricated a glucose sensor consisting of an array of PANI nanojunctions. Au nanoelectrode arrays were fabricated on oxidised Si substrate using electron beam lithography. PANI was electropolymerised in the presence of poly(acrylic acid) (PAA) to bridge the two nanoelectrodes separated with a nanoscale gap (20–60 nm). Glucose oxidase (GoX) is immobilised onto the PANI–PAA to provide specific detection of glucose. Forzani's group used this method to fabricate PANI nanojunction sensors for detection of dopamine (Forzani *et al.,* 2007) and ammonia (Aguilar *et al.,* 2008) in their following work. Other CP-based sensors including PPy and PTH have also been fabricated in this way (Wang *et al.,* 2006).

7.2.3 Template as a part of the nanocomposite

Besides the two templating approaches discussed above, some other nano scaled particles, sheets and crystals, such as graphene nanosheets, CNTs, metal particles and metal oxide particles have been used as templates to fabricate CP nanocomposites. Composites of CPs are interesting because of their potential for combining properties that are difficult to attain separately with the individual components. In this method, templates are often dispersed with monomers to create a uniform formulation, and then oxidised and polymerised by *in situ* chemical polymerisation.

The formation of nanocomposites of CPs/CNTs is often carried out by chemical polymerisation of monomers with functionalised CNTs. An *et al.* (2004) first reported a facile bulk method to produce PPy/single-walled CNT nanocomposite for gas sensing. PPy was prepared by a simple and straightforward *in situ* chemical polymerisation of pyrrole mixed with single-walled carbon nanotubes (SWCNTs), and the sensor electrodes were

fabricated by spin coating. PPy was uniformly coated on the wall of the SWCNTs to increase the specific surface area. The morphology of PPy was changed from a typical granular morphology (diameter: 0.2–0.3 μm) without SWCNTs to a fibrous morphology with the diameter around 20 nm with SWCNTs. This sensor has been used to detect NO_2 gas. Van Hieu *et al*. (2009) have also polymerised PPy/SWCNT nanocomposite using this method as a NH_3 chemical sensor. Other CPs including PANI (Ali *et al.,* 2008; Jeevananda *et al.,* 2008; Srivastava *et al.,* 2009), and poly (3-methylthiophene) (Santhanam *et al.,* 2005) have also been synthesised by this method to achieve a nanofibrous structure and enhanced properties.

As one of the fastest developing materials, graphene has attracted widespread attention in multiple fields. Thus, the possibility of using graphene nanosheets as the template to fabricate CPs/graphene nanocomposites has also been investigated. The method, which is very similar to the fabrication of CNT/CP composites, was reported by Al-Mashat's group in 2010. Graphite oxide (GO) was synthesised through graphite oxidation with sulphuric acid and potassium permanganate (H_2SO_4–$KMnO_4$). Reduction of GO to graphene was achieved via refluxing GO with hydrazine in N,N-dimethylformamide (DMF). The graphene was sonicated in ethylene glycol in the presence of aniline and N-phenyl-1,4-phenylenediamine. Then oxidant ammonium persulfate (APS) in HCl solution was rapidly added to the mixture to yield a graphene/PANI nanocomposite. Scanning electron microscopy (SEM) characterisation illustrated that PANI nanofibres on the order of 25–50 nm have been grown on the surface of the graphene nanosheets (Fig. 7.6). This composite has been used as a hydrogen sensor with sensitivity up to 16.57%.

Nanocomposites based on CP and transition metal oxides have been intensively investigated during recent years due to their potential applications as sensors (Tai *et al.,* 2007; Guo *et al.,* 2009; Rahman *et al.,* 2010). These composites were prepared by polymerisation of the monomers in the presence of dispersed oxide. The monomers can be oxidised by either external oxidants (Tai *et al.,* 2007; Deshpande *et al.,* 2009) or metal oxides themselves (Gemeay *et al.,* 2005). Tai *et al*. (2007) studied the sensing ability of PANI–titanium dioxide nanocomposite on CO and NH_3 gases. To prepare this nanocomposite, aniline was dissolved in HCl solution, then mixed with sonicated colloidal TiO_2. APS in HCl solution with an equal molar ratio of aniline was slowly added dropwise, with moderate manual stirring for 5 min. SEM characterisation showed that the film deposited on substrate showed a nanoporous mesh structure, enhancing the diffusion of gases to improve sensing capability. A similar approach has been used by Tandon *et al.* (2006) to fabricate PPy/iron oxide (Fe_3O_4) composites for humidity and gas sensor (Ray and Biswas, 2000). Fe_3O_4 nanoparticles were dispersed with pyrrole monomer and dodecylbenzene sulphuric acid (DBSA) in water and

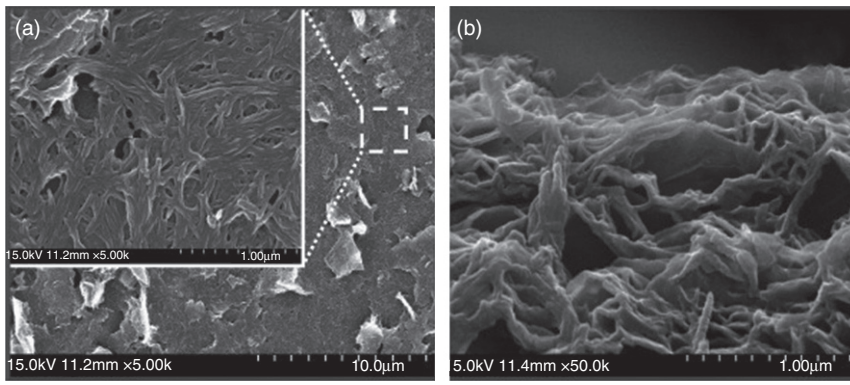

7.6 SEM images of graphene/PANI nanocomposite (a) top view, (b) tilted view (45°) (Al-Mashat *et al.,* 2010).

oxidised by $FeCl_3$ as oxidant. The conductivity of this composite can reach as high as more than 1000 S/cm, which was monitored to characterise the sensitivity of the sensor. The results illustrated that this sensor showed high sensitivity to humidity and gases (O_2, N_2 and CO_2). The amounts of PPy in the composite have great influence on the resulting structure and the conductivity value, as well as sensing behaviour. Other metal oxides and inorganic nanoparticles such as MnO_2 (Gemeay *et al.,* 2005), ZrO_2 (Ray and Biswas, 2000), CuO (Huang *et al*., 1995), MoO_3 (Posudievsky *et al.,* 2002), CdS and CuS (Chandrakanthi and Careem, 2002) have also been investigated as template and components in CP nanocomposites.

CP membranes have often been used as platforms to carry metal nanoparticles, especially noble metal particles, due to its ability to form good quality films. CP/metal composites have been extensively studied for their associated catalytic and redox behaviours and a wide variety have been employed as electrochemical sensors. Metallic particles can enhance the electrocatalytic behaviour of CPs due to their size, conductivity and step defects, which is very useful for sensing functionality. Most attention for chemical sensing applications has focussed on the use of noble metal catalysts such as Au, Pt and Ag, utilising principally voltammetric techniques. Sensors for the neurotransmitters dopamine and epinephrine have been constructed by the incorporation of Au nanoclusters through the reduction of $HAuCl_4$ onto the surface of an electropolymerised over-oxidised PPy film (Li and Lin, 2007a). The electrocatalytic oxidation of both dopamine and epinephrine was found to be enhanced significantly in the composite films as compared with either polymer, nanoparticles, or gold alone, and the enhancements have been ascribed to a combination of the ability of the over-oxidised film to accumulate dopamine and epinephrine due to the presence of greater numbers of carboxyl and carbonyl groups, as well

as the increased gold electrode surface area imparted by the embedded nanoparticles. Similar techniques using PPy and PEDOT have also been illustrated for the detection of uric acid at nanomolar concentrations (Li and Lin, 2007b; Mathiyarasu *et al*., 2008). Li and Lin (2007c) modified PPy nanowires with Pt nanoclusters and showed enhanced performance of the composite over an electrode modified by Pt nanoparticles alone with increased reduction current seen at −120 mV vs Ag/AgCl, compared to −144 mV for the Pt film alone.

7.3 Soft-template synthesis of conducting polymer nanomaterials

The soft-template method, which is also referred to as the template-free or self-assembly method, is another relatively simple, cheap, and powerful approach for fabricating conducting polymer nanostructures via a self-assembly process. To date, surfactants, colloidal particles, structure-directing molecules, oligomers, and colloids can all work as soft templates. Furthermore, strict non-template polymerisations have also been developed.

7.3.1 Non-template polymerisation

Kaner's group has studied the mechanism of PANI polymerisation and developed two approaches, interfacial polymerisation and the rapid mixing reaction, to fabricate intrinsic PANI nanofibres without either hard or soft templates used (Huang and Kaner, 2006). The mechanism of PANI polymerisation was studied by pumping initiator into aniline dispersion then recorded the morphologies of PANI products using TEM at 0, 25, 100 min. TEM results illustrated that at a very early stage of the polymerisation process (0 min), clean nanofibres with average diameters of 30–50 nm are obtained. As more APS solution is added into the aniline solution (25 min), the nanofibres become thicker and coarser, and the final reaction product (100 min) contains mostly irregularly-shaped agglomerates. These results indicate that the initial nanofibres formed may act as scaffolds for the overgrowth of irregularly-shaped PANI. Therefore, if the overgrowth of PANI can be suppressed after the initial nanofibrillar formation step, it should be possible to obtain a product of pure PANI nanofibres.

Interfacial polymerisation of PANI nanofibres is achieved by dissolving aniline monomer in organic solvent while dissolving oxidant APS in aqueous acidic solution. PANI forms at the interface, and then diffuses into the water layer, leaving the interface available for further reaction, as shown in Fig. 7.7. Further TEM analysis shows that the interfacial polymerisation produces pure PANI nanofibres, typically with average diameters between 30 and 50 nm (Huang *et al*., 2003; Huang *et al*., 2004; Huang and Kaner, 2004a).

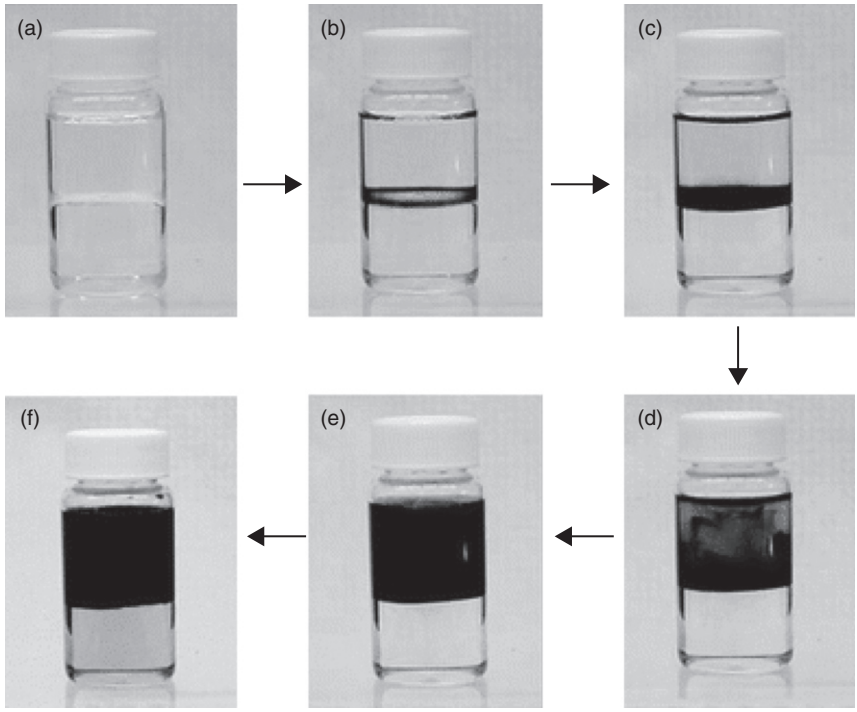

7.7 Snapshots showing the interfacial polymerisation of aniline. The reaction times are (a) 0 s, (b) 60 s, (c) 90 s, (d) 120 s, (e) 180 s, and (f) 2 h. The top layer is an aqueous solution of acid and oxidant; the bottom layer contains aniline dissolved in an organic solvent (Huang and Kaner, 2006).

Another method used to prevent PANI secondary overgrowth to obtain nanofibrillar structure is called 'rapid mixed reactions' (Huang and Kaner, 2004b). These can be achieved simply by pouring the initiator solution (e.g., APS) into the aniline solution all at once and rapidly mixing them (Fig. 7.8). As the polymerisation begins, the initiator molecules induce the formation of nanofibres by rapidly polymerising aniline monomers in their vicinity. If the initiator molecules are evenly distributed, then they should be consumed during the formation of nanofibres. Therefore, secondary growth of PANI will be very limited due to a lack of available reactants. The product created in a rapidly mixed reaction is pure nanofibres with a relatively uniform size distribution, comparable to that obtained in interfacial polymerisation.

The morphology and diameter of PANI nanofibres can be tuned by controlling polymerisation conditions, including dopants, solvents and purification methods, in both interfacial polymerisation and rapid mixed reactions, indicating that a nanofibrillar morphology appears to be intrinsic to chemically

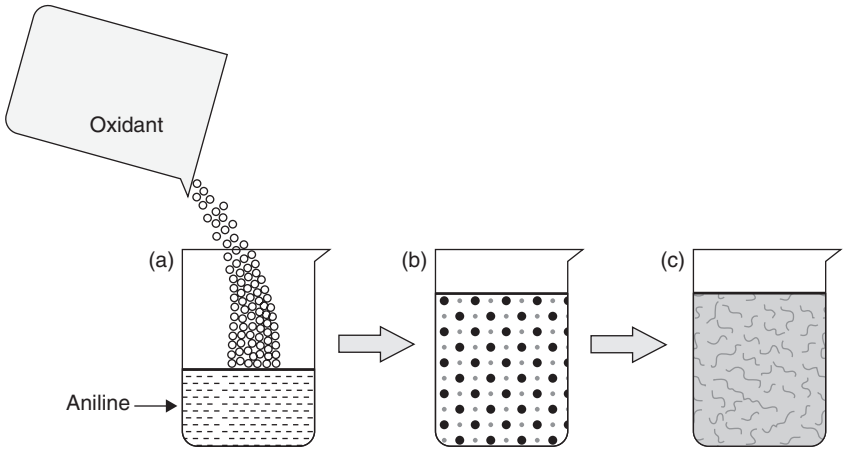

7.8 A schematic illustration of PANI nanofiber synthesis in a rapidly mixed reaction. (a) The oxidant (open circles) dopant solution is quickly added to the aniline (solid spheres) dopant solution and mixed. (b) A homogenous solution is obtained where the aniline and oxidant molecules are evenly distributed, leading to rapid polymerisation throughout the entire solution. (c) Since all the reactants are consumed in the formation of the nanofibres, secondary growth is suppressed (Huang and Kaner, 2006).

synthesised PANI, which can be made without any extra structural directing agents by interfacial polymerisation or by rapidly mixed reactions.

7.3.2 Surfactants as soft-template

Surfactants, which contain both a hydrophilic group and hydrophobic group in the one molecule, are extensively used as soft templates in emulsion polymerisation of nanostructured CPs with controlled dimensions. The size and shape of surfactant aggregates can be controlled by the volume and type of surfactants used, and the effective area occupied by each surfactant head group at the surface of the aggregate. The most common morphology of a surfactant in solution is spherical, cylindrical, or a flat bi-layer, depending on the parameters discussed above. Surfactant aggregates can shape CPs into the nanoscale by working as nanoreactors (Xia *et al.*, 2010). The shapes and diameters of CP nanostructures are determined by the surfactant and oxidant parameters.

Many investigations have been carried out on the synthesis of CP nanostructures with surfactants in aqueous solutions. Zhang and Manohar (2004a) successfully polymerised PANI nanofibres doped with D, L-camphorsulphonic acid (HCSA) and with 2-acrylamido-2-methyl-1-propanesulfonic acid (AMPSA) using TX100 as surfactant. The resulting

products had average fibre diameters in the range of 30–50 nm and exhibited a room temperature conductivity of 1–5 S/cm. The single molecule fibre of PANI/HCSA can be achieved by bath sonication during polymerisation. An inkjet printable PANI nanodispersion was synthesised by Ngamna *et al*. (2007) using DBAS as surfactant in HCl aqueous solution. The ratio of monomer to surfactant and oxidant was systematically controlled and the resulting nanodispersion showed a uniform particle size distribution of 82 nm, and ultraviolet-visible spectroscopy analysis indicated a high doping level. A similar approach has been utilised to synthesised PPy nanoparticles for printing purposes (Weng *et al*., 2011).

A reverse micro-emulsion, which is defined as an aggregate of surfactant molecules containing a nanometre-sized water pool in the oil phase, is another common route for preparation of micro- or nano-structures of CPs. Zhang *et al*. (2005) reported PEDOT nanotubes, 50–100 nm in diameter and

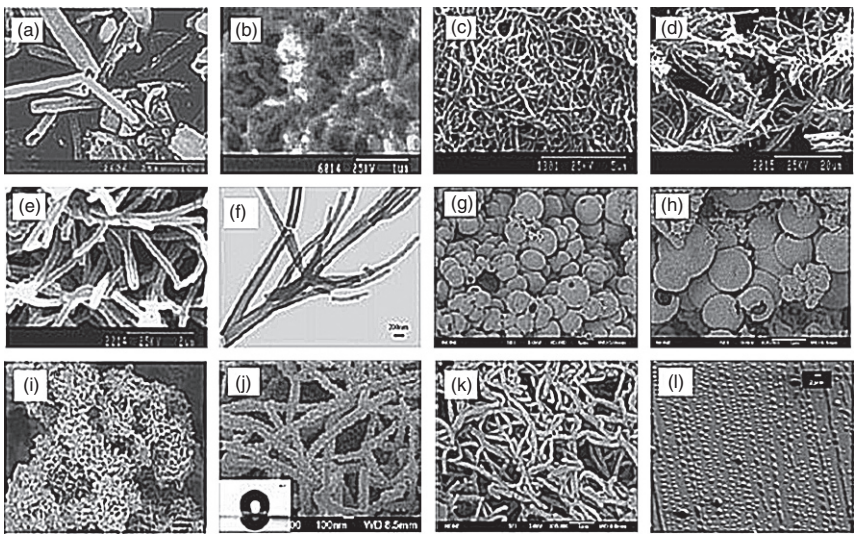

7.9 Various micro-/nano-structures of CPs, and composite micro-/nano-structures prepared by a soft-template method and associated other approaches: (a) PANI-β-NSA, (b) PANI-ANSA copolymers, (c) PPy-β-NSA prepared by chemical polymerisation, (d) PPy-β-NSA prepared by electrochemical polymerisation, (e) PANI-H_3PO_4 nanotubes, (f) PANI-CSA nanotube junctions, (g) PANI-SA hollow microspheres, (h) PANI-β-NSA hollow spheres prepared at a low temperature (−10°C), (i) electromagnetic nanofibres of PANI/γ-Fe_2O_3 by a one-step method, (j) electro-optic hydrophobic PANI-β-NSA/TiO_2 composite nanotubes by template-free method associated with TiO_2 nanoparticles as the additives, (k) electro-photoisomerisable PANI nanotubes produced by a photoisomerisable dopant and (l) mono-dispersed and oriented hollow spheres of a PANI-SA pre-oriented substrate by a template-free method associated with a deposition process (Wan, 2008).

with a conductivity of 3–6 S/cm, synthesised using a hexane/water reverse micro-emulsion consisting of sodium bis(2-ethylhexyl) sulphosuccinate (AOT) cylindrical micelles as the soft template. Wan (2008) obtained a nanotube structure of PANI by using b-naphthalene sulphuric acid (β-NSA) as both dopant and surfactant. The features of this nanostructure were determined by the amounts of monomer, dopant and oxidant used (Fig. 7.9).

7.3.3 Other materials as soft templates

As mentioned above, other materials including colloids, oligomers and DNA molecules can work as soft templates to guide the synthesis for nanostructures besides surfactants. The methods will be discussed as follows. Colloidal particles often work as micelle stabilisers in the reaction system of CPs and form core-shell structures consisting of CPs core and colloidal particles outer layer after polymerisation. Cruz-Silva *et al*. (2006) reported that PANI colloidal particles were enzymatically synthesised in aqueous media using poly(vinyl alcohol) (PVA) as steric stabiliser. Hydrochloric acid, toluenesulphonic acid, and camphorsulphonic acid were used as doping agents during polymerisation. X-ray diffraction (XRD) characterisation confirmed that PVA adsorbed at the surface of PANI particles.

CP oligomers are another soft template which is used to fabricate CP nanostructures. Li and Wang (2004) reported an approach to synthesise chiral PANI nanofibres in an aqueous solution with aniline oligomer used as template. APS and concentrated camphor sulfonic acid worked as oxidant and dopant, respectively. The high anisotropy factor of these PANI nanofibres is likely due to the 'autocatalytic effect' resulting from lower oxidation potentials of aniline oligomers (Li and Wang, 2004).

7.4 Physical methodologies for synthesis of conducting polymer nanomaterials

Besides chemical and electrochemical polymerisation, nanostructured CPs can also be created by mechanical fabrication methods, such as electrospinning and dip-pen nanolithography. In these methods, nanofibrillar structures and nanopatterns can be fabricated from CP solutions and are very important for sensing applications.

7.4.1 Electrospinning

Electrospinning is a process that produces continuous fibres with the diameters in the range of micron or nano scale. Kang *et al*. (2005) electrospun PPy nanofibres successfully from PPy/DBSA solution in chloroform. PPy

was first chemically polymerised using APS as the oxidant and DBSA as the dopant source. PPy solution with the appropriate concentration for the electrospinning was prepared by dissolving PPy powder in chloroform with extra DBSA. Electrospinning of the PPy fibre was then carried out by applying an electrical voltage of 30–45 kV. The material conductivity was around 0.5 S/cm. Pure polypyrrole nanofibres electrospun from organic solvent soluble polypyrrole were also reported by Chronakis *et al.* (2006) $[(PPy3)^{+}(DEHS)^{-}]x$, solution was prepared using the functional doping agent di(2-ethylhexyl) sulphosuccinate sodium salt (NaDEHS) to increase the solubility of PPy. Poly(ethylene oxide) (PEO) was added into solution and mixed with PPy to act as a carrier in order to improve PPy processability. Both the electrical conductivity and the average diameter of PPy nanofibres can be controlled with the ratio of PPy/PEO content (Fig. 7.10). Furthermore, PANI and PEDOT/PSS (polystyerene sulphonate) electrospun nanofibres have also been widely fabricated by the similar methods for sensing applications (Aussawasathien *et al.*, 2005; Choi *et al.*, 2010; Pinto *et al.*, 2011).

Nanocomposite CP fibres possess enhanced properties with the assistance of the other components. Thus, the utilisation of electrospinning to fabricate CP composite nanofibres has also attracted significant attention. To obtain composite CP fibres, the other components of the composites, such as metal oxides (Wang *et al.*, 2009b), biopolymers (Lee *et al.*, 2009) and CNTs (Ju *et al.*, 2008), were firstly electrospun for nanofibrillar structures. Then, CPs were chemically coated on the surface of these nanofibres by solution polymerisation or vapour polymerisation. PPy-coated TiO_2/ZnO nanofibre has been reported as an ammonia sensor by Wang *et al.* (2009b). The core TiO_2/ZnO nanofibres were prepared by electrospinning with average diameter of 100 nm. Then the electrospun fibres were immersed in $FeCl_3$ ethanol solution and dried. After drying in air for ten minutes, the TiO_2/ZnO nanofibres containing $FeCl_3$ were exposed to saturated pyrrole vapour at ambient conditions for five hours to yield PPy-coated TiO_2/ZnO nanofibres. Ji *et al.* (2008) reported a composite composed of poly(methyl methacrylate) (PMMA) nanofibres and PANI as gas sensors. The PMMA nanofibres were firstly electrospun on a glass slide which was attached on the copper template as collector to form a non-woven mat. The glass slide with non-woven PMMA mat was then put in to an aqueous solution of APS, aniline monomer and doping acid to achieve coating of the PANI on the PMMA mat. The diameter of the composite nanofibres was determined by the concentration of PMMA solution used for electrospinning.

7.4.2 Dip-pen nanolithography

Scanning probe-based lithography, which is also known as dip-pen nanolithography (DPN), has been used to fabricate conducting polymer

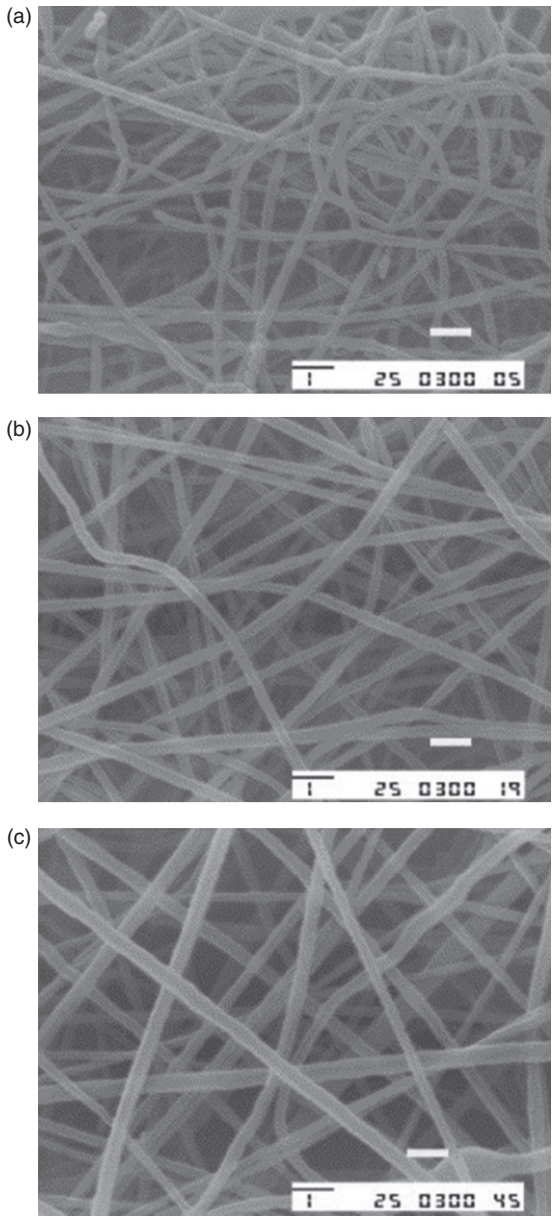

7.10 SEM micrographs of electrospun nanofibres from aqueous solutions of 1.5 wt.% PEO as carrier with various PPy concentrations. The PPy content of the nanofibres is (a) 45.5 wt.%, (b) 62.5 wt.% and (c) 71.5 wt.%. The scale bar is 1 μm (Chronakis *et al.*, 2006).

nanopatterns with precise spatial control. DPN operates by using existing atomic force microscopy (AFM) technology to deposit a wide variety of chemicals and materials onto a surface via a sharp probe tip (Moulton *et al*., 2012). The probe tip acts as an 'ink pen' by transferring molecules to the surface through a water meniscus that forms in ambient conditions as the tip nears the surface. Dot and line patterns with sizes down to 50 nm can be achieved.

Lim and Mirkin (2002) fabricated nanoscale PANI and PPy nanopatterns on modified semiconductor substrates using DPN. Electrostatic interactions between water-soluble ink materials and charged substrates are the driving force for the generation of stable DPN patterns. A series of investigations have been carried out by other groups on nanoscale writing or patterning of CPs or their corresponding monomers using AFM tips. Yang *et al*. (2006) developed a thermal DPN method for poly(3-dodecylthiophene) (PDDT) deposition on silicon oxide surfaces. The AFM tip with integrated tip heater was pre-coated with solid PDDT. The PDDT was precisely deposited onto the surface when the tip temperature was set close to PDDT's melting temperature. Finally a single monolayer film with the thickness of 2.6 nm was obtained. Maynor *et al*. (2002) used electrochemical DPN (e-DPN) to fabricate PEDOT nanowires under 50 nm on both semiconductive and isolative substrates. AFM was firstly coated with EDOT monomer, immersed in a solution of 1:1 v/v EDOT/$CHCl_3$ and dried. To pattern nanostructures, a negative bias voltage is applied between the AFM tip and the surface. The tip is translated across the surface in a pre-programmed pattern and the applied voltage electrochemically polymerises the monomer, resulting in tip-defined deposition of PEDOT on the substrate.

7.5 Chemical and biological sensing applications: nanofilms

Thin-film structures, such as those seen in nanofilms, are fundamental to gas sensing due to the small diffusion distance which accommodates fast response and recovery times. A nanocomposite nitrogen dioxide sensing device has been developed with a thin-film configuration using PANI with halogenated metallophthalocyanine (Azim-Araghi *et al*., 2011). The PANI-ClAlPc nanocomposite was able to determine 10 ppm of NO_2 within 70 s and recovered after 75 s. The sensitivity of the sensor increased with increased gas concentration but above 200 ppm saturation of the sensor was observed. The sensing mechanism here is based on the donor role of the aromatic rings of PANI and phthalocyanine and the acceptor role of NO_2, forming a charge-transfer complex. The combined components possess chemical moieties capable of transferring electronic charge to the analyte, and the speed

of this transmission is aided by the thin structural format produced during synthesis; this nanocomposite was observed to have a very rapid conductance response.

A nanofilm sensor for the determination of zinc ions has been developed using tartrazine (Tar)-doped polypyrrole (PPy) (Ansari *et al*., 2012). The doping process used this anionic azo dye to oxidise PPy monomers to form a thin conducting electrical film of PPy-Tar. The proposed reaction process in Equation [7.1] highlights the importance of this dopant in the determination of zinc ions. The device was able to determine Zn^{2+} linearly over a 0.01–100 mM concentration range and had a low detection limit of 0.008 mM. This nanofilm provided good metrological results in comparison to a similar bulk PPy-ion doped sensor developed by Pandey *et al*. (2002). This device had a higher LOD (0.1 mM) and was unable to achieve a linear determination range, demonstrating that the device's sensing abilities could be linked to the polymers synthesised dimensional format:

$$Py_{(aq)} + Tar^{3-}{}_{(aq)} \rightarrow PPy^{+} / Tar^{3-}{}_{(polym)} + e^{-}$$

$$PPy^{+} / Tar^{3-}{}_{(polym)} + Zn^{2+}{}_{(sol.)} \rightarrow PPy^{+} / Tar^{3-} / Zn^{2+}{}_{(polym)} \quad [7.1]$$

The synthesis of CPs in the nanofilm form has been heavily researched, and many synthesis routes have been developed; with each advance, more control over the film structure and properties has been realised. The ability to tailor the overall film and pore dimensions in a very precise manner allows for the very sensitive determination of analytes, particularly where the dimension control is used to enhance biomolecular loading.

A nanobioelectrode capable of determining free and total cholesterol (cholesterol oleate) has been fabricated using a nanodispersion of PANI, and the thin film was synthesised via a soft-template method (Chauhan *et al*., 2012). This method utilised sodium dodecyl sulphate (SDS) as the structural directing agent, which allowed for the controlled generation of a thin nanoporous surface for enhanced enzyme immobilisation. Enzyme kinetics studies found that the cholesterol esterase-cholesterol oxidase-PANI nanofilm has a low Michaelis-Menten constant, K_m, of 0.35 mM. This indicates that the immobilised enzymes have a high affinity for the analytes, which is a consequence of the highly uniform enzyme distribution that resulted from the uniform nanostructured polymeric matrix. It can be concluded that the uniform nanoporous conducting polymer film promotes the high enzyme loading exhibited. Response studies found the electrode to be capable of determining cholesterol at the low concentrations with a wide linear range (Table 7.1). The sensitive determination of cholesterol has great importance in the clinical studies of coronary heart disease, myocardial infarction, and arteriosclerosis. The device developed in this work

Table 7.1 Summary of data from referenced application material

Analyte	Core components	Measure method	Analytical range	LOD	Response time	Recovery time	Additional information	Reference
Ammonia	PVDF-PANI nanoparticle	Cond	–	100 ppb	2.5 m @ 1 ppm	–	PANI shell	Wojkiewicz *et al.* (2011)
	PBuA-PANI nanoparticle			250 ppb	2.5 m @ 1 ppm		PANI shell	
	PU-PANI nanofibres			20 ppb	5 m @ 1 ppm		PANI nanofibers embedded in PU	
	PPy nanowire	Cond	0.4–1.2 ppm	0.4 ppm	–	–	Magnetic alignment, electrodeposition, selective etching process	Kim and Yoo (2011)
	PPy/Ag nanotubes	Cond	10–150 ppm	10 ppm	–	500 s with N_2 purge	PVP required for uniform absorbance of Ag onto PPy	Yang *et al.* (2010)
	PPy nanowires	Cond	1.5–77 ppm	1.5 ppm	60 s @ 77 ppm	–	Electro-polymerisation	Zhang *et al.* (2009)
	PPy-TiO_2-ZnO nanofibres	Cond	50–450 ppm	0.06 ppm	15 m @ 450 ppm	30 m @ 450 ppm	Electrospinning, vapour phase polymerisation	Wang *et al.* (2009a)
	PPy-SWCNT nanocomposite	Cond	10–140 ppm 140–800 ppm	10 ppm	22 s @ 150 ppm	38 s @ 150 ppm	*In situ* chemical polymerisation, spin coating	Van Hieu *et al.* (2009)
	SnO_2/PANI nanocomposite	Cond	100–300 ppm	100 ppm	12–15 s @ 300 ppm	80 s @ 300 ppm	Chemical polymerisation	Deshpande *et al.* (2009)
Antigen/ Disease marker	PEDOT-M13 virus nanowires	Cond	20–100 nM	20 nM	–	–	Lithographically patterned electrodeposition	Arter *et al.* (2010)

Bisphenol A	PANI nanorods / MWCNT modified PGE	Amp	1–400 μM	10 nM	3 m	–	Template-directed electrodeposition	Poorahong *et al.* (2012)
Carbonyl chloride	PPy-amine* nanofibre array	Cond	0.01–2 ppm	<0.01 ppm	600 s @ 2 ppm	Single use	Temp/humidity interferences	Virji *et al.* (2009)
Cholesterol (and C. oleate)	ChET-ChOx-PANI-ITO nanofilm	LSV	250–5000 ppm	200 ppm	10 s	–	Soft-template-directed chemical polymerisation, Electrochemical deposition.	Chauhan *et al.* (2012)
Concanavalin A	MWCNT-PANI-D-glucose nanocomposite	DPV	3.3 pM – 9.3 nM	1.0 pM	–	–	*In situ* chemical polymerisation	Hu *et al.* (2012)
Copper	PPy_{ox}-GGH nanowires	SWV	20–300 nM	20 nM	–	–	Template-free polymerisation	Lin *et al.* (2010)
Dopamine	AuNP-$PANI_{ox}$-BDD nanocomposite	SWV	0.15–500 μM	0.03 μM	–	–	Electrochemical polymerisation and deposition, over-oxidation via amperometry	Song *et al.* (2012)
	Aptamer -Gp-PANI-GCE nanofilm	SWV	0.007–90 nM	1.98 pM	–	–	Chemical polymerisation, successful in human serum	Liu *et al.* (2012)
	Au nanocluster-PPy_{ox} nanocomposite coated GCE	DPV	75–20 000 nM	15 nM	–	–	Electrochemical polymerisation and deposition	Li and Lin (2007a)
	Au-PEDOT nanocomposite	DPV	20–80 μmol^{-1}	20 μmol^{-1}	–	–	Biphasic AuNP preparation, Self-assembly, chemical polymerisation, electrochemical deposition	Mathiyarasu *et al.* (2008)

(Continued)

Table 7.1 Continued

Analyte	Core components	Measure method	Analytical range	LOD	Response time	Recovery time	Additional information	Reference
Deoxyribo-nucleic acid	PPy-PANI nanotubes-AuNP-S-ssDNA nanocomposite	Imped	0.0001–1000 nM	0.1 pM	–	–	Chemical polymerisation, drop casting	Wilson *et al.* (2012)
	PPy- ssDNA single nanowire	Cond	0.001–100 pM	0.001 pM	–	–	Schottky barrier modulation, electrochemical deposition	Bangar *et al.* (2010)
[Adenine]	PTH-AuNP-MWCNT nanocomposite	DPV	0.2–1.0 μM 0.2–1.0 μM	0.01 μM 0.008 μM	–	–	Applied to calf thymus DNA	Liu *et al.* (2008)
[Guanine]	AuNP-PANI nanotubes	Imped	0.001–1000 nM	0.31 pM	–	–	Electrochemical deposition	Feng *et al.* (2008)
Dimethyl sulfoxide	PPy-HSO_3^- nanoparticles	Cond	0.1–500 μg	30 ng	–	–	*In situ* chemical polymerisation	Pirsa and Alizadeh (2012)
Epinephrine	Au nanocluster-PPy_{ox} nanocomposite coated GCE	DPV	0.3–21 μM	0.03 μM	–	–	Electrochemical polymerisation and deposition	Li an Lin (2007b)
Glucose	Nanostructured PANI- GOx Hydrogel	Amp	0.1–2.6 mM	0.1 mM	–	–	Phytic acid: gelator/ dopant	Pan *et al.* (2012)
	Nano PPy- GOx –ITO – Pt	Imped	5–70 mM	5 mM	Stable after 40 s	–	Pulsed electrodeposition,	Preethichandra *et al.* (2012)
Human serum albumin	PPPA- Anti-HSA nanowires	I-V	–	50 nM	4 m	–	Template-directed electrochemical polymerisation	Tolani *et al.* (2009)
Hydrogen	PPy nanowires	Cond	600–2500 ppm	12 ppm	72 s @ 600 ppm	–	CO interferent	Al-Mashat *et al.* (2012)
Hydrogen peroxide	PtNP-MWCNT-PANI nanocomposite	Amp	0.007–2.5 mM	2 μM	>5 s	–	*In situ* electrochemical polymerisation	Zhong *et al.* (2012)

Immuno-globulin G	Anti-IgG-PANI-ITO nanofilm	PPC	0.005–500 ppm	0.00187 ppm	–	–	Chemical polymerisation, electrodeposition	Bandodkar *et al.* (2010)
	PANI-Si nanofilm	Cond	5–500 ppm^{-1}	5 ppm^{-1}	–	–	Electrochemical polymerisation	Deep *et al.* (2012)
Neisseria gonor-rhoeae	aDNA-PANI-Fe_3O_4/ITO nanocomposite	Imped DPV	1×10^{-16}–1×10^{-6} M 1×10^{-18}–1×10^{-6} M	1×10^{-15} M 1×10^{-17} M	–	–	Electrochemical polymerisation	Singh *et al.* (2012)
Nitrogen dioxide	PANI-ClAlPc nanocomposite	Cond	10–200 ppm	10 ppm	70 s @ 10 ppm	75 s @ 10 ppm	Spin coating, Humidity interference	Azim-Araghi *et al.* (2011)
	TiO_2-PEDOT nanocables	Cond	0.1–0.4 ppm	0.007 ppm	5 m @ 0.3 ppm	15 m @ 0.3 ppm	Electrospun nanofibre template	Wang *et al.* (2009b)
Nitrite	Pt-PPy nanocomposite	CV	5.0×10^{-7}–1.0×10^{-3} M	1.5×10^{-7}	–	–	Electropolymerisation, electrochemical deposition	Li and Lin (2007c)
Prostate-Specific Antigen	Anti-PSA/Au-NP-PANI/Au nanocomposite	DPV	1 pg ml^{-1}–100 ng ml^{-1}	0.6 pg ml^{-1}	–	–	Chemical polymerisation, electrodeposition.	Dey *et al.* (2012)
Serotonin	Au nanocluster-PPy_{ox} nanocomposite coated GCE	DPV	7–2200 nM	1 nM	–	–	Electrochemical polymerisation and deposition	Li and Lin (2007a)
Triethylamine	PMMA-PANI nanofibres	Cond	20–500 ppm	20 ppm	131 s (average over range)	600 s (average over range)	Electrospinning (PMMA), chemical polymerisation (PANI)	Ji *et al.* (2008)
Uric acid	Au nanocluster-PPy_{ox} nanocomposite coated GCE	DPV	0.05–28 μM	0.012 μM	–	–	Electrochemical polymerisation and deposition	Li *et al.* (2007b)
	Au-PEDOT nanocomposite	DPV	20–130 μmol^{-1}	20 μmol^{-1}	–	–	Biphasic AuNP preparation, Self-assembly, chemical polymerisation, electrochemical deposition	Mathiyarasu *et al.* (2008)

(Continued)

Table 7.1 Continued

Analyte	Core components	Measure method	Analytical range	LOD	Response time	Recovery time	Additional information	Reference
Zinc	PPy-Tartrazine nanofilm	DP	0.01–100 nM	0.008 mM	50 s	–	Electropolymerisation	Ansari *et al.* (2012)
Pyridine deriv acetonitrile DMSO ROHs aldehydes ketones benzene deriv alkanes	PF-PPy nanocoating	Cond	450–1000 ng 500–800 ng 360–14500 ng 1.5–6.8 μg 1.5–220 μg 160–7800 μg 8–125 μg 312 μg–15 mg	8 ng 3 ng 75 ng 0.4 μg 5 μg 75 μg 0.8 μg 0.14 mg	<1 s	–	*In situ* chemical polymerisation, suitable GC sensor	Pirsa and Alizadeh (2010)

Analyte: DMSO: Dimethyl sulfoxide. TMB: 1,3,5, trimethylbenzene.
Core components:

PANI: Poly(aniline). PPy: Poly(pyrrole). PVDF: Poly(vinylidene fluoride). PBuA: Poly(butyl acrylate). PU: Polyurethane. DS: Dodecylsulphate. S-ssDNA: refers to DNA labelled at the 5′ end using 6-mercapto-1-hexane. GNs: Graphene nanosheets. ClAlPc: Chloroaluminium Phthalocyanine. PEDOT: Poly(3,4-ethylenedioxythiophene). PSSA: Poly(styrene sulfonic acid). PF: Polystyrene fibre. PPy_{ox}-GGH: Over-oxidised poly(pyrrole) – Gly-Gly-His tripeptide. TSA: Toluene-p-sulfonic acid. Amine*: Phenylenediamine. SWCNT: Single wall carbon nanotube. PPPA: Poly(pyrrole propylic acid). HSA: Human serum albumin. ITO: Indium tin oxide. MWCNT: Multiwalled carbon nanotubes. PGE: Pencil graphite electrode. PSiC: Porous silicon carbide. GOx: Glucose oxidase. BDD: Boron doped polycrystalline diamond. DBSA: Dodecylbenzene sulphonic acid. PTH: Poly(thionine). PMMA: Poly(methyl methacrylate).

Measurement method: Amp: Amperometric. Cond: Conductimetric. Imped: Impedimetric. CV: Cyclic voltammetric. SWV: Square wave voltammetric. PPC: Parallel plate capacitor. LSV: Linear sweep voltammetric. DPV: Differential pulse voltammetric. DP: Direct potentiometric.

has advantageous properties over other clinical diagnostics such as rapid response (10 s), diminutive size, reliability and reproducibility.

A dopamine aptasensor has been constructed using aniline and graphene (GR) oxide to produce a nanofilm with excellent conductivity and electron transfer properties (Liu *et al.*, 2012). Cyclic voltammetric (CV) characterisation highlighted the enhanced electron transport of the GR-PANI nanofilm in comparison to the individual nano-components. Effective enzyme immobilisation was provided via phosphoramidate bonding using the amino group of PANI and the phosphate group of dopamine. This sensor exhibited a low LOD (1.98 pM) with a linear current response in the concentration range 0.007–2.5 nM. Real human blood samples were trialled and the aptasensor showed good accuracy, which illustrated its great potential for use in clinical settings.

Bandodkar *et al.* (2010) have developed a reagentless, robust, and easy to use parallel plate capacitor-based immunosensor for the determination of human immunoglobulin G (IgG) antibody; determination of this biomolecule has an important role in settings such as clinical analyses, food detection, and environmental monitoring. The SEM images in Fig. 7.11 show the smooth, dense, uniform organisation of the PANI film, the inset in image (a) displays the nanoporous nature of the deposited polymeric matrix. Image (b) shows the uniform immobilisation of the anti-IgG biomolecules; this uniform configuration is a direct result of the nanoporous uniformity of the PANI surface. The anti-IgG-PANI nanofilm was subjected to various concentrations of human-IgG and the capacitance response data exhibited a 1.87 ng/mL detection limit and an analytical range of $5–5 \times 10^5$ ng/mL.

Another group has fabricated an immunosensor for the determination of human-IgG using a nanoPANI film; the anti-IgG biomolecules were attached to PANI through strong avidin–biotin interactions (Deep *et al.*, 2012). Figure 7.12 displays a cyclic voltammogram of the electrodeposition

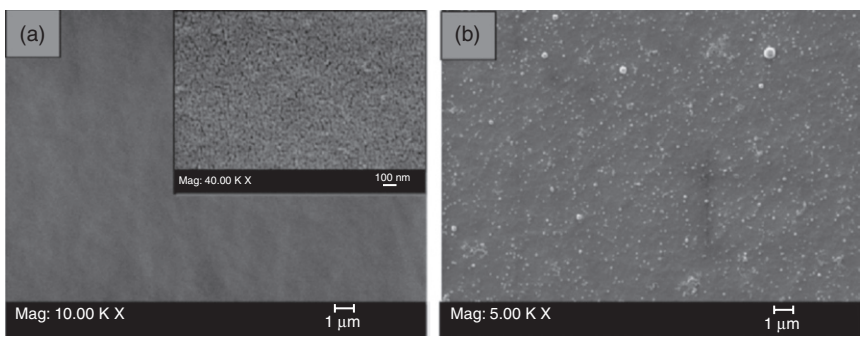

7.11 SEM images of (a) nanoPANI film (inset shows high magnification image) and (b) nanoPANI-Anti H IgG (Bandodkar *et al.*, 2010).

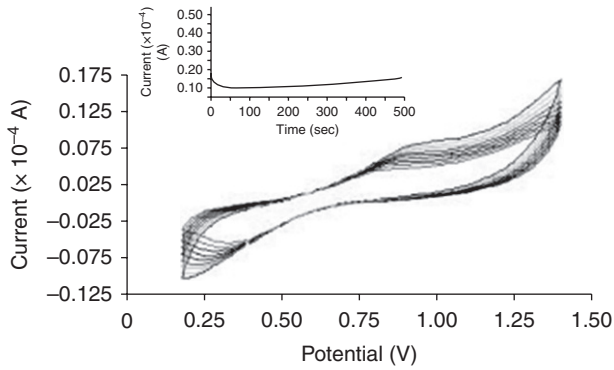

7.12 Cyclic voltammogram of PANI electrodeposition cycles. Inset: Growth curve of PANI (Deep *et al.,* 2012).

cycles of PANI. The inset shows a steady increase of charge flow with time, which indicates that the further growth of PANI resulted in improved charge-transfer characteristics; the inset also shows the control that this deposition technique holds, which prevents overloading of the conducting polymer. The optimum number of deposition cycles required to provide the smoothest film with the best charge transfer was established to be five using SEM characterisation. This sensor was found to have a linear conductance response between 5 and 550 μg/mL; above this concentration, a plateau in the response was observed due to the lack of available interaction sites. The authors noted that the most significant accomplishment of their work was found during the stability experiments. At low and high concentration ranges, little deviation in response was noted over time, and this suggested that the desired strong bonding had been achieved between the biomolecules and the conducting polymer.

7.6 Chemical and biological sensing applications: nanoparticle based sensors

The development of a dimethyl sulfoxide (DMSO) sensor highlighted the importance of the specific dopant chosen for the modification of CPs, in terms of conductivity, morphology, and sensor behaviour (Pirsa and Alizadeh, 2012). The SEM images displayed in Fig. 7.13 captured the different PPy nanoparticle morphologies formed on polyester fibres from five different sulfonate anion dopants; DS^- and PTS^- produced cabbage-like particles, whereas DBS^-, HSO_3^- and SS^- produced smaller spherical particles. Conductivity experiments found that doping with 5-sulpho salicylate (SS) gave the lowest resistance, but analyte response studies found the lowest detection limit for DMSO was achieved with the hydrogen sulphite anion

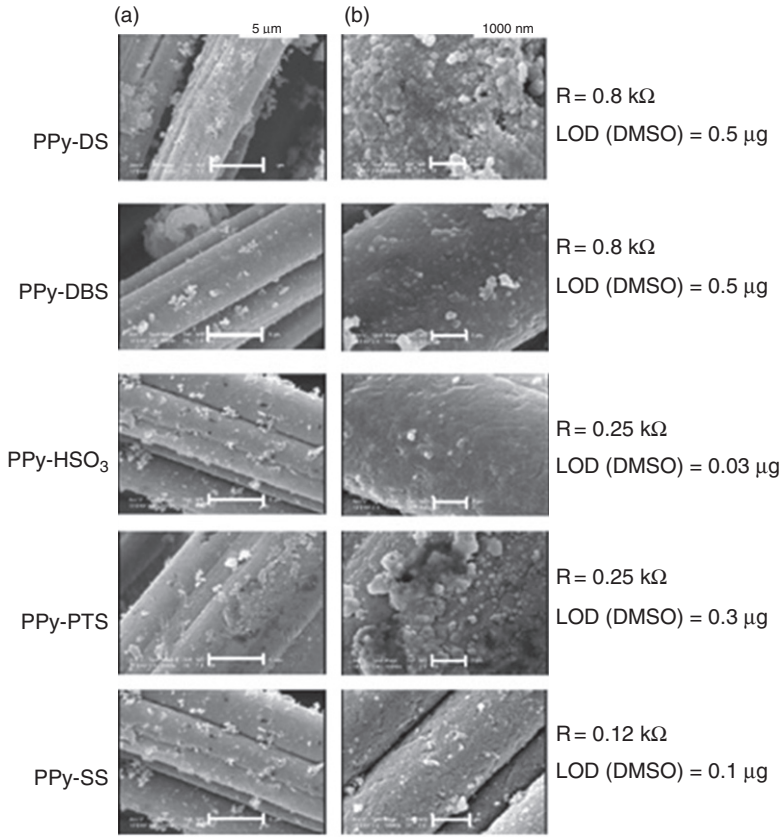

7.13 SEM images of PPy-S on the surfaces of the fibres with different sulphonate anions: (a) 5000×, scale bar 5 μm and (b) 15 000×, scale bar 1000 nm (Pirsa and Alizadeh, 2012).

(HSO^-_3) dopant. The three spherical conducting polymer structures synthesised provided higher sensitivty towards the analyte, indicating that smooth uniform conducting polymer structures can provide better sensing characteristics.

The authors of the above have also developed another PPy nanoparticle coated commercial polymer-based sensor capable of determining a wide range of volatile organic compounds (VOC) with high sensitivity (Pirsa and Alizadeh, 2010). This sensor used iron chloride doped PPy; Fig. 7.14b shows the SEM image displaying the uniform coverage of the spherical PPy nanoparticles on a polystyrene fibre. This PPy nanoparticle sensor was able to detect a large range of VOCs very quickly (around one second), and showed good stability with little morphological change after running continuously for 24 h at 100°C (Fig. 7.14c). This conducting polymer synthesised with the

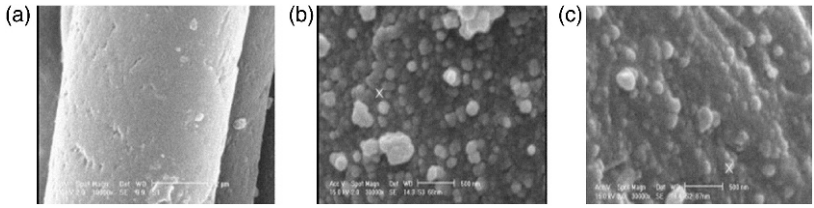

7.14 SEM images before introduction of PPy on the fibre surface (a) and PPy sensor before (b) and after (c) running at 100ºC for more than 24 h continuously (Pirsa and Alizadeh, 2010).

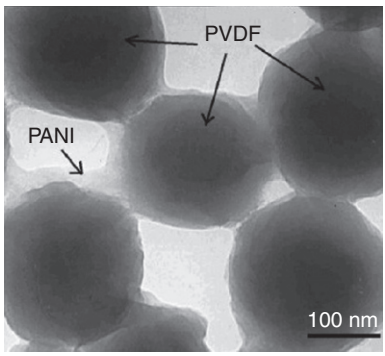

7.15 TEM image of PVDF–PANI core–shell particle (Wojkiewicz *et al.*, 2011).

chosen dopant produced a nanoparticle film with sensitive (Table 7.1) and stable characteristics.

Three types of nanoPANI-based thin-film composites have been investigated by Wojkiewicz *et al.* (2011) for their parts per billion sensing abilities for ammonia. Two of the composites utilise core–shell systems; poly(vinylidene fluoride) (PVDF) core (Fig. 7.15) and poly(butyl acrylate) (PBuA) with a PANI shell. The other composite consisted of PANI nanofibres embedded in a polyurethane (PU) matrix. The metrological parameters of the three sensor systems can be seen in Table 7.2. The low LOD exhibited by the nanofibre PU–PANI film is presumably a consequence of its superior conductivity, which enables enhanced charge-transfer characteristics. Although, the core–shell systems lacked the low LOD they did provide a faster response time and higher sensitivity, which could be attributed to the core–shell porosity. Overall, this study has demonstrated the importance of preparative techniques with regards to the resultant properties conducting polymer-based sensors can provide. The fibre-based composite secured one of the lowest ammonia detection limits of PANI-based sensors reported to date and all three systems exhibited high reproducibility and reversibility.

Table 7.2 Metrological parameters of the nanostructured materials (Wojkiewicz *et al.*, 2011)

Sensor	Detection limit (ppb)	Response time (min)	Sensitivity (% ppm^{-1})
PVDF-PANI (DBSA)	100	2.5 at 1 ppm	17
PBuA-PANI (HCl)	250	2.5 at 1 ppm	10
PU-PANI (CSA)	20	5 at 1 ppm	0.8

7.7 Chemical and biological sensing applications: metallic nanoparticles (NPs), carbon nanotubes (CNTs) and conducting polymer composites

Metallic nanoparticles (NP) are commonly used in CP composites as they provide enhanced electron-transport kinetics, which increases composite conductivity and thereby increasing sensitivity. Metallic nanoparticles can also provide redox altering properties; this has been demonstrated by Song *et al.* (2012) for the determination of dopamine principally in the presence of ascorbic acid. The square wave voltammograms (SWV) seen in Fig. 7.16 show that the addition of $PANI_{ox}$ enhances the current response to dopamine and reduces the response for ascorbic acid; the addition of AuNPs further enhances this effect to such an extent that the ascorbic acid response is negligible. Studies concluded that this sensor could operate linearly within a wide concentration range in the presence of 0.1 mM of ascorbic acid with a relatively low LOD (Table 7.1). This work illustrates the importance of combining core components to tailor an electrodes metrological performance to a specific analyte. The synergistic effects of the $PANI_{ox}$ film and the Au-NPs are seen to be an improvement in selectivity, catalytic activity, conductivity, and effective surface area. Mathiyarasu *et al.* (2008) fabricated an Au-PEDOT nanocomposite film capable of determining dopamine and uric acid; the authors attributed the selectivity exhibited to the PEDOT nanofibrillar matrix and the nanomolar sensitivity to the presence of the AuNPs.

A sensor also utilising gold has been developed by Li and Lin (2007a) for the simultaneous determination of dopamine and serotonin. This sensor (Au nanocluster-PPy_{ox} nanocomposite film modified GCE) provided a very low LOD and wide analytical range for both dopamine and serotonin (Table 7.1) in the presence of ascorbic acid. The growth of Au nanoclusters (~80 nm) was observed to be controlled by the nanoporous PPy_{ox} film which served as a deposition template. The incorporation of Au nanoclusters significantly increased electronic conductivity, effective surface area, and the catalytic activity towards the oxidation reaction for both analytes. This sensor was trialled using human blood and was found to provide satisfactory

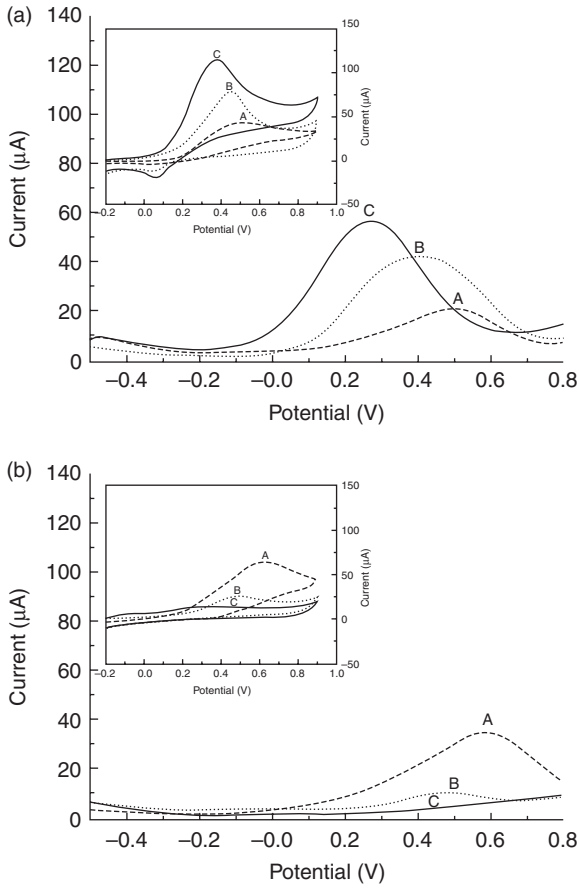

7.16 SWVs and CVs for the oxidation of (a) 0.5 mM dopamine and (b) 0.5 mM ascorbic acid at A. boron-doped diamond (BDD), B. $PANI_{ox}$-BDD, and C. AuNPs- $PANI_{ox}$-BDD electrodes (Song *et al.*, 2012).

results. This fabrication method has also been utilised for the sensitive simultaneous determination of epinephrine and uric acid in the presence of ascorbic acid (Li and Lin, 2007b). Here the modified component combination promoted selectivity by resolving any overlapping anodic peaks. The sensor was trialled and found to be successful in determining the analytes in both epinephrine hydrochloride injections and urine samples.

AuNPs have been utilised in several studies to enhance deoxyribonucleic acid (DNA) electrochemical sensing through improved biocompatibility, stability, and catalytic activity of the conducting polymer (Feng *et al.*, 2008; Liu *et al.*, 2008; Wilson *et al.*, 2012). In a recent study, bipolymer PPy-PANI nanotubes have been modified with AuNPs to permit electroactivity in neutral conditions (Wilson *et al.*, 2012). The AuNPs were utilised for

the covalent immobilisation of DNA capture probes through gold-thiol chemistry. The PPy-PANI-Au-S-ssDNA sensor was able to perform target hybridisation by immersion with the target DNA in a neutral-buffer solution for ~1.5 h; this allowed for efficient hybridisation for enhanced signal stability. The bipolymer nanotubes were noted for their enhanced hybridisation efficiency with a 2.5-fold improvement over plain AuNP electrodes. Impedance studies were carried out on four types of target DNA and it was observed that the combination of core components that were used in this sensor improved conductivity, and provided a good platform for the sensitive and selective detection of the different DNA target types. The sensor was found to have a 0.1 pM LOD and a 0.0001–1000 nM linear range. This fabrication method avoids the complex immobilisation chemistry usually required for the production of polymer-based DNA sensors and the PPy-PANI-Au platform accommodates a relatively high concentration of DNA molecules compared with other literature available at the time of publishing.

An AuNP-PANI composite has been used as the basis for a prostate-specific antigen immunosensor (Dey *et al*., 2012). The incorporation of AuNPs increased the electroactive surface area of the PANI therefore enhancing sensitivity towards the cancer biomarker. Using differential pulse voltammetry (DPV) a wide linear detection range of 1 pM–100 nM was established and a LOD of 0.6 pM was estimated. The high performance observed using this sensor was proposed to be due to the very uniform coating of AuNPs on the highly homogenous PANI nanowires displayed in SEM and TEM imaging. The use of this device for the analysis of real samples is currently in progress.

Metal oxides can also be used to enhance sensor performance; a study by Singh *et al.* (2012) saw the fabrication of a genosensor using iron oxide and DNA modified PANI for the specific determination of the bacteria Neisseria gonorrhoeae. Addition of Fe_3O_4 improved DNA immobilisation, catalytic activity, sensitivity, and selectivity of the genosensor. SEM imaging displayed a complex network of PANI nanotubes with Fe_3O_4 well embedded and stacked neatly in lattice planes with interplanar spacing of roughly 0.26 nm. This structure allowed for the successful immobilisation of probe DNA and response studies were undertaken using both electrochemical impedance spectroscopy and DPV; wide detection ranges and low detection limits were achieved (Table 7.1). The use of iron oxide as the enhancing NP has had further consideration and the trialling of other metallic nanoparticles or CNTs has been suggested as a possible route of future improvement for this sensor. A study by Deshpande *et al.* (2009) showed how the integration of a metal oxide (SnO_2) to a PANI micelle matrix enhanced the sensors recovery time by two fold while the analytical range and response time remained largely the same (Table 7.1).

Yang *et al.* (2010) have fabricated an ammonia sensor using AgNP-PPy nanotubes. The PPy nanotubes were prepared via a simple self-degrading template approach and the AgNPs were absorbed onto the tubes via the addition of an $AgNO_3$ and polyvinylpyrrolidone (PVP) mixture. The PVP played a crucial role in assuring that the silver particles did not form aggregates on the tubular structures. When PVP was present, the response was found to be almost reversible and reproducible, which was attributed to the small (30–40 nm) size and uniform distribution of the AgNPs. Here, AgNPs have been used to improve the electrical characteristics of the conducting polymer; with the aid of PVP a uniform NP coverage was achieved to optimise conductivity of the sensory material.

Many hydrogen peroxide electrochemical sensors exist and a fair proportion of these use enzyme recognition elements, which make them less amenable to the harsh environments which could be encountered during analyses. A PtNP-PANI-multi-walled CNT nanofilm has been developed for the non-enzymatic determination of H_2O_2 (Zhong *et al.*, 2012). PtNPs were deposited onto the surface of the MWCNT-PANI composite and it was observed that they adhered to the outer structures and the interspaces of the nanocomposite. CV studies displayed an improvement in PANIs redox characteristics with the addition of the PtNPs. Amperometry showed an increase in current response to H_2O_2 when PANI was combined with the MWCNTs and a further enhanced response when the PtNPs were incorporated. The sensor demonstrated a good analytical performance (Table 7.1); these results were due to the large specific surface, high redox electrochemical activity and good stable environment provided by the hybridised materials. A Pt-PPy nanocomposite fabricated by Li and Lin (2007c) showed excellent catalytic activity towards nitrite reduction with great storage stability and reproducibility; natural water samples were analysed with satisfactory results.

7.7.1 CNTs and conducting polymer nanocomposites

CNTs are exploited for their thermal and mechanical strength, biocompatibility, and unique electronic properties (Jorio *et al.*, 2008).The electronic properties can be metallic or semiconducting depending on the carbon atom arrangement (Dai *et al.*, 2002). Poorahong *et al.* (2011) have fabricated a pencil graphite electrode (PGE) modified with PANI nanorods and MWCNTs for the determine Bisphenol A (BPA). This chemical has recently been generating concern over its health effects, as it has been found to leach from products comprised of compounds such as epoxy resin, polycarbonate, and polyvinylchloride. CV studies using 0.1 mM BPA indicated that the MWCNTs have excellent electrocatalytic properties for this analyte, which can be further enhanced by the presence of PANI nanorods. This device was shown to have a LOD of 10 nM and a linear range of 1–400 μM, the

modified device showed a substantial increase in sensitivity compared to a bare PGE, PANI nanorod PGE, and MWCNT PGE. The hybrid device also proved to have great stability with only a 4.2% relative standard deviation over 95 analysis cycles.

SWCNTs have been used in conjunction with PPy in the form of thin films for the fast determination of ammonia (Van Hieu *et al.*, 2009). In this study a simple chemical polymerisation method was utilised for the synthesis of a PPy-SWCNT nanocomposite thin film. Response and recovery times noted for this sensor were shorter than for any other PPy-based sensor presented previously; several theories were considered as to how this hybrid composite achieved these results. The authors suggested that the thin-film configuration produced by the spin-coating synthesis aids the rapid diffusion of gaseous ammonia. This rapid diffusion was suggested to be aided further by the nanochannels present inside the CNTs. Regardless of the exact mechanism, this hybrid material in the presence of 150 ppm NH_3 had an impressive response time of 22 s and a recovery time of 38 s.

In a study by Hu *et al.* (2012) a sensor was developed for the determination on concanavalin A (Con A) using MWCNTs and PANI. The conducting polymer PANI was utilised for its efficient biomolecule immobilisation properties, while the MWCNTs were incorporated for their mechanical strength, which PANI lacks. The PANI-MWCNT nanocomposite allowed for the efficient immobilisation of D-glucose and BSA, in addition to providing sufficient transducer properties in the presence of these non-conducting biomolecules. Using DPV the detection limit and linear range were established to be 3.3 pM and 3.3 pM to 9.3 nM respectively; indicating that this hybrid configuration has efficient sensing properties for Con A.

7.8 Chemical and biological sensing applications: nanowires and nanotubes

CPs in the form of nanowires or nanotubes typically possess enhanced sensing abilities consequential of their 1-D structures. This structure allows for rapid analyte diffusion and signal transmission. Nanowire-based devices can be the product of a single-wire or multi-wire arrays. Both have their own advantages and disadvantages for different applications; a single nanowire simply has the advantage of allowing for an easier understanding and control of its structure, properties, and sensing mechanisms (Bangar *et al.*, 2010). Many synthesis methods have been developed for nanowires and nanotubes, Kim and Yoo (2011) have fabricated an ammonia gas sensor using a novel self-patterning method. This method uses a combination of magnetic alignment, electrodeposition, and a selective etching process. This new method allows for a larger contact area between the PPy nanowire and two gold electrodes; SEM images in

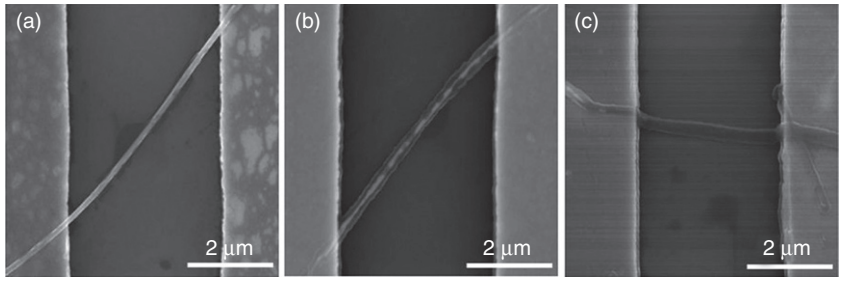

7.17 SEM images of (a) magnetically aligned Ni nanowire on Au electrodes, (b) after electropolymerisation of PPy and (c) PPy nanowire after Ni removal (Kim and Yoo, 2011).

Fig. 7.17 show the three fabrication steps. This device was able to detect ammonia at a 0.4 ppm concentration, which is the lowest reported at the date of publication using only PPy as the sensing material. One drawback of this single-wire device is the narrow linear range (0.4–1.2 ppm), but the novel fabrication methodology makes this device simple, fast and cost-effective to produce in comparison to conventional methods such as e-beam lithography.

An ammonia sensor utilising a nanowire array configuration was developed by Zhang *et al.* (2009) using perchlorate doped PPy. The wires were synthesised by electrochemical polymerisation in AAO templates; this generated a highly dense array of very smooth nanowires, which can be seen in Fig. 7.18. The sensor mechanism has been suggested in Equation [7.2] which highlights the necessity of the perchlorate doping. This sensor had a LOD of 1.5 ppm and a linear range of 1.5–77 ppm. In comparison to other reports the response time (60 s at 77 ppm) was relatively rapid; this was attributed to the very narrow wires in a dense array configuration, which promotes the rapid diffusion of ammonia.

$$PPy^{+} / ClO_4^{-} + NH_3\,(\delta^{-}) \rightleftharpoons PPy^{0} / NH_3\,(\delta^{-})^{+} + ClO_4^{-} \qquad [7.2]$$

A hydrogen sensor developed by Al-Mashat *et al.* (2012) utilised PPy nanowires deposited on gold electrodes via template-free electropolymerisation. This sensor was capable of detecting hydrogen with a fast response (72 s at 600 ppm), which is considered critical for hydrogen sensing due to its highly flammable nature. The alteration of anodic current during electropolymerisation was used to optimise the nanowire morphology; a low current of 13 mC produced nanowires of varying lengths which appeared to merge and form irregular shaped lumps, whereas nanowires produced at 90 mC had a uniform configuration. The uniform PPy nanowire array demonstrated a LOD of 12 ppm and a linear range of 600–2500 ppm; controlled synthesis of

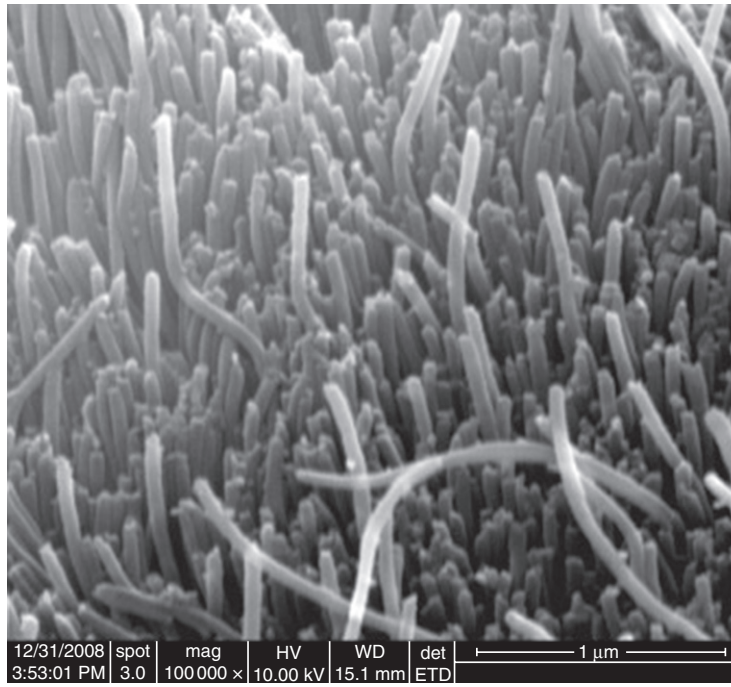

7.18 SEM image of PPy nanowires grown in AAO template (Zhang *et al.,* 2009).

this uniform nanowires array produced a hydrogen sensor with high sensitivity and rapid performance.

The electrochemical determination of copper has been significantly enhanced by the use of a biological recognition element; Gly-Gly-His (GGH) tripeptide which has a selective binding affinity for copper ions. The incorporation of this biological structure into the electrode has been demonstrated in several studies over the past decade; in a recent study by Lin *et al*. (2010) GGH was covalently bound to over-oxidised polypyrrole (PPy_{ox}) nanowires. The over-oxidation is required to prevent PPy oxidation during the SWV analyses, as the oxidation of PPy would generate a peak similar to that seen with Cu^0/Cu^{2+} oxidation. This sensor was shown to linearly determine copper ions in a 20–300 nM concentration range. The nanowire configuration benefits were demonstrated with a simple comparative SWV analysis between the nanowire and a nanofilm utilising the same materials; this clearly showed the nanowire had superior ligand functionalisation, this allowed for a higher concentration of tripeptide recognition elements to be immobilised which enhanced sensitivity. This PPy_{ox}-GGH nanowire biosensor uses a novel configuration which allows

for easy assembly and provides sensitive determination in a reproducible and stable manner.

The ability to integrate biological recognition molecules during conducting polymer synthesis could be advantageous for reasons of convenience of a one-step process (Ramanathan *et al*., 2004). A lithographically patterned nanowire electrodeposition (LPNE) method has been utilised for the synthesis of PEDOT- M13 bacteriophage nanowire arrays; this method does not require post-wire synthesis modification (Arter *et al*., 2010). A fluorescent microscopy image in Fig. 7.19 shows the virus coverage on the nanowires; the line trace below demonstrates the pattern of fluorescence corresponding to the virus incorporated nanowires. The virus–PEDOT hybrid has the potential to be altered and used for the determination of many biomolecules that are associated with specific disease processes. The appeal of the nanowire-based sensor lies in the ability to allow for label and reagent free, real-time sensing with low production costs and small device size. The resistance change was linear over a 20–100 nM concentration of positive antibodies; these results were obtained without device modification, therefore phage-loading, device configuration and nanowire diameter/length could potentially improve performance. This study indicates that the one-step process

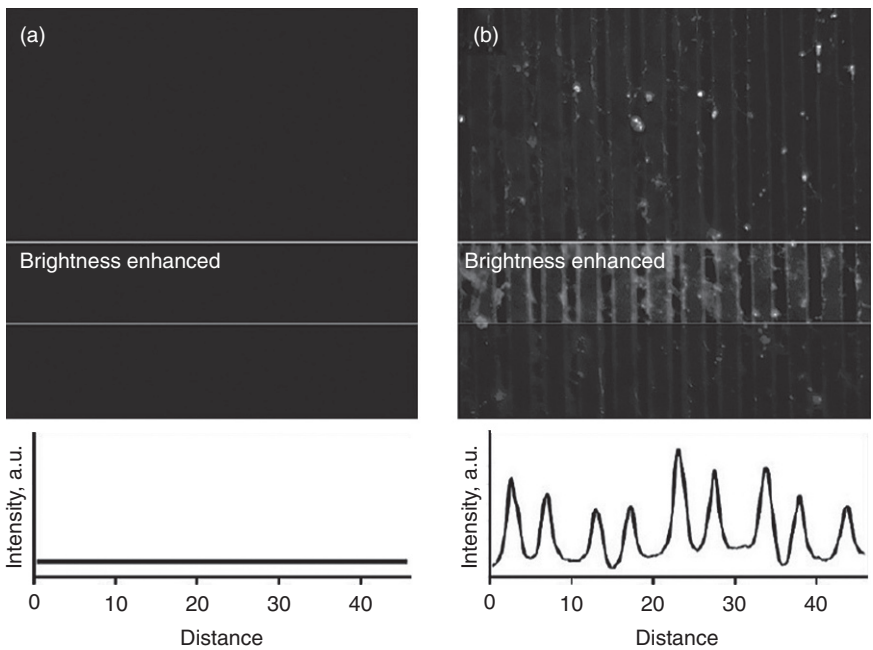

7.19 Fluorescent microscopy images (a) PEDOT nanowires after incubation with anti-M13 antibody and (b) PEDOT–virus nanowires after incubation with anti-M13 antibody (Arter*et al.,* 2010).

can successfully provide a sensitive device although, it has been noted that the two-step procedure can provide more scope for optimisation such as the selection of binding positions (Teles and Fonseca, 2008).

Poly(pyrrolepropylic) acid (PPPA) nanowires have been synthesised via a template-directed electrochemical polymerisation method and modified with anti-human serum albumin(HSA) antibody for the selective determination of HSA, a protein shown to play a significant role in the determination of impaired liver and or kidney function (Tolani *et al.*, 2009). The covalent attachment of the anti-HSA to the PPPA nanowires was aided by EDC/NHS cross-linking, which activates the carboxylic acid moieties of the polymer allowing binding to occur with the amine groups of the antibodies. The conducting polymer provided a stable organic conducting matrix for antibody immobilisation, and the device provided a significant current change to 100 nM HSA; this was achieved without parameter optimisation, and research is underway to generate more robust metrological data.

A single PPy nanowire genosensor was successfully developed for the sensitive determination of the human breast cancer gene (Bangar *et al.*, 2010). This study assessed the best immobilisation location for DNA using two different methods, which resulted in two different sensing mechanisms: gating effect and a work-function based sensor. The two immobilisation approaches were (1) immobilisation of DNA on the PPy nanowire bridge, and (2) immobilisation of DNA on the gold electrodes. The conducting polymer was found to be best suited to the role of conduction channel, as the immobilisation of the DNA to the PPy nanowire resulted in a much poorer metrological response.

7.9 Chemical and biological sensing applications: nanofibres, nanocables and other conducting polymer structures

A study by Chen *et al.* (2012) compared the properties of two nanoPANI sensors to the determination of ammonia: a single PANI nanofibre, and a thin nanoPANI film. The fibre exhibited superior sensitivity and response times; this was determined to be the result of the large surface area of the small diameter fibre, which permitted faster ammonia diffusion. The single PANI fibre was then compared to a CNT; the fibre showed high sensitivity at lower concentrations, 1–10 ppm, whereas the CNT had a wider sensing range at higher concentrations, 20–300 ppm. This research is aimed to be a platform for the development of a gas sensing array for ammonia which will combine high sensitivity with a wide sensing range.

Several studies have presented chemical sensors based on doped PANI nanofibres (Virji *et al.*, 2005a, 2005b, 2009). Each study utilises a fibre

modification agent which reacts with the analyte to produce an acid which dopes the conducting polymer producing a significant change in resistance, but this means the sensors are non-regenerative. Virji *et al.* (2009) developed a phosgene (carbonyl chloride) sensor using an amine-polyaniline nanofibre array. The PANI nanofibres were synthesised using a rapid mixing method, and water was used as the solvent which allowed for easy modification of the fibres with water-soluble amines. The chemical reaction relating to the amine-phosgene reaction is depicted in Equation [7.3]; the resultant hydrochloric acid dopes the PANI converting it from an emeraldine base to an emeraldine salt oxidation state. Many amines and amine chlorides were trialled; phenylenediamine provided the largest phosgene response. The sensor was able to detect phosgene well below the immediate danger to health and life limit of 2 ppm.

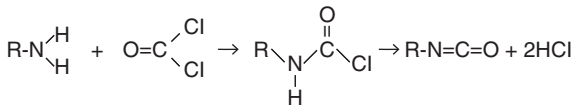

[7.3]

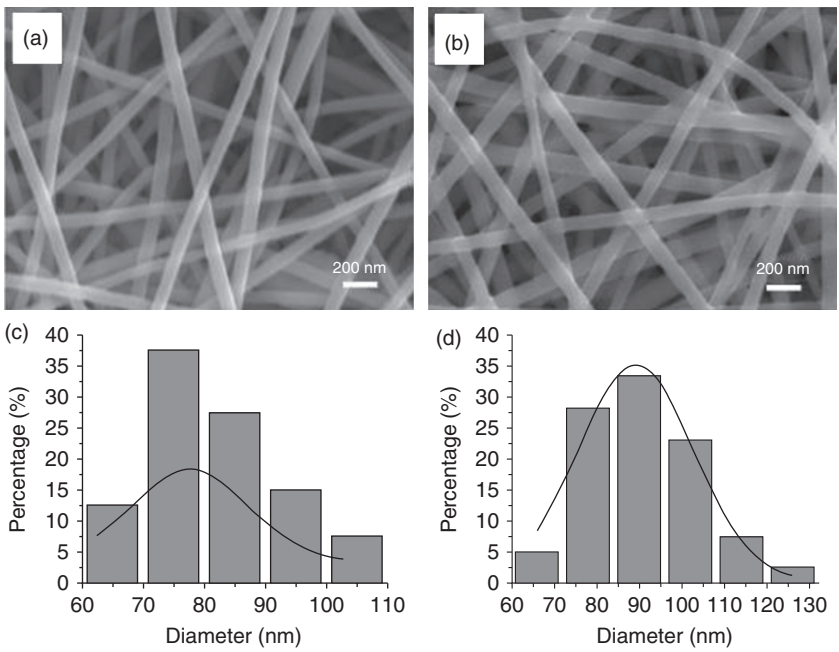

7.20 (a) SEM image of TiO_2 nanofibres. (b) SEM image of TiO_2-PEDOT nanocables. (c) and (d) Histograms showing the size distribution of TiO_2 nanofibres and TiO_2-PEDOT nanocables, respectively (Wang *et al.,* 2009a).

A simple cost-effective fabrication method was presented by Wang *et al.* (2009a) for the production of a core-sheath TiO_2-PEDOT nanocable capable of determining nitrogen dioxide and ammonia at very low concentrations. The cables were synthesised using an electrospun TiO_2 nanowire template coated with PEDOT using vapour phase polymerisation. The nanowire provides a supporting template for the ultrathin (~5.8 nm) PEDOT coating which gives the material a large surface to volume ratio which is required for sensitive detection of gaseous compounds. The sensor detection limit for NO_2 was estimated to be 7 ppb and 675 ppb for NH_3. It is speculated that the good detection limits observed are in part due to the ultrathin and very uniform coverage of the conducting polymer over the TiO_2 core (Fig. 7.20).

Ji *et al.* (2008) have developed a bipolymer gas sensor for the determination of triethylamine. The fabrication method utilised electrospinning for the production of PMMA nanofibres and chemical polymerisation for the PANI nanofibres. Fibre thickness was trialled during synthesis and an enhanced sensing magnitude was exhibited for smaller diameter fibres, thus supporting the theory that a thin fibre can achieve a higher surface to volume ratio therefore providing more sites for gas adsorption promoting higher sensitivity. This sensor provided a wide linear range with relatively fast recovery and response times (Table 7.1); cycle studies found the sensor to be reversible with good reproducibility.

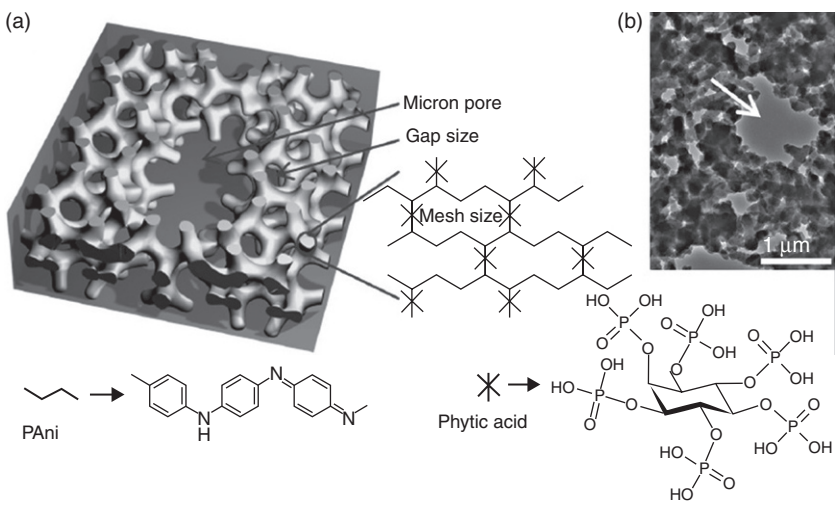

7.21 (a) Schematic illustration of the 3D hierarchal microstructure: three levels of hierarchal porosity from angstrom, nanometre to micron sized pores are highlighted by arrows. (b) TEM image showing the nanostructured network with a micron sized pore (Pan *et al.,* 2012).

7.9.1 Other conducting polymer structures

When CPs are integrated into a hydrogel structure they usually lose conductivity, but Pan *et al.* (2012) have demonstrated a PANI-hydrogel that possesses excellent electrochemical activity and superior conductivity over comparative methods reported to date. Phytic acid was used as the hydrogel support; this provided a stable platform for enzyme immobilisation due to the three-dimensional nanoporous structures. Figure 7.21a illustrates the hydrogel structure, and Fig. 7.21b is a TEM image of the nanostructured network. The PANI glucose oxidase hydrogel 3D hierarchical nanostructure exhibited a low detection limit but a narrow linear range (Table 7.1).

Preethichandra *et al.* (2012) have fabricated a nanobiosensor which utilised PPy to provide porous nanocavities capable of holding glucose oxidase. A pulsed electrodeposition technique allowed random growth of PPy islands, which improved the sensor's linear range. The effects of applied voltage, mark-to-space ratio, and pulse width allowed control over the physical dimensions of the pores, meaning they could be tailored to the enzyme's molecular size. A detection limit of 5 mM was found and a wide linear range of 5–70 mM was achieved with the possibility of enhancing this by widening the channel between the working and counter electrode.

7.10 Conclusion

Nanostructured CPs are continuously being utilised in electrochemical sensors, and will continue to be utilised as they possess many unique and modifiable properties. Many scientific fields, from clinical to environmental, will continue to gain from these advancements. Many of the sensors explored above provide the opportunity of sensitive, fast, reagentless, real-time sensing with simple and affordable fabrication methodologies and many of these have scope for further improvement.

7.11 References

Aguilar, A. D., Forzani, E. S., Nagahara, L. A., Amlani, I., Tsui, R. and Tao, N. (2008) A breath ammonia sensor based on conducting polymer nanojunctions. *IEEE Sensors J.*, **8** (3), 269–273.

Ali, S. R., Parajuli, R. R., Balogun, Y., Ma, Y. and He, H. (2008) A nonoxidative electrochemical sensor based on a self-doped polyaniline/carbon nanotube composite for sensitive and selective detection of the neurotransmitter dopamine: a review. *Sensors*, **8** (12), 8423–8452.

Al-Mashat, L., Debiemme-Chouvy, C., Borensztajn, S. and Wlodarski, W. (2012) Electropolymerised polypyrrole nanowires for hydrogen gas sensing. *J. Phys. Chem. C*, **166**, 13388–13394.

Al-Mashat, L., Shin, K., Kalantar-Zadeh, K., Plessis, J. D., Han, S. H., Kojima, R. W., Kaner, R. B., Li, D., Gou, X. and Ippolito, S. J. (2010) Graphene/polyaniline nanocomposite for hydrogen sensing. *J. Phys. Chem. C,* **114** (39), 16168–16173.

An, K. H., Jeong, S. Y., Hwang, H. R. and Lee, Y. H. (2004) Enhanced sensitivity of a gas sensor incorporating single-walled carbon nanotube–polypyrrole nanocomposites. *Adv. Mater.*, **16** (12), 1005–1009.

Ansari, R., Delavar, A. and Mohammed-Klan, A. (2012) Solid-state ion selective electrode based on polypyrrole conducting polymer nanofilm as a new potentiometric sensor for $Zn^{2\backslash+}$ ion. *J. Solid State Electrochem.*, **16** (10), 3315–3322.

Arter, J., Taggart, D., McIntire, T., Penner, R. and Weiss, G. (2010) Virus-PEDOT nanowires for biosensing. *Nano Lett.*, **10**, 4858–4862.

Aussawasathien, D., Dong, J. H. and Dai, L. (2005) Electrospun polymer nanofiber sensors. *Synth. Met.*, **154** (1), 37–40.

Azim-Araghi, M., Jafari, M., Barhemat, S. and Karimi-Kerdabadi, E. (2011) Gas mixture sensor based on polyaniline-chloroaluminium phthalocyanine nanocomposite thin films. *Sens. Lett.*, **9**, 1349–1355.

Bandodkar, A., Dhand, C., Arya, S., Pandey, M. and Malhotra, B. (2010) Nanostructured conducting polymer based reagentless capacitive immunosensor. *Biomed. Microdevices*, **12** (1), 63–70.

Bangar, M., Shirale, D., Purohit, H., Chen, W., Myung, N. and Mulchandani, A. (2010) Single conducting polymer nanowire based sequence-specific, base-pair-length dependant label-free DNA sensor. *Electroanalysis*, **23** (2), 371–379.

Chandrakanthi, R. and Careem, M. (2002) Preparation and characterization of CdS and Cu_2S nanoparticle/polyaniline composite films. *Thin Solid Films*, **417** (1), 51–56.

Chauhan, R., Deepshikha, and Basu, T. (2012) Development of a reusable transducer matrix based on nano structured conducting polyaniline and its application to cholesterol biosensor. *Sci. Adv. Mater.*, **4** (1), 96–105.

Choi, J., Lee, J., Jung, D. and Shim, S. E. (2010) Electrospun PEDOT: PSS/PVP nanofibers as the chemiresistor in chemical vapour sensing. *Synth. Met.,* **160** (13), 1415–1421.

Chronakis, I. S., Grapeson, S. and Jakob, A. (2006) Conductive polypyrrole nanofibres via electrospinning: electrical and morphological properties. *Polymer,* **47**, 1597–1603.

Cruz-Silva, R., Ruiz-Flores, C., Arizmendi, L., Romero-Garcia, J., Arias-Marin, E., Moggio, I., Castillon, F. and Farias, M. (2006) Enzymatic synthesis of colloidal polyaniline particles. *Polymer*, **47** (5), 1563–1568.

Dai, L., Soundarrajan, P. and Kim, T. (2002) Sensors and sensor arrays based on conjugated polymers and carbon nanotubes. *Pure Appl. Chem.*, **74** (9), 1753–1772.

Deep, A., Sharma, A., Kumar, P. and Bharadwaj, L. (2012) Nanostructured polyaniline–silicon substrate for protein biosensing. *Sens. Actuators B: Chem.*, **171**, 210–215.

Deshpande, N., Gudage, Y., Sharma, R., Vyas, J., Kim, J. and Lee, Y. (2009) Studies on tin oxide-intercalated polyaniline nanocomposite for ammonia gas sensing applications. *Sens. Actuators B: Chem.,* **138** (1), 76–84.

Dey, A., Kaushik, A., Arya, S. and Bhansali, S. (2012) Mediator free highly sensitive polyaniline–gold hybrid nanocomposite based immunosensor for prostate-specific antigen (PSA) detection. *J. Mater. Chem.*, **22** (29), 14 763–14 772.

Feng, Y., Yang, T., Zhang, W., Jiang, C. and Jiao, K. (2008) Enhanced sensitivity for deoxyribonucleic acid electrochemical impedance sensor: Gold nanoparticle/polyaniline nanotube membranes. *Anal. Chim. Acta*, **616** (2), 144–151.

Forzani, E. S., Li, X. and Tao, N. (2007) Hybrid amperometric and conductometric chemical sensor based on conducting polymer nanojunctions. *Anal. Chem.*, **79** (14), 5217–5224.

Forzani, E. S., Zhang, H., Nagahara, L. A., Amlani, I., Tsui, R. and Tao, N. (2004) A conducting polymer nanojunction sensor for glucose detection. *Nano Lett.*, **4** (9), 1785–1788.

Gemeay, A. H., Mansour, I. H., El-Sharkawy, R. G. and Zaki, A. B. (2005) Preparation and characterization of polyaniline/manganese dioxide composites via oxidative polymerization: Effect of acids. *Eur. Polym. J.*, **41** (11), 2575–2583.

Guo, Z., Shin, K., Karki, A. B., Young, D. P., Kaner, R. B. and Hahn, H. T. (2009) Fabrication and characterization of iron oxide nanoparticles filled polypyrrole nanocomposites. *J. Nanopart. Res.*, **11** (6), 1441–1452.

Han, M. G. and Foulger, S. H. (2005) 1-Dimensional structures of poly(3,4-ethylenedioxythiophene) (PEDOT): A chemical route to tubes, rods, thimbles, and belts. *Chem. Commun.*, **24**, 3092–3094.

Hu, F., Chen, S., Wang, C., Yuan, R., Xiang, Y. and Wang, C. (2012) Multi-wall carbon nanotube-polyaniline biosensor based on lectin–carbohydrate affinity for ultrasensitive detection of Con A. *Biosens. Bioelectron.*, **32** (1), 202–207.

Huang, C. L., Partch, R. E. and Matijević, E. (1995) Coating of uniform inorganic particles with polymers ii. polyaniline on copper oxide. *J. Colloid Interface Sci.*, **170** (1), 275–283.

Huang, J. and Kaner, R. B. (2004a) A general chemical route to polyaniline nanofibers. *JACS*, **126** (3), 851–855.

Huang, J. and Kaner, R. B. (2004b) Nanofiber formation in the chemical polymerization of aniline: a mechanistic study. *Angew. Chem. Int. Ed.*, **43**, 5817–5821.

Huang, J. and Kaner, R. B. (2006) The intrinsic nanofibrillar morphology of polyaniline. *Chem. Commun.*, **4**, 367–376.

Huang, J., Virji, S., Weiller, B. H. and Kaner, R. B. (2003) Polyaniline nanofibers: facile synthesis and chemical sensors. *JACS,* **125** (2), 314–315.

Huang, J., Virji, S., Weiller, B. H. and Kaner, R. B. (2004) Nanostructured polyaniline sensors. *Chem. Eur. J.,* **10** (6), 1314–1319.

Hulteen, J. C. and Martin, C.R. (1997) A general template-based method for the preparation of nanomaterials. *J. Mater. Chem.*, **7** (7), 1075–1087.

Jeevananda, T., Kim, N. H., Heo, S. B. and Lee, J. H. (2008) Synthesis and characterization of polyaniline-multiwalled carbon nanotube nanocomposites in the presence of sodium dodecyl sulfate. *Polym. Adv. Technol.*, **19** (12), 1754–1762.

Ji, S., Li, Y. and Yang, M. (2008) Gas sensing properties of a composite composed of electrospun poly (methyl methacrylate) nanofibers and *in situ* polymerized polyaniline. *Sens. Actuators B: Chem.,* **133** (2), 644–649.

Jiang, S., Chen, J., Tang, J., Jin, E., Kong, L., Zhang, W. and Wang, C. (2009) Au nanoparticles-functionalized two-dimensional patterned conducting PANI nanobowl monolayer for gas sensor. *Sens. Actuators B: Chem.*, **140** (2), 520–524.

Jorio, A., Dresselhaus, G. and Dresselhaus, M. (2008) Carbon nanotubes advanced topics in the synthesis, structure, properties and applications [online]. Germany: Springer. [Accessed 14 August 2012].

Ju, J. W., Choi, G. R., Jung, H. R. and Lee, W. J. (2008) Electrochemical properties of electrospun PAN/MWCNT carbon nanofibers electrodes coated with polypyrrole. *Electrochim. Acta*, **53** (19), 5796–5803.

Kang, T. S., Lee, S. W., Joo, J. and Lee, J. Y. (2005) Electrically conducting polypyrrole fibers spun by electrospinning. *Synth. Met.*, **153** (1–3), 61–64.

Killard, A. J. (2010) 'Nanostructured conducting polymers for (electro) chemical sensors' in Eftekhari A, *Nanostructured Conductive Polymers*, John Wiley & Sons, Chichester, 563–598.

Kim, D. and Yoo, B. (2011) A novel electropolymerization method for PPy nanowire-based NH3 gas sensor with low contact resistance. *Sens. Actuators B: Chem.*, **160** (1), 1168–1173.

Lee, J. Y., Bashur, C. A., Goldstein, A. S. and Schmidt, C. E. (2009) Polypyrrole-coated electrospun PLGA nanofibers for neural tissue applications. *Biomaterials*, **30** (26), 4325–4335.

Li, J. and Lin, X. (2007a) Simultaneous determination of dopamine and serotonin on gold nanocluster/overoxidized-polypyrrole composite modified glassy carbon electrode. *Sens. Actuators B: Chem.,* **124** (2), 486–493.

Li, J. and Lin, X. (2007b) Electrodeposition of gold nanoclusters on overoxidized polypyrrole film modified glassy carbon electrode and its application for the simultaneous determination of epinephrine and uric acid under coexistence of ascorbic acid. *Anal. Chim. Acta*, **596** (2), 222–230.

Li, J. and Lin, X. (2007c) Electrocatalytic reduction of nitrite at polypyrrole nanowire–platinum nanocluster modified glassy carbon electrode. *Microchem. J.*, **87** (1), 41–46.

Li, W. and Wang, H. L. (2004) Oligomer-assisted synthesis of chiral polyaniline nanofibers. *JACS*, **126** (8), 2278–2279.

Lim, J. H. and Mirkin, C. A. (2002) Electrostatically driven dip-pen nanolithography of conducting polymers. *Adv. Mater.,* **14** (20), 1474–1477.

Lin, M., Cho, M., Choe, W., Yoo, J. and Lee, Y. (2010) Polypyrrole nanowire modified with Gly-Gly-His tripeptide for electrochemical detection of copper ion. *Biosens. Bioelectron.,* **26** (2), 940–945.

Liu, H., Wang, G., Chen, D., Zhang, W., Li, C. and Fang, B. (2008) Fabrication of polythionine/NPAu/MWNTs modified electrode for simultaneous determination of adenine and guanine in DNA. *Sens. Actuators B: Chem.*, **128** (2), 414–421.

Liu, S., Xing, A., Yu, J., Lian, W., Li, J., Cui, M. and Huang, J. (2012) A novel label-free electrochemical aptasensor based on graphene–polyaniline composite film for dopamine determination. *Biosens. Bioelectron.*, **36** (1), 186–191.

Martin, C.R. (1994) Nanomaterials: a membrane-based synthetic approach. *Science*, **266** (5193), 1961–1966.

Martin, C.R. (1998), Template polymerization of conductive polymer nanostructures, In: Skotheim, T. A. (ed.), *Handbook of Conducting Polymers*, New York, Marcel Dekker, 409–422.

Martin, C. R., Parthasarathy, R. and Menon, V. (1993) Template synthesis of electronically conductive polymers-a new route for achieving higher electronic conductivities. *Synth. Met.*, **55** (2–3), 1165–1170.

Mathiyarasu, J., Senthilkumar, S., Phani, K. and Yegnaraman, V. (2008) PEDOT-Au nanocomposite film for electrochemical sensing. *Mater. Lett.*, **62** (4), 571–573.

Maynor, B. W., Filocamo, S. F., Grinstaff, M. W., and Liu, J. (2002) Direct-writing of polymer nanostructures: Poly (thiophene) nanowires on semiconducting and insulating surfaces. *JACS*, **124** (4), 522–523.

Moulton, S. E., Higgins, M. J., Kapsa, R. M. and Wallace, G. G. (2012) Organic bionics: A new dimension in neural communications. *Adv. Funct. Mater.,* **22** (10), 2003–2014.

Ngamna, O., Morrin, A., Killard, A. J., Moulton, S. E., Smyth, M. R. and Wallace, G. G. (2007) Inkjet printable polyaniline nanoformulations. *Langmuir*, **23** (16), 8569–8574.

Pan, L., Yu, G., Zhai, D., Lee, H., Zhao, W., Lin, N., Wang, H., Tee, B., Shi, Y., Cui, Y. and Bao, Z. (2012) Hierarchical nanostructured conducting polymer hydrogel with high electrochemical activity. *PNAS*, **109** (24), 9287–9292.

Pandey, P. C., Singh, G. and Srivastava, P. K. (2002) Electrochemical synthesis of tetraphenylborate doped polypyrrole and its applications in designing a novel zinc and potassium ion sensor. *Electroanalysis* **14** (6), 427–432.

Parthasarathy, R.V. and Martin, C.R. (1994) Template-synthesized polyaniline microtubules. *Chem. Mater.,* **6** (10), 1627–1632.

Pinto, N. J., Rivera, D., Melendez, A., Ramos, I., Lim, J. H. and Johnson, A. (2011) Electrical response of electrospun PEDOT-PSSA nanofibers to organic and inorganic gases. *Sens. Actuators B: Chem.*, **156** (2), 849–853.

Pirsa, S. and Alizadeh, N. (2010) Design and fabrication of gas sensor based on nanostructure conductive polypyrrole for determination of volatile organic solvents. *Sens. Actuators B: Chem.*, **147** (2), 461–466.

Pirsa, S. and Alizadeh, N. (2012) A selective DMSO gas sensor based on nanostructured conducting polypyrrole doped with sulfonate anion. *Sens. Actuators B: Chem.*, **168**, 303–309.

Poorahong, S., Thammakhet, C., Thavarungkul, P., Limbut, W., Numnuam, A. and Kanatharana, P. (2012) Amperometric sensor for detection of bisphenol A using a pencil graphite electrode modified with polyaniline nanorods and multiwalled carbon nanotubes. *Microchimica Acta*, **176**, 91–99.

Posudievsky, O. Y., Biskulova, S. A. and Pokhodenko, V. D. (2002) New polyaniline–MoO3 nanocomposite as a result of direct polymer intercalation. *J. Mater. Chem.*, **12** (5), 1446–1449.

Preethichandra, D., Ekanayake, E. and Kaneto, K. (2012) Enhanced glucose nanobiosensor by pulsed deposion of conducting polymer on ITO/Pt. In: IEEE. *Medical Measurements and Applications Proceedings*. Budapest, 18–19 May 2012.

Rahman, M. M., Ahammad, A., Jin, J. H., Ahn, S. J. and Lee, J. J. (2010) A comprehensive review of glucose biosensors based on nanostructured metal-oxides. *Sensors*, **10** (5), 4855–4886.

Ramanathan, K., Bangar, M., Yun, M., Chen, W., Mulchandani, A. and Myung, N. (2004) Individually addressable conducting polymer nanowires array. *Nano Lett.*, **4** (7), 1237–1239.

Ray, S. S. and Biswas, M. (2000) Water-dispersible conducting nanocomposites of polyaniline and poly (N-vinylcarbazole) with nanodimensional zirconium dioxide. *Synth. Met.*, **108** (3), 231–236.

Santhanam, K., Sangoi, R. and Fuller, L. (2005) A chemical sensor for chloromethanes using a nanocomposite of multiwalled carbon nanotubes with poly (3-methylthiophene). *Sens. Actuators B: Chem.*, **106** (2), 766–771.

Singh, R., Matharu, Z., Srivastava, A., Sood, S., Gupta, R. and Malhotra, B. (2012) Nanostructured platform for the detection of neisseria gonorrhoeae using electrochemical impedance spectroscopy and differential pulse voltammetry. *Microchim. Acta*, **177**, 201–210.

Song, M., Lee, S., Kim, J. and Lim, D. (2012) Dopamine sensor based on a boron-doped diamond electrode modified with a polyaniline/Au nanocomposites in the presence of ascorbic acid. *Anal. Sci.*, **28** (6), 583–587.

Srivastava, S., Sharma, S., Kumar, S., Agrawal, S., Singh, M. and Vijay, Y. (2009) Characterization of gas sensing behavior of multi walled carbon nanotube polyaniline composite films. *Int. J. Hydrogen Energ.*, **34** (19), 8444–8450.

Tai, H., Jiang, Y., Xie, G., Yu, J. and Chen, X. (2007) Fabrication and gas sensitivity of polyaniline-titanium dioxide nanocomposite thin film. *Sens. Actuators B: Chem.*, **125** (2), 644–650.

Tandon, R., Tripathy, M., Arora, A. and Hotchandani, S. (2006) Gas and humidity response of iron oxide-polypyrrole nanocomposites. *Sens. Actuators B: Chem.,* **114** (2), 768–773.

Teles, F. and Fonseca, L. (2008) Applications of polymers for biomolecule immobilization in electrochemical biosensors. *Mater. Sci. Eng. C*, **28**, 1530–1543.

Tolani, S., Craig, M., Delong, R., Ghosh, K. and Wanekaya, A. (2009) Towards biosensors based on conducting polymer nanowires. *Anal. Bioanal. Chem.*, **939**, 1225–1231.

Van Hieu, N., Dung, N. Q., Tam, P. D., Trung, T. and Chien, N. D. (2009) Thin film polypyrrole/SWCNTs nanocomposites-based NH3 sensor operated at room temperature. *Sens. Actuators B: Chem.*, **140** (2), 500–507.

Virji, S., Fowler, J., Baker, C., Huang, J., Kaner, R. and Weiller, B. (2005a) Polyaniline nanofiber composites with metal salts: chemical sensors for hydrogen sulfide. *Small*, **1** (6), 624–627.

Virji, S., Kaner, R. and Weiller, B. (2005b) Hydrazine detection by polyaniline using fluorinated alcohol additives. *Chem. Mater.*, **17** (5), 1256–1260.

Virji, S., Kojima, R., Fowler, J., Villanueva, J., Kaner, R. and Weillier, B. (2009) Polyaniline nanofiber composites with amines: novel materials for phosgene detection. *Nano Res.*, **2**, 135–142.

Wan, M. (2008) A template-free method towards conducting polymer nanostructures. *Adv. Mater.*, **20** (15), 2926–2932.

Wang, L., Fine, D., Khondaker, S. I., Jung, J. and Dodabalapur, A. (2006) Sub 10 nm conjugated polymer transistors for chemical sensing. *Sens. Actuators B: Chem.*, **113** (1), 539–544.

Wang, Y., Jia, W., Strout, T., Ding, Y. and Lei, Y. (2009a) Preparation, characterization and sensitive gas sensing of conductive core-sheath TiO_2-PEDOT nanocables. *Sensors,* **9** (9), 6752–6763.

Wang, Y., Jia, W. Strout, T. Schempf, A. Zhang, H. Li, B. Cui, J. and Lei, Y. (2009b) Ammonia gas sensor using polypyrrole-coated TiO_2/ZnO nanofibers. *Electroanalysis*, **21** (12), 1432–1438.

Weng, B., Shepherd, R., Chen, J. and Wallace, G. G. (2011) Gemini surfactant doped polypyrrole nanodispersions: an inkjet printable formulation. *J. Mater. Chem.*, **21** (6), 1918–1924.

Wilson, J., Radhakrishnan, S., Sumathi, C. and Dharuman, V. (2012) Polypyrrole–polyaniline-Au (PPy–PANi–Au) nano composite films for label-free electrochemical DNA sensing. *Sens. Actuators B: Chem.*, **171**, 216–222.

Wojkiewicz, J., Bliznyuk, V., Carquigny, S., Elkamchi, N., Redon, N., Lasri, T., Pud, A. and Reynaud, S. (2011) Nanostructured polyaniline-based composites for ppb range ammonia sensing. *Sens. Actuators B: Chem.*, **160** (1), 1394–1400.

Xia, L., Wei, Z. and Wan, M. (2010) Conducting polymer nanostructures and their application in biosensors. *J. Colloid Interface Sci.*, **341** (1), 1–11.

Xiong, S., Wang, Q., and Xia, H. (2004) Preparation of polyaniline nanotubes array based on anodic aluminium oxide template. *Mater. Res. Bull.*, **39** (10), 1569–1580.

Yang, M., Sheehan, P. E., King, W. P. and Whitman, L. J. (2006) Direct writing of a conducting polymer with molecular-level control of physical dimensions and orientation. *JACS,* **128** (21), 6774–6775.

Yang, X., Li, L. and Yan, F. (2010) Polypyrrole/silver composite nanotubes for gas sensors. *Sens. Actuators B: Chem.*, **145** (1), 495–500.

Zhang, L., Meng, F., Chen, Y., Liu, J., Sun, Y., Luo, T., Li, M. and Lin, J. (2009) A novel ammonia sensor based on high density, small diameter polypyrrole nanowire arrays. *Sens. Actuators B: Chem.*, **142** (1), 204–209.

Zhang, X. and Manohar, S. K. (2004a) Polyaniline nanofibers: chemical synthesis using surfactants. *Chem. Commun.,* **20**, 2360–2361.

Zhang, X. and Manohar, S. K. (2004b) Bulk synthesis of polypyrrole nanofibers by a seeding approach. *JACS*, **126** (40), 12714–12715.

Zhang, X., Lee, J. S., Lee, G. S., Cha, D. K., Kim, M. J., Yang, D. J. and Manohar, S. K. (2005) Chemical synthesis of PEDOT nanotubes. *Macromolecules*, **39** (2), 470–472.

Zhang, Z., Deng, J., Sui, J., Yu, L., Wan, M. and Wei, Y. (2006) Hollow microstructured polyaniline prepared using cuprous oxide crystals as templates. *Macromol. Chem. Phys.*, **207** (8), 763–769.

Zhong, H., Yuan, R., Chai, Y., Zhang, Y., Wang, C. and Jia, F. (2012) Non-enzymatic hydrogen peroxide amperometric sensor based on a glassy carbon electrode modified with an MWCNT/polyaniline composite film and platinum nanoparticles. *Microchimica Acta*, **176** (3), 389–395.

Zhu, Y., Li, J., Wan, M., Jiang, L. and Wei, Y. (2007) A new route for the preparation of brain-like nanostructured polyaniline. *Macromol. Rapid Commun.*, **28** (12), 1339–1344.

Part II

Spectrographic nanosensors

This page intentionally left blank

8

Surface-enhanced Raman scattering (SERS) nanoparticle sensors for biochemical and environmental sensing

L. RODRIGUEZ-LORENZO, University of Fribourg, Switzerland and R. A. ALVAREZ-PUEBLA, Rovira and Virgil University, Spain and Catalan Institution for Research and Advanced Studies, Spain and ICREA, Spain

DOI: 10.1533/9780857096722.2.197

Abstract: Metallic nanoparticles exhibit remarkable physical and chemical properties that are different from those of the bulk metals. In the context of nanophotonics, a key property of these nanostructures is the so-called localized surface plasmon resonance (LSPR), which is generated by the collective oscillation of conduction electrons upon excitation with the appropriate electromagnetic radiation (e.g. a laser beam). As a consequence of this excitation, a high electromagnetic field is generated at the surface of the nanoparticle which can be applied for the enhancement of spontaneous Raman scattering of the molecular species placed in close vicinity to these surfaces. This effect gives rise to a new powerful analytical tool, known as surface-enhanced Raman scattering (SERS) spectroscopy.

Key words: nanoparticles, plasmons, SERS, ultrasensitive analysis.

8.1 Introduction: Raman scattering

Raman scattering (RS) is the inelastic part of the light scattered by a molecule when illuminated. The energy difference between this scattered light and the incident light is due to the interaction of the photons with the vibrational states of the molecule under study. The effect was theoretically postulated in 1923 by A. Smekal *et al.* (Smekal, 1923) and experimentally demonstrated in 1928 by C. V. Raman (Raman and Krishnan, 1928) using the sun as the excitation source and some basic experimental set-up.

The Raman effect is produced when a monochromatic light with a certain frequency (ω_L) interacts with a molecule. The irradiated molecule scatters a fraction of radiation in all directions. Most of this light is scattered elastically, and only a millionth of the incident light is scattered inelastically (Fig. 8.1).

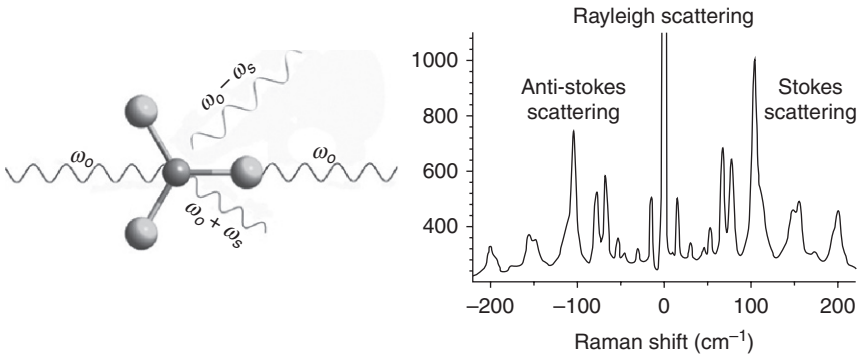

8.1 Schematic representation of Rayleigh and RS and their corresponding spectra.

Elastic scattering has the same frequency (ω_L) as the incident light and is called Rayleigh scattering. The frequency ($\omega_L \pm \omega_v$) of the inelastic scattering is called RS and its frequency shift (ω_v) is different from that of the incident light (ω_L). The Raman frequency shift corresponds to the excitation of the vibrational levels of the molecule, shifted to higher or lower frequencies from the incident light. If the frequency is shifted to lower frequencies ($\omega_L - \omega_v$), it is called Stokes shift. Otherwise, if the frequency is shifted to higher frequencies ($\omega_L + \omega_v$), it is known as anti-Stokes shift (Long, 2002; Smith and Dent, 2005).

An additional phenomenon in RS, which is also relevant in SERS, occurs when the energy of the incident (and scattered) photons is of the order of the electronic transitions of the molecule (Fig. 8.2). In this case, the virtual state becomes resonant with one of the electronic levels in the molecule, resulting in an increase of the scattering efficiency of the molecule of up to several orders of magnitude. Any molecule that absorbs in the vicinity of the incident laser wavelength is subject to this resonance Raman scattering (RRS). Many common probes in SERS (such as dye molecules) are used precisely because they have such electronic resonance contribution in the visible and, accordingly, have large Raman cross-sections (Long, 2002). Note that in Fig. 8.2 and the paragraph above, we refer to a *virtual state*. In fact, there is no physical reality to this state, but it is helpful for understanding the process and provides a link to the conception of Raman in a quantum mechanical context which is discussed in next section.

8.1.1 Classical theory behind Raman scattering

Within classical electromagnetic theory, the radiation of light from a localized source is treated as an electromagnetic wave. This wave can be

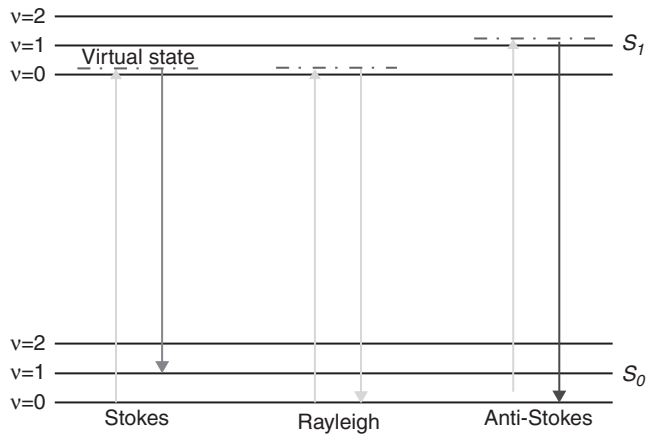

8.2 Simplified Jablonski diagram for the RRS, which results in an enhancement of the efficiency of the Raman process.

described in terms of its multipolar components, with the dominant contribution of the dipole. A standard approach to the Raman effect from a classical explanation consists in considering the RS as the induction of a Raman dipole within the molecule by an incident electric field, followed by the subsequent radiation of scattered light from this Raman dipole. To express this process mathematically, the intensity of the electric field of light (E) can be described by the following equation:

$$E(t,\omega) = E_L \cos(\omega_L t) \qquad [8.1]$$

where ω_L is the frequency of the incident monochromatic light. If the molecule is irradiated by this light, the electron cloud is distorted as a function of the ability of the electrons to be polarized. Then, an electric dipole moment $\mu_R(\omega)$ is induced:

$$\mu_R(\omega_R) = \alpha_R(\omega_L, \omega_v) \cdot E(\omega_L) \qquad [8.2]$$

$$\alpha_R(\omega) = \alpha(Q_k) \qquad [8.3]$$

where $\alpha_R(\omega_L,\omega_v)$ is the Raman polarizability tensor, which depends on both the laser and mode frequencies. This variable is a fully phenomenological parameter in this sense, and its components depend on the conformation of the molecule. If $\alpha_R(\omega_L,\omega_v)$ is specified for a given vibrational mode, then the RS process can be fully described classically as the induction of a Raman

dipole, which radiates the Raman scattered light. If the molecule is vibrating with a frequency ω_R, the perturbation in the linear optical polarizability can be considered as a consequence of the presence of these vibrations. The vibrations can be characterized by normal coordinates Q_k, which describe the scalar amplitude of the deformation according to the pattern of a given normal mode k. Taking a specific normal mode k characterized by Q_k and considering the perturbation in the linear optical polarizability, the following Taylor expansion is obtained:

$$\alpha_L(Q_k) = \alpha_L(0) + \left[\frac{\partial \alpha_L}{\partial Q_k}\right]_{Q_k=0} Q_k + \left[\frac{\partial^2 \alpha_L}{\partial Q_k^2}\right]_{Q_k=0} Q_k^2 + \cdots \qquad [8.4]$$

where the first term represents the unperturbed linear optical polarizability (or the Rayleigh scattering contribution) and the later terms are its first- and second-order perturbations. Substituting $\alpha_R(\omega_L,\omega_v)$ in Equation [8.2], the induced dipole can be calculated in the following way:

$$\mu_R(\omega) = \alpha_L E(\omega) + \frac{1}{2}\left[\frac{\partial \alpha_L}{\partial Q_k}\right]_{Q_k=0} \cdot Q_k \cdot E\left\{\cos\left[(\omega_L+\omega_v)t\right] + \cos\left[(\omega_L-\omega_v)t\right]\right\} \qquad [8.5]$$

Thus, the perturbations of the linear optical polarizability (the second term of Equation [8.5]) correspond to the RS of frequency $\omega_L + \omega_v$ (anti-Stokes) and $\omega_L - \omega_v$ (Stokes), as represented in Fig. 8.1 (Long, 2002; Le Ru and Etchegoin, 2009).

8.1.2 Quantum mechanical theory of Raman scattering

The classical theory includes the fully phenomenological description of RS in terms of a polarizability tensor with the microscopic interpretation of scattering by vibrational modes (Long, 2002). However, it is also useful to describe RS from a quantum point of view, in terms of the discrete vibration energy states of each molecular vibration mode. This description gives explanation to some effects such as the difference of intensities between Stokes and anti-Stokes scattering (Long, 2002; Smith and Dent, 2005).

When monochromatic light of frequency v_0 and energy ($E = h\,v_0$) interacts with a molecule which is in the state k (or n), the molecule is excited to a higher energy state (virtual state) as the first step of the process (Fig. 8.3). The virtual state is not a real state, but is created when the light interacts with the electrons and causes polarization. The energy of these states is

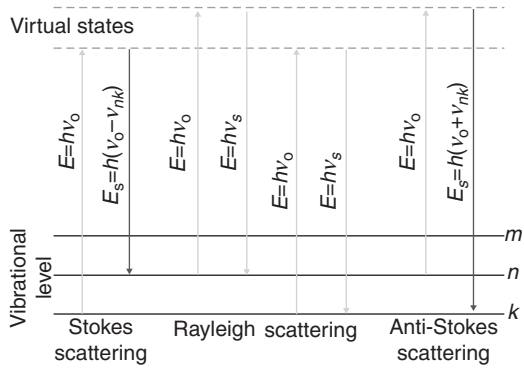

8.3 Simplified Jablonski diagram of the Raman process. Note that the virtual state is not a 'real' physical state.

determined by the frequency of the light source used. The second step of the process encompasses the emission of a photon, as the excited electron cannot stay long in the virtual state and immediately goes back to its initial state. Mostly the molecule returns back to the ground state. This scattering frequency v_S has the same frequency as the light source because there is no change in excitation energy, which is a function of hv_0. On the other hand, when the molecule leaves the virtual state and ends up at the first vibrational level (k) of the ground state, then E_{nk} is subtracted from the initial energy (E) of the light source:

$$E = E_0 - E_{nk} = h\nu_0 - h\nu_{nk} \qquad [8.6]$$

Since the energy (E_{nk}) is smaller, the frequency is lower (Fig. 8.3). This is known as Stokes emission. If the molecule starts off in the first vibrational level (n) of the ground state when it is irradiated, and the molecule travels back down to the lowest ground state, an increased change in energy is also observed

$$E = E_0 - E_{nk} = h\nu_0 + h\nu_{nk} \qquad [8.7]$$

indicating an emission of a higher frequency, known as anti-Stokes emission (Fig. 8.3).

In general, the Rayleigh scattering is 10^3 times more intense than the Stokes and anti-Stokes scattering. The intensity of the Stokes lines is usually higher than that of the anti-Stokes lines, because of the probability that the population in the ground state is always higher than that of the excited state at room temperature (Smith and Dent, 2005).

Both classical and quantum mechanical views of RS introduce some advantages in the understanding of the RS spectroscopy. Although the quantum picture is more vivid, it involves the understanding of the virtual state and it is hard to calculate. The classical description is more straightforward and provides some quantitative relationships. In this sense, the classical explanation is more often used by RS and SERS practitioners, and it has been further developed to explain the mechanism of the surface-enhanced phenomenon.

8.1.3 Cross-section

In order to quantify the efficiency of the Raman process, the concept of cross-section, $\sigma[m^2]$, is defined as the constant proportionality between the incident and the Raman scattered light. The cross-section, in this case, comes from an isotropically averaged version of the Raman tensor (as would occur in a liquid or a gas phase),

$$P = \sigma S_0 \qquad [8.8]$$

where P is the intensity in watts (proportional to the number of photons per unit of time) of the scattering events relative to the incident power density S_0 (W/m^2) at the molecule position.

However, this expression for the cross-section does not consider the directional profile of the scattering in a given molecule. In an experimental situation, usually the scattered radiation is detected in a particular direction, typically 90° or in back-scattering. Thus, a new term (Ω) is added for the absolute differential Raman cross-section (in m^2/sr):

$$\langle I_{RS} \rangle = \frac{d\sigma_{RS}}{d\Omega} S_0 \delta\Omega \qquad [8.9]$$

where S_0 is the incident laser intensity (W/m^2) at the molecule position; $\delta\Omega$, the solid angle for light collection in steradians (sr), which in turn relates to the numerical aperture of the collecting optics (Alvarez-Puebla, 2012), and $\langle I_{RS}^{SM} \rangle$ is the signal obtained for a given vibrational mode of a single molecule, averaged over all orientations of the molecule in space (Aroca, 2006; McCreery, 2000).

The cross-section for the RS is much smaller than those for other spectroscopic techniques. For example, a typical cross-section for fluorescence is about 10^{-16} cm^2 per molecule, while for RS it is only 10^{-28} cm^2 per molecule. Furthermore, the intensity of the Raman modes of a molecule is limited by

the concentration of molecules. This is the key disadvantage of Raman and is also the reason why Raman was not widely popular until the discovery of SERS.

Another important concept within the Raman effect is the possibility of determining whether the vibration would be active in a Raman spectrum. The existence of a given vibrational mode in a molecule does not necessarily guarantee the activity of that mode, which gives rise to the Raman selection rules. In infrared (IR) absorption spectroscopy the vibrations are detected when the dipole moment μ of a molecule changes during the normal vibration. Thus, the intensity of a band for IR absorption I_{IR} depends on the change of the dipole moment μ during the vibration

$$I_{\mathrm{IR}} \propto \left(\frac{\partial \mu}{\partial Q}\right)_0^2 \qquad [8.10]$$

In the case of RS spectroscopy, the vibrational modes are active if the polarizability α changes during the vibration. The intensity of a Raman active band I_R is proportional to a square of the polarizability change during the vibration:

$$I_R \propto \left(\frac{\partial \alpha}{\partial Q}\right)_0^2 \qquad [8.11]$$

To obtain Raman activity, the rate of change of α within the vibration must be different from zero. Thus, from the point group theory it is straightforward that, in centrosymmetric molecules, active vibrations in Raman will be 'weak' in IR spectroscopy, and vice versa. As a consequence, IR spectroscopy provides detailed information about polar functional groups, while Raman especially contributes to the characterization of the carbon backbone of organic substances or polymers.

8.2 Surface-enhanced Raman scattering (SERS)

The surface-enhanced Raman scattering (SERS) spectroscopy is based on the amplification of the Raman signal for molecules adsorbed on a nanostructured metallic surface (Fig. 8.4). The SERS effect was discovered in 1974 by Fleischman, Hendra and McQuillan (Fleischmann *et al.*, 1974). The group reported an abnormally large Raman signal of pyridine measured on top of a roughened silver electrode. The enhancement was initially attributed to a punctual high concentration of adsorbed pyridine due to the extra surface area generated by the redox cycles in the electrode.

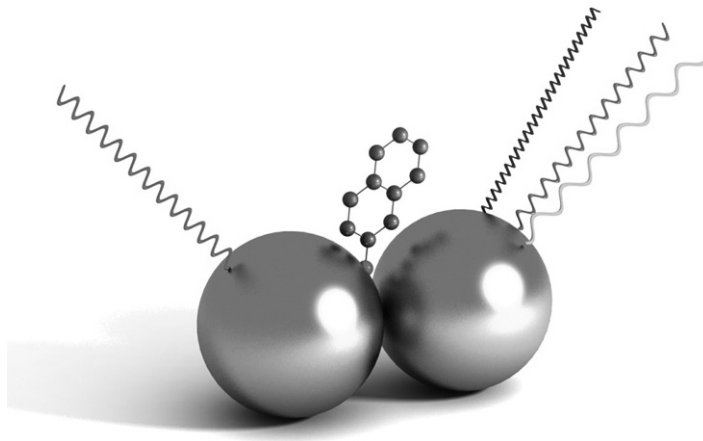

8.4 Schematic representation of the SERS phenomenon.

Notwithstanding, in 1977, two independent reports, by JeanMaire and Van Duyne (1977) and Albrecht and Creighton (1977), demonstrated that this intensity could not be accounted for by an increased surface. In fact, both papers reported on a new physical phenomenon, giving rise to the idea of the SERS cross-section. They also noted that the scattering intensity from the adsorbed molecules was 5–6 orders of magnitude stronger than that of conventional Raman signal (Jeanmaire and Van Duyne, 1977). Nowadays, enhancement factors (EF) have been reported up to 10^{14}–10^{15}-fold, which allows SERS to be sensitive enough to detect single molecules (Kneipp *et al.*, 1997; Nie and Emory, 1997). The EFs depend on the structure of the metal and on the nature of the molecule. The most commonly used metallic surfaces for SERS are based on silver and gold nanostructures, which bring together chemical stability with the appropriate optical properties (Smith and Dent, 2005; Banholzer *et al.*, 2008; Abalde-Cela *et al.*, 2010; Alvarez-Puebla and Liz-Marzan, 2010). Nevertheless, SERS has been extended to other metals (e.g. copper, platinum, lithium, sodium, potassium, indium, aluminium or rhodium) (Tian *et al.*, 2002; Kneipp *et al.*, 2006).

Much of the impetus behind the research in SERS relies on its potential applications. The signal enhancement provided by the metallic nanostructures resolves the problem of the intrinsic inefficiency of the Raman process, combining the ultrasensitive potential of this technique with the rich chemical and structural information characteristic of the vibrational spectroscopy. Further, the fact that SERS can be carried out under environmental or biological conditions make it an ideal detection platform for (bio) chemical sensing, diagnostics, (bio)analytical chemistry, or environmental

monitoring, among other applications. An additional benefit of SERS is that fluorescence is quenched for molecules close to the surface, due to the additional relaxation pathway available through transfer of energy to the metal surface, which facilitates signal detection.

The SERS effect has been deeply studied over the last 30 years. In general, two broad enhancement mechanisms have been proposed, the electromagnetic mechanism and the chemical (CT) mechanism. Nowadays, it is recognized that although EM is essential for SERS, CT plays a key role in the really ultrasensitive application of the technique (Moskovits and Suh, 1984; Otto, 2002; Moskovits, 2005; Smith and Dent, 2005; Le Ru and Etchegoin, 2009).

8.2.1 Electromagnetic enhancement (EM)

The SERS enhancement is due to an EM that is a direct consequence of the presence of the metallic nanostructures (also known as optical enhancers). In fact, the EM can be interpreted as, essentially, a redistribution of the electromagnetic field around the optical enhancer, resulting, in some cases, in strongly localized regions of high field intensities, the so-called *hot spots*. This effect is mediated through the resonance of the incident light with the surface plasmon resonances of the metal. Roughly speaking, plasmons are collective excitations of the surface conduction electrons that propagate along the metal surface. At certain frequencies of incident light, these electrons become highly polarizable, giving rise to large electromagnetic fields. The details of the plasmon resonance phenomenon are complicated and a variety of terms exist to describe different aspects of plasmons depending on the research emphasis; such terms include surface plasmon polaritons, radiative and non-radiative plasmons, and localized (LSPR) and propagating plasmons (Aroca, 2006; Le Ru and Etchegoin, 2009). Here, we present only some of the most basic theory needed to outline the SERS effect. It should be noted that, in this context, all plasmon-related effects can be understood as electromagnetic effects, and the relation to the free electrons of the metal is only secondary. In this sense, all characteristics of plasmons are contained within the dielectric function (and its wavelength dependence) and the geometry of a specific problem.

In terms of its basic properties, a material (usually a metal) would be suitable for use in SERS if its refractive index has:

1. A negative real part of the dielectric function (preferably large); and
2. A small imaginary part of the dielectric function.

The metals that can fulfil these conditions best are the alkaline and the noble metals (Cu, Ag, and Au). Silver is particularly appropriate for SERS

applications in the visible and near-infrared (NIR) because it has a very small imaginary component in this region and, thus, is less 'lossy' than other metals (Garcia de Abajo, 2007).

In simple words, the plasmon resonances of a metal can be considered in terms of certain electromagnetic modes that exist for a material described by a local dielectric function and a given geometry (Aroca, 2006; Kneipp *et al*., 2006; Le Ru and Etchegoin, 2009). When the electromagnetic modes of a substrate are resonant with the incident (or radiative) light of an external source, strong light scattering appears in the form of intense surface plasmon bands. Then, the enhancement of the local electromagnetic fields also occurs (Sepúlveda *et al*., 2009; Mayer and Hafner, 2011). This phenomenon can be observed in the spectral absorption of a SERS substrate (Fig. 8.5). It should be noted, however, that LSPRs cannot be simply used as an accurate indicator of the SERS enhancement of a given substrate at a given wavelength. First, the Raman effect involves enhancement of both the incident and radiative photons (at different energies); thus, the final enhancement depends on the convolution of these individual enhancements. In addition, for resonant molecules, pre-resonance effects may mean that SERS enhancements occur before the resonance shown by the absorption profile. Consequently,

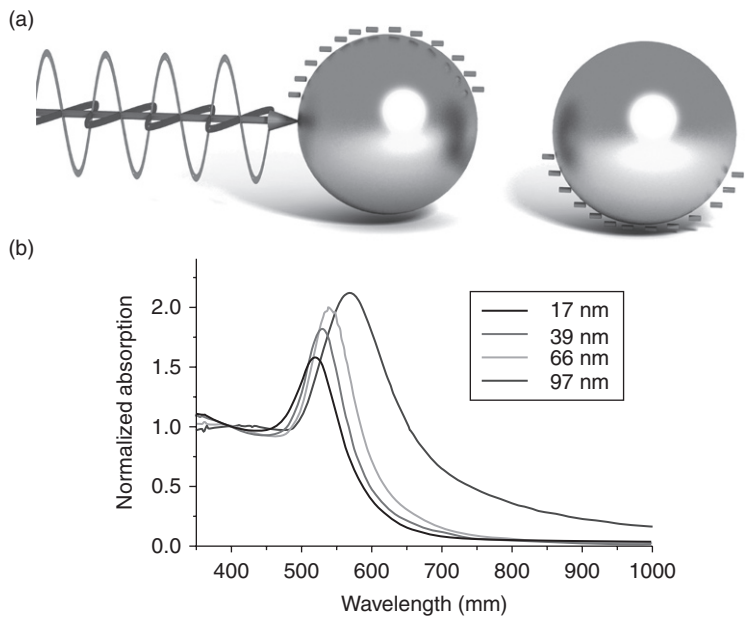

8.5 (a) Schematics for the plasmon oscillation in a metallic sphere, showing the displacement of the conduction electron charge cloud relative to the nuclei. (b) Extinction spectra of gold nanospheres with different sizes.

a common model to explore the EM enhancement relies on the E^4 approximation, which considers RS in the vicinity of a metallic surface (Moskovits and Suh, 1984; Moskovits, 2005). This model accounts for separate enhancement of the incident and the emitted radiation, inherent in the two-photon Raman process, by defining a local field intensity EF $M_{\text{Loc}} \cdot (\omega_L)$ and a directional radiation EF $M^d_{\text{Rad}} \cdot (\omega_R)$ (related to a given detection position). The EF in SERS is then given as:

$$\text{EF} \approx M_{\text{Loc}}(\omega_L) M^d_{\text{Rad}}(\omega_R) \qquad [8.12]$$

where $M_{\text{Loc}} \cdot (\omega_L)$ characterizes how much stronger the field intensity is with respect to the intensity in the absence of a metal substrate present, and can be determined by solving the electromagnetic problem under specific conditions with an incident field $\boldsymbol{E}_{\text{Inc.}}$. On the other hand, $M^d_{\text{Rad}} \cdot (\omega_R)$ relates to the enhancement experienced by the Raman emitting dipole, which is correspondingly at a different frequency from the incident laser.

The quantitative calculation of $M^d_{\text{Rad}} \cdot (\omega_R)$ is difficult; however, and for simplicity, it is generally assumed that $M^d_{\text{Rad}} \cdot (\omega_R) \approx M_{\text{Loc}} \cdot (\omega_R)$. This approximation can be formally justified when its range of validity is specified (Le Ru and Etchegoin, 2006). From the definition of $M_{\text{Loc}} \cdot (\omega_L)$, the EF can then be expressed as:

$$\text{EF} \approx M_{\text{Loc}}(\omega_L) M_{\text{Loc}}(\omega_R) \approx \frac{|E_{\text{Loc}}(\omega_L)|^2}{|E_{\text{Inc}}|^2} \frac{|E_{\text{Loc}} \cdot (\omega_R)|^2}{|E_{\text{Inc}}|^2} \qquad [8.13]$$

which at a zero-Stokes shift ($\omega_L = \omega_R$) yields the $|E|^4$ approximation as:

$$\text{EF}(\omega_L) \approx \frac{|E_{\text{Loc}}(\omega_L)|^4}{|E_{\text{Inc}}|^4} \qquad [8.14]$$

However, it is important to keep in mind that this approach only approximates the radiation enhancement, and does not account for polarization effects or surface selection rules in SERS (Le Ru and Etchegoin, 2006, 2009).

In general, for simple objects, such as an individual sphere or spheroid, it is possible to obtain analytical solutions for the EF using Mie theory as a basis (Aroca, 2006). Generalized Mie theory extends the solution to two closely spaced spheres (Xu, 1995; Garcia de Abajo, 2007; Myroshnychenko *et al.*, 2008). However, in most practical cases numerical approaches are the

only option. These include techniques such as the finite-element method (FEM), the finite-difference time domain (FDTD) and boundary element method (BEM), which provide the numerical solution to Maxwell's equations. Commonly, the simulations are simplified based on the electrostatic approximation (ESA). These methods treat the electric field as an electrostatic field, but still consider the metal in terms of its frequency-dependent complex dielectric function. This approximation works well for objects that are much smaller than the wavelength of light (20–40 nm), but should be used with caution for larger systems. Another common approximation is to reduce the problem to two dimensions (2D), which works for problems that are effectively 2D in nature due to symmetry. Otherwise, the 2D solution should only be used as a qualitative guide for the 3D cases (Le Ru and Etchegoin, 2009). Further, most numerical methods rely, at some point, on a discretization (meshing) of the objects under study into small cells. The characteristics of the EM fields inside each cell are then computed. As a result, the size and shape of the cell become one of the most important issues for the accuracy of the overall result. These factors place limits on the accuracy of the overall results, particularly at sizes that approach the cell size of the calculation, in which case the results are heavily dependent on the size and shape of the cell. In general, the results of such methods give us a theoretical calculation, based on Maxwell's equations, of the distribution of EFs around a particular object geometry and are of invaluable insight in SERS and plasmonics. One of the most important results is that maximum EFs up to ~10^{11} (sometimes 10^{12}) are obtained for the best cases (Kneipp *et al*., 2006; Le Ru and Etchegoin, 2009). In addition, simulations confirm that the optimum enhancements occur:

1. at the tip of objects with pointy curvatures, i.e. sharp features, and
2. in the gaps between closely spaced particles (with maximum EFs often for particles separated by less than 5 nm).

Further, in the vicinity of these regions of high enhancements, or *hot spots*, the enhancement changes dramatically even within a short distance of the regions of maximum intensity (Bidault *et al*., 2008; Myroshnychenko *et al*., 2008; Rodriguez-Lorenzo *et al*., 2009; Alvarez-Puebla *et al*., 2010). This implies that for most of the SERS substrates, the enhancements that mainly contribute to the SERS signal arise from extremely localized regions throughout the sample (see Fig. 8.6).

In terms of distance dependence, Mie theory using the ESA gives a distance dependence d for a simple sphere of radius a as $1/(a+d)^{12}$. In practice, EM enhancements typically extend to at least ≈10 nm from the surface (Aroca, 2006; Le Ru and Etchegoin, 2009). Thus, the effect can operate on non-bound molecules and extends beyond a monolayer for many molecules,

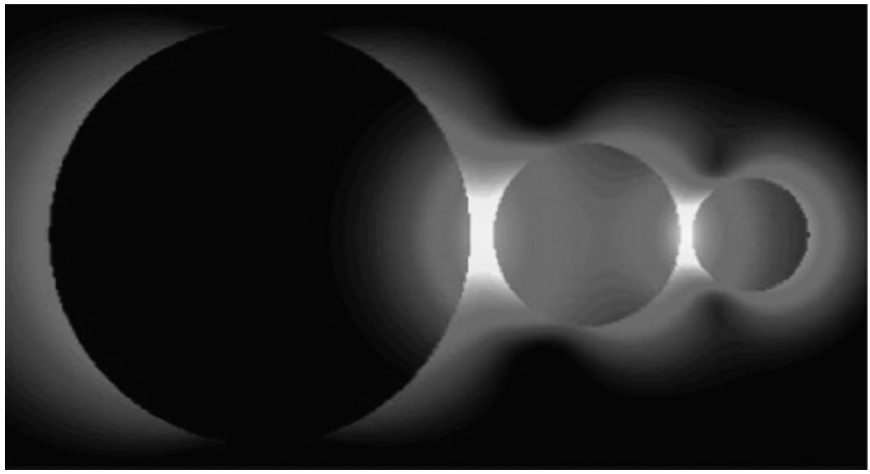

8.6 Calculated maximum enhancement intensity in aligned 18, 8 and 5 nm spheres with 1 and 0.5 nm spacing, respectively. (*Source*: Reproduced with permission from Bidault *et al.*, 2008. Copyright America Chemical Society 2008.)

which is an important distinction to the postulated chemical enhancements given in the next section.

8.2.2 Chemical enhancement (CT)

The other mechanism postulated to occur in SERS is chemical enhancement. This effect requires the vibrational probe to be chemically bound to the SERS substrate. Chemical effects have been proposed to explain changes in the relative intensities (and frequencies) in the vibrational modes of a molecule as compared with the normal Raman spectra, and to account for perceived discrepancies between the maximum EFs found experimentally and the maximum values from the electromagnetic calculations. The proposed chemical mechanism is associated with two processes (Otto, 2001b; Aroca, 2006):

1. Charge-transfer states involving transitions from the Fermi level of the metal to an unoccupied orbital of the molecule (or vice versa); and/or
2. Formation of a surface complex involving the metal and the analyte molecule, leading to a change in the properties of the molecule (such as the possibility of resonance RS).

The surface complexation of the analyte to the metallic nanostructure makes possible the transfer of charge (Fig. 8.7). Basically, the enhancement

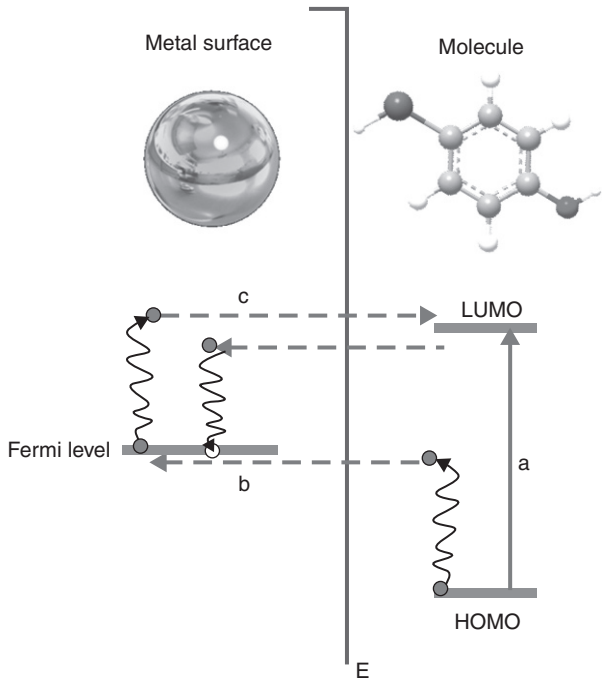

8.7 Diagram of energy levels for a 'metal-molecule system' and possible charge-transfer processes that can involve molecular states (a pathway) and/or both metallic and molecular states (b, c pathways).

proceeds via new electronic states, which arise from the formation of the molecule–metal complex. These new states are believed to be resonant intermediates in the RS. Thus, as opposed to the radiation being adsorbed or scattered through the plasmons on the surface (electromagnetic enhancement), the radiation is supposed to be absorbed into the metal. A hole is transferred into the adsorbate–metal atom cluster, then RS occurs and excitation is transferred back into the metal and re-radiation occurs from the metal surface (Smith and Dent, 2005; Kneipp *et al.*, 2006; Le Ru and Etchegoin, 2009).

A significant body of work has been dedicated to teasing out the details of charge-transfer processes and the change of properties resulting from the analyte–surface complex (Otto, 2002). Many of these studies have been performed on electrochemical set-ups and explain variations in analyte properties such as relative intensities that may not be able to be explained through electromagnetic mechanisms. However, it should be noted that in regard to the issue of chemical enhancement in SERS, there is considerable controversy (Natan, 2006; Le Ru and Etchegoin, 2009). Some of the effects attributed to chemical enhancement may actually be due to SERS

surface selection rules, which would also play an important role in the case of a molecule bound to a surface in a fixed orientation (Moskovits and Suh, 1984; Moskovits, 2005). Further, when examining some of the recent literature it may be concluded that some of the motivation for the discussion of chemical effects has been on the perceived need to 'bridge the gap' between EFs obtained theoretically and those reported experimentally (up to 10^{15}) in single-molecule studies (Kneipp *et al*., 1997; Nie and Emory, 1997).

In any case, in typical SERS conditions, it is always difficult to separate the chemical effects from possible contributions of electromagnetic origin, such as surface selection rules or other mechanisms. Also, chemical enhancement mechanisms exert a minor influence, up to 10^5 in the best cases (Otto, 2001a; Kneipp *et al*., 2010), in comparison to the EM, and are, by definition, a general phenomenon. For particular analytes, however, chemical enhancements may play an important role, and such surface effects are a topic of study by themselves.

8.2.3 Other mechanisms

Another possible source of enhancement in SERS, discussed very early after its discovery (King *et al*., 1978; Efrima and Metiu, 1979), involves the interaction of a dipole self-reaction field with its polarizability. This self-reaction field modifies the ability of the dipole to radiate energy (i.e. it can effectively oppose or amplify the dipole amplitude). This effect is effectively then defined as a 'chemical enhancement', given that it involves a change of polarizability upon adsorption; however, the origin is actually electromagnetic.

8.3 SERS-active substrates

In order to maximize the SERS effect, the optical enhancers should accomplish several requirements including: large EFs, good reproducibility from one sample to another, stable SERS signal with time, simple preparation process, and easiness to be applied to many analytes in parallel (Abalde-Cela *et al*., 2010, Alvarez-Puebla and Liz-Marzan, 2010). Moreover, these platforms should be inert, mechanically stable, and not lead to additional spurious peaks in the SERS spectrum. However, SERS cannot only be achieved and maximized through a detailed design of the optical substrates, but also by improving the adsorption of the molecules of interest (Alvarez-Puebla *et al*., 2005; Alvarez-Puebla and Liz-Marzan, 2012). For these reasons, the fabrication of active optical substrates with optimized properties has been a field of research with a great development during the last decades.

Nanotechnology shows potential applicability for the fabrication of new and specific SERS-active platforms by producing, assembling and ordering nanostructures. In fact, nanofabrication has solved two problems:

1. The engineering of well-defined structures which can be optimally tuned to maximize the EF; and
2. The fabrication of reproducible SERS platforms, which is a key request for SERS to be implemented as a quantitative analytical technique.

Normally, SERS has been obtained on electrodes, solid metal thin films and colloidal dispersions. Nowadays, metallic nanoparticles are considered one of the main SERS platforms. Since colloids are easy to produce in the laboratory and tend to generate large EFs, most researchers are still involved in the development of colloid-based SERS. Metallic nanoparticles are also of historical significance related to the development of SERS, as the first single-molecule SERS (SM-SERS) detections were reported using colloid particles (Kneipp *et al*., 1997; Nie and Emory, 1997). Besides, the utilization of nanoparticles allows direct SERS analysis within the analyte natural solution medium. The presence of the solvent and the Brownian motion of the analyte–particle complexes minimize damage to the sample, even when using more energetic laser lines and higher power at the sample for excitation. Finally, colloidal metals can also be used for the preparation of thin films, which add portability and versatility to 'on-field' SERS analysis, over the regular physical fabrication techniques such as sputtering, physical vapour deposition or electron beam lithography, which are difficult to find in conventional laboratories.

8.3.1 Colloidal solutions

Metallic nanoparticles are typically produced by a reduction reaction in solution. The existence of colloidal particles in solution is attributed to the stabilization caused by coulombic or steric repulsions among particles. Therefore, it is important to add stabilizing agent in a reaction mixture to prevent colloids from excessive aggregation and precipitation. However, in the most common SERS plasmonic substrates, such as citrate-reduced colloid, sodium citrate acts as both a reducing and stabilizing agent.

Citrate-reducing silver nanoparticles is a grey-yellow solution and has a UV-Vis absorption maximum at around 400–430 nm. The shape and size of the dispersion are highly disordered. Similarly, citrate-reduced gold nanoparticle solution is wine-red with maximum wavelength at around 520–539 nm. Several other chemical routes can be utilized for the production of silver or gold nanoparticles. Colloids produced by alternative reducing-stabilizing agents usually have different optical properties from that previously

described. The most common alternative to citrate-reducing agent is borohydride, which has been broadly used in SERS research. However, borohydride-reducing colloids are relatively less stable than citrate-reduced ones. Moreover, in some cases, controlled morphology metallic nanoparticles (cubes, rods, triangle, etc.) can be produced by careful reduction protocol (Jain *et al*., 2008; Ko *et al*., 2008; Lu *et al*., 2009).

In the last years, one of the most significant developments in SERS has been the exponential increase in synthetic capabilities for homogeneous anisotropic metal nanoparticles (Orenforff *et al*., 2005; Jana and Pal, 2007). Reliable synthesis of core–shell particles, rods, triangular prisms, dumbbells, stars, or cubes, and even more sophisticated morphologies, has been described (Mayer and Hafner, 2011). Controlling the morphology provides a method to tune the optical and spectroscopic properties of nanomaterials (Grzelczak *et al*., 2008), which is an essential requirement for a wide range of applications such as genetic diagnostics, immunoassay labelling and trace-detection of drugs, biomolecules and pesticides. To date, optical properties can be tuned from the UV to the IR just by controlling the morphology of the nanoparticles (Myroshnychenko *et al*., 2008). This has paved the way towards the generation of new families of advanced platforms for SERS ultrasensitive analysis, especially those related with biomedicine and sensing (Ochsenkühn *et al*., 2009; Alvarez-Puebla and Liz-Marzan, 2010; Rodriguez-Lorenzo *et al*., 2012).

Recent observations in anisotropic particles have demonstrated that LSPRs are not homogeneously distributed around the whole nanoparticle surface, but give rise to concentration of electromagnetic field in specific regions within it. This concentration of electromagnetic field has been experimentally observed at the corners of triangular platelets (Nelayah *et al*., 2007), the ends of nanorods (Chen *et al*., 2009), the edges and corners of nanorods and cubes (Cobley *et al*., 2008) and tips of nanostars (Rodriguez-Lorenzo *et al*., 2009) (Fig. 8.8). Numerical methods, including discrete dipole approximation (DDA), BEM, and FDTD methods, have been used to predict the field enhancements in the vicinity of single metal nanoparticles of a variety of shapes (Nelayah *et al*., 2007; Cobley *et al*., 2008; Chen *et al*., 2009; Rodriguez-Lorenzo *et al*., 2009; Alvarez-Puebla *et al*., 2010). The simulations for anisotropic nanoparticles have shown that sub-wavelength nonspherical metal nanostructures exhibit multiple resonances, and the field amplitudes associated with these resonances can be extremely large, up to several hundred times the incoming field amplitude (Zhao *et al*., 2008; Henry *et al*., 2011). Thus, in agreement with experimental results, these large electromagnetic fields are strongly concentrated at particular positions on the particle surface (Fig. 8.8). Notably, BEM calculations and electron energy loss spectroscopy (EELS) experiments of gold nanostars show clearly that the electromagnetic field is strongly localized at the apexes of

the nanostar tips (Rodriguez-Lorenzo *et al*., 2009). As a consequence, the SERS intensity of stars is substantially higher than that of spheres of similar dimensions (Rodriguez-Lorenzo *et al*., 2009, 2010). This enhancement has also been extended to more complex structures, such as thorn-shaped nanowires (Pazos-Perez *et al*., 2010a) and spiked particles derived from rods (Aldeanueva-Potel *et al*., 2012). Complementary to these latest approaches for electromagnetic field concentration, quite impressive progress has been made in the controlled fabrication of so-called hot spots. Until very recently, hot spots were commonly created by simply exploiting the small gaps between nanostructures originating from uncontrolled aggregation of colloids, promoted by changing the solvent, increasing the ionic strength of the suspension, decreasing solution pH, or just spontaneously due to the adsorption of the Raman label. However, this uncontrolled aggregation process is usually undesirable for quantitative applications as it leads to a random distribution of hot spots, and therefore the SERS intensity varies from spot to spot. Thus, several procedures have been developed for the controlled production of hot spots (Hu *et al*., 2002). Recent attempts to process quantitative, high-yield SERS relied on optical field concentration at the gaps between particles in controlled assembled dimers and trimers using wet chemical methods (Romo-Herrera *et al*., 2011). However, these systems are difficult to control and their reproducibility is marred by inescapable finite distributions of particle sizes and gap widths (Braun *et al*., 2007, 2009; Stoerzinger *et al*., 2010). Although the immobilization/assembly of colloidal nanoparticles onto solid supports could to some extent improve the controllable aggregation of the nanoparticles, the synthesis and fabrication processes for such assembled layers are usually laborious and time consuming, and commonly require the use of organic molecules acting as reductants, stabilizing reagents, or coupling reagents, with the consequent potential contamination of the vibrational spectrum with their spurious bands.

8.3.2 Colloidal particles immobilized on solid supports

Extensive efforts have been also dedicated to the development of stable nanostructured Ag or Au surfaces directly onto solid substrates using various physical or chemical techniques including vacuum evaporation (Pan *et al*., 2005), sputtering (Merlen *et al*., 2009), electrochemical deposition (Lee *et al*., 2006), thermal decomposition (Hou and Fang, 2007), and electroless plating (Xu *et al*., 2010b). For example, the fabrication of nanostructured metal films by mean electroless plating is attracting much attention due to its easy production, uniform coating, low cost, and no need for special and expensive equipment. A galvanic displacement reaction is a simple electroless plating process to prepared SERS-active metal (Ag or Au) films on metal and semiconductive substrates like copper, germanium, and silicon

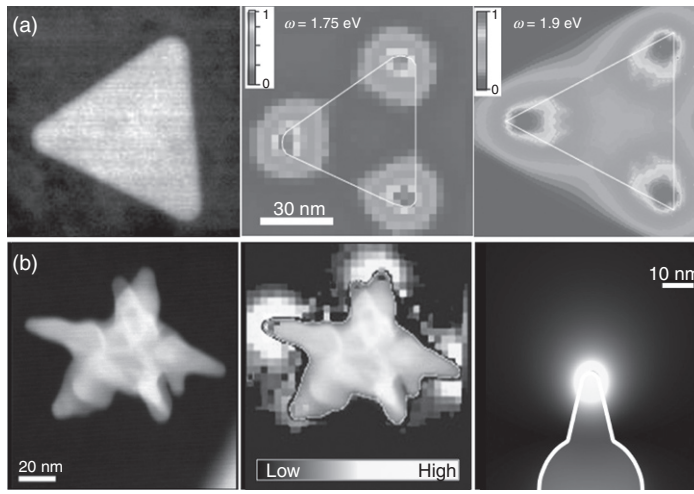

8.8 High resolution scanning transmission electron microscopy (STEM) dark-field image, EELS intensity mapping and calculated EELS intensity map of a single (a) Ag triangle and (b) Au nanostar. (*Source*: Reproduced with permission from Abalde-Cela *et al.*, 2010. Copyright Royal Society 2010.)

(Xu *et al.*, 2010b). However, this technique cannot be applied to dielectric substrates such as cheap glass slides. Although the well-known mirror reaction is suitable for the deposition of Ag nanofilms onto glass surfaces, this process includes multi-step reactions and requires complex reagents, with the subsequent difficulty in control of the surface roughness of the resulting metal films (Park *et al.*, 2006).

For practical applications, it is thus imperative to develop SERS-active substrates with reproducible and controllable SERS enhancement. To fulfil this goal, substrates that show better reproducibility are prepared by techniques such as nanosphere lithography (Zhang *et al.*, 2006b), laser ablation (Gamaly and Rode, 2004), dip-pen nanolithography (Zhang and Mirkin, 2004), oblique angle vapour deposition (OAD) (Driskell *et al.*, 2008), and atomic force microscopy (Yanagi and Ohno, 1999). As a result, advanced lithographic techniques such as focused ion beam (Min *et al.*, 2008) and electron beam lithographies (Oran *et al.*, 2008) have been applied for precision nanofabrication. Unfortunately, the use of these techniques does not permit the control of hot spots with small gap sizes smaller than 10 nm required to maximize the SERS enhancement (Alvarez-Puebla *et al.*, 2010). Recently, a new nanofabrication approach has been demonstrated, combining electron beam lithography (EBL), metal deposition, lift-off, and reactive ion etching, to produce highly ordered and elevated gold bowtie array substrates with controllable gap size to less than 8 nm. These ordered

SERS arrays have shown superior reproducibility and high sensitivity with an EF of 10^{11} (Hatab *et al*., 2010). Also, by using OAD the preparation of aligned nanoparticle arrays with surface morphologies required for SERS substrates is possible. The OAD method facilitates the selection of nanoparticle size, shape, density, alignment, orientation, and composition. However, although all these methods provide highly reproducible substrates with a controlled hot spot density, they result time consuming, expensive, require clean rooms and special nanofabrication tools and often cannot be sufficiently up-scaled.

More and more efforts are now focused on building two- and three-dimensional nanoarchitectures to improve the signal intensity and reproducibility (Ko *et al*., 2008). 2D periodic arrays of metal nanoparticles have two characteristic advantages for SERS applications. First, the surface density of hot spots can be maximized when the nanoparticles are organized in a close-packed manner and, second, the EFs of 2D periodic arrays can be several orders of magnitude higher than those of disordered metal nanoparticles films due to the reduced losses (retardation or damping effects). Theoretical calculations indicate that an average SERS EF of 2D periodic metal nanoparticle arrays with large diameter-spacing ratio (over 30) can approach 10^{11} for a Ag nanodisk array and 10^{9} for a Ag nanosphere array (Genov *et al*., 2004). The higher SERS EF for metal nanodisk arrays, compared to those for nanosphere arrays, can be ascribed to the electromagnetic field contribution along the depth. Notably, the intensity and distribution of electric fields on 2D metallic nanostructure arrays vary dramatically due to the coupling between LSPR and surface plasmon polaritons or propagating surface plasmon (SPP) (Willets and Van Duyne, 2007). On the other hand, quasi-3D arrayed nanostructures, fabricated via EBL, and involving a physically separated nanohole-patterned gold thin film on top and gold nanodisks at the bottom of wells, have been reported for SERS sensing applications (Yu *et al*., 2010). These 3D arrays present unique plasmonic properties and easy fabrication. The SPP and LSPR coupling between the top nanoholed gold thin film and the bottom gold nanodisks creates strong local electric fields and greatly enhances RS in comparison to 2D nanoholed gold thin films (Fig. 8.9) (Xu *et al*., 2011). In fact, the location of the strongest electric field (i.e. the *hot spot*) of quasi-3D gold plasmonic nanostructure arrays can be conveniently tailored by simply varying the diameter of the nanoholes in the film while maintaining the same spacing, depth and material properties. Moreover, the fabrication of robust 3D metallic nanostructures on solid substrates with open morphology for efficient light interaction is needed for efficient SERS-active chips. The solid 3D SERS substrates offer:

1. Large specific surface area for the adsorption of target analytes and provide a large density of hot spots with the laser illumination area;

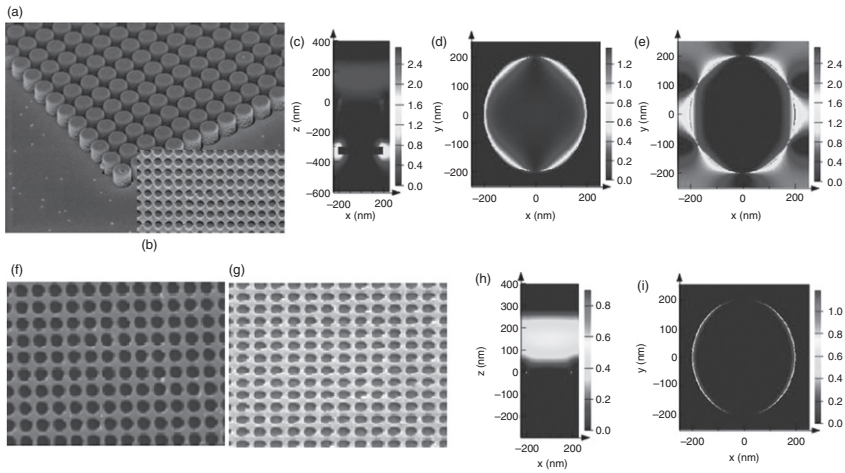

8.9 Quasi-3D nanostructure array. (a) A 45° view scanning electron microscopy (SEM) image of an Ma–N 2403 master with 500 nm tall nanopillars fabricated via EBL using 80 nC cm^{-2} area dosage. The designed nanopillar diameter is 500 nm and the pitch is 600 nm. The inset is the top view of this nanopillar array. (b) A top-view SEM image of the hard polydimethylsiloxane (hPDMS) replica with nanoholes. Calculated intensity of total electric fields $\left(|E|^2/|E_0|^2\right)$ in log scale for a gold quasi-3D nanostructure array on PDMS with a diameter of 400 nm, spacing of 100 nm and depth of 300 nm. (c) The x–z cross-section. (d) The x–y plane of the gold–air interface at the top gold nanohole film. (e) The x–y plane of the gold–air interface at the bottom gold disc. 2D nanohole array. SEM images of a gold 2D nanohole array on a silicon substrate fabricated via the lift-off nanopillars using a PDMS stamp, showing the top view of the array (f) and the 45° view (g) of a part of the array. Calculated intensity of total electric fields $\left(|E|^2/|E_0|^2\right)$ in log scale for a gold 2D nanohole array on silicon with a diameter of 400 nm and a spacing of 100 nm. (h) The x–z cross-section. (i), The x–y plane of the gold–air interface. (*Source*: Reproduced with permission from Yu *et al.*, 2010. Copyright Institute of Physics 2010.)

2. This advantage can be combined with other optical properties related to 3D geometry to assure additional Raman signal enhancement; and
3. These solid substrates are usually very stable under ambient conditions.

Thus, these optimized 2D- and 3D-nanostructured arrays make possible the quantitative and reproducible detection of chemical and biological species using SERS. This development is expected to lead to new sensing platforms with single-molecule sensitivity for potential applications in many important sectors including environmental monitoring, health care, food safety, and security (Xu *et al.*, 2010a; Alvarez-Puebla *et al.*, 2011). Notwithstanding,

SERS activity can be affected by the oxidation of the metal or the lack of stability of the nanostructures when exposed to liquid solutions. There are several methods to mitigate these undesired effects. For example, nanosphere lithography and reactive ion etching techniques may be combined to fabricate Ag nanoparticles arrays embedded in glass, which exhibit improved stability against mechanical force and solution flow (Hicks *et al.*, 2005). In addition, adding an alumina overlayer by atomic layer deposition (to NSL-fabricated particles dramatically increases their thermal stability (Whitney *et al.*, 2005) enabling SERS to be extended to high temperature studies such as those important in heterogeneous catalysis. It is also known that these alumina-coated substrates maintain their SERS activity under ambient conditions with little or no oxidation over months (Zhang *et al.*, 2006a; Yonzon *et al.*, 2007).

8.3.3 Hybrid materials

Although metal nanostructures and their organized arrays can provide high EFs while providing uniform intensities through large areas, several shortcomings are still to be resolved in the manufacture of SERS substrates. One of the main restrictions arises from close contact analyte–metallic surface to efficiently enhance the signal. Unfortunately, most molecular families show very low affinity towards nanostructured gold or silver surfaces. Thus, the integration of plasmonic nanoparticles into advanced hybrid materials is a key aspect in sensor engineering. As for example, efficiency of colloidal plasmonic particles towards the ultrasensitive SERS analysis of many molecular families with low affinity for gold and silver can be achieved through the rational design of materials where properties such as electrostatic charge,chemical compatibility, mechanical response, etc. are tuned to facilitate or even force the retention of the desired analyte onto the optical enhancer.

As a first approach, and maybe the simplest, electrostatic attraction can be favoured by tuning the nanoparticle charge as a function of the pH (Alvarez-Puebla *et al.*, 2005). This strategy has been employed with regular gold or silver citrate-reduced colloids. However, this method has only applicability for the analysis of implicitly positive analytes, especially because obtaining positive zeta potentials (i.e. surface charge) is limited. This drawback can be solved just by choosing the appropriate capping agent. For example, gold or silver nanoparticles can be reduced and stabilized with different amino acids. Thus, as a function of the amino acid nature (number of amino groups) and the pH of the media, the surface charge can be tuned from 30 to −50 mV (Alvarez-Puebla and Aroca, 2009). It is important to note that only certain amino acids can be used. As an example, all of those containing thiols passivate the gold or silver surface inhibiting the retention of the molecules under study. Hydrophobic affinity is a good option

to increment the retention of non-polar molecules. In this case materials are capped/functionalized with a hydrophobic monolayer that presents high affinity for the analyte. Examples of that can be the deposition of an aliphatic self-assembled monolayers as a partition interface, which has been successfully applied to the analysis of polycyclic aromatic hydrocarbons (PAH) (Jones *et al*., 2009) or polychlorinated biphenyls (Bantz and Haynes, 2009). Further, other hydrophobic molecules such as calixarenes, (Guerrini *et al*., 2006) viologen, (Guerrini *et al*., 2009a) and dithiocarbamates (Guerrini *et al*., 2009b) have been widely used for the detection of PAHs. Nevertheless, there are many analytes that cannot be detected by using these strategies. For example, metallic ions cannot be directly detected by Raman, a molecular spectroscopy. Thus, by coupling the appropriate molecule to the gold or silver surfaces, detection of metals can be achieved through the vibrational changes on the ligand after complexation (Zhao *et al*., 2009). In a more general scheme, hybrid materials able to unspecifically trap molecules from a given solution are highly desirable. Mechanical retention of analytes can be achieved by using stimuli responsive polymers, especially to temperature (i.e. pNIPAM) (Alvarez-Puebla *et al*., 2009; Contreras-Cáceres *et al*., 2011) or pH (i.e. lipoic acid- polyethylene glycol -polymethacrylic acid block-copolymer) (Qian *et al*., 2009). Unfortunately, these materials usually consist of coated single colloids. Thus, the same responsive coat, responsible for the mechanical trapping, hampers the interaction of the particles and so the generation of hot spots (Fig. 8.10a) (Markel *et al*., 1999). One advantage of colloids is that they can be used as prepared to fabricate solid thin films and bulk materials. In line with this trapping concept, colloidal silver particles have been imbibed into exponentially growth layer-by-layer films (Podsiadlo *et al*., 2008; Srivastava *et al*., 2008), generating a high density of hot spots (Fig. 8.10b). These materials allow for the direct ultrasensitive analysis of molecules that were not retained by other methods (Abalde-Cela *et al*., 2009). Further bulk polymers can be prepared by *in situ* reduction of silver particles, putting together benefits such as trapping properties, dynamic hot spots and reusability (Aldeanueva-Potel *et al*., 2009).

Besides the use of colloidal particles in solution, they can also be engineered into films. The easiest technique for film fabrication is undoubtedly by casting and air-drying a polymeric solution containing nanoparticles (dos Santos *et al*., 2004). This method is subject to the same drawbacks associated with the random generation of hot spots, as previously stated. This can be easily solved by applying modern thin film fabrication methods such as self-assembly (Gellner *et al*., 2009), Langmuir-Blodgett (Lu *et al*., 2004) or colloidal stamping (Pazos-Perez *et al*., 2010b; Schweikart *et al*., 2011; Mueller *et al*., 2012). Furthermore, these fabrication approaches can be also exploited for the fabrication of optical filters, able to monitor large volumes of sample in continuous flows or even discrete hybrid particles with size ranging

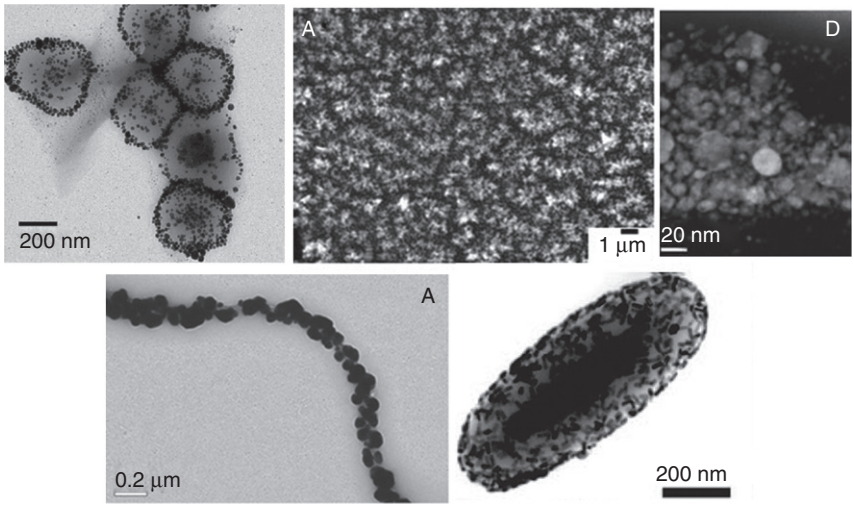

8.10 (a) Representative transmission electron microscopy (TEM) images of magnetite-Ag@pNIPAM composite microgels. (b) Right: Top view SEM images at different magnifications of the e-LBL AgNP film after 24 h of immersion. Left: Cross-sectional TEM and STEM images, respectively, of the film after focused ion beam (FIB) preparation. (c) Representative TEM image of silver-coated carbon nanotube (CNT@Ag). (d) Representative SEM image γ-Fe_2O_3@rod composite particles. (*Source*: Reproduced with permission from Abalde-Cela *et al.*, 2009; Spuch-Calvar *et al.*, 2009; Taladriz-Blanco *et al.*, 2009; Contreras-Cáceres *et al.*, 2011. Copyright Willey VCH, 2009; and, America Chemical Society 2009 and 2011.)

from the submicrometre to several micrometres. Though different in nature, both substrates accomplish the same function: the increment of the detection limit. The former, also called *optical accumulators*, are based on the continuous pass of the flow problem, retaining the analyte of interest until reaching a concentration sufficient for SERS detection (Ko and Tsukruk, 2008). This method has been demonstrated within the multiplex detection of several analytes at the same time with real concentrations as low as 10^{-18} M (Aldeanueva-Potel *et al.*, 2010). On the other hand self-assembly monolayers (SAMs), layer-by-layer (LbL) or even *in situ* reduction of adsorbed metal ions can be carried out on the surface of small particles, typically polymer or silica spheres, (Jiang and Tsukruk, 2006; Braun *et al.*, 2007; Farah *et al.*, 2009) but also on other substrates such as carbon nanotubes (Sanles-Sobrido *et al.*, 2009; Taladriz-Blanco *et al.*, 2009). These materials combine optical and colloidal stability of the supported gold or silver nanoparticles. Furthermore, the controlled aggregation of the colloidal suspensions on the particle surfaces allows the formation of stable and reproducible hot spots (Fig. 8.10c). Additionally, if these particles are big enough to be observed

under an optical microscope, it would allow for decreasing the amount of the optical enhancer required for the SERS analysis with the subsequent increase in the detection limit. Unfortunately just *looking for the bead* under the microscope is a very time-demanding process. Progress in multifunctional synthesis of materials has permitted the generation of bifunctional materials, either nanometric (Wei *et al*., 2009; Pazos-Perez *et al*., 2010c) or submicrometric (Spuch-Calvar *et al*., 2009) comprising optical properties together with magnetism (Fig. 8.10d). The last property offers the possibility of decreasing the amount of the optical substrate, which can be later concentrated upon application of a magnetic field.

8.4 Conclusion

To sum up, this chapter aims for a brief but clear exposition of the SERS effect and mechanisms in light of modern plasmonics. Also, the relation between SERS signal and the optical enhancer is studied, in order to provide tools to identify the possible advantages or disadvantages related to each substrate under each physical condition (in liquid or stabilized on a solid support). Then the methods for preparation of active substrates and their applications are critically reviewed. In fact, we can conclude that the preparation of optical substrates with optimized properties is a very dynamic field of research and, as there is no universal best SERS platform, careful consideration of the analytical problem is required before choosing/designing a SERS sensor.

8.5 Sources of further information and advice

To date, SERS is becoming a multidisciplinary area. Thus, the recommendation of further advanced lecture to gain information about the topic is complicated. Notwithstanding, three outstanding monographies have recently been published:

- Ewen Smith and Geoffrey Dent, *Modern Raman Spectroscopy: A Practical Approach*, Wiley, 2001.
- Ricardo Aroca, *Surface-Enhanced Vibrational Spectroscopy*, Wiley, 2006.
- Pablo Etchegoin and Eric Le Ru, *Principles of Surface-Enhanced Raman Spectroscopy and Related Plasmonic Effects, Elsevier*, 2008. In addition there are a number of highly recommended review papers summarizing different aspects of SERS:

Basic mechanisms

Moskovits, M. (2006). Surface-enhanced Raman spectroscopy: a brief perspective. *Surface-Enhanced Raman Scattering: Physics and Applications*, Springer-Verlag, Berlin Hidelberg, **103**, 1–17.

Otto, A. and Futamata, M. (2006). Electronic mechanisms of SERS. In: Kneipp, K., Moskovits, M. and Kneipp, H. (eds.) *Surface-Enhanced Raman Scattering: Physics and Applications*, Springer-Verlag, Berlin Hidelberg.

Schatz, G. C., Young, M. A. and Van Duyne, R. P. (2006). Electromagnetic mechanism of SERS. *Surface-Enhanced Raman Scattering: Physics and Applications*, Springer-Verlag, Berlin Hidelberg, **103**, 19–45.

Stiles, P. L., Dieringer, J. A., Shah, N. C. and Van Duyne, R. R. (2008). Surface-enhanced Raman spectroscopy. *Annual Review of Analytical Chemistry*, **1**, 601–626.

Bioapplications

Abalde-Cela, S., Aldeanueva-Potel, P., Mateo-Mateo, C., Rodriguez-Lorenzo, L., Alvarez-Puebla, R. A. and Liz-Marzan, L. M. (2010). Surface-enhanced Raman scattering biomedical applications of plasmonic colloidal particles. *Journal of the Royal Society Interface*, **7**, S435–S450.

Cialla, D., Maerz, A., Boehme, R., Theil, F., Weber, K., Schmitt, M. and Popp, J. (2012). Surface-enhanced Raman spectroscopy (SERS): progress and trends. *Analytical and Bioanalytical Chemistry*, **403**, 27–54.

Hering, K., Cialla, D., Ackermann, K., Doerfer, T., Moeller, R., Schneidewind, H., Mattheis, R., Fritzsche, W., Roesch, P. and Popp, J. (2008). SERS: a versatile tool in chemical and biochemical diagnostics. *Analytical and Bioanalytical Chemistry*, **390**, 113–124.

Porter, M. D., Lipert, R. J., Siperko, L. M., Wang, G. and Narayanana, R. (2008). SERS as a bioassay platform: fundamentals, design, and applications. *Chemical Society Reviews*, **37**, 1001–1011.

Environmental applications

Alvarez-Puebla, R. A. and Liz-Marzan, L. M. (2010). Environmental applications of plasmon assisted Raman scattering. *Energy & Environmental Science*, **3**, 1011–1017.

Fan, M., Andrade, G. F. S. and Brolo, A. G. (2011). A review on the fabrication of substrates for surface enhanced Raman spectroscopy and their applications in analytical chemistry. *Analytica Chimica Acta*, **693**, 7–25.

Jarvis, R. M. and Goodacre, R. (2008). Characterisation and identification of bacteria using SERS. *Chemical Society Reviews*, **37**, 931–936.

Materials

Brus, L. (2008). Noble metal nanocrystals: Plasmon electron transfer photochemistry and single-molecule Raman spectroscopy. *Accounts of Chemical Research*, **41**, 1742–1749.

Gordon, R., Sinton, D., Kavanagh, K. L. and Brolo, A. G. (2008). A new generation of sensors based on extraordinary optical transmission. *Accounts of Chemical Research*, **41**, 1049–1057.

Sharma, B., Frontiera, R. R., Henry, A.-I., Ringe, E. and Van Duyne, R. P. (2012). SERS: Materials, applications, and the future. *Materials Today*, **15**, 16–25.

Tripp, R. A., Dluhy, R. A. and Zhao, Y. (2008). Novel nanostructures for SERS biosensing. *Nano Today*, **3**, 31–37.

Single molecule

Kneipp, K., Kneipp, H. and Kneipp, J. (2006). Surface-enhanced Raman scattering in local optical fields of silver and gold nanoaggregates – From single-molecule Raman spectroscopy to ultrasensitive probing in live cells. *Accounts of Chemical Research*, **39**, 443–450.

Le Ru, E. C. and Etchegoin, P. G. (2012). Single-molecule surface-enhanced Raman spectroscopy. In: Johnson, M. A. and Martinez, T. J. (eds.) *Annual Review of Physical Chemistry*, Vol. 63.

Pieczonka, N. P. W. and Aroca, R. F. (2008). Single molecule analysis by surfaced-enhanced Raman scattering. *Chemical Society Reviews*, **37**, 946–954.

8.6 Acknowledgements

This work was funded by the Spanish Ministerio de Economia y Competitividad (CTQ2011-23167).

8.7 References

Abalde-Cela, S., Aldeanueva-Potel, P., Mateo-Mateo, C., Rodríguez-Lorenzo, L., Alvarez-Puebla, R. A. and Liz-Marzán, L. M. (2010). Surface-enhancement Raman scattering biomedical applications of plasmonic colloidal particles. *J. Royal Soc. Interface,* **7**, S435–S450.

Abalde-Cela, S., Ho, S., Rodriguez-Gonzalez, B., Correa-Duarte, M. A., Alvarez-Puebla, R. A., Liz-Marzan, L. M. and Kotov, N. A. (2009). Loading of exponentially grown LBL films with silver nanoparticles and their application to generalized SERS detection. *Angew. Chem. Int. Ed.,* **48**, 5326–5329.

Albrecht, M. G. and Creighton, J. A. (1977). Anomalously intense Raman spectra of pyridine at a silver electrode. *J. Am. Chem. Soc.,* **99**, 5215–5217.

Aldeanueva-Potel, P., Carbó-Argibay, E., Pazos-Pérez, N., Barbosa, S., Pastoriza-Santos, I., Alvarez-Puebla, R. A. and Liz-Marzán, L. M. (2012). Spiked gold beads as substrates for single-particle SERS. *ChemPhysChem,* **13**, 2561–2565.

Aldeanueva-Potel, P., Correa-Duarte, M. A., Alvarez-Puebla, R. and Liz-Marzan, L. M. (2010). Free-standing carbon nanotube films as optical accumulators for multiplex SERS. *ACS App. Mater. Interfaces,* **2**, 19–22.

Aldeanueva-Potel, P., Faoucher, E., Alvarez-Puebla, R. A., Liz-Marzan, L. M. and Brust, M. (2009). Recyclable molecular trapping and SERS detection in silver-loaded agarose gels with dynamic hot spots. *Anal. Chem.,* **81**, 9233–9238.

Alvarez-Puebla, R. A. (2012). Effects of the excitation wavelength on the SERS spectrum. *J. Phys. Chem. Lett.,* **3**, 857–866.

Alvarez-Puebla, R. A., Agarwal, A., Manna, P., Khanal, B. P., Aldeanueva-Potel, P., Carbó-Argibay, E., Pazos-Pérez, N., Vigderman, L., Zubarev, E. R., Kotov, N. A. and Liz-Marzán, L. M. (2011). Gold nanorods 3d-supercrystals as SERS substrates for the rapid detection of scrambled prions. *Proc. Natl. Acad. Sci. USA,* **108**, 8157–8161.

Alvarez-Puebla, R. A., Arceo, E., Goulet, P. J. G., Garrido, J. J. and Aroca, R. F. (2005). Role of nanoparticle surface charge in surface-enhanced Raman scattering. *J. Phys. Chem. B,* **109**, 3787–3792.

Alvarez-Puebla, R. A. and Aroca, R. F. (2009). Synthesis of silver nanoparticles with controllable surface charge and their application to surface-enhanced Raman scattering. *Anal. Chem.,* **81**, 2280–2285.

Alvarez-Puebla, R. A., Contreras-Caceres, R., Pastoriza-Santos, I., Perez-Juste, J. and Liz-Marzan, L. M. (2009). Au@pNIPAM colloids as molecular traps for surface-enhanced, spectroscopic, ultra-sensitive analysis. *Angew. Chem.Int. Ed.,* **48**, 138–143.

Alvarez-Puebla, R. A. and Liz-Marzan, L. M. (2010). SERS-based diagnosis and biodetection. *Small,* **6**, 604–610.

Alvarez-Puebla, R. A. and Liz-Marzan, L. M. (2012). Traps and cages for SERS detection. *Chem. Soc Rev.,* **41**, 43–51.

Alvarez-Puebla, R. A., Liz-Marzan, L. M. and Garcia De Abajo, F. J. (2010). Light concentration at the nanometer scale. *J. Phys. Chem. Lett.,* **1**, 2428–2434.

Aroca, R. (2006). *Surface-Enhancement Vibrational Spectoscopy,* New York, John Wiley and Sons, Ltd.

Banholzer, M. J., Millstone, J. E., Qin, L. and Mirkin, C. A. (2008). Rationally designed nanostructures for surface-enhanced Raman spectroscopy. *Chem. Soc. Rev.,* **37**, 885–897.

Bantz, K. C. and Haynes, C. L. (2009). Surface-enhanced Raman scattering detection and discrimination of polychlorinated biphenyls. *Vib. Spectrosc.,* **50**, 29–35.

Bidault, S., Garcia De Abajo, F. J. and Polman, A. (2008). Plasmon-based nanolenses assembled on a well-defined DNA template. *J. Am. Chem. Soc.,* **130**, 2750–2751.

Braun, G., Pavel, I., Morrill, A. R., Seferos, D. S., Bazan, G. C., Reich, N. O. and Moskovits, M. (2007). Chemically patterned microspheres for controlled nanoparticle assembly in the construction of SERS hot spots. *J. Am. Chem. Soc.,* **129**, 7760–7761.

Braun, G. B., Lee, S. J., Laurence, T., Fera, N., Fabris, L., Bazan, G. C., Moskovits, M. and Reich, N. O. (2009). Generalized approach to SERS-active nanomaterials via controlled nanoparticle linking, polymer encapsulation, and small-molecule infusion. *J. Phys. Chem. C,* **113**, 13622–13629.

Chen, X., Li, S., C, X., Banholzer, M. J., Schatz, G. C. and Mirkin, C. A. (2009). Plasmonic focusing in rod-sheath heteronanostructures. *ACS Nano,* **3**, 87–92.

Cobley, C. M., Skrabalak, S. E., Campbell, D. J. and Xia, Y. (2008). Shape-controlled synthesis of silver nanoparticles for plasmonic and sensing applications. *Plasmonics,* **4**, 171–179.

Contreras-Cáceres, R., Abalde-Cela, S., Guardia-Girós, P., Fernández-Barbero, A., Pérez-Juste, J., Alvarez-Puebla, R. A. and Liz-Marzán, L. M. (2011). Multifunctional microgel magnetic/optical traps for SERS ultradetection. *Langmuir,* **27**, 4520–4525.

Dos Santos, D. S., Goulet, P. J. G., Pieczonka, N. P. W., Oliveira, O. N. and Aroca, R. F. (2004). Gold nanoparticle embedded, self-sustained chitosan films as substrates for surface-enhanced Raman scattering. *Langmuir,* **20**, 10273–10277.

Driskell, J. D., Shanmukh, S., Liu, Y., Chaney, S. B., Tang, X.-J., Zhao, Y.-P. and Dluhy, R. A. (2008). The use of aligned silver nanorod arrays prepared by oblique angle deposition as surface enhanced Raman scattering substrates. *J. Phys. Chem. C,* **112**, 895–901.

Efrima, S. and Metiu, H. (1979). Classical theory of light scattering by an adsorbed molecule. I. Theory. *J. Chem. Phys.,* **70**, 1602–1613.

Farah, A. A., Bravo-Vasquez, J. P., Alvarez-Puebla, R. A., Cho, J.-Y. and Fenniri, H. (2009). Robust Au-PEG/PS microbeads as optically stable platforms for SERS. *Small,* **5**, 1283–1286.

Fleischmann, M., Hendra, P. J. and Mcquillan, A. J. (1974). Raman spectra of pyridine adsorbed at a silver electrode. *Chem. Phys. Lett.,* **26**, 163–166.

Gamaly, E. G. and Rode, A. V. (2004). Nanostructures created by lasers. *Encycl. Nanosci. Nanotechnol.,* **7**, 783–809.

Garcia De Abajo, F. J. (2007). Colloquium: Light scattering by particle and hole arrays. *Rev. Mod. Phys.,* **79**, 1267–1290.

Gellner, M., Kömpe, K. and Schlücker, S. (2009). Multiplexing with SERS labels using mixed SAMs of Raman reporter molecules. *Anal.Bioanal. Chem.,* **394**, 1839–1844.

Genov, D. A., Sarychev, A. K., Shalaev, V. M. and Wei, A. (2004). Resonant field enhancement from metal nanoparticle arrays. *Nano Lett.,* **4**, 153–158.

Grzelczak, M., Perez-Juste, J., Mulvaney, P. and Liz-Marzan, L. M. (2008). Shape control in gold nanoparticle synthesis. *Chem. Soc. Rev.,* **37**, 1783–1791.

Guerrini, L., Garcia-Ramos, J. V., Domingo, C. and Sanchez-Cortes, S. (2006). Functionalization of Ag nanoparticles with dithiocarbamate calix[4]arene as an effective supramolecular host for the surface-enhanced Raman scattering detection of polycyclic aromatic hydrocarbons. *Langmuir,* **22**, 10924–10926.

Guerrini, L., Garcia-Ramos, J. V., Domingo, C. and Sanchez-Cortes, S. (2009a). Nanosensors based on violagen functionalized silver nanoparticles: Few molecules surface-enhanced Raman detection of polycyclic aromatic hydrocarbons in interparticle hot spots. *Anal. Chem.,* **81**, 1418–1425.

Guerrini, L., Garcia-Ramos, J. V., Domingo, C. and Sanchez-Cortes, S. (2009b). Self-assembly of dithiocarbamate calixarene on Ag nanoparticles and its application in the fabrication of surface-enhanced Raman scattering based nanosensors. *Phys. Chem. Chem. Phys.,* **11**, 1787–1793.

Hatab, N. A., Hsueh., H. C., Gaddis, A. L., Retterer, S. T., Li, J. H., Eres, G., Zhang, Z. and Gu, B. (2010). An integrated portable Raman sensor with nanofabricated gold bowtie array substrates for energetics detection. *Nano Lett.,* **12**, 4952–4955.

Henry, A.-I., Bingham, J. M., Ringe, E., Marks, L. D., Schatz, G. C. and van Duyne, R. P. (2011). Correlated structure and optical property studies of plasmonic nanopartices. *J. Phys. Chem. C,* **115**, 9291–9395.

Hicks, E. M., Zhang, X. Y., Zou, S. L., Lyandres, O., Spears, K. G., Schatz, G. C. and Van Duyne, R. P. (2005). Plasmonic properties of film over nanowell surfaces fabricated by nanosphere lithography. *J. Phys. Chem. B,* **109**, 22351–22358.

Hou, X. and Fang, Y. (2007). Investigation of p-hydroxybenzoic acid from a new surface-enhanced Raman scattering system. *J. Colloid Interface Sci.,* **316**, 19.

Hu, J., Zhao, B., Xu, W., Fan, Y., Li, B. and Ozaki, Y. (2002). Simple method for preparing controllably aggregated silver particle films used as surface-enhanced Raman scattering active substrates. *Langmuir,* **18**, 6839.

Jain, P. K., Huang, X., El-Sayed, I. H. and El-Sayed, M. A. (2008). Noble metals on the nanoscale: Optical and photothermal properties and some applications in imaging, sensing, biology and medicine. *Acc. Chem. Res.,* **41**, 1578–1586.

Jana, N. R. and Pal, T. (2007). Anisotropic metal nanoparticles for use as surface-enhanced Raman substrates. *Adv. Mater.,* **19**, 1761–1763.

Jeanmaire, D. L. and Van Duyne, R. P. (1977). Surface Raman spectroelectrochemistry Part I. Heterocyclic, aromatic, and aliphatic amines adsorbed on the anodized silver electrode. *J. Electroanal. Chem.,* **84**, 1–20.

Jiang, C. and Tsukruk, V. V. (2006). Freestanding nanostructures via layer-by-layer assembly. *Adv. Mater.,* **18**, 829–840.

Jones, C. L., Bantz, K. C. and Haynes, C. L. (2009). Partition layer-modified substrates for reversible surface-enhanced Raman scattering detection of polycyclic aromatic hydrocarbons. *Anal. Bioanal. Chem.,* **394**, 303–311.

King, F. W., Van Duyne, R. P. and Schatz, G. C. (1978). Theory of Raman scattering by molecules adsorbed on electrode surfaces. *J. Chem. Phys.,* **69**, 4472–4481.

Kneipp, J., Wittig, B., Bohr, H. and Kneipp, K. (2010). Surface-enhanced Raman scattering: a new optical probe in molecular biophysic and biomedicine. *Theor. Chem. Acc.,* **125**, 319–327.

Kneipp, K., Kneipp, H. and Moskovits, M. (2006). *Surface-Enhanced Raman Scattering,* Berlin Heidelberg, Springer-Verlag.

Kneipp, K., Wang, Y., Kneipp, H., Perelman, L. T., Itzkan, I., Dasari, R. R. and Feld, M. S. (1997). Single molecule detection using surface-enhanced Raman scattering (SERS). *Phys. Rev. Lett.,* **78**, 1667–1670.

Ko, H., Singamaneni, S. and Tsukruk, V. V. (2008). Nanostructured surfaces and assemblies as SERS media. *Small,* **4**, 1576–1599.

Ko, H. and Tsukruk, V. V. (2008). Nanoparticle-decorated nanocanals for surface-enhanced Raman scattering. *Small,* **4**, 1980–1984.

Le Ru, E. C. and Etchegoin, P. G. (2006). Rigorous justification of the |E|4 enhancement factor in surface enhanced Raman scattering. *Chem. Phys. Lett.,* **423**, 63–66.

Le Ru, E. C. and Etchegoin, P. G. (2009). *Principles of Surface Enhanced Raman Spectroscopy and Related Plasmonic Effects,* Amsterdam, Elsevier.

Lee, S. J., Morrill, A. R. and Moskovits, M. (2006). Hot spots in silver nanowire bundles for surface-enhanced Raman spectroscopy. *J. Am. Chem. Soc.,* **128**, 2200.

Long, D. A. (2002). *The Raman Effect: A Unified Treatment of the Theory of Raman Scattering by Molecules*, New York, Jonh Wiley and Sons Ltd.

Lu, X., Rycenga, M., Skrabalak, S. E., Wiley, B. and Xia, Y. (2009). Chemical synthesis of novel plasmonic nanoparticles. *Annu. Rev. Phys. Chem.,* **60**, 167–192.

Lu, Y., Liu, G. L. and Lee, L. P. (2004). High-density silver nanoparticle film with temperature-controllable interparticle spacing for a tunable surface enhanced Raman scattering substrate. *Nano Lett.,* **5**, 5–9.

Markel, V. A., Shalaev, V. M., Zhang, P., Huynh, W., Tay, L., Haslett, T. L. and Moskovits, M. (1999). Near-field optical spectroscopy of individual surface-plasmon modes in colloid clusters. *Phys. Rev. B,* **59**, 10903.

Mayer, K. M. and Hafner, J. H. (2011). Localized surface plasmon resonance sensor. *Chem. Rev.,* **111**, 3828–3857.

McCreery, R. L. (2000). *Raman Spectroscopy for Chemical Analysis*, New York, John Wiley and Sons Inc.

Merlen, A., Gadenne, V., Romann, J., Chevallier, V., Patrone, L. and Valmalette, J. C. (2009). Surface-enhanced Raman spectroscopy of organic molecules deposited on gold sputtered substrates. *Nanotechnology,* **20**, 215705.

Min, Q., Santos, M. J. L., Girotto, E. M., Brolo, A. G. and Gordon, R. (2008). Localized Raman enhancement from a double-hole nanostructure in a metal film. *J. Phys. Chem. C,* **112**, 15098–15101.

Moskovits, M. (2005). Surface-enhanced Raman spectroscopy: A brief retrospective. *J. Raman Spectrosc.,* **36**, 485–496.

Moskovits, M. and Suh, J. S. (1984). Surface selection-rules for surface-enhanced Raman-spectroscopy – calculations and application to the surface-enhanced Raman spectrum of phthalazine on silver. *J. Phys. Chem.,* **88**, 5526–5530.

Mueller, M., Tebbe, M., Andreeva, D. V., Karg, M., Alvarez-Puebla, R. A., Pazos-Perez, N. and Fery, A. (2012). Large-area organization of pnipam-coated nanostars as SERS platforms for polycyclic aromatic hydrocarbons sensing in gas phase. *Langmuir,* **28**, 9168–9173.

Myroshnychenko, V., Rodriguez-Fernandez, J., Pastoriza-Santos, I., Funston, A. M., Novo, C., Liz-Marzan, L. M. and Garcia De Abajo, F. J. (2008). Modelling the optical response of gold nanoparticles. *Chem. Soc. Rev.,* **37**, 1792–1805.

Natan, M. J. (2006). Concluding remarks. surface enhanced Raman scattering. *Faraday Discuss,* **132**, 321–328.

Nelayah, J., Kociak, M., Stephan, O., Garcia De Abajo, F. J., Tencé, M., Henrard, L., Taverna, D., Pastoriza-Santos, I., Liz-Marzan, L. M. and Colliex, C. (2007). Mapping surface plasmons on a single metallic nanoparticle. *Nat. Phys.,* **3**, 348–353.

Nie, S. and Emory, S. R. (1997). Probing single molecules and single nanoparticles by surface-enhanced Raman scattering. *Science,* **275**, 1102–1106.

Ochsenkühn, M. A., Jess, P. R. T., Stoquert, H., Dholakia, K. and Campbell, C. J. (2009). Nanoshells for surface-enhanced Raman spectroscopy in eukaryotic cells: Cellular response and sensor development. *ACS Nano,* **3**, 3613–3621.

Oran, J., Hinde, R., Abu Hatab, N., Retterer, S. and Sepaniak, M. (2008). Nanofabricated periodic arrays of silver elliptical discs as SERS substrates. *J. Raman Spectrosc.,* **39**, 1811–1820.

Orenforff, C. J., Gearheart, L., Jana, N. R. and Murphy, C. J. (2005). Aspect ratio dependence on surface enhanced Raman scattering using silver and gold nanorod substrates. *Phys. Chem. Chem. Phys.,* **8**, 165–170.

Otto, A. (2001a). Theory of first layer and single molecule surface enhanced Raman scattering. *Phys. Status Solidi A,* **188**, 1455–1470.

Otto, A. (2001b). Theory of first layer and single molecule surface enhanced Raman scattering. *Phys. Status Solidi A-Appl. Res.,* **188**, 1455–1470.

Otto, A. (2002). What is observed in single molecule SERS, and why? *J. Raman Spectrosc.,* **33**, 593–598.

Pan, Z., Zavalin, A., Ueda, A., Guo, M., Groza, M., Burger, A., Mu, R. and Morgan, S. H. (2005). Surface-enhanced Raman spectroscopy using silver-coated porous glass-ceramic substrates. *Appl. Spectrosc.,* **59**, 782.

Park, H. K., Yoon, J. K. and Kim, K. (2006). Novel fabrication of Ag thin film on glass for efficient surface-enhanced Raman scattering. *Langmuir,* **22**, 1626.

Pazos-Perez, N., Barbosa, S., Rodriguez-Lorenzo, L., Aldeanueva-Potel, P., Perez-Juste, J., Pastoriza-Santos, I., Alvarez-Puebla, R. A. and Liz-Marzan, L. M. (2010a). Growth of sharp tips on gold nanowires leads to increased surface-enhanced Raman scattering activity. *J. Phys. Chem. Lett.,* **1**, 24–27.

Pazos-Perez, N., Ni, W., Schweikart, A., Alvarez-Puebla, R. A., Fery, A. and Liz-Marzan, L. M. (2010b). Highly uniform SERS substrates formed by wrinkle-confined drying of gold colloids. *Chem. Sci.,* **1**, 174–178.

Pazos-Perez, N., Rodriguez-Gonzalez, B., Hilgendorff, M., Giersig, M. and Liz-Marzan, L. M. (2010c). Gold encapsulation of star-shaped FePt nanoparticles. *J. Mater. Chem.*, **20**, 61–64.

Podsiadlo, P., Michel, M., Lee, J., Verploegen, E., Wong Shi Kam, N., Ball, V., Lee, J., Qi, Y., Hart, A. J., Hammond, P. T. and Kotov, N. A. (2008). Exponential growth of LBL films with incorporated inorganic sheets. *Nano Lett.,* **8**, 1762–1770.

Qian, X., Li, J. and Nie, S. (2009). Stimuli-responsive SERS nanoparticles: Conformational control of plasmonic coupling and surface Raman enhancement. *J. Am. Chem. Soc.,* **131**, 7540–7541.

Raman, C. V. and Krishnan, K. S. (1928). A new type of secondary radiation. *Nature,* **121**, 501–502.

Rodriguez-Lorenzo, L., Alvarez-Puebla, R. A., Garcia De Abajo, F. J. and Liz-Marzan, L. M. (2010). Surface enhanced Raman scattering using star-shape gold colloidal nanoparticles. *J. Phys. Chem. B,* **114**, 7336–7340.

Rodriguez-Lorenzo, L., Alvarez-Puebla, R. A., Pastoriza-Santos, I., Mazzucco, S., Stephan, O., Kociak, M., Liz-Marzan, L. M. and De Abajo, F. J. G. (2009). Zeptomol detection through controlled ultrasensitive surface-enhanced Raman scattering. *J. Am. Chem. Soc.,* **131**, 4616–4618.

Rodriguez-Lorenzo, L., Fabris, L. and Alvarez-Puebla, R. A. (2012). Multiplex optical sensing with SERS. A critical review. *Anal. Chim. Acta,* 10.1016/j.aca.2012.08.003.

Romo-Herrera, J. M., Alvarez-Puebla, R. A. and Liz-Marzan, L. M. (2011). Controlled assembly of plasmonic colloidal nanoparticle clusters. *Nanoscale,* **3**, 1304–1315.

Sanles-Sobrido, M., Exner, W., Rodríguez-Lorenzo, L., Rodríguez-González, B., Correa-Duarte, M. A., Álvarez-Puebla, R. A. and Liz-Marzán, L. M. (2009). Design of sers-encoded, submicron, hollow particles through confined growth of encapsulated metal nanoparticles. *J. Am. Chem. Soc.,* **131**, 2699–2705.

Schweikart, A., Pazos-Perez, N., Alvarez-Puebla, R. A. and Fery, A. (2011). Controlling inter-nanoparticle coupling by wrinkle-assisted assembly. *Soft Matter,* **7**, 4093–4100.

Sepúlveda, B., Angelomé, P. C., Lechuga, L. M. and Liz-Marzan, L. M. (2009). LSPR-based nanobiosensors. *Nano Today,* **4**, 244–251.

Smekal, A. (1923). The quantum theory of dispersion. *Naturwissenschaften,* **11**, 873–875.

Smith, E. and Dent, G. (2005). *Modern Raman Spectroscopy – A Practical Approach*, Chichester, John Wiley and Sons Ltd.

Spuch-Calvar, M., Rodriguez-Lorenzo, L., Morales, M. P., Alvarez-Puebla, R. A. and Liz-Marzan, L. M. (2009). Bifunctional nanocomposites with long-term stability as SERS optical accumulators for ultrasensitive analysis. *J. Phys. Chem. C,* **113**, 3373–3377.

Srivastava, S., Ball, V., Podsiadlo, P., Lee, J., Ho, P. and Kotov, N. A. (2008). Reversible loading and unloading of nanoparticles in a exponentially growing polyelectrolyte LBL films. *J. Am. Chem. Soc.,* **130**, 3748–3749.

Stoerzinger, K. A., Hasan, W., Lin, J. Y., Robles, A. and Odom, T. W. (2010). Screening nanopyramid assemblies to optimize surface enhanced Raman scattering. *J. Phys. Chem. Lett.,* **1**, 1046–1050.

Taladriz-Blanco, P., Rodriguez-Lorenzo, L., Sanles-Sobrido, M., Herves, P., Correa-Duarte, M. A., Alvarez-Puebla, R. A. and Liz-Marzan, L. M. (2009). SERS study of the controllable release of nitric oxide from aromatic nitrosothiols on bimetallic, bifunctional nanoparticles supported on carbon nanotubes. *ACS App. Mater. Interfaces,* **1**, 56–59.

Tian, Z. Q., Ren, B. and Wu, D. Y. (2002). Surface-enhanced Raman scattering: From noble to transition metals and from rough surfaces to ordered nanostructures. *J. Phys. Chem. B,* **106**, 9463–9483.

Wei, Q., Song, H.-M., Leonov, A. P., Hale, J. A., Oh, D., Ong, Q. K., Ritchie, K. and Wei, A. (2009). Gyromagnetic imaging: Dynamic optical contrast using gold nanostars with magnetic cores. *J. Am. Chem. Soc.,* **131**, 9728–9734.

Whitney, A. V., Elam, J. W., Zou, S. L., Zinovev, A. V., Stair, P. C., Schatz, G. C. and Van Duyne, R. P. (2005). Localized surface plasmon resonance nanosensor: A high-resolution distance-dependence study using atomic layer deposition. *J. Phys. Chem. B,* **109**, 20522–20528.

Willets, K. A. and Van Duyne, R. P. (2007). Localized surface plasmon resonance spectroscopy and sensing. *Annu. Rev. Phys. Chem.,* **58**, 267.

Xu, J., Kvasnička, P., Idso, M., Jordan, R. W., Gong, H., Homola, J. and Yu, Q. (2011). Understanding the effects of dielectric medium, substrate, and depth on electric fields and SERS of quasi-3D plasmonic nanostructures. *Opt. Express,* **19**, 20493–20505.

Xu, J., Zhang, L., Gong, H., Homola, J. and Yu, Q. (2010a). Tailoring plasmonic nanostructures for optimal SERS sensing of small molecules and large microorganisms. *Small,* **7**, 371–376.

Xu, Y.-L. (1995). Electromagnetic scattering by an aggregate of spheres. *Appl. Opt.,* **34**, 4573–4588.

Xu, Z., Hao, J., Li, F. and Meng, X. (2010b). Surface-enhanced Raman spectroscopy of arsenate and arsenite using Ag nanofilm prepared by modified mirror reaction. *J. Colloid Interface Sci.,* **347**, 90.

Yanagi, H. and Ohno, T. (1999). Nanofabrication of gold particles in glass films by AFM-assisted local reduction. *Langmuir,* **15**, 4773–4776.

Yonzon, C. R., Zhang, X., Zhao, J. and Van Duyne, R. P. (2007). Surface-enhanced nanosensors. *Spectroscopy,* **22**, 42.

Yu, Q., Braswell, S., Christin, B., Xu, J., Wallace, P. M., Gong, H. and Kaminsky, D. (2010). Surface-enhanced Raman scattering on gold quasi-3D nanostructure and 2D nanohole arrays. *Nanotechnology,* **21**, 355301.

Zhang, H. and Mirkin, C. A. (2004). DPN-generated nanostructures made of gold, silver, and palladium. *Chem. Mater.,* **16**, 1480–1484.

Zhang, X., Zhao, J., Whitney, A., Elam, J. and Van Duyne, R. P. (2006a). Ultrastable substrates for surface-enhanced Raman spectroscopy fabricated by atomic layer deposition: Improved anthrax biomarker detection. *J. Am. Chem. Soc.,* **128**, 10304–10309.

Zhang, X. Y., Yonzon, C. R. and Van Duyne, R. P. (2006b). Nanosphere lithography fabricated plasmonic materials and their applications. *J. Mater. Res.,* **21**, 1083–1092.

Zhao, J., Pinchuk, A. O., Mcmahon, J. M., Li, S., Ausman, L. K., Atkinson, A. L. and Schatz, G. C. (2008). Method for describing the electromagnetic properties of silver and gold nanoparticles. *Acc. Chem. Res.,* **41**, 1710–1720.

Zhao, Y., Newton, J. N., Liu, J. and Wei, A. (2009). Dithiocarbamate-coated SERS substrates: Sensitivity gain by partial surface passivation. *Langmuir,* **25**, 13833–13839.

9

The use of coated gold nanoparticles in high performance chemical sensors

N. LAZARUS, R. JIN and G. K. FEDDER,
Carnegie Mellon University, USA

DOI: 10.1533/9780857096722.2.231

Abstract: First demonstrated for chemical sensing by Wohltjen and Snow in 1998, coated gold nanoparticles have become one of the most promising technologies for creating high performance chemiresistive sensor systems. Chemical sensitivity for most nanoparticle sensors results from swelling when chemical is absorbed, varying the distance between neighboring conductive gold cores. By varying the coating material, a degree of selectivity can also be obtained, allowing differentiation between chemical analytes. This chapter reviews all aspects of sensing with gold nanoparticles, including synthesis, coating material choice, modeling, and demonstrations of other types of chemical sensors.

Key words: chemiresistor, gold nanoparticles, chemical sensing, synthesis.

9.1 Introduction

First demonstrated for chemical sensing by Wohltjen and Snow in 1998, coated gold nanoparticles have become one of the most promising technologies for creating high performance chemiresistive sensor systems. Chemical sensitivity for most nanoparticle sensors results from swelling when chemical is absorbed. Since conduction in the material occurs through tunneling between adjacent gold cores, expansion increases the core-to-core distance, causing an increase in resistivity (Steinecker *et al.*, 2007). The sensitivity can then be tuned by varying the dielectric coating material, allowing arrays of nanoparticles with different coatings to be used to distinguish between analytes (Garcia-Berrios *et al.*, 2011).

This chapter will begin by describing the methods that have been demonstrated for synthesizing gold nanoparticle materials for chemical sensing (Section 9.2). Section 9.3 focuses on the different coatings that have been successfully demonstrated for chemiresistive sensing. The following section, Section 9.3.1, presents models of the conductivity and chemical sensitivity of the material. Section 9.3.2 discusses the mechanisms of noise in

nanoparticle sensors and methods that have been developed for increasing the sensor limit of detection. Alternative types of sensors such as chemicapacitive and field effect transistor (FET) sensors based on gold nanoparticles are addressed in Section 9.4, followed by concluding remarks on future trends in Section 9.5.

9.2 Synthesis of gold nanoparticle materials

Most gold nanoparticles used for chemical sensing are synthesized chemically by reducing a metal salt with a reducing agent such as sodium borohydride, resulting in the formation of nanocrystals. A non-conducting capping agent, typically a surfactant, terminates the growth of the nanoparticle and prevents further agglomeration (Altavilla and Ciliberto, 2011). Thiol-based compounds are the main capping agents used for creating stable gold nanoparticles due to the chemical inertness of gold. The nanoparticles used in the original gold nanoparticle chemiresistor (Wohltjen and Snow, 1998) were synthesized using the technique commonly known as the Brust method, originally developed by Brust *et al*. in 1994. Chloroauric acid, $HAuCl_4$, is first dissolved in water to obtain $AuCl_4^-$ ions. Tetraoctylammonium bromide (TOAB) ($(C_8H_{17})_4NBr$) dissolved in toluene is then added to the solution. The addition of the TOAB results in a transfer of the gold chloride ions to the toluene solution according to the reaction (Leff *et al*., 1996):

$$AuCl^-_{4\,(aq)} + N\left(C_8H_{17}\right)^+_{4(toluene)} \rightarrow \left[N\left(C_8H_{17}\right)^+_4 AuCl^-_4\right]_{(toluene)}$$

The Cl^- may be displaced (at least partially) by Br^- from the TOAB. Once the ions have been transferred to the organic phase, the capping agent is added in toluene; the original Brust work used dodecanethiol ($C_{12}H_{25}SH$), but the process has since been demonstrated with numerous other thiols. Sodium borohydride ($NaBH_4$) in aqueous solution is added to the mixture (Terrill *et al*., 1995), serving primarily as an electron donor, resulting in the reaction (Brust *et al*., 1994):

$$mAuCl^-_{4(toluene)} + nC_{12}H_{25}SH_{(toluene)} + 3me^- \rightarrow 4mCl^-_{(aq)} + \left(Au_m\right)\left(C_{12}H_{25}S\right)_{n(toluene)}$$

The toluene phase is then separated, mixed with ethanol to remove excess thiol and the nanoparticle precipitate is filtered off. A similar procedure has since been developed for coating gold nanoparticles with amine groups, with the primary variation being the substitution of an alkylamine for the thiol capping agent (Leff *et al*., 1996).

Variations on the Brust two-phase method are used in most examples of gold nanoparticle chemical sensors in the literature. An alternative single phase technique called the Rowe method was developed at the University of Michigan (Rowe *et al.*, 2004). In the Rowe method, both the chloroauric acid and thiol capping agent are dissolved in the solvent tetrahydrofuran (THF). As with the Brust method, an electron donor, lithium borohydride ($LiBH_4$) is then added, resulting in a similar chemical reaction to create the thiol-capped nanoparticles. The primary advantages of this method are the elimination of possible contamination of TOAB in the final product and the reduction in the reaction time from 3 h to 3 min (Rowe *et al.*, 2004).

For coatings that are difficult to directly prepare using these synthesis methods, a 'place-exchange' process can also be used, where the materials are synthesized with other capping agents using the Rowe or Brust method. The nanoparticles are then added to a concentrated solution of a different alkylthiol, resulting in the replacement of the thiols on the nanoparticles with the more concentrated alkythiols from the solution (Smardzewski *et al.*, 2004). This method can also be used to obtain nanoparticles with a mixed coating of two different ligands, as in Kim *et al.* (2005).

9.3 Nanoparticle coatings

The dominant method for controlling the sensitivity and selectivity of gold-nanoparticle-based chemical sensors is the selection of the coating material. As a result, there has been significant research into a variety of different possible coating layers to target different chemicals.

9.3.1 Alkanethiols

The first gold nanoparticle chemiresistor used nanoparticles coated in octanethiol ($C_8H_{17}S$) (Wohltjen and Snow, 1998), referred to as C_8 from the number of carbons in the carbon chain of the alkanethiol (Fig. 9.1). A similar naming convention is used for the other alkanethiols; chain lengths between four and twelve carbons (C_4 to C_{12}) are most commonly used. Since the conduction is based on tunneling between neighboring gold cores, a longer carbon chain results in a higher resistivity, and is the main reason very long carbon chains are rarely used.

The study by Terrill *et al.* (1995) found that C_8, C_{12} and C_{16} had similar gold core radii distribution centered at 1.2 nm; the distance between cores upon deposition was found to be centered around 1.31, 1.48, and 1.83 nm for C_8, C_{12}, and C_{16}, respectively. During synthesis some variation occurs in the nanoparticle size. Figure 9.2a shows the size distribution of C_8 gold nanoparticles of a batch of C_8 gold nanoparticles synthesized at Carnegie Mellon

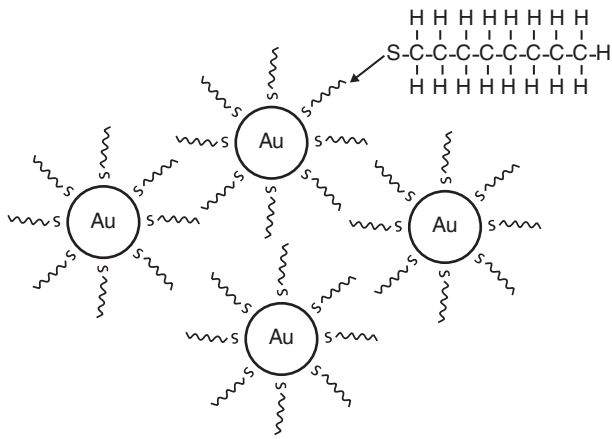

9.1 Octanethiol gold nanoparticles.

using the Rowe method. Figure 9.2b shows a transmission electron microscope (TEM) image of the gold nanoparticles.

Most types of thiol-coated nanoparticles are primarily used for measuring volatile organic carbon (VOC) vapors. Figure 9.3 shows the response to toluene of C_8 gold nanoparticles inkjetted in 1,2,4-trichlorobenzene on a spiral gold electrode, showing the linear rise in resistance as the concentration increases. Toluene is a common target analyte used to characterize nanoparticle chemiresistors, due to its large response and usage as both an industrial solvent and as a simulant for the chemically similar but highly hazardous solvent benzene. A more detailed discussion of the chemical sensitivity is presented in Section 9.3.

Over extended periods of time, alkanethiol-coated gold nanoparticles have been demonstrated to drop in resistance, possibly due to the decomposition due to interaction with ozone (Cai and Zellers, 2002). One method that can be used to improve the stability of the nanoparticles is to increase the binding strength between the gold nanoparticle core and the coating ligand groups, reducing the possibility of escape of the ligand groups and agglomeration of the particles. In the work by Garg *et al*. (2010), trithiol-coated gold nanoparticles were synthesized and used for chemiresistive sensing. For the trithiol material, the three thiol endings each bond to the gold, resulting in a stronger bond to the nanoparticle core. All three thiol endings must simultaneously dissociate from the gold for the ligand to escape the surface, resulting in a significantly lower chance of agglomeration and loss of sensitivity. A chemiresistor based on octanetrithiol coated nanoparticles was fabricated and compared to a comparable C_8 sensor. The sensitivity for both materials was similar after fabrication (Fig. 9.4a). However, when the response to a 500 ppm pulse of toluene was measured over a 6 month period

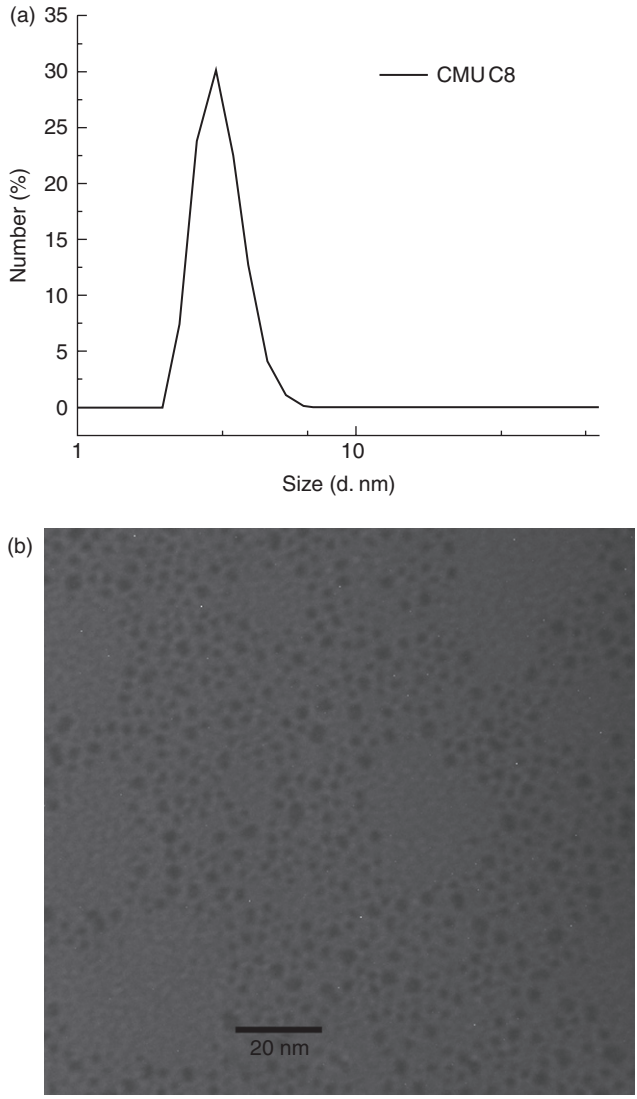

9.2 (a) Size distribution of synthesized C_8 nanoparticles measured using dynamic light scattering and (b) TEM image of the nanoparticles.

(Fig. 9.4b), the sensitivity of the C_8 sensor dropped by more than 45%, while the sensitivity of the trithiol sensor dropped by only 10%.

Varying the length of the coating carbon chain has also been shown to have important effects on the chemical sensor behavior. In one study, the chemical responses were measured for the alkanethiol coatings between 4 and 8 carbon atoms in length (C_4 through C_8) (Garcia-Berrios *et al.*, 2010), finding

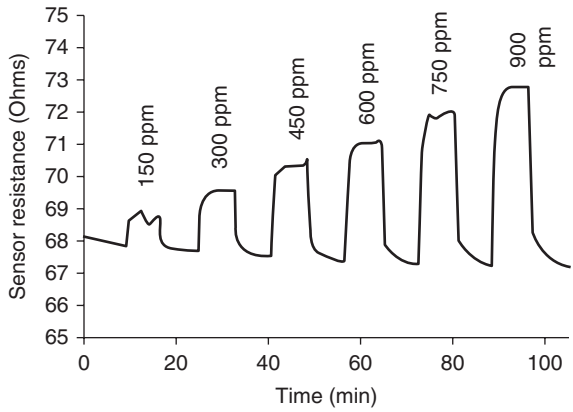

9.3 Test of C_8 gold nanoparticles with different concentrations of toluene.

that the sensitivity to hydrocarbons was larger as the chain length increased, due primarily due to the coating materials being a larger fraction of the total volume, resulting in a larger total uptake of chemical molecules.

9.3.2 Other coatings

One of the advantages of gold nanoparticle materials for chemiresistive sensing is the ability to vary the coating material to change the sensitivity to chemical analyte, allowing the creation of an array able to differentiate between chemicals using techniques such as principal component analysis and pattern recognition. As a result, nanoparticles with a number of different coatings have been synthesized and studied in an effort to control the chemical selectivity.

In addition to the chain length, the functional end of the thiol group can also be used to control the sensitivity to analyte. Ahn *et al*. (2005) measured the responses of gold nanoparticles coated with four different materials, two consisting of alkanethiols of different lengths and two with thiophene terminated thiol groups of comparable length. For the analytes tested, the non-polar solvent hexane was found to have almost identical responses for the thiophene and alkanethiol coatings of comparable length, while for the slightly more polar analytes of chloroform and toluene there were significant differences between the two types of function groups. In their study, the responses were found to correspond to the solubility of the nanoparticles in the solvents used in most cases. In another study of gold nanoparticles coated with branching dendrimer molecules (Krasteva *et al*., 2007), the sensitivity behavior of the nanoparticles were found to correspond to the solubility properties of pure dendrimer films.

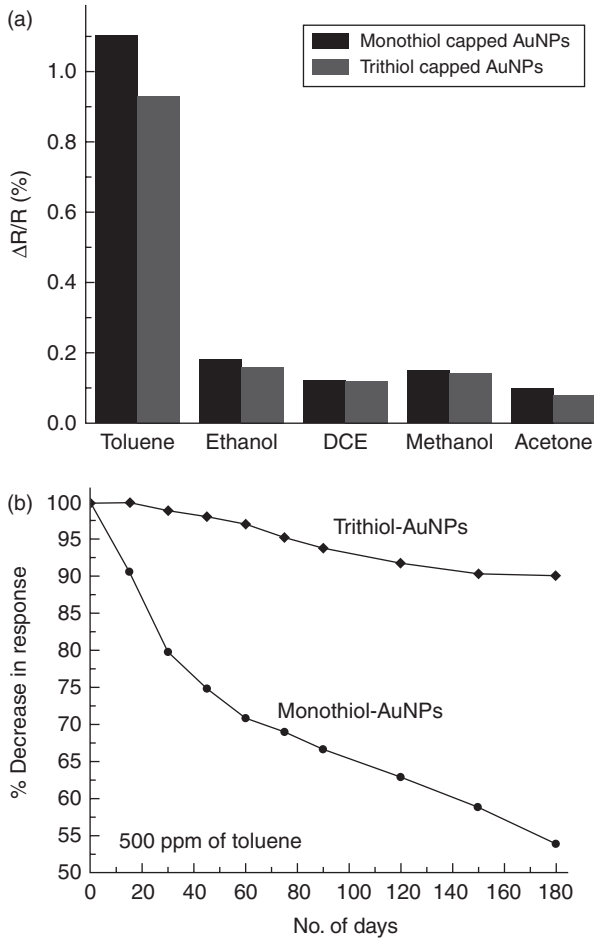

9.4 (a) Sensitivity and (b) response to 500 ppm of toluene for trithiol coated nanoparticles. (*Source*: Reprinted with permission from Garg *et al.*, 2010, copyright 2010, IOP Publishing.)

Since the response is based primarily on the swelling of the nanoparticle material, another factor that has been demonstrated to have a large impact on the chemical sensitivity is the rigidity of the coating material linking neighboring nanoparticles. The swelling can be controlled by using a place-exchange reaction to replace the traditional monothiol coating with a dithiol linker molecule. The dithiol group bonds to two neighboring gold cores with sulfur atoms on either end of a carbon chain. In Joseph *et al.* (2007), three different linker materials with comparable chain lengths but variable rigidity and conductivity were tested. The flexible dodecanedithiol coating was found to give a greater response than both rigid coating materials, even though similar

Table 9.1 Survey of gold nanoparticle coating materials

Group	Coatings	Target analytes	Synthesis	Reference
US Naval Research Laboratory	SC_4HFIP, SC_7OH, $SC_2OC_2OCH_3$, SC_6Cl, SC_2C_6, C_8, SC_5COOH	DMMP and toluene	Brust/place exchange	Smardzewski *et al.*, 2004
U. of Michigan	C_8, DPA, OPH, and HME	VOCs	Rowe	Scholten *et al.*, 2011
California Institute of Technology	20 coatings (alkanethiols, branched alkanethiols, aromatic ligands)	Hydrocarbons, polar aprotic vapors, and alcohols	Brust	Garcia-Berrios *et al.*, 2011
U. of Massachusetts-Lowell	C_3, C_{13} and two thiophene terminated alkanethiols	Toluene, chloroform and hexane	Brust	Ahn *et al.*, 2005
Sony	polyphenylene, poly(propylene imine), poly(amidoamine)	Toluene, IPA and water	Leff (amine for capping agent)/ place exchange	Krasteva *et al.*, 2002
Hungarian Acad. Of Sciences	C_8 and C_{10}	Toluene and CCl4	Brust	Voros *et al.*, 2008
University of Louisville	C_6	Toluene and IPA	Brust	Ibanez *et al.*, 2006
SUNY-Binghamton	1,9-nonanedithiol and 1,1-mercaptoundecanoic acid	Toluene, hexane, methanol, and water	Brust/place exchange	Han *et al.*, 2001
Pacific Northwest National Laboratory	C_{12}, benzenethiol, 4-chlorobenzenethiol, 4-(trifluoromethyl) benzenethiol	2-butanone, toluene, hexane, 1-butanol	Brust method; benzenethiolin methanol/water method (Brust *et al.*, 1995)	Grate *et al.*, 2003
Carnegie Mellon University	C_8 and octanetrithiol	Toluene, ethanol, DCE, methanol, acetone	Rowe (C_8) and Brust (trithiol)	Garg *et al.*, 2010

amounts of analyte were found to be absorbed using mass measurements with a quartz crystal microbalance. A relatively non-conductive rigid coating material, [4]-staffane-3,3‴-dithiol, was found to give a reduction, rather than an increase, in resistance upon chemical absorption, suggesting that dielectric constant change, rather than swelling, is the dominant mechanism. The dielectric constant of the coating material affects the energy barrier that must be overcome to charge neighboring particles, as will be discussed further in later sections. The third material, the more conductive rigid material 4,4′-terphenyldithiol, was found to give minimal response, since the effects of both swelling and dielectric constant changes were smaller.

A brief survey of some of the groups working on nanoparticle chemiresistors is shown in Table 9.1. The US Naval Research Laboratory was involved with the original development of the nanoparticle chemiresistor and has continued to do significant work in the area with an emphasis on the use of the sensors for detecting analytes with defense applications such as chemical weapons emulated by the chemical warfare agent simulant dimethyl methyl phosphonate (DMMP). The University of Michigan, another leading research group in the area, has focused on developing a chemiresistor array containing four different nanoparticle coatings aimed for use as a detector on a micro-gas chromatograph system. CalTech has been prominent in efforts to use large arrays of different coatings to differentiate between chemical analytes.

9.4 Modeling chemical sensing behavior

Understanding the mechanism for sensing behaviour through modelling of both the response magnitude and noise levels has been an important focus to improve the minimum detection limits of this type of chemical sensor.

9.4.1 Sensitivity

The behavior of several of the common alkanethiol materials (C_8, C_{12}, and C_{16}) was extensively studied by Terrill *et al.* (1995) to develop a conductivity model. Their model was based on an assumption of charge transfer by electron tunneling through the dielectric between conductive cores. The energy barrier between neighboring cores is given by (Terrill *et al.*, 1995):

$$E_{\mathrm{ET}} = \frac{N_A q^2 \delta_{\mathrm{edge}}}{\varepsilon_r \varepsilon_0 2R_{\mathrm{core}} \left[R_{\mathrm{core}} + \delta_{\mathrm{edge}} \right]} \qquad [9.1]$$

where N_A is Avogadro's number, q is the charge on an electron, δ_{edge} is the spacing between the edges of the conductive cores, ε_r is the relative permittivity of the dielectric matrix, ε_0 is the permittivity of free space, and R_{core}

is the radius of the core. The appearance of the relative permittivity of the dielectric in the denominator can have an important impact on the sensing behavior. If the absorbed chemical molecules have a higher dielectric constant than the matrix, this can result in a lowering of the energy barrier and a drop in resistance.

The conductivity of a gold nanoparticle film is related to the energy barrier by (Terrill *et al.*, 1995):

$$\sigma(T) = \sigma_0 e^{-\delta_{edge}\beta}\, e^{-E_{ET}/RT} \qquad [9.2]$$

where T is the temperature, β is the electron transfer coupling coefficient, R is the ideal gas constant, and σ_0 is a constant pre-exponential factor. For chemical sensing, the dependence of the tunneling probability on the edge-to-edge spacing results in the sensitivity to swelling of the dielectric matrix that increases the distance between the edges of the cores. This dependence also results in nanoparticles with longer chains in their thiol groups having higher resistance. The change in resistance upon chemical absorption (based on the equation in Steinecker *et al.*, 2007) is:

$$\frac{R + \Delta R}{R} = e^{\Delta\delta_{edge}\beta + \Delta E_{ET}/RT} \qquad [9.3]$$

In most cases, the swelling resulting in an increase in the edge-to-edge spacing is the dominant mechanism; however, there have been exceptions demonstrated, such as the rigid linker materials mentioned in Section 9.3.2.

Based on these results, two clear conclusions can be drawn about the chemical sensing behavior. The first is that the larger the quantity of analyte absorbing into the material, resulting in more swelling, the larger is the chemical response. One method of specifying this quantity is the partition coefficient K, defined as the ratio of the analyte concentration in the absorbent layer to the concentration of the analyte in the air at equilibrium (Steinecker *et al.*, 2007). A material with a larger partition coefficient for a specific chemical should, everything else being equal, have a larger response. The other main conclusion is that a higher dielectric constant of an absorbed analyte results in a reduction in the energy barrier that counteracts the rise in resistance due to swelling. For most gold nanoparticle materials, where swelling is the dominant mechanism, this result means that highly polar molecules such as alcohols have a lower response than would be expected from their partition coefficients.

Researchers at the University of Michigan performed an extensive study of the chemical response of C_8 gold nanoparticles to volatile organic compound analytes (Steinecker *et al.*, 2007), as shown in Fig. 9.5 (see also Table 9.2).

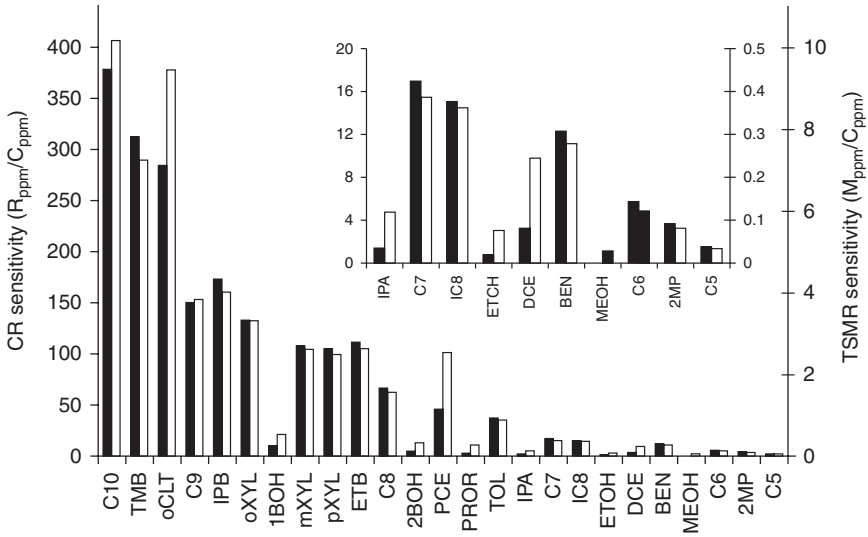

9.5 Sensitivity of C_8 coated nanoparticles. (*Source*: Reprinted with permission from Steinecker *et al.*, 2007, copyright 2007 American Chemical Society.) The acronyms for the analytes are summarized in Table 9.2

Table 9.2 Chemical acronyms for analytes tested in Fig. 9.5

Chemical	Symbol	Chemical	Symbol
n-decane	C10	Toluene	TOL
1,3,5-trimethylbenzene	TMB	2-propanol	IPA
o-chlorotoluene	oCLT	n-heptane	C7
n-nonane	C9	2,2,4-trimethylpentane	IC8
isopropylbenzene	IPB	Ethanol	ETOH
o-xylene	oXYL	1,2-dichloroethane	DCE
1-butanol	1BOH	Benzene	BEN
m-xylene	mXYL	1,1,1-trichloroethane	TCA
p-xylene	pXYL	Methanol	MEOH
ethylbenzene	ETB	n-hexane	C6
n-octane	C8	Chloroform	CHL
2-butanol	2BOH	2-methylpentane	2MP
perchloroethylene	PCE	n-pentane	C5
1-propanol	PROH	n-butane	C4

In their study, the nanoparticles were characterized both by measuring the chemiresistor (CR) response as well as by measuring the signal from a thickness shear mode resonator (TSMR) coated with the material. The TSMR measurement, which measures the mass of analyte absorbing into the layer, is one way of estimating the partition coefficient of a material. As expected, in most cases the two measurements roughly correspond; a similar mass of

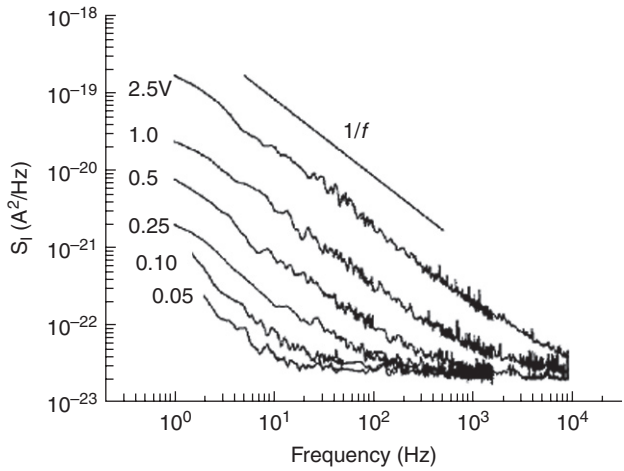

9.6 Current noise power density for a C_8 gold nanoparticle chemiresistor operated at different voltages (*Source*: Reprinted with permission from Kruppa *et al.*, 2006, copyright 2006, American Institute of Physics.)

analyte in the material results in a similar response for each analyte. There are two exceptions. The first is for the highly polar molecules such as alcohols, as expected from the model. For instance, for isopropyl alcohol, the chemiresistor response is several times lower than would be expected from the mass of analyte. The other exceptions are analytes that are non-polar, but have relatively high densities, such as perchloroethylene and 1,2-dichloroethane; for these analytes, the change in mass per molecule would be larger relative to the swelling, resulting in the diminished chemiresistor response.

9.4.2 Noise and limit of detection

One of the most important specifications for any chemical sensor is the limit of detection, or the minimum quantity of analyte that can be successfully differentiated from noise. The limit of detection can be defined as:

$$\mathrm{LOD} = \frac{\Delta R_{\min}}{S_{\mathrm{conc}}} \qquad [9.4]$$

where $\Delta R_{\min}$ is the minimum detectable change in resistance and S_{conc} is the concentration sensitivity of the sensor. The minimum detectable change in resistance is set by the noise of the sensor and measuring electronics. C_8 gold nanoparticle chemiresistors have been found to experience $1/f$ noise,

frequency dependent noise with increasing density at lower frequencies (Kurdak *et al*., 2005), as shown in Fig. 9.6. The normalized noise spectrum S_I/I^2 can be expressed in the form:

$$\frac{S_I}{I^2} = Af^{\alpha} \qquad [9.5]$$

where A is known as the noise prefactor setting the magnitude and α is the noise exponent and is approximately −1. In Kurdak *et al*. (2005), the dependence of the 1/*f* noise parameters on temperature was studied in an effort to understand the origins of the noise. The noise exponent was found to be roughly constant near −1 from a few degrees Kelvin up to room temperature. The noise prefactor was found to be heavily temperature dependent, with an order of magnitude increase above 40°K, and a local peak at 100°K, before leveling out above 200°K. The authors suggest that the complicated temperature dependence results from several noise processes present in the film, with possibilities including nanoparticle motion and changes in the conformality of the nanoparticles or charge offsets.

Since the 1/*f* noise is the primary limiting factor in the limit of detection of the sensors, there have been efforts to lower the noise prefactor using a number of different methods. To study the possibility that the 1/*f* noise was caused by motion of nanoparticles on the sensor surface, in Covington *et al*. (2008) the nanoparticles were crosslinked to lower the motion by exposure to different dosages from an electron beam source. Some dependence on the dosage was found, with a noise prefactor reduction of up to 30% in the film over the original uncrosslinked sensor; however, for larger doses the prefactor again rose. In the same work, thick nanoparticle layers deposited with an inkjet system were compared with a monolayer film, finding that the 1/*f* noise was heavily volume dependent and thicker films had noise prefactors lower by up to five orders of magnitude.

In addition to the volume, another factor in the limit of detection that has been studied is the effect on scaling the electrode dimensions of the resistor. Increasing the gap between neighboring electrodes has been demonstrated to result in an increase in the normalized noise power spectral density (Ancona *et al*., 2006), an effect attributed to the reduction in the number of electrons participating in the conduction. The normalized noise power density was studied for two C_6 nanoparticle chemiresistors with two different electrode spacings, 0.12 and 8 μm. The 1/*f* noise magnitude for the 8 μm device is three orders of magnitude lower than the device with narrower spacing.

The same study also examined the effects of the applied voltage on the 1/*f* noise levels of the sensor. For the range of voltages applied, the current noise power spectral density was proportional to the applied voltage

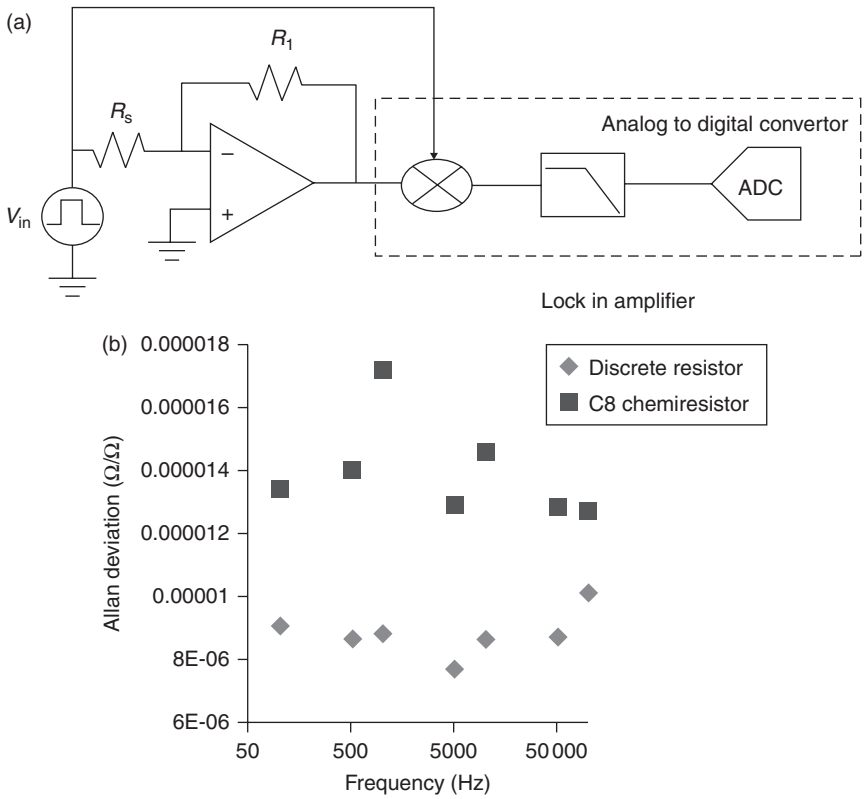

9.7 (a) Modulation testing circuit; R_s is the chemiresistor, R_1 is a fixed reference resistor. (b) Allan variance of system measured at 1 Hz integration time for different modulation frequencies for a chemiresistor, as well as for a discrete non-sensor resistor of comparable value (Lazarus, 2012).

squared, suggesting that the noise prefactor is independent of the voltage. This result means that the current noise power spectral density is increasing at the same rate as the current output, and testing at a higher voltage does not result in a higher signal-to-noise ratio.

In addition to techniques to lower the noise in the sensor itself, an alternative that was proposed in Ancona *et al*. (2006) was to modulate the input voltage on the sensor to higher frequencies with a lower spectral density, resulting in a lower limit of detection. This technique is used extensively in amplifier design, and is known as chopper stabilization (Enz and Temes, 1996). In order to test this approach, a C_8 chemiresistor was tested using a lock-in amplifier as shown in Fig. 9.7a. A lock-in amplifier takes a modulated input signal and demodulates the signal back to DC, followed by using a low pass filter to remove any noise occurring at other frequencies.

To characterize the limit of detection, the Allan deviation was measured for different modulation frequencies and compared to a similar measurement for a similarly sized discrete resistor (Fig. 9.7b). The Allan deviation is a statistical measure of the sample-to-sample variation in transient data, and gives the minimum step that can be successfully differentiated from noise; the Allan deviation is given by:

$$\sigma_R = \sqrt{\frac{1}{M}\sum_{k=1}^{M}\frac{1}{2}\frac{\left(R_k - R_{k-1}\right)^2}{R_0^2}} = \sqrt{\frac{1}{2M}\sum_{k=1}^{M}\left(\widetilde{R}_k - \widetilde{R}_{k-1}\right)^2} \qquad [9.6]$$

where R_0 is the baseline resistance, R_k is the kth sample, $\widetilde{R_k}$ is the normalized kth sample, and M is the number of samples.

The Allan deviation for the C_8 chemiresistor is approximately independent of the modulation frequency, and consistently higher than the discrete resistor; modulating the voltage across the chemiresistor does not appear to improve the limit of detection of the sensor. The reason for this behavior is shown graphically in Fig. 9.8, based on the analysis by

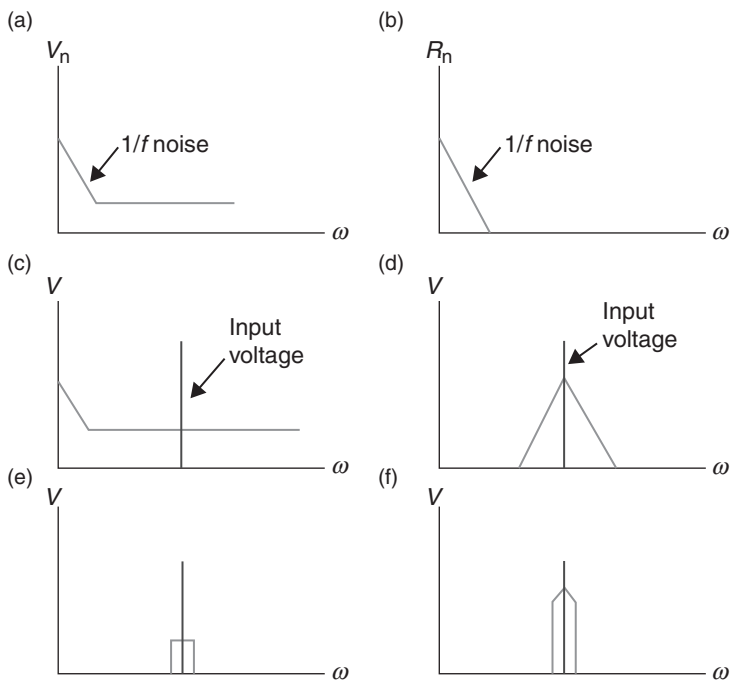

9.8 Modulation of a system (a–c) with input independent voltage noise and (d–f) a resistive sensor whose resistance varies with a 1/*f* noise relationship (Lazarus, 2012).

Senturia (2001). In conventional chopper stabilization, the input voltage can be controlled independently of the noise characteristic of a circuit element such as an amplifier; if the input is modulated to a higher frequency (Fig. 9.8b), the noise frequency response remains unchanged, and the $1/f$ noise can be filtered successfully (Fig. 9.8c). In a chemiresistive sensor, however, both the noise and signal are components of the resistance of the sensor. If a high frequency signal is applied to the sensor, both the signal and the noise will be modulated and shifted to higher frequencies (Fig. 9.8e). When the resulting signal is filtered, the $1/f$ noise region remains centered on the desired signal and the advantage of modulation is lost.

9.5 Other forms of gold nanoparticle chemical sensors

In addition to chemiresistive sensing, there have been a number of efforts to explore the possibility of using gold nanoparticles in other types of chemical sensing. In Cioffi *et al.* (2011), gold nanoparticles were deposited onto a thin oxide above a transistor channel to form a gate structure; absorbed analyte serves as charge donors, causing a charge buildup on the gate and influencing the current through the transistor. The optical properties of a nanoparticle film can also be used as a mechanism to measure the absorption of chemical. Karakouz *et al.* (2008), evaporated a very thin gold layer onto a glass substrate, forming isolated gold islands (Fig. 9.9) that were then coated with a thin layer of polymer. The absorption of chemical analyte was then measured based on changes in the refractive index of the layer.

The optical properties of gold nanoparticles loaded with nucleotides have also been successfully demonstrated for measuring DNA molecules. In Elghanian *et al.* (1997), a solution containing the nanoparticles was found to form a polymer matrix upon introduction of the appropriate nucleotide, resulting in a clear color change in the solution.

Highly resistive gold nanoparticles can also be used for chemicapacitive sensing, the measurement of changes in capacitance upon absorption of chemical analyte. Having conductive particles embedded in a dielectric material for capacitive sensing has several potential advantages. The particles act to effectively short portions of the dielectric, resulting in a narrower effective gap and allowing a higher capacitance per unit area and allowing the shrinking of the sensor. A nanoparticle film might also have more bonding sites for analyte absorption, resulting in a larger chemical response.

In Yao *et al.* (2010), gold nanoparticles of 10 nm in size were coated in thick layers of polyvinyl alcohol (PVA) to create particles 700 nm in

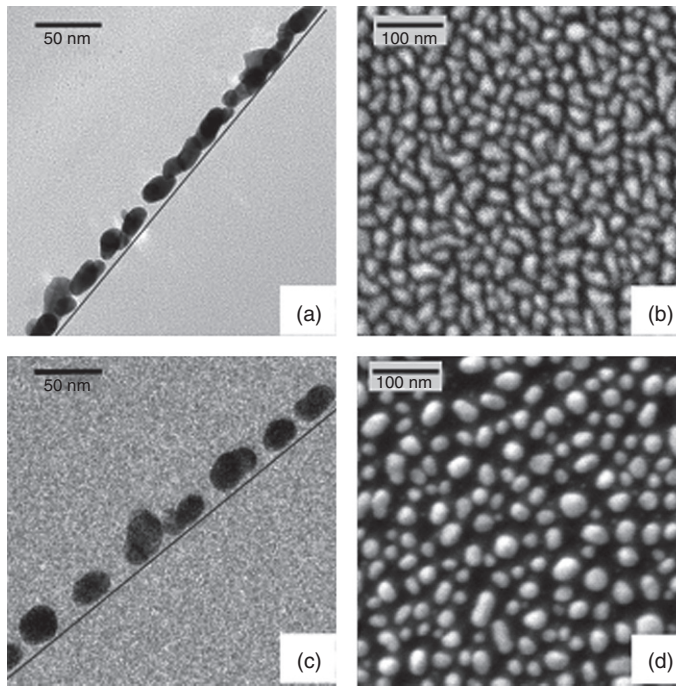

9.9 Gold islands for optical sensing, (a–b) before annealing, (c–d) after annealing. (*Source*: Reprinted with permission from Karakouz *et al.*, 2008, copyright 2008 American Chemical Society.)

diameter that were then used for measuring humidity. Since the gold core is a small fraction of the total volume, the response is likely dominated by the polymer layer in this case. In Lazarus (2012), chemicapacitive sensing with gold nanoclusters, semiconducting cores of a few tens of gold atoms with a thiol coating, was successfully demonstrated. $Au_{25}(SCH_2CH_2Ph)_{18}$, abbreviated as '$Au_{25}$', 25 gold atoms coated by 18 thiolate ligands, was deposited into the complementary metal-oxide-semiconductor–microelectromechanical systems (CMOS–MEMS) chemicapacitive structure presented in Lazarus and Fedder (2011).

The sensor response was measured for a number of analytes, and Table 9.3 shows the sensitivity along with the dielectric constant, vapor pressure and chemical family for each analyte. A representative response for ethanol is shown in Fig. 9.10. The highest sensitivity was measured for the alcohols isopropyl alcohol and ethanol, both highly polar analytes with low vapor pressures. A low vapor pressure results in an analyte being more likely to leave the vapor phase and enter the polymer, while a high dielectric constant results in a larger effective dielectric constant for the mixture upon absorption, resulting in a larger change in capacitance.

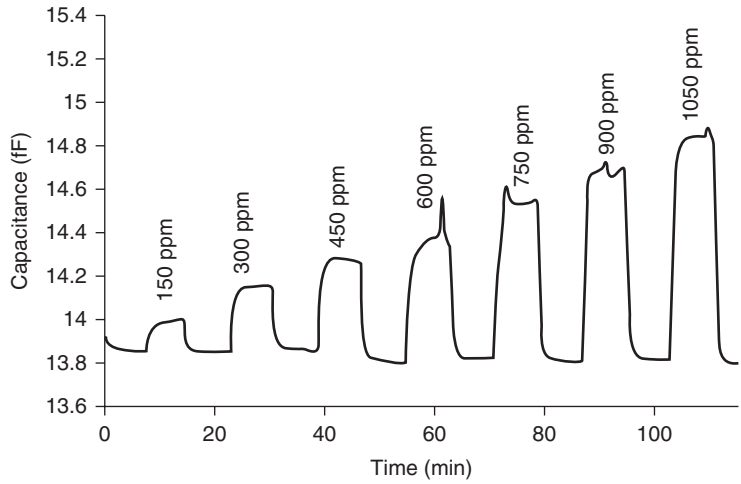

9.10 Sensor response to ethanol (Lazarus, 2012).

Table 9.3 Au_{25} analyte sensitivity (Lazarus, 2012)

Analyte	Dielectric constant	Vapor pressure at 20°C (Pa) (calculated from Green and Perry, 2008)	Chemical family	Sensitivity (% change in capacitance per ppm)
Acetone	20.7 (Kaye and Laby, 2009)	2.45×10^4	Ketone	0.002065
Toluene	2.39 (Kaye and Laby, 2009)	2.90×10^3	Aromatic	0.00616
IPA	19.92 (Cornila *et al.*, 1995)	4.34×10^3	Alcohol	0.006655
Ethanol	24.51 (Kaye and Laby, 2009)	5.85×10^3	Alcohol	0.00699
Methanol	32.65 (Kaye and Laby, 2009)	1.28×10^4	Alcohol	0.0033
Octane	1.95 (Kaye and Laby, 2009)	1.39×10^3	Alkane	0.0038
Pentane	1.84 (Kaye and Laby, 2009)	5.63×10^4	Alkane	0.0002

9.6 Conclusion and future trends

Since their original development in 1998, the numerous research groups focused on gold nanoparticle-based chemiresistors have demonstrated a variety of coatings and promising properties for sensing a wide range of analytes. Although individual sensors are generally not highly selective,

the work on using a number of coatings with different properties to obtain an array able to differentiate between chemicals is promising. The greatest challenge in the field, and a major focus for future research, has been making sensor systems based on gold nanoparticles able to operate successfully and consistently for the years necessary for most commercial applications. The dramatic changes in baseline due to the agglomeration inherent in most types of gold nanoparticles, such as the 45% change in resistance over 6 months shown in Fig. 9.4b for C_8, causes major problems in interpreting and using sensor responses.

The best approach for addressing the stability problem is still undetermined, and a subject of significant research. One possibility is to focus on modifying the nanoparticles and coatings to reduce agglomeration and minimize baseline drift, with methods such as the trithiol-based coatings mentioned in Section 9.2. The alternative approach has been to adapt sensor systems to allow the variation in behavior of the individual sensors to be addressed and removed from the final output of the system. Incorporating a method for periodic and inexpensive calibration is one means for performing this baseline correction. In Lu *et al*. (2005), a micro-gas chromatograph system with a gold nanoparticle chemiresistor detector incorporated a microfabricated reservoir of volatile liquid to generate a known concentration of analyte to allow performance correction of the sensor array.

A combination of both of these techniques will most likely be the most successful method for creating practical sensors with nanoparticle materials. A subset of the most stable materials, with resistances that vary on the order of a few percent over months or years, combined with carefully designed circuitry or calibration systems to correct for these modest variations, could be competitive with other similar sensors currently in the marketplace.

Improved interface circuitry can also be designed to measure accurately a resistance that can vary by an order of magnitude or more over the sensor lifetime. In Rairigh *et al*. (2009), a CMOS baseline correction chip was developed to eliminate the baseline variation of a C_8 gold nanoparticle sensor. During a period without chemical exposure, the output voltage obtained by sourcing a reference current into the sensor is measured, and is stored in an analog memory. This stored value is then used to modify the reference current and subtract away the stored value to remove the output baseline, allowing small changes in output resistance to be measured accurately and with high precision over a wide range of sensor resistance values.

9.7 Sources of further information and advice

For a reader interested in learning more about gold nanoparticle chemiresistive sensing, we recommend beginning with the Brust *et al*. (1994) paper that developed the original synthesis process primarily used and the Wohltjen

and Snow (1998) paper that first demonstrated thiol-coated nanoparticle chemiresistors. Both papers are widely cited in research throughout the field and provide a useful starting point for understanding the origins of nanoparticle chemiresistive sensing. The Steinecker *et al*. (2007) paper on developing an accurate theoretical model of the vapor response of a C_8 sensor is another excellent paper for a novice in the field. Steinecker presents a readable discussion of the mechanism of conduction in nanoparticle films and the effects of chemical exposure, summarized briefly here, as well as an extensive and detailed study of the response to dozens of common organic chemicals.

In addition to the above papers on the nanoparticle sensors themselves, we also recommend reading the Hierlemann and Guitierrez-Osuna (2008) review paper on chemical sensor arrays and data processing to understand the motivation behind making arrays of nanoparticle sensors to obtain selectivity. The review paper provides a good introduction to designing a sensor array to obtain maximum information, including selecting the number of sensors and types, and the pattern recognition techniques used to recognize analytes. The paper also discusses the issues of sensor stability and drift presented briefly here, and signal processing techniques that can also be used in many cases to compensate for the effects.

9.8 References

Ahn H., Chandekar A., Kang B., Sung C. and Whitten J. E. (2005) 'Comparison of solubility and vapor sensing properties of methyl- and thiophene-terminated alkanethiol-protected gold nanoparticle films', *J. Macromolecular Science A*, **42**, 1477–1487.

Altavilla C. and Ciliberto E. (2011) 'Inorganic nanoparticles: synthesis, applications, and perspectives – an overview', in *Inorganic Nanoparticles: Synthesis, Applications and Perspectives*, Boca Raton, FL, Taylor and Francis Group, 1–15.

Ancona M. G., Snow A. W., Foos E. E., Kruppa W. and Bass R. (2006) 'Scaling properties of gold nanocluster chemiresistor sensors', *IEEE Sensors J*., **6**, 1403–1414.

Brust M., Walker M., Bethell D., Schiffrin D. J. and Whyman R. (1994) 'Synthesis of thiol-derivatised gold nanoparticles in a two-phase liquid-liquid system', *J. Chem. Soc., Chem. Commun*., 801–802.

Brust M., Fink J., Bethall D., Schiffrin D. J. and Kiely C. (1995) 'Synthesis and reactions of functionalised gold nanoparticles', *J. Chem. Soc., Chem. Commun*., 1655–1656.

Cai Q. and Zellers E. T. (2002) 'Dual-chemiresistor GC detector employing monolayer-protected metal nanocluster interfaces', *Anal. Chem*., **74**, 3533–3539.

Cioffi N., Colaianni L., Ieva E., Pilolli R., Ditaranto N., Angione M., Cortrone S., Buchholt K., Spetz A., Sabbatini L. and Torsi L. (2011) 'Electrosynthesis and characterization of gold nanoparticles for electronic capacitance sensing of pollutants', *Electrochim. Acta*, **56**, 3713–3720.

Cornila C., Hierlemann A., Lenggenhager R., Malcovati P., Baltes H., Noetzel G., Weimar U. and Gopel W. (1995) 'Capacitive sensors in CMOS technology with polymer coating', *Sens. Actuators B*, **24/25**, 357–361.

Covington E. L., Turner R. W., Kurdak C., Rowe M. P., Xu C. and Zellers E. T. (2008) 'Electrical noise in gold nanoparticle chemiresistors', *Proc. IEEE Sensors*, Lecce, Italy, 26–29 October 2008, 102–105.

Elghanian R., Storhoff, Mucic R. C., Letsinger R. L. and Mirkin C. A. (1997) 'Selective colorimetric detection of polynucleotides based on the distance-dependent optical properties of gold nanoparticles', *Science*, **277**, 1078–1081.

Enz C. and Temes G. C. (1996) 'Circuit techniques for reducing the effects of op-amp imperfections: autozeroing, correlated double sampling, and chopper stabilization', *Proceedings of the IEEE*, **84**, 1584–1614.

Garcia-Berrios E., Gao T., Theriot J. C., Woodka M. D., Brunchwig B. S. and Lewis N. S. (2011) 'Response and discrimination performance of arrays of organothiol-capped Au nanoparticle chemiresistive vapor sensors', *J. Phys. Chem. C*, **115**, 6208–6217.

Garcia-Berrios E., Gao T., Woodka M. D., Maldanoado S., Bruncshwig S., Ellsworth M. W. and Lewis N. S. (2010) 'Response versus chain length of alkanethiol-capped Au nanoparticle chemiresistive chemical vapor sensors', *J. Phys. Chem. C*, **114**, 21914–21920.

Garg N., Mohanty A., Lazarus N., Schultz L., Rozzi T. R., Santhanam S., Weiss L., Snyder J. L., Fedder G. K. and Jin R. (2010) 'Robust gold nanoparticles stabilized by trithiol for application in chemiresistive sensors', *Nanotechnology*, **21**, 405501.

Grate J. W., Nelson D. A. and Skaggs R. (2003) 'Sorptive behavior of monolayer-protected gold nanoparticle films: implications for chemical vapor sensing', *Anal. Chem*., **75** 1868–1879.

Green D. W. and Perry R. H. (2008) *Perry's Chemical Engineers' Handbook*, 8th edn., New York, McGraw-Hill.

Han L., Daniel D. R., Maye M. M. and Zhong C.-J. (2001) 'Core-shell nanostructured nanoparticle films as chemically sensitive interfaces', *Anal. Chem*., **73**, 4441–4449.

Hierlemann A. and Gutierrez-Osuna R. (2008) 'Higher-order chemical sensing', *Chem. Rev*., **108**, 563–613.

Ibanez F. J., Gowrishetty U., Crain M. M., Walsh K. M. and Zamborini F. P. (2006) 'Chemiresistive vapor sensing with microscale films of gold monolayer protected clusters', *Anal. Chem*., **78**, 753–761.

Joseph Y., Peic A., Chen X., Michl J., Vossmeyer T. and Yasuda A. (2007) 'Vapor sensitivity of networked gold nanoparticle chemiresistors: importance of flexibility and resistivity of the interlinkage', *J. Phys. Chem. C*, **111**, 12855–12859.

Karakouz T., Vaskevich A. and Rubinstein I. (2008) 'Polymer-coated gold island films as localized plasmon transducers for gas sensing', *J. Phys. Chem. B*, **112**, 14530–14538.

Kaye and Laby (2009) Tables of physical and chemical constants, *Nat. Phys. Lab*, Teddington, U.K., http://www.kayelaby.npl.co.uk (accessed 2009).

Kim J. Y., Yang Y. S., Ha S.-C., Cho S. M., Kim Y. S., Kim H. Y., Yang H. and Kim Y. T. (2005) 'Mixed-ligand nanoparticles of chlorobenzenemethanethiol and n-octanethiol as chemical sensors', *Sens. Actuators B*, **106**, 189–198.

Krasteva N., Besnard I., Guse B., Bauer R. E., Mullen K., Yasuda A. and Vossmeyer T. (2002) 'Self-assembled gold-nanoparticle/dendrimer composite films for vapor sensing applications', *Nano Lett.*, **2**, 551–555.

Krasteva N., Fogel Y., Bauer R. E., Mullen K., Joseph Y., Matsuzawa N., Yasuda A. and Vossmeyer T. (2007) 'Vapor sorption and electrical response of Au-nanoparticle-dendrimer composites', *Adv. Funct. Mater*., **17**, 881–888.

Kruppa W., Ancona M. G., Rendell R. W., Snow A. W., Foos E. E. and Bass R. (2006) 'Electrical noise in gold nanocluster sensors', *Appl. Phys. Lett*., **88**, 053120.

Kurdak C., Kim J., Kuo A., Lucido J. J., Farina L. A., Bai X., Rowe M. P. and Matzger A. J. (2005) '1/f noise in gold nanoparticle chemosensors', *Appl. Phys. Lett*., **86**, 073506.

Lazarus N. (April 2012) 'CMOS-MEMS chemiresistive and chemicapacitive chemical sensor system', Ph.D. thesis, Carnegie Mellon University.

Lazarus N. and Fedder G. K. (2011) 'Integrated vertical parallel-plate capacitive humidity sensor', *J. Micromech. Microeng.*, **21**, 065028.

Leff D. V., Brandt L. and Heath J. R. (1996) 'Synthesis and characterization of hydrophobic, organically-soluble gold nanocrystals functionalized with primary amines', *Langmuir*, **12**, 4723–4730.

Lu C., Steinecker W. H., Tian W., Oborny M., Nichols J. M., Again M., Potkay J. A., Chan H. K. L., Driscoll J., Sacks R. D., Wise K. D., Pang S. W. and Zellers E. T. (2005) 'First-generation hybrid MEMS gas chromatograph', *Lab on a Chip*, **5**, 1123–1131.

Rairigh D. J., Warnell G. A., Xu C., Zellers E. T. and Mason A. J. (2009) 'CMOS baseline tracking and cancellation instrumentation for nanoparticle-coated chemiresistors', *IEEE Trans. Biomedical Circuits and Systems*, **3**, 267–276.

Rowe M. P., Plass K. E., Kim K., Kurdak C., Zellers E. T. and Matzger A. J. (2004) 'Single-phase synthesis of functionalized gold nanoparticles', *Chem. Mater*., **16**, 3513–3517.

Senturia S. D. (2001) *Microsystem Design*, Norwell, Massachusetts, Kluwer Academic Publishing.

Scholten K., Bohrer F. I., Dattoli E. Lu W. and Zellers E. T. (2011) 'Organic vapor discrimination with chemiresistor arrays of temperature modulated tin-oxide nanowires and thiolate-monolayer protected gold nanoparticles', *Nanotechnology*, **22**, 125501 (7pp).

Smardzewski R. R., Jarvis N. L., Snow A. W. and Wohltjen H. (2004) 'Nanoelectronic chemical sensors: theory and experiment', *Proc. Scientific Conference on CBD Research*, Hunt Valley, MD, 15–17 November 2004, 1300–1320.

Steinecker W. H., Rowe M. P. and Zellers E. T. (2007) 'Model of vapor-induced resistivity changes in gold-thiolate monolayer-protected nanoparticle sensor films', *Anal. Chem*., **79**, 4977–4986.

Terrill R. H., Postlethwaite T. A., Chen C., Poon C., Terzis A., Chen A.,. Hutchison J. E., Clark M. R., Wignall G., Londono J. D., Superfine R., Falvo M., Johnson C.S., Samulski E. T. and Murray R. W. (1995) 'Monolayers in three dimensions: NMR, SAXS, thermal and electron hopping studies of alkanethiol stabilized gold clusters', *J. Am. Chem. Soc*., **117**, 12537–12548.

Voros N., Patakfalvi R. and Dekany I. (2008) 'Alkylthiol-functionalized gold nanoparticles for sensing organic vapors: The connection between the adsorption isotherm and the sensor resistance', *Colloids Surf. A*, **329**, 205–210.

Wohltjen H. and Snow A. W. (1998) 'Colloidal metal-insulator-metal ensemble chemiresistor sensor', *Anal. Chem*., **70**, 2856–2859.

Yao W., Chen X. and Zhang J. (2010) 'A capacitive sensor based on gold-PVA core-shell nanocomposites', *Sens. Actuators B*., **145**, 327–333.

10

Nanoporous silicon biochemical sensors

T. SHIMOMURA, Funai Electric Advanced Applied Technology Research Institute Inc., Japan

DOI: 10.1533/9780857096722.2.254

Abstract: Enzyme encapsulation into the pores of nanoporous silicon material is an effective method for obtaining high-performance enzymatic sensors. This chapter first introduces the basic concept of enzyme encapsulation by nanoporous silicon material and its application to enzymatic sensor development. The chapter then applies this concept to the development of enzymatic sensors and demonstrates the analytical advantages to the performance that can be obtained, using the detection of formaldehyde as an example.

Key words: mesoporous silica materials, enzyme encapsulation, enzymatic sensor, high sensitivity, long-term stability.

10.1 Introduction

There is an increasing need to develop assays that are capable of selectively detecting low level concentrations of target substances in various fields including clinical chemistry, dairy and food industries and analysis of environmental pollutants. Standard methods for the detection of these substances use UV-visible absorption, high performance liquid chromatography (HPLC), gas chromatography, and fluorometry. However, these methods are either time consuming or require expensive apparatus and are not convenient for commercial use. From this point of view, the development of biological methods of detection combined with physical transducers, i.e., biosensors, has attracted considerable attention, because such methods enable direct, reliable, and reproducible measurements. In particular, enzyme-based, amperometric biosensors can offer high sensitivity, high selectivity, and a short response time without requiring any substantial or complicated instrumentation. Thus, biosensors are considered to be a promising method for the determination of target substances even when they are present at low concentrations. However, biosensors using enzyme electrodes have a problem that seriously affects the sensor performance: the enzyme itself has poor storage stability and the immobilization procedure causes a substantial decrease in the enzyme activity.

In order to solve this problem, we have paid attention to the use of nanoporous silicon material i.e., mesoporous silica, as a host material for enzyme immobilization for the electrochemical biosensors to enhance the enzyme stability. Mesoporous silica materials have inherent characteristics of high surface area and pore volume, tunable pore size accommodating dimensions of enzymes, and mechanical stability, and enzyme encapsulation within mesoporous silica materials can render enzymes more mechanically robust and stable with time (Blin *et al.*, 2005; Bornscheuer, 2003; Fan *et al.*, 2003; Shin *et al.*, 2002). It is expected that the encapsulation of enzymes in these mesoporous silica materials will make separation easier, and that it will improve the enzyme performance after the immobilization procedure, i.e., the activity, stability, and ability for the devices to be reused. Thus, by using these mesoporous silica materials as enzyme immobilization materials on the electrode in amperometric biosensors, we expect that a target substance can be detected and determined even at a low concentration with long-term stability.

In recent years, there have been some reports that mesoporous silica material enzyme systems obtained by physical adsorption and covalent-attachment procedures being applied to the development of biosensors for the detection of glucose, hemoglobin, myoglobin, phenolic compounds, and so on (details on the current state and development of mesoporous silica based biosensors can be found in several well documented review papers (Hasanzadeh *et al.*, 2012; Melde and Johnson, 2010; Walcarius, 2010)). However, in the literature so far, the relation between the pore size of the mesoporous silica material and the immobilized biomolecule has not been recognized as a key factor for achieving high-performance biosensor which satisfies high sensitivity, selectivity, and good stability. Therefore, the potential capacity of enzymatic activity has not previously been fully exploited for biosensor application.

In fact, our study in this chapter shows that the stability of the sensor, as well as its sensitivity, is improved drastically by encapsulating the enzyme into mesoporous silica materials with a pore diameter adjusted to the size of the enzyme, and that high-performance biosensors could be constructed easily by this entrapment method.

10.2 Synthesis of mesoporous silica materials and enzyme encapsulation

A number of synthesis methods that are able to accurately control the structure of mesoporous silica materials and produce a uniform pore diameter of between 2 and 15 nm have been developed (Hoffmann *et al.*, 2006; Kresge *et al.*, 1992; Yanagisawa *et al.*, 1990a, 1990b). A brief description of a typical synthesis route for the manufacture of mesoporous silica materials is given here. Water glass (sodium silicate powder) is calcinated at 800°C and we obtain a layered silica sheet, so-called kanemite. The kanemite is then

dispersed in water and surfactant is added and mixed. The ion exchange reaction occurs, the silicate layers of the kanemite form three-dimensional silicate networks, i.e., micelle/silica complex. The product is calcinated at 600°C, and the surfactant removed. The resulting micelle/silica complex is converted to mesoporous materials with uniform pore-size distributions. The specific surface areas of the mesoporous silica material are very large, typically 1000 m^2/g, and the pore size can be altered by variation of the alkyl-chain length of the surfactant. Figure 10.1 shows the schematic procedure of the synthesis and typical transmission electron microscope (TEM) image of the products. In this example, pore size of mesoporous silica material is about 3–4 nm.

An important feature of mesoporous silica material is that it has uniform pores comparable in size to large molecules such as proteins and DNA; taking advantage of this feature, we have encapsulated large-sized enzyme molecules that are very important for industrial use into mesoporous silicas for producing stabilized enzyme with high-density accumulation, and have applied them for sensing use. Indeed, we have successfully encapsulated a number of enzymes, such as formaldehyde dehydrogenase (FDH), choline oxidase, acetylcholinesterase, laccase, lactate oxidase, and 3-β-hydroxybutyrate dehydrogenase into the mesoporous silicas whose pore sizes are close to the molecular sizes of the enzymes, and developed high-performance biosensors by using these mesoporous silica–enzyme composites (Shimomura *et al.*, 2008, 2009a, 2009b, 2011, 2012a, 2012b, 2012c). This encapsulation method ensures the enzyme is encapsulated into the pores of mesoporous silica by equilibrium adsorption or by under air/vacuum due to capillary action, so

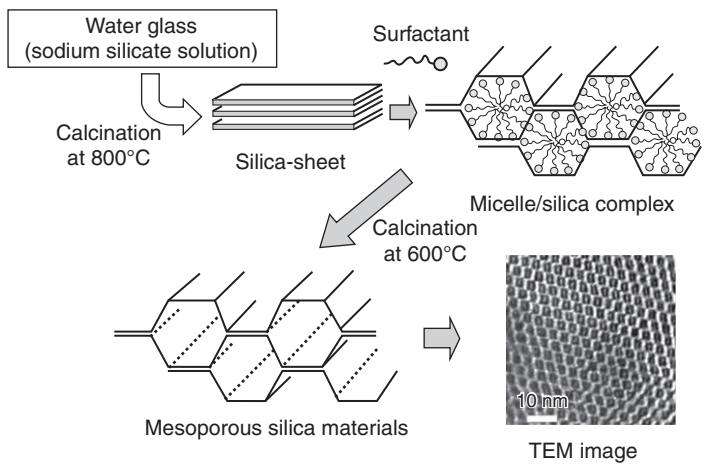

10.1 Schematic procedure of the synthesis and TEM images of the mesoporous silica material.

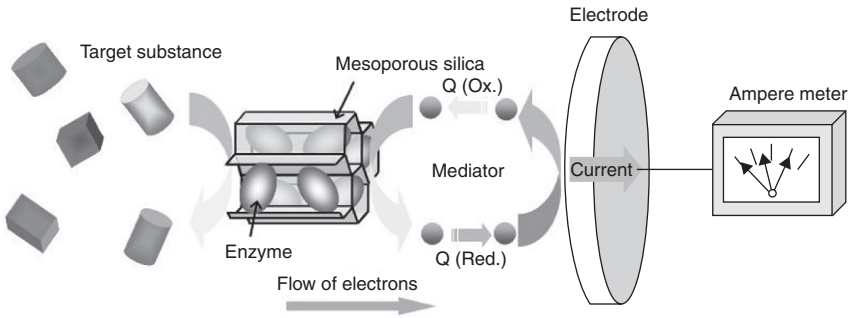

10.2 Schematic diagram of detection mechanism of our enzymatic sensor.

it requires no covalent bond immobilization. Thus, this method has the distinct advantage that the native properties of the enzymes are maintained, and the encapsulated enzymes show their intrinsic features such as high substrate specificity and reactive efficiency.

10.3 Application to enzymatic sensor and detection mechanism

Figure 10.2 shows the schematic diagram of a typical detection mechanism of our enzymatic sensor, where the sensor comprises an immobilized enzyme in a mesoporous silica material, electrodes in electrolytic solution, and measurement system such as the ampere meter.

Enzymes have high specificity, and react only with target substrates, catalyzing the oxidation of the target analyte, allowing for an electron to be transferred from target analyte to the electron mediator. Subsequently, the mediator transfers the electron from the enzyme to the electrode, and thus a concentration-dependent electrochemical current is obtained as a sensor response. Thus, we can determine the quantity of target substance in the environment or in biotic samples with high sensitivity.

10.4 Development of enzymatic sensor for formaldehyde detection

In this section, we provide an enzymatic sensor for formaldehyde detection as a successful example of our concept.

10.4.1 Formaldehyde detection at present

Formaldehyde (HCHO) is one of the harmful volatile organic compounds (VOCs); it has been reported to induce sick building syndrome (US EPA,

1996). Further, it has a risk of being highly toxic with an increased risk of impaired human health, including cancer (Chasnoff *et al.*, 1989; WHO, 1989). However, formaldehyde is widely used in many industrial processes to make other chemicals, building materials, and household products such as furniture, clothing, wallpaper, ceiling, flooring, carpet, and water cleaner (Patnaik, 1997; US EPA, 1996; WHO, 1989). Indeed, it often causes social/economic loss in the world. The maximum permitted concentration of formaldehyde vapor is defined by the World Health Organization (WHO) as 80 ppb, which corresponds to identify eight persons out of 100 million citizens! Therefore, a method is required for measuring formaldehyde with high sensitivity and selectivity.

Table 10.1 shows the summary of formaldehyde sensors at present. Each sensor is evaluated in terms of sensitivity, selectivity, measurement time, stability, cost, and size. For example, metal-oxide semiconductor sensors are low cost but have low sensitivity and low selectivity, while chromatography/mass spectrometry has high sensitivity and high selectivity but is expensive and requires expertise. In conclusion, they all exhibit merits and demerits, and we do not have a satisfactory formaldehyde sensor at present.

By using stabilized enzyme as a sensing material, we can expect the realization of high-performance sensor with high sensitivity, high selectivity, and long-term stability.

10.4.2 Sensor structure

We have successfully developed a measurement system containing an enzymatic biosensor for detecting formaldehyde.

Table 10.1 Summary of formaldehyde detection at present

Sensor type/ sensing method	Sensitivity	Selectivity	Measuring time	Stability	Cost	Size	Remarks
Metal-oxide-semiconductor sensor	×	×	△	○	○	○	Low sensitivity, selectivity
Electrochemical sensor	×	△	△	○	○	○	Sensitivity ~ 100 ppb
Surface plasmon resonance sensor	◎	△	○	×	×	×	Expensive, large
Colorimetric sensor	×	△	×	○	◎	◎	Sensitivity ~ 100 ppb
Chromatography/ mass spectrometry	◎	◎	×	○	×	×	Expensive, needs experts

◎ → Excellent; ○ → Enough; △ → Not enough; × → Inferior.

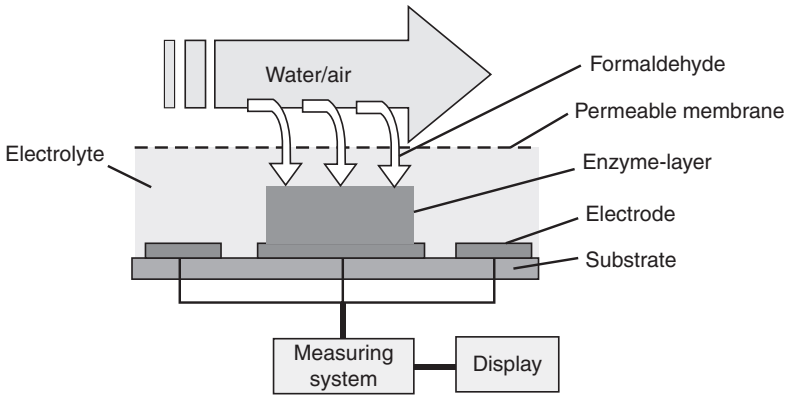

10.3 The schematic structure of our enzymatic sensor for formaldehyde detection.

Figure 10.3 shows the schematic structure of our enzymatic sensor. The electrodes are formed on the glass substrate and then the enzyme layer is formed. The enzyme layer comprises immobilized enzyme in mesoporous silica material. In this present example an enzyme FDH is utilized, and the enzyme molecules are immobilized by encapsulating them in mesoporous silica material whose pore size is close to the molecular size of the enzyme (≈8 nm (Tanaka *et al.*, 2002)). The electrodes are then immersed in an electrolyte and confined by a liquid/gas-permeable membrane. In the presence of water or air containing formaldehyde, the formaldehyde will diffuse into the supporting electrolyte solution via the permeable membrane, and can be detected directly without pretreatment.

Here, the sequence of reactions involved in the detection of formaldehyde can be described in terms of the following reactions (Shimomura *et al.*, 2008):

$$HCHO + NAD^+ + 3H_2O \rightarrow HCOO^- + NADH + 2H_3O^+ \quad [10.1]$$

$$H^+ + NADH + Q \rightarrow NAD^+ + QH_2 \quad [10.2]$$

$$QH_2 \xrightarrow{\text{electrode}} Q + 2e^- + 2H^+ \quad [10.3]$$

where immobilized FDH catalyzes the oxidation of formaldehyde to formic acid while NAD^+ is reduced to nicotinamide adenine dinucleotide, reduced form (NADH). The reaction can be monitored by the oxidation of NADH using quinone (Q) as an electrochemical mediator. The QH_2 is finally oxidized to Q by the working electrode. This reaction produces a flow of electrons to the working electrode and thus a measurable current, the magnitude of which is directly related to the formaldehyde concentration.

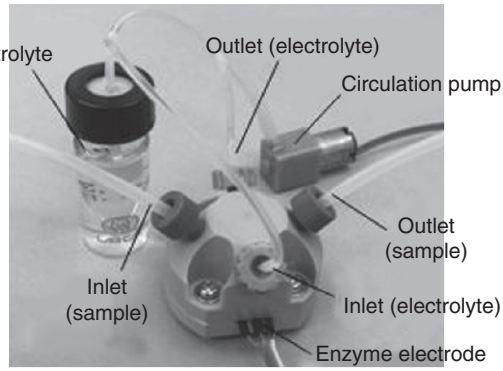

10.4 The external view of our sensor head.

Figure 10.4 show the external view of our sensor head. The sensor head is composed of enzyme electrode, the reservoir of the electrolyte, circulation pump, inlet/outlet of the electrolyte, and inlet/outlet of the sample. The electrolyte solution is circulated after each measurement by the small circulation pump for continuous measurement. The size of the sensor is about 4 cm × 4 cm × 3 cm. The electric signal (current response) is controlled and measured with the aid of a potentiostat, and recorded and displayed on a PC.

10.4.3 Evaluation result

In this section we explain the evaluation result of our sensor for the detection of formaldehyde in water/air.

Formaldehyde detection in water

The sensor response and its corresponding calibration curve for formaldehyde in water are shown in Fig. 10.5a and 10.5b. In these experiments, successive injections of different concentrations of formaldehyde solutions are introduced to our sensor. We can see from these figures that the sensor output is proportional to the amount of formaldehyde present in the solution, and formaldehyde is successfully detected at concentration below 80 ppb, the ambient criterion defined by the Ministry of Health, Labor and Welfare. In fact, it can detect sub-ppb (10^{-11}-level) formaldehyde in water. The response time is mostly less than one minute (90% of responses). The selectivity of the sensor is found to be excellent; the sensor system is specifically sensitive to formaldehyde, while it scarcely responds to other chemicals (see Fig. 10.6).

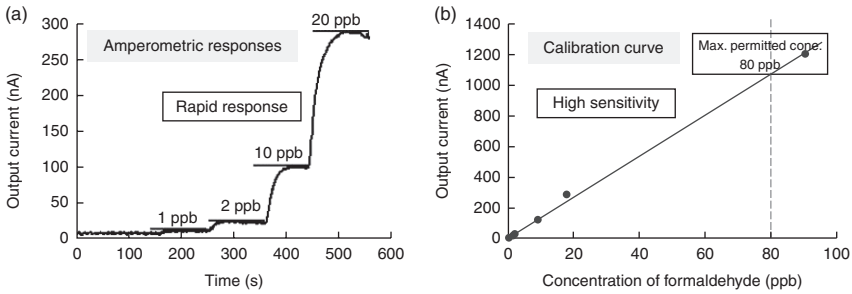

10.5 Amperometric responses (a) and calibration curve (b) of the sensor to formaldehyde in water, respectively.

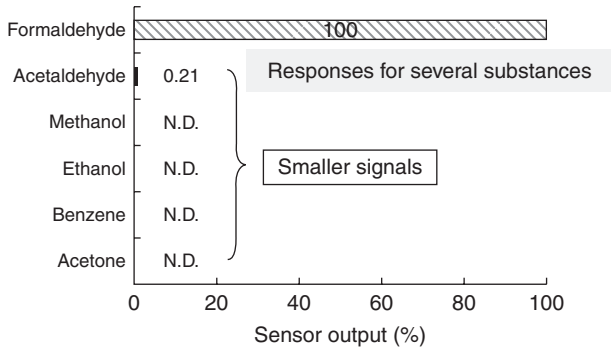

10.6 Selectivity of the sensor for various types of aqueous substances.

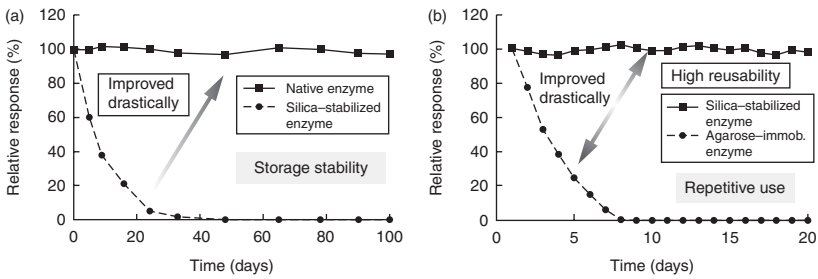

10.7 Storage stability (a) and reusability (b) of the sensor in water.

Figure 10.7a shows the storage stability of the sensor, where the output current of the sensor is expressed as a percentage of the initial response at day zero. We can see that no decrease was observed in the response of our sensor over a period of 100 days, whereas the native one loses its enzymatic activity and almost no response was observed over a period of 3 weeks. Thus, the storage stability is improved drastically and sensor shows remarkable

storage stability in the solution. Figure 10.7b shows the repeatability. We can see that the output of our sensor remains stable when the measurement is repeated 20 times, whereas the output of the enzyme immobilized biosensors with agarose shows an 80% decrease in response after five cycles. Thus, the reusability is very high and the sensor response is almost reversible for 20 repetitive uses.

Therefore, we have realized a high-performance formaldehyde sensor in water with high sensitivity, selectivity, reusability, and remarkable storage stability.

Formaldehyde detection in air

Next, we have used the biosensor for the detection of gaseous formaldehyde and evaluated its performance as a formaldehyde gas sensor. In this experiment, a low concentration of formaldehyde gas was generated using gas generation equipment that we have developed independently. The basic principle of gas generation and the validation method are as follows: standard formaldehyde gas was mixed and diluted with highly-purified air. After standing for another 24 h to achieve an equilibrium state, the resultant gas was sampled and extracted using a 2,4-dinitrophenylhydrazine (DNPH) collection tube, and then the concentration of formaldehyde gas was estimated and guaranteed by HPLC analysis (DNPH-HPLC method) (Fung and Grosejean, 1981)). The mixture ratio of standard formaldehyde gas and purified air was varied according to the target concentration of the gas, and this procedure was repeated until the target concentration of formaldehyde gas was obtained. The resultant formaldehyde gas was introduced to the sensor for evaluation. It should be noted that the sampling and concentration determination of the gas by this method needs considerable time and interpretation.

Figure 10.8a and 10.8b shows the typical response of our sensor to introducing of 10 ppb concentration of formaldehyde gas and the corresponding calibration curve, respectively. The sensor responses rapidly after the introduction of the sample gas and the initial slope of the response curve is sufficiently large. By using this, we successfully detected sub-ppb concentrations of formaldehyde gas within 2 min, representing an improvement over commonly used applications, as our sensor can expect to have a lower detection limit comparable to dog's nose for VOCs (Li, 2009). In addition, the calibration curve shows a wide dynamic range that ranges from sub-ppb to 1000 ppb, and one can say that this sensor possess sufficient measurement range as a gas sensor for environmental measurement.

Figure 10.9 shows the example of duplicate measurement with and without circulation technique. We introduced a 100 ppb concentration of

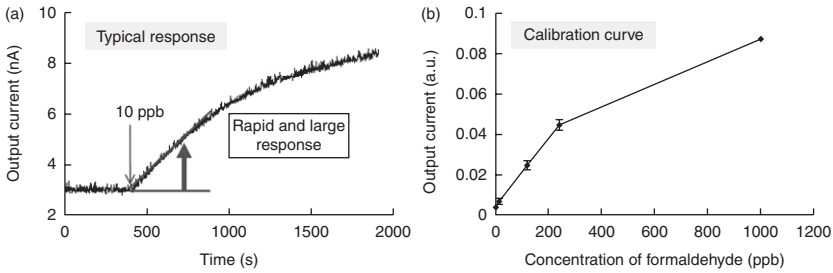

10.8 Amperometric responses (a) and calibration curve (b) of the sensor to gaseous formaldehyde in air, respectively.

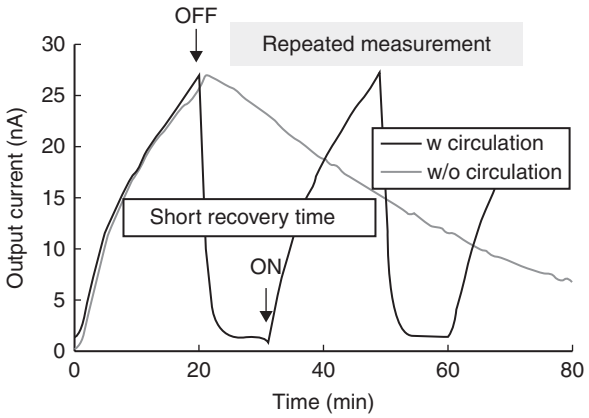

10.9 Duplicate measurement of gaseous formaldehyde in air.

formaldehyde gas in this experiment. As we can see from this figure, it is possible to repeat rapid measurement by circulating the electrolyte solution, i.e., one can achieve short recovery times and can start the next measurement. It takes about 4 min in this example to recover the baseline, but the baseline would be recovered more quickly in practice since the initial slope of the response curve is used.

Therefore, our sensor exhibits rapid response, high sensitivity, and wide detection range for formaldehyde in air as well as in water. In the above example, the superiority of the sensor is mainly a consequence of the following two points:

1. By controlling the pore size of the mesoporous silica material comparable to the enzyme size and by encapsulating and immobilizing the enzyme molecules into the pores, the aggregation of the enzyme molecules is prevented and their steric structure is stabilized; consequently, degradation of enzymatic activity is prevented. In addition,

the enzymes could be immobilized appropriately dispersed with a high density in this structured material so as to maximize their enzymatic activity.
2. By using an appropriate electron mediator to transfer electrons from the enzyme within the pores of mesoporous silica to the electrode, the rapid response and high sensitivity are obtained. In fact, our formaldehyde sensor operates as low operating potential as +30 mV at present, due to the improvement of electron mediator and electrode material.

These points successfully demonstrate the development of a high-performance formaldehyde sensor.

10.4.4 Application to other substances in our environment

Choosing proper enzymes for the purpose, and optimizing the pore size of mesoporous silica materials, the developed sensor and sensing techniques are generally applicable to the detection of various other substances. For example, we have successfully developed various high-performance aqueous and gaseous sensors (e.g. residual pesticides, phenolic compounds, alcohol, and ammonia) which can detect ultra-low concentration of target substances quickly. Based on this highly advanced sensing technique, we are now striving to make the systems suitable for the practical monitoring of harmful substances in the environment in order to protect our life from the 'attack' from these pollutant sources. Further details regarding this technology will be published elsewhere in the near future.

10.5 Conclusion

We have developed a high-speed, high-sensitivity enzymatic biosensor with long-term stability by using one of the silicon materials e.g., mesoporous silica. In particular, the stability of the sensor is improved drastically by encapsulating the enzyme into mesoporous silica material with a pore diameter adjusted to the size of the enzyme. As an example, using the enzyme FDH, we have successfully achieved direct and rapid detection of formaldehyde, which is known as a VOC, in water and in air with high sensitivity. The results presented here confirm that our methods are suitable for practical use in the area of detection requiring high sensitivity and selectivity. We expect that our sensing technology using silicon materials will make a huge contribution to the development of small-sized and high-performance sensing devices and to the realization of a secure and pleasant social environment for a comfortable and healthy life.

10.6 References

Blin, J.L., Gerardin, C., Carteret, D., Rondehuser, L., Selve, C. and Stebe, M.J. (2005) 'Direct one–step immobilization of glucose oxidase in well ordered meso-structured silica using a nonionic fluorinated surfactant', *Chem Mater,* **17**, 1479–1486.

Bornscheuer, U.T. (2003) 'Immobilizing enzymes: how to create more suitable biocatalysts', *Angew Chem Int Ed*, **42**, 3336–3337.

Chasnoff, I.J., Ellis, J.W. and Fainman, Z.S. (1989) '*Family Health and Medical Guide*', Publications International, Lincoln-Wood, Illinois.

Fan, J., Yu, C., Gao, F., Lei, J., Tian, B., Wang, L., Luo, Q., Tu, B., Zhou, W. and Zhao, D. (2003) 'Cubic mesoporous silica with large controllable entrance sizes and advanced adsorption properties', *Angew Chem Int Ed*, **42**, 3146–3150.

Fung, F. and Grosejean, D. (1981) 'Determination of nanogram amounts of carbonyls as 2,4-dinitrophenylhydrazines by high-performance liquid chromatography', *Anal Chem,* **53**, 168–171.

Hasanzadeh, M., Shadjou, N., Eskandani, M. and Guardia, M. (2012) 'Mesoporous materials for use in electrochemical enzyme nanobiosensors', *Trends Anal Chem*, **40**, 106–118.

Hoffmann, F., Cornelius, M., Morell, J. and Frba, M. (2006) 'Silica-based mesoporous organic–inorganic hybrid materials', *Angew Chem Int Ed*, **45**, 3216–3251.

Kresge, C.T., Leonowicz, M.E., Roth, W.J., Vartuli, J.C. and Beck, J.S. (1992) 'Ordered mesoporous molecular sieves synthesized by a liquid-crystal template mechanism', *Nature,* **359**, 710–712.

Li, S. (2009) 'Overview of Odor Detection Instrumentation and the Potential for Human Odor Detection in Air Matrices', MP090053, The MITRE Corporation, McLean, Virginia.

Melde, B.J. and Johnson, B.J. (2010) 'Mesoporous materials in sensing: morphology and functionality at the meso-interface', *Anal Bioanal Chem*, **398**(4), 1565–1573.

Patnaik, P. (1997) *Handbook of Environmental Analysis: Chemical Pollutants in Air, Water, Soil, and Solid Wastes* CRC Press, Boca Raton, Florida.

Shimomura, T., Itoh, T., Sumiya, T., Mizukami, F. and Ono, M. (2008) 'Electrochemical biosensor for the detection of formaldehyde based on enzyme immobilization in mesoporous silica materials', *Sen Actuators B: Chem*, **135**, 268–275.

Shimomura, T., Itoh, T., Sumiya, T., Mizukami, F. and Ono, M. (2009a) 'Amperometric determination of choline with enzyme immobilized in a hybrid mesoporous membrane', *Talanta,* **78**, 217–220.

Shimomura, T., Itoh, T., Sumiya, T., Mizukami, F. and Ono, M. (2009b) 'Amperometric biosensor based on enzymes immobilized in hybrid mesoporous membranes for the determination of acetylcholine', *Enzyme Microb Technol,* **45**, 443–448.

Shimomura, T., Itoh, T., Sumiya, T., Hanaoka, T., Mizukami, F. and Ono, M. (2011) 'Amperometric detection of phenolic compounds with enzyme immobilized in mesoporous silica prepared by electrophoretic deposition', *Sen Actuators B: Chem*, **153**, 361–368.

Shimomura, T., Sumiya, T., Ono, M., Ito, T. and Hanaoka, T. (2012a) 'Amperometric L-lactate biosensor based on screen-printed carbon electrode containing cobalt phthalocyanine, coated with lactate oxidase-mesoporous silica conjugate layer', *Anal Chim Acta*, **714**, 114–120.

Shimomura, T., Sumiya, T., Ono, M., Ito, T. and Hanaoka, T. (2012b) 'An electrochemical biosensor for the determination of lactic acid in expiration', *Procedia Chem,* **6**, 46–51.

Shimomura, T., Sumiya, T., Ono, M., Ito, T. and Hanaoka, T. (2012c) 'A novel, disposable, screen-printed amperometric biosensor for the ketone 3-β-hydroxybutyrate fabricated using a 3-β-hydroxybutyrate dehydrogenase-mesoporous silica conjugate', *Anal Bioanal Chem*, **405**, 297–305.

Shin, C.L.Y., Liu, J. and Ackerman, E.J. (2002) 'Entrapping enzyme in a functionalized nanoporous support', *J Am Chem Soc*, **124**, 11242–11243.

Tanaka, N., Kusakabe, Y., Ito, K., Yoshimoto, T. and Nakamura, K.T. (2002) 'Crystal structure of formaldehyde dehydrogenase from *Pseudomonas putida*: the structural origin of the tightly bound cofactor in nicotinoprotein dehydrogenases', *J Mol Biol*, **324**, 519–533.

US EPA (1996) 'National Air Quality and Emission Trend Report: Air Toxics (Chapter 5)', issued by the US Environmental Protection Agency, North Carolina.

Walcarius, A. (2010) 'Template-directed porous electrodes in electroanalysis', *Anal Bioanal Chem*, **396**(1), 261–272.

WHO (1989) 'World Health Organization, Environmental health criteria 89, Formaldehyde', issued by the World Health Organization, Geneva.

Yanagisawa, T., Shimizu, T., Kuroda, K. and Kato, C. (1990a) 'The preparation of alkyltrimethylammonium-kanemite complexes and their conversion to microporous materials', *Bull Chem Soc Jpn*, **63**, 988–992.

Yanagisawa, T., Shimizu, T., Kuroda, K. and Kato, C. (1990b) 'Trimethylsilyl derivatives of alkyltrimethylammonium-kanemite complexes and their conversion to microporous SiO2 materials', *Bull Chem Soc Jpn*, **63**, 1535–1537.

11

Semiconductor quantum dots in chemical sensors and biosensors

N. CHANIOTAKIS and R. BUICULESCU,
University of Crete, Greece

DOI: 10.1533/9780857096722.2.267

Abstract: A sensor, whether a chemisensor or a biosensor, is an integrated device capable of providing analytical information (such as concentration of an analyte) using a chemical or a biological recognition element, with most employed transduction methods used being the electrochemical and the optical. In the first part of this chapter, we will describe the fundamentals behind using semiconductor quantum dots (QDs) for the development of optically active chemical sensors and biosensors. In the second part we will focus on the most important applications of QDs so far in the field of sensor development.

Key words: semiconductor quantum dots (QDs), biosensor, optical, bioconjugation, fluorescence resonance energy transfer (FRET).

11.1 Introduction

The art of biochemical sensing is based on two fundamental scientific principles: biochemical recognition, and optoelectronic transduction. It is a discipline that from its early days was able to fuse biochemical with physicochemical principles for the development of the bioanalytical devices. In general, a sensor (whether a chemical sensor or a biosensor) is an integrated device which is capable of providing analytical information (such as concentration of an analyte) using a chemical or a biological recognition element. While the recognition or sensing element is responsible for probing the test solution for the analyte, it requires a second part in order to relay this information to the user. For this to be achieved, the sensing element is placed in close proximity to a transduction element or a transducer. The transducer, as used in chemical sensors and biosensors, is the device that converts the chemical energy to electrical energy. Since the early stages of sensor development, there have been two main transduction methods used, namely electrochemical and optical. When an electrochemical transducer is used, the signal is one of the three parameters of Ohm's law ($V = I \times R$).

Thus we have potentiometric, amperometric, conductometric and impedometric sensors. When optical transduction is used, the signal obtained is either radiation intensity decrease (absorption), increase (fluorescence, chemiluminescence), or wavelength shift (change of colour). Optical transduction seems to be much more attractive, since our optical detection systems (our eyes) are very sensitive light detectors and can be used to screen the signal produced. On the other hand, when the optical biosensor is to be designed and applied, many serious operational problems arise. For example, the detection limit is not good enough, or the sample interferes with the signal, or the reproducibility and stability of the signal are very low. For these reasons, electrochemical sensors are more widely used. It is thus of great importance to the sensor community that optical transduction systems are developed that can rival the characteristics of electrochemical transduction. It is believed that the development of quantum dots (QDs) will be able to provide these characteristics, and thus give a boost to optical biochemical sensors.

QDs are nanometre-scale (10^{-9} m) semiconductor crystals. Due to size confinement of the energy (light) they absorb, intense and in many cases controllable light absorption and emission (fluorescence) characteristics are exhibited. In comparison to organic dyes such as rhodamine 6G or fluorescein, QDs show similar quantum yields but they have larger absorption

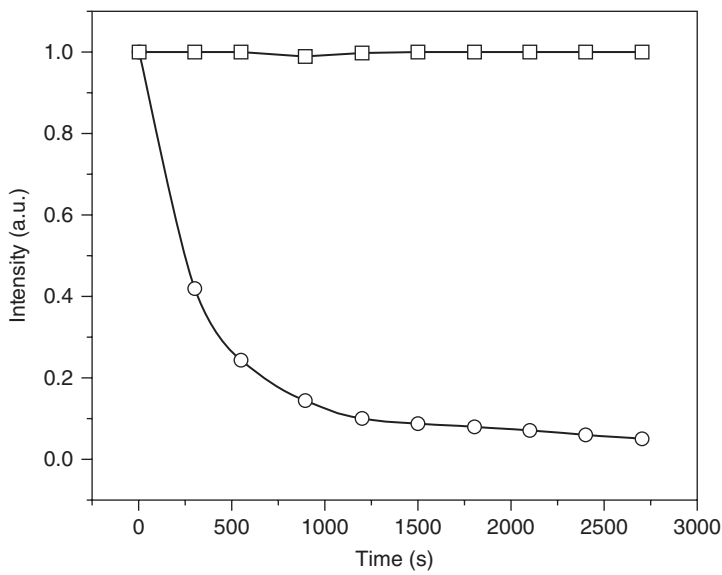

11.1 Photostability of QDs (squares) compared to the organic dye Texas Red (circles). Note the drastic decrease of the dyes intensity over time, compared to the QD. (*Source*: Adapted from Smith *et al.*, 2006.)

cross-sections i.e. they are more efficient absorbers, and most importantly, they are usually much more stable (Fig. 11.1) and resistant to photobleaching. For these reasons, they are suitable for the development of novel chemical sensors and biosensors, substituting the organic dyes. In addition, if the optical characteristics of the QDs can be influenced in a direct and reproducible manner by the surface chemistry, then there is a new platform for the development of stable and highly sensitive biosensors. In this chapter we will describe the fundamentals behind the use of QDs for the development of optically active chemical sensors and biosensors.

11.2 Quantum dots (QDs): synthesis and optical properties

QDs are very small (2–10 nm) spherical particles of inorganic semiconductor material, such as CdSe, CdS, CdS/ZnS, CdSe/ZnS, CdSe/CdS, or InAs/CdSe, that can form a clear coloured suspension or a colloidal solution with water. Their size, in the order of nanometres, can be precisely controlled during their synthesis. They are called QDs because they possess unique properties due to the 'quantum confinement effect'. These quantum properties appear as the physical size of certain classes of materials (such as semiconductors) is smaller in magnitude than the wavelength of the electron wave function. A material that exhibits this effect has electronic and optical properties that are fundamentally different from those of its corresponding normal (bulk) material. QDs have very broad continuous absorption spectra, and high quantum yields for fluorescence. The light emitted by QDs can be tuned to cover a wide wavelength range, extending from the ultraviolet to the visible (e.g., CdSe can emit in the 450–650 nm range, CdTe in the 500–700 nm range, while InAs or PbSe can emit above 800 nm), depending on the particle size (Michalet *et al.*, 2005) (Fig. 11.2).

They can be excited over a broad wavelength range (they can be excited with any wavelength shorter than the wavelength where they emit fluorescent light). They give narrow and symmetric size-tunable emission spectra (usually 20–40 nm full width at half maximum intensity). They are resistant to photobleaching and chemical degradation, and show high photochemical stability (Bruchez *et al.*, 1998; Chan and Nie, 1998). Their molar extinction coefficients are 10–100 times higher than those of organic dyes. All these unique characteristics have opened the way for their use in a large number of analytical and bioanalytical applications.

Due to their small size, the energy states of semiconductor QDs are size dependent as in an atom, due to the confinement of charge carriers (electrons, e^-, and holes, h^+) in all three dimensions. As a consequence, their bandgap energies vary as a function of size. As the size increases, the bandgap energy decreases. The bandgap energy can be defined as the minimum

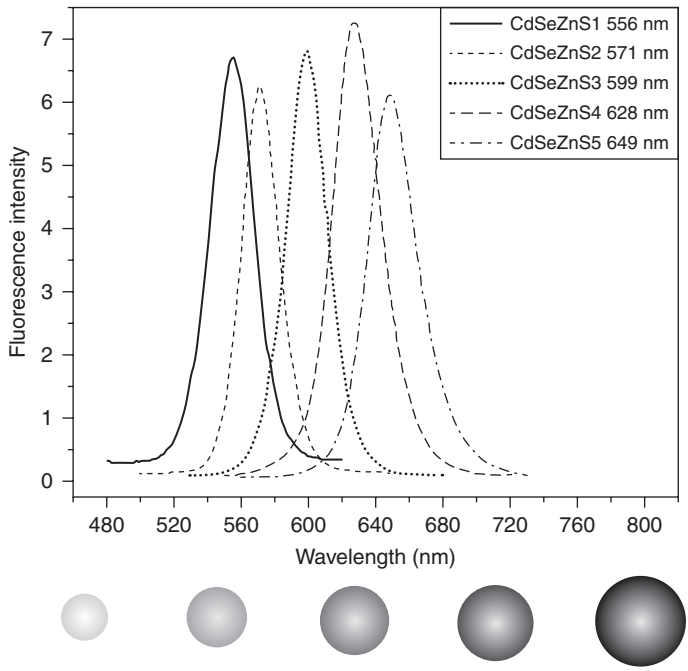

11.2 Size dependent emission spectra of CdSe/ZnS QDs. (*Source*: Adapted from Frasco and Chaniotakis, 2009.)

energy an electron must absorb in order to be excited from the valence to the conduction band, thus leaving a hole behind. The excited electron can return to the ground state, where upon recombination with the hole it emits energy (equal to the bandgap energy) in the form of heat or light (fluorescence). Nevertheless, there is a high probability that energy states within the material will trap either the electron or the hole (Fig. 11.3).

A QD is never a perfect sphere. Structural defects in the QD crystal structure can also act as temporary 'traps' for the electron or hole. For example, atomic vacancies (atoms missing from the surface), local lattice mismatches, dangling bonds, or adsorbates at the surface (Murphy, 2002) are some of the conditions which drastically affect the photoluminescence of the QDs. All these defects can prevent the radiative recombination of the electron–hole pair. The alternation of trapping and untrapping events results in intermittent fluorescence, also called blinking (Bakalova *et al*., 2007). Blinking causes a drop in the quantum yield (the ratio of emitted to absorbed photons). In order to eliminate defects and consequently decrease the possibility of charge carriers being kept in trap states, surface passivation is used (Dabbousi *et al*., 1997). This is achieved by coating the dot with another semiconductor material with wider band gaps. In addition, surface

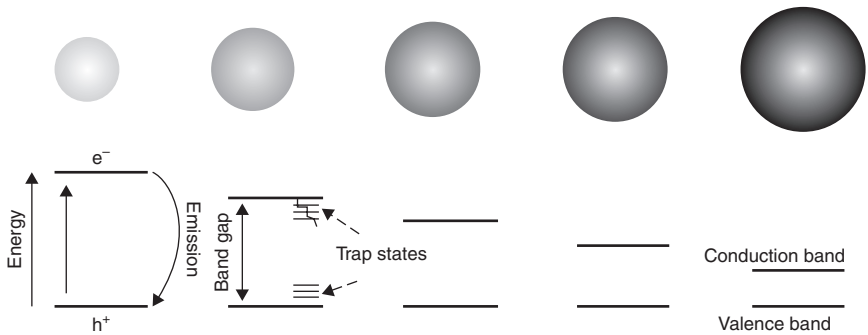

11.3 The photoexcitative creation of an electron–hole pair and the following radiative relaxation through trap states. (*Source*: Adapted from Frasco and Chaniotakis, 2009.)

passivation increases the photostability of the QDs' core, and subsequently their quantum yield. These stabilized QDs are called core–shell structures and are more robust, and thus more useful for fluorescence-based applications (Jaiswal *et al.*, 2003).

The synthesis of QDs requires the presence of organic molecules named surfactants (Fig. 11.4). They are amphiphilic compounds, trioctylphosphine (TOPO/TOP) being a very common example. They are molecules comprising one hydrophilic part (a polar or a charged functional group) and one hydrophobic part (in the simplest case, one or several hydrocarbon chains). The surfactant provides the QDs with charged surface, prevents their aggregation and renders them soluble in organic solvents. The choice of the surfactant depends on its chemical stability and its binding strength to the QD surface. Too strong a binding does not allow for the growth of the QD, while too weak will lead to the formation of large particles and aggregates (Comparelli *et al.*, 2007). Using a mixture of surfactants will result in the synthesis of a wide range of QDs sizes and shapes (rod-like, disc-like, arrow- or zigzag-shaped nanocrystals, and even inorganic dendrimers).

Due to the availability of precursors and the simplicity of crystallization, Cd-chalcogenide nanocrystals have been the most widely studied colloidal QDs. The breakthrough in the synthesis of high quality colloidal semiconductor QDs was realized in 1993 by Bawendi's group from the Massachusetts Institute of Technology (Murray *et al.*, 1993) that managed the synthesis of highly crystalline CdSe QDs with a narrow size distribution, by a hot-injection method. The kinetic control of the reaction conditions, such as the growth time, temperature, and monomer concentration, led to monodisperse nanocrystals of high quality. Extensive reviews detailing the synthesis of a range of QDs can be found in the literature (Park *et al.*, 2007; Reiss *et al.*, 2009; Mattoussi *et al.*, 2012).

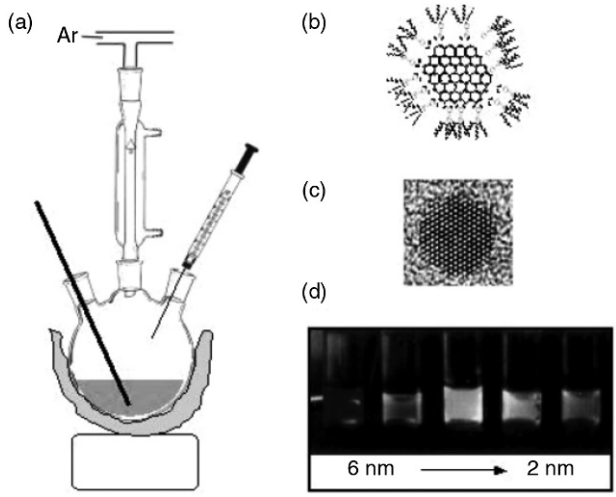

11.4 Synthesis of colloidal nanocrystals. (a) Typical set-up. The surfactant is placed in a three-neck flask and heated under an Ar atmosphere, with continuous stirring. The precursor is quickly injected with a syringe and stirring is continued until nanocrystals are formed. (b) Schematic of a semiconductor QD (CdSe) with surface surfactant molecules (TOPO). (c) High resolution transmission electron microscopy (HR-TEM) image of one CdSe nanocrystal. Each dot corresponds to a column of atoms in the CdSe lattice. The TOPO layer is not visible due to its low contrast. The diameter of the nanocrystal is about 5 nm. (d) Colloidal CdSe nanocrystals dissolved in toluene. Depending on their size, when excited with UV light, the CdSe nanocrystals emit another colour. (*Source:* From Parak *et al.*, 2003.)

11.3 Bioconjugation and capping strategies

Since biological processes are typically taking place in aqueous environments, the nanocrystals that are used in biological applications need to have a hydrophilic surface. As mentioned earlier, QDs are synthesized with the help of organic compounds (hydrophobic) that make them water insoluble. For this reason, a number of methods exist (Smith *et al.*, 2006) which increase their hydrophilicity, making them water-soluble. This is achieved by either ligand exchange or by functionalization with a molecule that can provide both water solubility and bioconjugation sites. Functionalization with a ligand relies on the exchange of the hydrophobic surfactant groups on the surface of the QDs with ligand molecules that carry functional groups at both ends – one end being reactive towards the nanocrystal surface, and one hydrophilic end that ensures water solubility. Other methods include the growth of a hydrophilic silica shell through surface silanization, and the use of amphiphilic polymers or incorporation into micelles (Frasco and

Chaniotakis, 2009). Although there is yet to be found the optimum method that contains all the advantages of individual procedures, state of the art semiconductor QDs have reached a degree of performance regarding water solubility that is sufficient for biological experiments.

The methods used to conjugate or attach biomolecules to the surface of QDs can be divided into three primary categories, as determined by Mattoussi and co-workers (2006): (a) covalent modification by attaching of biomolecules to a functional group (e.g. amines, thiols, carboxyls) present on the surface of the QDs; (b) direct attachment to the QD surface (e.g. through a dative thiol bond or by metal-affinity coordination) and (c) electrostatic interactions between the QD surface and oppositely charged biomolecules.

The fascinating optoelectronic properties mentioned in an earlier paragraph make these nanomaterials ideal for a large number of applications, such as in biomedical areas. Water-soluble QDs possessing a wide range of surface functional groups (COOH-, SH-, NH_2-, etc.) can be easily conjugated with different biomolecules (oligonucleotides, proteins, enzymes, antibodies, etc.). The resulting structures combine the chemical properties of the surface moieties and the biological function of the surface-attached biomolecule with the optical ones of the semiconductor QDs.

Depending on the size of the QD with respect to the biomolecule, two types of conjugates can be obtained. If QDs with sizes considerably larger than that of the biomolecule are used, nano-bio-hybrids consisting of a single QD surrounded by a large number of biomolecules on its surface can be produced. In this case, since the QD offers an important number of surface attachment groups, different functionalities can be attached, resulting in multifunctional probes. If small sized QDs are used, nano-bio-hybrids consisting of a biological molecule surrounded by a number of QDs can be obtained (Zhelev *et al*., 2005). If this is the case, a strong fluorescent signal resulting from the nano-bio-hybrid can be registered, and the biomolecule is easily tracked. This is the reason why QDs with sizes of 2–4 nm are preferred for bio-applications and thus are the most studied. In theory, QDs decorated with ligands with specific molecular orientation and molar ratios can be produced. At this time however, these conjugates are still not readily available. Nevertheless, a number of commercially available QDs coated with proteins such as biotin, avidin, protein A or G, and other proteins, can be found.

The research work published by Chan and Nie (1998) pioneered the conjugation of semiconducting QDs to biological molecules and their application to biological detection. Their method involved conjugation of CdSe/ZnS QDs to transferrin, an iron-binding protein found in blood plasma that controls the levels of free iron in biological fluids. Through receptor-mediated endocytosis, the bioconjugates are being transported into the cell, and as a result, the cells exhibited high fluorescent signals. CdSe QDs have also

been conjugated to antibodies to be used for the detection of specific antigens such as proteins and cell fragments, these bioconjugates proving to be very valuable for applications in flow cytometric and western blot analyses (Zhelev *et al*., 2006). More details about these applications will be given further down.

11.4 Applications of QDs to biosensors

Biosensors are devices that can monitor the analyte continuously, using a sensing element, usually a protein or other biomolecule, with a transduction system close by. In the case of biosensors based on fluorescent QDs, the transduction will have to be optical. Biosensors play an important role in the development and improvement of public health, finding applications in areas where rapid detection, high sensitivity and specificity are important. As presented above, the most important characteristic of QDs is their fluorescence. For this reason, QDs are used mainly as fluorescent probes in biosensing systems (Medintz *et al*., 2006). As fluorescent labels, QDs can be used to simply label the cell wall or to partition into the cells, allowing for flow cytometry or microscopy applications. A simple staining procedure, though not adequate by itself for biosensor development, the research in this area has provided various surface modification methods which have laid out the ground for the development of QD-based biosensors and related biochemical applications (Costa-Fernandez *et al*., 2006). We are now at the point where the required know how and QD-related technologies allow for the design of novel biosensors. Figure 11.5 illustrates some bioconjugation methods employed now for biosensor applications.

11.4.1 pH and ion sensing

QDs systems that are pH-sensitive have been obtained by capping QDs with organic ligands. These nano-conjugates have very promising applications for a variety of analytical purposes, in particular for the development of luminescent chemisensors. Within this strategy, the surface of CdSe/ZnS QDs was capped with pH-sensitive organic ligands incorporating 1,3-oxazine rings in their skeleton (Tomasulo *et al*., 2006). The addition of base determines the formation of coloured compounds called chromophores, that transfer energy from the excited QDs to the ligands. This process results in a decrease of the quantum yield (Fig. 11.6). On the other hand, the addition of acid controls the formation of a different chromophore that is not able to receive the excitation energy of the QDs, resulting in an increase of the quantum yield. The modulation of this reversible switch of the luminescence is thus very promising for the design of sensing devices towards other

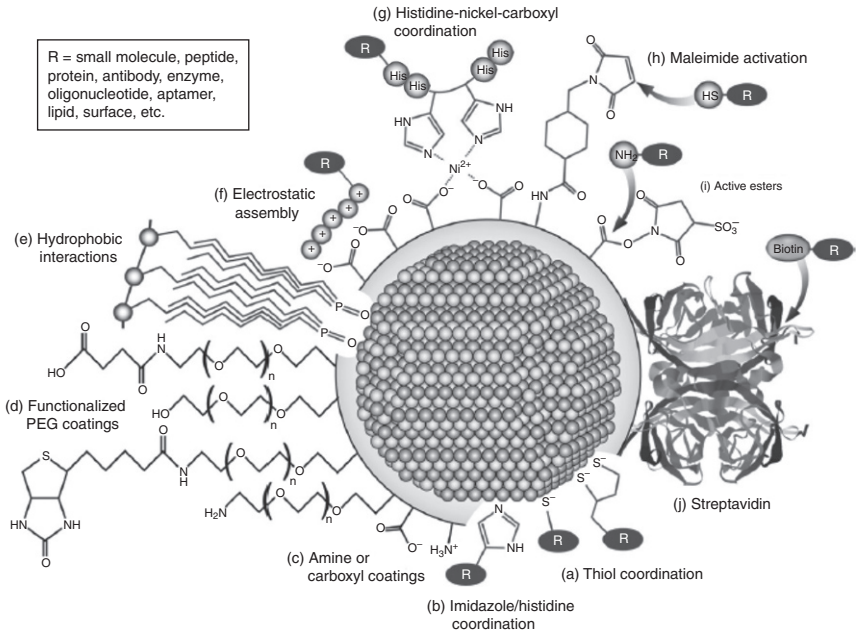

11.5 An illustration of some selected surface chemistries and conjugation strategies that are applied to QDs. (*Source:* From Algar *et al.*, 2010.) The grey periphery of the QD represents a general coating. This coating can be associated with the surface of the QD via ligand coordination (for example monodentate (a) or bidentate thiols (b) groups) or hydrophobic interactions (e). The surface functionalities offer water solubility by the display of amine or carboxyl groups (c) or functionalized polyethylene glycol (PEG) (d). Common strategies for bioconjugation include thiol modifications (a), imidazole/histidine coordination (b), electrostatic association with the coating (f), nickel mediated assembly of polyhistidine to carboxyl coatings (g), maleimide activation and coupling (h), active ester formation and coupling (i) or biotin-labelling and streptavidin–QD conjugates (j). Figure not to scale.

analytes. Other pH-sensitive ligands have also been successfully used in the construction of QD-based pH-sensing systems such as squaraine dye (Snee *et al.*, 2006), thioalkyl groups (Susha *et al.*, 2006), mercaptoacetic acid (Liu *et al.*, 2007), mercaptopropionic acid (Yu *et al.*, 2007; Wang *et al.*, 2008) or mercaptosuccinic acid (Huang *et al.*, 2007).

There are many different compounds that can be used as surface capping agents for the QDs, with the thioalkyl acid ligands being the most widely used ones. This capability opened the way for using QDs in ion sensing via analyte-induced changes in their photoluminescence. As the self-assembly proceeds via metal–thiol affinity interactions, the carboxyl groups are exposed to the surrounding environment. As such, the ligand

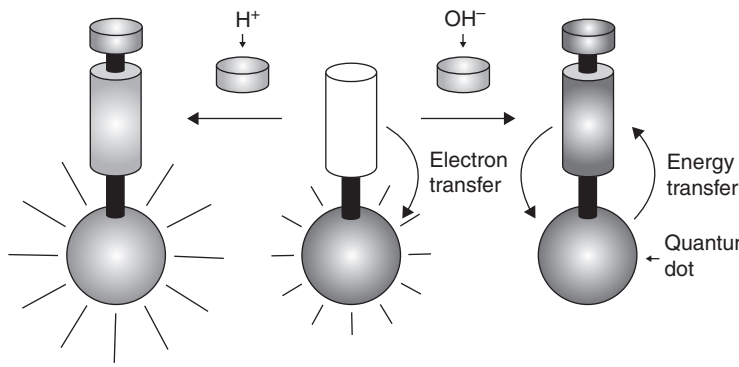

11.6 The influence of acid or base on CdSe/ZnS QDs capped with pH-sensitive organic ligands incorporating 1,3-oxazine rings in their skeleton. (*Source:* From Tomasulo *et al.,* 2006.)

plays a double role: it increases the water solubility of the QDs, and represents the sensing moiety for ions. As the ligand interacts with the ions in solution, there is an induced strong fluorescence quenching. This effect can be attributed to inner-filter effects, non-radiative recombination pathways and electron transfer processes (Wang *et al*., 2007), or to passivation of trap states or defects on the surface of the QDs (Moore and Patel, 2001).

Based on this simple idea, optical sensors for the detection of ions such as mercury (Hg^{2+}) or zinc (Zn^{2+}), based on the conjugation of calixarenes onto the surface of CdSe/ZnS QDs (Li *et al*., 2007) have been developed. In this way, the detection of mercury ions in acetonitrile with high sensitivity was possible. The selective sensing of Hg^{2+} was also achieved based on the fluorescence resonance energy transfer (FRET) between thioglycolic acid-capped CdTe QDs as donors and butyl-rhodamine B as acceptor. The presence of the surfactant cetyltrimethylammonium bromide proved to be very important, since it aids in increasing the FRET efficiency (Li *et al*., 2008). More details regarding the fluorescence resonance energy transfer process, or FRET, will be given further down. Efficient Zn^{2+} sensing was developed based on another optical process called photoinduced electron transfer (PET). In this case, azamacrocycles were covalently linked via an amide bond to mercaptopropionic acid-capped CdSe/ZnS QDs (Ruedas-Rama and Hall, 2008). Azamacrocycles are a class of nitrogen-containing analogues to crown ethers that can complex zinc ions with a high binding constant. In the absence of Zn^{2+}, the photogenerated hole on the QD is transferred to an energy level on the ligand and becomes trapped, thus preventing the recombination with the QD. This leads to charge separation and, as a consequence, the emission of the QDs is turned off. In the

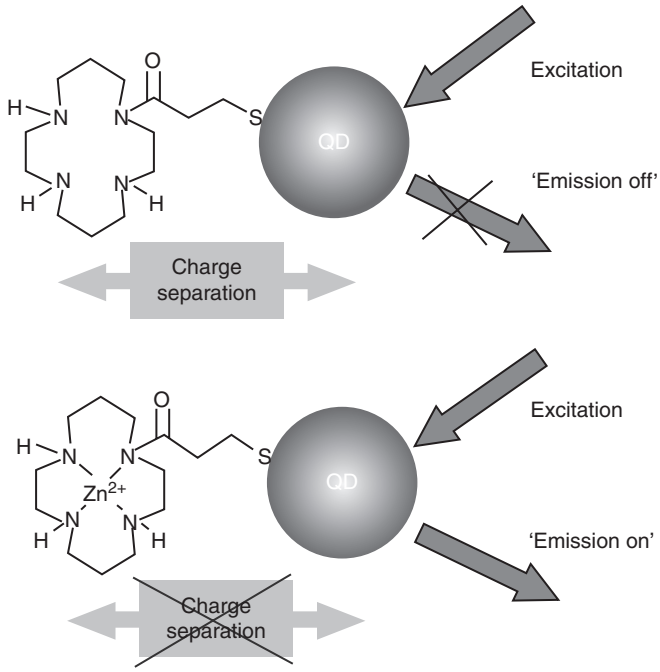

11.7 Schematic of the on–off switching of the QDs' emission in the presence/absence of the Zn^{2+} metal ion. (*Source:* From Ruedas-Rama and Hall, 2008.)

presence of Zn^{2+}, the energy level of the ligand is no longer available and the emission is again turned on (Fig. 11.7).

Larger charged ions have also been detected based on this simple PET-based platform. For example, tetrabutylammonium salts of fluoride, chloride and acetate were detected with a method based on CdSe/ZnS QDs capped with a charge neutral thiourea receptor (Callan *et al*., 2008). The selective multi-analyte sensing of silver (Ag^{+}) and copper (Cu^{2+}) (Gattás-Asfura and Leblanc, 2003) has been achieved with CdS QDs coated with Gly–His–Leu–Leu–Cys penta-peptide. In addition, core/shell CdSe/ZnS QDs conjugated with a Schiff base (2-[(2-mercaptophenylimino)methyl]phenol) has allowed for the chromogenic selective detection of copper (Cu^{2+}) and iron (Fe^{3+}) simultaneously in semi-aqueous solution (Singh *et al*., 2008).

The zinc ion was also detected using CdSe QDs functionalized with a cation-selective carrier, namely the tetrapyridyl-substituted porphyrin (Frasco *et al*., 2010). The porphyrin ion carrier is able to coordinate with the Cd atoms of the CdSe QDs through the Lewis basic pyridyl groups (Fig. 11.8). Addition of zinc ions into the solution leads to their coordination with the porphyrin capping of the QDs. It is shown that this interaction strongly

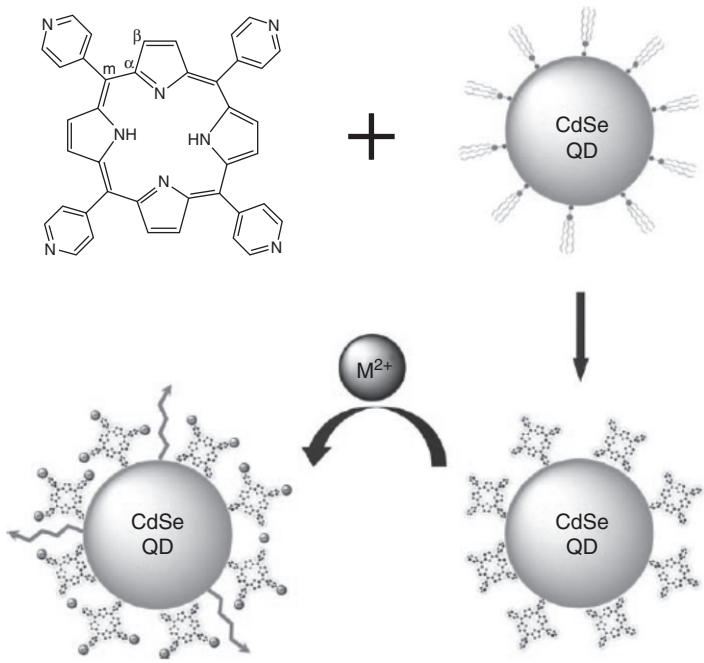

11.8 Schematic of the porphyrin–QD detection system of metal ions. Functionalization of fluorescent QDs with a tetra-pyridyl-porphyrine and direct metal sensing. (*Source:* From Frasco *et al.*, 2010.)

contributes to the increase in the fluorescence efficiency of CdSe, thus providing a highly fluorescent and selective nanosensor system for the detection of zinc ions from organic media.

11.4.2 Detection of organic compounds

Organic compounds, including drugs, pesticides, pollutants, explosives, food additives and others, must be monitored regularly as they may pose a threat to human health, public safety and the environment. Fluorescent QDs have been shown to be suitable for a rapid and sensitive detection of such analytes, thus extensive research has been carried out for this purpose. Organophosphoric pesticide residues were detected with the help of CdTe QDs coordinated with dithizone. In basic solutions, dithizone quenches the fluorescence of the QDs. The addition of organophosphorothioate pesticides results in the replacement of the dithizone ligands by the product of hydrolysis of the pesticide. As a consequence, the fluorescence of the QDs is re-established (Zhang *et al.*, 2010). The response time of the sensor to the pesticide is very fast, with an instantaneous fluorescence turn on and with

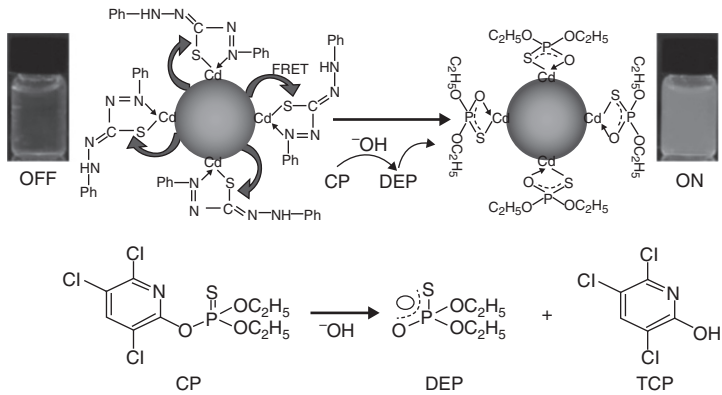

11.9 Pesticide detection. The fluorescence of CdTe QDs is quenched by coordination with dithizone and subsequently turned on with the replacement of dithizone by diethylphosphorothioate (DEP) ligand. Schematic of chlorpyrifos (CP) hydrolysis to DEP and trichloro-2-pyridinol (TCP) in basic media. (*Source:* From Zhang *et al.*, 2010.)

a limit of detection as low as ~0.1 nM (Fig. 11.9). Other pollutants, such as the herbicide 2,4-dichlorophenoxyacetic acid (Vinayaka *et al.*, 2009) and the insecticide paraoxon (Ji *et al.*, 2005), have also been successfully determined with the help of QDs and fluoro-immunological techniques.

Nitroaromatic compounds like trinitrotoluene (TNT) are dangerous to humans and toxic to the environment, and this is why their detection even in trace amounts is of crucial interest for the society. QD-based biosensing systems have been proposed for the detection of some of these species with excellent results. Acid-base pairing electrostatic interactions has been the basis for the development of these sensors. TNT binds selectively the amine-capped QDs and, as a result, there is an electron transfer between the electron-rich amino ligands and the electron-deficient aromatic rings of TNT. This electron transfer affects the photoluminescence signal of the QDs. For example, manganese (Mn^{2+}) doped ZnS QDs with amino capping have been used for the detection of TNT (Tu *et al.*, 2008) down to 1 nM in solutions or even parts-per-billion (ppb) in the atmosphere (Fig. 11.10). It has been shown that, even in such small amounts, the presence of TNT produces the immediate quenching of the strong orange QDs' photoluminescence.

TNT has also been detected by a very ingenious method involving the attachment of anti-TNT specific antibody fragments to the surface of hydrophilic CdSe/ZnS QDs via metal-affinity coordination. Subsequently, a dye-labelled TNT analogue immobilized in the antibody binding site quenches the photoluminescence of the QDs via proximity-induced FRET (Goldman *et al.*, 2005). Modifications of the ratio dye-labelled analogue: QDs provided an insight into how the antibody fragments self-assemble on the QD. It was

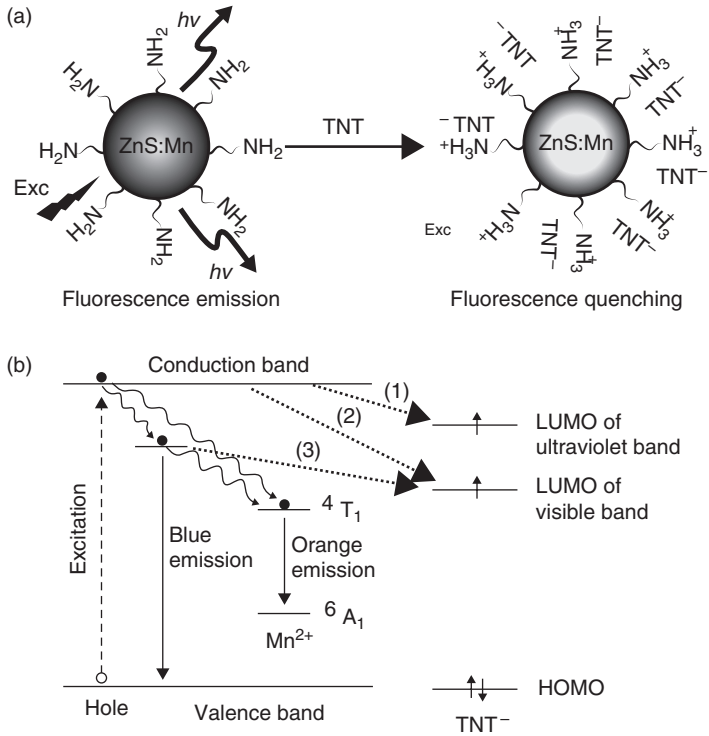

11.10 Schematic of the amine-capped ZnS-Mn^{2+} sensor for the detection of TNT (a) and the mechanism of fluorescence quenching by the charge transfer from nanocrystals to TNT analyte (b). (*Source:* From Tu *et al.*, 2008.)

discovered that the addition of soluble TNT resulted in the displacement of the dye-labelled analogue, eliminating FRET and resulting in a concentration-dependent recovery of QD photoluminescence.

The need for selective organic compounds detection is continuous, but due to the weak nature of the interactions involved, their recognition presents a greater challenge than recognition of charged ionic species. Fortunately, the constant development of new nanomaterials, such as semiconductor QDs, provides the research community with new sensitive and selective tools.

11.4.3 Förster (fluorescence) resonance energy transfer (FRET) biosensors

One of the most promising optical detection techniques is based on the fluorescence (Förster) resonance energy transfer (or FRET) technique. This is a non-radiative process that relies on the distance-dependent transfer of

energy from a donor (usually a fluorophore) found in an excited state, to a proximal acceptor found in its ground state. The donor is excited with incoming light at a certain wavelength and, as a consequence, emits energy that is absorbed by the acceptor. The rate of energy transfer is highly dependent on many factors, such as the extent of the donor–acceptor spectral overlap, the relative orientation of the transition dipoles and, most importantly, the distance between the donor and acceptor molecules (usually 10–100 Å) (Sapsford *et al*., 2006). The energy transfer from the donor to the acceptor results in a decrease of the fluorescent emission of the donor and an increase in the fluorescent emission of the acceptor.

QDs have broad absorption spectra and large Stokes shifts. This means that they can be excited at wavelengths far from their emission wavelengths. In addition, size tuning allows for the fine tuning of their spectral overlap to specific systems. QDs have a broad absorption and can thus be excited at almost any wavelength below their emission band. For this reason, an excitation wavelength can be chosen that corresponds to the absorption minimum of the acceptor so that direct excitation is minimized. The possibility of QDs to act as energy acceptors in FRET assays has been investigated quite extensively (Willard *et al*., 2001; Clapp *et al*., 2005) (Fig. 11.11). For example, two proteins, one attached to CdSe-ZnS QDs and the other attached to an organic acceptor dye, have been used for this purpose. The specific interaction of the two proteins results in the decrease of the QDs' fluorescence and the strong enhancement of the dyes' fluorescence.

FRET represents a simple and effective detection method. It is for this reason the basis of a large number of studies relying on specific protein binding processes (Willard *et al*., 2001; Medintz *et al*., 2003) (Fig. 11.12), antibodies (Nikiforov and Beechem, 2006; Kattke *et al*., 2011) or DNA aptamer hybridization (Bagalkot *et al*., 2007; Freeman *et al*., 2009; Chi *et al*., 2011) in order to bring the donor and acceptor into close proximity. Both single- and multicolour FRET assays have been reported (Algar and Krull, 2007). In the multicoloured schemes, the different ligands act relatively independently of each other, but due to non-specific adsorption processes, these optical detection schemes can provide reduced sensitivities compared to the single-colour system (Fig. 11.13). This problem was solved with the successful utilization of an intercalating acceptor dye. These highly sophisticated monitoring systems are used for monitoring the dynamics of DNA replication and telomerization (Patolsky *et al*., 2003). For this, oligonucleotide-modified QDs are incubated with a mixture of organic dye-labelled deoxyribonucleotides in the presence of telomerase or polymerase and, as the telomerization or replication advances, there is a constant decrease of the QD fluorescence and a concomitant increase of the dye's emission due to FRET processes.

The use of aptamers in QD-based analyses is also an area of continuous advancement. Recently, the first QD-aptamer bioprobe for FRET-based

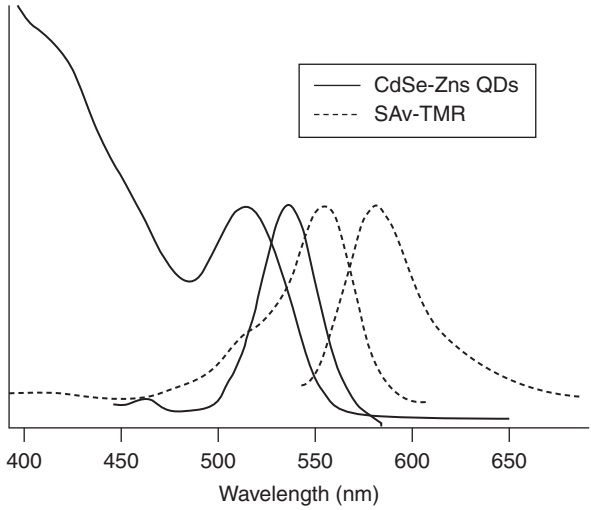

11.11 Normalized absorption and emission spectra of pure solutions of biotinylated bovine serum albumin (bBSA) conjugated CdSe-ZnS QDs and tetramethylrhodamine-labelled streptavidin (SAv-TMR). (*Source:* From Willard *et al.*, 2001.)

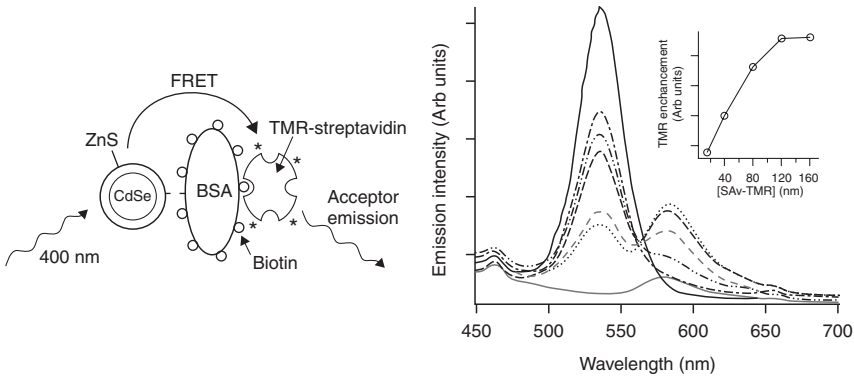

11.12 Schematic of the FRET binding assay between the biotinylated bovine serum albumin (bBSA) conjugated CdSe-ZnS QDs and tetramethylrhodamine-labelled streptavidin (SAv-TMR) (a). Evolution of the FRET assay through fluorescence emission spectra from solutions containing ~15 nM QD-bBSA and different concentrations of SAv-TMR (excitation wavelength 400 nm). The inset displays the enhanced TMR fluorescence intensity at 585 nm from the QD-bBSA/SAv-TMR solutions as a function of SAv-TMR concentration. (*Source:* From Willard *et al.*, 2001.)

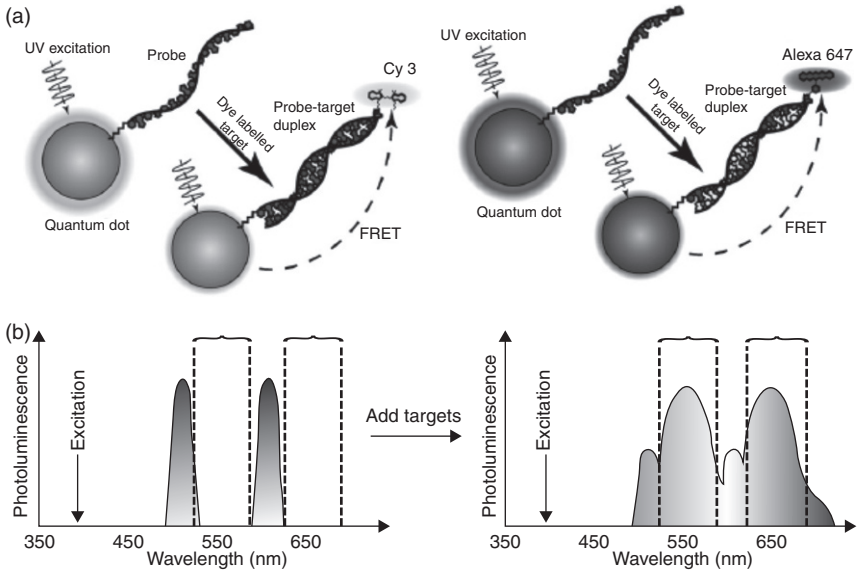

11.13 The proposed FRET mechanism for nucleic acid detection using a two-colour scheme with simultaneous and efficient excitation of green and red QDs (dyes used: Cy3 and Alexa647) in solution (a). A cartoon of the expected emission profiles of the QDs. (*Source:* From Algar and Krull, 2007.)

sensing of thrombin was developed (Levy *et al*., 2005). For this, QDs are conjugated with an anti-thrombin aptamer and an oligonucleotide quencher. When the oligonucleotide quencher hybridizes with its complementary strand, it causes the disruption of the aptamers' structure. The introduction into the system of the target protein thrombin results in the displacement of the quencher and formation of a quadruplex conformation of the aptamer, and a concomitant increase in the fluorescence of the QDs. The practically unlimited number of aptamers allows for an extensive number of possible applications in analytical systems.

The on–off state switching ability of the FRET phenomenon can also be achieved upon binding of the probe molecule leading to dislocation of the acceptor dye (Chen *et al*., 2008), hybridization with dark quenchers (Kim *et al*., 2009) or even configurations using both a dye acceptor and a dark quencher (Zhang and Johnson, 2009).

One major challenge in analytical chemistry is multiplex sensing of a number of analytes, with each analyte displaying a different signal. In order to meet such a challenge, an aggregative/dispersive method using aptamers as crosslinkers between gold nanoparticles (Au NPs) and streptavidin-coated QDs (Liu *et al*., 2007) for the detection of cocaine and adenosine was developed. In this method, each inorganic nanoparticle was conjugated

to an oligonucleotide sequence that was complementary to different sites of the aptamer (Fig. 11.14). The hybridization resulted in the formation of a compact structure containing both NPs species, which alters the magnitude of the fluorescence quenching by the Au NPs.

When the target analyte is introduced into the system, the 3-D structure is disrupted and the QDs fluorescence, as well as the Au NPs' plasmon resonance, is restored. In this way, simultaneous colorimetric and fluorescent detection and quantification of both molecules in one pot can be achieved.

Saccharides, such as glucose or galactose, were also used in FRET system assays. A glucose bioprobe was the basis for the development of a QD–AuNPs system based on the specific interaction of concanavalin A (ConA) and β-cyclodextrin (β-CD) (Tang *et al*., 2008). The proximity

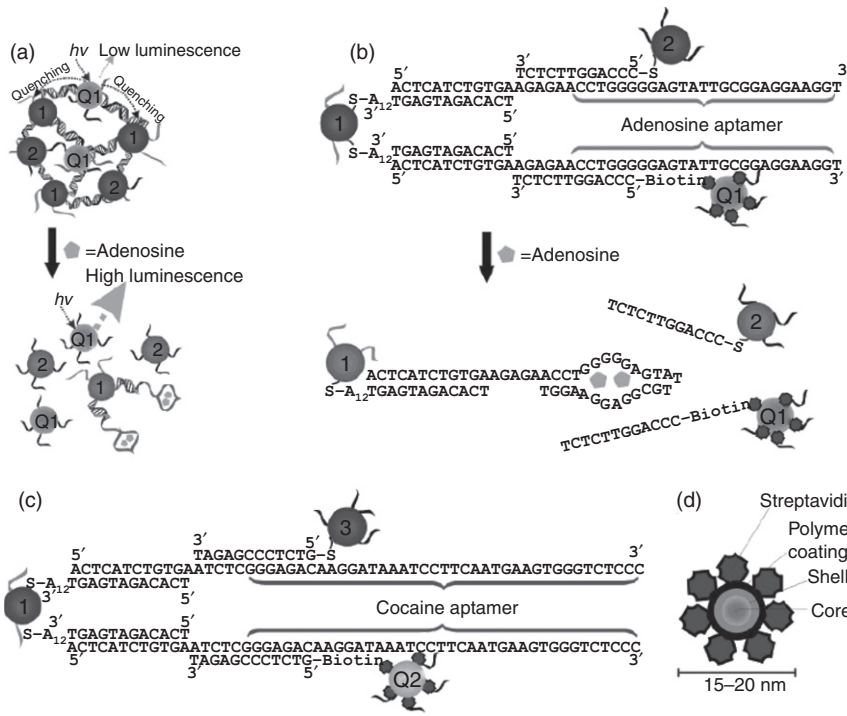

11.14 QD-encoded aptamer-linked nanostructures for multiplex detection. (a) Assembly of QDs and Au NPs with the adenosine aptamer DNA, resulting in quenched QD emission. Addition of adenosine disassembles the aggregates and restores the fluorescence of the QDs. (b) and (c) the DNA sequences and nanoparticle linkages and modifications for the adenosine sensor and the cocaine sensor respectively. (d) Schematic of the overall structure of the QDs used in this work. (Q1 and Q2 = QDs, 1, 2 and 3 = gold nanoparticles) (Q1 emits at 525 nm and Q2 emits at 585 nm). (*Source:* From Liu *et al*., 2007.)

induced by the interaction of the QD–ConA and the AuNP–β-CD conjugates resulted in fluorescence quenching. On the other hand, the presence of glucose leads to its competition with β-CD for the ConA binding sites and the restoration of the QDs' fluorescence proportional to the glucose concentration. The biosensor constructed in this was proved to be successful in retaining its function in human serum.

11.4.4 Detection of proteins and enzymatic activities

FRET is a useful tool for both the identification of proteins and determination of their activities. Due to the high importance of several enzymes and proteins in the biomedical field, they have been intensively studied in conjunction with QDs for the development of FRET systems. For example, a system for the detection of protease activity by conjugating Au NPs with QDs through a protease degradable peptide has been developed (Chang *et al*., 2005). This system can detect the presence of micrococcal nuclease (MNase), which is an extracellular nuclease of *Staphylococcus aureus*. Mono-maleimide functionalized Au NPs were covalently linked to the sulfhydryl group on the cysteine residue of the peptide-modified QDs, leading to the formation of a nano-structure that brings the two NPs into close proximity to each other. This close proximity provides a strong fluorescence quenching of the QDs. When the protease is introduced into the test solution, it cleaves the protein sequence, the Au NPs are no longer found in the vicinity of the QDs, and thus the fluorescence of the QDs is regained. Green fluorescent QDs and MNase degradable oligonucleotides labelled with a fluorescent die were used for the construction of a similar biosensor (Huang *et al*., 2008). Upon conjugation of the oligonucleotide to the surface of the QDs, there is an intense colour change of the sensing element from green to orange-red. The presence of the MNase resulted in the cleavage of the oligonucleotide and the regaining of the systems' initial green fluorescence.

Recently the presence of caspases, a class of essential enzymes involved in programmed cell death, was detected using a similar methodology (Boeneman *et al*., 2009). The idea is to take a fluorescent protein, mCherry in this case, and to modify it in order to express a target peptide sequence with a caspase 3 cleavage site and a histidine tag. The protein is attached to the surface of the QDs through the histidine tag, thus creating a FRET system with the energy flowing from the QDs to the fluorescent mCherry. This energy flow is disrupted when caspase is introduced into the system, due to its cleavage of the linker.

Similarly, the activity of the casein kinase (CK2), an enzyme that plays key roles in signal transduction and regulation of intracellular processes, or

of the alkaline phosphatase (ALP), could be selectively measured with the help of different-sized CdSe/ZnS QDs linked to a serine-containing peptide (Freeman *et al*., 2010). The CK2 catalyses the phosphorylation of the peptide, the newly created phosphorylated site allowing for the attachment of a dye-labelled antibody and thus generating an energy transfer from the QDs to the dye. Likewise, the hydrolytic activity of ALP was followed using CdSe QDs modified with phosphotyrosine. The presence of tyrosinase triggers a cascade of reactions by cleaving the phosphotyrosine to tyrosine units. The newly formed tyrosine units are further oxidized by O_2/tyrosinase to a respective dopaquinone product which quenches the fluorescence of the QDs. The proposed methods are noteworthy, in particular the modification of different-sized QDs with peptide substrates specific for different kinases providing an attractive approach for their multiplexed analysis.

A system with obvious applications in sensing, imaging, immunoassay, and other diagnostics applications was obtained through the use of newly designed maltose binding proteins based on *Escherichia coli*. These maltose binding protein-basic leucine zipper (MBP-zb) fusion proteins (Mattoussi *et al*., 2000) are able to bind onto the oppositely charged surface of QDs through electrostatic interactions. This method presents the advantage of avoiding a large number of steps for conjugating the biomolecule to the surface of the QDs, the conjugates being ready for use within a few minutes. On the other hand, the cloning and preparation of the protein is time consuming and requires specific techniques and instrumentation. The self-assembled conjugation approach described can be applied to a number of different nanoparticle systems. It can also be employed with other variants of engineered recombinant proteins, for use in the sensitive detection of reagents, for use in cell surface labelling and intracellular tracking studies, and for a variety of other imaging applications (Mattoussi *et al*., 2000) (Fig. 11.15).

In another study, recombinant proteins have been identified and isolated with the help of immobilized metal ion clusters using a nitrilotriacetic acid (NTA)-chelator (Bae *et al*., 2009). For this purpose, highly luminescent CdTe/CdS QDs were conjugated with nickel–NTA (Ni-NTA), via metal chelating adsorbents. These clusters target selectively the 6× histidine (His)-tagged proteins due to the Ni-NTA moiety's high affinity for this His tag. This technique is extensively used for purification, immobilization, and detection of recombinant proteins. It is believed that this approach will provide a more convenient methodology for the intracellular localization of histidine-tagged protein, as compared with current methods (Bae *et al*., 2009). Similarly, the use of mercaptoundecanoic acid-modified CdSe/ZnS QDs can be employed for the direct detection of acetylcholinesterase activity. The enzyme is conjugated to the surface of the QDs, and further covered with a biomimetically synthesized silica shell (Buiculescu *et al*., 2010) in order to ensure its protection from proteases. The enzyme cleaves its substrate,

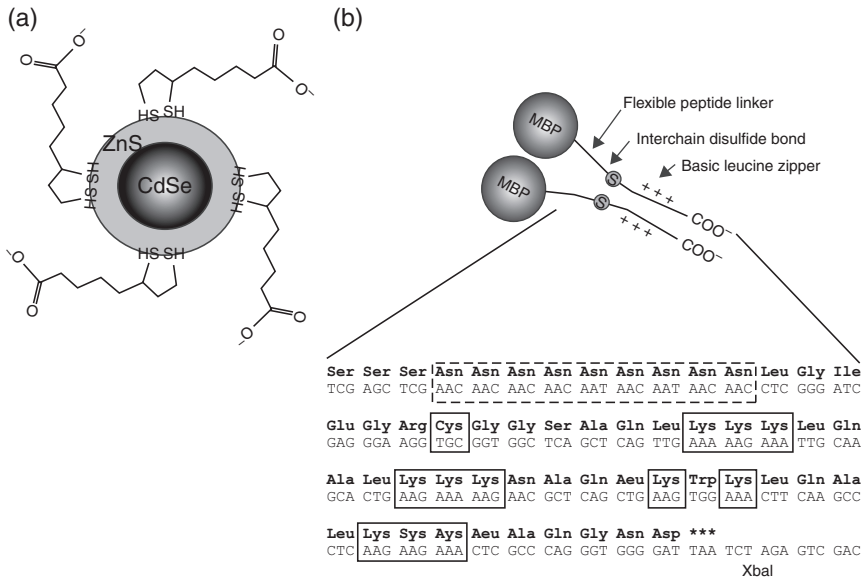

11.15 (a) Schematic of the CdSe-ZnS core–shell nanoparticle with dihydrolipoic acid surface capping groups; (b) cartoon of the maltose binding protein-basic leucine zipper (MBP-zb) fusion protein homodimer with detail showing the nucleotides and the primary amino acid sequences of the C-terminal basic leucine zipper interaction domain. (*Source:* From Mattoussi *et al.*, 2000.)

acetylcholine chloride, determining a drop in the pH of the surrounding environment and subsequently, the modification of the fluorescence intensity of the pH-sensitive QDs.

11.4.5 Nucleic acid detection

As mentioned in the section dedicated to the FRET mechanism, nucleic acid detection is a field that has benefited enormously from the use of QDs based methods. The basis for the development of the DNA sensing approaches has been the specificity of the hybridization process. Most reports focus on fluorescent detection of the targets after hybridization with a QD-conjugate probe oligonucleotide or on the use of FRET processes between two QDs, a QD and a fluorophore, or finally the quenching of the QDs fluorescence emission by metallic gold NPs.

Multicolour targeting of oligonucleotides based on the selective hybridization of oligonucleotides has been achieved (Gerion *et al.*, 2002) by conjugating four different single-stranded DNA sequences onto QDs of different sizes, which implicitly emit light at different wavelengths. All conjugates

are combined in one solution, and the mixture is then passed over a substrate with immobilized complementary single-stranded DNA (ss-DNA). The Watson–Crick interactions between the immobilized ss-DNA and the DNA-nanocrystal conjugates allows for the sorting of the QDs and probing by fluorescence confocal microscopy. These results are very important for biomedical applications, permitting for gene mapping of combed DNA, with resolutions below a few kilobases (Gerion *et al*., 2002).

The FRET mechanism between QDs and organic dyes has been successfully applied in the study of RNA-peptide interaction by employing the regulatory protein Rev in conjunction with the Rev responsive element (RRE). The binding between the two is essential for the expression of two HIV structural genes and for the replication of the virus (Zhang and Johnson, 2006). The specific interaction between biotinylated RRE RNA and cyanine dye-labelled Rev peptide originated a complex that is then assembled with streptavidin-QDs (Fig. 11.16). In this way the QDs function both as nanoscaffold and FRET donor, and the obtained nanosensor can be used to study the effect of inhibitors upon the Rev-RRE interaction and may have a wide applicability in the development of new drugs against HIV-1 infection (Zhang and Johnson, 2006).

Fluorescent *in situ* hybridization (FISH) is another method taking advantage of the QDs and their conjugates with oligonucleotides strands,

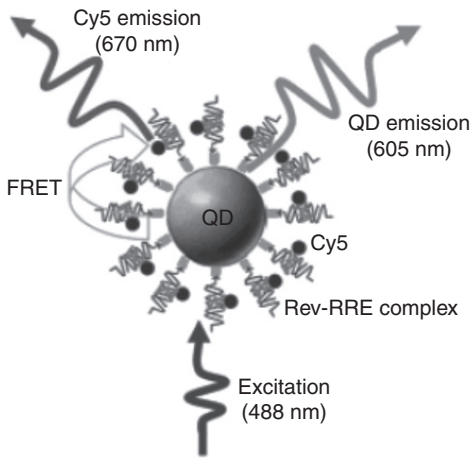

11.16 Schematic of the nanosensor based on the interaction between the Rev protein and the RRE. The binding of a Cy5-labelled Rev to a biotinylated RRE RNA gives rise to a Rev-RRE complex that is conjugated to the surface of QDs to form through specific streptavidin-biotin binding. Upon light excitation, a FRET phenomenon takes place with the energy flowing from the QDs towards the Cy5 dye. (*Source:* From Zhang and Johnson, 2006.)

the method being based on the specific Watson–Crick base interactions. Hydroxyl-terminated CdSe/ZnS–oligonucleotide conjugates are obtained via carbamate linkage and used to follow the *in situ* chromosome abnormalities or mutations. For this, a 'Y-specific' sequence was used to conduct FISH experiments with sperm cells (Pathak *et al*., 2001). Half of these cells contain a Y chromosome and are thus hybridizing with the oligonucleotide–QD conjugates. Multiplexed studies based on FISH detection were reported by Chan *et al*. (2005) who studied specific mRNA transcripts with the help of fluorescent QDs. Streptavidin modified QDs were specifically bound to biotinylated DNA probes. Subsequently new protocols were developed for the combined direct QD-FISH and QD-immunohistochemical labelling within the same neurons as well as for simultaneous study of the subcellular distribution of multiple mRNA targets (Chan *et al*., 2005). This technique was validated in mouse brainstem sections.

Electrochemical biosensors based on the assembly of nucleotide-crosslinked CdS QDs arrays on surfaces have been investigated (Xu *et al*., 2006). Nucleotides are known to form specific hydrogen-bonding by themselves and this property is then used for bridging the layers, with the resulting structures proving to be highly stable. The specific guanine–cytosine (G–C) and adenine–tyrosine (A–T) bonding generate photocurrents that increase linearly with the number of aggregated layers, providing an efficient tunnelling interface for transporting conduction-band electrons to the electrode.

11.5 Conclusion and future trends

QDs are unique materials, with extraordinary electronic and optical properties. Since their discovery they have been used in numerous applications, and have been studied in great depth, making them one of the most prolific nanomaterials. These colourful nanocrystals have a broad variety of applications that include their use as a new type of tuneable fluorescent probes as well as active components in nanostructure-biomolecule complexes. Various optical transduction schemes have already been successfully explored for sensing of a wide range of molecules, allowing low levels of detection and reduced interference of other compounds in complex samples. Currently a reality, multiplex detection is an ever-expanding research tool for QDs in optical arrays. Despite their toxicity, which limits their applications for *in vivo* diagnostics, they are still at this time leading the way in quantum nanomaterial discoveries and applications. As the scientific world discovers new ways to manipulate and control their properties, combined with continuous progress in their synthesis, conjugation and functionalization for increased stability, sensitivity and binding specificity, we will experience a

continuous increase of QD-nanoassemblies incorporated in chemical sensors, biosensors, as well as in other optical and electronic detection devices.

11.6 References

Algar, W. R. and Krull, U. J. (2007) 'Towards multi-colour strategies for the detection of oligonucleotide hybridization using quantum dots as energy donors in fluorescence resonance energy transfer (FRET)', *Anal. Chim. Acta*, **581**, 193–201.

Algar, W. R., Tavares, A. J. and Krull, U. J. (2010) 'Beyond labels: A review of the application of quantum dots as integrated components of assays, bioprobes, and biosensors utilizing optical transduction', *Anal. Chim. Acta*, **673**, 1–25.

Bae, P. K., Kim, K. N., Lee, S. J., Chang, H. J., Lee, C. K. and Park, J. K. (2009) 'The modification of quantum dot probes used for the targeted imaging of his-tagged fusion proteins', *Biomaterials*, **30**, 836–842.

Bagalkot, V., Zhang, L., Levy-Nissenbaum, E., Jon, S., Kantoff, P. W., Langer, R. and Farokhzad, O. C. (2007) 'Quantum dot-aptamer conjugates for synchronous cancer imaging, therapy, and sensing of drug delivery based on bi-fluorescence resonance energy transfer', *Nano Lett.*, **7**, 3065–3070.

Bakalova, R., Zhelev, Z., Ohba, H. and Baba, Y. (2007) 'Quantum dot-based nanobiohybrids for fluorescent detection of molecular and cellular biological targets', in *Nanomaterials for Biosensors*, Weinheim, Wiley-VCH.

Boeneman, K., Mei, B. C., Dennis, A. M., Bao, G., Deschamps, J. R., Mattoussi, H. and Medintz, I. L. (2009) 'Sensing caspase 3 activity with quantum dot-fluorescent protein assemblies', *J. Am. Chem. Soc.*, **131**, 3828–3829.

Bruchez Jr., M., Moronne, M., Gin, P., Weiss, S. and Alivisatos, A. P. (1998) 'Semiconductor nanocrystals as fluorescent biological labels', *Science*, **281**, 2013–2016.

Buiculescu, R., Hatzimarinaki, M. and Chaniotakis, N. A. (2010) 'Biosilicated CdSe/ZnS quantum dots as photoluminescent transducers for acetylcholinesterase-based biosensors', *Anal. Bioanal. Chem.*, **398**, 3015–3021.

Callan, J. F., Mulrooney, R. C., Kamila, S. and McCaughan, B. (2008) 'Anion sensing with luminescent quantum dots-a modular approach based on the photoinduced electron transfer (PET) mechanism', *J. Fluoresc.*, **18**, 527–532.

Chan, P. M., Yuen, T., Ruf, F., Gonzalez-Maeso, J. and Sealfon, S. C. (2005) 'Method for multiplex cellular detection of mRNAs using quantum dot fluorescent in situ hybridization', *Nucl. Acid. Res.*, **33**, e161.

Chan, W. C. W. and Nie, S. (1998) 'Quantum dot bioconjugates for ultrasensitive nonisotopic detection', *Science*, **281**, 2016–2018.

Chang, E., Miller, J. S., Sun, J., Yu, W. W., Colvin, V. L., Drezek, R. and West, J. L. (2005) 'Protease-activated quantum dots', *Biochem. Biophys. Res. Co.*, **334**, 1317–1321.

Chen, Z., Li, G., Zhang, L., Jiang, J., Li, Z., Peng, Z. and Deng, L. (2008) 'A new method for the detection of ATP using a quantum-dot-tagged aptamer', *Anal. Bioanal. Chem.*, **392**, 1185–1188.

Chi, C.-W., Lao, Y.-H., Li, Y.-S. and Chen, L.-C. (2011) 'A quantum dot-aptamer beacon using a DNA intercalating dye as the FRET reporter: Application to label-free thrombin detection', *Biosens. Bioelectron.*, **26**, 3346–3352.

Clapp, A. R., Medintz, I. L., Fisher, B. R., Anderson, G. P. and Mattoussi, H. (2005) 'Can luminescent quantum dots be efficient energy acceptors with organic dye donors?', *J. Am. Chem. Soc.*, **127**, 1242–1250.

Comparelli, R., Curri, M. L., Cozzoli, P. D. and Striccoli, M. (2007) 'Optical biosensing based on metal and semiconductor colloidal nanocrystals', in *Nanomaterials for Biosensors*, Weinheim, Wiley-VCH.

Costa-Fernandez, J. M., Pereiro, R. and Sanz-Medel, A. (2006) 'The use of luminescent quantum dots for optical sensing', *Tr. Anal. Chem.*, **25**, 207–218.

Dabbousi, B. O., Rodriguez-Viejo, J., Mikulec, F. V., Heine, J. R., Mattoussi, H., Ober, R., Jensen, K. F. and Bawendi, M. G. (1997) '(CdSe)ZnS core-shell quantum dots: Synthesis and characterization of a size series of highly luminescent nanocrystallites', *J. Phys. Chem. B*, **101**, 9463–9475.

Frasco, M. F. and Chaniotakis, N. (2009) 'Semiconductor quantum dots in chemical sensors and biosensors', *Sensors*, **9**, 7266–7286.

Frasco, M. F., Vamvakaki, V. and Chaniotakis, N. (2010) 'Porphyrin decorated CdSe quantum dots for direct fluorescent sensing of metal ions', *J. Nanopart. Res.*, **12**, 1449–1458.

Freeman, R., Finder, T., Gill, R. and Willner, I. (2010) 'Probing protein kinase (CK2) and alkaline phosphatase with CdSe/ZnS quantum dots', *Nano Lett.*, **10**, 2192–2196.

Freeman, R., Li, Y., Tel-Vered, R., Sharon, E., Elbaz, J. and Willner, I. (2009) 'Self-assembly of supramolecular aptamer structures for optical or electrochemical sensing', *Analyst*, **134**, 653–656.

Gattás-Asfura, K. M. and Leblanc, R. M. (2003) 'Peptide-coated CdS quantum dots for the optical detection of copper (II) and silver (I)', *Chem. Commun.*, **21**, 2684–2685.

Gerion, D., Parak, W. J., Williams, S. C., Zanchet, D., Micheel, C. M. and Alivisatos, A. P. (2002) 'Sorting fluorescent nanocrystals with DNA', *J. Am. Chem. Soc.*, **124**, 7070–7074.

Goldman, E. R., Medintz, I. L., Whitley, J. L., Hayhurst, A., Clapp, A. R., Uyeda, H. T., Deschamps, J. R., Lassman, M. E. and Mattoussi, H. (2005) 'A hybrid quantum dot-antibody fragment fluorescence resonance energy transfer-based TNT sensor', *J. Am. Chem. Soc.*, **127**, 6744–6751.

Huang, C.-P., Li, Y.-K. and Chen, T.-M. (2007) 'A highly sensitive system for urea detection by using CdSe/ZnS core-shell quantum dots', *Biosens. Bioelectron.*, **22**, 1835–1838.

Huang, S., Xiao, Q., He, Z. K., Liu, Y., Tinnefeld, P., Su, X. R. and Peng, X. N. (2008) 'A high sensitive and specific QDs FRET bioprobe for Mnase', *Chem. Commun.*, **45**, 5990–5992.

Jaiswal, J. K., Mattoussi, H., Mauro, J. M. and Simon, S. M. (2003) 'Long-term multiple color imaging of live cells using quantum dot bioconjugates', *Nat. Biotechnol.*, **21**, 47–51.

Ji, X., Zheng, J., Xu, J., Rastogi, V. K., Cheng, T.-C., DeFrank, J. J. and Leblanc, R. M. (2005) '(CdSe)ZnS quantum dots and organophosphorus hydrolase bioconjugate as biosensors for detection of paraoxon', *J. Phys. Chem. B,* **109**, 3793–3799.

Kattke, M. D., Gao, E. J., Sapsford, K. E., Stephenson, L. D. and Kumar, A. (2011) 'FRET-based quantum dot immunoassay for rapid and sensitive detection of *Aspergillus amstelodami*', *Sensors* **11**, 6396–6410.

Kim, G.-I., Kim, K.-W., Oh, M.-K. and Sung, Y.-M. (2009) 'The detection of platelet derived growth factor using decoupling of quencher oligonucleotide from aptamer/quantum dot bioconjugates', *Nanotechnology,* **20**, 175503.

Levy, M., Cater, S. F. and Ellington, A. D. (2005) 'Quantum-dot aptamer beacons for the detection of proteins', *Chem. Biol. Chem*., **6**, 2163–2166.

Li, H., Zhang, Y., Wang, X., Xiong, D. and Bai, Y. (2007) 'Calixarene capped quantum dots as luminescent probes for Hg^{2+} ions', *Mater. Lett*., **61**, 1474–1477.

Li, J., Mei, F., Li, W.-Y., He, X.-W. and Zhang, Y.-K. (2008) 'Study on the fluorescence resonance energy transfer between CdTe QDs and butyl-rhodamine B in the presence of CTMAB and its application on the detection of Hg(II)', *Spectrochim. Acta A*, **70**, 811–817.

Liu, J., Lee, J. H. and Lu, Y. (2007a) 'Quantum dot encoding of aptamer-linked nanostructures for one-pot simultaneous detection of multiple analytes', *Anal. Chem*., **79**, 4120–4125.

Liu, Y.-S., Sun, Y., Vernier, P. T., Liang, C.-H., Chong, S. Y. C. and Gundersen, M. A. (2007b) 'pH-sensitive photoluminescence of CdSe/ZnSe/ZnS quantum dots in human ovarian cancer cells', *J. Phys. Chem. C,* **111**, 2872–2878.

Mattoussi, H., Mauro, J. M., Goldman, E. R., Anderson, G. P., Sundar, V. C., Mikulec, F. V. and Bawendi, M. G. (2000) 'Self-assembly of CdSe-ZnS quantum dot bioconjugates using an engineered recombinant protein', *J. Am. Chem. Soc.*, **122**, 12142–12150.

Mattoussi, H., Palui, G. and Na, H. B. (2012) 'Luminescent quantum dots as platforms for probing *in vitro* and *in vivo* biological processes', *Adv. Drug Deliv. Rev*., **64**, 138–166.

Medintz, I. L., Clapp, A. R., Brunel, F. M., Tiefenbrunn, T., Uyeda, H. T., Chang, E. L. Deschamps, J. R., Dawson, P. E. and Mattoussi, H. (2006) 'Proteolytic activity monitored by fluorescence resonance energy transfer through quantum-dot–peptide conjugates', *Nature Mater*., **5**, 581–589.

Medintz, I. L., Goldman, E. R., Lassman, M. E. and Mauro, J. M. (2003) 'A fluorescence resonance energy transfer sensor based on maltose binding protein', *Bioconj. Chem*., **14**, 909–918.

Michalet, X., Pinaud, F. F., Bentolila, L. A., Tsay, J. M., Doose, S., Li, J. J., Sundaresan, G., Wu, A. M., Gambhir, S. S. and Weiss, S. (2005) 'Quantum dots for live cells, *in vivo* imaging, and diagnostics', *Science,* **307**, 538–544.

Moore, D. E. and Patel, K. (2001) 'Q-CdS photoluminescence activation on Zn^{2+} and Cd^{2+} salt introduction', *Langmuir,* **17**, 2541–2544.

Murphy, C. J. (2002) 'Optical sensing with quantum dots', *Anal. Chem.*, **74**, 520A–526A.

Murray, C. B., Norris, D. J. and Bawendi, M. G. (1993) 'Synthesis and characterization of nearly monodisperse CdE (E = sulphur, selenium, tellurium) semiconductor nanocrystallites', *J. Am. Chem. Soc.,* **115**, 8706–8715.

Nikiforov, T. T. and Beechem, J. M. (2006) 'Development of homogeneous binding assays based on fluorescence resonance energy transfer between quantum dots and Alexa Fluor fluorophores', *Anal. Biochem*., **357**, 68–76.

Parak, W. J., Gerion, D., Pellegrino, T., Zanchet, D., Micheel, C., Williams, S. C., Boudreau, R., Le Gros, M. A., Larabell, C. A. and Alivisatos, A. P. (2003) 'Biological applications of colloidal nanocrystals', *Nanotechnology*, **14**, R15–R27.

Park, J., Joo, J., Kwon, S. G., Jang, Y. and Hyeon, T. (2007) 'Synthesis of monodisperse spherical nanocrystals', *Angew. Chem. Int. Ed.*, **46**, 4630–4660.

Pathak, S., Choi, S. K., Arnheim, N. and Thompson, M. E. (2001) 'Hydroxylated quantum dots as luminescent probes for in situ hybridization', *J. Am. Chem. Soc.*, **123**, 4103–4104.

Patolsky, F., Gill, R., Weizmann, Y., Mokari, T., Banin, U. and Willner, I. (2003) 'Lighting-up the dynamics of telomerization and DNA replication by CdSe-ZnS quantum dots', *J. Am. Chem. Soc*., **125**, 13918–13919.

Reiss, P., Protière, M. and Li, L. (2009) 'Core/shell semiconductor nanocrystals', *Small*, **5**, 154–168.

Ruedas-Rama, M. J. and Hall, E. A. H. (2008) 'Azamacrocycle activated quantum dot for zinc ion detection', *Anal. Chem.*, **80**, 8260–8268.

Sapsford, K. E., Berti, L. and Medintz, I. L. (2006a) 'Materials for fluorescence resonance energy transfer analysis: Beyond traditional donor–acceptor combinations', *Angew. Chem. Int. Ed.*, **45**, 4562–4588.

Sapsford, K. E., Pons, T., Medintz, I. L. and Mattoussi, H. (2006b) 'Biosensing with luminescent semiconductor quantum dots', *Sensors,* **6**, 925–953.

Singh, N., Mulrooney, R. C., Kaur, N. and Callan, J. F. (2008) 'A nanoparticle based chromogenic chemosensor for the simultaneous detection of multiple analytes', *Chem. Commun.*, **40**, 4900–4902.

Smith, A. M., Dave, S., Nie, S., True, L. and Gao, X. (2006a) 'Multicolor quantum dots for molecular diagnostics of cancer', *Expert Rev. Mol. Diagn*., **6**, 231–244.

Smith, A. M., Ruan, G., Rhyner, M. N. and Nie, S. (2006b) 'Engineering luminescent quantum dots for *in vivo* molecular and cellular imaging', *Ann. Biomed. Eng.*, **34**, 3–14.

Snee, P. T., Somers, R. C., Nair, G., Zimmer, J. P., Bawendi, M. G. and Nocera, D. G. (2006) 'A ratiometric CdSe/ZnS nanocrystal pH sensor', *J. Am. Chem. Soc.*, **128**, 13320–13321.

Susha, A. S., Javier, A. M., Parak, W. J. and Rogach, A. L. (2006) 'Luminescent CdTe nanocrystals as ion probes and pH sensors in aqueous solutions', *Colloid Surf. A,* **281**, 40–43.

Tang, B., Cao, L., Xu, K., Zhuo, L., Ge, J., Li, Q. and Yu, L. (2008) 'A new nanobiosensor for glucose with high sensitivity and selectivity in serum based on fluorescence resonance energy transfer (FRET) between CdTe quantum dots and Au nanoparticles', *Chem. Eur. J.*, **14**, 3637–3644.

Tomasulo, M., Yildiz, I., Kaanumalle, S. L. and Raymo, F. M. (2006) 'pH-sensitive ligand for luminescent quantum dots', *Langmuir,* **22**, 10284–10290.

Tu, R., Liu, B., Wang, Z., Gao, D., Wang, F., Fang, Q. and Zhang, Z. (2008) 'Amine-capped ZnS-Mn^{2+} nanocrystals for fluorescence detection of trace TNT explosive', *Anal. Chem.,* **80**, 3458–3465.

Vinayaka, A. C., Basheer, S. and Thakur, M. S. (2009) 'Bioconjugation of CdTe quantum dot for the detection of 2,4-dichlorophenoxyacetic acid by competitive fluoroimmunoassay based biosensor', *Biosens. Bioelectron.*, **24**, 1615–1620.

Wang, X., Ruedas-Rama, M. J. and Hall, E. A. H. (2007) 'The emerging use of quantum dots in analysis', *Anal. Lett.*, **40**, 1497–1520.

Wang, Y.-Q., Ye, C., Zhu, Z.-H. and Hu, Y.-Z. (2008) 'Cadmium telluride quantum dots as pH-sensitive probes for tiopronin determination', *Anal. Chim. Acta*, **610**, 50–56.

Willard, D. M., Carillo, L. L., Jung, J. and Van Orden, A. (2001) 'CdSe-ZnS quantum dots as resonance energy transfer donors in a model protein-protein binding assay', *Nano Lett.*, **1**, 469–474.

Xu, J. P., Weizmann, Y., Krikhely, N., Baron, R. and Willner, I. (2006) 'Layered hydrogen-bonded nucleotide-functionalized CdS nanoparticles for photoelectrochemical applications', *Small,* **2**, 1178–1182.

Yu, D., Wang, Z., Liu, Y., Jin, L., Cheng, Y., Zhou, J. and Cao, S. (2007) 'Quantum dot-based pH probe for quick study of enzyme reaction kinetics', *Enzyme Microb. Technol.*, **41**, 127–132.

Zhang, C.-Y. and Johnson, L. W. (2006) 'Quantum-dot-based nanosensor for RRE IIB RNA-Rev peptide interaction assay', *J. Am. Chem. Soc.*, **128**, 5324–5325.

Zhang, C.-Y. and Johnson, L. W. (2009) 'Single quantum-dot-based aptameric nanosensor for cocaine', *Anal. Chem.*, **81**, 3051–3055.

Zhang, K., Mei, Q., Guan, G. J., Liu, B. H., Wang, S. H. and Zhang, Z.P. (2010) 'Ligand replacement-induced fluorescence switch of quantum dots for ultrasensitive detection of organophosphorothioate pesticides', *Anal. Chem.,* **82**, 9579–9586.

Zhelev, Z., Bakalova, R., Ohba, H., Jose, R., Imai, Y. and Baba, Y. (2006) 'Uncoated, broad fluorescent, and size-homogeneous CdSe quantum dots for bioanalyses', *Anal. Chem*., **78**, 321–330.

Zhelev, Z., Ohba, H., Bakalova, R., Jose, R., Fukuoka, S., Nagase, T., Ishikawa, M. and Baba, Y. (2005) 'Fabrication of quantum dot-lectin conjugates as novel fluorescent probes for microscopic and flow cytometric identification of leukemia cells from normal lymphocytes', *Chem. Commun.*, **15**, 1980–1982.

12

Nanosensors and other techniques for detecting nanoparticles in the environment

Y. PICÓ, Universitat de València, Spain and V. ANDREU, Research Center on Desertification-CIDE (CSIC-UV-GV), Spain

DOI: 10.1533/9780857096722.2.295

Abstract: Detecting nanomaterials in the environment is a demanding task, not only because of the extremely small size of the particles and their potential sequestration and agglomeration, but also because of their unique physical and chemical characteristics. The aim of this review is to recommend a way forward on tackling the challenge of engineered nanomaterial detection in the environment. An overview will be presented of the available analytical techniques used for the detection and characterization of nanoparticles in environmental matrices including particle-size analysis, particle-fraction concentration counts, surface-area analysis, morphology, and particle chemical composition analysis. Sample preparation aspects, imaging techniques (electron microscopy, scanning electron microscopy, or X-ray microscopy), separation methods (e.g. flow field fractionation, electrophoresis, liquid chromatography, hydrodynamic chromatography), and detection/characterization techniques (e.g. light scattering, inductive coupled plasma, mass spectrometry) have been included. This review also introduces what is known concerning their fate, behavior, disposition, and toxicity.

Key words: nanoparticles, engineered nanoparticles, environment, analysis, separation techniques, single-particle detection.

12.1 Introduction

The European Union have recently defined nanomaterial (NM) as '… a natural, incidental or manufactured material containing particles, in an unbound state or as an aggregate or as an agglomerate and where, for 50% or more of the particles in the number size distribution, one or more external dimensions is in the size range 1–100 nm' (Anon, 2012c). This definition is based on the size of the particles because it determines that nanoparticles (NPs) exhibit greater relative surface areas than the corresponding conventional forms, which often results in higher reactivity and different surface characteristics (Aschberger *et al.*, 2011; Atha *et al.*, 2012; Eckelman *et al.*, 2012; Elzey and Grassian, 2010).

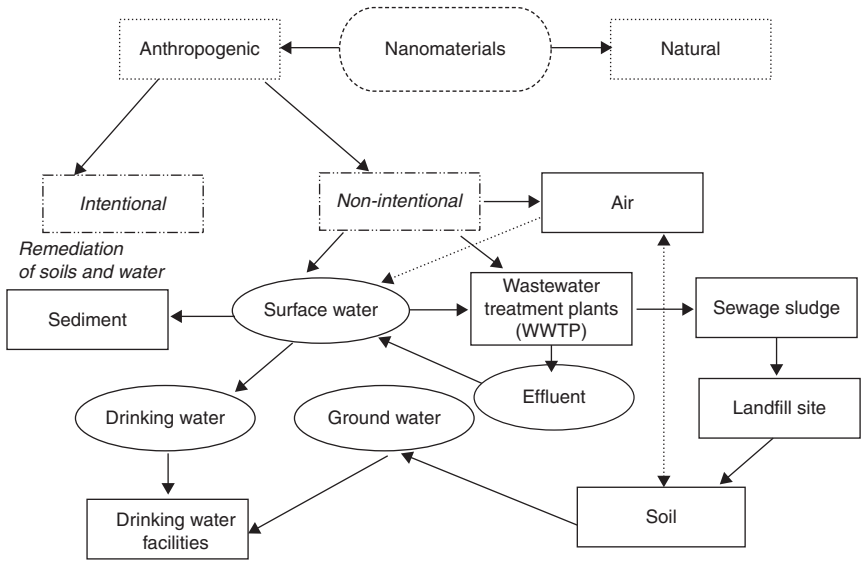

12.1 Sources and fate of NMs in the environment. (*Source*: Reproduced from Perez *et al.,* 2009 with permission of Elsevier Ltd.)

Figure 12.1 shows the different sources of NMs in the environment. NMs can occur in nature, such as clay minerals and humic acids; they can be incidentally produced by human activity, such as diesel emissions or welding fumes; or they can be specifically engineered to exhibit unique optical, electrical, physical, or chemical characteristics (Bernhardt *et al*., 2010; Chen *et al*., 2011; Coutris *et al*., 2012; Eckelman *et al*., 2012; Jiménez *et al*., 2011). Depending on their chemical and physical characteristics, the engineered nanomaterials (ENMs) exhibit greater physical strength, enhanced magnetic properties, conduction of heat or electricity, greater chemical reactivity or size-dependent optical properties (Felekis and Katsaros, 2009; Gao *et al*., 2008; Ghosh *et al*., 2011). These attributes are exploited in a variety of consumer products, such as medicines, food, cosmetics and suntan lotions, paints, and electronics, as well as applications that directly release NMs into the environment, such as remediation of polluted environments (O'Brien and Cummins, 2008, 2010).

Due to the unique characteristics of ENMs compared to other environmental contaminants, limited information concerning their transport, fate, exposure, dose, and potential effects is now available (Handy *et al*., 2008; Jiang *et al*., 2011; Kennedy *et al*., 2008; Lin *et al*., 2010; Quik *et al*., 2011). The approach for prediction of environmental concentrations through life-cycle assessment modeling requires validation through measurement of actual environmental concentrations (Gottschalk *et al*., 2010; Grieger *et al*., 2011;

Hotze *et al*., 2010; Kohler *et al*., 2008). Accurately assessing the environmental risks posed by NPs requires use of effective quantitative analytical methods to obtain the required information, many of which still have to be developed. In the last 5 years, some reviews have examined the existing information about analytical developments to assess the occurrence, fate, and behavior of NMs in the environment (Albella *et al*., 2011; Anon, 2012a; Bandyopadhyay *et al*., 2012; Brar and Verma, 2011; da Silva *et al*., 2011; Farre *et al*., 2009; Farre *et al*., 2011; Gallego-Urrea *et al*., 2011; Jiménez *et al*., 2011; Simonet and Valcarcel, 2009; Tiede *et al*., 2008; von der Kammer *et al*., 2012; Yu and Andriola, 2010). All of them conclude that engineered nanoparticles (ENPs) differ from most conventional 'dissolved' chemicals in terms of their heterogeneous distributions in size, shape, surface charge, composition, and degree of dispersion. Therefore, it is not only important to determine their concentrations, but also other characteristics, such as shape, size distribution, and chemical composition. This chapter describes some methodological aspects relating to the field of ENM analysis.

12.2 Overview of nanomaterials

ENMs encompass those NPs synthesized and modified in order to enhance their performance in several technological and industrial processes (Peralta-Videa *et al*., 2011). ENPs are often classified according to their chemical composition, occasionally complemented with a few size or morphology characteristics, due to lack of information regarding other relevant properties such as surface reactivity or mechanism of toxicity (Stone *et al*., 2010). The simplest division is between carbon-based (e.g. nanotubes and fullerenes) and mineral ENPs (e.g. Au, Ag, Fe, or TiO_2). A more detailed classification is illustrated in Fig. 12.2.

Carbon-based NMs are very stable against degradation and consequently accumulate in the environment (Farre *et al*., 2009). This group includes carbon black, fullerenes, and carbon nanotubes (CNTs) (Peralta-Videa *et al*., 2011; Stone *et al*., 2010).

Carbon black or soot is a by-product of combustion (e.g. a major constituent of car tires), and is also formed naturally during fires. Some reports confirm that stable organic matter in soils and sediments contains 5–10% of this material (Li *et al*., 2008; Peralta-Videa *et al*., 2011). Carbon black has also been demonstrated to have low potential for toxicity to aquatic organisms and has been used as a reference substance (control treatment) in studies of toxicity and ecotoxicity of CNT and fullerenes (Brausch *et al*., 2010; Lyon *et al*., 2006; Yan *et al*., 2008).

Fullerenes are molecules composed entirely of carbon, in the form of a hollow sphere, ellipsoid, or tube (Hyung *et al*., 2007). The simplest fullerene, C_{60}, is a ball made up of 60 C atoms, also known as buckminster fullerenes

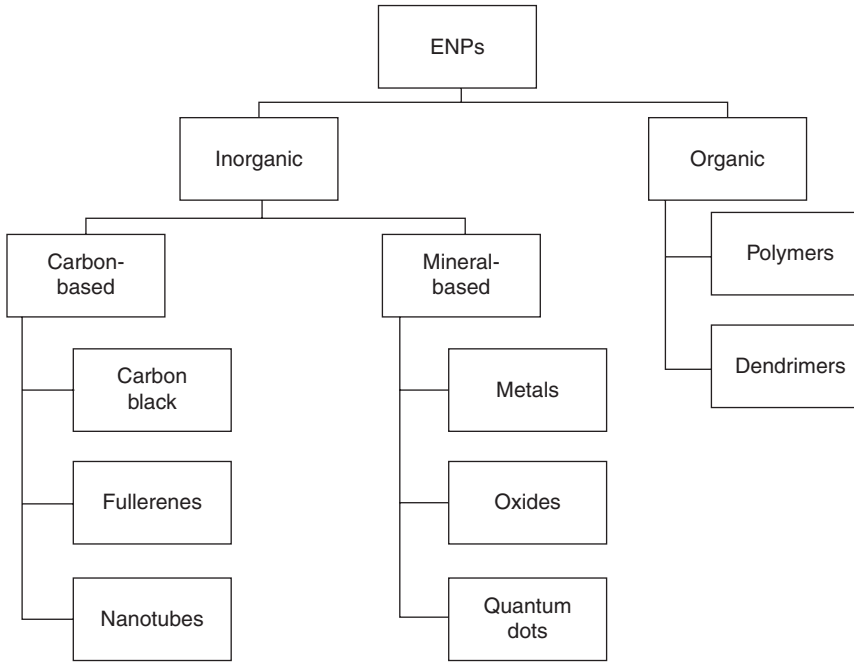

12.2 Nanomaterial classification according to their physical and chemical properties.

or 'bucky balls' (Johansen *et al.*, 2008). The next stable fullerene is C_{70} and has an oblong form (Liu *et al.*, 2009). Fullerenes are hydrophobic and soluble in organic solvents such as toluene (2.8 mg L^{-1} for C_{60}) (Wiesner *et al.*, 2008). Fullerenes may: (i) contain atoms, ions, or small clusters inside their spherical structure; (ii) their surface could be modified by functionalization (functional groups as hydroxyls are attached covalently to a C atom of the fullerene); or (iii) form highly stable hydrophilic nanosized aggregates (n–C_{60}; 100–200 nm diameter) that can exist as stable aqueous suspensions at low ionic strength (Park *et al.*, 2010).

Carbon nanotubes (CNTs) are cylindrical fullerenes consisting of rolled-up grapheme sheets that sometimes are capped at the ends by a half-fullerene sphere (Eckelman *et al.*, 2012; Farre *et al.*, 2009; Gottschalk *et al.*, 2009). They are obtained from graphite by laser ablation, or from methane or other carbon containing gases as a starting material through chemical vapor deposition (Hotze *et al.*, 2010; Koelmans *et al.*, 2009; Mattison *et al.*, 2011). CNTs are light and have high mechanical strength and conductive properties. There are two main types of nanotubes: single-walled nanotubes (SWNTs) and multi-walled nanotubes (MWNTs) (Li *et al.*, 2008; Peralta-Videa *et al.*, 2011). The former have superior mechanical strength, and thermal and electric

conductivity, compared to the latter (nanofibers are relatively short and thin, while nanoropes and nanowires are thicker and longer, up to a mm scale) (Petersen and Henry, 2012; Wiench *et al*., 2009).

Inorganic NMs comprise zero-valence NMs, oxides, and quantum dots. Zero-valence metals are typically obtained by reducing solutions of metal salts (Peralta-Videa *et al*., 2011; Tiede *et al*., 2008). Their physical properties can be controlled by varying the reduction conditions. Most applications using zero-valence NPs have involved iron NPs (for the remediation of waters, sediments, and soils), silver NPs (because of their bactericidal properties), and gold NP (due to the catalytic activity of AuNPs and their possible use in bioanalytic and medical applications) (Albella *et al*., 2011; Mitrano *et al*., 2012a, 2012b). Metal-oxide (or binary compounds when including carbides, nitrides, etc.) NPs are among the most used NMs. Relevant metal-oxide NPs are based on titanium dioxide (TiO_2), aluminum oxide (Al_2O_3), iron oxides (magnetite (Fe_3O_4) and its oxidized form maghemite (γ-Fe_2O_3)), zinc oxide (ZnO), cerium dioxide (CeO_2), chromium dioxide (CrO_2), molybdenum trioxide (MoO_3), bismuth trioxide (Bi_2O_3), silicon dioxide (SiO_2), and binary oxides (e.g., lithium-cobalt dioxide ($LiCoO_2$) or indium-tin oxide (LiSnO)) (Peralta-Videa *et al*., 2011; Tan *et al*., 2012; Wang *et al*., 2011a). Metal-oxide NPs can be used to optimize UV absorption and to enhance the stiffness, toughness, and probably the service life of polymeric materials.

Quantum dots (Q-dots) are fluorescent semiconductor nanocrystals, commonly made up of a 3–6 nm diameter core of CdS, CdSe, PbSe, CdHg or a range of other metals, and coated by an organic polymer (to protect against oxidation and to permit linking to biologically active moieties, such as antibodies) (Aruguete and Hochella, 2010; Ingle *et al*., 2008; Lee *et al*., 2011). Due to their small size, they can emit light (i.e. photons) with a specific wavelength that is limited by quantum confinement and determined by particle size and composition (i.e. the resulting band gap energy) (Navarro *et al*., 2011; Peralta-Videa *et al*., 2011). Within biology/medicine Q-dots are mainly used for fluorescence imaging to localize specific cells (e.g. tumor cells) (Sandin *et al*., 2012; Tervonen *et al*., 2009).

In recent years, a new structural class of macromolecules, the organic polymers, has attracted attention. These nanometer-sized, polymeric systems are hyperbranched materials having compact hydrodynamic volumes in solution and high, surface, functional group content. They may be water-soluble but, because of their compact dimensions, they do not have the usual rheological thickening properties that many polymers have in solution. Among them, dendrimers are 3D nanostructures engineered to carry molecules encapsulated in their interior void spaces or attached to the surface. Size, shape, and reactivity are determined by their generation, chemical composition of the core, interior branching, and surface functionalities. The most common organic ENPs are dendrimers, which

are constructed through a set of repeated chemical-synthesis procedures that build up from the molecular level to the nanoscale. They are very uniform with extremely low polydispersities, and are commonly created with dimensions incrementally grown in approximately 1 nm steps from 1 nm to over 10 nm (Hernando *et al*., 2012). Control of size, shape, and surface functionality makes dendrimers one of the customizable nanotechnologies commercially available (Suarez *et al*., 2011). These applications include mostly drug-delivery systems but also polymer materials (e.g., nanolatex), chemical sensors and modified electrodes, DNA-transfecting agents, and therapeutic agents for prion diseases (Albertazzi *et al*., 2013; Casado *et al*., 2013; Mendez *et al*., 2012).

Environmental contamination of NMs results from their growing use in an increasing number of industries. Nanowaste streams are most likely to contain the dominantly used NMs in the fabrication of nanoproducts in applications such as cosmetics, pharmaceuticals, pesticides, and sunscreens. An analysis of the NMs mostly used in the nanoproducts reported by the Woodrow Wilson International Center for Scholars and their distribution by type from the Nanowerk database shows that the most common material mentioned in the product descriptions is now silver (313 products). Carbon, which includes fullerenes, is the second most referenced (91), followed by titanium (including titanium dioxide) (59), silica (43), zinc (including zinc oxide) (31), and gold (28) (Anon, 2011a; Woodrow Wilson International Center for Scholars, 2013).

12.3 The regulatory context

Currently, there is no widely agreed international or EU definition of NM or nanotechnology. NM is just a commonly used term covering manufactured nanosized, nanostructured NMs and materials with specific properties due to their small particle size. However, the EU Commission adopted a recommendation on the definition of NMs (2011/696/EU), which will be reviewed in 2014 (2012c), and some specific designations have been introduced in sector specific EU legislative instruments, with the possibility to adapt them in the future (Anon, 2011b).

The situation is similar regarding legislation of NMs in the environment. There is no specific law regulating NMs, and provisions in EU regulations do not always explicitly refer to NMs (Bleeker *et al*., 2013; Gogos *et al*., 2012; Zea, 2012). However, the EU considers, at least at this moment, that potential risks related to NMs are covered by the existing regulatory framework (Hansen, 2010; Hansen and Baun, 2012; Liden, 2011). Indeed, the safety protection and health of workers legislation, product requirements for health and safety of workers, consumers' legislation, and environment legislation

apply to NMs. In its Second Regulatory Review (COM/2012/572) (Anon, 12 A.D.), the Commission stated that NMs are covered by the definition of substances given by the REACH Regulation (Anon, 2010b), which represents 'the best possible framework for risk management of NMs' and by regulation on Classification, Labeling and Packaging (CLP) of substances (Anon, 2008b).

NMs are also covered by all product-related legislation that requires the carrying out of risk assessment and the adoption of risk management measures (Plant Protection Products, Biocidal Products, Cosmetics, etc.) (Bleeker *et al*., 2013; Hansen, 2010; Zea, 2012) and the environmental protection legislation (IED Directive (Anon, 2010a), Seveso III Directive (Anon, 2012b), the Water Framework Directive (Anon, 2000) and Waste legislation (Anon, 2008a)). However, NMs are not specified in this legislation. This is currently a controversial position.

The situation is the same in the USA. Two principal laws govern chemicals regulation in the USA: the Toxic Substances Control Act (TSCA) and the Federal Insecticide, Fungicide and Rodenticide Act (FIFRA). The former provides authority to regulate most chemicals, while the latter addresses pesticides in particular. Neither of them has adopted a nano-specific regulatory framework (Breggin *et al*., 2011).

NMs are also regulated in Canada under existing legislation including the Canadian Environmental Protection Act, 1999, the Pest Control Products Act, the Fertilizers Act, the Feeds Act, and the Food and Drugs Act. It is recognized that, due to the unique properties associated with NMs, the science surrounding the risk assessment of these substances needs to be developed further. To that end, the Federal Government is funding NM health and safety research within Canada, and actively participating in international efforts to study, quantify, and understand the behavior and toxicity of NMs (Government of Canada, 2013).

As the use of NMs is predicted to continue growing in many industries, many regulatory agencies are working to evaluate the environmental impact of NMs and to establish requirements for environmental assessments of novel NMs prior to approve the commercialization of products. These investigations will be further enhanced through improved detection and monitoring tools, some of which will be further discussed below.

12.4 Analytical methodology: measurements of nanoparticles (NPs) in environmental media

Several books (Breggin *et al*., 2011; Farre and Barceló, 2012), special issues (Farre and Barceló, 2011a, 2011b; Lowry *et al*., 2012) and reviews (Brar *et al*., 2011; Bystrzejewska-Piotrowska *et al*., 2009; Chen *et al*., 2011; da Silva

et al., 2011; Darlington *et al*., 2009; Domingos *et al*., 2009; Duester *et al*., 2011; Farre *et al*., 2011; Felekis *et al*., 2009; Gallego-Urrea *et al*., 2011; Handy *et al*., 2008; Hotze *et al*., 2010; Howard, 2010; Jiang *et al*., 2011; Jiménez *et al*., 2011; Lin *et al*., 2010; Lowry *et al*., 2012; Majestic *et al*., 2010; Peralta-Videa *et al*., 2011; Perez *et al*., 2009; Petersen *et al*., 2012; Schmidt *et al*., 2011; Simonet *et al*., 2009; Stone *et al*., 2010; Tiede *et al*., 2008; von der Kammer *et al*., 2012; Wiesner *et al*., 2008; Yu *et al*., 2010) have summarized the recent developments in this field. Methods for assessing ENP concentration and particle-size distribution include electron microscopy, chromatography, centrifugation, laser-light scattering, ultrafiltration, and spectroscopy. Composition, structure, particle shape and size, surface area and charge, and concentration, along with agglomeration and particle-size distribution, need to be measured to fully describe a NM. Table 12.1 outlines the techniques and which key characteristics are able to measure.

The detection and analysis of NPs can be carried out in different environments and ecosystems that have different media, mainly, solid, liquid or gas. However within these main types of media are variations such as plant tissue and cells, and soil types. These provide challenges for methods of detection and analysis. Furthermore, different types of data will be required depending on the aim of the study. An example of a routine commercially available method to successfully measure NPs in different environments is the scanning mobility particle sizer (SMPS), used for measuring particle-size distribution in aerosols, which can be applied to measure NPs in the gas phase. There are also techniques for detection of NPs in the liquid phase, such as optical chromophore counting, resonant light scattering, and Raman scattering, as well as electron microscopy such as scanning transmission electron microscopy (STEM), or high resolution transmission electron microscopy (HRTEM). A problem with these techniques is that often sampling and extraction are required before the analysis. This not only increases error in quantitative analysis, but also prevents *in situ* analysis of the NPs in their own environment.

When considering ENMs in the environment, toxicology studies might focus on the size distribution and effects, while environmental studies might focus on detection and quantitation. The methods can be classified into those that allow detection and the measure of size distribution and those that characterize the NMs. In addition to these methods mentioned in the following sections, there are a number of other analytical techniques that might be used as complementary methods to detect NMs, such as flow-cytometry, elemental analysis (EA), nuclear magnetic resonance (NMR), X-ray crystallography (XRD) and infrared spectroscopy. These techniques are rarely used to quantify NMs in environmental samples, probably because they need mgs of the analyte to operate effectively.

Table 12.1 Nanomaterial characteristics and applicable analytical technologies

Analytical technique		Conc	Particle size	Particle distribution	Surface charge	Surface area	Shape	Aggregation	Structure	Composition
Electrical mobility										
Scanning mobility particle sizer	SMPS	++	+++	+++	–	–	–	++	–	–
Imaging techniques										
Scanning electron microscopy	SEM	+	+++	+++	+	+	+++	+++	+++	+
Transmission electron microscopy (+EDS)	TEM	+	+++	+++	+	+++	+++	+++	+++	+++
Atomic force microscopy	AFM	+	+++	+++	+++	+++	+++	+++	+	+
Two-Photon excitation microscopy	TPEM	+	+++	+++	+	+	+++	+++	+++	+
Coherent anti-Stokes Raman scattering	CARS	+	+++	+++	+	+	+++	+++	+++	+
Diffraction techniques										
Dynamic light scattering	DLS	+	+++	+++	+	+	+++	+++	+	+
NTA	NTA	+	+++	+++	+	+	+	+++	+	+
Static light scattering	SLS	+	+++	+	+	+	+++	+++	+	+
X-ray diffraction	XRE	+	+	+	+	+	+	+	+++	+
Extraction techniques										
Dialysis		+	+++	+	+	+	+	+	+	+
Ultrafiltration		+	+++	+++	+++	+	+	+	+	+
Centrifugation		+	+++	+++	+	+	+	+++	+	+
Filtration		+	+++	+++	+	+	+	+	+	+

(Continued)

Table 12.1 Continued

Analytical technique		Conc	Particle size	Particle distribution	Surface charge	Surface area	Shape	Aggregation	Structure	Composition
Separation techniques										
Capillary electrophoresis		+	+++	+++	+	+	+	+	+	+
Size exclusion chromatography	SEC	+	+	+++	+	+	+	+	+	+
HC	HC	+	—	—	+	+	+	+	+	
FFF	FFF	+	+++	+++	+	+	+++	+++	+	+
Spectroscopy techniques										
X-ray photoelectron spectroscopy	XPS	+	+	+	+++	+++	+	+	+	—
Optical spectroscopy-UV/Vis	UV/Vis	+++	+++	+	+	+	+	+	+	+++
Fluorescence spectroscopy	FL	+	+++	+	+	+	+	+++	+	+++
MS techniques										
Inductively coupled plasma-MS	ICP-MS	+++	+	+	+	+	+	+	+	+++
LC-MS	LC-MS	+++	+	+	+	+	+	+	+	+++
TGA coupled with gas chromatography-MS	TGGA-GC/MS	+	+	+	+	+	+	+	+	+++

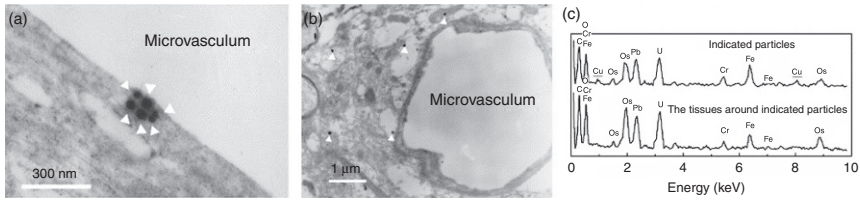

12.3 Intratissular distribution of labeled NPs with the T-80 coating in the brain tissue probed with analytical electron microscopy (AEM): (a) at the wall of the microvasculum (indicated by the white triangles), (b) around the microvasculum (indicated by the white triangles), (c) representative EDS of indicated particles in (a)–(b) and the brain tissues around particles. (*Source*: Reproduced from Sun *et al.*, 2006 with permission of Elsevier Ltd.)

12.5 Analytical methodology: detection and size distribution

There are a number of techniques that can be used to detect NPs and determine their size distribution. This section outlines the main differences in results, specifications and requirements for each technique.

12.5.1 Scanning mobility particle sizer (SMPS)

An SMPS is a spectrometer that can automatically measure particles from 2.5 to 1000 nm and a total concentration of up to 105 particles/cm^3 transient. These systems comprise a differential mobility analyzer (DMA) for the classification of particles, a condensation particle counter (CPC) as detection system, and a software package. The particles that are investigated can be of biological or chemical nature. The spectrometer can be applied in situations such as air quality measurement indoors, vehicle exhaust pipes, research in bioaerosols, atmospheric studies, toxicology testing, etc.

SMPS spectrometry is widely used as the standard method to measure airborne particle-size distributions all over the world (Wang *et al.*, 2010b; Watson *et al.*, 2011). These particle sizers, at least in theory, can also be routinely used to make accurate NP size measurements of particles suspended in liquids. The main inconvenience is that this technique does not provide information on the chemical nature of the NPs.

12.5.2 Imaging techniques

The most efficient tool to characterize submicron dimensions and morphology in a number of ENPs is high resolution imaging, which comprises electron microscopy and non-linear optical microscopy.

The most used electron microscopy techniques are transmission electron microscopy (TEM) and scanning electron microscopy (SEM) (Al-Salim *et al*., 2011; Domingos *et al*., 2009; Garcia-Negrete *et al*., 2013; Lopez-Lorente *et al*., 2012; Tiede *et al*., 2009). Atomic force electron microscopy (AFM) has also some applications within the ENMs (Domingos *et al*., 2009). These methods provided the most direct information on the size distribution and shape of the individual ENPs. However, the sample requires tedious treatments, and the sample preparation phases (drying, frozen or exposure to vacuum) can induce an agglomeration of the particles changing the size that they had in the original environment. In addition, organic ENPs are not visible without staining, which can lead to errors in the measurement of the particle diameters.

SEM produces images of a sample by scanning it with a focused beam of electrons. It can achieve resolution better than 1 nm. Specimens can be observed in high vacuum, low vacuum and, in environmental SEM specimens, can be observed in wet conditions (da Silva *et al*., 2011; Kaegi *et al*., 2008). TEM is a microscopy technique whereby a beam of electrons is transmitted through an ultra-thin specimen, interacting with the specimen as it passes through (Garcia-Negrete *et al*., 2013). This technique can resolve in the order of 0.5 nm, and has already proved suitable for imaging inorganic and organic NPs (Duester *et al*., 2011). TEM requires high vacuum and thin sample sections for electron-beam penetration (Suarez *et al*., 2011). This technique has been applied to metal oxides ZnO, CeO_2, and TiO_2 in fish and nano-Fe in excised mussel gills (Al-Salim *et al*., 2011; Tiede *et al*., 2009). TEM may supply either morphological information or chemical information with high spatial resolution. There are different TEM variants that tend to improve the resolution, such as STEM or HRTEM (Lopez-Lorente *et al*., 2012; Sun *et al*., 2006). Sun *et al*. (2006) directly trace polymeric NPs by STEM using copper chlorophyll as the contrast agent, based on the experiments concerned with the copper chlorophyll labeled poly-DL-lactide NPs and the *in vivo* distribution of the T-80-coated NPs in brain tissues. Figure 12.3 further illustrates the results measured with STEM in detail. Some particles with the information of copper are located at the wall of the microvasculum (i.e. the layer of the brain micro-vessel endothelial cells) in the brain (Fig. 12.3a), or around the microvasculum in the brain (Fig. 12.3b). Only the labeled NPs with the T-80 coating and the brain tissues containing copper are among those that may appear in the STEM image.

In environmental analysis, these electron microscopy imaging techniques are mainly applied to the validation of other detection and quantification methods. The identification and location of individual NP sample by electron microscopy is not easy, due to the time-consuming analysis of small sample volumes and the issues of representativeness and reproducibility, the wide range of natural nanostructures present in the sample, and

probably also because the visual observation is biased by subjective evaluation. Furthermore, these approaches are extremely expensive, difficult to use, cannot observe live specimens, and do not provide information on the chemical nature of the NP. This last drawback can be solved combining electron microscopy with ICP-MS or X-ray, which give some chemical information on the ENPs composition. This gave place to the so-called analytical EM, which allows the determination of the elemental composition of a specimen or specific areas or spots of a sample. This is often done by scanning the electron beam over the sample. The most common example is energy-dispersive X-ray spectroscopy (EDS). Figure12.3c also shows the representative EDS of indicated particles in (a)–(b) and the brain tissues around particles.

Non-linear optical microscopy provides a nonintrusive tool for the *in vivo* visualization of NM fate, interactions, and behavior. Non-linear optical microscopy is generally divided into two categories: incoherent (optical signal whose phase is random and whose power is proportional to the concentration of radiating molecules) or coherent (optical signal whose phase is rigorously prescribed by a variety of factors including the excitation light phase and the geometric distribution of the radiating molecules). Incoherent microscopy, such as two-photon excitation microscopy (TPEM) combined with autofluorescence, can be used to detect NM multi-walled carbon nanotubes (MWCNT), TiO_2, and CeO_2^- interacting with vegetation and to monitor the interactions between these nanotubes and polycyclic aromatic hydrocarbons *in vivo* in roots. Coherent anti-Stokes Raman scattering (CARS) microscopy can be applied in living cells and provides vibrational contrast. Definitive uptake from the water column and location of TiO_2 NPs in gills was demonstrated for the first time using CARS microscopy. CARS imaging of rainbow trout gill tissues clearly showed large aggregates of TiO_2 (up to 3 μm) on the surface of the gill epithelium following 24–96 h exposure.

The above examples demonstrate that imaging techniques can detect and characterize ENPs in a wide range of matrices. Their potential for detecting interactions of ENMs with complex environmental matrices is improving with refinement of existing systems and the development of new procedures (e.g., wet-state imaging systems or non-linear optical techniques).

12.5.3 Light absorbance or emission

Others techniques used to measure the size of NMs are based on light, and absorbance or emission of light through back-scattering of the light and use of software to track the Brownian motion of the light using the Stokes-Einstein equation, such as dynamic light scattering (DLS) and *nanoparticle tracking analysis* (NTA).

DLS is used to characterize size of various particles including proteins, polymers, micelles, carbohydrates, and NPs, while these particles are in motion. It has been applied to the determination of size distribution of ZnO, TiO_2 and CeS in aqueous suspension (Domingos *et al.*, 2009). Despite being a powerful and accessible tool, DLS is also known to have several drawbacks, which are mainly inherent in the principles of the technique. The fact that the intensity of the scattered light is proportional to the sixth power of the particle diameter makes this technique very sensitive to the presence of large particles. This can be of advantage if the purpose is to detect small numbers of large particles, but it can be a major drawback for accurate size determination. Dust particles or small amounts of large aggregates can impede the size determination if the main component exhibits a distinctly smaller size.

NTA, which was first commercialized in 2006, is an innovative system for sizing particles from about 30 to 1000 nm, with the lower detection limit being dependent on the refractive index of the NPs. This technique combines laser-light scattering microscopy with a charge-coupled device (CCD) camera, which enables the visualization and recording of NPs in solution. Applications of this technique for environmental, food, and biological analysis have been recently reviewed (Gallego-Urrea *et al.*, 2011). This method has already been tested for environmental application to determine particle-size and aggregate-size distributions of Ag-NPs from leachate after washing silver nanotextiles and standards (Geranio *et al.*, 2009). This technique has also been applied to evaluate the effect of

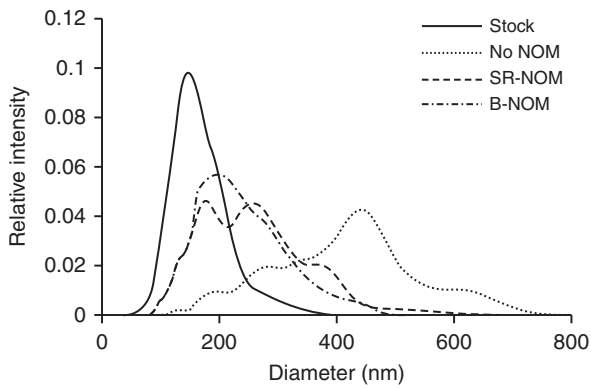

12.4 The particle-size distribution (PSD) of cerium dioxide (CeO_2) NPs as measured by NTA. Giving the PSD for the stock suspension of CeO_2 NPs used to prepare all suspensions. The PSD in algae medium without NOM after 1 d of settling. The PSD in algae medium with SR-NOM and B-NOM after 12 d of settling. (*Source*: Reproduced from Quik *et al.,* 2010 with permission of Elsevier Ltd.)

natural organic matter on CeO_2 NPs settling in model fresh water to determine particle-size distribution variation with time (Quik *et al*., 2010). The particle-size distribution of the CeO_2 NPs in deionized water and algae medium showed the formation of aggregates, with an average diameter of 301 and 417 nm, respectively, after 1 d of settling. This is larger than the average particle diameter of 169 nm found for the stock suspension at pH 4 (Fig. 12.4).

NTA feasibility to determine size distribution and concentration of sub-μm-sized particles in different aquatic environments has been compared with standard nephelometric turbidity measurements (Gallego-Urrea *et al*., 2010) as well as with TEM, AFM, DLS, fluorescence correlation spectroscopy, and flow field flow fractionation (F^4) (Domingos *et al*., 2009). In this last example, the determination of average and mode size of titanium dioxide, zinc oxide, and carboxy-functionalized CdS-capped CdTe are reported. However, the nominal size of the particles tested was below the detection limit, and the measured sizes corresponded mostly to aggregates.

12.6 Analytical methodology: chemical composition and quantification

The analytical methods currently used to identify and quantify ENMs in environmental samples need to be coupled to an efficient extraction and/or clean-up procedure to eliminate interferences within the sample matrices (Brar *et al*., 2011; Bystrzejewska-Piotrowska *et al*., 2009; Chen *et al*., 2011; da Silva *et al*., 2011; Darlington *et al*., 2009; Domingos *et al*., 2009; Farre *et al*., 2011; Felekis *et al*., 2009; Gallego-Urrea *et al*., 2011; Handy *et al*., 2008). Separation of ENMs according to size distribution is also very important (Duester *et al*., 2011; Hotze *et al*., 2010; Howard, 2010; Jiang *et al*., 2011; Jiménez *et al*., 2011; Lin *et al*., 2010; Lowry *et al*., 2012; Majestic *et al*., 2010; Peralta-Videa *et al*., 2011; Perez *et al*., 2009; Petersen *et al*., 2012; Schmidt *et al*., 2011; Simonet *et al*., 2009; Stone *et al*., 2010; Tiede *et al*., 2008; von der Kammer *et al*., 2012; Wiesner *et al*., 2008; Yu *et al*., 2010).

12.6.1 Sample preparation

NMs are often insoluble but exist in suspension. NP dispersions in the environment could be unstable and, ideally, NMs should be determined *in situ* with no or minimal sample treatment (Duester *et al*., 2011; Hotze *et al*., 2010; Howard, 2010; Schmidt *et al*., 2011). This, however, is impossible, since equipment sensitive enough for this purpose is not currently available (Simonet *et al*., 2009). Extraction procedures are as important as the analytical instrumentation used (Lowry *et al*., 2012; Majestic *et al*., 2010). The trend within

NP extraction is toward the implementation of new procedures that cause minimal sample perturbation (Simonet *et al*., 2009; Stone *et al*., 2010).

Removing the particles contained in environmental samples frequently entails their prefractionation by centrifugation or filtration (Hernando *et al*., 2012; Schmidt *et al*., 2011; Suarez *et al*., 2008). Centrifugation is more efficient in removing denser mineral particles, but microfiltration and/or ultrafiltration are widely used (Schmidt *et al*., 2011). Today, it is possible to use membranes with pore size less than 1 nm for so-called nanofiltration. These membranes therefore possess a high potential for the analysis of environmental NPs. Separating NPs from soil components is, in fact, difficult. In general, centrifugation is the recommended method, but this can induce some aggregation (Hernando *et al*., 2012). Recently, the ability of sequential size selective precipitation (SSSP) to successfully separate Au nanoclusters from larger to smaller ones by progressively increasing the concentration of acetone in the aqueous AuNC solution has been demonstrated. The study shed light on the potential use of SSSP for simple and large-scale preliminary separation of polydispersed water-soluble AuNCs into different fractions with a relatively narrower size distribution. However, it is far away from being applicable as a routine method for environmental samples

In addition, the extraction of NPs in soils, sediments, and biota is further complicated by the presence of natural solid particles of size similar to that of the target NPs (e.g. humic and fulvic acids, clays, proteins, carbohydrates, or lipids). These methods still need some improvement because, often, they cannot guarantee to preserve the nanoform of the material.

The use of dispersive methods involving chemical dispersants (e.g. surfactants) or sonication (Chen and Ding, 2012; Geranio *et al*., 2009; Lopez-Lorente *et al*., 2012) can help release NPs to an aqueous phase; for example, Lozano *et al*. (Lopez-Lorente *et al*., 2012) developed a method of purification of NPs from water or liver based on the stabilization of gold NPs with a cationic surfactant followed by a microliquid–liquid extraction in ionic liquid. Finally, the extracted NPs can be analyzed by UV/Vis detection or Raman spectroscopy. No changes were observed in the nanoform showing that liquid–liquid extraction with ionic liquids is a good approach to the analysis of these kind of samples and analytes.

There are other methods already well established, such as wet digestion for metals-based compounds (Bigorgne *et al*., 2011; Bradford *et al*., 2009; Garcia-Negrete *et al*., 2013; Johnston *et al*., 2010; Luo *et al*., 2011; Tedesco *et al*., 2010; Zhao *et al*., 2011). Fullerenes can be extracted from environmental matrices including water by exploiting their solubility in toluene (Bouchard and Xin, 2008; Carrillo-Carrion *et al*., 2011; Chen *et al*., 2008; Hendrickson *et al*., 2012; Hoon and Jae-Hong, 2009; Isaacson

and Bouchard, 2010; Jiménez *et al.*, 2011; Myojo *et al.*, 2011; Wang *et al.*, 2010a, 2011b; Xia *et al.*, 2006); however, CNTs are poorly soluble, even in organic solvents, complicating their purification. One recent approach to the extraction of SWCNTs from surface water uses a filter modified with MWCNTs as a pre-concentrator (Suarez *et al.*, 2008). Under these conditions, separation was completed in only 5 min. Recoveries for the analysis of spiked samples ranged from 70% to 85%, and the precision from 6.4% to 7.3%. After preconcentration, the samples were analyzed by capillary electrophoresis, which has the disadvantage of low sensitivity.

12.6.2 Separation techniques

Separating NPs is one of the most critical steps in their analytical processing. Available methods for this purpose are still under study. However, all the techniques used to this moment assume that it is useful to separate molecules into size, mass, and mass/charge relations. Field flow fractionation (FFF), liquid chromatography (LC), capillary electrophoresis (CZE), and hydrodynamic chromatography (HC) have been tested in some practical applications, showing interesting prospects.

The most frequently applied technique for the separation of ENPs is LC, using octadecylsilane as stationary phase and a fairly polar mobile phase. The most important property of the molecule involved in the separation is its polarity, which is slightly related to molecule size. Furthermore, structural properties of the analyte molecule play an important role in its retention characteristics. In general, an analyte with a larger hydrophobic surface area (C–H, C–C, and generally non-polar atomic bonds) is retained longer. Such interactions are also subjected to steric effects, in that very large molecules may have only restricted access to the pores of the stationary phase, where the interactions with surface ligands (alkyl chains) take place. Such surface hindrance typically results in less retention. It has been widely used to determine fullerenes in water and biota (Bouchard *et al.*, 2008; Chen *et al.*, 2008; Chen *et al.*, 2012; Hoon *et al.*, 2009; Isaacson *et al.*, 2010; Jiménez *et al.*, 2011; Myojo *et al.*, 2011; Wang *et al.*, 2010a; Xia *et al.*, 2006). The most useful stationary phase for the separation of fullerenes is octadecylsilane bonded phase (ODS) (using n-hexane or toluene based mobile phases). However, there are a number of reports in which different types of stationary phases have been proposed for fullerene separation (Bouchard *et al.*, 2008; Hoon *et al.*, 2009; Jiménez *et al.*, 2011). These reports show that monomeric ODS phases are better suited than polymeric, which have very high planarity recognition capability. Fullerenes have basically ball-type structures and are weakly retained with polymeric ODS phases. Dendrimers can also be separated by LC performed with a reversed-phase

C_5 and a more conventional reverse mobile phase of acetonitrile-water modified with 1% of acetic acid (Hernando *et al.*, 2012; Ucles *et al.*, 2013; Ulaszewska *et al.*, 2013).

HC is another technique for particle-size determination in the 30–60 000 nm range at a high dilution without being affected by their density. It has some similarities to size exclusion chromatography (SEC) and FFF. The separation takes place in a packet or an open tubular column. In the most common way to perform HC, the column is packed with non-porous microparticles, and separation is achieved by flow velocity and the velocity gradient across them. Components are eluted in order of the decreasing size. This has been applied to the analysis of metal-based NPs in environmental samples (Tiede *et al.*, 2009).

FFF is a single-phase chromatography technique in which separation is achieved within a very thin channel, against a perpendicular force field. One of the most common forms of FFF is asymmetrical-F^4 or (AF^4), in which the field is generated by a cross-flow applied perpendicularly to the channel. The sample separation occurs in a thin, ribbon-like, channel in which there are an inlet flow and a perpendicular field flow. The inlet flow is where the carrier liquid is pumped into the channel, and it creates a parabolic flow profile propelling the sample toward the outlet of the channel. F^4 has been used in combination with UV to determine size distribution of TiO_2, ZnO and quantum dots in aqueous suspension. However, it does not provide enough sensitivity (Domingos *et al.*, 2009). An analytical platform coupling AF^4 with multiangle light scattering (MALS), DLS, and ICP-MS was established and used for separation and quantitative determination of size and mass concentration of NPs in aqueous suspensions, achieving limits of detection between 0.04 and 0.2 ng of Au. The fractograms corresponding to a mixture of Au NPs (Fig. 12.5) showed that separation into their components was successfully achieved. However, a peak from 'residual' AuNPs occurred when the cross-flow of the AF^4 program, in its final stage, was set to zero (Schmidt *et al.*, 2011).

One of the most important separation techniques for the characterization of ENPs is capillary electrophoresis. However, in spite of the potential of capillary electrophoresis, to date, it has been scarcely used to separate and characterize ENPs. In fact, capillary zone electrophoretic separations have been limited to SWCNTs (Suarez *et al.*, 2008). The limit of detection referring to 250 mL of the sample was established as only 0.8 mg/L (ppm). The combination of this technique with detectors more sensitive to CNTs will provide in the near future a powerful tool to control the presence of carbon NPs in the environment.

These separation techniques work well with ENPs. However, their combination with traditional detectors, such as UV/Vis does not achieve enough sensitivity to determine ENPs in environmental matrices. The choice of detector is very important.

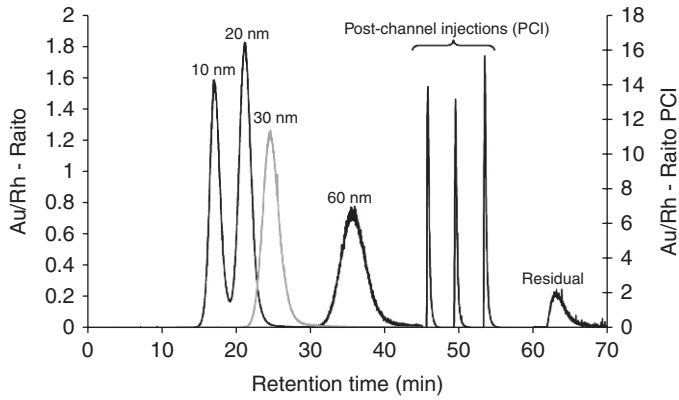

12.5 AF⁴-ICP-MS fractogram of a mixture of 10, 20, and 60 nm AuNPs (black line) superimposed on a fractogram corresponding to 30 nm NIST Au NPs (gray line) all at ca. 1000 μg/L concentrations. The signal intensities of post-channel injections of 10, 20, and 60 nm Au NPs have been indicated on the secondary y-axis. 'Residual' AF⁴ peak corresponded to released Au NPs that were adhered to the membrane or were associated with nonspecific particulate matter, which originated from the carrier liquid or bled from the membrane. Injected volumes, 50 μL. (*Source*: Reproduced from Schmidt *et al.*, 2011 with permission of American Chemical Society.)

12.6.3 Quantitative determination

The techniques in this group are also used to assess chemical composition or structure (Brar *et al.*, 2011; Bystrzejewska-Piotrowska *et al.*, 2009; Chen *et al.*, 2011; da Silva *et al.*, 2011; Darlington *et al.*, 2009; Domingos *et al.*, 2009; Duester *et al.*, 2011; Farre *et al.*, 2011; Felekis *et al.*, 2009; Gallego-Urrea *et al.*, 2011; Handy *et al.*, 2008; Hotze *et al.*, 2010; Howard, 2010; Jiang *et al.*, 2011; Jiménez *et al.*, 2011; Lin *et al.*, 2010; Lowry *et al.*, 2012; Majestic *et al.*, 2010; Peralta-Videa *et al.*, 2011; Perez *et al.*, 2009; Petersen *et al.*, 2012; Schmidt *et al.*, 2011; Simonet *et al.*, 2009; Stone *et al.*, 2010; Tiede *et al.*, 2008; von der Kammer *et al.*, 2012; Wiesner *et al.*, 2008; Yu *et al.*, 2010). The most common techniques that have been reported for the quantitative determination of ENPs are:

- AAS
- ICP-AES or ICP-MS
- UV/Vis
- Fluorescence
- Raman
- Mass spectrometry (MS).

The average bulk chemical composition of metal ENPs can be determined by using spectroscopic techniques such as atomic absorption spectroscopy

(AAS), inductively coupled plasma atomic emission spectroscopy (ICP-AES), and ICP-MS (Bradford *et al*., 2009; Garcia-Negrete *et al*., 2013; Johnston *et al*., 2010; Navarro *et al*., 2009; Tedesco *et al*., 2010). These techniques feature good limits of detection; also, the composition results they provide are sample averages and they afford multi-element analysis. On the other hand, they are destructive and subject to matrix interferences. These techniques are especially recommended for the analysis of metallic NPs. Because of its element-specific detection and high sensitivity, inductively coupled plasma–mass spectrometry (ICP-MS) is ideal to study AgNP and other inorganic NPs.

These techniques commonly require wet digestion of the sample, which destroys the nanoform of the metal. To solve this drawback, particularly in the case of ICP-MS, several digestion-free possibilities have been published for ICP-MS, e.g. direct-in-torch vaporization, laser ablation (LA), and graphite furnace electrothermal vaporization (GF-ETV), or coupling with a separation technique, such as hydrodynamic chromatography (HD) or asymmetric flow field flow fractionation (AF^4) (Judy *et al*., 2011; Schmidt *et al*., 2011; Tiede *et al*., 2009). The strength of LA-ICP-MS is the spatial resolution of the elemental composition, whereas the ETV-ICP-MS may only indirectly deliver spatial information by using small sample parts, but as a major benefit, shows lower limits of detection (Judy *et al*., 2011).

Recently, the operation of ICP-MS in the single-particle mode (SP-ICP-MS) has provided a means of detecting individual NPs. Single-particle ICP-MS relies on the sensitive metal detection capability of ICP-MS, but, in contrast to traditional ICP analysis techniques, thousands of individual intensity readings are acquired, each with a very short dwell time (10–20 ms). Instead of measuring metal concentration representative of the bulk sample, the intensity readings can be collected as a function of time, where pulses above the background represent the measurement of an individual NP. Versions of the SP-ICP-MS concept have been used to detect AgNP in unprocessed environmental water (Mitrano *et al*., 2012a, 2012b). Mitrano *et al*. (2012a) compared the ability of SP-ICP-MS and AF^4-ICP-MS to detect silver ENPs and examined their overall applicability to environmental studies with respect to their (a) size and concentration detection limits, (b) resolution, and (c) multi-form EA. In terms of concentration detection limit (on both a mass basis and particle number basis) SP-ICP-MS was considerably more sensitive than AF^4-ICP-MS (ng L^{-1} vs μg L^{-1}, respectively), and offers the unique ability to differentiate dissolved and nanoparticulate fractions of total metal. On the other hand, AF^4-ICP-MS can detect a much smaller NP size (2 nm vs 20 nm for SP-ICP-MS), providing the possibility for greater size resolution. Figure 12.6 illustrated the results obtained using SP-ICP-MS.

UV/visible spectroscopy is usually applied to the characterization of NMs. However, it lacks specificity and sensitivity to determine NMs in the environment. It was applied to determine CNTs and fullerenes commonly

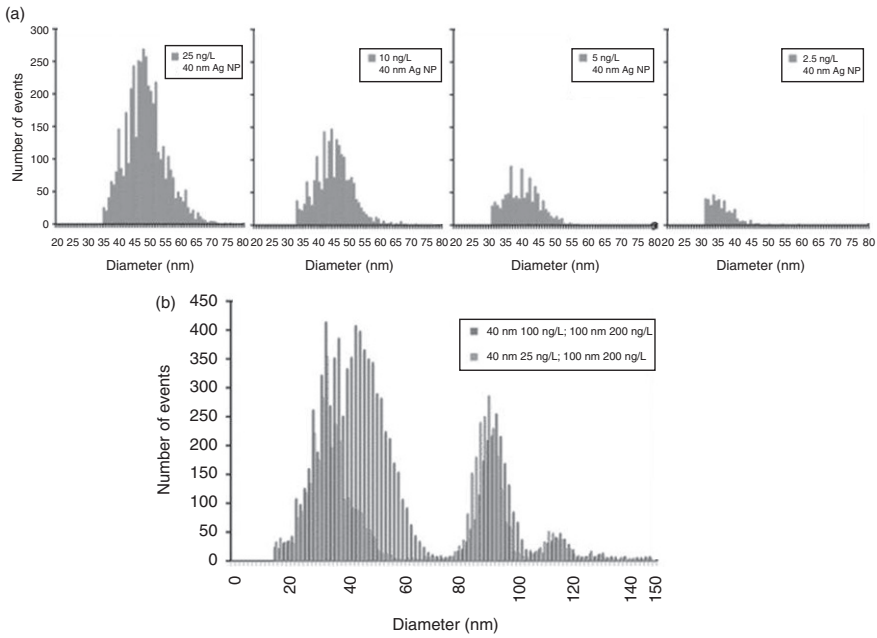

12.6 (a) Dilution scheme of 40 nm Ag NP, using SP-ICP-MS, with approximate detection limit of 2.5 ng L^{-1}. (b) 40 and 100 nm Ag NP mix. 40 nm particles at 100 ng L^{-1} are outside SP-ICP-MS dynamic range, observed coincidence of particles. The 40 nm at 25 ng L^{-1} and 100 nm particles are within the acceptable range for the SP-ICP-MS technique. (*Source*: Reproduced from Mitrano *et al.*, 2012a with permission of The Royal Society of Chemistry.)

coupled to a separation technique, such as CZE (Suarez *et al.*, 2008) or HPLC (Bouchard *et al.*, 2008; Xia *et al.*, 2006).

Fluorescence-based techniques can be an interesting choice for the analysis of NPs with a strong native fluorescence, which can be characterized from their adsorption or fluorescence spectra. Thus, the position of emission bands can be correlated with particle size and is commonly used to monitor size in the synthesis of quantum dots. Al-Salim *et al.* (2011) reported on a study of the transport of quantum dot NPs through soils, their uptake into plants, and their passage through insects following ingestion. The monitor of these compounds was done tracing the red fluorescence characteristic of the selenium. Also, particle concentrations can be quantified from adsorption or fluorescence measurements, provided the optical constants for the NPs are known (Carrillo-Carrion *et al.*, 2011; Domingos *et al.*, 2009).

X-ray diffraction and scattering are considered important for two essential reasons: X-ray diffraction is virtually non-destructive, and X-ray photons

with a wavelength in the nm range are the ideal sensors for the nanocosmos. X-ray diffraction offers a number of different dedicated methods to investigate nanostructures (Geranio *et al*., 2009; Judy *et al*., 2011).

Vibrational spectroscopies, both Raman and infrared, are useful for the analysis of NPs (particularly carbon NPs). The two techniques differ in the excitation source used, the way signals are monitored, and the selection rules employed on vibrational modes. Raman spectroscopy using portable equipment has been recently reported to determine AuNPs in water and liver (Lopez-Lorente *et al*., 2012).

The last technique widely applied to determine ENPs in environment is MS, which has emerged as a powerful tool for characterizing various types of NMs. Yang *et al*. (2012) have shown that laser desorption/ionization-MS, matrix-assisted laser desorption/ionization (MALDI)-MS, is not the only effective approach for nanocluster/NP core size determination but can also assist in tracking the progress of fractionation/precipitation of AuNCs.

A large number of works have reported the use of liquid chromatography–mass spectrometry (LC-MS) for the identification and quantification of fullerenes. Most of these studies used electrospray ionization (ESI) and atmospheric pressure chemical ionization (APCI) for mass-selective analysis (Chen *et al*., 2008, 2012; Isaacson *et al*., 2010; Jiménez *et al*., 2011). Due to the particular nature of C_{60} and C_{70} fullerenes, cage fragmentation cannot be achieved using tandem MS (Jiménez *et al*., 2011). The low fragmentation is a limitation in confirming the identity of these compounds using instrumental techniques like LC-MS/MS.

In contrast to the fullerene behavior, ESI-MS has been shown to efficiently promote ionization of dendrimers ranging from low to high generations. However, owing to the unit mass resolution, multiple charging of the molecules cannot be fully resolved in the MS spectra. MS offers sensitivity and selectivity for unambiguous identification with a high degree of confidence. With the primary focus of identifying any structural deviations in polyamidoamine (PAMAM) dendrimers, most recent studies have reported how ESI mass spectra increases in complexity for increasing generations, due to multiple charging phenomena induced by the electrospray process, as illustrated Fig. 12.7. Owing to random Na impurities in the sample, adducts of this series of peaks were observed in the spectrum (Fig. 12.7a). The multiply charged ions +9, +8, and +7 also correspond to a defective protonated dendrimer (Fig. 12.7b).

This makes characterization by ESI-MS of PAMAM dendrimer of third or upper generations to be unresolved due to the unit resolution mass analysis where multiple charging of the molecules cannot be detected in the MS spectra, and potentially might limit the LC-ESI-MS analysis of PAMAM dendrimers. In real applications such as bio analysis or environmental impact, there is a broad consensus on the lack a quantitative understanding

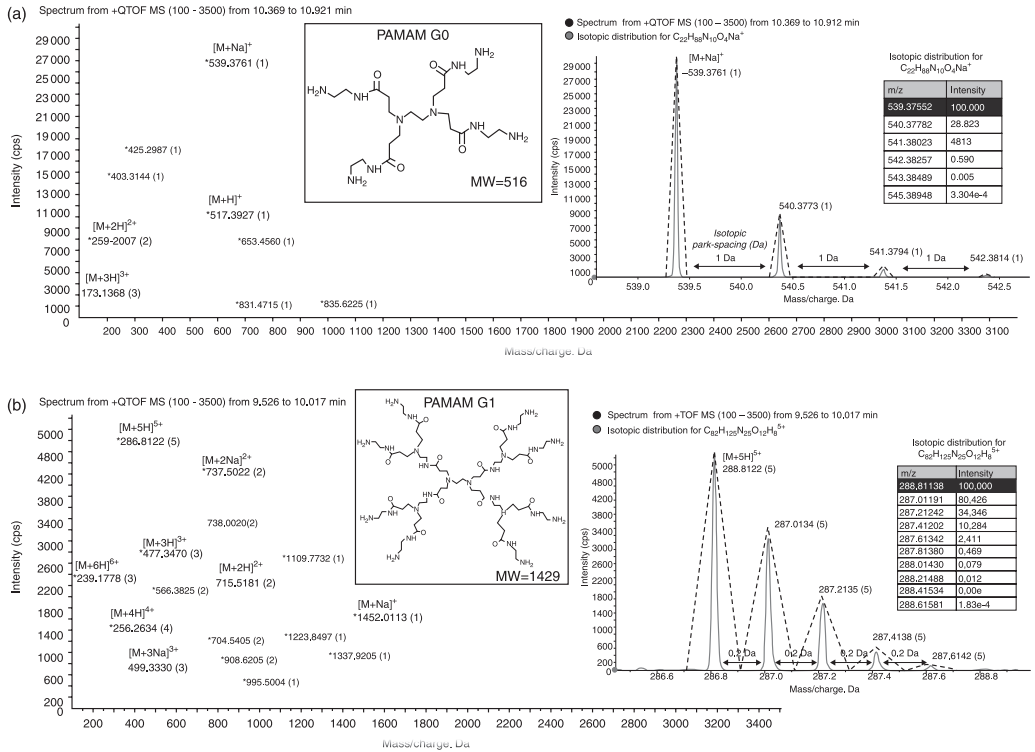

12.7 LC-ESI-QTOFMS spectrum of PAMAM dendrimer of generations (a) G0 and (b) G1. Resolution of isotopic clusters of (a) G0, [M+Na]+ and (b) G1, [M+5H]5+. 13C/12C isotopic distribution and isotopic peak spacing (*Source*: Reproduced from Ucles *et al.*, 2013 with permission of Springer.)

and need for addressing some of the analytical challenges that allow not just reliable identification but also an accurate and robust measure to cover many aspects, such as safety of NMs.

12.7 Applications

Table 12.2 reports the selected applications to determine ENMs in the environment. NMs are highly reactive and dynamic in the environment and can undergo a range of physical, chemical, and biological transformations. Some examples of transformations include hetero-aggregation, adsorption of biomacromolecules, biodegradation, and sulfidation. These transformations will affect the NM properties and environmental behaviors and impacts.

12.7.1 Air

Air contains large numbers of naturally occurring nanosized particles, frequently reaching concentrations of 10 000–500 000 particles/cm^3 (Kumar *et al*., 2010). The detection of a comparatively low number of ENPs released into air is a demanding task for which no proper methods have been developed yet (Zhang *et al*., 2012). This lack of analytical methods is mainly a problem in relation to surveillance of workers' health during manufacturing of ENPs, and in quantifying ENPs released into the atmosphere or the stratosphere (Majestic *et al*., 2010). The most common approach is the use of solid phase membrane samplers (SPMS), which establish the particle number, size and distribution of ultrafine particles (UFPs) with diameter <100 nm. Extensive measurement programs of urban and regional submicron particle number size distribution have been carried out at several locations: e.g. in the US (Watson *et al*., 2011), Europe (Wang *et al*., 2010b), Australia, as well as China. However, these systems do not distinguish natural and engineering NPs and do not give information on their chemical nature. Some attempts have been made to characterize size-resolved particles, including the NPs fraction with a diameter of 29–58 nm in roadside atmosphere (Ochiai *et al*., 2007). The method is based on thermal desorption (TD) of a sample followed by comprehensive two-dimensional gas chromatography (GC × GC) with novel detection capabilities, including high resolution time-of-flight mass spectrometry (HRTOF-MS) and simultaneous detection with a nitrogen phosphorous detector (NPD) and a quadrupole mass spectrometer (qMS). Increased selectivity with the GC × GC–HRTOF-MS allows a group type separation of a selected chemical class, e.g. oxygenated polycyclic aromatic hydrocarbons (oxy-PAHs), using mass chromatography with a 0.05 Da wide window in the complex sample matrix. Also, exact mass measurements provide candidate elemental compositions as well as NIST library search results for tentative identifications of 50 compounds. Moreover, the

Table 12.2 Selected applications to determine NMs in the environment 2008–2012

Matrix	Analytes	Extraction	Recovery (%)	EF	Determination	LODs ng/g	Reference
Size distribution of NMs							
Ambient aerosols at the Fresno supersite	NPs 10–10000 nm	Do not require extraction, analysis is carried out directly in air	–	–	Four different types of SMPS	–	Watson *et al.*, 2011
Aerosol size distribution in the city of Rome	NPs 10–10000 nm	Do not require extraction, analysis is carried out directly in air	–	–	SMPS	–	Wang *et al.*, 2010b
NPs suspension	TiO_2, ZnO, carboxy-functionalized CdS-capped CdTe	Do not required extraction, analysis is carried out directly in the suspension	–	–	TEM; AFM; DLS; fluorescence correlation spectroscopy; NTA; F^4	AFM: 1–30 mg L^{-1} Fluorescence: 30 mg L^{-1} NTA: 30 mg L^{-1} DLS: 30 and 100 mg L^{-1} F^4-UV: 100 mg L^{-1}	Domingos *et al.*, 2009
Environmental water	AgNP	Ultrasonication for 5 min with an ultrasonication probe	–	–	NTA ICP-OES XRF	–	Geranio *et al.*, 2009
Environmental water	NPs	–	–	–	NTA Standard nephelometry	–	Gallego-Urrea *et al.*, 2010
Environmental water	CeO_2NPs	–	–	–	NTA HR-ICP-MS	–	Quik *et al.*, 2010
Brain tissue Cells	Polymer NMs (poly-dl-lactide and polysorbate 80 (T-80)-coated NPs)	–	–	–	STEM X-ray EDS	–	Sun *et al.*, 2006

(Continued)

Table 12.2 Continued

Matrix	Analytes	Extraction	Recovery (%)	EF	Determination	LODs ng/g	Reference
Identification and chemical characterization of NMs							
Mineral based NMs							
Aqueous samples	Au Nanocluster	–	–	–	MALDI-TOF-MS	–	Yang *et al.*, 2012
Aqueous samples	Ag-NPs	–	–	–	SP-ICP-MS AF^4-ICP-MS	ng L^{-1} (SP-ICP-MS) μg L^{-1} (AF^4-ICP-MS)	Mitrano *et al.*, 2012a
Environmental waters and rat tissues	AuNPs	Ultrafiltration (water) Alkaline (TMAH) extraction (rat liver)	50%, 95%, and 67% for the 10, 20, and 60 nm Au NPs (water) 86–123% for total Au (liver)	1	SEM and TEM AF^4-DLS/MALS-ICP-MS	0.02–0.4 ng	Schmidt *et al.*, 2011
Estuarine waters and sediments	Ag-NPs	Wet digestion HNO_3 (waters) Aqua regia [HCl + HNO_3] (sediments)	–	–	ICP-OES	–	Bradford *et al.*, 2009
Wastewater effluents	Ag-NPs	–	–	–	SP-ICP-MS	–	Mitrano *et al.*, 2012b

Water	Ag-NPs	Addition of NaCl				≈ μg/L	Raz *et al.*, 2012
Water and liver tissue	AuNPs	Water: extraction with ionic liquid (BMIM PF6) Liver: previous treatment with trichloroacetic acid (TCA) and Ácido etilendiamino-tetraacético (EDTA)	87–90%	1:3	UV/Vis measurements HRTEM portable Raman spectrometer	1.17 1012 M	Lopez-Lorente *et al.*, 2012
Sea Water and tissues (*Ruditapes philippinarum)*	AuNPs	HNO_3 (Wet digestion)	–	–	ICP-MS SEM and TEM	–	Garcia-Negrete *et al.*, 2013
Juvenile carp (*Cyprinus carpio*)	CuO NPs	HNO_3 (Wet digestion)	–	–	AAS (GF)	–	Zhao *et al.*, 2011
Surface sediments	TiO_2	Acid digestion (HNO_3 + H_2SO_4)	–	–	ICP-OES	–	Luo *et al.*, 2011
Earthworm *Eisenia fetida*	TiO_2 byproducts	2 mL HNO_3 (68%) 2 mL H_2O_2 (30%)		–	ICP-AES		Bigorgne *et al.*, 2011
Pumpkin plants (*Cucurbita maxima*)	Fe_3O_4 NPs	–	–	–	Vibrating sample magnetometry (VSM)	–	Zhu *et al.*, 2008
Natural surface waters	TOPO-capped CdSe QDs	–	–	–	AS-DLS +ICP-OES	–	Navarro *et al.*, 2009
Fish *(Mytilus edulis)*	AuNPs	Wet digestion (HNO_3+H_2O_2)	–	–	ICP-OES	–	Tedesco *et al.*, 2010

(Continued)

Table 12.2 Continued

Matrix	Analytes	Extraction	Recovery (%)	EF	Determination	LODs ng/g	Reference
Fish (*Rainbow trout*)	TiO_2, CeO_2 and ZnO	Wet digestion	_	_	CARS (confirmation of nano size) ICP-OES ICP-MS	–	Johnston *et al.*, 2010
Water and sewage sludge	AuNPs, Ag-NPs TiO_2, SiO_2, Al_2O_3 and Fe_2O_3	–	–	–	TEM HD-ICP-MS	2.3 ng mL^{-1} (Ag in water)	Tiede *et al.*, 2009
Soil, plants, and insects (study of the transport)	CdSe/ZnS/Cys CdSe/ZnS/MPA CdSe/ZnS/MSA	–	–	–	TEM Fluorescence microscopy	–	Al-Salim *et al.*, 2011
Nicotiana tabacum L. cv Xanthi and *Manduca sexta* (tobacco hornworm)	AuNPs	–	–	–	ICP-MS LA-ICP-MS XRF	–	Judy *et al.*, 2011
Zebra fish (*Danio rerio*)	SWCNTs	–	–	–	SEM	–	Cheng *et al.*, 2007
Carbon-based NMs							
Bovine serum and plasma	C_{60}fullerene	Toluene + glacial acetic acid	94–100%	3.1	HPLC-UV	34 μg/L	Xia *et al.*, 2006
Synthetic and natural waters	C_{60} and C_{70} fullerenes, and [6,6]-phenyl C_{61}-butyric acid methyl ester	Toluene +acetonitrile (SPE)	98.5	10	HPLC-UV	2.87 μg/L 2.48 μg/L 6.54 μg/L	Bouchard *et al.*, 2008
Water	C_{60} fullerene	A) Toluene B) NaCl (20%w/w) + Toluene C) SPE (Strata C_{18}-E) Toluene	35 39 42	360 180 10^3	HPLC-MS	2.78 μg/L 3.33 μg/L 0.30 μg/L	Chen *et al.*, 2008
Natural water	C_{60} fullerene	Toluene	> 98%	50	HPLC	–	Hoon *et al.*, 2009

Surface water	C_{60}, C_{70} fullerenes and N-methylfullero-pyrrolidine C_{60}	Toluene	70–77	200	LC-QqLIT-MS	0.2–0.1 ng/L	Farre *et al.*, 2010
Water	C_{60} fullerene	Toluene +NaCl	29–80	–	LC–APPI–MS	–	Isaacson *et al.*, 2010
Ultrapure water and wastewater	C_{60} fullerene	Toluene + NaCl (LLE) Toluene (SPE)	89–94	10 1000	HPLC-UV-MS	3–4 μg/L 0.42–0.64 μg/L	Wang *et al.*, 2010a
Aerosols filters	C_{60} fullerenes	Toluene Toluene/methanol	–	–	HPLC-UV	0.15–1 μg/cm^2	Myojo *et al.*, 2011
Artificial sediments	C_{60} fullerenes	Toluene (normal shaking)	90–93.8	5	HPLC-UV	0.15 mg/kg	Wang *et al.*, 2011b
River waters	C_{60} fullerenes	a) Toluene b) p-tertbutylcalix[8] areneCdSe/ZnS QDs	85.97–98.98 70.20–92.70	100	Absorption and fluorescence emission (Spectro-fluorometry)	100 μg/L 5 μg/L	Carrillo-Carrion *et al.*, 2011
Water	Aqueous fullerene aggregates: nC_{60}, nC_{70}, and aqueous [6,6]-phenyl C_{61} butyric acid methyl ester (nPCBM)	UA-DLLME NaCl + (Isopropyl alcohol + 10 μL of benzyl bromide)	70–86	–	LC–APPI–MS/MS	60 ng/L 8 ng/L 150 ng/L	Chen *et al.*, 2012
Organ homogenates of rats	C_{60} fullerenes	Toluene	–	–	ELISA	2 μg/L	Hendrickson *et al.*, 2012
in airborne particulate from the Mediterranean Sea	Fullerenes (C-60, C-70, N-methylfulleropyrrolidine, C-60 pyrrolidinetris-acid ethyl ester, [6,6]-Phenyl-C-61 butyric acid butyl ester and [6,6]-Thienyl C-61 butyric acid methyl ester)	Toluene	90–98	4	LC-QqQ-MS	5.4–20.9 pg/m^3	Sanchis *et al.*, 2012

(Continued)

Table 12.2 Continued

Matrix	Analytes	Extraction	Recovery (%)	EF	Determination	LODs ng/g	Reference
Environmental water samples	SWCNTs	Filtration using a filter modified with MWNTs and eluted with HCl in methanol	82–92	125	CZE-UV	0.8 mg/L	Suarez *et al.*, 2008
Wheat tissues	MWCNTs, TiO_2 and CeO_2 NPs	–	–	1	TPEM + autofluorescence	–	Wild and Jones, 2009
Polymeric NPs							
Aqueous matrices	PAMAM dendrimers				LC-QqTOF-MS		Ulaszewska *et al.*, 2013
Aqueous matrices (surface and waste water)	PAMAM dendrimers	Direct injection of water and wastewater in the system	–	1	LC-QqTOF-MS	0.006–0.53 μM	Ucles *et al.*, 2013
Cell lines	PAMAM dendrimers	LLE with methanol–water (50:50) and centrifugation at 3500 rpm for 30 min	–	–	LC-QqTOF-MS	0.43–1.82 μM	Hernando *et al.*, 2012
Identification of different types of NPs							
Atmosphere	Identification of compounds in the NP fraction D_p: 29–58 nm	–	–	–	TD, GC × GC, HRTOF-MS, NPD, qMS	–	Ochiai *et al.*, 2007
Atmospheric particles and diesel exhaust particles	Determine the non-polar organic composition	–	–	–	TD–GC/MS	–	Fushimi *et al.*, 2007

simultaneous detection with the NPD and the qMS elucidate the presence of 15 nitrogen-containing compounds.

12.7.2 Surface and groundwater

Water can be extremely rich in natural NPs in the form of organic and inorganic colloids, mostly originating from soil. These are commonly natural dissolved or condensed humic substances, inorganic colloids (clays, silicate and iron oxides/hydroxides) or humic-mineral complexes formed from these. There are a number of works that study the interactions within this ENPs and organic matter. In general, the methods developed for water are focused on the quantification of NMs. Some of the studies focus on the determination of the amount and the form of NPs using NTA (Gallego-Urrea *et al*., 2010; Geranio *et al*., 2009; Quik *et al*., 2010) or on the determination of the metal concentration using ICP-MS but losing nanoform in coastal waters (Bradford *et al*., 2009; Coutris *et al*., 2012). Other studies try to determine the concentration and nanoform using a separation technique combined with ICP-MS or by single-particle ICP-MS (Mitrano *et al*., 2012a, 2012b; Tiede *et al*., 2009). Fullerenes have also been determined in different types of waters in their nanoform (Bouchard *et al*., 2008; Carrillo-Carrion *et al*., 2011; Chen *et al*., 2008, 2012; Farre *et al*., 2010; Hoon *et al*., 2009; Isaacson *et al*., 2010; Wang *et al*., 2010a) as well as dendrimers (Ucles *et al*., 2013; Ulaszewska *et al*., 2013).

12.7.3 Soil and sediments

Sediments contain naturally occurring NPs primary particles (single, free particles that are not aggregated) and agglomerated particles (loose clusters of a few primary particles) as well as particles that are far larger than NPs, as colloids (particles that do not settle by sedimentation, even in non-disturbed water). However, NPs in sediments tend to aggregate into larger particles which will fall out by sedimentation when they reach a certain size (Bradford *et al*., 2009).

Soil is the environmental matrix that is richest in natural NPs, both as primary particles and agglomerates/aggregates. This is due to constant physical/chemical weathering and re-arrangement of its geogenic constituents, coupled with a high biological activity that transforms both dead organic matter and minerals. Soils and sediments are the ultimate recipients and reservoirs of all sorts of particulate matter, and this is where ENPs will ultimately end up if they are not re-used or destroyed. The question that remains is to what extent ENPs can be mobilized or resuspended from soils and sediments, and herein lies one of the main challenges in environmental risk assessment of

spreading ENPs. There are some studies on the translocation of engineered NMs between soil and plant material (Al-Salim *et al*., 2011; Bradford *et al*., 2009).

12.7.4 Biota

Much of the research has focused on fundamental aspects of ecotoxicity, such as estimates of lethal concentrations, documenting sublethal effects on organisms, identifying potential mechanisms of toxicity, as well as describing the fate and behavior of ENMs. Inevitably, researchers have customized exposure protocols and selecting biological endpoints to match their research objectives; therefore, they have used a variety of methods. Although it is still poorly understood, the uptake, translocation, and transmission of NMs from their growth environment to plants and biota have been demonstrated (Al-Salim *et al*., 2011). The identification of NPs is the most important part (Zhao *et al*., 2011; Zhu *et al*., 2008).

12.8 Conclusion and future trends

Methods for the screening of ENMs in environmental samples are still in their infancy. However, the results presented in this chapter, if compared with those presented in the sources of further information and advice, reveal technological developments of major importance for the detection, characterization, monitoring and quantification of these compounds in environmental samples. The analysis of NPs in the environment is not question of a single analytical technique, but rather a combination of multiple sophisticated procedures and instrumentation. Many of these methods rely on chromatographic separations that lack stationary phases because of the surface reactivity of particles (for example, FFF techniques). Detectors such as TOF and ICP-MS are being adapted to provide sensitive and specific detection of ENMs. X-ray-based techniques provide sensitivity and specificity. Traditional electron and optical microscopy-based approaches are being augmented by minimally invasive techniques, such as environmental scanning electron microscope (ESEM), STEM or coherent anti-Stokes Raman spectroscopy (CARDS), which are simpler to apply and less invasive. STEM holds promise for internal imaging and 3D reconstruction with samples held under minimally destructive cryogenic conditions. The availability of routine analytical methods that address these issues is already key to gaining a better understanding of the mechanisms of NP formation and reactivity.

Despite not being completely resolved yet, there are already a few protocols established for the determination of some of them. For example, wet metal digestion followed by ICP-MS and complemented by SEM or TEM to demonstrate that these metals were present as nanoforms, and fullerene

extraction with toluene followed by LC-MS, are well-established routine protocols. As mentioned, existing methods are not perfect, and there is still much work to be done. There are a number of methods in development based on the determination of unique particles (e.g. single-particle ICP-MS) or particle separation according to size (e.g. HC) that promise to revolutionize this field of determination of NMs in the next few years and to improve substantially on the methods that exist at this time, because until very recently chemical analysis of individual NPs in gases and liquids was impossible time due to their low mass. The enormous diversity of engineered NMs with different sizes, shapes, compositions, and coatings matches, and possibly exceeds, that of conventional chemicals. Further development and application of these promising methods will provide research opportunities and challenges for the foreseeable future.

Other important challenges that remain unsolved in the analysis and characterization of NPs are the development of methods able to differentiate between ENMs against background level of incidental or naturally occurring NMs, and the determination of transformation products. Possible modifications that could determine key transformation products include biodegradation/chemical transformation, and physical attenuation such as aggregation and surface modifications. Development of analytical schemes (e.g. techniques and methodology) is needed for characterization of transformed engineering NMs in environmental matrices such as air, water, soil, sediments, biota, etc. As with conventional chemicals, to understand transport, degradation, and fate, it is essential to first look the NM from a life-cycle perspective.

Future advance in these topics will help a deeper understanding of nanotechnology's environmental footprint and potential toxicity – areas little understood, despite a rapid increase of NMs used in consumer products, from cellphones and laptops to sunscreen and beer bottles.

12.9 Sources of further information and advice

Bandyopadhyay *et al*. (2012) includes the most recent literature about the methods applied to the measurement of NPs and ENPs in the environment. The review covers methods to determine size distribution, shape, structure, surface charge, chemical composition, surface area, agglomeration, surface chemistry, porosity, and solubility.

Farre and Barceló (2011a, 2011b), editing a two volume special issue on this topic, covered different aspects, including analytical techniques for separation and characterization of NMs. However, the greater part is devoted to applications to environmental and food samples, covering a broad range of matrices and also NMs (e.g., Magnetic nanoparticles (MNPs), CNTs, fullerenes, and quantum dots).

Farré and Barceló (2012) published a book that covers most of the aspects of the analysis, characterization, and risk of NMs in the environment and for food safety.

Lowry *et al*. (2012) presented a series of papers in a special issue of *Environ. Sci. Technol*. that highlight several transformations of natural and engineered NMs that are critical processes affecting their behavior in the environment. It begins to make connections between the nanoscale properties and features of various NP types and their macromolecular coatings, and their behavior and effects in natural systems. The papers also illustrate that additional research and the development of novel tools for characterizing NMs *in situ*.

Peralta-Videa *et al*. (2011) compiled and analyzed publications on NMs in the biennium 2008–2010. This review includes the most recent publications in risk assessment/toxicity, characterization and stability, toxicity, fate, and transport of NMs in terrestrial ecosystems, and new ENMs. CNTs, metallic, metal oxides and hydroxides nanoparticles, quantum dots, and polystyrene NPs are included.

Simonet and Valcarcel (2009) describe some methodological aspects relating to the fields of NP analysis, nanometrology, and analytical chemistry.

Tiede *et al*. (2008) provided the first overview of the characteristics of NPs that could affect their behavior and toxicity, as well as techniques available for their determination.

Von der Kammer *et al*. (2012) pointed out how advances in the study of the environmental fate, transport, and ecotoxicological effects of ENMs have been hampered by a lack of adequate techniques for the detection and quantification of ENMs at environmentally relevant concentrations in complex media.

Yu and Andriola (2010) summarized the most recent chemical and particle quantitative analysis methods that have been used to characterize the concentration (in number of moles of gold per liter) or population (in number of particles per mL) of AuNPs. This review includes mass spectroscopy, electroanalytical methods, spectroscopic methods, and particle counting methods.

12.10 Acknowledgements

This work has been supported by the Spanish Ministry of Economy and Competitiveness through the Program Consolider-Ingenio 2010 (Project No. CSD2009-00065) and Program on Fundamental Research (Projects No. CGL2011-29703-C02-00, CGL2011-29703-C02-01 and CGL2011-29703-C02-02).

12.11 References

Al-Salim, N, Barraclough, E, Burgess, E, Clothier, B, Deurer, M, Green, S, Malone, L and Weir, G (2011) Quantum dot transport in soil, plantsand insects, *Science of the Total Environment*, **409**, 3237–3248.

Albella, P, Saiz, J M, Gonzalez, F and Moreno, F (2011) Surface monitoring based on light scattering by metal nanosensors, *Journal of Quantitative Spectroscopy and Radiative Transfer*, **112**, 2046–2058.

Albertazzi, L, Gherardini, L, Brondi, M, Sato, S S, Bifone, A, Pizzorusso, T, Ratto, G M and Bardi, G (2013) *In vivo* distribution and toxicity of PAMAM dendrimers in the central nervous system depend on their surface chemistry, *Molecular Pharmaceutics*, **10**, 249–260.

Aruguete, D M and Hochella, M F (2010) Bacteria-nanoparticle interactions and their environmental implications, *Environmental Chemistry*, **7**, 3–9.

Aschberger, K, Micheletti, C, Sokull-Kluttgen, B and Christensen, F M (2011) Analysis of currently available data for characterising the risk of engineered nanomaterials to the environment and human health – lessons learned from four case studies, *Environment International*, **37**, 1143–1156.

Atha, D H, Wang, H H, Petersen, E J, Cleveland, D, Holbrook, R D, Jaruga, P, Dizdaroglu, M, Xing, B S and Nelson, B C (2012) Copper oxide nanoparticle mediated DNA damage in terrestrial plant models, *Environmental Science and Technology*, **46**, 1819–1827.

Bandyopadhyay, S, Peralta-Videa, J R, Hernandez-Viezcas, J A, Montes, M O, Keller, A A and Gardea-Torresdey, J L (2012) Microscopic and spectroscopic methods applied to the measurements of nanoparticles in the environment, *Applied Spectroscopy Reviews*, **47**, 180–206.

Bernhardt, E S, Colman, B P, Hochella, M F, Cardinale, B J, Nisbet, R M, Richardson and C J, Yin, L Y (2010) An ecological perspective on nanomaterial impacts in the environment, *Journal of Environmental Quality*, **39**, 1954–1965.

Bigorgne, E, Foucaud, L, Lapied, E, Labile, J, Botta, C, Sirguey, C, Falla, J, Rose, J, Joner, E J, Rodius, F and Nahmani, J (2011) Ecotoxicological assessment of TiO(2) byproducts on the earthworm *Eisenia fetida*, *Environmental Pollution*, **159**, 2698–2705.

Bleeker, E A J, de Jong, W H, Geertsma, R E, Groenewold, M, Heugens, E H W, Koers-Jacquemijns, M, Van De Meent, D, Popma, J R, Rietveld, A G, Wijnhoven, S W P, Cassee, F R and Oomen, A G (2013) Considerations on the EU definition of a nanomaterial: Science to support policy making, *Regulatory Toxicology and Pharmacology*, **65**, 119–125.

Bouchard, D and Xin, M (2008) Extraction and high-performance liquid chromatographic analysis of C_{60}, C_{70} and [6,6]-phenyl C_{61}-butyric acid methyl ester in synthetic and natural waters, *Journal of Chromatography A*, **1203**, 153–159.

Bradford, A, Handy, R D, Readman, J W, Atfield, A and Muhling, M (2009) Impact of silver nanoparticle contamination on the genetic diversity of natural bacterial assemblages in estuarine sediments, *Environmental Science and Technology*, **43**, 4530–4536.

Brar, S K and Verma, M (2011) Measurement of nanoparticles by light-scattering techniques, *Trac-Trends in Analytical Chemistry*, **30**, 4–17.

Brausch, K A, Anderson, T A, Smith, P N and Maul, J D (2010) Effects of functionalized fullerenes on bifenthrin and tribufos toxicity to *Daphnia magna*: Survival,

reproduction, and growth rate, *Environmental Toxicology and Chemistry*, **29**, 2600–2606.

Breggin, L K, Falkner, R, Pendergrass, J, Porter, R and Jaspers, N (2011) Chapter 8 – Addressing the risks of nanomaterials under United States and European Union regulatory frameworks for chemicals, In: *Assessing Nanoparticle Risks to Human Health*, Oxford: William Andrew Publishing, 195–272.

Bystrzejewska-Piotrowska, G, Golimowski, J and Urban, P L (2009) Nanoparticles: Their potential toxicity, waste and environmental management, *Waste Management*, **29**, 2587–2595.

Carrillo-Carrion, C, Lendl, B, Simonet, B M and Valcarcel, M (2011) Calix[8]arene coated CdSe/ZnS quantum dots as C 60-nanosensor, *Analytical Chemistry*, **83**, 8093–8100.

Casado, M P, Macken, A and Byrne, H J (2013) Ecotoxicological assessment of silica and polystyrene nanoparticles assessed by a multitrophic test battery, *Environment International*, **51**, 97–105.

Chen, H C and Ding, W H (2012) Determination of aqueous fullerene aggregates in water by ultrasound-assisted dispersive liquid–liquid microextraction with liquid chromatography–atmospheric pressure photoionization-tandem mass spectrometry, *Journal of Chromatography A*, **1223**, 15–23.

Chen, Z, Westerhoff, P and Herckes, P (2008) Quantification of C 60 fullerene concentrations in water, *Environmental Toxicology and Chemistry*, **27**, 1852–1859.

Chen, Z, Yadghar, A M, Zhao, L and Mi, Z T (2011) A review of environmental effects and management of nanomaterials, *Toxicological and Environmental Chemistry*, **93**, 1227–1250.

Cheng, J P, Flahaut, E and Cheng, S H (2007) Effect of carbon nanotubes on developing zebrafish (*Danio rerio*) embryos, *Environmental Toxicology and Chemistry*, **26**, 708–716.

Communication from the Commission to the European Parliament, the Council and the European Economic and Social Committee – Second Regulatory Review on Nanomaterials Brussels, COM(2012) 572 final.

Coutris, C, Joner, E J and Oughton, D H (2012) Aging and soil organic matter content affect the fate of silver nanoparticles in soil, *Science of the Total Environment*, **420**, 327–333.

da Silva, B F, Perez, S, Gardinalli, P, Singhal, R K, Mozeto, A A and Barceló, D (2011) Analytical chemistry of metallic nanoparticles in natural environments, *Trac-Trends in Analytical Chemistry*, **30**, 528–540.

Darlington, T K, Neigh, A M, Spencer, M T, Nguyen, O T and Oldenburg, S J (2009) Nanoparticle characteristics affecting environmental fate and transport through soil, *Environmental Toxicology and Chemistry*, **28**, 1191–1199.

Directive 2000/60/EC of the European Parliament and of the Council of 23 October 2000 establishing a framework for Community action in the field of water policy. *Official Journal of the European Communities*, **L 327**, 1–72. Brussels.

Directive 2008/98/EC of the European Parliament and of the Council of 19 November 2008 on waste and repealing certain Directives. *Official Journal of the European Communities*, **L 312**, 3–30. 22 November 2008a. Brussels.

Directive 2010/75/EU of the European Parliament and of the Council of 24 November 2010 on industrial emissions (integrated pollution prevention and control) Text with EEA relevance. *Official Journal of the European Communities*, **L 334**, 0017–0119. 2010a. Brussels.

Directive 2012/18/EU of the European Parliament and of the Council of 4 July 2012 on the control of major-accident hazards involving dangerous substances, amending and subsequently repealing Council Directive 96/82/EC. *Official Journal of the European Communities*, **L 197**, 1–37. 2012b. Brussels.

Domingos, R F, Baalousha, M A, Ju-Nam, Y, Reid, M M, Tufenkji, N, Lead, J R, Leppard, G and G, Wilkinson, K J (2009) Characterizing manufactured nanoparticles in the environment: Multimethod determination of particle sizes, *Environmental Science and Technology*, **43**, 7277–7284.

Duester, L, Rakcheev, D, Bayer, J V, Abraham, P M, Dabrunz, A, Schulz, R and Schaumann, G E (2011) A robust, particle size independent, method for quantifying metal(loid oxide) nanoparticles and their agglomerates in complex environmental matrices by electrothermal vaporisation coupled to ICP-MS, *Journal of Analytical Atomic Spectrometry*, **26**, 450–455.

Eckelman, M J, Mauter, M S, Isaacs, J A and Elimelech, M (2012) New perspectives on nanomaterial aquatic ecotoxicity: production impacts exceed direct exposure impacts for carbon nanotubes, *Environmental Science and Technology*, **46**, 2902–2910.

Elzey, S and Grassian, V H (2010) Agglomeration, isolation and dissolution of commercially manufactured silver nanoparticles in aqueous environments, *Journal of Nanoparticle Research*, **12**, 1945–1958.

European Commission Recommendation of 18 October 2011 on the definition of nanomaterial (2011/696/EU). *Official Journal of the European Communities*, **L 275**, 38–40. 2012c. Luxembourg.

Farre, M and Barceló, D. (2011a) Characterization, analysis and risks of nanomaterials in environmental and food samples II. *Trac-Trends in Analytical Chemistry*, **30**, 415–568.

Farre, M and Barceló, D. (2011b) Characterization, analysis and risks of nanomaterials in environmental and food samples I. *Trac-Trends in Analytical Chemistry*, **30**, 1–164.

Farre, M and Barceló, D.(2012) *Analysis and Risk of Nanomaterials in Environmental and Food Samples*, Amsterdam, Elsevier.

Farre, M, Gajda-Schrantz, K, Kantiani, L and Barceló, D (2009) Ecotoxicity and analysis of nanomaterials in the aquatic environment, *Analytical and Bioanal Chem*, **393**, 81–95.

Farre, M, Sanchis, J and Barceló, D (2011) Analysis and assessment of the occurrence, the fate and the behavior of nanomaterials in the environment, *Trac-Trends in Analytical Chemistry*, **30**, 517–527.

Farre, M, Perez, S, Gajda-Schrantz, K, Osorio, V, Kantiani, L, Ginebreda, A and Barceló, D (2010) First determination of C_{60} and C_{70} fullerenes and N-methylfulleropyrrolidine C_{60} on the suspended material of wastewater effluents by liquid chromatography hybrid quadrupole linear ion trap tandem mass spectrometry, *Journal of Hydrology*, **383**, 44–51.

Felekis, T A and Katsaros, N (2009) Environment and nanotechnology: A promising challenge, *Journal of Environmental Protection and Ecology*, **10**, 1146–1154.

Fushimi, A, Tanabe, K, Hasegawa, S and Kobayashi, S (2007) Investigation of characterization method for nanoparticles in roadside atmosphere by thermal desorption–gas chromatography/mass spectrometry using a pyrolyzer, *Science of the Total Environment*, **386**, 83–92.

Gallego-Urrea, J A, Tuoriniemi, J and Hassellov, M (2011) Applications of particle-tracking analysis to the determination of size distributions and concentrations of nanoparticles in environmental, biological and food samples, *Trac-Trends in Analytical Chemistry*, **30**, 473–483.

Gallego-Urrea, J A, Tuoriniemi, J, Pallander, T and Hassellöv, M (2010) Measurements of nanoparticle number concentrations and size distributions in contrasting aquatic environments using nanoparticle tracking analysis, *Environmental Chemistry*, **7**, 67–81.

Gao, J, Bonzongo, J C J, Bitton, G, Li, Y and Wu, C Y (2008) Nanowastes and the environment: Using mercury as an example pollutant to assess the environmental fate of chemicals adsorbed onto manufactured nanomaterials, *Environmental Toxicology and Chemistry*, **27**, 808–810.

Garcia-Negrete, C A, Blasco, J, Volland, M, Rojas, T C, Hampel, M, Lapresta-Fernandez, A, Jimenez de Haro, M C, Soto, M and Fernandez, A (2013) Behaviour of Au-citrate nanoparticles in seawater and accumulation in bivalves at environmentally relevant concentrations, *Environmental Pollution*, **174**, 134–141.

Geranio, L, Heuberger, M and Nowack, B (2009) The behavior of silver nanotextiles during washing, *Environmental Science and Technology*, **43**, 8113–8118.

Ghosh, M, Chakraborty, A, Bandyopadhyay, M and Mukherjee, A (2011) Multi-walled carbon nanotubes (MWCNT): Induction of DNA damage in plant and mammalian cells, *Journal of Hazardous Materials*, **197**, 327–336.

Gogos, A, Knauer, K and Bucheli, T D (2012) Nanomaterials in plant protection and fertilization: Current state, foreseen applications, and research priorities, *Journal of Agriculture and Food Chemistry*, **60**, 9781–9792.

Gottschalk, F, Sonderer, T, Scholz, R W and Nowack, B (2009) Modeled environmental concentrations of engineered nanomaterials (TiO(2), ZnO, Ag, CNT, fullerenes) for different regions, *Environmental Science and Technology*, **43**, 9216–9222.

Gottschalk, F, Sonderer, T, Scholz, R W and Nowack, B (2010) Possibilities and limitations of modeling environmental exposure to engineered nanomaterials by material flow analysis, *Environmental Toxicology and Chemistry*, **29**, 1036–1048.

Government of Canada (2013) Nanoportal-NanoRegulations. http://nanoportal.gc.ca/default.asp?lang=En&n=23410D1F-1.

Grieger, K D, Hansen, S F, Sorensen, P B and Baun, A (2011) Conceptual modeling for identification of worst case conditions in environmental risk assessment of nanomaterials using nZVI and C(60) as case studies, *Science of the Total Environment*, **409**, 4109–4124.

Handy, R D, Owen, R and Valsami-Jones, E (2008) The ecotoxicology of nanoparticles and nanomaterials: current status, knowledge gaps, challenges, and future needs, *Ecotoxicology*, **17**, 315–325.

Hansen, S F (2010) A global view of regulations affecting nanomaterials, *Wiley Interdisciplinary Reviews-Nanomedicine and Nanobiotechnology*, **2**, 441–449.

Hansen, S F and Baun, A (2012) European regulation affecting nanomaterials – Review of limitations and future recommendations, *Dose-Response*, **10**, 364–383.

Hendrickson, O, Fedyunina, N, Zherdev, A, Solopova, O, Sveshnikov, P and Dzantiev, B (2012) Production of monoclonal antibodies against fullerene C 60 and development of a fullerene enzyme immunoassay, *Analyst*, **137**, 98–105.

Hernando, M D, Rosenkranz, P, Ulaszewska, M M, Fernandez-Cruz, M L, Fernandez-Alba, A R and Navas, J M (2012) *In vitro* dose-response effects of poly(amidoamine) dendrimers [amino-terminated and surface-modified with N-(2-hydroxydodecyl) groups] and quantitative determination by a liquid chromatography-hybrid quadrupole/time-of-flight mass spectrometry based method, *Anal Bioanal Chem*, **404**, 2749–2763.

Hoon, H and Jae-Hong, K (2009) Dispersion of C_{60} in natural water and removal by conventional drinking water treatment processes, *Water Research*, **43**, 2463–2470.

Hotze, E M, Phenrat, T and Lowry, G V (2010) Nanoparticle aggregation: challenges to understanding transport and reactivity in the environment, *Journal of Environmental Quality*, **39**, 1909–1924.

Howard, A G (2010) On the challenge of quantifying man-made nanoparticles in the aquatic environment, *Journal of Environmental Monitoring*, **12**, 135–142.

Hyung, H, Fortner, J D, Hughes, J B and Kim, J H (2007) Natural organic matter stabilizes carbon nanotubes in the aqueous phase, *Environmental Science and Technology*, **41**, 179–184.

Ingle, T M, Alexander, R, Bouldin, J and Buchanan, R A (2008) Absorption of semiconductor nanocrystals by the aquatic invertebrate Ceriodaphnia dubia, *Bulletin of Environmental Contamination and Toxicology*, **81**, 249–252.

Isaacson, C W and Bouchard, D (2010) Asymmetric flow field flow fractionation of aqueous C_{60} nanoparticles with size determination by dynamic light scattering and quantification by liquid chromatography atmospheric pressure photo-ionization mass spectrometry, *Journal of Chromatography A*, **1217**, 1506–1512.

Jiang, G X, Shen, Z Y, Niu, J F, Zhuang, L P and He, T D (2011) Nanotoxicity of engineered nanomaterials in the environment, *Progress in Chemistry*, **23**, 1769–1781.

Jiménez, M S, Gómez, M T, Bolea, E, Laborda, F and Castillo, J (2011) An approach to the natural and engineered nanoparticles analysis in the environment by inductively coupled plasma mass spectrometry, *International Journal of Mass Spectrometry*, **307**, 99–104.

Johansen, A, Pedersen, A L, Jensen, K A, Karlson, U, Hansen, B M, Scott-Fordsmand, J J and Winding, A (2008) Effects of C(60) fullerene nanoparticles on soil bacteria and protozoans, *Environmental Toxicology and Chemistry*, **27**, 1895–1903.

Johnston, B D, Scown, T M, Moger, J, Cumberland, S A, Baalousha, M, Linge, K, van Aerle, R, Jarvis, K, Lead, J R and Tyler, C R (2010) Bioavailability of nanoscale metal oxides TiO(2), CeO(2), and ZnO to Fish, *Environmental Science and Technology*, **44**, 1144–1151.

Judy, J D, Unrine, J M and Bertsch, P M (2011) Evidence for biomagnification of gold nanoparticles within a terrestrial food chain, *Environmental Science and Technology*, **45**, 776–781.

Kaegi, R, Ulrich, A, Sinnet, B, Vonbank, R, Wichser, A, Zuleeg, S, Simmler, H, Brunner, S, Vonmont, H, Burkhardt, M and Boller, M (2008) Synthetic TiO(2) nanoparticle emission from exterior facades into the aquatic environment, *Environmental Pollution*, **156**, 233–239.

Kennedy, A J, Hull, M S, Steevens, J A, Dontsova, K M, Chappell, M A, Gunter, J C and Weiss, C A (2008) Factors influencing the partitioning and toxicity of nanotubes in the aquatic environment, *Environmental Toxicology and Chemistry*, **27**, 1932–1941.

Koelmans, A A, Nowack, B and Wiesner, M R (2009) Comparison of manufactured and black carbon nanoparticle concentrations in aquatic sediments, *Environmental Pollution*, **157**, 1110–1116.

Kohler, A R, Som, C, Helland, A and Gottschalk, F (2008) Studying the potential release of carbon nanotubes throughout the application life cycle, *Journal of Cleaner Production*, **16**, 927–937.

Kumar, P, Robins, A, Vardoulakis, S and Britter, R (2010) A review of the characteristics of nanoparticles in the urban atmosphere and the prospects for developing regulatory controls, *Atmospheric Environment*, **44**, 5035–5052.

Lee, S, Kim, K, Shon, H K, Kim, S D and Cho, J (2011) Biotoxicity of nanoparticles: effect of natural organic matter, *Journal of Nanoparticle Research*, **13**, 3051–3061.

Li, D, Lyon, D Y, Li, Q and Alvarez, P J J (2008) Effect of soil sorption and aquatic natural organic matter on the antibacterial activity of a fullerene water suspension, *Environmental Toxicology and Chemistry*, **27**, 1888–1894.

Liden, G (2011) The European Commission tries to define nanomaterials, *Annals of Occupational Hygiene*, **55**, 1–5.

Lin, D H, Tian, X L, Wu, F C and Xing, B S (2010) Fate and transport of engineered nanomaterials in the environment, *Journal of Environmental Quality*, **39**, 1896–908.

Liu, X Y, Vinson, D, Abt, D, Hurt, R H and Rand, D M (2009) Differential toxicity of carbon nanomaterials in drosophila: Larval dietary uptake is benign, but adult exposure causes locomotor impairment and mortality, *Environmental Science and Technology*, **43**, 6357–6363.

Lopez-Lorente, A I, Simonet, B M and Valcarcel, M (2012) Rapid analysis of gold nanoparticles in liver and river water samples, *Analyst*, **137**, 3528–3534.

Lowry, G V, Gregory, K B, Apte, S C and Lead, J R. (2012) Transformation of nanomaterials in the environment, *Environmental Science and Technology,* **46**, 6891–7434.

Luo, Z X, Wang, Z H, Li, Q Z, Pan, Q K, Yan, C Z and Liu, F (2011) Spatial distribution, electron microscopy analysis of titanium and its correlation to heavy metals: Occurrence and sources of titanium nanomaterials in surface sediments from Xiamen Bay, China, *Journal of Environmental Monitoring*, **13**, 1046–1052.

Lyon, D Y, Adams, L K, Falkner, J C and Alvarez, P J J (2006) Antibacterial activity of fullerene water suspensions: Effects of preparation method and particle size, *Environmental Science and Technology*, **40**, 4360–4366.

Majestic, B J, Erdakos, G B, Lewandowski, M, Oliver, K D, Willis, R D, Kleindienst, T E and Bhave, P V (2010) A review of selected engineered nanoparticles in the atmosphere sources, transformations and techniques for sampling and analysis, *International Journal of Occupational and Environmental Health*, **16**, 488–507.

Mattison, N T, O'Carroll, D M, Rowe, R K and Petersen, E J (2011) Impact of porous media grain size on the transport of multi-walled carbon nanotubes, *Environmental Science and Technology*, **45**, 9765–9775.

Mendez, P F, Sepulveda, S, Manriquez, J, Rodriguez, F J, Bustos, E, Rodriguez, A and Godinez, L A (2012) Growth dynamics of polyamidoamine dendrimer encapsulated CdS nanoparticles, *Journal of Crystal Growth*, **361**, 108–113.

Mitrano, D M, Barber, A, Bednar, A, Westerhoff, P, Higgins, C P and Ranville, J F (2012a) Silver nanoparticle characterization using single-particle ICP-MS

(SP-ICP-MS) and asymmetrical flow field flow fractionation ICP-MS (AF4-ICP-MS), *Journal of Analytical Atomic Spectrometry*, **27**, 1131–1142.

Mitrano, D M, Lesher, E K, Bednar, A, Monserud, J, Higgins, C P and Ranville, J F (2012b) Detecting nanoparticulate silver using single-particle inductively coupled plasma-mass spectrometry, *Environmental Toxicology and Chemistry*, **31**, 115–121.

Myojo, T, Oyabu, T, Ogami, A, Hirohashi, M, Murakami, M, Yamamoto, M, Todoroki, M, Kadoya, C, Nishi, K, Yamasaki, S, Morimoto, Y, Tanaka, I, Shimada, M and Endoh, S (2011) Monitoring of C 60 aerosol concentrations during 4-week inhalation study using a carbon aerosol analyzer with adjusted analytical protocol, *Journal of Nanoparticle Research*, **13**, 2063–2071.

Nanowerk: Nanotechnology and Emerging Technologies. (Available at www.nanowerk.com) last access 2013.

Navarro, D A, Depner, S W, Watson, D F, Aga, D S and Banerjee, S (2011) Partitioning behavior and stabilization of hydrophobically coated HfO(2), ZrO(2) and Hf(x)Zr(1-x)O(2) nanoparticles with natural organic matter reveal differences dependent on crystal structure, *Journal of Hazardous Materials*, **196**, 196–302.

Navarro, D A G, Watson, D F, Aga, D S and Banerjee, S (2009) Natural organic matter-mediated phase transfer of quantum dots in the aquatic environment, *Environmental Science and Technology*, **43**, 677–682.

O'Brien, N and Cummins, E (2008) Recent developments in nanotechnology and risk assessment strategies for addressing public and environmental health concerns, *Human and Ecological Risk Assessment*, **14**, 568–592.

O'Brien, N and Cummins, E (2010) Ranking initial environmental and human health risk resulting from environmentally relevant nanomaterials, *Journal of Environmental Science and Health Part a-Toxic/Hazardous Substances and Environmental Engineering*, **45**, 992–1007.

Ochiai, N, Ieda, T, Sasamoto, K, Fushimi, A, Hasegawa, S, Tanabe, K and Kobayashi, S (2007) Comprehensive two-dimensional gas chromatography coupled to high-resolution time-of-flight mass spectrometry and simultaneous nitrogen phosphorous and mass spectrometric detection for characterization of nanoparticles in roadside atmosphere, *Journal of Chromatography A*, **1150**, 13–20.

Park, J W, Henry, T B, Menn, F M, Compton, R N and Sayler, G (2010) No bioavailability of 17 alpha-ethinylestradiol when associated with nC(60) aggregates during dietary exposure in adult male zebrafish (*Danio rerio*), *Chemosphere*, **81**, 1227–1232.

Peralta-Videa, J R, Zhao, L, Lopez-Moreno, M L, de la Rosa, G, Hong, J and Gardea-Torresdey, J L (2011) Nanomaterials and the environment: A review for the biennium 2008–2010, *Journal of Hazardous Materials*, **186**, 1–15.

Perez, S, Farre, M and Barcelo, D (2009) Analysis, behavior and ecotoxicity of carbon-based nanomaterials in the aquatic environment, *TrAC Trends in Analytical Chemistry*, **28**, 820–832.

Petersen, E J and Henry, T B (2012) Methodological considerations for testing the ecotoxicity of carbon nanotubes and fullerenes: Review, *Environmental Toxicology and Chemistry*, **31**, 60–72.

Quik, J T K, Lynch, I, Hoecke, K V, Miermans, C J H, Schamphelaere, K A C D, Janssen, C R, Dawson, K A, Stuart, M A C and Meent, D V D (2010) Effect of

natural organic matter on cerium dioxide nanoparticles settling in model fresh water, *Chemosphere*, **81**, 711–715.

Quik, J T K, Vonk, J A, Hansen, S F, Baun, A and Van De Meent, D (2011) How to assess exposure of aquatic organisms to manufactured nanoparticles?, *Environment International*, **37**, 1068–1077.

Raz, S R, Leontaridou, M, Bremer, M G E G, Peters, R and Weigel, S (2012) Development of surface plasmon resonance-based sensor for detection of silver nanoparticles in food and the environment, *Anal Bioanal Chem*, **403**, 2843–2850.

Regulation (EC) No 1272/2008 of the European Parliament and of the Council of 16 December 2008 on classification, labelling and packaging of substances and mixtures, amending and repealing Directives 67/548/EEC and 1999/45/EC, and amending Regulation (EC) No 1907/2006. *Official Journal of the European Communities*, **L 353**, 1–1355. 2008b. Brussels.

Regulation (EC) No 1907/2006 of the European Parliament and of the Council of 18 December 2006 concerning the Registration, Evaluation, Authorisation and Restriction of Chemicals (REACH), establishing a European Chemicals Agency, amending Directive 1999/45/EC and repealing Council Regulation (EEC) No 793/93 and Commission Regulation (EC) No 1488/94 as well as Council Directive 76/769/EEC and Commission Directives 91/155/EEC, 93/67/EEC, 93/105/EC and 2000/21/EC. *Official Journal of the European Communities*, **L 396**, 1–849. 2010b.

Regulation (EU) No 1169/2011 of the European Parliament and of the Council of 25 October 2011 on the provision of food information to consumers, amending Regulations (EC) No 1924/2006 and (EC) No 1925/2006 of the European Parliament and of the Council, and repealing Commission Directive 87/250/EEC, Council Directive 90/496/EEC, Commission Directive 1999/10/EC, Directive 2000/13/EC of the European Parliament and of the Council, Commission Directives 2002/67/EC and 2008/5/EC and Commission Regulation (EC) No 608/2004 Text with EEA relevance. *Official Journal of the European Communities*, **L 304**, 18–63. 2011b. Brussels.

Sanchis, J, Berrojalbiz, N, Caballero, G, Dachs, J, Farre, M and Barcelo, D (2012) Occurrence of aerosol-bound fullerenes in the mediterranean sea atmosphere, *Environmental Science and Technology*, **46**, 1335–1343.

Sandin, P, Fitzpatrick, L W, Simpson, J C and Dawson, K A (2012) High-speed imaging of rab family small GTPases reveals rare events in nanoparticle trafficking in living cells, *Acs Nano*, **6**, 1513–1521.

Schmidt, B, Loeschner, K, Hadrup, N, Mortensen, A, Sloth, J J, Koch, C B and Larsen, E H (2011) Quantitative characterization of gold nanoparticles by field-flow fractionation coupled online with light scattering detection and inductively coupled plasma mass spectrometry, *Analytical Chemistry*, **83**, 2461–2468.

Simonet, B M and Valcarcel, M (2009) Monitoring nanoparticles in the environment, *Analytical and Bioanalytical Chemistry*, **393**, 17–21.

Stone, V, Nowack, B, Baun, A, van den Brink, N, von der Kammer, F, Dusinska, M, Handy, R, Hankin, S, Hassellöv, M, Joner, E and Fernandes, T F (2010) Nanomaterials for environmental studies: Classification, reference material issues and strategies for physico-chemical characterisation, *Science of the Total Environment*, **408**, 1745–1754.

Suarez, B, Moliner-Martínez, Y, Cardenas, S, Simonet, B M and Valcarcel, M (2008) Monitoring of carboxylic carbon nanotubes in surface water by

using multiwalled carbon nanotube-modified filter as preconcentration unit, *Environmental Science and Technology*, **42**, 6100–6104.

Suarez, I J, Rosal, R, Rodriguez, A, Ucles, A, Fernandez-Alba, A R, Hernando, M D and Garcia-Calvo, E (2011) Chemical and ecotoxicological assessment of poly(amidoamine) dendrimers in the aquatic environment, *Trac-Trends in Analytical Chemistry*, **30**, 492–506.

Sun, W, Wang, H, Xie, C, Hu, Y, Yang, X and Xu, H (2006) An attempt to directly trace polymeric nanoparticles *in vivo* with electron microscopy, *Journal of Controlled Release*, **115**, 259–265.

Tan, C, Fan, W H and Wang, W X (2012) Role of titanium dioxide nanoparticles in the elevated uptake and retention of cadmium and zinc in *Daphnia magna*, *Environmental Science and Technology*, **46**, 469–476.

Tedesco, S, Doyle, H, Blasco, J, Redmond, G and Sheehan, D (2010) Oxidative stress and toxicity of gold nanoparticles in *Mytilus edulis*, *Aquatic Toxicology*, **15**, 178–186.

Tedesco, S, Doyle, H, Blasco, J, Redmond, G and Sheehan, D (2010) Exposure of the blue mussel, *Mytilus edulis*, to gold nanoparticles and the pro-oxidant menadione, *Comparative Biochemistry and Physiology C*, **151**, 167–174.

Tervonen, T, Linkov, I, Figueira, J R, Steevens, J, Chappell, M and Merad, M (2009) Risk-based classification system of nanomaterials, *Journal of Nanoparticle Research*, **11**, 757–766.

Tiede, K, Boxall, A B A, Tear, S P, Lewis, J, David, H and Hassellöv, M (2008) Detection and characterization of engineered nanoparticles in food and the environment, *Food Additives and Contaminants Part A-Chemistry Analysis Control Exposure and Risk Assessment*, **25**, 795–821.

Tiede, K, Boxall, A B A, Tiede, D, Tear, S P, David, H and Lewis, J (2009) A robust size-characterisation methodology for studying nanoparticle behaviour in 'real' environmental samples, using hydrodynamic chromatography coupled to ICP-MS, *Journal of Analytical Atomic Spectrometry*, **24**, 964–972.

Ucles, A, Ulaszewska, M M, Hernando, M D, Ramos, M J, Herrera, S, Garcia, E and Fernandez-Alba, A R (2013) Qualitative and quantitative analysis of poly(amidoamine) dendrimers in an aqueous matrix by liquid chromatography-electrospray ionization-hybrid quadrupole/time-of-flight mass spectrometry (LC-ESI-QTOF-MS). *Analytical and Bioanalytical Chemistry*, **405**, 5901–14

Ulaszewska, M M, Hernando, M D, Moreno, A U, Garcia, A V, Calvo, E G and Fernandez-Alba, A R (2013) Identification and quantification of poly(amidoamine) PAMAM dendrimers of generations 0 to 3 by liquid chromatography/hybrid quadrupole time-of-flight mass spectrometry in aqueous medium, *Rapid Communications in Mass Spectrometry*, **27**, 747–762.

von der Kammer, F, Ferguson, P L, Holden, P A, Masion, A, Rogers, K R, Klaine, S J, Koelmans, A A, Horne, N and Unrine, J M (2012) Analysis of engineered nanomaterials in complex matrices (environment and biota): General considerations and conceptual case studies, *Environmental Toxicology and Chemistry*, **31**, 32–49.

Wang, C, Shang, C and Westerhoff, P (2010a) Quantification of fullerene aggregate nC_{60} in wastewater by high-performance liquid chromatography with UV–vis spectroscopic and mass spectrometric detection, *Chemosphere*, **80**, 334–339.

Wang, D M, Hu, J, Irons, D R and Wang, J M (2011a) Synergistic toxic effect of nano-TiO(2) and As(V) on Ceriodaphnia dubia, *Science of the Total Environment*, **409**, 1351–1356.

Wang, F, Costabileb, F, Li, H, Fang, D and Alligrini, I (2010b) Measurements of ultrafine particle size distribution near Rome, *Atmospheric Research*, **98**, 69–77.

Wang, J, Cai, Q, Fang, Y, Anderson, T A and Cobb, G P (2011b) Determination of fullerenes (C_{60}) in artificial sediments by liquid chromatography, *Talanta*, **87**, 35–39.

Watson, J G, Chow, J C, Sodeman, D A, Lowenthal, D H, Chang, M-C O, Park, K and Wang, X (2011) Comparison of four scanning mobility particle sizers at the Fresno Supersite, *Particuology*, **9**, 204–209.

Wiench, K, Wohlleben, W, Hisgen, V, Radke, K, Salinas, E, Zok, S and Landsiedel, R (2009) Acute and chronic effects of nano- and non-nano-scale TiO_2 and ZnO particles on mobility and reproduction of the freshwater invertebrate *Daphnia magna*, *Chemosphere*, **76**, 1356–1365.

Wiesner, M R, Hotze, E M, Brant, J A and Espinasse, B (2008) Nanomaterials as possible contaminants: The fullerene example, *Water Science and Technology*, **57**, 305–310.

Wild, E and Jones, K C (2009) Novel method for the direct visualization of *in vivo* nanomaterials and chemical interactions in plants, *Environmental Science and Technology*, **43**, 5290–5994.

Woodrow Wilson International Center for Scholars (2013) The project on emerging technologies: Agrifood Nanotechnology Research and Development, http://www.nanotechproject.org/inventories/.

Xia, X, Monteiro-Riviere, N A and Riviere, J E (2006) Trace analysis of fullerenes in biological samples by simplified liquid–liquid extraction and high-performance liquid chromatography, *Journal of Chromatography A*, **1129**, 216–222.

Yan, X M, Shi, B Y, Wang, D S and Tang, H X (2008) The eco-toxic aspects of aqueous nano-C-60 fullerenes, *Progress in Chemistry*, **20**, 422–428.

Yang, X, Su, Y, Paau, M C and Choi, M M F (2012) Mass spectrometric identification of water-soluble gold nanocluster fractions from sequential size-selective precipitation, *Analytical Chemistry*, **84**, 1765–1771.

Yu, L and Andriola, A (2010) Quantitative gold nanoparticle analysis methods: A review, *Talanta*, **82**, 869–875.

Zea, H R (2012) Nanomaterials: Health effects and legislation, *Ingenieria e Investigacion*, **32**, 36–41.

Zhang, R Y, Khalizov, A, Wang, L, Hu, M and Xu, W (2012) Nucleation and growth of nanoparticles in the atmosphere, *Chemical Reviews*, **112**, 1957–2011.

Zhao, J, Wang, Z Y, Liu, X Y, Xie, X Y, Zhang, K and Xing, B S (2011) Distribution of CuO nanoparticles in juvenile carp (*Cyprinus carpio*) and their potential toxicity, *Journal of Hazardous Materials*, **197**, 304–310.

Zhu, H, Han, J, Xiao, J Q and Jin, Y (2008) Uptake, translocation, and accumulation of manufactured iron oxide nanoparticles by pumpkin plants, *Journal of Environmental Monitoring*, **10**, 713–717.

Index